

PROCEEDINGS OF THE TWENTY-FIRST WORKSHOP
ON
GENERAL RELATIVITY AND GRAVITATION
IN JAPAN

SAKURA HALL, TOHOKU UNIVERSITY
SENDAI, JAPAN

SEPTEMBER 26-29, 2011

Edited by
Yousuke Itoh

Organising Committee

Scientific Organising Committee

Hideki Asada (Hirotsuki University)
Takeshi Chiba (Nihon University)
Tomohiro Harada (Rikkyo University)
Kunihito Ioka (High Energy Accelerator Research Organization)
Hideki Ishihara (Osaka City University)
Hideo Kodama (High Energy Accelerator Research Organization)
Yasufumi Kojima (Hiroshima University)
Kei-ichi Maeda (Waseda University)
Shinji Mukohyama (Institute for the Physics and Mathematics of the Universe, University of Tokyo)
Takashi Nakamura (Kyoto University)
Ken-ichi Nakao (Osaka City University)
Yasusada Nambu (Nagoya University)
Ken-ichi Oohara (Niigata University)
Misao Sasaki (Yukawa Institute for Theoretical Physics, Kyoto University)
Naoki Seto (Kyoto University)
Masaru Shibata (Yukawa Institute for Theoretical Physics, Kyoto University)
Tetsuya Shiromizu (Kyoto University)
Jiro Soda (Kyoto University)
Naoshi Sugiyama (Nagoya University)
Takahiro Tanaka (Yukawa Institute for Theoretical Physics, Kyoto University)
Shoichi Yamada (Waseda University)
Masahide Yamaguchi (Tokyo Institute of Technology)
Jun'ichi Yokoyama (Research Center for the Early Universe, University of Tokyo)

Local Organizing Committee

Toshifumi Futamase [Chair](Astronomical Institute, Tohoku University)
Yousuke Itoh (Astronomical Institute, Tohoku University)
Sumio Yamada (Mathematical Institute, Tohoku University)
Masahiro Yamaguchi (Particle Theory and Cosmology Group, Tohoku University)
Shijun Yoshida (Astronomical Institute, Tohoku University)

Preface

The year 2011 may be remembered by many of us as the year of the East Japan Great Earthquake and the fatal accident of the Fukushima Daiichi nuclear power-plants which seriously affect life mainly in Tohoku area, Japan. Even around the registration period for the workshop participation in the last July, aftershocks happened frequently and safety of the power-plants was not perfectly. In this circumstance, it was a great pleasure of the organizing committee to see more than 120 participants attended the workshop and enjoyed 7 invited talks, 46 contributed talks and 28 poster presentations, some of whom were from abroad. The talks and posters cover a wide range of active research topics including experimental hints of the Higgs particle from the LHC, possible use of gravitational waves as probes of the universe and modifications of gravity theory, and inflation with large non-Gaussianity to name a few. “**The twenty-first workshop on General Relativity and Gravitation in Japan**” was thus successfully held at the Tohoku University, 26-29 September 2011, in the year when the university celebrated its 100 years anniversary on the 10th of September. Regarding this success, we appreciate very much all the participants for their warm support for the workshop and their remarkable patience when the LOC asked them accept the profound changes of the workshop program. ¹

This workshop is supported by the following Grants-in-Aid for Scientific Research from the Japan Society for the Promotion of Science (JSPS) and the Ministry of Education, Culture, Sports, Science, and Technology in Japan (MEXT). The grants in alphabetical order of the research representatives’ names are the JSPS Grant-in-Aid for Creative Scientific Research No. 19GS0219 (Tohru Eguchi), the MEXT Grant-in-Aid for Scientific Research on Priority Areas No. 18072001 (Toshifumi Futamase), the MEXT Grant-in-Aid for Scientific Research on Innovative Areas No. 21111006 (Hideo Kodama), and the JSPS Grant-in-Aid for Scientific Research (A) No. 20244009 (Takayoshi Ogawa) and No. 21244033 (Misao Sasaki). The MEXT Tohoku University Global COE Program Scienceweb also supports this workshop. Edamatsu-Kosaka-Mitumori group of Research Institute of Electrical Communication (RIEC), Tohoku University is greatly acknowledged, for they kindly allowed us to use the conference room in the Laboratory for Nanoelectronics and Spintronics building. The LOC thanks Prof. M. Hotta of Tohoku Univ. very much for his helpful advices regarding the workshop managements. We thank Ms. Kiyoe Yokota (Kyoto University), Satomi Miyata, and Junko Nagasawa (Tohoku University) for their administrative works including visa and reimbursement issues. Graduate students in the Astronomical students of Tohoku University, K. Fujio, R. Kuroshima, Y. Mochizuki, M. Morioka, S. Ogawa, T. Okamura, N. Uchikata, and N. Sugiyama, have taken care of the conference palce preparation during the workshop. We thank Prof. T. Murayama (Tohoku University) for his arranging the wireless lan services available in the Sakura Hall. The LOC is grateful to the management office members of the Sakura Hall, the members of the Astronomical Institute and the Faculty of Science Tohoku University for their kindful help of both financial supports and administrative works.

May 21, 2012
Yousuke Itoh
(on behalf of the JGRG21 LOC)

¹After all, we could not figure out what caused the nasty gas smell spread out in the conference hall in the afternoon of the 28th, September. According to the Sendai city gas company, it was not due to any town gas leak within the conference hall.

List of Participants

No	Family Name	First Name	Affiliation
1	Adachi	Masaru	Hiroisaki University
2	Arakida	Hideyoshi	Iwate University
3	Asada	Hideki	Hirosaki University
4	Asai	Shoji	University of Tokyo
5	Bamba	Kazuharu	Nagoya University
6	Cao	Li-Ming	Kinki University
7	Chiba	Takeshi	Nihon University
8	Figueras	Pau	University of Cambridge
9	Fujii	Shunsuke	Iwate Prefectural Morioka First high School
10	Fujio	Kazuya	Tohoku University
11	Futamase	Toshifumi	Tohoku University
12	Gümrukçüoğlu	Ahmet	Institute for the Physics and Mathematics of the Universe (IPMU) University of Tokyo
13	Harada	Tomohiro	Rikkyo University
14	Hikichi	Takayuki	Nagoya University
15	Hirano	Koichi	Ichinoseki National College of Technology
16	Hiranuma	Yuta	Niigata University
17	Hotokezaka	Kenta	Kyoto University
18	Hotta	Masahiro	Tohoku University
19	Igata	Takahisa	Osaka City University
20	Iguchi	Hideo	Nihon University
21	Ishihara	Hideki	Osaka City University
22	Isoyama	Soichiro	Yukawa Institute for Theoretical Physics (YITP) Kyoto University
23	Itoh	Yousuke	Tohoku University
24	Izumi	Koji	Hirosaki University
25	Kamata	Masaru	Kisarazu National College of Technology
26	Kan	Nahomi	Yamaguchi Junior College
27	Kaneyama	Masato	Niigata University
28	Kato	Yoshiaki	National Astronomical Observatory Japan (NAOJ)
29	Khabibullina	Margarita	Kazan (Volga Region) Federal University
30	Kimura	Masashi	Yukawa Institute for Theoretical Physics (YITP) Kyoto University
31	Kinoshita	Shunichiro	Kyoto University
32	kitamura	takao	Hirosaki University
33	Kitazume	Atsushi	Tohoku University
34	Kiuchi	Kenta	Yukawa Institute for Theoretical Physics (YITP) Kyoto University
35	Kobayashi	Koichiro	Yamaguchi university
36	Kobayashi	Tsutomu	Kyoto University
37	Kodama	Hidewo	High Energy Accelerator Research Organization (KEK)
38	Koike	Tatsuhiko	Keio University
39	Kojima	Yasufumi	Hiroshima University
40	Komatsu	Eiichiro	University of Texas at Austin
41	Kozaki	Hiroshi	Ishikawa National College of Technology
42	Kuroshima	Risa	Tohoku University
43	Kyutoku	Koutarou	Kyoto University
44	Lin	Chunshan	Institute for the Physics and Mathematics of the Universe (IPMU) University of Tokyo
45	Maeda	Hideki	Centro de Estudios Científicos (CECS)
46	Maeda	Kei-ichi	Waseda University
47	Maeda	Satoshi	Kyoto University
48	Martínez	Cristián	Centro de Estudios Científicos (CECS)
49	Matsumoto	Mitsuhiro	Sokendai
50	Mishima	Takashi	Nihon University

No	Family Name	First Name	Affiliation
51	Misonoh	Yosuke	Waseda University
52	Miyamoto	Umpei	Rikkyo University
53	Miyazaki	Akihito	University of Nagasaki
54	Miyoshi	Makoto	National Astronomical Observatory Japan (NAOJ)
55	Mochizuki	Yuuki	Tohoku University
56	Morioka	Masayo	Tohoku University
57	Morisawa	Yoshiyuki	Osaka University of Economics and Law
58	Motohashi	Hayato	Research Center for the Early Universe (RESCEU) University of Tokyo
59	Nakamura	Atsushi	Kitazato University
60	Nakamura	Kouji	National Astronomical Observatory of Japan (NAOJ)
61	Nakao	Ken-ichi	Osaka City University
62	Nambu	Yasusada	Nagoya University
63	Naruko	Atsushi	Yukawa Institute for Theoretical Physics (YITP) Kyoto University
64	Nishikawa	Ryusuke	Osaka City University
65	Nitta	Daisuke	Nagoya University
66	Nozawa	Masato	High Energy Accelerator Research Organization (KEK)
67	Ogawa	Shinpei	Tohoku University
68	Ohashi	Seiju	Kyoto University
69	Ohsumi	Yuji	Nagoya University
70	Okamura	Tomohiro	Tohoku University
71	Okawara	Hiroki	Hirosaki University
72	Oohara	Ken-ichi	Niigata University
73	Pavluchenko	Sergey	Special Astrophysical Observatory of the Russian Academy of Sciences
74	Peloso	Marco	University of Minnesota
75	Saida	Hiromi	Daido University
76	Saijo	Motoyuki	Rikkyo University
77	Saikawa	Ken'ichi	Institute for Cosmic Ray Research (ICRR) University of Tokyo
78	Saito	Keiki	Sokendai
79	Saito	Ryo	Yukawa Institute for Theoretical Physics (YITP) Kyoto University
80	Sakai	Nobuyuki	Yamagata University
81	Sasaki	Misao	Yukawa Institute for Theoretical Physics (YITP) Kyoto University
82	Sato	Ginpei	Tohoku University
83	Sekiguchi	Yuichiro	Yukawa Institute for Theoretical Physics (YITP) Kyoto University
84	Sendouda	Yuuiti	Hirosaki University
85	shibata	masaru	Yukawa Institute of Theoretical Physics (YITP) Kyoto University
86	Shimano	Masahiro	Jumonji Junior and Senior High School
87	Shinkai	Hisaaki	Osaka Institute of Technology
88	Shiraishi	Kiyoshi	Yamaguchi University
89	Shiraishi	Maresuke	Nagoya University
90	Shiromizu	Tetsuya	Kyoto University
91	Siino	Masaru	Tokyo Institute of Technology
92	Soda	Jiro	Kyoto University
93	Sotani	Hajime	National Astronomical Observatory of Japan (NAOJ)
94	Sugimura	Kazuyuki	Yukawa institute for theoretical physics (YITP) Kyoto University
95	Sugiyama	Naonori	Tohoku University
96	Suyama	Teruaki	Research Center for the Early Universe (RESCEU) University of Tokyo
97	Suzuki	Takayuki	Yamaguchi University
98	Tagoshi	Hideyuki	Osaka University
99	Takahashi	Fuminiobu	Tohoku University
100	Takahashi	Masaaki	Aichi University of Education

No	Family Name	First Name	Affiliation
101	Takahashi	Tomohiro	Kyoto University
102	Takami	Kentaro	Max-Planck-Institute for Gravitational Physics Albert-Einstein-Institute
103	Takamizu	Yuichi	Waseda University
104	Tamaki	Takashi	Nihon University
105	Tanabe	Kentaro	Yukawa Institute for Theoretical Physics (YITP) Kyoto University
106	Tanaka	Takahiro	Yukawa Institute for Theoretical Physics (YITP) Kyoto University
107	Taniguchi	Keisuke	University of Tokyo
108	Tomizawa	Shinya	High Energy Accelerator Research Organization (KEK)
109	Torii	Takashi	Osaka Institute of Technology
110	Tsuchiya	Takuya	Waseda University
111	Tsukamoto	Naoki	Rikkyo University
112	Uchikata	Nami	Tohoku University
113	Uzawa	Kunihito	Kinki University
114	Wang	Mu-Tao	Columbia University
115	Watanabe	Masaaki	Kyoto University
116	Yagi	Kent	Kyoto University
117	Yamada	Kei	Hirosaki University
118	Yamada	Sumio	Tohoku University
119	Yamada	Yuta	Osaka Institute of Technology
120	Yamaguchi	Masahide	Tokyo Institute of Technology
121	Yamaguchi	Masahiro	Tohoku University
122	Yamauchi	Daisuke	Institute for Cosmic Ray Research (ICRR) University of Tokyo
123	Yokota	Kiyoe	Kyoto University
124	Yokoyama	Jun'ichi	Research Center for the Early Universe (RESCEU) University of Tokyo
125	Yoshida	Shijun	Tohoku University
126	Yoshino	Hirohata	High Energy Accelerator Research Organization (KEK)
127	Yunes	Nicolás	Massachusetts Institute of Technology (MIT)
128	Zhang	Ying-li	Yukawa Institute for Theoretical Physics (YITP) Kyoto University

Programme of the Workshop and Table of Contents

	Page
Sep. 26 Mon.	
Morning session (Chair: Tetsuya Shiromizu)	
10:40-10:40 Opening address: Toshifumi Futamase (LOC Chair)	
10:40-11:25 Sumio Yamada (Tohoku University, Japan) Riemannian geometric aspects of Penrose-type inequalities	1
11:25-12:10 Mu-Tao Wang (Colombia University, USA) Quasilocal mass in general relativity	9
12:10-14:00 Poster exhibition at the 1st floor of the Sakura Hall and Lunch	
Afternoon session	
14:00-15:00 (Chair: Yasusada Nambu)	
1. Kunihito Uzawa (Kinki) Warped de Sitter compactifications	14
2. Cristián Martínez (CECS) Exact solutions of Einstein gravity with a negative cosmological constant coupled to a massless scalar field in arbitrary spacetime dimensions	18
3. Teruaki Suyama (RESCEU) Black hole perturbation in parity violating gravitational theories	22
4. Sergey Pavluchenko (Special Astrophysical Observatory, Russia) New features of black hole solutions in $f(R; G)$ theories	26
15:00-15:20 COFFEE BREAK 20min	
15:20-16:20 (Chair: Jiro Soda)	
5. Keiki Saito (Sokendai) The high frequency limit in $f(R)$ gravity	30
6. Hayato Motohashi (RESCEU) The unification of inflation and dark energy in extended $f(R)$ gravity	34
7. Ahmet Emir Gümrükçüoğlu (IPMU) Nonlinear perturbations in the IR limit of Horava-Lifshitz gravity	38
8. Naoki Tsukamoto (Rikkyo) There are no stationary axisymmetric star solutions in Horava-Lifshitz gravity	42
16:20-16:40 COFFEE BREAK 20min.	
16:40-17:40 Chair: Takeshi Chiba	
9. Seiju Ohashi (Kyoto) Spherical collapse of inhomogeneous dust cloud in the Lovelock theory	46
10. Kent Yagi (Kyoto) Binary Inspiral in Quadratic Gravity	50

11. Takayuki Suzuki (Yamaguchi)
N-body simulation of cosmic structure formation on the MOffat Gravity
12. Kazuharu Bamba (Nagoya)
Screening scenario for cosmological constant in de Sitter solutions; phantom-divide crossing and finite-time future singularities in non-local gravity 54

Sep. 27 Tue.

Page

Morning session (Chair: Masahiro Yamaguchi)

10:30-11:15

Shoji Asai (University of Tokyo, Japan)

The latest results of LHC - Hint of Higgs and Dark matter

11:15-12:00

Pau Figueras (University of Cambridge, UK)

[Braneworld black holes](#)

58

12:00-13:30 Lunch

Afternoon session

13:30-14:45 (Chair: Ken-ichi Nakao)

1. Umpei Miyamoto (Rikkyo)

[Astrophysical censorship](#)

76

2. Soichiro Isoyama (YITP)

[Cosmic censorship in overcharging a charged black hole with a charged particle](#)

80

3. Tomohiro Harada (Rikkyo)

[High-velocity collision of particles around a rapidly rotating black hole](#)

84

4. Hirotaka Yoshino (KEK)

[Bosenova collapse of axion cloud around a rotating black hole](#)

88

5. Ryo Saito (YITP)

[Constraints on Particle Dark Matter Models by the Presence of Primordial Black Holes](#)

92

14:45-15:00 BREAK 15min

15:00-16:00 (Chair: Shijun Yoshida)

6. Kentaro Takami (AEI Potsdam)

[A quasi-radial stability criterion for rotating relativistic stars](#)

96

7. Hajime Sotani (NAOJ)

[Effect of Pasta Phase on Oscillations in Neutron Stars](#)

100

8. Motoyuki Saijo (Rikkyo)

[Dynamical Approaches for Secular Instabilities in Rotating Stars](#)

104

9. Takashi Tamaki (Nihon)

[What are universal features of gravitating Q-balls?](#)

108

16:00-17:30 Poster session (2) at the 1st floor of the Sakura Hall

Sep. 28 Wed.

Page

Morning session (Chair: Takahiro Tanaka)

10:30-11:15

Eiichiro Komatsu (University of Texas at Austin, USA)
Cosmology in the Next Decade

11:15-12:00

Nicolás Yunes (Massachusetts Institute of Technology, USA)
[Gravitational Waves from Compact Binaries as Probes of the Universe](#)

112

12:00-13:30 Lunch

Afternoon session

13:30-14:45 (Chair: Masaru Shibata)

1. Takuya Tsuchiya (Waseda)

[Constraint propagation and constraint-damping for \$C^2\$ -adjusted formulations](#)

126

2. Yuichiro Sekiguchi (YITP)

[Effects of hyperon in binary neutron star mergers](#)

130

3. Kenta Hotokezaka (Kyoto)

Gravitational waves from binary neutron star mergers: measuring of the equation of state

4. Kenta Kiuchi (YITP)

[Gravitational waves and neutrino emission from the merger of binary neutron stars](#)

134

5. Ken'ichi Saikawa (ICRR)

[Gravitational waves from cosmic string-domain wall networks](#)

138

14:45-14:55 BREAK 10min

14:55-16:10 (Chair: Jun'ichi Yokoyama)

6. Maresuke Shiraishi (Nagoya)

[Violation of the Rotational Invariance in the CMB Bispectrum](#)

142

7. Daisuke Yamauchi (ICRR)

[Weak lensing of CMB from cosmic \(super-\)strings](#)

146

8. Satoshi Maeda (Kyoto)

[Generation of the primordial magnetic fields from the non-adiabatic fluctuations at the pre-recombination era](#)

150

9. Kouji Nakamura (NAOJ)

[Construction of gauge-invariant variables of linear metric perturbation on general background space-time](#)

154

10. Masaru Adachi (Hirosaki)

No Dark Energy is required if we accept a slightly inhomogeneous viewpoint

16:10-16:40 COFFEE BREAK 30min.

16:40-17:25 (Chair: Hideki Ishihara)

11. Li-Ming Cao (Kinki)

Deformation of Codimension-2 surfaces and Horizon thermodynamics

12. Shunichiro Kinoshita (Kyoto)
[Hawking temperature for near-equilibrium black holes](#) 158
13. Hiromi Saida (Dido)
[Universal Property of Quantum Gravity implied Uniqueness Theorem of Bekenstein-Hawking Entropy](#) 163
- 17:25-17:35 BREAK 10min
- 17:35-18:20 (Chair: Kei-ichi Maeda)
14. Mitsuhiro Matsumoto (Sokendai)
[Time Evolution of Evaporating Black Rings](#) 167
15. Masahiro Hotta (Tohoku)
[Quantum Energy Teleportation and Black Hole](#) 171
16. Shinya Tomizawa (KEK)
New solution generation utilizing $SL(2;R)$ -duality and new black holes

Banquet at the 1st floor of the Sakura Hall (18:30-20:30)

Sep. 29, Thur.

Page

Morning session (Chair: Misao Sasaki)

10:30-11:15

Marco Peloso (University of Minnesota, USA)

Phenomenology of a pseudoscalar inflaton: naturally large nongaussianity

11:15-12:00

1. Kazuyuki Sugimura (YITP)

[Multi-field open inflation and instanton](#)

172

2. Tsutomu Kobayashi (Kyoto)

Generalized G-inflation

3. Fuminiobu Takahashi (Tohoku)

[Non-Gaussianity from Hilltop Curvaton](#)

176

12:00-13:30 Lunch

Afternoon session

13:30-14:15 (Chair: Masahide Yamaguchi)

4. Atsushi Naruko (YITP)

[Beyond \$\delta N\$ formalism](#)

178

5. Yuichi Takamizu (Waseda)

[Gradient expansion approach to multi-field inflation](#)

182

6. Masato Nozawa (KEK)

[Parity violation in graviton non-Gaussianity](#)

186

14:15-14:25 BREAK 10min

14:25-15:05 (Chair: Toshifumi Futamase)

7. Margarita Khabibullina (Kazan)

[The estimation of black-hole masses in distant radio galaxies](#)

190

8. Yoshiaki Kato (NAOJ) Exploring the Growth History of Massive Black Holes by Measuring the Spin of the Massive Black Hole Sagittarius A*

9. Makoto Miyoshi (NAOJ)

[Oscillation Phenomena in the Disk around the Massive Black Hole Sagittarius A*](#)

194

Poster contributions

P01	Hideyoshi Arakida (Iwate) Effect of cosmological constant on light deflection	198
P02	Takayuki Hikichi (Nagoya) Numerical simulation of quantum gravity	202
P03	Koichi Hirano (Ichinoseki National College of Technology) Constraining Galileon gravity from observational data with growth rate	206
P04	Takahisa Igata (Osaka City) Stationary Closed Strings in 5d Minkowski Spacetime	
P05	Koji Izumi (Hirosaki) Perturbative solutions to the lens equation for multiple lens planes: With some numerical examples	210
P06	Nahomi Kan (Yamaguchi Junior College) Equations of motion in Double Field Theory: from classical particles to quantum cosmology	213
P07	Masashi Kimura (YITP) Analyticity of event horizons of extremal Kaluza-Klein black holes	
P08	Takao Kitamura (Hirosaki) Astrometric microlensing by the Ellis wormhole	217
P09	Koichiro Kobayashi (Yamaguchi) Flux vacua in DBI type Einstein-Maxwell theory	221
P10	Yasufumi Kojima (Hiroshima) Off-equatorial orbits of charged particles in strong gravity with magnetic dipole field	225
P11	Koutarou Kyutoku (Kyoto) Extracting equation of state parameters from black hole-neutron star mergers	228
P12	Yosuke Misonoh (Waseda) Oscillating Bianchi IX Universe in Horava-Lifshitz Gravity	232
P13	Yoshiyuki Morisawa (Osaka U. of Economics and Law) Geometry and symmetry of target space of 5-dimensional Einstein-Maxwell-Chern-Simons theory with non-SUGRA coupling	236
P14	Daisuke Nitta (Nagoya) Shadows of Colliding Black Holes	
P15	Yuji Ohsumi (Nagoya) Possibility of observing entanglement in primordial fluctuation	
P16	Hiroki Okawara (Hirosaki) Quantum interference in Chern-Simon gravity	240
P17	Ken-ichi Oohara (Niigata) Effectiveness of Empirical Mode Decomposition in Search for Gravitational Wave Signals II	243
P18	Nobuyuki Sakai (Yamagata) Cosmic microwave background anisotropy produced by network of nonlinear super-structures	247
P19	Yuuiti Sendouda (Hirosaki) Ghostfree Lorentz-violating Weyl gravity	251

P20	Kiyoshi Shiraishi (Yamaguchi) Einstein Universe under Deconstruction: the case with degenerate fermions	255
P21	Hideyuki Tagoshi (Osaka) The cross-correlation search for a hot spot of gravitational waves	
P22	Masaaki Takahashi (Aichi U. of Education) Isothermal MHD Shocks in Accretion onto a Black Hole	
P23	Tomohiro Takahashi (Kyoto) Instability of Charged Lovelock Black Holes under Tensor Perturbations	
P24	Kentaro Tanabe (YITP) Asymptotic rigidity of black holes	259
P25	Masaaki Watanabe (Kyoto) The anisotropic inflation	
P26	Kei Yamada (Hirosaki) Three-body-interaction effects on the relativistic perihelion precession	263
P27	Yuta Yamada (Osaka Institute of Technology) Gravitational Collapse of Ring Object in Five-dimensional Space-time	266
P28	Ying-li Zhang (YITP) Screening the Cosmological Constant in non-local gravity	270

Table of Contents

Riemannian geometric aspects of Penrose-type inequalities Sumio Yamada	1
Quasilocal mass in general relativity Mu-Tao Wang	9
Warped de Sitter compactifications Kunihito Uzawa	14
Exact solutions of Einstein gravity with a negative cosmological constant coupled to a massless scalar field in arbitrary spacetime dimensions Cristián Martínez	18
Black hole perturbation in parity violating gravitational theories Teruaki Suyama	22
New features of black hole solutions in $f(R; G)$ theories Sergey Pavluchenko	26
The high frequency limit in $f(R)$ gravity Keiki Saito	30
The unification of inflation and dark energy in extended $f(R)$ gravity Hayato Motohashi	34
Nonlinear perturbations in the IR limit of Horava-Lifshitz gravity Ahmet Emir Gümrukçüoğlu	38
There are no stationary axisymmetric star solutions in Horava-Lifshitz gravity Naoki Tsukamoto	42
Spherical collapse of inhomogeneous dust cloud in the Lovelock theory Seiju Ohashi	46
Binary Inspiral in Quadratic Gravity Kent Yagi	50
Screening scenario for cosmological constant in de Sitter solutions; phantom-divide crossing and finite-time future singularities in non-local gravity Kazuharu Bamba	54
Braneworld black holes Pau Figueras	58
Astrophysical censorship Umpei Miyamoto	76
Cosmic censorship in overcharging a charged black hole with a charged particle Soichiro Isoyama	80
High-velocity collision of particles around a rapidly rotating black hole Tomohiro Harada	84
Bosenova collapse of axion cloud around a rotating black hole Hirotaka Yoshino	88
Constraints on Particle Dark Matter Models by the Presence of Primordial Black Holes Ryo Saito	92

A quasi-radial stability criterion for rotating relativistic stars Kentaro Takami	96
Effect of Pasta Phase on Oscillations in Neutron Stars Hajime Sotani	100
Dynamical Approaches for Secular Instabilities in Rotating Stars Motoyuki Saijo	104
What are universal features of gravitating Q-balls? Takashi Tamaki	108
Gravitational Waves from Compact Binaries as Probes of the Universe Nicolás Yunes	112
Constraint propagation and constraint-damping for C^2 -adjusted formulations Takuya Tsuchiya	126
Effects of hyperon in binary neutron star mergers Yuichiro Sekiguchi	130
Gravitational waves and neutrino emission from the merger of binary neutron stars Kenta Kiuchi	134
Gravitational waves from cosmic string-domain wall networks Ken'ichi Saikawa	138
Violation of the Rotational Invariance in the CMB Bispectrum Maresuke Shiraishi	142
Weak lensing of CMB from cosmic (super-)strings Daisuke Yamauchi	146
Generation of the primordial magnetic fields from the non-adiabatic fluctuations at the pre-recombination era Satoshi Maeda	150
Construction of gauge-invariant variables of linear metric perturbation on general background spacetime Kouji Nakamura	154
Hawking temperature for near-equilibrium black holes Shunichiro Kinoshita	158
Universal Property of Quantum Gravity implied Uniqueness Theorem of Bekenstein-Hawking Entropy Hiromi Saida	163
Time Evolution of Evaporating Black Rings Mitsuhiro Matsumoto	167
Quantum Energy Teleportation and Black Hole Masahiro Hotta	171
Multi-field open inflation and instanton Kazuyuki Sugimura	172
Non-Gaussianity from Hilltop Curvaton Fuminiobu Takahashi	176

Beyond δN formalism Atsushi Naruko	178
Gradient expansion approach to multi-field inflation Yuichi Takamizu	182
Parity violation in graviton non-Gaussianity Masato Nozawa	186
The estimation of black-hole masses in distant radio galaxies Margarita Khabibullina	190
Oscillation Phenomena in the Disk around the Massive Black Hole Sagittarius A* Makoto Miyoshi	194
Effect of cosmological constant on light deflection Hideyoshi Arakida	198
Numerical simulation of quantum gravity Takayuki Hikichi	202
Constraining Galileon gravity from observational data with growth rate Koichi Hirano	206
Perturbative solutions to the lens equation for multiple lens planes: With some numerical examples Koji Izumi	210
Equations of motion in Double Field Theory: from classical particles to quantum cosmology Nahomi Kan	213
Astrometric microlensing by the Ellis wormhole Takao Kitamura	217
Flux vacua in DBI type Einstein-Maxwell theory Koichiro Kobayashi	221
Off-equatorial orbits of charged particles in strong gravity with magnetic dipole field Yasufumi Kojima	225
Extracting equation of state parameters from black hole-neutron star mergers Koutarou Kyutoku	228
Oscillating Bianchi IX Universe in Horava-Lifshitz Gravity Yosuke Misonoh	232
Geometry and symmetry of target space of 5-dimensional Einstein-Maxwell-Chern-Simons theory with non-SUGRA coupling Yoshiyuki Morisawa	236
Quantum interference in Chern-Simon gravity Hiroki Okawara	240
Effectiveness of Empirical Mode Decomposition in Search for Gravitational Wave Signals II Ken-ichi Oohara	243
Cosmic microwave background anisotropy produced by network of nonlinear super-structures Nobuyuki Sakai	247
Ghostfree Lorentz-violating Weyl gravity Yuuiti Sendouda	251

Einstein Universe under Deconstruction: the case with degenerate fermions Kiyoshi Shiraishi	255
Asymptotic rigidity of black holes Kentaro Tanabe	259
Three-body-interaction effects on the relativistic perihelion precession Kei Yamada	263
Gravitational Collapse of Ring Object in Five-dimensional Space-time Yuta Yamada	266
Screening the Cosmological Constant in non-local gravity Ying-li Zhang	270

Riemannian geometric aspects of Penrose-type inequalities

Sumio Yamada ^{2(a)}

^(a)*Mathematical Institute, Tohoku University, Sendai 980-8578, Japan*

Abstract

We investigate a series of inequalities which gives bounds on a set of asymptotically defined invariant associated with blackhole geometries.

1 Introduction

We suppose that \mathcal{S}^4 is a smooth manifold with a Lorentz signature metric g , representing a space-time.

Matter in relativity is represented by tensor fields over \mathcal{S} , and the spacetime metric g represents the gravitational field. The matter fields evolve from initial data via their equations of motion, and the gravitational field evolves via the Einstein equation

$$\text{Ric}(g) - \frac{1}{2}R_g = 8\pi T$$

where Ric denotes the Ricci curvature and $R = \text{Tr}_g(\text{Ric}(g))$ is the scalar curvature. When there are no matter fields present the right hand side T is zero, and the equation reduces to $\text{Ric}(g) = 0$. These equations are called the vacuum Einstein equation.

The solution to the Einstein equation is determined by initial data given on a spacelike hypersurface M^3 in \mathcal{S}^4 . The fields at a point x_0 in the space-time \mathcal{S}^4 are determined by initial data in the part of M^3 which lies in the past of x_0 . The initial data for g are the induced (Riemannian) metric $g|_M$, also denoted g for simplicity, and the second fundamental form p . These play the role of the initial position and velocity for the gravitational field. An initial data set is a triple (M, g, p) . With this set of data, solving the Einstein equation amounts to finding the integral curve with the initial position and the initial velocity. That p describes how M^3 sits inside \mathcal{S} , and hence it cannot be chosen arbitrarily.

Using the Einstein equations together with the Gauss and Codazzi equations, the constraint equations g and p need to satisfy are

$$\mu = \frac{1}{16\pi}(R_M + \text{Tr}_g(P)^2 - \|p\|^2), \quad J_i = 8\pi \sum_{j=1}^3 \nabla^j \pi_{ij}$$

where μ is the local energy density, J is the local current energy with respect to an adapted frame $\{e_i\}_{i=0}^3$ to $M^3 \subset \mathcal{S}^4$ with e_1, e_2, e_3 tangential to M . where $\pi_{ij} = p_{ij} - \text{Tr}_g(p)g_{ij}$, and ∇ is the covariant derivative with respect to g . In case there is no matter present, the vacuum constraint equations become

$$R_M + \text{Tr}_g(p)^2 - \|p\|^2 = 0, \quad \nabla^j \pi_{ij} = 0$$

for $i = 1, 2, 3$ where R_M is the scalar curvature of M^3 . For spacetimes with matter, the stress-energy tensor is normally required to satisfy the dominant energy condition

$$\mu \geq \|J\|^2$$

The most natural boundary condition for the Einstein equations is the condition of asymptotic flatness [1, 21]. This boundary condition describes isolated systems which are the analogues of finite mass distributions in Newtonian gravity. The requirement is that the initial manifold M outside a compact set be diffeomorphic to the exterior of a ball in \mathbb{R}^3 and that there be coordinates $x = (x^1, x^2, x^3)$ in which g and p have appropriate fall of

$$g_{ij} = \delta_{ij} + O_2(|x|^{-1}), \quad p_{ij} = O_1(|x|^{-2})$$

²Email address: yamada@math.tohoku.ac.jp

where $O_i(|x|^{-j})$ means that the function falls off like $C/|x|^j$ and its i -th derivative falls off like $C'/|x|^{j+i}$. The following are two basic examples of asymptotically flat spacetimes:

- The Minkowski space-time is \mathbb{R}^4 with the flat metric $g = -dx_0^2 + \sum_{i=1}^3 dx_i^2$. It is the space-time of special relativity.
- The Schwarzschild space-time with mass $m > 0$ is $\mathbb{R} \times (2m, \infty) \times S^2$ with metric

$$g = -\left(1 - \frac{2m}{r}\right)dt^2 + \left(1 - \frac{2m}{r}\right)^{-1}dr^2 + r^2g_0$$

where g_0 is the standard metric on the unit sphere S^2 , $r = \sqrt{\sum_{i=1}^3 x_i^2}$. It is a vacuum solution describing the exterior of a static black hole with mass m . It is the analogue of the exterior field in Newtonian gravity induced by a point mass.

For general asymptotically flat initial data sets, there is a notion of total energy-momentum which was defined by Arnowitt, Deser, and Misner (ADM) [1]. There is no energy density for the gravitational field so these quantities are computed in terms of the asymptotic behavior of g and p . For these definitions we fix asymptotically flat coordinates $x = (x^1, \dots, x^n)$. Then the ADM-mass M is defined as

$$M = \frac{1}{2(n-1)\omega_{n-1}} \lim_{r \rightarrow \infty} \int_{|x|=r} \sum_{i,j=1}^n (g_{ij,i} - g_{ii,j}) \nu_0^j d\sigma_0$$

where ν_0 is the unit outer normal vector to the $(n-1)$ -dimensional standard Euclidean unit sphere S^{n-1} , σ_0 is the area element of S^{n-1} , and ω_{n-1} is the volume of that sphere.

2 Variational Formulations of Mass Inequalities

In the above setting, there have been several important results in Riemannian geometric contexts. The first is the so-called positive mass/energy theorem.

The Positive Mass Theorem (Schoen-Yau 1979 [19, 20], Witten 1981 [23])

Among all time-symmetric asymptotically flat initial data sets for the Einstein-Vacuum Equations, flat Euclidean n -space is the unique minimizer of the total ADM-mass. Namely the following inequality holds

$$m \geq 0.$$

We make the following remarks regarding the history.

- For $3 \leq n \leq 7$ this theorem was proven by R. Schoen and S.-T. Yau around 1980 [19, 20]. The proof uses variational properties of minimal hypersurfaces.
- For spin manifolds of any dimension the theorem follows from an argument of E. Witten in the early 1980's [23]. The proof uses the Dirac operator.
- For $n = 3$, a new proof was given in 2000 by G. Huisken and T. Ilmanen [13]. It uses the inverse mean curvature flow, making rigorous an argument proposed by R. Geroch [10]. We will come back to this argument.

Based on the conjectured picture of gravitational collapse to a black hole, Penrose [17] proposed a sharp strengthening of the positive mass/energy theorem, which is the so-called Riemannian Penrose inequality. In what follows, we restrict our attention to the case $n = 3$.

The Riemannian Penrose Inequality (Huisken-Ilmanen 2001 [13], Bray 2001 [2])

Among all time-symmetric asymptotically flat initial data sets for the Einstein-Vacuum Equations with

an outermost minimal surface Σ of area A , the Schwarzschild slice is the unique minimizer of the total mass. Namely we always have the inequality

$$m \geq \frac{1}{2}R$$

where R is the area radius $\sqrt{\frac{A}{4\pi}}$.

Recall that the event horizon and the apparent horizon coincided in time-symmetric settings, and the horizon consist of a collection of minimal spheres. This follows from the stability of the minimal surfaces, namely the second variations of the area functional of the horizon are positive definite. We also make the following remarks concerning the Penrose inequality.

- Around 2000 this was proven by G. Huisken and T. Ilmanen using the inverse mean curvature flow. This made rigorous a proof originally proposed by P. Jang and R. Wald [14].
- Shortly after the Huisken/Ilmanen proof [13], a very different proof was given by H. Bray [2] which extends the result to the case of a possibly disconnected boundary surface. The inverse mean curvature flow approach does not work in that case, namely, in the Huisken/Ilmanen argument, what they showed is the ADM mass is bounded below by the area radius of the largest connected component of the outermost minimal surfaces. Bray's proof also involved a flow, but it was a conformal flow of the metric which deformed the given metric to a Schwarzschild metric.

3 Natural Questions

We ask the following set of questions, naturally led by the variational interpretation of the preceding two inequalities. Those inequalities share the property that in each case, the equality is realized by one of the exact solutions of the Einstein equation. Incidentally a good exposition on these subjects, whose scope is much wider than the current article is Marc Mars's article [16].

3.1 The Angular Momentum Case

Question: *Is the Kerr slice the unique minimizer of the total mass among all asymptotically flat axisymmetric maximal gauge initial data sets for the Einstein-Vacuum Equations with an outermost minimal surface Σ of area A and (Komar) angular momentum J ? Namely does the following inequality always hold?*

$$m \geq \frac{1}{2} \left(R^2 + \frac{4J^2}{R^2} \right)^{1/2}$$

Here the Komar angular momentum $J(S)$ for a surface S is defined for axisymmetric data as

$$J(S) = \frac{1}{8\pi} \int_S p_{ij} X^i n_S^j d\sigma_S$$

where S is a sphere homological to the two-sphere at the infinity, X is the Killing vector field which generates the axisymmetry, n_S is the unit normal vector to the surface S , and $d\sigma_S$ is the area element of S . This quantity is known to be a homological quantity, and is equal to the total angular momentum J in this setting. The equality is assumed for the Kerr slice.

This question remains open. Technically this is due to the fact that the setting is no longer Riemannian, as the effect of Killing vector field X and the extrinsic curvature p have to be taken into account.

3.2 The Charged Case I

Question (cf. Jang 1979 [15]): *Is the Reissner-Nordstrom slice the unique minimizer of the total mass among all asymptotically flat time-symmetric initial data sets for the Einstein-Maxwell Equations with*

an outermost minimal surface Σ of area A and charge Q ? Namely does the following inequality always hold?

$$m \geq \frac{1}{2} \left(R + \frac{Q^2}{R} \right)$$

where the total charge Q is defined by $Q(S) = \int_{S^2_\infty} E_i n^i d\sigma_S$ for S a sphere homological to the sphere at the asymptotically flat end. This represents the sum of the charges $\{Q_i\}$ each trapped inside the horizons Σ_i .

Recall that the Time-Symmetric Einstein-Maxwell Constraints

$$S_g = 2(|E|_g^2 + |B|_g^2), \quad \operatorname{div}_g E = \operatorname{div}_g B = 0, \quad E \times_g B = 0$$

as well as the nonexistence of magnetic monopole $\int_S B_i n^i d\sigma_S = 0$ for a sphere S homological to the sphere at the asymptotically flat end.

3.3 The Charged Case II

Question (Gibbons 1984 [12]): Is the Majumdar-Papapetrou slice with the horizon consisting of two components of opposite charges the unique minimizer of the total mass among all asymptotically flat time-symmetric initial data sets for the Einstein-Maxwell Equations with an outermost minimal surface $\Sigma = \cup \Sigma_i$ of area $A = \sum A_i$ and charges $\{Q_i\}$? Namely does the following inequality always hold?

$$m \geq \sum_i \frac{1}{2} \left(R_i + \frac{Q_i^2}{R_i} \right)$$

4 Answers to Questions

In this section, we present answers to each of the two questions concerning the charged cases I and II.

4.1 Charged Case I

For the Penrose-type inequality $m \geq \frac{1}{2} \left(R + \frac{Q^2}{R} \right)$, the following is known:

- **Yes**, provided Σ is connected (Jang 1979 [15], Huisken-Ilmanen 2001 [13]).
- **No**, in general (Weinstein-Yamada 2004 [22]).

It is interesting to note that the topological conditions affect the Penrose-type inequality in an essential manner. We will outline the arguments for the two cases now.

4.1.1 Jang/Huisken-Ilmanen argument for Σ connected

As was done for the proof of the Riemannian Penrose inequality, flow the connected component Σ of the horizon of the biggest area by Inverse Mean Curvature; $\frac{\partial x}{\partial t} = \frac{1}{H} \nu$. Then use the Geroch Monotonicity (sharpened by Jang to incorporate the electric field E) which says

$$\frac{dm_H(\Sigma(t))}{dt} \geq \frac{R}{32\pi} \int_{\Sigma(t)} S_g \geq 0$$

where $m_H(\Sigma) = \frac{R}{2} \left(1 - \frac{1}{16\pi} \int_{\Sigma} H^2 \right)$ is the Hawking Mass and the scalar curvature of (M^3, g) has the following expression $S_g = 2(|E|^2 + |B|^2)$ from the Einstein constraint equation. The Hawking mass converges to ADM mass as $\Sigma \rightarrow S^2_\infty$, while the Cauchy-Schwarz inequality and $Q = \int_{S^2_\infty} E_i n^i d\sigma$ gives the expression for the right hand side of the inequality $m \geq \frac{1}{2} \left(R + \frac{Q^2}{R} \right)$. In taking the limit of the evolution $\Sigma \rightarrow S^2_\infty$ via the inverse mean curvature flow, and jump over discontinuities with Huisken-Ilmanen's weak flow as necessary. By backtracking the argument, one can check that the equality holds if and only if the initial data set is that of Reissner-Nordstrom with the appropriate mass and charge.

4.1.2 Weinstein-Yamada argument for Σ of two components

We recall the so-called Majumdar-Papapetrou Metric [6], or sometimes better known as the extremal Reissner-Nordstrom metric in the sense that the usual inequality $M \geq |Q|$ is saturated $M = |Q|$. We are here concerned with the case when Σ is of two components, and the charge is split evenly and of the same sign causing the repulsive force. To be precise, the underlying differential manifold is $\mathbb{R}^3 \setminus \{p_1, p_2\}$ with $p_1 = (0, 0, 1), p_2 = (0, 0, -1)$ on which we have the following gravitational and electric fields

- $g_{ij} = u^4 \delta_{ij}, u = \left(1 + \frac{\mu}{r_1} + \frac{\mu}{r_2}\right)^{1/2}$
- $E_i = 2\nabla_i \log u, B_i = 0$

where r_1, r_2 are the distances to p_1 and p_2 . Then the scalar curvature is $S_g = 2\|E\|_g^2$

The total mass of this initial data is $m = 2\mu$ and the total asymptotic area of Σ is $A = 8\pi\mu^2$, while the total charge is $Q = 2\mu$. This gives a counterexample to the inequality $m \geq \frac{1}{2}\left(R + \frac{Q^2}{R}\right)$ as

$$m - \frac{1}{2}\left(R + \frac{Q^2}{R}\right) = \mu\left(2 - \frac{3}{\sqrt{2}}\right) < 0.$$

However, we are not quite done yet, for this manifold $(\mathbb{R}^3 \setminus \{p_1, p_2\}, g, E, B = 0)$ is not asymptotically flat. It has two ends, one of which is asymptotically flat, but the Majumdar-Papapetrou slice $(\mathbb{R}^3 \setminus \{p_1, p_2\}, g)$ has no horizon, as there are two infinite cylinders centered at p_1 and p_2 . In [22], two copies of Majumdar-Papapetrou are truncated at their necks, and glued to rectify those features.

We note that the so-called Cosmic Censorship proposed by Penrose [17] is intact. The Cosmic Censorship says that the evolution of space-time driven by the Einstein equation would force singularities to be hidden behind the event horizons which is the surface of the blackhole regions, so that there is no naked singularities to the observer in this part of the space-time. As those blackholes would coalesce together by the gravitational effect, the time-asymptotic behavior of the universe would settle down to the Kerr-Newman solution.

Setting aside the angular momentum, Jang [15] has adapted the Cosmic Censorship statement to the Penrose-type inequality. First he notes that

$$m \geq \frac{1}{2}\left(R + \frac{Q^2}{R}\right)$$

is equivalent to the following pair of inequalities

$$m - \sqrt{m^2 - Q^2} \leq R \leq m + \sqrt{m^2 - Q^2}$$

Only the upper bound on R follows from Cosmic Censorship using Penrose's heuristic argument, as the coalescing process would cause the increase of the size of the horizon, whose upper bound is set by the asymptotic invariants from the Hamiltonian formulation by Arnowitt, Deser, and Misner [1].

Note that our counter-example violates the lower bound.

4.2 Charged Case II

For the Penrose-type inequality

$$m \geq \sum_i \frac{1}{2}\left(R_i + \frac{Q_i^2}{R_i}\right)$$

the following is known: the so-called Brill-Lindquist initial data set [3] satisfies $m < \frac{1}{2}\sum_{i=1}^2 R_i$ (Dain-Weinstein-Yamada 2010 [9]), which violates the proposed inequality when $Q_i = 0$.

By setting quasi-local mass-like quantities m_i , the same inequality $m < \frac{1}{2}\sum_{i=1}^2 R_i$ functions as a counterexample for each of the following cases.

Namely by defining

$$m_i = \frac{1}{2}\left(R_i + \frac{Q_i^2}{R_i}\right), \quad \text{or} \quad \sqrt{\frac{1}{4}R_i^2 + \frac{J_i^2}{R_i^2}}$$

the inequalities

$$m \geq \sum m_i.$$

do not hold, as they reduce to $m \geq \frac{1}{2} \sum R_i$ in vacuum.

We will explain the counterexample to $m \geq \frac{1}{2} \sum_{i=1}^2 R_i$ now.

4.2.1 Brill-Lindquist initial data

The so-called Brill-Lindquist initial data [3] has been known for many years, which models a time-symmetric initial data set $(\mathbb{R}^3 \setminus \{p_1, p_2\}, g)$ with $p_1 = (0, 0, 1), p_2 = (0, 0, -1)$, which has three asymptotically flat ends, which are linked by two Einstein-Rosen bridges. To be precise,

$$\bullet \quad g_{ij} = u^4 \delta_{ij}, \quad u = \left(1 + \frac{\mu}{2r_1} + \frac{\mu}{2r_2} \right)$$

where r_1, r_2 are the distances to the punctures p_1 and p_2 in \mathbb{R}^3 . The metric has zero scalar curvature, as the function u is harmonic.

Seen from afar, the metric g looks like a Schwarzschild metric of mass $\mu + \mu$. Hence the total mass is $m = 2\mu$. By a simple comparison argument, the area radii are $R_1 = R_2 > 2\mu$ (Gibbons 1972 [11]) Once we establish that the outermost horizon is not connected for μ sufficiently small, we have

$$m - \frac{1}{2} \sum_i R_i < 0.$$

To check that for μ sufficiently small, the horizon cannot be a single minimal sphere, we use the following properties of the stable minimal surfaces in three dimensional manifolds of bounded geometry.

If the outermost horizon is connected, then there exists $x \in \Sigma \cap \{z = 0\}$. Then an estimate by Schoen [18] says there exists some $\varepsilon > 0$ such that

$$\sup_{\Sigma_1 \cap B(x, \varepsilon)} |A| \leq C \int_{\Sigma_1 \cap B(x, 2\varepsilon)} |A|^2 dx$$

where C is independent of $\mu \ll 1$. Note that the right hand side is $o(\mu)$ as $\mu \rightarrow 0$ as the space becomes increasingly flatter. This means that the piece of the surface $\Sigma_1 = \Sigma \cap B(x, r)$ with $r < 1$ becomes a graph over a two-dimensional disc centered at x , as the pointwise small extrinsic curvature implies the bound of turning of the normal vector to the surface. This says $|\Sigma_1| > C$, with C independent of μ .

On the other hand, Bray's Penrose inequality [2]

$$2\mu \geq \sqrt{\frac{|\Sigma|}{16\pi}}$$

says $|\Sigma_1| \rightarrow 0$ as $\mu \rightarrow 0$, a contradiction.

5 Concluding Remarks

We have seen the following set of results concerning the Penrose-type inequalities involving the Einstein-Maxwell Constraints:

- Σ connected $\Rightarrow m \geq \frac{1}{2} \left(R + \frac{Q^2}{R} \right)$ always holds by inverse mean curvature flow and the monotonicity of Hawking mass.
- Σ not connected $\Rightarrow m - \frac{1}{2} \left(R + \frac{Q^2}{R} \right) < 0$ is possible, in fact achieved by an asymptotic time-symmetric initial data set obtained by glueing and perturbing a pair of the Majumdar-Papapertou data.

- Σ not connected $\Rightarrow m - \frac{1}{2} \sum_i \left(R_i + \frac{Q_i^2}{R_i} \right) < 0$ is possible, and achieved by the Brill-Lindquist initial data when the two neck are sufficiently apart compared to the assigned masses.

This would lead to the following open problems

Open Problem 1: The Charged Case for the asymptotically flat time-symmetric initial data set (M^3, g, p, E) without any topological assumption.

$$R \leq m + \sqrt{m^2 - Q^2}$$

Note this is the part consistent with the Cosmic Censorship, of the two inequalities proposed by Jang. The variational interpretation is that the Reissner-Nordstrom slice *maximizes* the area of the horizon among all asymptotically flat time-symmetric initial data satisfying the Einstein-Maxwell constraint with ADM mass m and the total charge Q .

Open Problem 2: For the axisymmetric maximal ($\text{Tr}_g p = 0$) initial data set whose the horizon Σ is connected,

$$m \geq \frac{1}{2} \left(R^2 + \frac{4J^2}{R^2} \right)^{1/2}.$$

Note that the equality here is realized by the Kerr slice. Note the Einstein-Maxwell setting, the analogous result was obtained by inverse mean curvature flow. However, the difficulty here is the fact that the time-symmetry is no longer assumed, and there is a nontrivial Killing vector field around the symmetry axis.

We also remark that S. Dain recently obtained a series of results [8] which address the inequality

$$m \geq \sqrt{|J|}$$

where the equality is achieved by the extremal Kerr initial data set, using the technique of harmonic maps with singularities.

Open Problem 3: When one relaxes the topological type of the horizon, we ask the following stronger inequality than Open Problem 3 for axisymmetric maximal ($\text{Tr}_g p = 0$) initial data sets

$$\frac{R^2}{2} \leq m^2 + \sqrt{m^4 - J^2}.$$

The variational interpretation is that the Kerr slice *maximizes* the area of the horizon among all asymptotically flat time-symmetric initial data satisfying the Einstein constraint with ADM mass m and the total angular momentum J . The challenge here is that one needs to capture the lack of symmetry of the space, caused by inhomogeneity of the metric or by multiple horizons, in terms of the deviation of the right hand side from the left hand side of the inequality. Such was achieved in Bray's ingenious proof [2] of the Riemannian Penrose inequality by means of a conformal change trick by Bunting-Masood-ul-Alam [4].

References

- [1] R. Arnowitt, S. Deser, C. Misner. (Republication of:) The dynamics of general relativity. *General Relativity and Gravitation* 40, 1997–2027, 2008.
- [2] H. Bray. Proof of the Riemannian Penrose inequality using the positive mass theorem. *J. Differential Geometry*, 59, 177–367, 2001.
- [3] D. Brill and R. Lindquist. Interaction energy in geometrostatics. *Phys. Rev.*, 131, 471–476, 1963.
- [4] G. Bunting and A. Masood-ul-Alam. Nonexistence of multiple black holes in asymptotically Euclidean static vacuum space-time *General Relativity and Gravitation* 19, 147–154, 1987.

-
- [5] P. T. Chruściel, J. Corvino and J. Isenberg. Construction of N -body time-symmetric initial data sets in general relativity. *Proceedings of Complex Analysis and Dynamical Systems IV. Intl. Conf. on Complex Analysis and Dynamical Systems*. Ed. by Mark Agranovsky et al. American Mathematical Society, 2011.
- [6] P. Chruściel and N. Nadirashvili. All Majumdar-Papapetrou black holes with a non-singular domain of outer communication. *Classical and Quantum Gravity* 12, L17–L23 (1995).
- [7] S. Dain. Extreme throat initial data set and horizon area-angular momentum inequality for axisymmetric black holes. *Phys. Rev. D*, 82, 2010.
- [8] S. Dain. Proof of the angular momentum-mass inequality for axisymmetric black holes. *J. Differential Geometry*, 79, 33–67 (2008).
- [9] S. Dain, G. Weinstein and S. Yamada. A counterexample to a Penrose inequality conjectured by Gibbons. *Class. Quantum Grav.* 28, (2011).
- [10] R. Geroch. *Ann. N. Y. Acad. Sci.* 224, 108 (1973).
- [11] G. Gibbons. The time symmetric initial value problem for black holes. *Commun. Math. Phys.*, 27, 87–102, 1972.
- [12] G. Gibbons. The isoperimetric and bogomolny inequalities for black holes. In T.J. Willmore and N. Hitchin, editors, *Global Riemannian Geometry*, pages 194–202. John Wiley & Sons, New York, 1984.
- [13] G. Huisken and T. Ilmanen. The inverse mean curvature flow and the Riemannian Penrose inequality. *J. Differential Geometry*, 59, 352–437, 2001.
- [14] P. Jang and R. Wald. *J. Math. Phys.* 18, 41 (1977).
- [15] P. Jang. Note on cosmic censorship. *Phys. Rev. D*, 20, 834–837, 1979.
- [16] M. Mars. Present status of the Penrose inequality. *Class. Quant. Grav.*, 26, 2009.
- [17] R. Penrose. Naked singularities. *Ann. New York Acad. Sci.*, 224:125–134, 1973.
- [18] R. Schoen. Estimates for stable minimal surfaces in three-dimensional manifolds. In *Seminar on minimal submanifolds*, volume 103 of *Ann. of Math. Stud.*, pages 111–126. Princeton Univ. Press, Princeton, NJ, 1983.
- [19] R. Schoen and S.-T. Yau. On the proof of the positive mass conjecture in general relativity. *Comm. Math. Phys.*, 65, 45–76, 1979.
- [20] R. Schoen and S.-T. Yau. Proof of the positive mass theorem. II. *Comm. Math. Phys.*, 79, 231–260, 1981. August 2005.
- [21] R. Wald. *General Relativity* Univ. Chicago Press, 1984.
- [22] G. Weinstein and S. Yamada. On a Penrose inequality with charge. *Commun. Math. Phys.*, 257, 703–723, 2005.
- [23] E. Witten. A new proof of the positive energy theorem. *Communications in Mathematical Physics*, 80, 381–402, 1981.

Constraints on total conserved quantities in general relativity

Mu-Tao Wang^{3(a),(b)}

^(a) *Department of Mathematics, Columbia University, New York, NY 10027, USA*

^(b) *Department of Mathematics, National Taiwan University, Taipei, Taiwan*

Abstract

This note discusses the recent work of Huang-Schoen-Wang [13] on specifying total conserved quantities of a vacuum initial data set.

1 Conserved quantities in special relativity

Conserved quantities in special relativity are associated with symmetry in the Minkowski space $\mathbb{R}^{3,1}$. The isometry group of $\mathbb{R}^{3,1}$ consists of spacetime translations and Lorentz rotations. An infinitesimal isometry corresponds to a Killing vector field of $\mathbb{R}^{3,1}$. In term of standard coordinates t, x^1, x^2, x^3 on $\mathbb{R}^{3,1}$, they are:

- Constant vector fields.
- Boost vector fields: $t \frac{\partial}{\partial x^i} + x^i \frac{\partial}{\partial t}, i = 1, 2, 3$.
- Rotation vector fields: $Y_i = \frac{\partial}{\partial x^i} \times \vec{x}, i = 1, 2, 3$.

For example, $Y_{(3)} = x^1 \frac{\partial}{\partial x^2} - x^2 \frac{\partial}{\partial x^1}$ corresponds to rotation about the x^3 axis.

A Killing vector field K satisfies the Killing equation

$$K_{a;b} + K_{b;a} = 0. \quad (1.1)$$

Given a timelike geodesic γ with 4-velocity V (thus $V^b V_{;b}^a = 0$) and energy-momentum 4-vector $p = mV$. By the geodesic equation and the Killing equation (1.1), we have $\langle p, K \rangle = p^a K_a$ is a constant along γ and thus conserved. In case when K is a future timelike unit constant vector field as the 4-velocity of an observer, $E = -\langle p, K \rangle$ is interpreted as the energy seen by the corresponding observer.

Each continuous distribution of matter field is attached with an energy-momentum stress tensor of matter density T_{ab} . For example, for electromagnetic field,

$$T_{ab} = \frac{1}{4\pi} (F_{ac} F_{bd} g^{cd} - \frac{1}{4} g_{ab} F_{cd} F_{ef} g^{ce} g^{df}).$$

T satisfies the conservation equation as a result of coordinate invariance of the associated Lagrangian:

$$T^a_{b;a} = 0.$$

For any spacelike hypersurface Ω in $\mathbb{R}^{3,1}$ which represents a time slice, the energy seen by an observer K and intercepted by Ω is the integral

$$\int_{\Omega} T(K, u) = \int_{\Omega} T_{ab} K^a u^b \quad (1.2)$$

where u^b is the future unit timelike normal of Ω . This is a conserved quantity by the Killing field equation for K , the conservation equation for T , and Stoke's theorem, i.e.

$$\int_{\Omega_1} T(K, u_1) = \int_{\Omega_2} T(K, u_2)$$

if $\partial\Omega_1 = \partial\Omega_2$.

Therefore, this expression depends only on the boundary 2-surface $\Sigma = \partial\Omega$ and is the quasi-local energy of Σ seen by the observer K if K is a future timelike Killing field.

³Email address: mtwang@math.columbia.edu

2 Energy in general relativity

In general relativity, spacetime is a 4-dimensional manifold with a Lorentz metric g , the gravitational field. Thus local causal structure is the same, and each tangent space is isometric to the Minkowski space. Gravitational force is represented by the spacetime curvature of g . Einstein's field equation relates gravitation field and matter fields by

$$Ric - \frac{1}{2}Rg = 8\pi T \quad (2.1)$$

where Ric is the Ricci curvature, and R is the scalar curvature of g , respectively. T represents the energy-momentum stress tensor of all matter fields. This is the Euler-Lagrange equation of the Hilbert-Einstein action.

It turns out first derivatives of g are all coordinate dependent, and thus there is no density for gravitational energy. This is manifestly Einstein's equivalence principle. If we try to form the same energy expression (1.2) by integrating T over a spacelike hypersurface as in special relativity, we encounter two difficulties:

Firstly, a generic spacetime does not have any Killing field and the expression is not conserved. Though T in (2.1) still satisfies the conservation equation $T^a_{b;a} = 0$. Secondly, the expression would give only the energy contribution from matters. There exists vacuum spacetime, i.e. $T = 0$, with nonzero energy such as the Kerr solution. There is gravitational energy by the sheer presence of spacetime curvature.

We recall the Kerr metric in Boyer-Lindquist coordinates is of the form:

$$ds^2 = -\frac{\Delta}{U} (dt - a \sin^2 \theta d\phi)^2 + U \left(\frac{dr^2}{\Delta} + d\theta^2 \right) + \frac{\sin^2 \theta}{U} (a dt - (r^2 + a^2) d\phi)^2$$

$$U = r^2 + a^2 \cos^2 \theta$$

$$\Delta = r^2 - 2mr + a^2$$

This is a stationary vacuum solution which is axially symmetric solution and $\frac{\partial}{\partial \phi}$ is the corresponding Killing field. The total mass is m and the total angular momentum with respect to $\frac{\partial}{\partial \phi}$ is a . When $a = 0$, this reduces to the Schwarzschild solution which is a static vacuum solution that is also spherically symmetric.

Einstein's field equation is derived from variation of the Einstein-Hilbert action on a spacetime domain M :

$$\frac{1}{16\pi} \int_M R + \frac{1}{8\pi} \int_{\partial M} \mathfrak{K} + \int_M L(g, \Phi)$$

where \mathfrak{K} is the trace of the second fundamental form of ∂M and Φ represents all the matter fields. The variation of the last term with respect to g gives T . The second term is indeed a divergence term $\int_M \partial^a I_a$, where I_a consists of first derivatives of g . Formally applying Hamilton-Jacobi analysis to this action, one obtains T^*_{ab} , the so called Einstein pseudo tensor, which is expressed in terms of first derivatives of g and satisfies the conservation equation $T^*_{;ba} = 0$.

Here is Weyl's [17] comment on T^*_{ab} (see chapter 3 of [6] for the English translation quoted here)

Nevertheless it seems to be physically meaningless to introduce the T^*_{ab} as energy components of the gravitational field; for, these quantities are neither a tensor nor are they symmetric. In fact by choosing an appropriate coordinate system all the T^*_{ab} can be made to vanish at any given point; for this purpose one only needs to choose a geodesic (normal) coordinate system. And on the other hand one gets $T^*_{ab} \neq 0$ in a 'Euclidean' completely gravitationless world when using a curved coordinate system, but where no gravitational energy exists. Although the differential relations ($\nabla^a T^*_{ab} = 0$) are without a physical meaning, nevertheless by integrating them over an isolated system one gets invariant conserved quantities.

3 Isolated systems and total conserved quantities

An isolated system is modeled on an asymptotically flat spacetime where gravitation is weak at spatial infinity. Arnowitt-Deser-Misner [1] applied Hamilton-Jacobi analysis of the Einstein-Hilbert action to such a system, and obtained total conserved quantities. It turns out the application of Noether's theorem to general relativity requires a reference system which is taken to be $\mathbb{R}^{3,1}$. These include the total energy and linear momentum, as well as the angular momentum and center of mass which altogether correspond to the 10-dimensional Killing vector fields of the Minkowski space.

Let (M, g, p) be an unbounded spacelike hypersurface in spacetime, where g is the induced Riemannian metric and p is the second fundamental form, we usually use the canonical momentum $\pi = p - (tr_g p)g$ instead of p . (M, g, π) is called an initial data set as it represents a Cauchy data for the Einstein equation as a hyperbolic PDE system. We say (M, g, π) is asymptotically flat if outside a compact set there exists an asymptotically flat coordinate system $\{x^i\}_{i=1,2,3}$ so that $g_{ij} - \delta_{ij} = O(|x|^{-1})$ and $\pi_{ij} = O(|x|^{-2})$ and derivatives of g_{ij} and p_{ij} satisfy appropriate decay conditions.

Let (M, g, π) be an asymptotically flat initial data set. Let $E, \mathbf{C}, \mathbf{P}, \mathbf{J}$ denote the energy, center of mass, linear momentum, and angular momentum of (g, π) . They are defined as limits of flux integrals over coordinate spheres S_ρ of radius ρ with respect to the asymptotic flat coordinate system.

$$\begin{aligned} E &= \frac{1}{16\pi} \lim_{\rho \rightarrow \infty} \int_{S_\rho} \sum_{i,j} (g_{ij,i} - g_{ii,j}) \nu^j \\ \mathbf{P}_i &= \frac{1}{8\pi} \lim_{\rho \rightarrow \infty} \int_{S_\rho} \sum_j \pi_{ij} \nu^j \\ \mathbf{J}_i &= \frac{1}{8\pi E} \lim_{\rho \rightarrow \infty} \int_{S_\rho} \sum_{j,k} \pi_{jk} Y_{(i)}^j \nu^k \\ \mathbf{C}^k &= \frac{1}{16\pi E} \lim_{\rho \rightarrow \infty} \int_{S_\rho} \left[x^k \sum_{i,j} (g_{ij,i} - g_{ii,j}) \nu^j - \sum_i (g_{ik} \nu^i - g_{ii} \nu^k) \right] \end{aligned}$$

Here ν^i is the outward unit normal of S_ρ and $Y_{(i)}, i = 1, 2, 3$ is the rotation Killing field with respect to the x^i axis.

It turns out the well-definedness of \mathbf{J}_i and \mathbf{C}_k rely on extra assumptions at spatial infinity. We impose the Regge-Teitelboim [14] condition that

$$g_{ij}(x) - g_{ij}(-x) = O(|x|^{-2}) \text{ and } \pi_{ij}(x) + \pi_{ij}(-x) = O(|x|^{-3})$$

and similar parity conditions on ∂g_{ij} and $\partial \pi_{ij}$. These quantities are conserved under the evolution of Einstein's equation of a maximal slice with appropriate assumptions on the decay rate of (g, π) , see chapter 3 of Christodoulou [6]. There are other different conditions (see for example, Ashtekar-Hansen [2]) to ensure the finiteness of angular momentum and center of mass. An important property of the Regge-Teitelboim condition is, by a theorem of Corvino-Schoen [10], that initial data sets satisfying this condition are dense, and thus a generic initial data set can be approximated by these sets.

(M, g, π) as a hypersurface in spacetime satisfies the constraint equation

$$\frac{1}{2}(R(g) + \frac{1}{2}(Tr_g \pi)^2 - |\pi|^2) = \mu, \text{ and } div_g(\pi) = \mathfrak{J} \quad (3.1)$$

where μ, \mathfrak{J} are from the energy-momentum stress tensor of matter fields which is assumed to satisfy the dominant energy condition $\mu \geq |\mathfrak{J}|$. We shall assume both μ and \mathfrak{J} vanish and thus (M, g, π) is a vacuum initial data set.

Question: Given a vacuum initial data set which is asymptotically flat, is there any constraint on the conserved quantities $E, \mathbf{C}, \mathbf{P}, \mathbf{J}$?

Schoen-Yau's positive mass theorem [15, 16] [3] imposes the most important constraint on these quantities, namely that the energy-momentum vector is a future timelike vector. In particular, this says

that the magnitude of the linear momentum vector is bounded above by the energy:

$$E \geq |\mathbf{P}|$$

and thus the total mass $m = \sqrt{E^2 - |\mathbf{P}|^2}$ is always non-negative.

For the Kerr solutions which describe rotating stationary axially symmetric vacuum black holes, we have the mass-angular momentum inequality

$$m \geq |\mathbf{J}|.$$

It has been shown by Dain [11, 12] and Chruściel et al. [7, 8] that such an inequality is also satisfied by general axially symmetric black hole solutions of the Einstein equations (see also work of Zhang [18]).

4 Specifying total conserved quantities

In [13], we show that the mass-angular inequality does not hold true in general.

Theorem There are no constraints on the angular momentum and center of mass in terms of the energy-momentum vector for general vacuum solutions of the Einstein equations.

In fact, given any 10 real numbers $E, \mathbf{C}, \mathbf{P}, \mathbf{J}$ with $E \geq |\mathbf{P}|$, we can construct a vacuum initial data set that has them as conserved quantities.

An effective procedure was given for adding a specified amount of angular momentum to a solution of the vacuum Einstein equations, producing a new solution with specified angular momentum but with only slightly perturbed energy-momentum vector. A similar result was obtained for the center of mass. Then, by considering a family of initial data set near the given one, and by doing the construction continuously and a degree argument, we obtain a perturbation with arbitrarily specified angular momentum and center of mass, while leaving the energy-momentum vector unchanged.

From a technical point of view the reason it is possible to make these constructions is that the angular momentum and center of mass are determined by terms in the expansion of the solution which are of lower order than those which determine the energy and linear momentum.

The idea then is to make perturbations near infinity which affect only the lower order terms in the expansion. We do this by explicitly constructing linear perturbations supported in a shell near infinity which impose the required change in angular momentum (or center of mass), and then by finding a solution of the vacuum constraint equations which is sufficiently close to the perturbed system so that the change in angular momentum (or center of mass) persists. This is an application of the Corvino-Schoen [9, 10] gluing construction of initial data set.

The added term in the perturbation vanishes in the axially symmetric case, and we cannot increase the angular momentum while keeping the axially symmetric condition. Thus the result is consistent with the mass-angular momentum inequality of Dain and Chruściel et al.

References

- [1] Arnowitt, R., Deser, S., and Misner, C. W. *The dynamics of general relativity*. 1962 Gravitation: An introduction to current research pp. 227–265 Wiley, New York.
- [2] Ashtekar, A. and Hansen, R. O. *A unified treatment of null and spatial infinity in general relativity. I. Universal structure, asymptotic symmetries, and conserved quantities at spatial infinity*. J. Math. Phys. 19 (1978), no. 7, 1542–1566.
- [3] Witten, E., *A new proof of the positive energy theorem*. Comm. Math. Phys. 80 (1981), no. 3, 381–402.
- [4] Beig, R. and Ó Murchadha, N. *The Poincaré group as the symmetry group of canonical general relativity*, Ann. Physics 174 (1987), no. 2, 463–498.
- [5] Christodoulou, D. and Klainerman, S., *The global nonlinear stability of the Minkowski space*, Princeton Mathematical Series, 41. Princeton University Press.

-
- [6] Christodoulou, D., *Mathematical problems of general relativity. I.* Zürich Lectures in Advanced Mathematics. European Mathematical Society (EMS), Zürich, 2008. x+147 pp.
- [7] Chruściel, P. T., *Mass and angular-momentum inequalities for axi-symmetric initial data sets. I. Positivity of mass*, Ann. Physics 323 (2008), no. 10, 2566–2590.
- [8] Chruściel, P. T., Li, Y., and Weinstein, G., *Mass and angular-momentum inequalities for axi-symmetric initial data sets. II. Angular momentum*, Ann. Physics 323 (2008), no. 10, 2591–2613.
- [9] Corvino, J., *Scalar curvature deformation and a gluing construction for the Einstein constraint equations*, Comm. Math. Phys. 214 (2000), no. 1, 137–189.
- [10] Corvino, J. and Schoen, R., *On the asymptotics for the vacuum Einstein constraint equations*, J. Diff. Geom. Volume 73, Number 2 (2006), 185–217.
- [11] Dain, S. *Angular-momentum inequality for axisymmetric black holes*. Phys. Rev. Lett. 96 (2006), no. 10, 101101, 3 pp.
- [12] Dain, S., *Proof of the angular momentum-mass inequality for axisymmetric black holes*, J. Diff. Geom. 79 (2008), 33–67.
- [13] Huang, L.-H., Schoen R. and Wang, M.-T., *Specifying angular momentum and center of mass for vacuum initial data sets* Comm. Math. Phys. 306 (2011), no. 3, 785–803.
- [14] Regge, T. and Teitelboim, C., *Role of Surface Integrals in the Hamiltonian Formulation of General Relativity*, Ann. Phys. Volume 88 (1974), 286–318.
- [15] Schoen, R. and Yau, S.-T. *Positivity of the total mass of a general space-time*. Phys. Rev. Lett. **43** (1979), no. 20, 1457–1459.
- [16] Schoen, R. and Yau, S.-T. *On the proof of the positive mass conjecture in general relativity*. Comm. Math. Phys. 65 (1979), no. 1, 45–76.
- [17] Weyl, H., *Raum-Zeit-Materie* (1921) Springer-Verlag.
- [18] Zhang, X., *Angular momentum and positive mass theorem*. Comm. Math. Phys. 206 (1999), no. 1, 137–155.

Warped de Sitter compactifications

Kunihito Uzawa⁴

Department of Physics, Kinki University, Higashi-Osaka 577-8502, Japan.

Abstract

We show that the warped de Sitter compactifications are possible under certain conditions in D -dimensional gravitational theory coupled to a dilaton, a form field strength, and a cosmological constant. We find that the solutions of field equations give de Sitter spacetime with the warped structure, and discuss cosmological model directly obtained from the solution. We also construct a cosmological model in the lower-dimensional effective theory. If there is a field strength having non-vanishing components along the internal space, the moduli can be fixed at the minimum of the effective potential where a de Sitter vacuum can be obtained.

1 Introduction

The de Sitter compactification of higher-dimensional theory is an important cosmological issue. Such a solution has been explored from several points of view because this provides a fairly direct explanation of the accelerating expansion of four-dimensional universe. The inflation and accelerating expansion with warped compactifications can be constructed in a variety of ways from higher-dimensional cosmology or string theory. A road to obtain the warped de Sitter compactification has appeared recently in a study of the higher-dimensional pure gravity theory in [1]. It was shown that warped structure of the spacetime realizes a de Sitter universe, but the pay is that one of the internal space dimensions has to have an infinite volume rather than small and finite one. For such a class of solutions, a way of the construction of a cosmological model is to insert a brane world boundary in the noncompact direction whose world volume contains all the remaining compact directions of the internal space which is discussed more explicitly in [1]. It may be regarded as a generalization of the five-dimensional brane world models. The details of the brane world models obtained from our solutions are argued in [2].

We will first focus on the derivation of the new warped de Sitter solutions obtained as the generalization of Ref. [1]. We discuss the warped de Sitter compactification which include the metric, the scalar fields, the cosmological constant in D dimensions, and re-examine possible generalizations of the de Sitter compactification [1]. This gives the logically simple treatment of this topic and the clearest explanation of warped compactifications. In the case with a positively curved internal space and pure gravity, this will be a simpler expression of the solution [1]. We will next investigate a stabilization mechanism of the internal space via some kinds of matter fields in the D -dimensional theory, and present another way to construct a cosmological model adding matter fields after integrating over the compact directions and involving the noncompact direction in the higher-dimensional solution into our Universe. We consider the matter fields with a cosmological constant in order to stabilize the scale of internal space. Many works suggest that the field strength might provide a physical mechanism which is capable of accounting for the extreme smallness of the extra dimensions.

We present the solutions to be de Sitter warped compactification with several matter fields following [2, 3] in Sec. 2. In Sec. 3, we discuss the stabilization of moduli degrees of freedom in the lower-dimensional effective theories for the warped compactification. Sec. 4 is devoted to giving concluding remarks.

2 Compactifications with matter fields

In this section, we discuss the warped de Sitter compactification which includes several fields and the cosmological constant.

⁴Email address: uzawa@phys.kindai.ac.jp

The action we consider in the Einstein frame is given by

$$S = \frac{1}{2\kappa^2} \int \left[\left\{ R - 2e^{-\alpha\phi/(p-1)} \Lambda \right\} * \mathbf{1} - \frac{1}{2} d\phi \wedge *d\phi - \frac{1}{2 \cdot p!} e^{\alpha\phi} F \wedge *F \right], \quad (2.1)$$

where κ^2 is the D -dimensional gravitational constant, $*$ is the Hodge operator in the D -dimensional spacetime, and ϕ is the scalar field, and F is p -form field strength, and Λ , α are constants. We adopt the following ansatz for the D -dimensional metric:

$$ds^2 = e^{2A(y)} [q_{\mu\nu}(X) dx^\mu dx^\nu + dy^2 + \gamma_{ab}(Z) dz^a dz^b], \quad (2.2)$$

where $q_{\mu\nu}$ is the n -dimensional metric which depends only on the n -dimensional coordinates x^μ , and γ_{ab} is the $p(= D - n - 1)$ -dimensional metric which depends only on the p -dimensional coordinates z^a . As for the scalar field and the p -form field strength, we take

$$\phi = \frac{2}{\alpha}(p-1)A(y), \quad F = f \sqrt{\gamma} dz^1 \wedge \cdots \wedge dz^p, \quad (2.3)$$

where f is a constant, and γ denotes the determinant of the metric $\gamma_{ab}(Z)$.

Let us first consider the gauge field. Under the assumption (2.3), the Bianchi identity and equation of motion for the gauge field are automatically satisfied. Next we consider the scalar field equation. Substituting the fields (2.3), and the metric (2.2) into the equation of motion for the scalar field, we obtain

$$2(p-1)\alpha^{-1}e^{-2A} \left[A'' + (D-2)(A')^2 - \frac{\alpha^2}{p-1} \left(-\frac{\Lambda}{p-1} + \frac{f^2}{4} \right) \right] = 0, \quad (2.4)$$

where $'$ denotes the ordinary derivative with respect to the coordinate y .

In terms of Eq. (2.4), the Einstein equations are reduced to

$$R_{\mu\nu}(X) - \beta \left(-\frac{\Lambda}{p-1} + \frac{f^2}{4} \right) q_{\mu\nu}(X) = 0, \quad R_{ab}(Z) - \left[\beta \left(-\frac{\Lambda}{p-1} + \frac{f^2}{4} \right) + \frac{f^2}{2} \right] \gamma_{ab}(Z) = 0, \quad (2.5)$$

$$(D-1)A'' + \frac{2(p-1)^2}{(D-2)\alpha^2} \left[(D-2)(A')^2 - \frac{\alpha^2}{p-1} \left(-\frac{\Lambda}{p-1} + \frac{f^2}{4} \right) \right] = 0, \quad (2.6)$$

where $R_{\mu\nu}(X)$ and $R_{ab}(Z)$ are the Ricci tensors of the metrics $q_{\mu\nu}$ and γ_{ab} , respectively, and the constant β is defined by $\beta = \alpha^2(p-1)^{-1} - 2(p-1)(D-2)^{-1}$. So the field equations lead to the D -dimensional metric

$$ds^2 = e^{2\ell(y-y_0)} [-dt^2 + e^{2Ht} \delta_{mn} dx^m dx^n + dy^2 + \gamma_{ab}(Z) dz^a dz^b], \quad (2.7)$$

where y_0 is constant, and ℓ , H is given by

$$\ell = \pm \alpha \sqrt{\frac{1}{(p-1)(D-2)} \left(-\frac{\Lambda}{p-1} + \frac{f^2}{4} \right)}, \quad H^2 = \frac{\beta}{n-1} \left(-\frac{\Lambda}{p-1} + \frac{f^2}{4} \right). \quad (2.8)$$

If we choose α so that $\beta > 0$, it follows that $\alpha > (p-1)\sqrt{2/(D-2)}$, $\alpha < -(p-1)\sqrt{2/(D-2)}$. Hence, the internal space Z has the positive curvature which is clear from an inspection of Eq. (2.5). In the limit of $H \rightarrow 0$, we see that the Ricci tensor of the Z space leads to $R_{ab}(Z) \rightarrow \frac{1}{2}f^2\gamma_{ab}(Z)$. As the internal space is essentially supported by the field strength, we can keep the geometrical property of the internal space in the limit $H \rightarrow 0$.

Before concluding this subsection, we comment about the ansatz for the field strength F . We have simply assumed that the indices of non-vanishing components of the field strength could be along the internal space Z to obtain the de Sitter spacetime for warped compactifications. If the constant field strength F has the components along our $(n+1)$ -dimensional spacetime M , the Ricci tensor on M is proportional to the $(n+1)$ -dimensional metric with negative sign that is no longer de Sitter spacetime.

3 Lower-dimensional effective theory

In this section, we will consider another construction of our de Sitter Universe as well as fixing the moduli in the lower-dimensional effective theory, following the ordinary compactification approach. For simplicity, we consider the internal moduli degrees of freedom of the metric of internal space Z . Now, we assume the D -dimensional metric

$$ds^2 = e^{2A(v)} \left[w_{PQ}(M) dv^P dv^Q + e^{2\psi(v)} \gamma_{ab}(Z) dz^a dz^b \right], \quad (3.1)$$

where $\psi(v)$ is the moduli degrees of freedom on the Z space, and $w_{PQ}(M)$ is the $(n+1)$ -dimensional metric, and $\gamma_{ab}(Z)$ is the metric of the $(D-n-1)$ -dimensional Einstein space Z .

In contrast to the previous section, M contains the direction of the infinite line y in the previous sections, which is regarded as an external direction in the effective theory approach. Furthermore, we assume that the scalar and gauge fields are expressed as in Eq. (2.3). Hence, the moduli ψ and the function A are the only dynamical variables in the effective theory. In the following, we construct the $(n+1)$ -dimensional effective theory after compactifying the Z space. However, in contrast to the brane world model constructed from the higher-dimensional solution (2.7) where the n -dimensional spacetime X becomes our external directions, now the $(n+1)$ -dimensional spacetime M including the noncompact direction y is assumed to be our external directions. The $(n+1)$ -dimensional effective action for these variables can be obtained by evaluating the D -dimensional action (2.1). We assume that the internal space Z satisfies the condition $R_{ab}(Z) = \lambda \gamma_{ab}(Z)$, where λ characterizes the internal space curvature. Inserting the Eqs. (2.3) and (3.1) into (2.1), we get

$$S = \frac{1}{2\tilde{\kappa}^2} \int_{\bar{M}} \left[\{R(\bar{M}) - V(\bar{A}, \bar{\psi})\} *_{\bar{M}} \mathbf{1}_{\bar{M}} - \frac{1}{2} d\bar{A} \wedge *_{\bar{M}} d\bar{A} - \frac{1}{2} \frac{c_2}{\sqrt{c_1 c_3}} d\bar{A} \wedge *_{\bar{M}} d\bar{\psi} - \frac{1}{2} d\bar{\psi} \wedge *_{\bar{M}} d\bar{\psi} \right], \quad (3.2)$$

where we used the conformal transformation $w_{PQ}(M) = e^{-2[(D-2)A+p\psi]/(n-1)} w_{PQ}(\bar{M})$, and $*_{\bar{M}}$ is the Hodge operator on the \bar{M} space and $\tilde{\kappa}$ is given by $\tilde{\kappa} = (\int_Z *_{\mathbf{Z}} \mathbf{1}_{\mathbf{Z}})^{-1/2} \kappa$, with the Hodge operator on the Z space $*_{\mathbf{Z}}$, and $R(\bar{M})$ is the Ricci scalar with respect to the metric $w_{PQ}(\bar{M})$, and we have dropped the surface terms coming from $\Delta_{\bar{M}} A$, $\Delta_{\bar{M}} \psi$, and the potential $V(\bar{A}, \bar{\psi})$, fields \bar{A} , $\bar{\psi}$, the constants c_i ($i = 1, 2, 3$) are defined by

$$V(\bar{A}, \bar{\psi}) = \exp \left[-\frac{2(D-2)\bar{A}}{(n-1)\sqrt{c_1}} \right] \left[2\Lambda \exp \left\{ -\frac{2p\bar{\psi}}{(n-1)\sqrt{c_3}} \right\} + \frac{f^2}{2} \exp \left\{ -\frac{2np\bar{\psi}}{(n-1)\sqrt{c_3}} \right\} - p\lambda \exp \left\{ -\frac{2(D-2)\bar{\psi}}{(n-1)\sqrt{c_3}} \right\} \right], \quad (3.3)$$

$$c_1 = 2 \left[\frac{n}{n-1} (D-2) - 2(D-1) \right] (D-2) + 2 \left[n-1 + \frac{2}{\alpha^2} (p-1) \right] (p-1) + 2p(D-1), \quad (3.4)$$

$$c_2 = \frac{4(D-2)p}{n-1}, \quad c_3 = 2p \left(\frac{n-1}{p} + 1 \right), \quad \bar{A} = \sqrt{c_1} A, \quad \bar{\psi} = \sqrt{c_3} \psi. \quad (3.5)$$

Here $\Delta_{\bar{M}}$ is the Laplace operator constructed from the metric $w_{PQ}(\bar{M})$. The form of the potential (3.3) implies that the warp factor \bar{A} cannot be fixed by the background fields. This is consistent with the fact that the analysis of the the scalar perturbations for the solutions which have been discussed in the previous section is unstable. We have explained these in [2].

Then, in the following, we fix the value of \bar{A} by assuming some additional stabilization mechanism which does not affect the dynamics of the other moduli $\bar{\psi}$, and consider the stabilization of $\bar{\psi}$. In order to fix the moduli degrees of freedom $\bar{\psi}$, the moduli potential has to have a minimum or at least a local minimum. In the present model, setting $n = 3$, $p = 6$, $\bar{A} = 1$, $f = 0.17$, $\lambda = 0.229$ and $\alpha = 0.5$ in the unit of $\Lambda = 1$, we find the stable minimum point $\bar{\psi}_0 = -1.1000$, where $\Lambda^{-1} V(1, \bar{\psi}_0) = 0.0365$. Since the potential energy is proportional to the warp factor $e^{-\bar{A}}$, the $(n+1)$ -dimensional effective cosmological constant can be dropped exponentially as \bar{A} increases. Hence, if we choose the value of the function \bar{A} appropriately, we get the small energy value of the potential at $\bar{\psi} = \bar{\psi}_0$. We illustrate the moduli potential in Fig. 1.

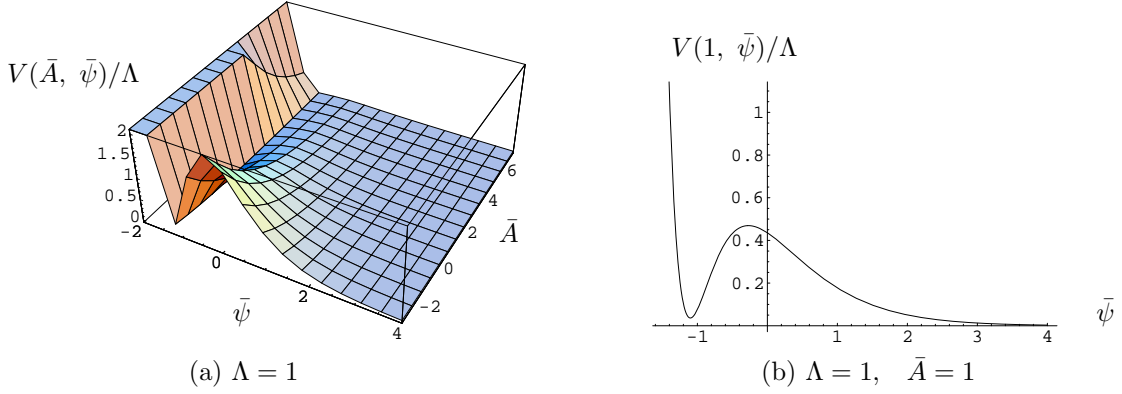


Figure 1: The moduli potential given in (11) is depicted. We set $n = 3$, $p = 6$, $f = 0.17$, $\lambda = 0.229$ and $\alpha = 0.5$ in the unit of $\Lambda = 1$. We can find the minimum of the potential with respect to the field $\bar{\psi}$ while there is not local minimum of the potential for the direction of \bar{A} . If we fix the value of the function \bar{A} , we get the small energy value of the moduli potential at the local minimum. The minimum of the potential is located at $\bar{\psi}_0 = -1.1000$ and its value is $\Lambda^{-1}V(1, \bar{\psi}_0) = 0.0365$.

4 Discussions

We have discussed the warped de Sitter compactifications in higher-dimensional theory. We presented the n -dimensional warped de Sitter compactification due to the contribution of the matter fields. The solution gives the accelerating expansion of the n -dimensional universe. An important consequence of this is obtaining the de Sitter spacetime from warped compactifications. If the constant field strength F goes through our n -dimensional spacetime X , the Ricci tensor on X is proportional to the n -dimensional metric with negative sign that is no longer de Sitter spacetime [3]. Hence we were only concerned with the field strength along Z . We have also presented another construction of a de Sitter spacetime in terms of the $(n+1)$ -dimensional effective theory after integrating over the Z space. The $(n+1)$ -dimensional spacetime M was regarded as our Universe. We have calculated the moduli potential and discussed its stability using the moduli potential. Assuming some stabilization mechanism of the volume moduli which does not affect the dynamics of the internal space moduli the cosmological constant and field strengths force the internal space to expand, while the curvature of the internal spacetime forces it to contract. These combination produces a local minimum of the moduli potential. In the $(n+1)$ -dimensional effective theory, the scale of the compact internal space Z is stabilized by balancing the gauge field strength wrapped around the internal space and the curvature term of the internal space with the cosmological constant. For some choices of the parameters, these contributions could produce a local minimum of the effective potential with a positive value which corresponds to the $dS_{n+1} \times Z$ background in the effective theory, while the solution in the original higher-dimensional gravitational theory gave the geometry of $dS_n \times \mathbb{R} \times Z$. If the $(n+1)$ -dimensional universe is created near the top of the potential hill, the moduli rolls down the potential hill and finds a stable minimum point. Since the moduli potential eventually turns out to be positive or negative, the $(n+1)$ -dimensional background geometry becomes dS_{n+1} or AdS_{n+1} spacetime. As the moduli potential without the cosmological constant leads to the AdS_{n+1} at the local minimum even if we have a field strength, we need the contribution of the cosmological constant to obtain de Sitter compactifications [3].

References

- [1] I. P. Neupane, Nucl. Phys. B **847** (2011) 549 [arXiv:1011.5007 [hep-th]].
- [2] M. Minamitsuji and K. Uzawa, arXiv:1103.5325 [hep-th].
- [3] M. Minamitsuji and K. Uzawa, arXiv:1103.5326 [hep-th].

Exact solutions of Einstein gravity with a negative cosmological constant coupled to a massless scalar field in arbitrary spacetime dimensions

Cristián Martínez^{5(a),(b)} and Sebastián García Sáenz^{6(c)}

^(a) *Centro de Estudios Científicos (CECs), Av. Arturo Prat 514, Valdivia, Chile*

^(b) *Universidad Andrés Bello, Av. República 440, Santiago, Chile*

^(c) *Department of Physics, Columbia University, New York, NY 10027, USA*

Abstract

Static d -dimensional spacetimes in Einstein gravity with a negative cosmological constant in the presence of a minimally coupled massless scalar field are considered. The spacetimes have a $(d - 2)$ -dimensional transverse space-like section given by an Einstein Ricci-flat space and the massless scalar field depends only on the radial coordinate. The field equations are decoupled and solved exactly. The solution has a curvature singularity located at the origin, where also the scalar field diverges. Since there is no event horizon surrounding this singularity, the solution describes a naked singularity dressed with a non-trivial scalar field. This spacetime is an asymptotically locally anti-de Sitter one when the Ricci-flat transverse space has constant curvature. The mass of the solutions is computed using the canonical generator of the time-translation invariance, as well as the asymptotic form of the metric and scalar field, and it is shown to be finite. The contribution of the scalar field at infinity to the mass is also discussed.

1 Introduction

In this paper we study the d -dimensional static solutions of the Einstein field equations in the presence of a minimally coupled massless scalar field and a negative cosmological constant. The search for exact solutions in the presence of a negative cosmological constant is well motivated, for the reason that they are asymptotically anti-de Sitter (AdS), and may therefore be of interest in the context of the gravity/gauge correspondence [1].

For the case of a vanishing cosmological constant, the general static and spherically symmetric solution to the problem was first found in four dimensions by Fisher [2], and later rediscovered in [3] and [4] (see also [5]). The higher-dimensional generalization was found by Xanthopoulos and Zannias in [6], and further studied in detail in [7], while the solution for the 3-dimensional case was reported in [8]. Regardless of the number of spacetime dimensions, the results dictate that the static and spherically symmetric solution, with a non-trivial massless scalar field, corresponds to a spacetime containing a naked singularity, as it is expected by virtue of the no-hair theorem for asymptotically flat spacetimes.

The problem with a negative cosmological constant was first considered in [9], where the general solution for $d = 3$ spacetime dimensions was found, and later independently rediscovered in [1] and [10]. In four dimensions we can mention the existence of a particular plane-symmetric solution with non-zero cosmological constant (of arbitrary sign) given in [11]. As far as we know, there are no exact results for this model in higher dimensions. The main purpose of this paper is to generalize previous results in two different ways: (i) by including a non-vanishing cosmological constant term in arbitrary dimension, and (ii) by studying the case in which the transverse space is a $(d - 2)$ -dimensional Ricci flat Einstein manifold rather than the usual $(d - 2)$ -sphere.

⁵Email address: martinez@cecs.cl

⁶Email address: sg2947@columbia.edu

2 Action and field equations

We consider a real massless scalar field minimally coupled to Einstein gravity in $d > 2$ spacetime dimensions in the presence of a cosmological constant Λ , which is written in terms of the AdS radius l as $\Lambda = -(d-1)(d-2)/(2l^2)$. The action for this model is given by

$$I[g_{\mu\nu}, \phi] = \int d^d x \sqrt{-g} \left(\frac{R - 2\Lambda}{2\kappa} - \frac{1}{2} g^{\mu\nu} \partial_\mu \phi \partial_\nu \phi \right), \quad (2.1)$$

where κ is the Einstein constant. The corresponding field equations are

$$R^\mu{}_\nu + \frac{(d-1)}{l^2} \delta^\mu{}_\nu = \kappa \partial^\mu \phi \partial_\nu \phi, \quad (2.2)$$

and

$$\square \phi = 0. \quad (2.3)$$

We are interested in static configurations defined by the following Ansatz:

$$ds^2 = -e^{2h(r)} f^2(r) dt^2 + \frac{dr^2}{f^2(r)} + r^2 \gamma_{mn} dz^m dz^n, \quad \text{with } \phi = \phi(r). \quad (2.4)$$

Here γ_{mn} is the metric of a $(d-2)$ -dimensional Einstein manifold Σ of Euclidean signature, whose Ricci tensor vanishes. The manifold Σ is assumed to have a finite volume, denoted by $V(\Sigma)$.

For this class of static configurations the field equations can be reduced to a system of three ordinary nonlinear differential equations for the metric functions $h(r)$, $f^2(r)$, and the scalar field $\phi(r)$. Following [1], we define a new variable $a(r) := r^{d-3} e^h f^2$, and the system becomes a decoupled set of differential equations:

$$a^2 \left[r \frac{a''}{a'} - (d-2) \right] = \frac{\kappa c_0^2}{(d-2)}. \quad (2.5a)$$

$$h' = \frac{\kappa c_0^2}{(d-2)} \frac{1}{ra^2}, \quad (2.5b)$$

$$\phi' = \frac{c_0}{ra}. \quad (2.5c)$$

In the above equations $'$ denotes derivation with respect to r , and c_0 is an arbitrary constant that comes from the integration of the field equation (2.3).

3 Exact general solution

We find the general solution of (2.5a) to be implicitly given by

$$r^{d-1} = l^{d-1} (a - a_1)^{\frac{a_1}{a_1+a_2}} (a + a_2)^{\frac{a_2}{a_1+a_2}}. \quad (3.1)$$

Here a_1, a_2 are integration constants, which are related to the constant c_0 above. There is no restriction to assume that they are non-negative. Thus, the coordinate range $r \geq 0$ implies the condition $a \geq a_1$ for the variable a .

A simple expression for the solution can be obtained by defining the variable $x := a + (a_2 - a_1)/2$, and the constants $b := (a_1 + a_2)/2$ and $p := (a_2 - a_1)/(a_1 + a_2)$. Then the solution can be written in the form

$$ds^2 = - (x-b)^{\frac{1+(d-2)p}{(d-1)}} (x+b)^{\frac{1-(d-2)p}{(d-1)}} dt^2 + \frac{l^2}{(d-1)^2} \frac{dx^2}{(x^2 - b^2)} + l^2 (x-b)^{\frac{1-p}{(d-1)}} (x+b)^{\frac{1+p}{(d-1)}} \gamma_{mn} dz^m dz^n, \quad (3.2)$$

$$\phi(x) = \phi_0 + \sqrt{\frac{d-2}{d-1}} \sqrt{\frac{1-p^2}{4\kappa}} \ln \left(\frac{x-b}{x+b} \right). \quad (3.3)$$

Now, the constants b , p , and ϕ_0 are the parameters of the family of solutions to this problem. Note that $|p| \leq 1$, and $b \geq 0$. The range $r > 0$ implies that $x > b$.

The existence of curvature singularities can be shown through the Ricci scalar, which reads

$$R = -\frac{(d-1)}{l^2} \left[d - (d-2) \frac{b^2(1-p^2)}{(x^2-b^2)} \right]. \quad (3.4)$$

Assuming that $b \neq 0$ and $p^2 \neq 1$, we see that there is a curvature singularity at $x = b$, which corresponds to $r = 0$. Moreover, there are no horizons in this spacetime. This implies the existence of a naked singularity at the origin.

The causal structure of the solution is the same as in AdS spacetime, except that the surface $r = 0$ is now a curvature singularity. As in the case of AdS, future null geodesics can reach infinity, while future timelike geodesics cannot. In contrast to AdS spacetime, however, geodesics do not reach timelike infinities i^+ and i^- in this solution.

4 Asymptotic solution and mass

We now turn to study the asymptotic behavior of the solutions. We find

$$a(r) = \left(\frac{r}{l}\right)^{d-1} - \mu + O\left(\left(\frac{l}{r}\right)^{d-1}\right), \quad (4.1)$$

where μ is an arbitrary constant. In terms of the integration constants of the exact solution (3.2) the constant μ is equal to $2bp$. With the result of Eq. (4.1) we obtain the asymptotic expansion of the metric:

$$ds^2 = - \left[\left(\frac{r}{l}\right)^2 - \mu \left(\frac{l}{r}\right)^{d-3} + O\left(\left(\frac{l}{r}\right)^{2(d-2)}\right) \right] dt^2 \\ + \left[\left(\frac{r}{l}\right)^2 - \mu \left(\frac{l}{r}\right)^{d-3} + O\left(\left(\frac{l}{r}\right)^{2(d-2)}\right) \right]^{-1} dr^2 + r^2 \gamma_{mn} dz^m dz^n. \quad (4.2)$$

Strictly speaking, the spacetime is an asymptotically locally AdS spacetimes only if the transverse section Σ is a constant curvature space. This condition is automatically satisfied in four and five spacetime dimensions.

Replacing (4.1) in (2.5c), we compute the asymptotic form of the scalar field,

$$\phi = \phi_0 - \phi_1 \left(\frac{l}{r}\right)^{d-1} + O\left(\left(\frac{l}{r}\right)^{d+1}\right), \quad (4.3)$$

where ϕ_0 and ϕ_1 are arbitrary constants. For the exact solution (3.3), $\phi_1 = \sqrt{\frac{d-2}{d-1}} \sqrt{\frac{1-p^2}{\kappa}} b$. The full family of asymptotic solutions is thus parametrized by the three constants μ , ϕ_0 , and ϕ_1 .

We now turn to the problem of computing the mass of these configurations. We address this issue following the Regge-Teitelboim approach [12].

The mass is the conserved charge associated with time-translation symmetry. We then write the variation of the mass as $\delta M = \delta M_G + \delta M_\phi$ [13], and from Eqs. (4.2) and (4.3) we obtain

$$\delta M_G = - \lim_{r \rightarrow \infty} \frac{(d-2)}{2\kappa} V(\Sigma) \frac{r^{d-2}}{l} (g^{rr})^{-1/2} \delta g^{rr} = \frac{(d-2)}{2\kappa} V(\Sigma) l^{d-3} \delta \mu, \quad (4.4)$$

$$\delta M_\phi = - \lim_{r \rightarrow \infty} V(\Sigma) \frac{r^{d-1}}{l} (g^{rr})^{1/2} \phi' \delta \phi = (d-1) V(\Sigma) l^{d-3} \phi_1 \delta \phi_0, \quad (4.5)$$

where $V(\Sigma)$ denotes the volume of the Einstein base manifold.

The next step is to integrate Eqs. (4.4) and (4.5) in order to obtain the value of the mass M . The gravitational contribution can be directly integrated, giving the result

$$M_G = \frac{(d-2)}{2\kappa} V(\Sigma) l^{d-3} \mu = \frac{(d-2)}{\kappa} V(\Sigma) l^{d-3} bp. \quad (4.6)$$

The above expression corresponds to the standard mass formula for a spacetime with a metric of the form (4.2) in vacuum.

The issue of the scalar field contribution to the mass is more subtle, since now δM_ϕ depends on the two integration constants ϕ_0 and ϕ_1 through the combination $\phi_1 \delta \phi_0$. In general, the integration of this variation requires a functional relation between ϕ_0 and ϕ_1 . Consequently, the scalar field contribution M_ϕ will be determined by this relation, and so will be the total mass as well. Here we are considering solutions having a subset of the AdS symmetries at infinity. In particular, system (2.5) possesses a scaling symmetry [14]. Thus, if one restricts the functional variations at infinity to be compatible with the variations generated by an infinitesimal scaling, the condition $\delta \phi_0 = 0$ must hold. This condition is satisfied provided that ϕ_0 is a constant without variation. Under this condition we have $\delta M_\phi = 0$, and then the total mass is just $M = M_G$. In summary, if the functional variations at infinity are restricted to be compatible with those coming from the scaling invariance, we can conclude that the scalar field does not contribute to the mass. On the contrary, for a generic variation of the scalar field at infinity one should expect a nonzero contribution.

Acknowledgments. The authors thank Hideki Maeda and Ricardo Troncoso for useful discussions. This work has been partially funded by the Fondecyt grants 1085322, 1095098, 1100755 and by the Conicyt grant ACT-91: “Southern Theoretical Physics Laboratory” (STPLab). The Centro de Estudios Científicos (CECS) is funded by the Chilean Government through the Centers of Excellence Base Financing Program of Conicyt.

References

- [1] S. Das, J. Gegenberg and V. Husain, *Phys. Rev. D* **64**, 065027 (2001) [arXiv:hep-th/0101169].
- [2] I. Z. Fisher, *Zh. Eksp. Teor. Fiz.* **18**, 636-640 (1948). [gr-qc/9911008].
- [3] A. I. Janis, E. T. Newman, J. Winicour, *Phys. Rev. Lett.* **20**, 878-880 (1968).
- [4] M. Wyman, *Phys. Rev.* **D24**, 839-841 (1981).
- [5] K. S. Virbhadra, *Int. J. Mod. Phys. A* **12**, 4831 (1997) [arXiv:gr-qc/9701021].
- [6] B. C. Xanthopoulos, T. Zannias, *Phys. Rev.* **D40**, 2564-2567 (1989).
- [7] S. Abdolrahimi and A. A. Shoom, *Phys. Rev. D* **81**, 024035 (2010) [arXiv:0911.5380 [gr-qc]].
- [8] K. S. Virbhadra, *Pramana* **44**, 317-322 (1995). [gr-qc/9408035].
- [9] G. Clément, A. Fabbri, *Class. Quant. Grav.* **17**, 2537-2546 (2000). [gr-qc/9912023].
- [10] D. Daghan, A. H. Bilge, *Gen. Rel. Grav.* **37**, 1289-1296 (2005). [gr-qc/0505130].
- [11] C. Vuille, *Gen. Rel. Grav.* **39**, 621 (2007).
- [12] T. Regge, C. Teitelboim, *Annals Phys.* **88**, 286 (1974).
- [13] M. Henneaux, C. Martínez, R. Troncoso and J. Zanelli, *Annals Phys.* **322**, 824 (2007) [arXiv:hep-th/0603185].
- [14] M. Bañados, S. Theisen, *Phys. Rev.* **D72**, 064019 (2005). [hep-th/0506025].

Stability of Schwarzschild-like spacetime in parity violating gravitational theories

Hayato Motohashi^(a,b) and Teruaki Suyama^(b)

^(a)*Department of Physics, Graduate School of Science, The University of Tokyo, Tokyo 113-0033, Japan*

^(b)*Research Center for the Early Universe (RESCEU), Graduate School of Science, The University of Tokyo, Tokyo 113-0033, Japan*

Abstract

We study linear perturbations around static, spherically-symmetric spacetimes in $f(R, C)$ gravitational theories whose Lagrangians depend on the Ricci scalar R and the parity violating Chern-Simons term C . By an explicit construction, we show that the Hamiltonian for the perturbation variables is not bounded from below, suggesting that such a background spacetime is unstable against perturbations. This gives a strong limit on a phenomenological gravitational model which violates parity. We also show that either $R = \text{const}$ or $\frac{\partial^2 f}{\partial R \partial C} = 0$ is a necessary and sufficient condition for the stability. We then implement in detail the perturbation analysis for such theories which satisfy the stability conditions and find that the no-ghost conditions and no-tachyon conditions are the same as those in $f(R)$ theories.

1 Introduction

General relativity (GR) in the weak gravitational field regime has been tested both experimentally and observationally over many decades. In the forthcoming decade, the test of GR in the strong gravitational regime will be also available, for example, by observing the gravitational waves coming from the vicinity of black holes (BHs). These facts have provoked alternative theories of gravity and have led us to understand theoretically what kinds of different phenomena are expected in such theories. In light of this situation, it is interesting to consider gravitational theories which violate parity due to the so-called Chern-Simons(CS) term, or the Pontryagin density, $C \equiv \frac{1}{2} \epsilon_{\alpha\beta\gamma\delta} R^{\alpha\beta}{}_{\mu\nu} R^{\gamma\delta\mu\nu}$, where $\epsilon_{\alpha\beta\gamma\delta}$ is the totally antisymmetric tensor. For a recent review on the Chern-Simons gravity, see Ref. [1].

In this paper, we consider the gravitational theories whose Lagrangian is a general function of R and C , $f(R, C)$, and develop linear perturbation theory around the static and spherically symmetric spacetime. Unlike in the case of $f(R)$ theories which can be mapped into equivalent theories where a scalar field having self-interacting potential is minimally coupled to Einstein-Hilbert gravity, $f(R, C)$ theories cannot be mapped into theories where C is coupled solely to a dynamical scalar field due to nontrivial transformation property of the CS term under the conformal transformation. Our aim is to clarify both quantitative and qualitative behaviors of the perturbations. To be more precise, we will derive no-ghost and no-tachyon conditions which are necessary to ensure stability of the background spacetime against perturbation, obtain dispersion relations for the propagating modes and find features that are characteristic to parity violating theories.

2 BH perturbation for $f(R, C)$ theories

We study $f(R, C)$ theory, where the action is described by a general function of Ricci scalar R and the CS term $C \equiv \frac{1}{2} \epsilon_{\alpha\beta\gamma\delta} R^{\alpha\beta}{}_{\mu\nu} R^{\gamma\delta\mu\nu}$,

$$S = \frac{M_P^2}{2} \int d^4x \sqrt{-g} f(R, C). \quad (2.1)$$

Here, $M_P = 1/\sqrt{8\pi G_N} \simeq 4.34 \times 10^{-6} \text{g}$ is the reduced Planck mass. We can rewrite the action (2.1) as

$$S = \frac{M_P^2}{2} \int d^4x \sqrt{-g} (RF(\lambda, s) + W(\lambda, s)C - V(\lambda, s)), \quad (2.2)$$

where λ and s are auxiliary fields and

$$F(\lambda, s) = \frac{\partial f(\lambda, s)}{\partial \lambda}, \quad W(\lambda, s) = \frac{\partial f(\lambda, s)}{\partial s}, \quad V(\lambda, s) = \lambda F(\lambda, s) + sW(\lambda, s) - f(\lambda, s). \quad (2.3)$$

In this section, we calculate the perturbative action around a static and spherically symmetric space-time whose metric is given by

$$ds^2 = -A(r)dt^2 + \frac{dr^2}{B(r)} + r^2 (d\theta^2 + \sin^2 \theta d\varphi^2). \quad (2.4)$$

There are gauge degrees of freedom for the metric perturbations $h_{\mu\nu}$ [2, 3]. For the odd-type perturbations, we take a gauge in which spherical component $h_{ab}(a, b = \theta, \varphi)$ vanishes. For the even-type perturbations, we impose that both h_{ab} and h_{ta} vanish. As a result of the parity violation term, the odd and even modes do not decouple from each other within the system of equations and we have to deal with it all together. In addition to the metric perturbations, we also need to perturb the other functions λ and s that appear in the action. Just for later convenience, instead of perturbing λ and s as the fundamental fields, we treat δF and δW as perturbation variables.

With these perturbation variables, expanding the action (2.2) to second order yields the quadratic action for the perturbation variables. It then turns out that not all of the variables are dynamical. Actually, we find that H_0 , H_1 and δW are auxiliary fields. Therefore, they can be eliminated from the action by using their equations of motion. After substituting the constraints and many integration by parts, we end up with the following Lagrangian density (for the detailed calculations, see Ref. [4]):

$$\begin{aligned} \mathcal{L} = & p_1 \ddot{h}_1^2 + p_2 \ddot{h}_1 (r \dot{h}'_0 - 2\dot{h}_0) + p_3 \dot{h}_0'^2 + p_4 \dot{h}_0^2 + p_5 \dot{h}_1^2 + p_6 \delta F'^2 + p_7 \dot{\beta}^2 + p_8 \dot{h}_0 \delta F + p_9 \dot{h}_0 \dot{\beta} + p_{10} \dot{\beta} \delta F + p_{11} h_0'^2 \\ & + p_{12} \delta F'^2 + p_{13} \beta'^2 + p_{14} h_0' \delta F' + p_{15} h_0' \beta' + p_{16} \beta' \delta F' + p_{17} h_0' \dot{h}_1 + p_{18} \dot{h}_0 h_1 + p_{19} h_0' \delta F + p_{20} h_0' \beta \\ & + p_{21} \dot{h}_1 \delta F + p_{22} \dot{h}_1 \beta + p_{23} \delta F \beta' + p_{24} h_0^2 + h_0 (p_{25} \delta F + p_{26} \beta) + p_{27} h_1^2 + p_{28} \delta F^2 + p_{29} \delta F \beta + p_{30} \beta^2 \end{aligned} \quad (2.5)$$

Since all the fields (h_0 , h_1 , β , δF) have time derivatives that are not removed by any integration by parts, all of them are dynamical fields. Hence, this is our final Lagrangian. Explicit expressions of the background dependent coefficients p_1, \dots are given in the appendix of Ref. [4].

Contrary to the corresponding Lagrangian in $f(R)$ gravity, the above Lagrangian contains a term \ddot{h}_1^2 . This term results in fourth order differential equations for h_1 with respect to time. We can confirm this fact by looking at the explicit expressions for p_1 , p_2 and p_3 , which are given by

$$p_1 = -\frac{32\pi\ell(\ell+1)M_P^2 W'^2}{(2\ell+1)F\left(\frac{A}{B}\right)^{3/2}}, \quad p_2 = -\frac{2p_1}{r}, \quad p_3 = p_1.$$

The presence of the \ddot{h}_1 term in the general $f(R, C)$ gravity is a signal that the theory is plagued by instability [5]. In particular, the Hamiltonian can take arbitrary negative values and hence it is not bounded from below. This result shows that the general $f(R, C)$ gravity has the problem of having a ghost around the static and spherically symmetric background and provides a severe condition on the functional form of $f(R, C)$.

There are two possible cases where the presence of the ghost does not become problematic. The first one is to assume that the $f(R, C)$ theory under consideration is an effective theory which is valid only on length scales larger than a certain length d_c . From this point of view, the presence of the ghost does not matter if its mass is larger than the energy scale d_c^{-1} since the dynamics of the ghost cannot be described by the low energy $f(R, C)$ theory. The more fundamental theory which is valid above d_c^{-1} may cure the problem. To see this, let us pick up terms in the Hamiltonian relevant to the ghost mode,

$$\begin{aligned} \mathcal{H}_{\text{sub}} = & -\cos \delta \left(K_{11} \bar{M}_{11} \cos \delta + 2K_{13} \sqrt{\bar{M}_{11} \bar{M}_{33}} \sin \delta \right) \bar{P}_1^2 \\ & -\sin \delta \left(K_{11} \bar{M}_{11} \sin \delta - 2K_{13} \sqrt{\bar{M}_{11} \bar{M}_{33}} \cos \delta \right) \bar{P}_3^2 - \bar{Q}_1^2 - \bar{Q}_3^2, \end{aligned}$$

where δ is determined from the equation

$$\tan 2\delta = -\frac{2K_{13}}{K_{11}} \sqrt{\frac{\bar{M}_{33}}{\bar{M}_{11}}} = \sqrt{\frac{3}{\ell^2 + \ell - 2}} \operatorname{sgn}(r^4 F_\lambda - 64\ell(\ell+1)F_s^2 F'^2).$$

Here, the sign function is defined as $\text{sgn}(x) = +1, 0, -1$ for $x > 0, x = 0, x < 0$, respectively. The coefficients in front of \bar{P}_1 and \bar{P}_3 must be larger than d_c^{-2} in order for those fields to be in the high energy regime where the effective $f(R, C)$ theory does not work. This leads to a condition,

$$|K_{11}M_{11}| \simeq \left| \frac{r^4 F_\lambda - 64\ell(\ell+1)F_s^2 F'^2}{64r^4 F_\lambda W'^2} \right| \gtrsim d_c^{-2}.$$

In particular, when the second term in the numerator is negligible, we obtain the very simple condition for W' ,

$$|W'| \lesssim d_c.$$

Since W' , which has dimensions of length, represents how large the effects of the Chern-Simons term are, this condition says these effects are suppressed on distances larger than d_c .

The second possibility where the presence of the ghost does not become problematic is that $f(R, C)$ belongs to the special class in which $W' = 0$ is satisfied identically. Using the background metric, W' can be written as

$$W' = F_s R' + W_s C' = F_s R', \quad (2.6)$$

where we have used an identity $C = 0$ for the background metric. Therefore, if $f(R, C)$ satisfies either $F_s = 0$ or $R = \text{const}$, we have $W' = 0$ identically. For example, $F_s = 0$ is trivially satisfied if $f(R, C)$ takes a separable form, *i.e.*, $f(R, C) = f_1(R) + f_2(C)$, where f_1 and f_2 are arbitrary functions of R and C , respectively. $f(R)$ gravity is included in this case. The second case $R = \text{const}$ is satisfied, for example, if the Schwarzschild metric is a solution of the model. In either case, we have still many $f(R, C)$ theories. We deal with this class of $f(R, C)$ theories in the next section.

3 Study of special cases with $W' = 0$.

As we have shown in the previous section, the general $f(R, C)$ theories with nonvanishing W' have the problem of instability. Thus, the cases with $W' = 0$ are more phenomenologically interesting and deserve further investigation. The Lagrangian for the general $f(R, C)$ theories (2.5) can be also used for the special case $W' = 0$ as well. We find that even for the special cases, the odd and even modes are still coupled as long as $F_s = 0$.

By introducing a new variable q , we can rewrite the Lagrangian so that it contains only q , δF and β ,

$$\mathcal{L} = k_{ij} \dot{q}_i \dot{q}_j - d_{ij} q'_i q'_j - e_{ij} q'_i q_j - m_{ij} q_i q_j, \quad (3.1)$$

where we have defined $(q_1, q_2, q_3) = (\delta F, \beta, q)$. A determinant of the kinetic matrix k_{ij} is found to be

$$\det(k_{ij}) = \frac{384\pi^3 \ell^2 (\ell+1)^2 M_P^6 r^4 Y^2}{(2\ell+1)^3 A^3 F^3 \left(\frac{A}{B}\right)^{3/2} (rBA' (rF' + 2F) + 2A (F(-2B + \ell^2 + \ell) - rBF'))^2}, \quad (3.2)$$

where the definition of Y is given in Ref. [4]. This is not zero in general. Therefore, all the variables are dynamical and there are three propagating modes, one of which is odd (*i.e.*, q) and the remaining two are even (*i.e.*, δF and β). This structure is the same as that of the $f(R)$ gravity theories where there is one propagating odd mode and two propagating even modes. This result shows that the condition $W' = 0$ kills all the pathological modes which exist in the general $f(R, C)$ theories. By evaluating k_{33} and $k_{22}k_{33} - k_{23}^2$, we find that $F > 0$ is needed to ensure their positivity. Therefore, as is the case with $f(R)$ theories, $F > 0$ is the no-ghost condition for $f(R, C)$ theories that satisfy $W' = 0$.

We can derive the dispersion relations for the three modes from an equation,

$$\det(-\omega^2 k_{ij} + k^2 d_{ij}) = \frac{768\pi^3 \ell^2 (-\ell^3 - 2\ell^2 + \ell + 2)^2 M_P^6 r B F^3 q_1^2 \sqrt{\frac{A}{B}} (\omega^2 - k^2 AB)^3}{(2\ell+1)^3 q_{13} (2rq_{11} - rq'_8 - 2q_8) (rBA' (rF' + 2F) + 2A (F(-2B + \ell^2 + \ell) - rBF'))^2}.$$

We see all the modes obey a dispersion relation $\omega^2 = ABk^2$. The appearance of the factor AB is due to the fact that t and r are coordinate time and distance. In terms of the physical time and distance, the

dispersion relation says all the modes propagate at the speed of light, which is exactly the same as in the case of $f(R)$ theories. Although there are no new contributions to the propagation speeds due to the Chern-Simons term, the coupling between δF and q means that we cannot consider the propagation of the odd and even modes separately as we can do in the case of $f(R)$ theories, which is a clear difference from $f(R)$ theories. This shows the potential usefulness of using the distinct nature of mode propagation in $f(R, C)$ theories for putting constraints on $f(R, C)$ models using observations of gravitational waves from compact astrophysical objects.

We can also evaluate the mass for each eigenmode. However, since each matrix element of m_{ij} is too lengthy to obtain analytic expressions for the mass eigenvalues, we will make an assumption that the background is very close to GR, *i.e.*, $F = 1$, $A = B = 1 - \frac{r_g}{r}$ and also expand the eigenvalues in $\varepsilon \equiv \frac{r_g}{r}$ (weak field approximation). Under these assumptions, three eigenvalues are given by

$$\begin{aligned} m_1^2 &= \frac{1}{3F_\lambda} - \frac{\ell^2(\ell+1)^2 r_g - 2(\ell^2 + \ell - 2)^2 (\ell^2 + \ell + 2) r}{3(\ell^2 + \ell - 2)^2 r^3} + \mathcal{O}(\varepsilon^2), \\ m_2^2 &= \frac{\ell(\ell+1)}{r^2} - \frac{\ell^2(\ell+1)^2 r_g}{(\ell^2 + \ell - 2)^2 r^3} + \mathcal{O}(\varepsilon^3), \\ m_3^2 &= \frac{\ell^2 + \ell + 4}{r^2} - \frac{192\ell(\ell^5 + 3\ell^4 + 7\ell^3 + 9\ell^2 - 4) r_g^2 F_s^2}{(\ell^2 + \ell - 2)^2 r^8 F_\lambda^2} + \mathcal{O}(\varepsilon^3). \end{aligned}$$

Since m_1^2 is inversely proportional to F_λ at leading order, this mode corresponds to the scalar graviton that exists in the general $f(R)$ theories. To avoid the tachyonic mode, we need to impose a condition $F_\lambda > 0$. The Chern-Simons corrections, F_s , appear in m_1^2 and m_3^2 , but only in a combination with r_g . This means those corrections are important only in the vicinity of the BH and are suppressed compared to the standard terms that exist in GR far from the BH.

4 Conclusion

We have studied linear perturbations around the static, spherically-symmetric spacetime for general $f(R, C)$ theories, where C is the parity violating Chern-Simons term. By explicitly constructing the second order action, we showed that one odd mode appears in the action as a quadratic in its second time derivative. Irrespective of its sign, this results in an Hamiltonian that is not bounded from below. Therefore, the static and spherically symmetric spacetime is unstable in general $f(R, C)$ theories. This gives a strong limit on any phenomenological gravitational model which violates parity.

We also showed that either $R = \text{const}$ or $\frac{\partial^2 f}{\partial R \partial C} = 0$ for the background metric is a necessary and sufficient condition to avoid the instability mentioned above. For such theories, the number of propagating modes for $\ell \geq 2$ is three, one from the odd and the other two from the even. Unlike in the case of $f(R)$ theories, those modes are coupled, which can be used as a distinctive feature to test the parity violating theories from observations. All the modes propagate at the speed of light. The no-ghost condition is $\frac{\partial f}{\partial R} > 0$ and the no-tachyon condition is $\frac{\partial^2 f}{\partial R^2} > 0$, which are the same as in the case of $f(R)$ theories.

References

- [1] S. Alexander and N. Yunes, Phys. Rept. **480**, 1 (2009) [arXiv:0907.2562 [hep-th]].
- [2] T. Regge and J. A. Wheeler, Phys. Rev. **108**, 1063 (1957).
- [3] F. J. Zerilli, Phys. Rev. Lett. **24**, 737 (1970).
- [4] H. Motohashi and T. Suyama, Phys. Rev. D **84**, 084041 (2011) [arXiv:1107.3705 [gr-qc]].
- [5] R. P. Woodard, Lect. Notes Phys. **720**, 403 (2007) [arXiv:astro-ph/0601672].

New features of black hole solutions in $f(R, \mathcal{G})$ theories

Sergey Pavluchenko⁷

Special Astrophysical Observatory of the Russian Academy of Sciences, Nizhnij Arkhyz, Russia 369167

Abstract

Our report reflects new features of the black-hole (BH)-like (spherically-symmetric) solutions in $f(R, \mathcal{G})$ theories. Since BH-like solutions are an important tool for testing GR; it might be the same for the generalizations of GR and $f(R, \mathcal{G})$ theories are one of the best candidate for it. So we report our findings for BH-like solutions for several partial cases of $f(R, \mathcal{G})$ theories as well as we attempt to construct generic solution and find out its properties.

1 Introduction

With the Nobel Prize in Physics in 2011 [1] granted for the discovery of the current accelerated expansion of the Universe, the source of this expansion – the mysterious *dark energy* – yet awaits its nature to be unveiled. One class of the dark energy models imply modifications of gravity and $f(R)$ (with the Lagrangian density contains not the Ricci scalar but some function of it) is one of the oldest models of the kind. In this way, $f(R, \mathcal{G})$ theory is natural generalization of $f(R)$ model. There are all kinds of the dark energy models, but almost all of them possess the same difficulty – they are hard to be distinguished from one another using cosmological tests. We propose to use spherically-symmetric solutions (and their divergence from known ones) as a test of the $f(R, \mathcal{G})$ theory viability.

2 Equations of motion

Let us consider the theory with an action in form

$$S = \int d^4x \sqrt{-g} f(R, \mathcal{G}), \quad (2.1)$$

where $\mathcal{G} = R_{\mu\nu\alpha\beta}R^{\mu\nu\alpha\beta} - 4R_{\mu\nu}R^{\mu\nu} + R^2$ is the Gauss-Bonnet invariant and R is the Ricci (curvature) scalar.

By varying this action with respect to the metric components one can retrieve the field equations:

$$\begin{aligned} & -\frac{1}{2}f g_{\mu\nu} + f_R R_{\mu\nu} - \nabla_\mu \nabla_\nu f_R + g_{\mu\nu} \square f_R + 2f_{\mathcal{G}} (R_\mu^{\alpha\beta\gamma} R_{\nu\alpha\beta\gamma} + 2R_{\mu\alpha\beta\nu} R^{\alpha\beta} - 2R_{\alpha\mu} R^\alpha_\nu + R R_{\mu\nu}) \\ & - 4 \left(R_{\mu\alpha\beta\nu} + R_{\mu\nu} g_{\alpha\beta} + R_{\alpha\beta} g_{\mu\nu} - R_{\alpha\mu} g_{\beta\nu} - R_{\alpha\nu} g_{\beta\mu} + \frac{1}{2} R (g_{\alpha\mu} g_{\beta\nu} - g_{\mu\nu} g_{\alpha\beta}) \right) \nabla^\alpha \nabla^\beta f_{\mathcal{G}} = 0. \end{aligned} \quad (2.2)$$

In (3+1)-dimensional model the second Lovelock tensor is always zero:

$$2 (R_\mu^{\alpha\beta\gamma} R_{\nu\alpha\beta\gamma} + 2R_{\mu\alpha\beta\nu} R^{\alpha\beta} - 2R_{\alpha\mu} R^\alpha_\nu + R R_{\mu\nu}) - \frac{1}{2} \mathcal{G} g_{\mu\nu} = 0.$$

Hence we can rewrite (2.2) as

$$\begin{aligned} & -\frac{1}{2}f g_{\mu\nu} + f_R R_{\mu\nu} - \nabla_\mu \nabla_\nu f_R + g_{\mu\nu} \square f_R + \frac{1}{2} f_{\mathcal{G}} \mathcal{G} g_{\mu\nu} - 4 (R_{\mu\alpha\beta\nu} + R_{\mu\nu} g_{\alpha\beta} + \\ & + R_{\alpha\beta} g_{\mu\nu} - R_{\alpha\mu} g_{\beta\nu} - R_{\alpha\nu} g_{\beta\mu} + \frac{1}{2} R (g_{\alpha\mu} g_{\beta\nu} - g_{\mu\nu} g_{\alpha\beta})) \nabla^\alpha \nabla^\beta f_{\mathcal{G}} = 0. \end{aligned} \quad (2.3)$$

⁷Email address: sergey.pavluchenko@gmail.com

Now considering the spherically-symmetric metric

$$g_{\mu\nu} = \text{diag}\{-A(r), B(r), r^2, r^2 \sin^2 \theta\}$$

we obtain expressions for Christoffel symbols, Riemann and Ricci tensors components as well as Ricci scalar and Gauss-Bonnet invariant. Substituting derived functions into (2.3) one can get 00-component in the form:

$$\begin{aligned} & \frac{1}{2}Af - f_R \left(\frac{1}{4} \frac{\dot{A}^2}{AB} - \frac{1}{2} \frac{\ddot{A}}{B} + \frac{1}{4} \frac{\dot{A}\dot{B}}{B^2} - \frac{\dot{A}}{Br} \right) + f_G \left(\frac{\dot{A}^2}{AB^2r^2} + \frac{3\dot{A}\dot{B}}{B^3r^2} - \frac{\dot{A}\dot{B}}{B^2r^2} + \frac{2\ddot{A}}{Br^2} - \frac{2\ddot{A}}{B^2r^2} - \right. \\ & \left. - \frac{\dot{A}^2}{ABr^2} \right) - \frac{A}{B} \ddot{f}_R - \dot{f}_R \left(\frac{2A}{Br} + \frac{1}{2} \frac{\dot{A}}{B} - \frac{1}{2} \frac{\dot{A}\dot{B}}{B^2} + \frac{1}{2} \frac{\dot{A}}{A} \right) + \frac{4A}{B^2r^2}(1-B)\ddot{f}_G + \frac{2\dot{B}A}{B^2r^2}(1+B)\dot{f}_G; \end{aligned} \quad (2.4)$$

where $A \equiv A(r)$, $B \equiv B(r)$, and dot above designate the derivative with respect to the radial coordinate r . Similarly 11-component have the form:

$$\begin{aligned} & -\frac{1}{2}Bf + f_R \left(\frac{1}{4} \frac{\dot{A}^2}{A^2} - \frac{1}{2} \frac{\ddot{A}}{A} + \frac{1}{4} \frac{\dot{A}\dot{B}}{AB} + \frac{\dot{B}}{Br} \right) - f_G \left(\frac{\dot{A}^2}{A^2Br^2} + \frac{3\dot{A}\dot{B}}{AB^2r^2} - \frac{\dot{A}\dot{B}}{ABr^2} + \frac{2\ddot{A}}{Ar^2} - \right. \\ & \left. - \frac{2\ddot{A}}{ABr^2} - \frac{\dot{A}^2}{A^2r^2} \right) + \dot{f}_R \left(\frac{2}{r} + \frac{1}{2} \frac{\dot{A}}{A} - \frac{1}{2} \frac{\dot{B}}{B} + \frac{1}{2} \frac{\dot{B}}{A} \right) - \frac{2\dot{A}}{Ar^2}(B-3)\dot{f}_G. \end{aligned} \quad (2.5)$$

By multiplying (2.4) on B/A and adding the result to (2.5) we obtain “mixed” equation with a lot of terms that are common in (2.4) and (2.5) being cancelled:

$$\ddot{f}_R + \dot{f}_R \left(\frac{\dot{A}B}{2A} - \frac{1}{2} \frac{\dot{B}}{B} \right) - f_R \left(\frac{\dot{B}}{Br} + \frac{\dot{A}}{Ar} \right) = \frac{4}{Br^2}(1-B)\ddot{f}_G + \frac{2}{r^2} \left(3 \frac{\dot{A}}{A} - \frac{\dot{A}B}{A} + \frac{\dot{B}}{B} + \dot{B} \right) \dot{f}_G. \quad (2.6)$$

3 Horizon existence

First of, let us find out about the possibility of the existence of the horizon for our problem. Similarly to the classical Schwarzschild solution we define the horizon as ($A \rightarrow 0$, $B \rightarrow \infty$). Hence, the terms \dot{B} ($\equiv B \frac{\dot{B}}{B}$) and $\frac{B\dot{A}}{A}$ will diverge obviously faster than $\frac{\dot{B}}{B}$ and $\frac{\dot{A}}{A}$, so Eq.(2.6) takes a form⁸:

$$\frac{2\dot{f}_G\dot{B}}{r^2} - \frac{2B\dot{A}\dot{f}_G}{Ar^2} - \frac{1}{2} \frac{B\dot{A}\dot{f}_R}{A} + \frac{1}{2} \dot{f}_R\dot{B} = 0; \quad (3.1)$$

it could be further simplified to

$$\left(\frac{2\dot{f}_G}{r^2} + \frac{\dot{f}_R}{2} \right) \left(\dot{B} - \frac{B\dot{A}}{A} \right) = 0. \quad (3.2)$$

The second multiplier imply $A = \text{const} \times B$ which is obviously impossible to construct the horizon since A and B would diverge simultaneously. Hence the first parenthesis imply

$$\dot{f}_R = -\frac{4\dot{f}_G}{r^2}. \quad (3.3)$$

Taking a derivative with respect to r of (3.3) gives us one more condition:

$$\ddot{f}_R = -\frac{4\ddot{f}_G}{r^2} + \frac{8\dot{f}_G}{r^3}. \quad (3.4)$$

⁸We assume $f(R, \mathcal{G})$ and its derivatives are be smooth enough to not create additional singularities; possible zeros and divergences of $f(R, \mathcal{G})$ and its derivatives will be discussed below.

Let us note that conditions (3.3) and (3.4) are derived under most general assumptions on the $A(r)$ and $B(r)$.

Equation (3.3) has an interesting consequence that worth mentioning: for a wide class of $f(R, \mathcal{G})$ functions⁹ we can express \dot{f}_R and \dot{f}_G as

$$\dot{f}_R = \dot{R}f_{RR} + \dot{\mathcal{G}}f_{RG}; \quad \dot{f}_G = \dot{R}f_{RG} + \dot{\mathcal{G}}f_{GG}; \quad (3.5)$$

if we substitute it into (3.3), apply the horizon conditions ($\dot{R} \rightarrow -4/r^3$ and $\dot{\mathcal{G}} \rightarrow 0$) and we will get

$$f_{RR} = -\frac{4}{r^2}f_{RG}. \quad (3.6)$$

One can notice an interesting thing from (3.6) – if there are no cross-terms in $f(R, \mathcal{G})$ (i.e., $f(R, \mathcal{G}) = f_1(R) + f_2(\mathcal{G})$), this immediately imply either $f_{RR} = 0$ or $\dot{R} = 0$. Similarly one can demonstrate that in the absence of the cross-terms we have either $f_{GG} = 0$ or $\dot{\mathcal{G}} = 0$. Hence, in the absence of cross-terms, the function $f(R, \mathcal{G})$ can either have only linear contributions from R and \mathcal{G} (first one gives the Einstein-Hilbert contribution while the second will nullify its impact since being Euler topological invariant in (3+1)) or should both $\dot{R} = 0$ and $\dot{\mathcal{G}} = 0$ being satisfied. Now let us consider different $f(R, \mathcal{G}) = f_1(R) + f_2(\mathcal{G})$ cases.

4 $R + f(R)$ case

From (3.3) one can see that in this case $\dot{f}_R = 0$ and hence from (3.5) we have either $f_{RR} = 0$ or $\dot{R} = 0$. With the former being trivial case (it is equal to the Einstein-Hilbert action) we will consider the latter. So we have $f = R + F(R)$, $f_R = 1 + F_R$, $\dot{f}_R = \dot{f}_R = 0$, $f_G = \dot{f}_G = \ddot{f}_G = 0$ ¹⁰, after substituting all this into (2.6) we will get

$$\frac{1}{r} \left(\frac{\dot{A}}{A} + \frac{\dot{B}}{B} \right) (1 + F_R) = 0, \quad (4.1)$$

with the solution

$$A(r) = \frac{C_0}{B(r)}. \quad (4.2)$$

Now if we apply the conditions of the derivatives of $f(R, \mathcal{G})$ and (4.2) to (2.5) we get

$$-\frac{\dot{B}}{Br} - \frac{B}{r^2} + \frac{1}{r^2} - \frac{1}{2}BF - \frac{\dot{B}^2 F_R}{B^2} + \frac{\ddot{B} F_R}{2B} + \frac{\dot{B} F_R}{Br} = 0; \quad (4.3)$$

solving (4.3) together with $R = R_0$ one will obtain general solution in the form

$$B(r) = \frac{6r(1 + F_R)}{r^3(F - R_0 F_R) + 6r(1 + F_R) + 6C_1(1 + F_R)}; \quad (4.4)$$

and under reassigning $F_R = -1/2$, $C_1 = -2m$ and $F = \Lambda - R_0/2$ we get the solution in the usual Schwarzschild-de Sitter form

$$B(r) = \frac{3r}{\Lambda r^3 + 3r - 6m}. \quad (4.5)$$

The similar result was obtained in [2] with the difference that they took $AB = \text{const}$ and $R = \text{const}$ as given while we demonstrated that there are no other cases.

⁹Analitic functions; but if the functional notation of $f(R, \mathcal{G})$ contain some differential operators, the following expression might not holds true

¹⁰One can easily demontrate that in the considered case $F = \text{const}$ as well as $F_R = \text{const}$.

5 $R + f(\mathcal{G})$ case

Similarly to the previous case, to have nontrivial solution we consider $\dot{\mathcal{G}} = 0$, which leads to the $\mathcal{G} = \text{const}$. In this case we have $f = R + f(\mathcal{G})$, $f_R = 1$, $\dot{f}_R = \dot{f}_R = 0$, $\dot{f}_{\mathcal{G}} = \dot{f}_{\mathcal{G}} = 0$ (and again $F = \text{const}$ and $f_{\mathcal{G}} = \text{const}$). Equation (2.6) reads

$$\frac{1}{r} \left(\frac{\dot{A}}{A} + \frac{\dot{B}}{B} \right) = 0, \quad (5.1)$$

and the solution is the same as in previous case (4.2). Again, substituting everything into (2.5) and $\mathcal{G} = \mathcal{G}_0$ (from $\dot{\mathcal{G}} = 0$) we obtain the solution in the form

$$B(r) = \frac{6r}{r^3(F - \mathcal{G}_0 f_{\mathcal{G}}) + 6r + 6C_1}; \quad (5.2)$$

and under reassigning $C_1 = -2m$ and $F = 2\Lambda + \mathcal{G}_0 f_{\mathcal{G}}$ we get the solution in the usual Schwarzschild-de Sitter form (4.5).

6 $R + f(R) + F(\mathcal{G})$ case

In this case both conditions $R = R_0$ and $\mathcal{G} = \mathcal{G}_0$ are applied, we have $f = R + f(R) + F(\mathcal{G})$, $f_R = 1 + f_R$, $\dot{f}_R = \dot{f}_R = \dot{f}_{\mathcal{G}} = \dot{f}_{\mathcal{G}} = 0$; Eq. (2.6) will be the same as in $R + f(R)$ case (4.1) so will be the solution (4.2). Similarly to the previous cases we substitute everything into (2.5) and $R = R_0$ with $\mathcal{G} = \mathcal{G}_0$ and derive the answer

$$B(r) = \frac{12r}{r^3(f + F - \mathcal{G}_0 f_{\mathcal{G}} - R_0 f_R) + 12r + 12C_1} \quad (6.1)$$

that could be rewritten in the usual Schwarzschild-de Sitter form (4.5) after redefinitions $C_1 = -2m$ and $f + F - \mathcal{G}_0 f_{\mathcal{G}} - R_0 f_R = 4\Lambda$.

7 Conclusions

This finalizes our study of the simplest case of the BH with horizons existence in the $f(R, \mathcal{G})$ gravity – similar to the $R + f(R)$ case [2], there is only Schwarzschild-de Sitter solution. Our simplest case is “detached” one, i.e., $f(R, \mathcal{G}) = f_1(R) + f_2(\mathcal{G})$. The same may not be true in the general case, so the problem requires additional investigation and we carry it on.

8 Acknowledgements

I would like to thank the Organizing Committee for the financial support, which made it possible to present these results. The research was also supported partially via RFBR grants nos. 11-02-09704-mob_z and 11-02-00643-a.

References

- [1] Nobelprize.org (2011).
- [2] A. de La Cruz-Dombriz, A. Dobado, and A.L. Maroto, *Phys. Rev. D* **80**, 124011, (2009).

The high frequency limit in $f(R)$ gravity

Keiki Saito^{11(a)} and Akihiro Ishibashi^(b)

^(a)*Department of Particles and Nuclear Physics,
The Graduate University for Advanced Studies (SOKENDAI),
1-1 Oho, Tsukuba, Ibaraki 305-0801, Japan*

^(b)*Department of Physics, Kinki University, Higashi-Osaka 577-8502, Japan*

Abstract

In general relativity, the effective gravitational stress-energy tensor for short wavelength metric perturbations acts just like that for a radiation fluid and in particular cannot provide any effects that mimic dark energy. However, it is far from obvious if this property of the effective gravitational stress tensor hold for any theories of gravity, or is a specific nature held only in the Einstein gravity. In this paper, we consider the effective stress-energy tensor of short-wavelength perturbations in $f(R)$ gravity and investigate its property to compare with the case of the Einstein gravity.

1 Introduction

Our observable universe appears, on large scales, to be homogeneous and isotropic but highly inhomogeneous on small scales. It is therefore interesting to consider whether (and, if so, how) local inhomogeneities can affect global dynamics of the universe. Such a backreaction effect of local inhomogeneities may be described in terms of an effective stress-energy tensor for perturbations.

In general relativity, a consistent expansion scheme for short-wavelength perturbations and the corresponding effective stress-energy tensor were first developed by Isaacson [1, 2], in which the small parameter corresponds to the amplitude and at the same time the wavelength of perturbations. Isaacson's expansion scheme is called the high frequency limit or the short-wavelength approximation. In this expansion, the first-order Einstein equation corresponds to the equation of motion for linearized gravitational waves. The second-order expansion of the Einstein equation provides the Einstein equation for the zeroth-order metric with an effective stress-energy tensor, which is essentially given as the second-order Einstein tensor averaged over several wavelengths of metric perturbations. Since taking a derivative of perturbations corresponds to multiplying the inverse of the smallness parameter (or the inverse of the wavelength of perturbations), the effective stress-energy tensor consisting of the square of derivatives of the first-order metric perturbations can have non-negligible effects on the background dynamics. Furthermore, it was shown that this effective gravitational stress-energy tensor is traceless and satisfies the weak energy condition, i.e. acts like radiation [3, 4], and in particular, cannot provide any effects that imitate the dark energy in general relativity.

In this paper, we consider an effective gravitational stress-energy tensor in the context of $f(R)$ gravity, in which the Einstein-Hilbert action is modified by replacing the Ricci scalar R with an arbitrary function $f(R)$. Since $f(R)$ gravity theory contains higher order derivative terms, one can anticipate the effective gravitational stress-energy tensor to be generally modified in high frequency limit [5, 6]. For simplicity, we restrict our attention to the R^2 model ($f(R) = R + cR^2$).

In the next section, we briefly summarize the high frequency limit in general relativity. In Sec. 3, we derive the effective gravitational stress-energy tensor in $f(R)$ gravity. Sec. 4 is devoted to summary and points to future research.

2 The high frequency limit in general relativity

Let g_{ab} be the metric with linear perturbation h_{ab} ; it is described by $g_{ab} = \gamma_{ab} + h_{ab}$ with γ_{ab} being the background metric including the backreaction from perturbations, and is normalized: $\gamma_{ab} \sim O(1)$. h_{ab} is

¹¹Email address: saitok@post.kek.jp

of order $h_{ab} \sim O(\epsilon)$, and its derivatives are

$$\nabla_{a_1} \nabla_{a_2} \cdots \nabla_{a_m} h_{bc} \sim O\left(\frac{\epsilon}{(\lambda/L)^m}\right) \sim O(\epsilon^{1-m}), \quad (2.1)$$

where ∇_a denotes the covariant derivative with respect to γ_{ab} , so that $\nabla_a \gamma_{bc} = 0$, and ϵ is the smallness parameter, and λ is the wavelength of perturbations. One may bear in mind perturbations of the form $h \sim \epsilon \sin(x/\lambda)$ and $\lambda/L \sim O(\epsilon)$. L is a characteristic length over the background and we normalize $L \sim 1$. The inverse metric takes the form $g^{ab} = \gamma^{ab} - h^{ab} + h^a_c h^{cb} + \cdots$, where $h^{ab} \equiv \gamma^{ac} \gamma^{bd} h_{cd}$.

We cannot in general have $\nabla_a h_{bc} \rightarrow 0$ pointwise $\lambda \rightarrow 0$, but suitable spacetime averages of $\nabla_a h_{bc}$ will go to 0. More precisely, if f^{abc} is any smooth tensor field of compact support, we have

$$\int f^{abc} \nabla_a h_{bc} = - \int (\nabla_a f^{abc}) h_{bc} \xrightarrow{\lambda \rightarrow 0} 0. \quad (2.2)$$

If this equation holds for all test tensor fields f^{abc} , we say that $\nabla_a h_{bc} \rightarrow 0$ *weakly*.

There is the general relationship between the Ricci tensor of g_{ab} and of γ_{ab} , namely $R_{ab} = R_{ab}[\gamma] + 2\nabla_{[c} C_{b]a}^c + 2C_{d[c}^c C_{b]a}^d$, where $C_{bc}^a \equiv \Gamma_{bc}^a - \Gamma_{bc}^a[\gamma] = g^{ad} (\nabla_b g_{dc} + \nabla_c g_{bd} - \nabla_d g_{bc}) / 2$. Because R_{ab} includes $g^{-1} \nabla \nabla g$, $\nabla g^{-1} \nabla g$ and $g^{-1} g^{-1} \nabla g \nabla g$, we can find

$$R_{ab}^{(n)}[h] \sim O(\epsilon^{n-2}), \quad (2.3)$$

where n is the number of h_{ab} included in R_{ab} . We also find

$$R^{(n)}[h] \sim G_{ab}^{(n)}[h] \sim O(\epsilon^{n-2}), \quad \nabla_{a_1} \nabla_{a_2} \cdots \nabla_{a_m} R^{(n)}[h] \sim O(\epsilon^{n-2-m}), \quad (2.4)$$

where $R = g^{ab} R_{ab}$, $G_{ab} = R_{ab} - g_{ab} R / 2$ is the Einstein tensor, and $R^{(n)}[h]$ and $G_{ab}^{(n)}[h]$ do not include $R_{ab}[\gamma]$.

The vacuum Einstein equation is

$$G_{ab} = R_{ab} - \frac{1}{2} g_{ab} R = 0. \quad (2.5)$$

We can derive the vacuum Einstein equation of $O(\epsilon^{-1})$:

$$G_{ab}^{(1)}[h] = R_{ab}^{(1)}[h] - \frac{1}{2} \gamma_{ab} R^{(1)}[h] = 0, \quad \text{i.e.} \quad R_{ab}^{(1)}[h] = 0, \quad (2.6)$$

and that of $O(1)$:

$$G_{ab}[\gamma] = - \text{w-lim}_{\lambda \rightarrow 0} G_{ab}^{(2)}[h] \equiv \kappa^2 T_{ab}^{\text{eff}}, \quad (2.7)$$

where "w-lim" means the weak limit and T_{ab}^{eff} is the effective gravitational stress-energy tensor, and $\kappa^2 = 8\pi G$. Then, T_{ab}^{eff} becomes

$$\begin{aligned} \kappa^2 T_{ab}^{\text{eff}} &= - \text{w-lim}_{\lambda \rightarrow 0} \left(R_{ab}^{(2)}[h] - \frac{1}{2} \gamma_{ab} \gamma^{cd} R_{cd}^{(2)}[h] \right) \\ &= \frac{1}{4} \text{w-lim}_{\lambda \rightarrow 0} (\nabla_a h^{cd} \nabla_b h_{cd}), \end{aligned} \quad (2.8)$$

where indices are raised and lowered with γ^{ab} and γ_{ab} . We can also check T_{ab}^{eff} is traceless and satisfies the weak energy condition, i.e. acts like radiation [3, 4]. Thus, it cannot provide any effects that mimic the dark energy in the general relativity.

3 The high frequency limit in $f(R)$ gravity

In this section, we consider the vacuum R^2 model for simplicity. The action is

$$S = \frac{1}{2\kappa^2} \int d^4x \sqrt{-g} (R + cR^2), \quad (3.1)$$

where c is constant, and the vacuum Einstein equation is

$$G_{ab}^{f(R)} = G_{ab} + 2c \left(RR_{ab} - \frac{1}{4} g_{ab} R^2 - \nabla_a \nabla_b R + g_{ab} g^{cd} \nabla_c \nabla_d R \right) = 0. \quad (3.2)$$

In R^2 model, we should consider the second order perturbation H_{ab} , and therefore expand the metric as $g_{ab} = \gamma_{ab} + h_{ab} + H_{ab}$. We normalize $H_{ab} \sim \mathcal{O}(\epsilon^2)$, and its derivatives are of order

$$\nabla_{a_1} \nabla_{a_2} \cdots \nabla_{a_m} H_{bc} \sim \mathcal{O} \left(\frac{\epsilon^2}{(\lambda/L)^m} \right) \sim \mathcal{O}(\epsilon^{2-m}), \quad (3.3)$$

where one may bear in mind second-order perturbations of the form $H \sim \epsilon^2 \sin(x/\lambda)$. The inverse metric takes the form $g^{ab} = \gamma^{ab} - h^{ab} + (h^a_c h^{cb} - H^{ab}) - (h^a_c h^c_d h^{db} - 2h^a_c H^{cb}) + \cdots$, where $H^{ab} \equiv \gamma^{ac} \gamma^{bd} H_{cd}$.

In the $f(R)$ gravity, the first order perturbation h_{ab} takes the form $h_{ab} = h_{ab}^{(+)} + h_{ab}^{(\times)} + h_f \gamma_{ab}$, where $h_{ab}^{(+)}$ and $h_{ab}^{(\times)}$ describe the two standard polarizations of gravitational waves which arise from general relativity, and h_f is the massive field arising from the generic high order $f(R)$ gravity [7]. We will focus on h_f from now on. Especially in the R^2 model we have $\square h_f = m^2 h_f = h_f/6c \sim \mathcal{O}(\epsilon)$. Thus, we have

$$\tilde{R}^{(1)}[h_f] = -(R[\gamma] + 3m^2)h_f \sim \mathcal{O}(\epsilon), \quad (3.4)$$

$$\tilde{R}^{(2)}[h_f] = \frac{3}{2} \nabla^a h_f \nabla_a h_f + (R[\gamma] + 6m^2)h_f^2 \sim \mathcal{O}(1) + \mathcal{O}(\epsilon^2), \quad (3.5)$$

$$\tilde{R}^{(3)}[h_f] = -\frac{9}{2} h_f \nabla^a h_f \nabla_a h_f - (R[\gamma] + 9m^2)h_f^3 \sim \mathcal{O}(\epsilon) + \mathcal{O}(\epsilon^3), \quad (3.6)$$

where $\tilde{R}^{(n)}$ includes $R[\gamma]$ differently from $R^{(n)}$. The vacuum Einstein equation of $\mathcal{O}(\epsilon^{-2})$ is

$$\nabla_a \nabla_b R^{\mathcal{O}(1)}[h_f] - \gamma_{ab} \square R^{\mathcal{O}(1)}[h_f] = 0, \quad \text{i.e.} \quad \nabla_a \nabla_b R^{\mathcal{O}(1)}[h_f] = 0. \quad (3.7)$$

If $R^{\mathcal{O}(1)}$ becomes 0 at infinity, we can find

$$R^{\mathcal{O}(1)}[h_f] \equiv \frac{3}{2} \nabla^a h_f \nabla_a h_f + R^{(1)}[H] = 0. \quad (3.8)$$

That of $\mathcal{O}(\epsilon^{-1})$ is

$$R_{ab}^{\mathcal{O}(\epsilon^{-1})}[h_f] + 2cR[\gamma]R_{ab}^{\mathcal{O}(\epsilon^{-1})}[h_f] - 2c\nabla_a \nabla_b R^{\mathcal{O}(\epsilon)}[h_f] + 2c\eta_{ab} \square R^{\mathcal{O}(\epsilon)}[h_f] = 0, \quad (3.9)$$

where

$$R_{ab}^{\mathcal{O}(\epsilon^{-1})}[h_f] \equiv -\nabla_a \nabla_b h_f, \quad R^{\mathcal{O}(\epsilon)}[h_f] \equiv -\frac{9}{2} h_f \nabla^a h_f \nabla_a h_f - (R[\gamma] + 3m^2)h_f. \quad (3.10)$$

From this equation, we derive

$$\nabla_a \nabla_b (h_f \nabla^c h_f \nabla_c h_f) = 0. \quad (3.11)$$

If $h_f \nabla^c h_f \nabla_c h_f$ becomes 0 at infinity,

$$\nabla^c h_f \nabla_c h_f = -\frac{2}{3} R^{(1)}[H] = 0, \quad (3.12)$$

where we use (3.8). From this equation, $\tilde{R}^{(2)}[h_f]$ and $\tilde{R}^{(3)}[h_f]$ become

$$\tilde{R}^{(2)}[h_f] = (R[\gamma] + 6m^2)h_f^2 \sim \mathcal{O}(\epsilon^2), \quad (3.13)$$

$$\tilde{R}^{(3)}[h_f] = -(R[\gamma] + 9m^2)h_f^3 \sim \mathcal{O}(\epsilon^3). \quad (3.14)$$

The effective stress-energy tensor for h_f is

$$\begin{aligned} \kappa^2 T_{ab}^{\text{eff}} &= -\text{w-lim}_{\lambda \rightarrow 0} \left\{ R_{ab}^{\mathcal{O}(1)}[h_f] + 2cR[\gamma]R_{ab}^{\mathcal{O}(1)}[h_f] \right. \\ &\quad \left. + 2cR^{\mathcal{O}(\epsilon)}[h_f]R_{ab}^{\mathcal{O}(\epsilon^{-1})}[h_f] + (-\eta_{ab}h_f \eta^{cd} + h_f \eta_{ab} \eta^{cd}) \nabla_c \nabla_d R^{\mathcal{O}(\epsilon)} \right\} \\ &= \text{w-lim}_{\lambda \rightarrow 0} \left\{ \left(\frac{1}{2} + cR[\gamma] \right) \nabla_a h_f \nabla_b h_f \right\}, \end{aligned} \quad (3.15)$$

and the trace of $\kappa^2 T_{ab}^{\text{eff}}$ is

$$\begin{aligned}\kappa^2 T^{\text{eff}a}{}_a &= -\left(\frac{1}{2} + cR[\gamma]\right) m^2 h_f^2 \\ &\sim \mathcal{O}(\epsilon^2).\end{aligned}\tag{3.16}$$

Thus, we can find that the effective stress-energy tensor for h_f is proportional to the square of first partial derivatives of metric perturbation h_f as in the case of general relativity, i.e. proportional to the square of the frequency of gravitational waves. Therefore it acts like radiation fluid as in the high frequency limit in general relativity, and in particular, cannot provide any effects that imitate dark energy in R^2 model.

4 Summary

We have here addressed the effective stress-energy tensor for short wavelength perturbations in $f(R)$ gravity. We focused on the R^2 model especially. The Einstein equation is expanded to third order in metric perturbations about an arbitrary background. The Einstein equation of $\mathcal{O}(\epsilon^{-2})$ describes the evolution for the second order perturbation H_{ab} . The Einstein equation of $\mathcal{O}(\epsilon^{-1})$ represents the evolution for the first order perturbation h_{ab} . The Einstein equation of $\mathcal{O}(1)$ serves as the source of the zeroth-order Einstein equation and depends only on the square of first order derivatives of first-order perturbations, like the effective stress-energy tensor in Isaacson's formula in general relativity, .

In this paper, we have restricted our attention to the R^2 model only. It would be interesting to consider an extension of the work presented here to general $f(R)$ gravity (or the scalar-tensor theory). This is left for future work [8].

Acknowledgements

We would like to thank Hideo Kodama, Hirotaka Yoshino, Robert M. Wald, and Stephen R. Green for useful discussions and comments. This work was supported in part by a Grant-in-Aid for JSPS Fellows under Grant No. 23-4465 (KS) and by the JSPS Grant-in-Aid for Scientific Research (C)No. 22540299 (AI).

References

- [1] R. A. Isaacson, Phys. Rev. **166**, 1263 (1968).
- [2] R. A. Isaacson, Phys. Rev. **166**, 1272 (1968).
- [3] G. A. Burnett, J. Math. Phys. **30**, 90 (1989).
- [4] S. R. Green and R. M. Wald, Phys. Rev. D **83**, 084020 (2011).
- [5] L. C. Stein and N. Yunes, Phys. Rev. D **83** 064038 (2011).
- [6] C. P. L. Berry and J. R. Gair, Phys. Rev. D **83**, 104022 (2011).
- [7] S. Capozziello, C. Corda and M. F. De Laurentis, Phys. Lett. B **669**, 255 (2008).
- [8] K. Saito and A. Ishibashi, work in progress.

Joint description of inflation and dark energy in extended $f(R)$ gravity

Hayato Motohashi^{12(a),(b)}, Alexei A. Starobinsky^{13(b),(c)}, Jun'ichi Yokoyama^{14(b),(d)}

^(a)*Department of Physics, Graduate School of Science, The University of Tokyo, Tokyo 113-0033, Japan*

^(b)*Research Center for the Early Universe (RESCEU), Graduate School of Science, The University of Tokyo, Tokyo 113-0033, Japan*

^(c)*L. D. Landau Institute for Theoretical Physics RAS, Moscow 119334, Russia*

^(d)*Institute for the Physics and Mathematics of the Universe (IPMU), The University of Tokyo, Kashiwa, Chiba 277-8568, Japan*

Abstract

We have constructed a $f(R)$ gravity model which avoids weak singularities and satisfies viability conditions even for negative values of the Ricci scalar, and which describes accelerated expansion both in the primordial and present Universe. We constrain the model parameters from the stability of the late time de Sitter solution and we solve the evolution at early time regimes numerically. As a result, we found characteristic strongly anharmonic oscillations of the Universe scale factor after the end of the inflationary stage.

1 Introduction

It is of great interest to consider the possibility for the theoretical model which explains the two accelerated expansion regimes in the Universe: primordial inflation and current cosmic acceleration. $f(R)$ gravity, where R is the scalar curvature, is one of the most attractive candidates. It is a phenomenological macroscopic way to describe both of primordial dark energy (DE) and present DE.

The simplest R^2 inflationary model proposed in Ref. [1] is internally consistent, has a graceful exit to the radiation-dominated Friedmann-Robertson-Walker (FRW) stage via the period of reheating in which all matter in the Universe arises as a result of gravitational particle creation, and remains in agreement with the most recent observational data [2]. Moreover, this form of $f(R)$ may be justified by a number of microscopic models[3].

We are also capable to construct $f(R)$ models which describe the present DE and satisfy all present observational tests[4–6]. In the previous works, we have found that we can distinguish $f(R)$ gravity from concordance Λ -Cold-Dark-Matter (Λ CDM) model by using time evolution of equation-of-state (EoS) parameter for DE and both time and scale dependencies of the matter density fluctuations[7]. However, these models require a much more complicated form of $f(R)$ and a very low energy scale, so we do not have any reasonable microscopic justification of them at present. More critical is that these models generically cannot reproduce the correct evolution of the Universe in the past due to formation of additional weak singularities and other problems. Thus, to construct complete cosmological models of present DE not destroying all previous achievements of the early Universe cosmology including the recombination, the correct BBN and inflation of any kind, one has to change the behaviour of $f(R)$ at large positive R and to extend $f(R)$ to the region of negative R .

First example of combined $f(R)$ model, which avoids weak singularities, is extended to negative R correctly, and explain both primordial and present DE is proposed in Ref. [8]. In this paper, we describe how to construct such new functions $f(R)$ in general. Furthermore, we investigate one of the models in detail. We provide reasonable parameter constraint and numerically solve the evolution in the early Universe. As a result, it leads to completely different reheating after inflation during which strongly non-linear oscillations of R occur.

¹²Email address: motohashi@resceu.s.u-tokyo.ac.jp

¹³Email address: alstar@landau.ac.ru

¹⁴Email address: yokoyama@resceu.s.u-tokyo.ac.jp

2 Conditions

We study the special class of $f(R)$ gravity theories for both primordial and present DE which is defined by the following action

$$S = \frac{M_{\text{Pl}}^2}{2} \int d^4x \sqrt{-g} f(R) + S_m \quad \text{with} \quad f(R) = R + \lambda \nu M^2 \varphi(x) + \frac{R^2}{6M^2}. \quad (2.1)$$

Here, S_m denotes matter action, $M_{\text{Pl}} \equiv (8\pi G)^{-1/2}$, and λ , ν , M are the model parameters. R leads Einstein gravity, and R^2 term describes the primordial DE, which drives inflation in the early Universe[1]. The model parameter M^2 has a dimension of curvature and should be chosen so that R^2 term contributes only at high curvature regime $R \geq R_{\text{inf}}$, and provides proper amplitude of the primordial power spectrum, which is consistent with the observational data. On the other hand, second term $\varphi(x)$ controls the present DE, which triggers late time acceleration. We choose the function $\varphi(x)$ so that it contributes only when $R \lesssim \nu M^2$. Namely, νM^2 is the order of present curvature. $x \equiv R/\nu M^2$ is normalized Ricci scalar, and λ is a positive parameter by which we adjust the deviation from R^2 model.

The function $\varphi(x)$ should satisfy the following viable conditions:

$$(V1) \quad \forall |x| < R_{\text{inf}}/R_s, \quad \varphi''(x) > 0, \quad (2.2)$$

$$(V2) \quad \forall |x| < R_{\text{inf}}/R_s, \quad \lambda \varphi'(x) > -1, \quad (2.3)$$

$$(V3) \quad 1 \ll x \lesssim R_{\text{inf}}/R_s, \quad \varphi'(x) \rightarrow 0, \quad (2.4)$$

$$(V4) \quad 1 \ll x \lesssim R_{\text{inf}}/R_s, \quad \varphi(x) \rightarrow -\text{const.} + x^{-m}, \quad (2.5)$$

$$(V5) \quad \varphi(0) = 0. \quad (2.6)$$

Notice that we impose (V1) and (V2) even for negative R . We also have to care the de Sitter conditions[7],

$$(dS1) \quad \exists x_1 > 0, \quad \alpha(x_1) \equiv x_1 + \lambda(2\varphi_1 - x_1\varphi_1') = 0, \quad (2.7)$$

$$(dS2) \quad \beta(x_1) \equiv \frac{1 + \lambda\varphi_1'}{\lambda\varphi_1''} - x_1 > 0, \quad (2.8)$$

$$(dS3) \quad \gamma(x_1) \equiv \frac{1 + \lambda\varphi_1'}{\lambda\varphi_1''} - \frac{25}{16}x_1 > 0, \quad (2.9)$$

by which we can obtain the de Sitter solution and read its future behavior. For given function $\varphi(x)$, (dS1) provides the de Sitter solution, $x = x_1$. We can check its future stability by (dS2). Also, (dS3) allows us to know the existence of the oscillation. We demand at least the existence of one future stable de Sitter solution because the observational value of the equation of state (EoS) parameter w_{DE} for DE is very close to -1 , so the Universe should be approaching stable de Sitter solution.

3 Specific model

We can construct the family of functions which satisfy the above conditions[9]. From here forward, we focus on one of these models for the specific analysis:

$$\varphi(x) = \frac{1}{\pi} \left[(x - \mu) \text{Arctan}(x - \mu) - \mu \text{Arctan} \mu - \frac{\pi x}{2} \right]. \quad (3.1)$$

First, we constrain the model parameter λ and μ from the future stability of de Sitter solution. Since $\varphi'' > 0$, the stability condition (dS2) is equivalent with $\alpha'(x) > 0$. The equation $\alpha(x) = 0$ has one root, $x = 0$, or three roots, $x = 0$ and two positive roots, depending on the values of model parameters. $x = 0$ corresponds to Minkowski solution and it is always stable because it has positive gradient $\varphi'(x)$. When there are three roots, smaller positive root and larger one are always unstable and stable, respectively. This maximal root is stable de Sitter solution which we needed. Thus, to satisfy the de Sitter stability condition, we choose the model parameters λ and μ for which $\alpha(x) = 0$ has three roots. There is lower bound for μ for each value of $0 < \lambda < 1$ as in Fig. 1. And the upper bound for μ is obtained from the stability of high curvature regime such as matter dominated regime in the past.

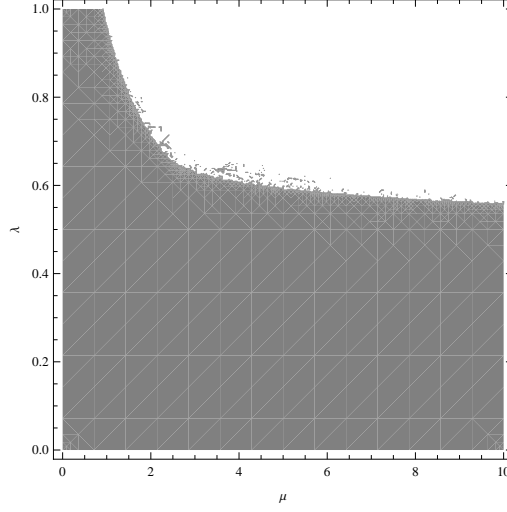


Figure 1: Allowed parameter region for the model (3.1) to keep the future stability of de Sitter solution. Shaded region is prohibited because there is no stable de Sitter solution. λ is restricted $0 < \lambda < 1$ by the viable conditions.

Next, we explore the inflationary dynamics. By moving from physical Jordan frame to Einstein frame, we can regard additional degree of freedom in $f(R)$ gravity as a scalar field. We define Einstein frame metric by conformal transformation $g_{\mu\nu}^E = f'(\xi)g_{\mu\nu}^J$ and scalaron ϕ by $f'(\xi) = e^{\sqrt{\frac{2}{3}}\frac{\phi}{M_{\text{Pl}}}}$. We then obtain

$$S = \int d^4x \sqrt{-g_E} \left(\frac{M_{\text{Pl}}^2}{2} R_E - \frac{1}{2} g_E^{\mu\nu} \nabla_\mu \phi \nabla_\nu \phi - V(\phi) \right) + \int d^4x \mathcal{L}_m \left(g_{\mu\nu}^E e^{-\sqrt{\frac{2}{3}}\frac{\phi}{M_{\text{Pl}}}} \right), \quad (3.2)$$

with a potential

$$V(\phi) = \frac{M_{\text{Pl}}^2}{2} \frac{\xi(\phi) f'(\xi(\phi)) - f(\xi(\phi))}{f'^2(\xi(\phi))}, \quad (3.3)$$

where auxiliary field $\xi = \xi(\phi)$ is obtained as a solution of the defining equation of ϕ . In general, matter has a coupling with scalar field ϕ in Einstein frame via argument of \mathcal{L}_m in Eq. (3.2). We do not consider matter term when we calculate inflationary regime.

Fig. 2 (a) illustrates the inflaton potential for model parameter set $\lambda = 0.9, \mu = 4, \nu = 10^{-12}$. There is a flat slope for $\phi/M_{\text{Pl}} \gg 1$, where inflaton starts slow rolling. However, unlike original R^2 inflation, there is a long plateau and a false vacuum at $\phi/M_{\text{Pl}} = 0$, whose height is remarkably small compared to that of the slope. The global minimum is at $\phi/M_{\text{Pl}} \simeq -2.8$. It is this structure that induces characteristic oscillations during inflation and reheating regime as in Fig. 2 (b)–(d). We can see that there is anharmonic oscillation regime. In terms of Einstein frame dynamics, this regime amounts to the oscillation in the plateau.

4 Conclusion

We have investigated a new class of $f(R)$ models, which can explain both accelerating expansion in the early Universe and late time Universe. Contrary to the previous models, our model is also valid for negative R , which occurs at the end of the inflation. We have studied one of such models in some detail. We have constrained parameter region from the stability of de Sitter solution, and carried out numerical calculation for inflation and reheating regime without backreaction from particle creation. In terms of the inflaton in Einstein frame, it turns out that there is anharmonic oscillation regime. As a result, Hubble parameter and Ricci scalar exhibit characteristic oscillatory behaviour.

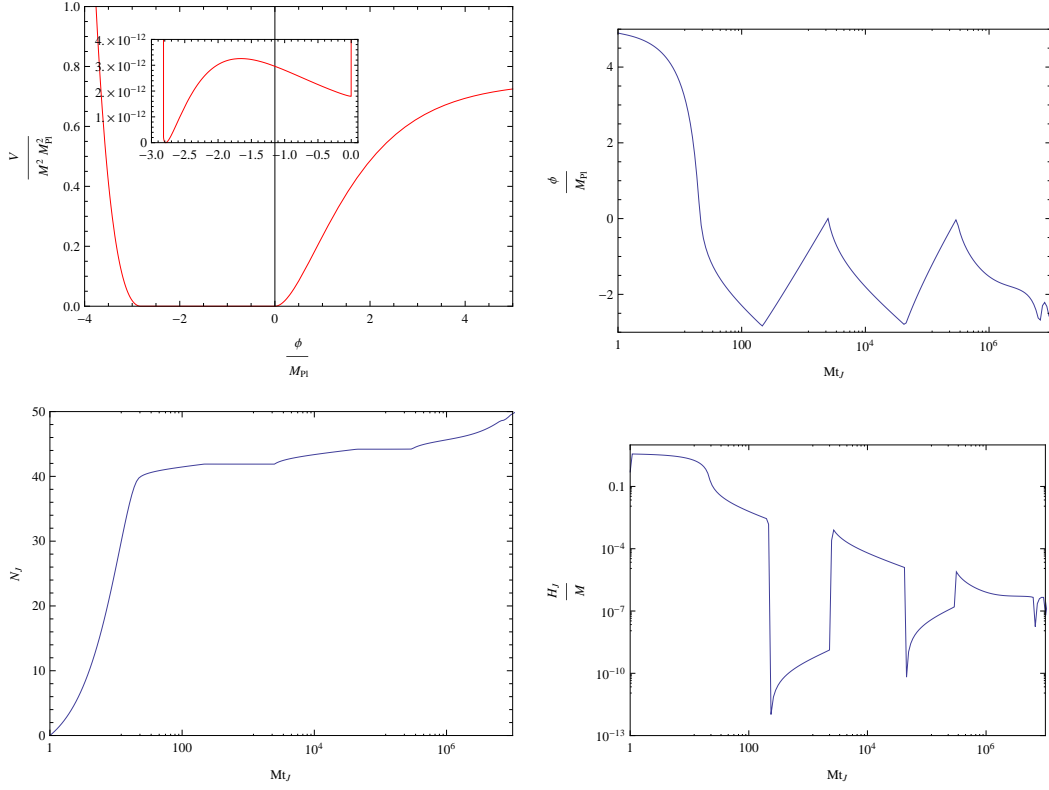


Figure 2: (a): Inflation potential in Einstein frame for model parameter set $\lambda = 0.9, \mu = 4, \nu = 10^{-12}$. Unlike original R^2 inflation, it has a long plateau and a false vacuum at $\phi/M_{\text{Pl}} = 0$. (b), (c), and (d): Time evolution of inflaton, e -folding number, and Hubble parameter in terms of Jordan frame time t_J during inflation and the beginning of reheating for $\lambda = 0.9, \mu = 4, \nu = 10^{-12}$. There is characteristic anharmonic oscillation phase.

References

- [1] A. A. Starobinsky, *Phys. Lett. B* **91** (1980) 99.
- [2] E. Komatsu *et al.*, [arXiv:1001.4538](#).
- [3] S. V. Ketov, A. A. Starobinsky, *Phys. Rev. D* **83**, 063512 (2011) [[arXiv:1011.0240](#)].
- [4] A. A. Starobinsky, *JETP Lett.* **86**, 157 (2007) [[arXiv:0706.2041](#)].
- [5] W. Hu and I. Sawicki, *Phys. Rev. D* **76**, 064004 (2007) [[arXiv:0705.1158](#)].
- [6] S. A. Appleby and R. A. Battye, *Phys. Lett. B* **654**, 7 (2007) [[arXiv:0705.3199](#)].
- [7] H. Motohashi, A. A. Starobinsky, J. Yokoyama, *Int. J. Mod. Phys. D* **18**, 1731 (2009) [[arXiv:0905.0730](#)]; H. Motohashi, A. A. Starobinsky, J. Yokoyama, *Prog. Theor. Phys.* **123**, 887 (2010) [[arXiv:1002.1141](#)]; H. Motohashi, A. A. Starobinsky, J. Yokoyama, *Prog. Theor. Phys.* **124**, 541 (2010) [[arXiv:1005.1171](#)]; H. Motohashi, A. A. Starobinsky, J. Yokoyama, *JCAP* **1106**, 006 (2011) [[arXiv:1101.0744](#)].
- [8] S. A. Appleby, R. A. Battye, A. A. Starobinsky, *JCAP* **1006**, 005 (2010) [[arXiv:0909.1737](#)].
- [9] H. Motohashi, A. A. Starobinsky, J. Yokoyama, in preparation.

Nonlinear perturbations in the General Relativity limit of Hořava-Lifshitz Gravity

A. Emir Gümrukçüoğlu¹⁵

IPMU, The University of Tokyo, Kashiwa, Chiba 277-8582, Japan

Abstract

The power-counting renormalizable theory of gravitation, proposed by Hořava, has attracted significant attention. In the projectable version of the theory, the lack of a local Hamiltonian constraint gives rise to an additional scalar degree of freedom. Although in the UV, this component has very simple dynamics and is coupled weakly, a major problem arises in the IR limit where it becomes strongly coupled. Although the perturbative expansion breaks down, the nonlinear cosmological solutions are regular in this limit, where general relativity, coupled to a dark matter-like component is recovered. This is in sharp contrast with the results of the naïve perturbative approach, where the action becomes divergent and the scalar mode strongly couples. Here, we summarize the analysis on the source of the divergences and show that they originate from an inconsistent application of the momentum constraint. In addition to the standard solution, valid only away from the expected IR fixed point, we find a new solution for the low energy regime. We argue that the latter branch is responsible for the recovery of general relativity in this limit.

About two years ago, Hořava introduced a quantum field theory of gravity, which is power counting renormalizable [1]. This is realized by the anisotropic scaling between space and time:

$$t \rightarrow b^{-z}t, \quad \vec{x} \rightarrow b^{-1}\vec{x}, \quad (0.1)$$

where b is the momentum scale, and $z \geq 3$ is the critical exponent. The UV behavior is improved by the additional high spatial curvature terms, but in contrast to the previous attempts [2], the action has no more than two time derivatives, avoiding the emergence of obvious ghosts.

The Hořava-Lifshitz (HL) gravity is defined by requiring invariance under the foliation-preserving diffeomorphism

$$t \rightarrow t'(t), \quad \vec{x} \rightarrow \vec{x}'(t, \vec{x}). \quad (0.2)$$

Due to the anisotropy between space and time, the Arnowitt-Deser-Misner formalism [3] provides a convenient framework for studying the metric

$$ds^2 = -N^2 dt^2 + g_{ij}(dx^i + N^i dt)(dx^j + N^j dt), \quad (0.3)$$

where N_i is the shift vector and N is the lapse function. In the present text, we focus on the version of the theory with the *projectability condition* $N = N(t)$, which stems from the fundamental symmetry (0.2). Using the 3-d induced metric g_{ij} , the extrinsic curvature K_{ij} , covariant derivative compatible with the induced metric D_i and the curvature of the induced metric R_{ij} as the building blocks, the power-counting renormalizable action can be written as follows

$$S = \frac{M_{Pl}^2}{2} \int N dt \sqrt{g} d^3\vec{x} (K^{ij}K_{ij} - \lambda K^2 - 2\Lambda + R + L_{z>1}), \quad (0.4)$$

where we include higher spatial derivative terms up to $z = 3$ through

$$\frac{M_{Pl}^2}{2} L_{z>1} = \left(c_1 D_i R_{jk} D^i R^{jk} + c_2 D_i R D^i R + c_3 R_i^j R_j^k R_k^i + c_4 R R_i^j R_j^i + c_5 R^3 \right) + \left(c_6 R_i^j R_j^i + c_7 R^2 \right). \quad (0.5)$$

¹⁵Email address: emir.gumrukcuoglu@ipmu.jp

For the minimal value of the critical exponent $z = 3$, these are all the possible marginal and relevant terms allowed by the projectability condition, spatial parity and time reflection. We note that in general relativity (GR), the 4d diffeomorphism invariance fixes λ to be 1, while in HL gravity, it is a coupling constant which runs under renormalization group (RG) flow. Thus, for the theory to be a viable description of gravity at low energies, GR (or something close to GR) needs to be recovered. In the IR, the higher curvature terms are suppressed and the gravitational action has exactly the same form as the Einstein-Hilbert action, only if $\lambda = 1$. Unfortunately the RG flow of the various couplings has not been investigated yet. Therefore, the recovery of GR relies on the assumption (or, the hope) that the parameter λ flows to 1 in the IR. However, even though the action has the same form as GR when $\lambda \rightarrow 1$, the symmetry of the theory is different. This difference originates from the space independent lapse function, which leads schematically to an action of the form

$$S \ni \int dt N(t) \left(\int d^3x \sqrt{g} \mathcal{H} \right). \quad (0.6)$$

The variation of the above with respect to $N(t)$ does not produce a local Hamiltonian constraint, but rather a constraint that is integrated over all space

$$\int d^3x \sqrt{g} \mathcal{H} = 0. \quad (0.7)$$

At the level of equations of motion, the $\lambda = 1$ theory was shown to mimic general relativity with some dust fluid, dubbed “dark matter as an integration constant” [4]. We also note that since the shift vector has the same properties as in GR, the momentum constraint

$$\frac{\delta S}{\delta N_i} = 0, \quad (0.8)$$

stays intact.

As mentioned above, the more relaxed symmetry of HL gravity results in an additional propagating degree of freedom, the scalar graviton. The nature of the scalar graviton depends on the details of the RG flow of the λ parameter, and some pathologies associated with it have been noted. For instance, for values $1/3 < \lambda < 1$, the scalar graviton has a wrong sign kinetic term, and is a ghost [5]. Forbidding this range and enforcing the recovery of GR at low energies suggest that λ should run in the interval $1 < \lambda < \infty$, flowing to GR with “dark matter” in the IR, and to ∞ in the UV [6].

Although the extra degree can be shown to be weakly coupled under some conditions in the UV [6], the IR behavior suffers from strong coupling, where the perturbative expansion seems to break down [7]. On the other hand, the breakdown of perturbations does not necessarily imply that the predictive power is lost. Indeed, if the theory is renormalizable, the coefficients of infinite number of interactions should be expressed in terms of the finite parameters in the full action. For an accurate analysis, one needs to employ nonlinear tools to determine the fate of the scalar graviton mode. In the IR, this mode is expected to decouple in order to ensure sensible low energy physics in agreement with GR. This is reminiscent of the Vainshtein mechanism [8], which plays a similar role in massive gravity theories. For the strong coupling problem in HL, a few analogues of this effect have been noted. For instance, by solving the full equations of motion, static and spherically symmetric vacuum configurations have been shown to be continuously connected to GR in the $\lambda \rightarrow 1$ limit [9].

In the cosmological context, such exact nonlinear realizations become extremely difficult. A convenient approximation is to adopt the gradient expansion technique [10]. This approach is valid for perturbations whose characteristic length scale L is much larger than the Hubble length H^{-1} . Since all terms from the perturbative expansion contribute to each order in the gradient expansion, it provides a consistent way for accounting for the nonlinearities. The technique was successfully applied to an empty, flat Friedmann-Robertson-Walker (FRW) cosmology in HL in [11] and the solutions were shown to be regular in the limit $\lambda \rightarrow 1$. By adding a scalar field as a matter source example, the coupling between matter sector and the scalar graviton was shown to lead to a similar situation: in the $\lambda \rightarrow 1$ limit, one recovers GR, sourced by the scalar field, along with the dark matter-like component [12].

These results are in contrast with the conclusion of the perturbative calculation, where, as discussed above, the perturbative expansion of the action breaks down and the scalar graviton mode becomes

strongly coupled in the expected GR limit $\lambda \rightarrow 1$. In the remainder of this paper, we present a simple discussion on the source of the apparent breakdown of the perturbative expansion and determine the origin of the problem as an improper application of the momentum constraint for $\lambda - 1 \ll 1$. We find a previously overlooked solution, which is valid in this range. The calculation is based on our paper [12].

We start by sketching the breakdown of naïve perturbation theory and discussing the role of the momentum constraint. We introduce linear perturbations to a FRW universe in vacuum,¹⁶

$$N = 1, \quad N_i = \partial_i B + n_i, \quad g_{ij} = a^2 [\delta_{ij}(1 + \zeta) + h_{ij}], \quad (0.9)$$

where $\partial_i n_i = 0$, $h_{ii} = 0$, and as a gauge choice, we set $\partial_i h_{ij} = 0$ (transverse gauge). With this decomposition, the momentum constraint (0.8) at first order in perturbations can be found as

$$\partial_i [a^2(3\lambda - 1)\partial_t \zeta - (\lambda - 1)\Delta B] + \frac{1}{2}\Delta n_i = 0, \quad (0.10)$$

which can be solved by

$$\Delta B = \frac{3\lambda - 1}{\lambda - 1} a^2 \partial_t \zeta, \quad n_i = 0. \quad (0.11)$$

As B and n_i are nondynamical degrees of freedom, the above solutions can be inserted back into the action. For the current discussion, we only focus on the kinetic part of the action, since the dependence on the parameter λ arises there. The part of the action which contains the scalar degrees of freedom can be written schematically as [6]

$$S_{\text{kin}} \ni \int dt d^3x a^3 \left[\frac{(\dots)}{\lambda - 1} \dot{\zeta}^2 + \frac{(\dots)}{(\lambda - 1)^2} \dot{\zeta}^2 \zeta \right]. \quad (0.12)$$

The convergence of the above series is preserved if formally,

$$|\zeta| \ll \min(1, \lambda - 1). \quad (0.13)$$

At first sight, Eq.(0.12) seems to suggest that in the limit $\lambda \rightarrow 1$, the terms of higher order in perturbative expansion become larger. However, the solution to the momentum constraint (0.11) implicitly assumes that $\lambda - 1$ is finite, i.e. this solution is not valid in the $\lambda \rightarrow 1$ limit. Rather, we found that there is a second branch of solution, valid in the latter limit.

To demonstrate that the solution (0.11) does not apply in the $\lambda \rightarrow 1$ limit, we take a different approach than the above. We keep the assumption of small perturbations for the dynamical modes

$$\zeta = \mathcal{O}(\epsilon), \quad h_{ij} = \mathcal{O}(\epsilon), \quad (0.14)$$

with $\epsilon \ll 1$, while keeping the shift vector nonlinear

$$B = \mathcal{O}(\epsilon^0), \quad n_i = \mathcal{O}(\epsilon^0). \quad (0.15)$$

Then the momentum constraint at leading order can be written as

$$a^2(3\lambda - 1)\partial_i \partial_t \zeta + \mathcal{O}(\epsilon^2) + \frac{1}{2}[\Delta + \mathcal{O}(\epsilon)]n_i - \left\{ (\lambda - 1) \left[\delta_i^j \Delta + \mathcal{O}(\epsilon) \right] + \left(\frac{1}{2} \Delta h^j_i + \partial^j \partial_i \zeta + \delta_i^j \Delta \zeta + \mathcal{O}(\epsilon^2) \right) \right\} \partial_j B = 0. \quad (0.16)$$

Depending on the value of λ , there are two branches of solutions to the above equation. The first one, valid in the regime $\epsilon \ll \min(1, \lambda - 1)$, is

$$\Delta B = \frac{3\lambda - 1}{\lambda - 1} a^2 \partial_t \zeta + \mathcal{O}(\epsilon^2), \quad n_i = \mathcal{O}(\epsilon^2), \quad \text{for } \epsilon \ll \min(1, \lambda - 1), \quad (0.17)$$

¹⁶Throughout this paper, we exploit the (space-independent) time reparametrization to set $N = 1$.

which, at $\mathcal{O}(\epsilon)$, is nothing but Eq.(0.11). On the other hand, for the regime where $\lambda - 1 \ll \epsilon \ll 1$, the terms $\mathcal{O}(\epsilon^2)$ dominate over the $\mathcal{O}(\epsilon)$ terms, giving the second branch solution

$$B = 2a^2 \left[\frac{1}{2} \Delta h_j^i + \partial^i \partial_j \zeta + \delta_j^i \Delta \zeta + 2 (\partial^i \Delta \zeta) \partial_i \right]^{-1} \Delta \partial_t \zeta + \mathcal{O} \left(\frac{\lambda - 1}{\epsilon} \right) + \mathcal{O}(\epsilon), \quad \text{for } \lambda - 1 \ll \epsilon \ll 1, \quad (0.18)$$

which does not suffer from infinities in the limit $\lambda \rightarrow 1$.

The existence of the two mutually exclusive branches of solution to the momentum constraint provides a justification of the regularity and continuity observed in the gradient expansion approach, despite the breakdown of perturbation theory. An interesting implication of this result is that a fully nonlinear analysis in this limit is still consistent with small perturbations, except for the longitudinal part of the shift vector B which becomes nonlinear. Formally,

$$B = \begin{cases} \mathcal{O}(\zeta), & \text{for } |\zeta| \ll \min(\lambda - 1, 1) \\ \mathcal{O}(1), & \text{for } \lambda - 1 \ll |\zeta| \ll 1 \end{cases}, \quad (0.19)$$

while in both cases, $\zeta \ll 1$. This opens the possibility that substituting this nonlinear solution, then applying the perturbative expansion for ζ may provide a healthy perturbative action.

References

- [1] P. Horava, Phys. Rev. D **79**, 084008 (2009) [arXiv:0901.3775 [hep-th]].
- [2] K.S. Stelle, Phys. Rev. D **16**, 953 (1977).
- [3] R. Arnowitt, S. Deser, and C. W. Misner, *The dynamics of general relativity*, in Gravitation: An Introduction to Current Research, L. Witten, edited (Wiley, New York, 1962), p. 227.
- [4] S. Mukohyama, Phys. Rev. D **80**, 064005 (2009) [arXiv:0905.3563 [hep-th]].
- [5] T. P. Sotiriou, M. Visser, and S. Weinfurtner, J. High Energy Phys., **10**, 033 (2009) [arXiv:0905.2798].
- [6] A. E. Gumrukcuoglu and S. Mukohyama, Phys. Rev. D **83**, 124033 (2011) [arXiv:1104.2087].
- [7] C. Charmousis, G. Niz, A. Padilla, and P.M. Saffin, JHEP, **08**, 070 (2009) [arXiv:0905.2579]; D. Blas, O. Pujolas, and S. Sibiryakov, JHEP, **03**, 061 (2009) [arXiv:0906.3046]; K. Koyama and F. Arroja, JHEP, **03**, 061 (2010) [arXiv:0910.1998]; A. Papazoglou and T.P. Sotiriou, Phys. Lett. **B685**, 197 (2010) [arXiv:0911.1299]; I. Kimpton and A. Padilla, JHEP, **07**, 014 (2010) [arXiv:1003.5666]; A. Wang and Q. Wu, Phys. Rev. D **83**, 044025 (2011) [arXiv:1009.0268].
- [8] A. I. Vainshtein, Phys. Lett. B **39**, 393 (1972).
- [9] S. Mukohyama, Class. Quant. Grav. **27**, 223101 (2010) [arXiv:1007.5199 [hep-th]].
- [10] D. S. Salopek and J. R. Bond, Phys. Rev. D **42**, 3936 (1990); D. H. Lyth, K. A. Malik and M. Sasaki, JCAP **0505**, 004 (2005) [arXiv:astro-ph/0411220].
- [11] K. Izumi and S. Mukohyama, Phys. Rev. D **84**, 064025 (2011) [arXiv:1105.0246 [hep-th]].
- [12] A. E. Gumrukcuoglu, S. Mukohyama and A. Wang, arXiv:1109.2609 [hep-th].

There are no stationary axisymmetric star solutions in Hořava-Lifshitz gravity

Naoki Tsukamoto¹⁷ and Tomohiro Harada¹⁸

Department of Physics, Rikkyo University, Tokyo 171-8501, Japan

Abstract

Hořava-Lifshitz gravity has covariance only under the foliation-preserving diffeomorphism. This implies that the quantities on the constant-time hypersurfaces should be regular. In this theory, the projectability condition which strongly restricts the lapse function is required. We assume that a star is filled with a perfect fluid, that it has the reflection symmetry about the equatorial plane. As a result, we find that there are no stationary axisymmetric star solutions in Hořava-Lifshitz gravity under the physically reasonable assumptions on the matter sector. This is a serious problem in this theory from the view point of astrophysics. It seems that the invariance under the foliation-preserving diffeomorphism and the projectability condition are questionable since our result is derived from them.

1 Introduction

Recently, Hořava proposed a power-counting renormalizable gravitational theory [1, 2]. The theory is called Hořava-Lifshitz gravity because it exhibits the Lifshitz-type anisotropic scaling in the ultraviolet, $t \rightarrow b^z t$, $x^i \rightarrow b x^i$, where z is the dynamical critical exponent.

The first study of stars in Hořava-Lifshitz gravity was done by Izumi and Mukohyama [3]. Surprisingly, they found that no spherically symmetric and static solution with a perfect fluid exists in this theory under the assumption that the energy density is a piecewise-continuous and non-negative function of the pressure and that the pressure at the center is positive.

However, it seems that their assumption is too simple to describe realistic stars because of their rotations. We investigate a stationary axisymmetric star in Hořava-Lifshitz gravity. Here we use the units in which $c = 1$.

2 Properties of Hořava-Lifshitz gravity

Hořava-Lifshitz gravity does not have general covariance since the Lifshitz-type anisotropic scaling treats time and space differently. Instead this theory is invariant under the foliation-preserving diffeomorphism: $t \rightarrow \tilde{t}(t)$, $x^i \rightarrow \tilde{x}^i(t, x^j)$. This means that the foliation of the spacetime manifold by constant-time hypersurfaces has a physical meaning. Thus the quantities on the constant-time hypersurfaces such as the extrinsic curvature tensor and the shift vector must be regular.

The field variables are the lapse function $N(t)$, the shift vector $N^i(t, x)$ and the spatial metric $g_{ij}(t, x)$. Note that the shift vector N^i and the spatial metric g_{ij} depend on both t and x^i but that the lapse function N only does on t . This requirement, called the projectability condition, is imposed on Hořava's original paper [1] from a view point of quantization. It is useful to describe the line element in the Arnowitt-Deser-Misner(ADM) form,

$$ds^2 = -N^2 dt^2 + g_{ij}(dx^i + N^i dt)(dx^j + N^j dt). \quad (2.1)$$

By the invariance of matter action I_m under the infinitesimal transformation $\delta x^i = \zeta^i(t, x)$, we get the momentum conservation

$$0 = \frac{1}{N}(\partial_t - N^j D_j)\mathcal{H}_{mi} + K\mathcal{H}_{mi} - \frac{1}{N}\mathcal{H}_{mj}D_i N^j - D^j \mathcal{E}_{mij}, \quad (2.2)$$

¹⁷Email address: 11ra001t@rikkyo.ac.jp

¹⁸Email address: harada@scphys.kyoto-u.ac.jp

where D_i is the covariant derivative compatible with g_{ij} ,

$$\mathcal{H}_{mi} \equiv -\frac{1}{\sqrt{g}} \frac{\delta I_m}{\delta N^i} = T_{i\mu} n^\mu, \quad \mathcal{E}_{mij} \equiv g_{ik} g_{jl} \frac{2}{N\sqrt{g}} \frac{\delta I_m}{\delta g_{kl}} = T_{ij}, \quad (2.3)$$

K is the extrinsic curvature and n^μ is defined as $n_\mu dx^\mu = -N dt$.

3 No stationary axisymmetric star solutions

In this section, we show that there are no stationary axisymmetric star solutions in Hořava-Lifshitz gravity. To prove it, we assume that a star is filled with a perfect fluid, that it has the reflection symmetry about the equatorial plane, that the energy density is a piecewise-continuous and non-negative function of the pressure, that the pressure is a continuous function of r , and that the pressure at the center of the star is positive.

3.1 Stationary And Axisymmetric Configuration

We consider stationary and axisymmetric configurations with the timelike and spacelike Killing vectors respectively given by $t^\mu \partial_\mu = \partial_t$, $\phi^\mu \partial_\mu = \partial_\phi$. The timelike Killing vector t^μ implies everywhere $N^2 - N_i N^i > 0$. The spacelike Killing vector ϕ^μ implies that $\phi^\mu \phi_\mu = g_{\phi\phi}$ is a geometrical invariant.

As a part of the gauge condition, we take $g_{r\theta} = g_{r\phi} = 0$. Under this gauge condition, the general form for the spatial line element is described by [4]

$$dl^2 = \psi^4 [A^2 dr^2 + \frac{r^2}{B^2} d\theta^2 + r^2 B^2 (\sin \theta d\phi + \xi d\theta)^2], \quad (3.1)$$

where ψ , A , B , and ξ are functions of r and θ , but neither t nor ϕ for stationarity and axisymmetry. Now we assume that the spacetime has a rotation axis, where $\sin \theta = 0$. This means $\phi^\mu \phi_\mu = g_{\phi\phi} = 0$ there.

We define triad basis vectors $\{\mathbf{e}_{(i)}\}$. $\mathbf{e}_{(1)}$ is along the radial direction, $\mathbf{e}_{(3)}$ is along the axial Killing vector and $\mathbf{e}_{(2)}$ is fixed by the orthonormality and the right-hand rule. The coordinate components for the orthonormal triad are

$$e_{(1)}^i = \frac{1}{\psi^2} \left[\frac{1}{A}, 0, 0 \right], \quad e_{(2)}^i = \frac{1}{\psi^2} \left[0, \frac{B}{r}, -\frac{\xi B}{r \sin \theta} \right], \quad e_{(3)}^i = \frac{1}{\psi^2} \left[0, 0, \frac{1}{r B \sin \theta} \right], \quad (3.2)$$

where we have used the spatial line element (3.1). The projection of the shift vector on the triad is related to its coordinate components by

$$N_{(1)} = \frac{N_r}{\psi^2 A}, \quad N_{(2)} = \frac{N_\theta B}{\psi^2 r} - \frac{N_\phi \xi B}{\psi^2 r \sin \theta}, \quad N_{(3)} = \frac{N_\phi}{\psi^2 r B \sin \theta}. \quad (3.3)$$

3.2 Regularity Conditions At The Origin

Here we give the regularity conditions of the shift vector N^i near the origin. A tensorial quantity is regular at $r = 0$ if and only if all its components can be expanded in non-negative integer powers of x , y and z in locally Cartesian coordinates, defined by $x \equiv r \sin \theta \cos \phi$, $y \equiv r \sin \theta \sin \phi$ and $z \equiv r \cos \theta$. The Lie derivative of the shift vector N^i along the spacelike Killing vector vanishes, or

$$N^i{}_{;j} \phi^j - \phi^i{}_{;j} N^j = 0. \quad (3.4)$$

In locally Cartesian coordinates, the spacelike Killing vector is written as $\phi^i \partial_i = -y \partial_x + x \partial_y$. Then its components of eq.(3.4) are

$$-N^x{}_{;x} y + N^x{}_{;y} x + N^y = 0, \quad -N^y{}_{;x} y + N^y{}_{;y} x - N^x = 0, \quad -N^z{}_{;x} y + N^z{}_{;y} x = 0. \quad (3.5)$$

The general regular solution of these equations is

$$N^x = F_1(z, \rho^2) x - F_2(z, \rho^2) y, \quad N^y = F_1(z, \rho^2) y + F_2(z, \rho^2) x, \quad N^z = F_3(z, \rho^2), \quad (3.6)$$

where F_1, F_2 and F_3 are independent and regular functions which depend on z and $\rho^2 \equiv x^2 + y^2$.

Now transforming N^i back to the spherical coordinates r, θ and ϕ , we get the spherical components

$$\frac{N^r}{r} = \sin^2 \theta F_1 + \frac{1}{r} \cos \theta F_3, \quad \frac{N^\theta}{\sin \theta} = \cos \theta F_1 - \frac{F_3}{r}, \quad N^\phi = F_2. \quad (3.7)$$

On the rotation axis ($\sin \theta = 0$), thus, we obtain $N^\theta = 0$.

Here we additionally assume the reflection symmetry about the equatorial plane $z = 0$ or $\theta = \pi/2$. Then N^x and N^y must be even functions of z , and N^z must be an odd function of z . This implies that F_1, F_2 must be even functions of z , and F_3 must be an odd function of z . Since N^r is an odd function of z on the rotation axis ($\sin \theta = 0$), we get $N^r = 0$ at the origin.

3.3 Matter Sector And Momentum Conservation

For simplicity we assume that the matter consists of a perfect fluid. The stress-energy tensor is given by $T_{\mu\nu} = (\rho + P)u_\mu u_\nu + P g_{\mu\nu}$, where P and ρ represent the pressure and the energy density, respectively. We assume the four-velocity given by $u^\mu \partial_\mu = \frac{1}{D}(t^\mu + \omega \phi^\mu) \partial_\mu$ where $D \equiv (N^2 - N_i N^i - 2\omega N_\phi - \omega^2 g_{\phi\phi})^{\frac{1}{2}}$ is the normalization factor and ω is a function of r and θ . For the four-velocity u^μ to be timelike, we shall have $N^2 - N_i N^i - 2\omega N_\phi - \omega^2 g_{\phi\phi} > 0$.

After some calculation, the r component the momentum conservation (2.2) becomes Now and this equation becomes

$$0 = -P_{,r} + \frac{\rho + P}{D^2} \left\{ \frac{1}{2}(-N^2 + N_i N^i)_{,r} + \omega N_{\phi,r} + \frac{1}{2}\omega^2 g_{\phi\phi,r} \right\}. \quad (3.8)$$

Here we have used the projectability condition $N = N(t)$.

Now we concentrate on the r component of the momentum conservation of the matter on the rotation axis $\sin \theta = 0$. On the rotation axis, $g_{\phi\phi}$ and $g_{\phi\phi,r}$ vanish. From eq. (3.3), the regularity of the triad component of the shift vector $N_{(3)}$ implies

$$N_\phi = 0 \quad (3.9)$$

on the rotation axis. Thus $N_{\phi,r} = 0$. Thus the r component of the momentum conservation (3.8) on the rotation axis becomes

$$0 = -P_{,r} - \frac{1}{2} \frac{(\rho + P)(N^2 - N_i N^i)_{,r}}{N^2 - N_i N^i}. \quad (3.10)$$

3.4 Contradiction Of Momentum Conservation

We assume that the star has the reflection symmetry about the equatorial plane $\theta = \frac{\pi}{2}$, that the energy density ρ is a piecewise-continuous and non-negative function of the pressure P , that the pressure P is a continuous function of r and that the pressure at the center of the star $P_c \equiv P(r = 0)$ is positive. Thus, $\rho + P$ is a piecewise-continuous function of r . We have assumed that the energy density ρ is non-negative everywhere and that the pressure at the center P_c is positive, hence $\rho + P$ is positive at the center. We define r_s as the minimal value of r for which at least one of $(\rho + P)|_{r=r_s}$, $\lim_{r \rightarrow r_s-0}(\rho + P)$ and $\lim_{r \rightarrow r_s+0}(\rho + P)$ is nonpositive.

Dividing the momentum conservation (3.10) by $\frac{1}{2}(\rho + P)$, we have

$$\left\{ \log(N^2 - N_i N^i) \right\}_{,r} = -2 \frac{P_{,r}}{\rho + P}. \quad (3.11)$$

Under the assumption that the energy density is a function of the pressure, $\rho = \rho(P)$, integrating the momentum conservation (3.11) over the interval $0 \leq r < r_s$, we obtain

$$\log(N^2 - N_i N^i)|_{r=r_s} - \log(N^2 - N_i N^i)|_{r=0} = -2 \int_{P_c}^{P_s} \frac{dP}{\rho + P}, \quad (3.12)$$

where $P_s \equiv P(r = r_s)$.

The definition of r_s implies that at least one of $(\rho + P)|_{r=r_s}$, $\lim_{r \rightarrow r_s - 0}(\rho + P)$ and $\lim_{r \rightarrow r_s + 0}(\rho + P)$ is nonpositive. Since we have assumed that $P(r)$ is a continuous function and that ρ is non-negative everywhere, $P_s = \lim_{r \rightarrow r_s - 0} P = \lim_{r \rightarrow r_s + 0} P$ is non-positive. Thus, we get

$$P_s \leq 0 < P_c. \quad (3.13)$$

This implies that the right-hand side of eq. (3.12) is positive. However, the left-hand side of eq. (3.12) is nonpositive since we have the projectability condition $N = N(t)$ and we obtain from eqs. (3.7) and (3.9) and the reflection symmetry

$$N_i N^i|_{r=0} = 0 \quad (3.14)$$

at the center of the star. This contradicts that the right-hand side of eq. (3.12) is positive.

4 Discussion and conclusion

Hořava-Lifshitz gravity is only covariant under the foliation-preserving diffeomorphism. This means that the foliation of the spacetime manifold by the constant-time hypersurfaces has a physical meaning. As a result, the regularity condition at the center of a star is more restrictive than the one in a theory which has general covariance.

Under the assumption that a star is filled with a perfect fluid, that it has the reflection symmetry about the equatorial plane, and that the matter sector obeys the physically reasonable conditions, we have shown that the momentum conservation is incompatible with the projectability condition and the regularity condition at the center for stationary and axisymmetric configurations. Since we have not used the gravitational action to prove it, our result is also true in other projectable theories [5, 6]. Note that our result is true under not only strong-gravity circumstances like neutron stars but also weak-gravity ones like planets or moons. However, it is not certain that star solutions can exist in non-projectable theories. Since we have used both the covariance under the foliation-preserving diffeomorphism and the projectability condition to prove the non-existence of stationary axisymmetric star, our proof will not apply if we assume just one of the two.

The non-existence of stationary axisymmetric star solutions gives a serious problem in this theory from the view point of astrophysics. It seems that the invariance under the foliation-preserving diffeomorphism and the projectability condition are questionable since our result is derived from them.

Acknowledgements:

The authors would like to thank M. Saijo and U. Miyamoto for valuable comments and discussion. TH was supported by the Grant-in-Aid for Scientific Research Fund of the Ministry of Education, Culture, Sports, Science and Technology, Japan [Young Scientists (B) 21740190].

References

- [1] P. Hořava, Phys. Rev. **D79**, 084008 (2009).
- [2] P. Hořava, JHEP **0903**, 020 (2009).
- [3] K. Izumi and S. Mukohyama, Phys. Rev. **D81**, 044008 (2010).
- [4] J.M. Bardeen and T. Piran, Phys. Rep. **96**, 205 (1983).
- [5] T.P. Sotiriou, M. Visser and S. Weinfurtner, Phys. Rev. Lett. **102**, 251601 (2009).
- [6] T.P. Sotiriou, M. Visser, S. Weinfurtner, JHEP **0910**, 033 (2009).

Spherical collapse of inhomogeneous dust cloud in Lovelock gravity

Seiju Ohashi^{19(a)} and Tetsuya Shiromizu^{20(a)} Sanjay Jhingan^{21(b)}

^(a)*Department of Physics, Kyoto University, Kyoto 606-8502, Japan*

^(b)*Centre for Theoretical Physics, Jamia Millia Islamia, New Delhi 110025, India*

Abstract

We study gravitational collapse of a spherically symmetric inhomogeneous dust cloud in the Lovelock theory without cosmological constant. We show that singularities which are formed under gravitational collapse can be naked in all dimensions. We also show that the nature of singularities depends on the spacetime dimensions. In odd dimensions the naked singularities formed are found to be massive. In the even dimensions, on the other hand, the naked singularities are found to be massless.

1 Introduction

Whether gravitational collapse results in a black hole or a naked singularity is one of the crucial issues in classical general relativity. A singularity is not a “*point*” in the spacetime and information from such a place is in fact an end of causality in the theory. In order to avoid such a breakdown of physics, it is often believed that naked singularities cannot be formed under physically reasonable conditions in classical general relativity (GR). This is known as the cosmic censorship conjecture (CCC) [1].

In 1939 Oppenheimer and Snyder studied the gravitational collapse of a spherically symmetric homogeneous dust cloud and found that the collapse ends in a black hole [2]. However, in absence of a general proof of the CCC there have been studies on collapse using various matter models like dust, radiation, scalar fields, and so on. In these exact solutions of Einstein equations several counterexamples to the CCC have been found.

Recently, higher-dimensional spacetimes have generated considerable interest in theoretical physics. These higher-dimensional models are motivated by string/M theory which are believed to describe high energy phenomena. It is expected that spacetime should be extremely curved near singularities putting in doubt the validity of classical GR in these regions. Indeed the string/M theory predicts the higher curvature corrections to the Einstein equation in its low-energy limit. In view of the above facts it is important to study gravitational collapse in such a theory. In this paper we shall adopt a special combination of higher curvature corrections so that the field equations do not include the higher derivative terms of the metric than the third order, that is, the Lovelock theory [3] because string theory predicts Lovelock type corrections to Einstein gravity.

2 Lovelock gravity

In this section we give an overview of the Lovelock theory in $D = n + 2$ -dimensional spacetimes. This is the most general theory of gravity satisfying following three conditions: (i) The field equations are written in terms of a symmetric rank-2 tensor. (ii) The theory is consistent with the conservation law of the energy-momentum tensor. (iii) The theory does not include higher than third order derivatives.

The Lagrangian of the theory is given by

$$\mathcal{L} = \sum_{m=1}^k \frac{a_m}{m} \mathcal{L}_m, \quad (2.1)$$

¹⁹Email address: ohashi@tap.scphys.kyoto-u.ac.jp

²⁰Email address: shiromizu@tap.scphys.kyoto-u.ac.jp

²¹Email address: sanjay.jhingan@gmail.com

where

$$\mathcal{L}_m = \frac{1}{2^m} \delta_{\mu_1 \mu_2 \dots \mu_{2m-1} \mu_{2m}}^{\nu_1 \nu_2 \dots \nu_{2m-1} \nu_{2m}} R_{\nu_1 \nu_2}^{\mu_1 \mu_2} \dots R_{\nu_{2m-1} \nu_{2m}}^{\mu_{2m-1} \mu_{2m}}. \quad (2.2)$$

In the above, $R_{\mu\nu}{}^{\rho\sigma}$ is the Riemann curvature tensor, k is a constant depending on the spacetime dimensions, defined by $k = [(D-1)/2]$ ($[x]$ is the integer part of x) and $\delta_{\mu_1 \mu_2 \dots \mu_{2m-1} \mu_{2m}}^{\nu_1 \nu_2 \dots \nu_{2m-1} \nu_{2m}}$ is the generalized and totally antisymmetric Kronecker delta. $\{a_m\}$ are arbitrary constants which cannot be determined by the theory itself. Throughout this paper we suppose that a_m are positive.

3 Spherical collapse of dust clouds

In this section, we will consider the spherical collapse of dust clouds in the Lovelock theory [5]. We first write down the basic equations.

The energy-momentum tensor of dust cloud is

$$T_\nu^\mu = \varepsilon(t, r) u_\nu u^\mu, \quad (3.1)$$

where $\varepsilon(t, r)$ is the energy density, which is supposed to be positive, and u^μ is the velocity. The metric for spherically symmetric spacetime is

$$ds^2 = -B(t, r)^2 dt^2 + A(t, r)^2 dr^2 + R(t, r)^2 d\Omega_n^2. \quad (3.2)$$

Here $A(t, r)$, $B(t, r)$ and $R(t, r)$ are arbitrary functions of t and r , and $d\Omega_n^2$ is the line element of the n -dimensional unit sphere. From the conservation equations and field equations, we can derive the metric and basic equation as

$$ds^2 = -dt^2 + \frac{R'^2}{W(r)^2} dr^2 + R^2 d\Omega_n^2 \quad (3.3)$$

$$\sum_{m=1}^k c_m \left(\dot{R}^2 + 1 - W^2 \right)^m \frac{1}{R^{2m}} = \frac{F(r)}{R^{n+1}} \quad (3.4)$$

where $W(r)$ is a arbitrary function of r , $F(r)$ is a mass function defined as $F(r) = \frac{2}{n} \int_0^r \varepsilon R^n R' dr$ and c_l are constants defined as

$$c_l = \begin{cases} 1 & \text{if } l = 1 \\ \frac{a_l}{l} \prod_{p=1}^{2l-2} (n-p) & \text{if } 2 \leq l \leq k. \end{cases} \quad (3.5)$$

4 Apparent horizons and singularities

In this section we analyze the structure of spacetimes obtained in the previous section [5]. We shall focus on the behavior of trapped surfaces and apparent horizons surrounding the singularities. If singularities are covered by apparent horizon, they cannot be naked. And if singularities are not covered by apparent horizon, they can be naked.

We shall investigate the even and odd-dimensional cases separately since they have quite different features. As stated in Sec. 2, we assume that all coefficients c_l are positive. Here we also take $W(r) = 1$, which corresponds to the ‘‘marginally bound case’’.

A trapped surface is described by the surfaces which satisfy $dR/dt|_{\pm} < 0$, where $d/dt|_+$ and $d/dt|_-$ are derivatives along the outgoing and ingoing null geodesics respectively. For the current metric form, $dR/dt|_{\pm}$ becomes

$$\left. \frac{dR}{dt} \right|_+ = \dot{R} + \left. \frac{dr}{dt} \right|_+ R' = \dot{R} + 1, \quad (4.1)$$

$$\left. \frac{dR}{dt} \right|_- = \dot{R} + \left. \frac{dr}{dt} \right|_- R' = \dot{R} - 1, \quad (4.2)$$

where we used the fact of $dr/dt|_{\pm} = \pm R'^{-1}$. The apparent horizon is defined to be the boundary of trapped regions. In our case it is easy to see that the location of the apparent horizons can be found through the solving of

$$g^{\mu\nu} R_{,\mu} R_{,\nu} = 0. \quad (4.3)$$

For the metric of Eq. (3.3), this condition becomes

$$\dot{R}^2 = 1. \quad (4.4)$$

4.1 Even dimensions

We first consider the apparent horizon in even dimensions. Using Eq. (4.4), Eq. (3.4) implies

$$H_{\text{even}}(R) \equiv \sum_{m=1}^{k=n/2} c_m R^{n-2m+1} = F(r), \quad (4.5)$$

which determines the location of the apparent horizons. Note that the left-hand side of the equation above is an odd function of R , and $F(r)$ is a monotonically increasing function of r , with $\lim_{r \rightarrow 0} F(r) = 0$. We depict the behavior of the left-hand side of Eq. (4.5) in Fig. 1.

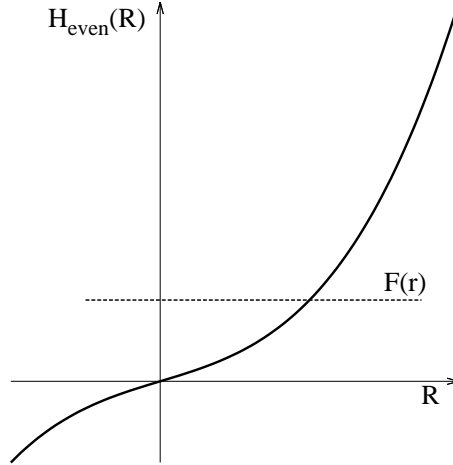


Figure 1: The profile of function $H_{\text{even}}(R)$. The thick line is $H_{\text{even}}(R)$ and the dotted line is $F(r)$. $H_{\text{even}}(R)$ is the odd function and we assume that all coefficients are positive. Therefore, H_{even} is monotonically increasing function for $R > 0$ and $H_{\text{even}}(0) = 0$.

As shown in the figure, for any given finite r , we always have a solution to Eq. (4.5). This implies that the apparent horizons always exist in these spacetimes and all singularities which occur at finite $r > 0$ (but, $R = 0$) will be the inside of the apparent horizon. Therefore, only the central singularity at $r = 0$ could be naked. In addition, they are massless because $F(0) = 0$, in even dimensions. (Note that $F(r)$ is proportional to a quasilocal mass.) This is the same property as in the Gauss-Bonnet case. In the Gauss-Bonnet case, all singularities except for $r = 0$ were found to be covered by apparent horizons in any dimensions higher than six [4].

4.2 Odd dimensions

As in even dimensional cases, Eqs. (4.4) and (3.4) give

$$H_{\text{odd}}(R) \equiv \sum_{m=1}^{k=(n+1)/2} c_m R^{n-2m+1} = F(r), \quad (4.6)$$

which determines the location of the apparent horizons. Contrary to what we had in even dimensions, the left-hand side of Eq. (4.6) is the even function of R (See Fig. 2). In the range of $0 \leq r \leq r_{ah}$, we see

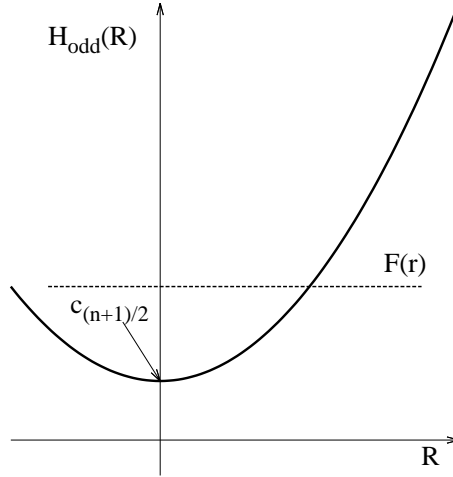


Figure 2: The profile of the function $H_{odd}(R)$. The thick line is $H_{odd}(R)$ and the dotted line is $F(r)$. $H_{odd}(R)$ is the even function and we assume that all coefficients are positive. Therefore H_{odd} is monotonically increasing function of $R > 0$ and $H_{odd}(0) = c_{(n+1)/2} > 0$. The figure shows that r satisfying $F(r) < c_{(n+1)/2}$ have no solution to Eq. (4.6).

that there are no solutions, where r_{ah} is determined through

$$F(r_{ah}) = c_{(n+1)/2}. \quad (4.7)$$

Hence the singularities which occurs in the range $0 \leq r \leq r_{ah}$ are not wrapped by the apparent horizons. They could be naked and massive ($F(r^*) \geq 0$ where $0 \leq r^* \leq r_{ah}$) in odd dimensions. This result is in agreement with what is observed in the five-dimensional Gauss-Bonnet case [4]. For the Gauss-Bonnet case in any dimensions higher than six, however, the singularities at finite r shall always be safely wrapped.

5 Conclusion

We considered gravitational collapse of a spherical inhomogeneous dust cloud in the Lovelock gravity in any dimension. We found that the formation of apparent horizon and nature of singularities depend on the dimensions, that is, odd or even. In even dimensions, noncentral singularities ($r \neq 0$) will be safely wrapped by apparent horizons and only “central” singularity at $r = 0$ could be naked and massless. In odd dimensions, on the other hand, even those singularities which form at $0 \leq r \leq r_{ah}$ may not be wrapped by apparent horizons and they could be naked and massive.

References

- [1] R. Penrose, Riv. Nuovo Cim. **1**, 252 (1969) [Gen. Rel. Grav. **34**, 1141 (2002)].
- [2] J. R. Oppenheimer and H. Snyder, Phys. Rev. **56**, 455 (1939).
- [3] D. Lovelock, J. Math. Phys. **12**, 498 (1971).
- [4] H. Maeda, Phys. Rev. D **73**, 104004 (2006) [arXiv:gr-qc/0602109].
- [5] S. Ohashi, T. Shiromizu and S. Jhingan, Phys. Rev. D **84**, 024021 (2011) [arXiv:1103.3826 [gr-qc]].

Binary Inspiral in Quadratic Gravity

Kent Yagi^{22(a)}, Leo Stein^(b), Nicolas Yunes^{(b),(c)} and Takahiro Tanaka^(d)

^(a)*Department of Physics, Kyoto University, Kyoto 606-8502, Japan*

^(b)*Department of Physics and MIT Kavli Institute, Cambridge, MA 02139, USA*

^(c)*Department of Physics, Montana State University, Bozeman, MT 59717, USA*

^(d)*Yukawa Institute for Theoretical Physics, Kyoto University, Kyoto, 606-8502, Japan.*

Abstract

We consider a general class of quantum-gravity-inspired theories, where the Einstein-Hilbert action is extended through the addition of all terms quadratic in the curvature tensor coupled to a scalar field. This class of theories includes Einstein-Dilaton-Gauss-Bonnet (EDGB) and dynamical Chern-Simons gravity. We consider scalar and gravitational radiation from compact binaries in this theory. We analytically solve the wave equations for the scalar and gravitational radiation under the post-Newtonian formalism and derive the correction in the radiated energy flux. Then, we estimate the expected constraint on this theory from ground-based gravitational wave detectors such as adv. LIGO. We found that they can place considerably stronger constraints on EDGB theory compared to the current solar system experiment.

1 Introduction

Gravitational theory has been tested with great precisions in the solar system experiments and from binary pulsar observations in the weak field regime [1]. On the other hand, future gravitational wave (GW) observations would allow us to perform precise tests of general relativity (GR) in the *strong field regimes*. Among various alternative theories of gravity, in this paper, we consider the so-called *quadratic gravity* [2, 3] which is a general class of theories that contain additional quadratic curvature invariants coupled to a dynamical scalar fields in their actions. This theory can be considered as an *effective* theory of more fundamental theories such as superstring theory, and it contains some well-studied theories such as Einstein-Dilaton-Gauss-Bonnet (EDGB) theory [4] and Dynamical Chern-Simons (CS) gravity [5].

We solved field equations for the scalar and perturbed metric under post-Newtonian (PN) formalism [6, 7]. Although PN approach is an expansion in the weak field or slow motion limit, it is known that in GR, it can also describe strong field regions thanks to the effacement principle or strong equivalence principle. (i.e. Point-particle limit can be safely taken and the results do not depend on the internal structure of sources.) However, in alternative theories of gravity where these principles do not hold, point-particle limit is no longer assured and PN formalism cannot be applied in the strong field regimes. In order to take the effect of strong field into account, we first performed asymptotic matching between the weak field PN and the known strong field (i.e. black hole (BH)) solutions. Then, we derived the effective source terms that correctly reproduce these strong field solutions under PN formalism. Next, we obtained far zone field point solution for the wave equations sourced by these effective source terms and estimated the corrections in the energy flux. Finally, we mapped our modified waveforms to the parameterized post-Einsteinian (PPE) [8] ones and obtained the possible constraints with future GW interferometers such as adv. LIGO.

Due to the limitation of the paper, we focus on explaining the PN approach for the scalar fields in the even parity sector. Then, we comment about the contributions from the metric and the odd parity case at the end. We use the geometrical units $c = G = 1$ throughout.

²²Email address: kent@tap.scphys.kyoto-u.ac.jp

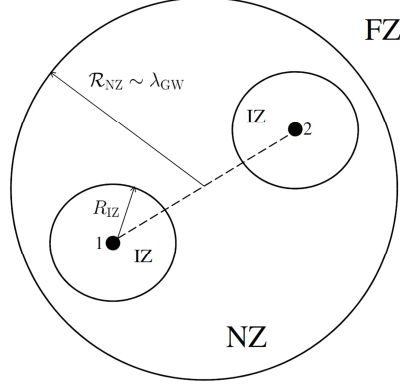


Figure 1: We consider three zones, inner zone (IZ), near zone (NZ) and far zone (FZ). The IZs are centered at each object and their radii \mathcal{R}_{IZ} satisfy $\mathcal{R}_{\text{IZ}} \ll a$, where a denotes the separation of the binary. The NZ is centered at the center of mass of the two bodies and the radius \mathcal{R}_{NZ} satisfies $\mathcal{R}_{\text{NZ}} \sim \lambda_{\text{GW}}$, where λ_{GW} is the GW wavelength.

2 PN Approach for Scalar Radiation in the Even Parity Sector

2.1 Action of Quadratic Gravity

The action for the quadratic gravity that we consider is given as [2, 3]

$$S \equiv \int d^4x \sqrt{-g} [\kappa R + \alpha_1 f_1(\vartheta) R^2 + \alpha_2 f_2(\vartheta) R_{\mu\nu} R^{\mu\nu} + \alpha_3 f_3(\vartheta) R_{\mu\nu\delta\sigma} R^{\mu\nu\delta\sigma} + \alpha_4 f_4(\vartheta) R_{\mu\nu\delta\sigma} {}^* R^{\mu\nu\delta\sigma} - \frac{\beta}{2} \{ \nabla_\mu \vartheta \nabla^\mu \vartheta + 2V(\vartheta) \} + \mathcal{L}_{\text{mat}}]. \quad (2.1)$$

Here, g stands for the determinant of the metric $g_{\mu\nu}$. R , $R_{\mu\nu}$, $R_{\mu\nu\delta\sigma}$ and ${}^* R_{\mu\nu\delta\sigma}$ are the Ricci scalar and tensor, the Riemann tensor and its dual, respectively, with the latter defined as ${}^* R^\mu{}_\nu{}^\delta{}_\sigma = (1/2)\epsilon_{\delta\sigma}{}^{\alpha\beta} R^\mu{}_\nu{}_{\alpha\beta}$ and with $\epsilon^{\mu\nu\delta\sigma}$ the Levi-Civita tensor. The quantity \mathcal{L}_{mat} is the external matter Lagrangian, ϑ is a scalar field, (α_i, β) are coupling constants and $\kappa = (16\pi)^{-1}$. For simplicity, we assume $f_i(\vartheta) = \vartheta$ and $V(\vartheta) = 0$. When we set $\alpha_4 = 0$, while $(\alpha_1, \alpha_2, \alpha_3) = (1, -4, 1)\alpha_{\text{EDGB}}$, quadratic gravity reduces to Einstein-Dilaton-Gauss-Bonnet theory [4]. Alternatively, when we set $\alpha_4 = -\frac{1}{4}\alpha_{\text{CS}}$ and all other $\alpha_i = 0$, it reduces to dynamical CS gravity [5]. Throughout this paper, we take our small dimensionless deformation parameters as $\zeta_i \equiv \alpha_i^2 / (\beta \kappa m^4) \ll 1$ where m is a typical mass parameter.

2.2 Asymptotic Matching and Effective Source Terms

As shown in Fig. 1, let us decompose the geometry into three regions: an inner zone (IZ), a near zone (NZ) and a far zone (FZ). One can only apply the PN formalism when the gravitational field is weak and velocities are small. Hence, when we apply it to strong field sources like BHs and NSs, the fields in the IZs are too strong that PN application becomes invalid. In this case, we have to asymptotically match our PN solution in the NZ with the known strong field solutions valid in the IZs.

When we take variation of the action with respect to the scalar field and perturb the GR metric as $g_{\mu\nu}^{\text{GR}} = \eta_{\mu\nu} + h_{\mu\nu}$, the evolution equation for the scalar field in the even-parity sector becomes

$$\square_\eta \vartheta = -64\pi^2 \frac{\alpha_1}{\beta} \rho^2 - 64\pi^2 \frac{\alpha_2}{\beta} \rho^2 - \frac{2\alpha_3}{\beta} \left(h_{\alpha\beta,\mu\nu} h^{\alpha[\beta,\mu]\nu} + h_{\alpha\beta,\mu\nu} h^{\mu[\nu,\alpha]\beta} \right), \quad (2.2)$$

where $\rho \equiv \rho_1 + \rho_2$ with ρ_A representing the density of each object and remainders of $\mathcal{O}(h^3)$. We can apply the PN formalism to compact binary systems and the leading NZ solution can be obtained as [3]

$$\vartheta^{(\text{NZ})} = \frac{q_1}{r_1} + (1 \leftrightarrow 2), \quad q_A \equiv \frac{16\pi}{\beta} (\alpha_1 + \alpha_2 + 3\alpha_3) \int_{\text{IZ}} \rho_A'^2 d^3x', \quad (2.3)$$

where q_A ($A = 1, 2$) represents the scalar monopole charge and r_A is the distance from each source to the field point. Notice that this dominant monopole contribution vanishes in the case of EDGB theory. For neutron stars, the scalar monopole charge vanishes independently of the equation of state. Notice also that our NZ solution depends on the internal structure of the source. This is due to the fact that the point-particle limit is not always valid in alternative theories of gravity.

We match this NZ solution to the isolated BH solution (valid in the IZs) found by Yunes and Stein [2], $\vartheta_{\text{YS}} = \frac{2\alpha_3}{\beta m_A^2} \frac{m_A}{r_A}$, with m_A representing the mass of the body, to yield $q_A = \frac{2\alpha_3}{\beta m_A}$. Notice that this monopole charge does not depend on (α_1, α_2) . This is because these parameters couple to Ricci tensor and scalar which vanish in vacuum. This is to be contrasted with the NS case, in which q_A depends on all of α_1 , α_2 and α_3 but vanishes for the EDGB combination. Interestingly, BHs do not have scalar hair in more traditional (Brans-Dicke type) scalar-tensor theories [9, 10], while NSs do possess them. This situation is opposite in EDGB theory. We can now treat BHs in even-parity, quadratic modified gravity as delta function sources of matter energy density, and with effective scalar charge density $\rho_\vartheta = q_A \delta^{(3)}(\mathbf{x} - \mathbf{x}_A)$. In the PN expansion such sources reproduce the BH solution found by Yunes and Stein [2] at leading order.

By applying the PN formula [6, 7], the far zone field point solution for the wave equation sourced by the effective source terms (multiplied by -4π) can be calculated as [3]

$$\vartheta^{\text{FZ}} = \frac{1}{r} \left(q_1 \frac{m_2}{m} - q_2 \frac{m_1}{m} \right) v_{12i} n^i + \mathcal{O}(v^2). \quad (2.4)$$

Here we have defined the relative velocity $v_{12}^k \equiv v_1^k - v_2^k$, and the total mass of the binary $m \equiv m_1 + m_2$. r is the distance from the center of mass of the binary to the field point and n_i is defined as $n_i \equiv -(t - r)_i$.

2.3 Correction in the Energy Flux and Mapping to the PPE Waveform

By using Eq. (2.4), the correction in the energy flux due to the scalar radiation can be given as $\delta \dot{E}^{(\vartheta)} = -\frac{1}{3} \zeta_3 \frac{1}{\eta^2} \frac{\delta m^2}{m^2} v^8$. By comparing this with the contribution in GR (obtained from the quadrupole radiation formula), $\dot{E}^{\text{GR}} = -\frac{32}{5} \eta^2 v^{10}$ with the symmetric mass ratio $\eta \equiv m_1 m_2 / m^2$, we obtain [3]

$$\frac{\delta \dot{E}^{(\vartheta)}}{\dot{E}^{\text{GR}}} = \frac{5}{96} \zeta_3 \frac{1}{\eta^4} \frac{\delta m^2}{m^2} v^{-2}, \quad (2.5)$$

a relative -1PN effect. We found that contribution from metric perturbation is of 0PN order [3], hence Eq. (2.5) gives the dominant correction in the even parity sector.

By denoting the Fourier waveform in GR as \tilde{h}_{GR} , the correction can be mapped to the PPE waveform [8]

$$\tilde{h}(f) \equiv \tilde{h}_{\text{GR}}(f) [1 + \alpha_{\text{PPE}} u^{a_{\text{PPE}}}] \exp(i\beta_{\text{PPE}} u^{b_{\text{PPE}}}) \quad (2.6)$$

with $u \equiv \pi \mathcal{M} f$ and the chirp mass $\mathcal{M} \equiv m \eta^{3/5}$, as

$$\alpha_{\text{PPE}} = 0, \quad \beta_{\text{PPE}} = -\frac{5}{7168} \zeta_3 \eta^{-18/5} \frac{\delta m^2}{m^2}, \quad b_{\text{PPE}} = -\frac{7}{3}, \quad (2.7)$$

where δm is defined by $\delta m = m_1 - m_2$.

2.4 Constraints on EDGB Theory

Although we currently lack any GW detections, we can still estimate the projected constraints that such detections would place on quadratic gravity. We consider EDGB theory as a simple sub-case of the even-parity sector. For adv. LIGO, if we detect GW signals of a non-spinning BH binary with masses $(m_1, m_2) = (6, 12) M_\odot$ at a signal-to-noise ratio (SNR) of 20, Cornish *et al.* [11] obtained the projected bound $|\beta_{\text{PPE}}| \lesssim 5 \times 10^{-4}$ for $b_{\text{PPE}} = -\frac{7}{3}$, which implies $|\alpha_{\text{EDGB}}|^{1/2} \lesssim 4 \times 10^5$ cm. This bound corresponds to $\zeta_{\text{EDGB}} \sim 3 \times 10^{-2}$, hence this satisfies our assumption of $\zeta_i \ll 1$.

Comparing this results with the current constraint obtained by the Cassini satellite, $|\alpha_{\text{EDGB}}|^{1/2} < 1.3 \times 10^{12}$ cm [4], we see that the former is more than six orders of magnitude stronger than the latter! Unfortunately, it seems difficult to put constraints on EDGB theory with binary pulsar observations, since NSs have no scalar monopole charge in this theory.

3 Summary and Discussions

In this paper, we described how to apply PN formalism to alternative theories of gravity in deriving modified gravitational waveforms from compact binaries. Since PN formalism can only be applied in the weak field regime, in order to take the strong field effect into account, we asymptotically matched our PN solution with the known (isolated) BH solutions. Then, we obtained the effective source terms (proportional to the delta functions of the positions of the sources) that successfully reproduce the BH solutions under PN formalism. Then, we solve the wave equations sourced by these effective source terms and obtained far zone field point solutions. With these at hand, we can calculate the corrections in the energy flux and can map the modified waveforms to the PPE ones.

For the even parity sector, we found that there generically exists scalar dipole radiation which modifies the waveform at -1PN order relative to GR. Since the metric perturbation gives 0PN correction at best, we conclude that the scalar radiation gives the dominant modification. However, the interesting point is that in EDGB theory, NSs do not possess scalar hair while BHs do. This is opposite to scalar-tensor theories [9, 10]. Therefore, unfortunately, we cannot constrain EDGB theory from current binary pulsar observations. We found that future GW interferometers such as adv. LIGO can place more than six orders of magnitude stronger constraint relative to the current strongest one obtained from the solar system experiment.

We can perform similar analysis for the odd parity sector. By matching the PN solution with the BH solution found by Yunes and Pretorius [12], we found that a spinning BH possesses scalar dipole hair which leads to 2PN correction. We also found 2PN correction from the metric part, and both of these corrections are at quadratic order in spins. There also exists 3.5PN correction at the linear order in spins. This may overwhelm the above 2PN ones for slowly rotating BHs. A non-spinning BH cannot have a scalar hair and scalar radiation only leads to 7PN correction. Our analytic calculation matches beautifully with numerical one obtained by Pani *et al.* [13] under BH perturbation (see Fig. 3 of Ref. [3]). We expect the metric part gives 6PN correction which is also shown by Pani *et al.* [13].

There are many possibilities for future works including (i) finding isolated BH solution at the quadratic order in spins for dynamical CS gravity, (ii) taking the BH deformation by the other BH into account, (iii) considering non-dissipative corrections such as scalar force induced by the scalar charges, (iv) performing BH perturbation in quadratic gravity instead of PN formalism, and (v) calculating the structures of NSs in this theory so that we can obtain the constraints from current binary pulsar observations.

References

- [1] C. M. Will, Living Rev. Rel. **9**, 3 (2005).
- [2] N. Yunes and L. C. Stein, Phys. Rev. D **83**, 104002 (2011).
- [3] K. Yagi, L. C. Stein, N. Yunes and T. Tanaka, arXiv:1110.5950 [gr-qc].
- [4] L. Amendola, C. Charmousis and S. C. Davis, JCAP **0710**, 004 (2007).
- [5] S. Alexander and N. Yunes, Phys. Rept. **480**, 1 (2009).
- [6] C. M. Will and A. G. Wiseman, Phys. Rev. D **54**, 4813 (1996).
- [7] M. E. Pati and C. M. Will, Phys. Rev. D **62**, 124015 (2000) [arXiv:gr-qc/0007087].
- [8] N. Yunes and F. Pretorius, Phys. Rev. D **80**, 122003 (2009).
- [9] S. W. Hawking, Commun. Math. Phys. **25**, 167 (1972).
- [10] T. P. Sotiriou and V. Faraoni, arXiv:1109.6324 [gr-qc].
- [11] N. Cornish, L. Sampson, N. Yunes and F. Pretorius, Phys. Rev. D **84**, 062003 (2011).
- [12] N. Yunes and F. Pretorius, Phys. Rev. D **79**, 084043 (2009)
- [13] P. Pani, V. Cardoso and L. Gualtieri, Phys. Rev. D **83**, 104048 (2011).

Screening scenario for cosmological constant in de Sitter solutions, phantom-divide crossing and finite-time future singularities in non-local gravity

Kazuharu Bamba^{23(a)}, Shin'ichi Nojiri^{24(a),(b)}, Sergei D. Odintsov^{25(c)26} and Misao Sasaki^{27(d),(e)}

^(a)*Kobayashi-Maskawa Institute for the Origin of Particles and the Universe, Nagoya University, Nagoya 464-8602, Japan*

^(b)*Department of Physics, Nagoya University, Nagoya 464-8602, Japan*

^(c)*Institució Catalana de Recerca i Estudis Avançats (ICREA) and Institut de Ciències de l'Espai (IEEC-CSIC), Campus UAB, Facultat de Ciències, Torre C5-Par-2a pl, E-08193 Bellaterra (Barcelona), Spain*

^(d)*Yukawa Institute for Theoretical Physics, Kyoto University, Kyoto 606-8502, Japan*

^(e)*Korea Institute for Advanced Study 207-43 Cheongnyangni 2-dong, Dongdaemun-gu, Seoul 130-722, Republic of Korea*

Abstract

We investigate de Sitter solutions in non-local gravity. We examine a condition to avoid a ghost and discuss a screening scenario for a cosmological constant in de Sitter solutions. Furthermore, we explicitly demonstrate that three types of the finite-time future singularities can occur in non-local gravity and explore their properties.

1 Introduction

It has been suggested that the current expansion of the universe is accelerating by recent cosmological observations such as Supernovae Ia (SNe Ia), cosmic microwave background (CMB) radiation, large scale structure (LSS), baryon acoustic oscillations (BAO), and weak lensing. There are two representative approaches to account for the late time cosmic acceleration. One is the introduction of cosmological constant dark energy in the framework of general relativity. The other is the modification of gravity, for example, $F(R)$ gravity, where $F(R)$ is an arbitrary function of the scalar curvature R (for recent reviews on $F(R)$ gravity, see, e.g., [1]). As a possible modification of gravity, non-local gravity produced by quantum effects has been proposed in Ref. [2]. There was a proposal on the solution of the cosmological constant problem by non-local modification of gravity [3]. Recently, an explicit mechanism to screen a cosmological constant in non-local gravity has been discussed in Ref. [4]. Furthermore, it is known that so-called matter instability [5] occurs in $F(R)$ gravity. This implies that the curvature inside matter sphere becomes very large and hence the curvature singularity could appear. It is important to examine whether there exists the curvature singularity in non-local gravity. The curvature singularity is called “the finite-time future singularities” throughout this paper. In this paper, we review our results in Ref. [6]. We explore de Sitter solutions in non-local gravity. We also study a condition to avoid a ghost and present a screening scenario for a cosmological constant in de Sitter solutions. In addition, we explicitly show that three types of the finite-time future singularities can occur in non-local gravity and examine their properties. We use units of $k_B = c = \hbar = 1$ and denote the gravitational constant $8\pi G$ by $\kappa^2 \equiv 8\pi/M_{\text{Pl}}^2$ with the Planck mass of $M_{\text{Pl}} = G^{-1/2} = 1.2 \times 10^{19} \text{GeV}$.

²³Email address: bamba@kmi.nagoya-u.ac.jp

²⁴Email address: nojiri@phys.nagoya-u.ac.jp

²⁵Email address: odintsov@ieec.uab.es

²⁶Also at Tomsk State Pedagogical University.

²⁷Email address: misao@yukawa.kyoto-u.ac.jp

2 de Sitter solution in non-local gravity

The starting action of non-local gravity is given by

$$S = \int d^4x \sqrt{-g} \left\{ \frac{1}{2\kappa^2} [R(1 + f(\square^{-1}R)) - 2\Lambda] + \mathcal{L}_{\text{matter}}(Q; g) \right\}. \quad (2.1)$$

Here, g is the determinant of the metric tensor $g_{\mu\nu}$, f is some function, $\square \equiv g^{\mu\nu} \nabla_\mu \nabla_\nu$ with ∇_μ being the covariant derivative is the covariant d'Alembertian for a scalar field, Λ is a cosmological constant, and $\mathcal{L}_{\text{matter}}(Q; g)$ is the matter Lagrangian, where Q stands for the matter fields. The above action in Eq. (2.1) can be rewritten by introducing two scalar fields η and ξ in the following form:

$$S = \int d^4x \sqrt{-g} \left\{ \frac{1}{2\kappa^2} [R(1 + f(\eta)) - \partial_\mu \xi \partial^\mu \eta - \xi R - 2\Lambda] + \mathcal{L}_{\text{matter}} \right\}. \quad (2.2)$$

We take the flat Friedmann-Lemaître-Robertson-Walker (FLRW) metric $ds^2 = -dt^2 + a^2(t) \sum_{i=1,2,3} (dx^i)^2$. We consider the case in which the scalar fields η and ξ only depend on time. In this background, the gravitational field equations are given by

$$0 = -3H^2(1 + f(\eta) - \xi) + \frac{1}{2} \dot{\xi} \dot{\eta} - 3H(f'(\eta)\dot{\eta} - \dot{\xi}) + \Lambda + \kappa^2 \rho_m, \quad (2.3)$$

$$0 = (2\dot{H} + 3H^2)(1 + f(\eta) - \xi) + \frac{1}{2} \dot{\xi} \dot{\eta} + \left(\frac{d^2}{dt^2} + 2H \frac{d}{dt} \right) (f(\eta) - \xi) - \Lambda + \kappa^2 P_m, \quad (2.4)$$

where $H = \dot{a}/a$ is the Hubble parameter, the dot denotes the time derivative of $\partial/\partial t$, and ρ_m and P_m are the energy density and pressure of a perfect fluid of matter, respectively. Furthermore, the equations of motion for the scalar fields η and ξ are given by $0 = \ddot{\eta} + 3H\dot{\eta} + 6\dot{H} + 12H^2$ and $0 = \ddot{\xi} + 3H\dot{\xi} - (6\dot{H} + 12H^2)f'(\eta)$, respectively, where we have used $R = 6\dot{H} + 12H^2$. We now assume a de Sitter solution $H = H_0$, where H_0 is a constant. Then, the equation of motion for η can be solved as $\eta = -4H_0 t - \eta_0 e^{-3H_0 t} + \eta_1$, with constants of integration, η_0 and η_1 . For simplicity, we only consider the case that $\eta_0 = \eta_1 = 0$. We also suppose $f(\eta)$ is given by $f(\eta) = f_0 e^{\eta/\beta} = f_0 e^{-4H_0 t/\beta}$, where f_0 and β are constants. In this case, the equation of motion for ξ can be solved as follows, $\xi = -[3f_0\beta/(3\beta - 4)]e^{-4H_0 t/\beta} + [\xi_0/(3H_0)]e^{-3H_0 t} - \xi_1$, where ξ_0 and ξ_1 are constants. For the de Sitter space, a behaves as $a = a_0 e^{H_0 t}$, where a_0 is a constant. Hence, for the matter with the constant equation of state $w_m \equiv P_m/\rho_m$, we find $\rho_m = \rho_{m0} e^{-3(w_m+1)H_0 t}$, where ρ_{m0} is a constant. By substituting this expression of ρ_m , a solution of η and a solution of ξ with putting $\xi_0 = 0$ into Eq. (2.3), we obtain $0 = -3H_0^2(1 + \xi_1) + 6H_0^2 f_0(2/\beta - 1)e^{-4H_0 t/\beta} + \Lambda + \kappa^2 \rho_{m0} e^{-3(w_m+1)H_0 t}$. For $\rho_{m0} = 0$, if we choose $\beta = 2$, $\xi_1 = -1 + \Lambda/(3H_0^2)$, de Sitter space can be a solution. Even if $\rho_m \neq 0$, by taking $\beta = 4/[3(1 + w_m)]$, $f_0 = -\kappa^2 \rho_{m0}/[3H_0^2(1 + 3w_m)]$, $\xi_1 = -1 + \Lambda/(3H_0^2)$, we find that there is a de Sitter solution. The equation $\xi_1 = -1 + \Lambda/(3H_0^2)$ implies that $H_0^2 = \Lambda/[3(1 + \xi_1)]$. This means that the cosmological constant Λ is effectively screened by ξ . This is one of main results in this paper. We include the cosmological term in the action (2.1) in order to show that the cosmological constant is surely screened by the non-local effect. We should note that in the case that there does not exist the cosmological constant, i.e., $\Lambda = 0$, if we choose $\xi_1 = -1$, H_0 can be arbitrary. Thus, H_0 can be determined by an initial condition. Since H_0 can be small or large, the theory with the function in $f(\eta) = f_0 e^{\eta/\beta} = f_0 e^{-4H_0 t/\beta}$ with $\beta = 2$ could describe the early-time inflation or current cosmic acceleration. In the presence of matter with $w_m \neq 0$, for $\Lambda = 0$, we may also have a de Sitter solution $H = H_0$.

To examine the ghost-free condition, we make a conformal transformation to the Einstein frame: $g_{\mu\nu} = \Omega^2 g_{\mu\nu}^{(E)}$, where $\Omega^2 = 1/(1 + f(\eta) - \xi)$ and $R = (1/\Omega^2) [R^{(E)} - 6(\square \ln \Omega + g^{(E)\mu\nu} \nabla_\mu \ln \Omega \nabla_\nu \ln \Omega)]$. We use a superscription (E) to represent quantities in the Einstein frame. We may discard the $\square \ln \Omega$ term because it is a total divergence, and introduce the expression of $\phi = \ln \Omega = -(1/2) \ln(1 + f(\eta) - \xi)$. Instead of η and ξ , we may regard ϕ and η to be independent fields. Inserting $\xi = -e^{-2\phi} + (1 + f(\eta))$ into the action, which is obtained from the action in Eq. (2.2), we finally arrive at

$$S = \int d^4x \sqrt{-g^{(E)}} \left\{ \frac{1}{2\kappa^2} \left[R^{(E)} - 6\nabla^\mu \phi \nabla_\mu \phi - 2\nabla^\mu \phi \nabla_\mu \eta - e^{2\phi} f'(\eta) \nabla^\mu \eta \nabla_\mu \eta - 2e^{4\phi} \Lambda \right] + e^{4\phi} \mathcal{L}_{\text{matter}}(Q; e^{2\phi} g^{(E)}) \right\}. \quad (2.5)$$

In order to avoid a ghost, the determinant of the kinetic term must be positive, which means [4]

$$\det \begin{vmatrix} 6 & 1 \\ 1 & e^{2\phi} f'(\eta) \end{vmatrix} = 6e^{2\phi} f'(\eta) - 1 > 0. \quad (2.6)$$

This condition is assumed to be satisfied. In particular, $f'(\eta) > 0$ is a necessary condition. Thus, the ghost-free condition is expressed as $f'(\eta) > 1/(6e^{2\phi}) = (1 + f(\eta) - \xi)/6 > 0$, where in the equality of the middle term, we have used $\phi = -(1/2) \ln(1 + f(\eta) - \xi)$. Then, we may introduce a new field χ , given by $\chi = \int^\eta \sqrt{f'(\eta)} d\eta$, and rewrite the action in Eq. (2.5) in the form,

$$S = \int d^4x \sqrt{-g^{(E)}} \left\{ \frac{1}{2\kappa^2} \left[R^{(E)} - 6\nabla^\mu \phi \nabla_\mu \phi - \frac{2}{\sqrt{f'}} \nabla^\mu \phi \nabla_\mu \chi - e^{2\phi} \nabla^\mu \chi \nabla_\mu \chi - 2e^{4\phi} \Lambda \right] + e^{4\phi} \mathcal{L}_{\text{matter}}(Q; e^{2\phi} g^{(E)}) \right\}, \quad (2.7)$$

where f' should be regarded as a function of χ , $f'(\eta) = f'(\eta(\chi))$. In case of the model $f(\eta) = f_0 e^{\eta/\beta} = f_0 e^{-4H_0 t/\beta}$ with $\beta = 2$, for the solution $\eta = -4H_0 t - \eta_0 e^{-3H_0 t} + \eta_1$ with $\eta_0 = \eta_1 = 0$ and in $\xi = -[3f_0\beta/(3\beta - 4)] e^{-4H_0 t/\beta} + [\xi_0/(3H_0)] e^{-3H_0 t} - \xi_1$ with $\xi_0 = 0$ and ξ_1 , the condition (2.6) to avoid a ghost has the following form: $3/\{4 + [\Lambda/(3H_0^2 f_0)] e^{2H_0 t}\} > 1$, which suggests the two cases. One is f_0 is positive but the bare cosmological constant Λ is negative and therefore $\xi_1 < -1$ from $\xi_1 = -1 + \Lambda/(3H_0^2)$. Another is f_0 is negative and Λ is positive and therefore $\xi_1 > -1$. We note that in the model $f(\eta) = f_0 e^{\eta/\beta} = f_0 e^{-4H_0 t/\beta}$ with $\beta = 2$, $f'(\eta) = (f_0/2) e^{\eta/2}$ and from a necessary condition in order to avoid a ghost $f'(\eta) > 0$ we find $f_0 > 0$, which corresponds to the former case. In this case, the condition described above suggests that the de Sitter universe is stable in a period $1/(2H_0) \ln(-3H_0^2 f_0/\Lambda) < t < 1/(2H_0) [\ln 4 + \ln(-3H_0^2 f_0/\Lambda)]$, where we have also used the condition $(1 + f(\eta) - \xi)/6 > 0$. Hence the length of the ghost-free period is given by $\Delta t = \ln 4/(2H_0) = \ln 2/H_0 \simeq 0.69/H_0$. Thus unfortunately the period is less than one e -folding time. So this cannot give inflation in the early universe provided that the appearance of a ghost has to be avoided.

3 Finite-time future singularities in non-local gravity

In this section, we examine whether there exists the finite-time future singularities in non-local gravity. In the flat FLRW space-time, we analyze an asymptotic solution of the gravitational field equations (2.3) and (2.4) in the limit of the time when the finite-time future singularities appear. We consider the case in which the Hubble parameter H is expressed as $H \sim h_s (t_s - t)^{-q}$, where h_s is a positive constant, q is a non-zero constant larger than -1 ($q > -1, q \neq 0$), and t_s is the time when the finite-time future singularity appears. We only consider the period $0 < t < t_s$ because H should be real number. When $t \rightarrow t_s$, for $q > 1$, $H \sim h_s (t_s - t)^{-q}$ as well as $\dot{H} \sim q h_s (t_s - t)^{-(q+1)}$ become infinity and hence the scalar curvature R diverges. For $-1 < q < 0$ and $0 < q < 1$, H is finite, but \dot{H} becomes infinity and therefore R also diverges. From $H \sim h_s (t_s - t)^{-q}$, we obtain $a \sim a_s \exp\left\{[h_s/(q-1)](t_s - t)^{-(q-1)}\right\}$, where a_s is a constant. By using $\ddot{\eta} + 3H\dot{\eta} = a^{-3} d(a^3 \dot{\eta})/dt$ and $0 = \ddot{\eta} + 3H\dot{\eta} + 6\dot{H} + 12H^2$, η is described as $\eta = -\int^t (1/a^3) \left(\int^{\bar{t}} R a^3 d\bar{t}\right) dt$. In the limit $t \rightarrow t_s$, for $q > 1$, $\dot{H} \ll H^2$ and hence $R \sim 12H^2$, whereas for $-1 < q < 0$ and $0 < q < 1$, $\dot{H} \gg H^2$ and hence $R \sim 6\dot{H}$. By applying these relations to the integral expression of η shown above and taking the leading term in terms of $(t_s - t)$, we obtain $\eta \sim -[4h_s/(q-1)](t_s - t)^{-(q-1)} + \eta_c$ ($q > 1$), $\eta \sim -[6h_s/(q-1)](t_s - t)^{-(q-1)} + \eta_c$ ($-1 < q < 0, 0 < q < 1$), where η_c is an integration constant. From the expression of a , we see that when $t \rightarrow t_s$, for $q > 1$, $a \rightarrow \infty$, whereas for $-1 < q < 0$ and $0 < q < 1$, $a \rightarrow a_s$. Moreover, it follows from $H \sim h_s (t_s - t)^{-q}$ and $\rho_{\text{eff}} = 3H^2/\kappa^2$ that for $q > 0$, $H \rightarrow \infty$ and therefore $\rho_{\text{eff}} = 3H^2/\kappa^2 \rightarrow \infty$, whereas for $-1 < q < 0$, H asymptotically becomes finite and also ρ_{eff} asymptotically approaches a finite constant value ρ_s . On the other hand, from $\dot{H} \sim q h_s (t_s - t)^{-(q+1)}$ and $P_{\text{eff}} = -(2\dot{H} + 3H^2)/\kappa^2$ we find that for $q > -1$, $\dot{H} \rightarrow \infty$ and hence $P_{\text{eff}} = -(2\dot{H} + 3H^2)/\kappa^2 \rightarrow \infty$. Here, ρ_{eff} and P_{eff} are the effective energy density and pressure of the universe, respectively. It is known that the finite-time future singularities can be classified in the following manner [7]:

Table 1: Range and conditions for the value of parameters of $f(\eta)$, H , and η_c and ξ_c in order that the finite-time future singularities can exist.

Case	$f(\eta) = f_s \eta^\sigma$	$H \sim h_s (t_s - t)^{-q}$	η_c, ξ_c
	$f_s \neq 0$	$h_s > 0$	$\eta_c \neq 0$
	$\sigma \neq 0$	$q > -1, q \neq 0$	
(ii)	$\sigma < 0$	$q > 1$ [Type I (“Big Rip”) singularity]	$\xi_c = 1$
(iii)	$f_s \eta_c^{\sigma-1} (6\sigma - \eta_c) + \xi_c - 1 = 0$	$0 < q < 1$ [Type III singularity] $-1 < q < 0$ [Type II (“sudden”) singularity]	

- Type I (“Big Rip” [8]): In the limit $t \rightarrow t_s, a \rightarrow \infty, \rho_{\text{eff}} \rightarrow \infty$ and $|P_{\text{eff}}| \rightarrow \infty$. The case in which ρ_{eff} and P_{eff} becomes finite values at $t = t_s$ is also included.
- Type II (“sudden” [9]): In the limit $t \rightarrow t_s, a \rightarrow a_s, \rho_{\text{eff}} \rightarrow \rho_s$ and $|P_{\text{eff}}| \rightarrow \infty$.
- Type III: In the limit $t \rightarrow t_s, a \rightarrow a_s, \rho_{\text{eff}} \rightarrow \infty$ and $|P_{\text{eff}}| \rightarrow \infty$.
- Type IV: In the limit $t \rightarrow t_s, a \rightarrow a_s, \rho_{\text{eff}} \rightarrow 0, |P_{\text{eff}}| \rightarrow 0$, and higher derivatives of H diverge. The case in which ρ_{eff} and/or $|P_{\text{eff}}|$ asymptotically approach finite values is also included.

For $q > 1$, the Type I (“Big Rip”) singularity, for $0 < q < 1$, the Type III singularity, and for $-1 < q < 0$, the Type II (“sudden”) singularity. In Table 1, we show the range and conditions for the value of parameters of $f(\eta)$, H , and η_c and ξ_c in order that the finite-time future singularities can exist. If $\eta_c \neq 0$ and $\xi_c = 1$, in a model with $\sigma < 0$, there can exist the finite-time future singularities with the property of the Type I (“Big Rip”) singularity for $q > 1$. If $\eta_c \neq 0$, in a model with satisfying the condition $f_s \eta_c^{\sigma-1} (6\sigma - \eta_c) + \xi_c - 1 = 0$, there can exist the finite-time future singularities with the property of the Type III singularity for $0 < q < 1$ and that of the Type II (“sudden”) singularity for $-1 < q < 0$. In the special case of $\eta_c = 0$, the finite-time future singularities described by $H \sim h_s (t_s - t)^{-q}$ cannot occur.

4 Summary

We have studied a screening scenario for a cosmological constant in de Sitter solutions as well as a condition to avoid a ghost. In addition, we have explicitly shown that three types of the finite-time future singularities can occur in non-local gravity and examined their properties.

References

- [1] S. Nojiri and S. D. Odintsov, Phys. Rept. **505**, 59 (2011).
- [2] S. Deser and R. P. Woodard, Phys. Rev. Lett. **99**, 111301 (2007).
- [3] N. Arkani-Hamed, S. Dimopoulos, G. Dvali and G. Gabadadze, arXiv:hep-th/0209227.
- [4] S. Nojiri, S. D. Odintsov, M. Sasaki and Y. I. Zhang, Phys. Lett. B **696**, 278 (2011).
- [5] A. D. Dolgov and M. Kawasaki, Phys. Lett. B **573**, 1 (2003).
- [6] K. Bamba, S. Nojiri, S. D. Odintsov and M. Sasaki, arXiv:1104.2692 [hep-th].
- [7] S. Nojiri, S. D. Odintsov and S. Tsujikawa, Phys. Rev. D **71**, 063004 (2005).
- [8] R. R. Caldwell, M. Kamionkowski and N. N. Weinberg, Phys. Rev. Lett. **91**, 071301 (2003); B. McInnes, JHEP **0208** (2002) 029.
- [9] J. D. Barrow, Class. Quant. Grav. **21**, L79 (2004); S. Nojiri and S. D. Odintsov, Phys. Lett. B **595**, 1 (2004).

Braneworld black holes

Pau Figueras^{28(a)}

^(a)*Department of Applied Mathematics and Theoretical Physics, University of Cambridge
Centre for Mathematical Sciences, Wilberforce Road, Cambridge CB3 0WA, United Kingdom*

Abstract

In this note we review the latest developments in the numerical construction of localised black holes on a four-dimensional Randall-Sundrum II (RSII) braneworld model. We argue that arbitrarily large black holes on the brane can be constructed as perturbations of a solution of the Einstein equations in five-dimensional anti-de Sitter (AdS₅) space whose boundary metric is conformal to the four-dimensional asymptotically flat Schwarzschild solution. Using the newly developed harmonic formulation of the Einstein equations for elliptic problems we construct RSII static black holes with radii ranging from $\sim 5 \times 10^{-3}\ell$ up to $\sim 100\ell$, where ℓ is the radius of AdS₅.

1 Introduction

The major goal in theoretical physics is to formulate a consistent theory of quantum gravity. String theory (or the poorly understood M-theory) is meant to be such a theory of quantum gravity but its consistency requires the existence more than four spacetime dimensions. Kaluza and Klein (KK), almost a century ago, showed that if these extra dimensions are curled up so that the typical radius of the *compact* dimensions is sufficiently small (compared to the length scale probed in experiments) then $4d$ physics would be unaffected. Therefore, string theory is perfectly consistent with the present experimental data if we assume that the extra dimensions are sufficiently small. In standard KK theory the existence of such compact extra dimensions would manifest itself in experiments with the appearance of new massive particles, with an energy gap proportional to the inverse compactification radius squared.

In [1, 2] Randall and Sundrum proposed a remarkable alternative to KK compactification in which the extra dimensions are non-compact. In the Randall-Sundrum infinite braneworld model (RSII) one takes two copies of AdS₅ and glues them together along a boundary, which corresponds to the brane. Our $4d$ world is given by this hypersurface (the brane) embedded in the higher-dimensional spacetime and all Standard model particles (and their interactions) are confined to the brane except for gravity, which can propagate in the extra dimensions. This construction can also be motivated from string theory, where the existence of dynamical $(d + 1)$ -dimensional objects, known as d -branes, with gauge fields living in their worldvolume is common place.

Considering small fluctuations of the metric around the aforementioned background, Randall and Sundrum showed that there is a zero mode of the graviton, which is localised on the brane, together with a *continuum* of massive KK modes. Indeed, the fact that the extra dimension is non-compact is responsible for the absence of a mass gap in the KK spectrum. Moreover, [2] argued (and later [3, 4] explicitly verified) that for an observer sitting on the brane gravity at large distances from the sources would look like standard $4d$ gravity, with the usual $1/r$ potential, plus corrections that go like ℓ^2/r^3 , where ℓ is the radius of the ambient AdS₅ space. Therefore, at least at the linearised level it would seem that the RSII model offers a viable and attractive alternative to KK compactification.

Of course, an obvious question that one can ask is what happens in the strong field regime. More specifically, how does a black hole on the brane look like? This is an important question that has to be addressed in the context of the RSII models if they have to be phenomenologically viable. This issue is especially relevant because in the near future we expect to be able to test $4d$ general relativity (GR) in the strong field regime, and more precisely its predictions for black hole physics, through the detection of gravitational waves. One would hope that if gravity on the brane has to reduce to standard $4d$ GR then a large (compared to ℓ) static black hole on the brane should look like $4d$ asymptotically flat Schwarzschild.

²⁸Email address: p.figueras@damtp.cam.ac.uk

For phenomenological reasons in this paper we will focus on the case of (3+1)-dimensional brane. The first (unsuccessful) attempt to construct a black hole on a 4-brane was made in [5] but so far very little progress has been made in terms of finding an explicit solution and most of the work has been numerical.²⁹ Furthermore, refs. [8, 9] used AdS/CFT to argue that the difficulties in finding large and *static* (non-extremal) braneworld black holes were not a mere accident. According to these references, black holes on a brane in an AdS_{d+1} braneworld that are obtained by solving the classical bulk equations of motion correspond to quantum corrected black holes from the brane point of view. The reason is that applying AdS/CFT to the RSII model one is led to conclude that classical gravity in the bulk is dual to a strongly interacting conformal field theory (CFT) in the planar limit that lives on the brane and which is coupled to dynamical gravity. Moreover, this CFT is cut off in the UV but the full conformal invariance is recovered in the IR. Therefore, the induced geometry on the brane is sourced by the stress tensor of the CFT, which includes all quantum effects in the planar limit. It is well-known that quantum effects can survive when we take the $\hbar \rightarrow 0$ and $N_c \rightarrow \infty$ limit if they are coherent among the $O(N_c^2)$ colour degrees of freedom in the CFT as the total effect would go like $\sim \hbar N_c^2$. Indeed, recall that in the large N_c limit the 't Hooft coupling $\lambda = g_s N_c = (\ell/\ell_s)^4$ is kept fixed, where g_s is the bulk string coupling constant and ℓ_s is the string length. The $4d$ Planck length is given by $\ell_4 = \ell/N_c$ and since $\hbar = \ell_4^2/G_4$, where G_4 is the $4d$ Newton's constant, then the product

$$\hbar N_c^2 = \left(\frac{\ell}{\ell_4}\right)^2 \left(\frac{\ell_4^2}{G_4}\right) = \frac{\ell^2}{G_4}, \quad (1.1)$$

remains finite when we take $\hbar \rightarrow 0$ while keeping ℓ and G_4 fixed in the RSII model. This led the authors of [8, 9] to make the remarkable conjecture that a large, static and non-extremal black hole on the brane could not exist as it would Hawking radiate and therefore it could not be static.³⁰ At this point we should mention that [10] provided a counter-argument for the non-existence of a large braneworld black hole. Their reasoning is as follows. Although the theory on the brane is conformal in the infrared (there is no mass gap), the presence of a black hole should effectively introduce a mass gap in the spectrum because of the presence of a new length scale in the theory, namely the size of the black hole. Ref. [10] argued that in the large N_c and strong coupling limit, the energy of most of the $O(N_c^2)$ states in the theory is lifted to stringy scales and only $O(1)$ states remain accessible to be radiated by a finite energy object such as a localised black hole. Therefore, Hawking radiation should be an $O(1)$ effect and therefore not visible in the classical bulk gravity limit.

Most of the previous attempts in constructing localised braneworld black holes have been numerical. Using the methods of [11, 12], localised black holes on a 4-brane with radius up to $\sim 0.2\ell$ and on a 5-brane with radius up to $\sim 2.0\ell$ were constructed in [13, 14] and [15] respectively. Therefore, none of these results could be used to test the aforementioned conjecture. More recently, using the same numerical methods as the previous references, [16] (see also [17]) revisited the problem and could not find a solution at all, no matter the size of the black hole. It was then argued that even arbitrarily small static braneworld black holes could not exist. Finally, we should point out that [18] (see also [19]) constructed the near-horizon geometry of *extremal* (*i.e.*, zero temperature) localised black holes on a 4-brane and they could find black holes of arbitrary radius, either very small or very large compared to the radius of AdS_5 . However, in this case the non-existence conjecture can be bypassed because the black holes in question have zero temperature and therefore they are not expected to Hawking radiate and thus they should be static.

So far we have summarised the state of the art concerning the existence (or non-existence) of localised braneworld black holes previous to our work [20, 21]. In these articles we used the new (and better) formulation of the numerical problem of [22] (see [23] for a review) to construct five-dimensional localised braneworld black holes in the RSII model with radii ranging from $\sim 5 \times 10^{-3}\ell$ up to $\sim 100\ell$, and thereby solving the long-standing existence problem of these objects. The rest of this article is devoted to review these papers. In §2 we will briefly review the numerical method of [22] which has proven to be crucial in our work. Then, in §3 we will consider its application to the numerical construction of localised black holes in the RSII braneworld model. Somewhat as an aside, we will first discuss in §3.1 the construction of a

²⁹ However, refs. [6, 7] found an analytic solution for the case of a (2+1)-dimensional brane.

³⁰ Only when the black hole on the brane is large compared to the radius ℓ of AdS_5 one can sensibly describe it as a CFT-corrected black hole.

solution in AdS₅ whose boundary metric is 4d Schwarzschild. We then argue in §3.2 that large braneworld black holes can be viewed as perturbations of the previous AdS/CFT solution. In this subsection we also consider the numerical construction of braneworld black holes of arbitrary radius. In §4 we present our conclusions.

2 The Harmonic Einstein equation

In this section we will provide a short review of the new formulation of the Einstein equations introduced in [22] (see [23] for a thorough review) for finding static (or stationary) spacetimes and which is especially well-suited for numerics. This formulation played a key role in our numerical construction of braneworld black holes.

Suppose that we want to solve the Einstein equations,

$$R_{ab} = 0, \quad (2.1)$$

on a d -dimensional spacetime (\mathcal{M}, g) . For simplicity we will start considering the vacuum case but, as we shall see, we can (and we will) incorporate a cosmological constant Λ . Including matter fields should not be difficult as long as they obey elliptic equations. In this article we will only consider static spacetimes and therefore we can Wick-rotate the time direction and consider the associated Riemannian problem. The generalisation of the formulation of the Einstein equations that we will outline below to the stationary case can be found in [24]. Furthermore, we will be interested in spacetimes containing a black hole and hence, in the Euclidean setting, they possess a $U(1)$ isometry generated by the Killing vector field ∂_τ . The period of τ is chosen so that there are no conical singularities and the horizon corresponds to the fixed point set of ∂_τ and there is no boundary there.

Since we are interested in finding static spacetimes we would expect to be able to solve the equations as a boundary value problem. But in order to be able to do that we first need to cast the equations (2.1) in a manifestly elliptic form. The character of a certain equation is determined by the so called principal symbol. To see what this is, lets think of (2.1) as an operator acting on the metric and lets linearise it around a fixed background:

$$\delta R_{ab} \equiv \Delta_R h_{ab} = \Delta_L h_{ab} + \nabla_{(a} v_{b)}, \quad (2.2)$$

where

$$\Delta_L h_{ab} = -\frac{1}{2} \Delta h_{ab} - R_a{}^c{}_b{}^d h_{cd} \quad (2.3)$$

is the Lichnerowicz operator and $v_a = \nabla^b h_{ba} - \frac{1}{2} \partial_a h$. Then the principal symbol of the *linear* operator Δ_R is obtained from the highest derivative terms in Δ_R ,

$$P_g h_{ab} = \frac{1}{2} g^{cd} (\partial_a \partial_c h_{bd} + \partial_b \partial_c h_{ad} - \partial_c \partial_d h_{ab} - \partial_a \partial_b h_{cd}), \quad (2.4)$$

and substituting the derivatives by vectors $\xi^a \in \mathbb{R}^d$ to get

$$P_g(\xi) h_{ab} = \frac{1}{2} (\xi_a \xi^c h_{cb} + \xi_b \xi^c h_{ca} - \xi^2 h_{ab} - \xi_a \xi_b h). \quad (2.5)$$

Then, an operator is said to be elliptic if $P_g(\xi) h_{ab} \neq 0$ for *all* ξ and for every point x in \mathcal{M} . Physically this means that locally it should not be possible to find short wavelength perturbations that propagate as waves. But clearly (2.5) is not elliptic because for perturbations of the form $h_{ab} = \xi_{(a} v_{b)}$, which in real space correspond to the usual short distance behaviour of pure gauge modes $\nabla_{(a} v_{b)}$, we have $P_g(\xi) h_{ab} = 0$ for all ξ . In practice the lack of ellipticity of (2.1) implies that we cannot solve it as a boundary value problem.

From the previous discussion, we have seen that the obstruction to ellipticity comes from the pure gauge modes. Therefore, in order to turn (2.1) into a manifestly elliptic system of equations we have to fix the gauge. The proposal of [22] basically consists on adding a gauge-fixing term to (2.1) while preserving the general covariance. More specifically, instead of solving (2.1) we will solve the so called *Harmonic Einstein equation*:

$$R_{ab}^H = 0, \quad R_{ab}^H \equiv R_{ab} - \nabla_{(a} \xi_{b)}, \quad \xi^a = g^{bc} (\Gamma_{bc}^a - \bar{\Gamma}_{bc}^a), \quad (2.6)$$

where Γ is the Levi-Civita connection associated to the spacetime metric g and $\bar{\Gamma}$ is a reference connection on \mathcal{M} . For simplicity we will consider $\bar{\Gamma}$ to be the Levi-Civita connection associated to a reference metric \bar{g} on \mathcal{M} , but one could be more general. The great advantage in considering the Harmonic Einstein equations is that (2.6) is manifestly elliptic; the principal symbol of this operator is given by

$$P_g^H h_{ab} = -\frac{1}{2} g^{cd} \partial_c \partial_d h_{ab}, \quad (2.7)$$

which is manifestly elliptic for any Riemannian background metric g . We should mention that the Harmonic Einstein equation (2.6), with $\bar{\Gamma}$ chosen as the Levi-Civita connection associated to a reference metric \bar{g} on \mathcal{M} , was used in the early 80's by DeTurck to show that Ricci flow is parabolic. We will come back to this point later.

The proposal of [22] is to solve (2.6) instead of (2.1), and since the former is manifestly elliptic, it can be solved as a boundary value problem. Therefore, a basic question that we have to address is to determine under which conditions or, more precisely, for which boundary conditions the solutions to (2.6) are Einstein, and hence $\xi^a = 0$.³¹ Solutions to (2.6) with a non-vanishing vector ξ^a are known in the literature as Ricci solitons. Their existence is controlled by the equation

$$\nabla^2 \xi_a + R_a{}^b \xi_b = 0, \quad (2.8)$$

which follows from contracting (2.6) with ∇^a and using the contracted Bianchi identity. In the context of the dynamical (time-evolution) problem, ξ^a satisfies a wave equation. Then, in order for the solutions to the Harmonic Einstein equation be Einstein it suffices to choose initial data for which ξ and its time derivative vanish on the initial Cauchy surface. Then the above wave equation guarantees that ξ vanishes throughout the time-evolution and the Harmonic Einstein equation gives rise to an Einstein metric in harmonic coordinates. However, in the present context we are interested in the elliptic problem and the situation is more delicate.³²

Before we continue with the discussion on the existence of Ricci solitons, note that the cosmological constant term in the Einstein equations has no derivatives of the metric and therefore it does not affect the character of the equations, and the same is true for the Harmonic Einstein equation. Therefore, from now on will consider the Harmonic Einstein equation augmented with a non-positive cosmological constant term. The reason for the importance of the sign of the cosmological constant will become apparent in a moment.

In favourable circumstances it is possible to prove the non-existence of Ricci solitons on certain manifolds with suitable boundary conditions. Indeed, Bourguignon [27] proved that there are no Ricci solitons on a compact manifold without boundary for any choice of vector ξ^a . For non-compact manifolds and for different asymptotic boundary conditions of interest (flat, Kaluza-Klein and AdS), ref. [20] could show the non-existence of Ricci solitons. Their argument is as follows. Contracting (2.8) with ξ^a and using (2.6) one finds,

$$\nabla^2 \phi + \xi^a \partial_a \phi = -2\Lambda \phi + 2(\nabla^a \xi^b)(\nabla_a \xi_b) \geq 0, \quad \phi \equiv \xi^a \xi_a. \quad (2.9)$$

Note that in order for this inequality to hold it is crucial to work in the Riemannian setting and that $\Lambda \leq 0$. Ref. [20] showed that solutions to this equation are governed by a maximum principle, so that if ϕ is non-constant then its maximum must be attained at the boundary of the manifold and the normal outer gradient there must be positive. Then, imposing suitable regularity conditions and that the spacetime metric is asymptotically flat, AdS or KK it is possible to show that in fact ϕ must be zero everywhere. From this and the fact that the metric is Riemannian one then deduces that $\xi^a = 0$ (see [20] for the details).

Although the maximum principle described above allows one to show that in some situations the solutions to the Harmonic Einstein equation must in fact be Einstein, there are situations in which it does not apply. For instance, that is the case for the braneworld black hole, where the Israel junction conditions allow for the existence of a maximum of ϕ on the brane. However, even in these adverse cases, since the Harmonic Einstein equations are elliptic the solutions should be locally unique as long as the problem is well-posed. Therefore, if one finds a solution to (2.6) numerically it is always possible to check whether ξ^a vanishes or not.

³¹Note that for $\xi^a = 0$, the spacetime coordinates satisfy a harmonic-type equation: $\Delta_g x^a = -g^{bc} \bar{\Gamma}_{bc}^a$.

³²Ricci solitons are known to exist on manifolds with a positive cosmological constant [26].

Methods for solving the Harmonic Einstein equations

In the following we will briefly describe the methods that can be used to solve (2.6) numerically. These are to simulate Ricci flow and a Newton's method. We will discuss each of them in turn.

Since (2.6) is elliptic, a general method for solving this equation is to consider the associated parabolic equation,

$$\frac{\partial}{\partial \lambda} g_{ab} = -2 R_{ab}^H, \quad (2.10)$$

where λ is the (fictitious) flow time. This equation is known as the Ricci-DeTurck flow equation, and it has been used in the context of Ricci flow. The basic idea is to start with some initial guess for the metric, $g_{ab}|_{\lambda=0}$ and let it evolve according to this equation until one reaches a fixed point. Clearly fixed points of this equation are solutions to the original Harmonic Einstein equation (2.6).

As discussed in [22], a remarkable property of the Ricci-DeTurck flow (2.10) is that it is diffeomorphic to the Ricci flow,

$$\frac{\partial}{\partial \lambda} g_{ab} = -2 R_{ab}, \quad (2.11)$$

which is independent of the vector field ξ^a . This implies that given some initial metric, while its evolution under (2.10) in the space of metrics on \mathcal{M} depends on the choice of reference metric \bar{g} , its path on the space of geometries (*i.e.*, metrics up to diffeomorphisms) in \mathcal{M} is independent of \bar{g} . This allows one to address, in an invariant manner, the existence or non-existence of fixed points, and therefore solutions to (2.6). This will be important later when we provide numerical evidence for the existence of braneworld black holes.

Another question that we have to address is that given some generic initial data, under which conditions the Ricci-DeTurck flow (2.10) will converge to it? It turns out that an Einstein metric is an attractive fixed point of the Ricci flow if and only if the Lichnerowicz operator Δ_L around this particular background is positive, *i.e.*, it has no negative eigenvalues [22]. However, for many of the known black holes spacetimes Δ_L possess negative modes, which are the analogue of the negative mode of the Euclidean Schwarzschild black hole discovered by Gross, Perry and Yaffe [28]. Therefore they are unstable fixed points of Ricci flow and *generic* initial data will *not* converge to these Einstein metrics. It may seem then that Ricci flow is not a very useful method in practice for finding new types of black holes if the latter have negative modes. We will now explain that this is not quite the case if the black hole that we are trying to find has one, and only one, negative mode. In this case, as explained in [22] (see also [23]), the positive modes lie on a co-dimension one surface Σ in the space of geometries around the fixed point that we are interested in. Then, if we start the flow on Σ (or very close to Σ), the flow will remain on this hypersurface and it will tend to the desired fixed point asymptotically in flow time. Therefore, the main difficulty consists on constructing suitable initial data that lies on Σ . In §3.2 we will see how this can be implemented in practice for the case in which the black hole of interest has one negative mode. If the number of negative modes is greater than one, then Ricci flow becomes more difficult to implement (because finding initial data that lies sufficiently close to Σ is more difficult) and therefore less useful.

As we have seen, Ricci flow is a very elegant method for numerically constructing new types of black holes but it becomes less useful if the latter have negative modes. There is another standard method to solve (2.6) numerically which does not depend on whether the fixed point has positive or negative modes. This method is known as Newton's method. Its main disadvantage is that it is not geometric in nature, it explicitly depends on the choice of reference metric and it is more difficult to implement. In practice it works very well if the initial guess is sufficiently close to the fixed point.

The idea of Newton's method is to start with some initial guess g_{ab} that does not solve (2.6), and iteratively correct this guess $g_{ab} \rightarrow g_{ab} + \epsilon h_{ab}$, where the correction satisfies

$$\Delta_H h_{ab} = -R_{ab}^H(g), \quad (2.12)$$

and Δ_H is the linearisation of R_{ab}^H around the initial guess. Here ϵ is a parameter that can be taken between 0 and 1 depending on how close we are to the fixed point. Clearly the only requirement for this algorithm to work is that Δ_H has to be invertible, which implies that this operator cannot have zero modes. In general this should not be a problem since the boundary conditions should take care of eliminating any zero modes and rendering the fixed point locally unique. In the results that we will present in the coming sections we used this method extensively.

3 Braneworld black holes

In this section we will present our results for the numerical construction of braneworld black holes in the RSII model. But before we do that, in §3.1 we will pause to describe a seemingly unrelated solution in AdS₅. More specifically, we will describe a black hole solution in AdS₅ such that the boundary metric is conformal to 4d asymptotically flat Schwarzschild. As we shall see, this solution will allow us to understand the existence of large braneworld black holes in RSII. The actual construction of these solutions will be described in §3.2.

3.1 AdS₅-CFT₄ solution

In this subsection we will numerically construct a static and axisymmetric spacetime in AdS₅ such that the boundary metric is conformal to the 4d asymptotically flat (AF) Schwarzschild black hole. Moreover, we will require that the metric deep in the interior asymptotes to the Poincare horizon of AdS. This solution can be trivially uplifted to 10d taking the product with an S⁵ and therefore, using the AdS/CFT correspondence, it should be the gravitational dual of $\mathcal{N} = 4$ super Yang-Mills (SYM) in the background of Schwarzschild in a certain vacuum state. With this boundary conditions, we conjecture that the dual field theory should not correspond to a thermal state, which typically corresponds to the Hartle-Hawking state; we believe that this geometry is the classical dual of the CFT in the Unruh or the Boulware states. This has important implications for the existence of braneworld black holes in the RSII model.

3.1.1 Metric ansatz and boundary conditions

We want to find a static Einstein metric which is asymptotically locally AdS such that the boundary metric is in the same conformal class as the 4d asymptotically flat Schwarzschild black hole. Considering the Wick-rotated Euclidean section, the spacetime manifold will be asymptotically locally hyperbolic (ALH) with a conformal boundary metric given by 4d Schwarzschild, whose isometry group is $U(1) \times SO(3)$. It has been shown that a regular static ALH Einstein metrics must inherit the isometries of the boundary metric [29] and therefore we do not need to assume these isometries. Furthermore, we will require that the metric approaches the Poincare horizon of AdS far from the conformal boundary.

Taking into account the previous considerations we are now ready to write down our ansatz for the metric:

$$ds^2 = \frac{\ell^2}{(1-x^2)^2} \left(4r^2 f(r)^2 e^T d\tau^2 + x^2 g(x) e^S d\Omega_{(2)}^2 + \frac{4}{f(r)^2} e^{T+r^2 f(r)A} dr^2 + \frac{4}{g(x)} e^{S+x^2 B} dx^2 + \frac{2rx}{f(r)} F dr dx \right), \quad (3.1)$$

where $f(r) = 1 - r^2$, $g(x) = 2 - x^2$ and the range of the coordinates can be chosen to be $r, x \in [0, 1]$ without loss of generality. $X = \{T, S, A, B, F\}$ are smooth functions which depend on r and x only and they are the unknowns. Recall that in order to solve (2.6) we have to specify a reference metric on \mathcal{M} ; here we will choose the reference metric to be as in (3.1) with $X = 0$.

In these coordinates, $r = 0$ corresponds to the horizon and smoothness of the manifold there requires X to be smooth in r^2 . Therefore, all functions X will have a Neumann condition at $r = 0$. Notice that we have constructed the metric ansatz (3.1) in such a way that $g_{\tau\tau} = \kappa^2 g_{rr}$ at $r = 0$ without any further condition on X , where κ is a constant so that the period of τ is $2\pi/\kappa$. This ensures the absence of conical singularities at $r = 0$. Having 4d Schwarzschild with unit horizon radius as the conformal boundary metric fixes $\kappa = 1$. Similarly, $x = 0$ is the axis of spherical symmetry and all functions X should be smooth in x^2 and hence obey a Neumann condition. Again, the absence of conical singularities at $x = 0$ is ensured by the form our ansatz (3.1). $r = 1$ corresponds to the Poincare horizon of AdS and, as discussed in [20], we have to impose a Dirichlet boundary condition there so that $X = 0$. Finally, $x = 1$ is the conformal boundary of AdS and in order to obtain a metric in the same conformal class as 4d AF Schwarzschild we have to impose $X = 0$ there.

Notice that the problem has two length scales, namely the radius of AdS₅ ℓ and the radius of the boundary black hole R_0 . Fixing $\ell = 1$ there is one scale left, namely R_0 . But since R_0 only appears as an

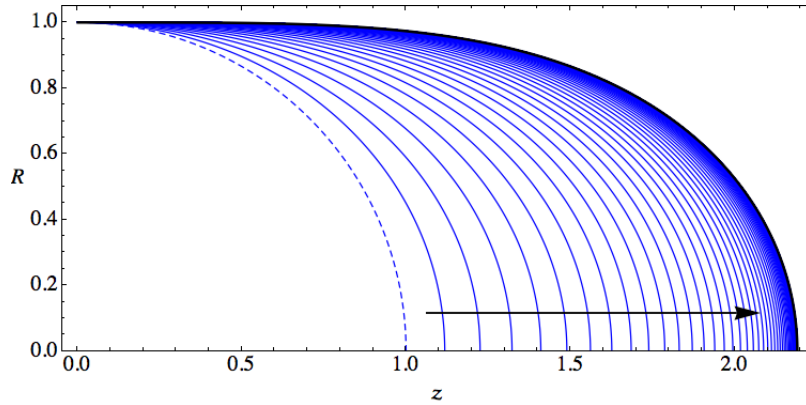


Figure 1: Evolution of the radius of the horizon S^2 , $R(z)$, of the embedding along the flow. The dashed line corresponds to the initial data and the solid black line is the fixed point. The snapshots are drawn at intervals of $\Delta\lambda = 0.05$.

overall factor in the boundary metric and since it is only the conformal class of the latter that is relevant, we can always set $R_0 = 1$ without loss of generality and we shall do that henceforth.

3.1.2 Ricci-DeTurck flow

In this subsection we will describe how we can numerically construct the desired solution using Ricci Flow. Ref. [20] proved that for our metric (3.1) with the boundary conditions previously described, a solution to the Einstein Harmonic equation (2.6) cannot be a Ricci soliton. We should emphasise though that *a priori* we do not know whether an Einstein metric satisfying the desired boundary conditions exists on \mathcal{M} . Therefore, if such a solution does not exist then the Ricci-DeTurck flow will inevitably form a singularity in finite flow time or expand indefinitely for *any* initial data. Moreover, there is a second complication: we do not know *a priori* if the desired solution will be an attractive fixed point of Ricci flow, *i.e.*, it will not have negative modes. In the present situation we could expect that the fixed point, if it exists, will not have negative modes. The heuristic argument is that in AdS/CFT the boundary geometry is non-dynamical and although in our case the boundary metric is $4d$ Schwarzschild, which is known to have a negative mode [28], the fact that it is pinned on the boundary should project out any potential negative modes. In practice we will see that this is indeed what happens. However, *a priori* it is not possible to know whether the fixed point of interest will have negative modes or not; one has to simulate the flow and see if it converges to a fixed point for *generic* initial data. Because we could prove that no Ricci solitons can exist with our boundary conditions, if the flow converges to a fixed point then it must be the Einstein solution we are seeking.

The details of the numerical implementation of the Ricci-DeTurck flow can be found in [20]. It suffices to say that for results presented here we chose as initial data the reference metric and we found that it converged to a fixed point without having to perform any fine-tuning. This fixed point is the solution that we are seeking and, furthermore, since generic initial converges to it we immediately deduce that it is an attractive fixed point and therefore it cannot have negative modes. A direct calculation confirms this latter fact. To present our results, we may embed the horizon of the geometry along the flow into hyperbolic space with the same radius ℓ in axisymmetric coordinates, $ds^2 = \frac{\ell^2}{z^2}(dz^2 + dR^2 + R^2 d\Omega_{(2)}^2)$ as a surface of revolution $R = R(z)$. We fix $R(0) = 1$ and in Fig. 1 we present the evolution of R along the flow.

Now that we have found the Einstein metric that we were seeking, we can extract the boundary stress tensor of the dual field theory using the standard prescription of holographic renormalisation [30]. The

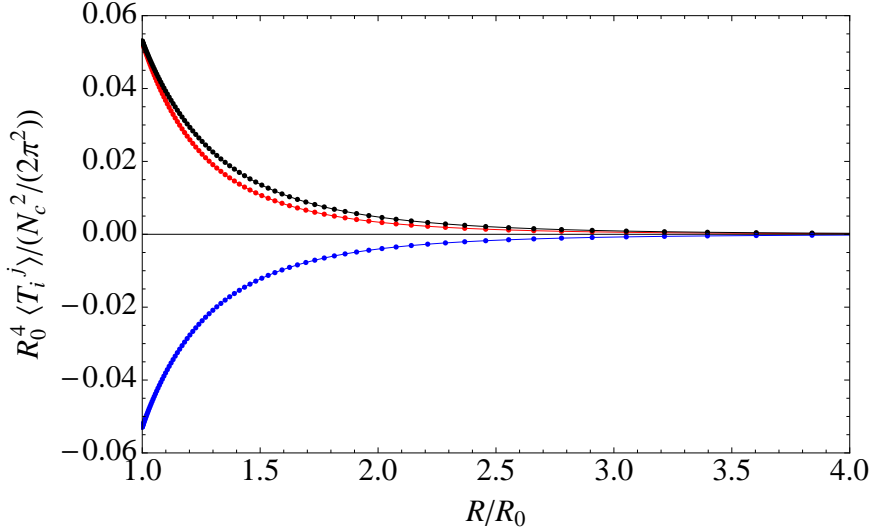


Figure 2: Expectation value of the stress tensor of the dual field theory. In black we depict the $\langle T_\tau^\tau \rangle$ component, in red the $\langle T_R^R \rangle$ component and in blue the $\langle T_\Omega^\Omega \rangle$ components. As this figure shows, at $R = R_0$ we have $\langle T_\tau^\tau \rangle = \langle T_R^R \rangle$, which guarantees the regularity of the stress tensor on the horizon. At large distances, $R \rightarrow \infty$, the various components of the stress tensor decay like $1/R^5$.

calculation is standard (see [20] for the details) and the result, in Schwarzschild coordinates, is

$$\langle T_i^j \rangle = \frac{N_c^2}{2\pi^2} \frac{1}{R^4} \text{diag} \left\{ \frac{3R_0}{4R} \left(1 - \frac{R_0}{R} \right) + t_4(R), \frac{3R_0^2}{4R^2} - (t_4(R) + 2s_4(R)), \right. \\ \left. - \frac{3R_0}{8R} + s_4(R), - \frac{3R_0}{8R} + s_4(R) \right\} \quad (3.2)$$

where the entries correspond to the $\tau\tau$, RR and 2-sphere components respectively. The functions $t_4(R)$ and $s_4(R)$ are related by the conservation of the stress energy tensor (which is implied by the bulk equations of motion) and therefore they are not independent. In any case, they can be determined from fitting the bulk (numerical) solution to the near boundary ($x \rightarrow 1$) expansion.

We note that the stress tensor is traceless, as it should be since the boundary metric is Ricci flat and therefore there is no anomaly in the dual CFT. Also, on the horizon $R = R_0$ we find that all the components of $\langle T_i^j \rangle$ are finite and that $\langle T_\tau^\tau \rangle = \langle T_R^R \rangle$, which guarantees that the stress tensor is regular there. At large distances from boundary black hole, the various components of the stress tensor decay like $1/R^5$. This behaviour matches precisely that linear results of [3].

At the beginning of the section we claimed that our boundary conditions in the IR should imply that the vacuum state of the dual CFT should be either the Unruh or the Boulware vacuum. We will now argue why this is the case. First, one should bear in mind that in the bulk we have performed a classical gravity computation and therefore we only have access to the $O(N_c^2)$ piece of the stress tensor, not the full quantum stress tensor. And, as we shall see, at this order we cannot distinguish between the Unruh and the Boulware vacua. On the other hand, if in the IR we had a horizon with some finite temperature then these other boundary conditions would be the relevant ones the Hartle-Hawking state. Moreover, the $O(N_c^2)$ piece of the stress tensor would differ from ours, among other things because at $R \rightarrow \infty$ there should be finite energy density. For our stress tensor, the energy density decays like $1/R^5$, indicating that at far distances the theory is in the vacuum.

The $O(N_c^2)$ piece of our stress tensor is very interesting since it is regular on both the future and the past event horizons. This must be attributed to a strong coupling effect since for free field theories the Unruh state is time dependent and singular in the past event horizon whereas for the Boulware state it is static but singular both horizons. Moreover, we conjecture that our stress tensor should correspond to

the Unruh state since this is the only physically relevant one captured by our solution. We expect that the time dependence is an $O(1)$ effect that could be detected including 1-loop graviton corrections in the bulk. Since, as this AdS/CFT solution explicitly demonstrates, strong coupling effects significantly alter the behaviour of field theories in black hole backgrounds, then this should also apply to the existence of braneworld black holes in the RSII model. In particular, the non-existence conjecture of [8, 9] was based on free field theory intuition and our results show that this does not apply at strong coupling and large N_c .

The physical picture for this strongly interacting CFT in the Schwarzschild background in our vacuum state is the following. The self-interactions of the CFT are attractive since they are dual to gravity in the bulk which is attractive. On the other hand, there should be Hawking radiation coming out of the black hole, and the pressure created by this radiation perfectly balances the attractive self-interactions of the CFT at every radius. Therefore, there is a static equilibrium at every radius between the radiation and CFT plasma giving rise to an $O(N_c^2)$ stress tensor. Also, note that since the boundary geometry is non-dynamical the black hole should be regarded as being a source with infinite energy. Finally, at asymptotic infinity there is no flux of energy since $\frac{1}{N_c^2}\langle T_\tau^\tau \rangle = O(R^{-5})$ at large R .

We close this subsection discussing the stability of our solution. From the shape of the horizon (see black curve in Fig. 1), it could be that there is an instability of the Gregory-Laflamme type. However, it turns out that the proper length of the horizon in the direction orthogonal to the boundary is too small for the unstable modes to fit. In addition, our solution has no negative modes and therefore we expect that it will be stable. However, we have not performed a proper study of the perturbations and it is important to include the possibility of instabilities that involve the internal space in the full $10d$ solution or that are localised near the tip of the horizon in the bulk.

3.2 Black holes in the RSII model

In this subsection we will review the numerical construction of [21] of braneworld black holes in the RSII model, together with some new results [31].

3.2.1 Large braneworld black holes from AdS/CFT

Consider first the near boundary expansion of the AdS₅-CFT₄ solution described in the previous subsection in the standard Fefferman-Graham coordinates:

$$ds^2 = \frac{1}{z^2} (dz^2 + \tilde{g}_{\mu\nu}(z, x) dx^\mu dx^\nu), \quad (3.3)$$

with

$$\begin{aligned} \tilde{g}_{\mu\nu}(z, x) = & g_{\mu\nu}^{(0)}(x) + z^2 \left(R_{\mu\nu}^{(0)}(x) - \frac{1}{4} g_{\mu\nu}^{(0)}(x) R^{(0)}(x) \right) + z^4 \left(g_{\mu\nu}^{(4)}(x) + t_{\mu\nu}(x) \right) \\ & + 2z^4 \log z h_{\mu\nu}^{(4)}(x) + O(z^6), \end{aligned} \quad (3.4)$$

and the expressions for $g^{(4)}$ and $h^{(4)}$ are given in [30]. Here $g_{\mu\nu}^{(0)}$ is the boundary metric ($4d$ Schwarzschild in our case), $R_{\mu\nu}^{(0)}$ is the Ricci tensor corresponding to this metric, and $t_{\mu\nu}$ is related to the vev of the stress tensor of the boundary CFT by $\langle T_{\mu\nu}^{CFT} \rangle = t_{\mu\nu}/(4\pi G_5)$. In our case the boundary stress tensor is given by (3.2).

Now *assume* that there exists a smooth solution in AdS₅ such that its boundary metric is given by a perturbation of $4d$ Schwarzschild, $g_{\mu\nu}^{(0)} = g_{\mu\nu}^{Schw} + \epsilon^2 h_{\mu\nu}$ and deep in the IR it asymptotes to the Poincare horizon of AdS₅.³³ Ref. [21] argued that if such a perturbation exists then it is possible to slice the resulting spacetime with a RSII brane located at $z = \epsilon$. Moreover, the induced metric on the brane is given by

$$\gamma_{\mu\nu} = \frac{\ell^2}{\epsilon^2} (g_{\mu\nu}^{Schw} + \epsilon^2 h_{\mu\nu}). \quad (3.5)$$

From this equation it is clear that the radius of the black hole on the brane is parametrically much larger than the radius of AdS₅. Furthermore, the induced geometry on the brane is given by $4d$ Schwarzschild

³³For a well-posed boundary value problem one expects to be able to slightly deform the boundary data and find a nearby solution.

plus a small, $O(\epsilon^2)$, perturbation. Therefore, we conclude that in RSII $4d$ gravity is recovered on the brane for black holes whose size is much larger than the radius of AdS_5 .

In the absence of brane matter, [21] showed that the perturbation $h_{\mu\nu}$ satisfies the perturbed Einstein equations with a source given precisely by the CFT stress tensor computed in §3.1 (see also [32]):

$$\delta G_{\mu\nu} = 16\pi G_4 \langle T_{\mu\nu}^{CFT} \rangle, \quad (3.6)$$

where $\delta G_{\mu\nu}$ is the perturbation of the Einstein tensor around $4d$ Schwarzschild and the right-hand-side is given by (3.2). Finally we mention that including matter on the brane then the CFT stress tensor does not give rise to the main correction (see [21] for the details).

3.2.2 Large braneworld black holes in RSII

In the previous subsection we argued that given the existence of the $\text{AdS}_5\text{-CFT}_4$ solution described in §3.1, then it should be possible to perturb it and construct a large black hole on the brane. In this subsection we will describe how this can be done in practice.

Since we expect that large braneworld black holes should be well-approximated by the $\text{AdS}_5\text{-CFT}_4$ solution, we start by making an ansatz that is “close” to the AdS/CFT solution (3.1):

$$ds^2 = \frac{\ell^2}{\Delta(r, x)^2} \left(4r^2 f(r)^2 e^T d\tau^2 + x^2 g(x) e^S d\Omega_{(2)}^2 + \frac{4}{f(r)^2} e^{T+r^2 f(r)A} dr^2 + \frac{4}{g(x)} e^{S+x^2 B} dx^2 + \frac{2rx}{f(r)} F dr dx \right), \quad (3.7)$$

$$\Delta(r, x) = (1 - x^2) + \epsilon(1 - r^2),$$

and $f(r) = 1 - r^2$, $g(x) = 2 - x^2$ as before. Here ϵ is a parameter that effectively measures the radius of AdS_5 with respect to the radius of the black hole on the brane. Therefore, taking $\epsilon \rightarrow 0$ we recover the $\text{AdS}_5\text{-CFT}_4$ solution described in §3.1. In our calculation we will vary this parameter to effectively move along the branch of solutions and therefore it need not be small when the black hole on the brane is small compared to the radius of AdS_5 . As in §3.1, the functions $X = \{T, S, A, B, F\}$ are the unknowns and they depend on the coordinates r and x only. The coordinate ranges can be taken to be the same as in §3.1, and similarly for the boundary conditions. The main difference though is that now we will place the brane at $x = 1$ by imposing the usual Israel junction conditions there. Notice that the form of the function $\Delta(r, x)$ is such that it does not vanish at $x = 1$ and hence there is no UV conformal boundary there.

On the other hand, when the black hole on the brane is very small the expectation is that the full spacetime should be “close” to that of $5d$ asymptotically flat Schwarzschild black hole (see for instance [13, 16]). Then we can also construct an ansatz which is well suited for the small black hole limit by building in it the $5d$ AF Schwarzschild geometry as follows:

$$ds^2 = \frac{\ell^2}{\Delta(r, x)^2} \left(4r^2 g(r) f(r)^2 e^T d\tau^2 + x^2 g(x) e^S d\Omega_{(2)}^2 + \frac{4}{f(r)^2 g(r)} e^{T+r^2 f(r)A} dr^2 + \frac{4}{g(x)} e^{S+x^2 B} dx^2 + \frac{2rx}{f(r)} F dr dx \right), \quad (3.8)$$

where the functions $f(\xi)$, $g(\xi)$ and $\Delta(r, x)$ have the same definitions as above and similarly for the coordinate ranges and boundary conditions. The virtue of this ansatz (3.8) is that stripping off the conformal factor $\ell^2/\Delta(r, x)^2$ and setting $X = 0$ it reduces to $5d$ AF Schwarzschild with a unit horizon radius, and therefore it should be well-suited for finding small RSII black holes.

We will solve numerically the Harmonic Einstein equations with a negative cosmological constant,

$$R_{ab} + \frac{4}{\ell^2} - \nabla_{(a} \xi_{b)} = 0, \quad \xi^a = g^{bc} (\Gamma_{bc}^a - \bar{\Gamma}_{bc}^a), \quad (3.9)$$

where $\bar{\Gamma}$ is a reference connection associated to a reference metric \bar{g} . For the latter we will take (3.7) or (3.8), depending on the situation, with $X = 0$ in either case. The boundary conditions for the metric are

the usual regularity at the horizon ($r = 0$) and at the axis of symmetry ($x = 0$), and at $r = 1$ we will require that the metric reduces to the extremal Poincare horizon of AdS₅. We want to place the brane at $x = 1$ and therefore will impose the Israel junction conditions with no matter on the brane,

$$K_{ij} = \frac{1}{\ell} \gamma_{ij} \quad (3.10)$$

where K_{ij} is the extrinsic curvature of the $x = 1$ hypersurface and γ_{ij} is the corresponding induced metric. Notice that (3.10) only imposes conditions on the components of the metric tangent to the brane, namely T , S and A . Therefore we still need to provide extra boundary conditions for the remaining metric components. Since we want to find solutions to (3.9) which are Einstein, one would be tempted to require $\xi^r = \xi^x = 0$ at $x = 1$ in order to fully specify the boundary value problem while ensuring the vanishing of the DeTurck vector field. It turns out though that these boundary conditions are not compatible with ellipticity, that is to say, there is not a locally unique solution that satisfies these boundary conditions. As shown in [20], it turns out that the correct (*i.e.*, compatible with a regular elliptic problem) boundary conditions are $F = 0$ and $\xi^x = 0$ at $x = 1$. The condition on ξ^x can be understood from the fact that ξ^x generates diffeomorphisms in the directions orthogonal to the brane and requiring the vanishing of this component of the DeTurck vector fixes the location of the brane. However, with these boundary conditions a complication arises, and it is that the maximum principle argument of [20] cannot be used to rule out the existence of Ricci solitons on \mathcal{M} . The reason is that (3.10) together with $\xi^x = 0$ and $F = 0$ at $x = 1$ imply that $\partial_n \xi_r = \frac{2}{\ell} \xi_r$ on the brane, where ∂_n denotes the outward pointing normal derivative. Although this condition is compatible with $\xi_r = 0$, it does not imply it and, furthermore, is compatible with the existence of a maximum of ϕ on the brane. Therefore, we will have to check a posteriori if the solutions to (3.9) are Ricci solitons. At this stage it suffices to say that we did not find any evidence for the latter.

3.2.3 Results: Ricci flow

As we have explained in §2 we can numerically solve (3.9) simulating the associated Ricci flow equation, (2.10). This method works particularly well if the fixed point is attractive but, as we will now argue, large braneworld black holes, if they exist, should be *unstable* fixed points of the flow. The reason is that, contrary to the AdS/CFT situation in §3.1 where the boundary geometry is non-dynamical, now gravity on the brane is dynamical. Moreover, we have argued in §3.2.1 that large braneworld black holes should be well-approximated by $4d$ Schwarzschild, which is known to have a negative mode. Therefore, by continuity one should expect them to have at least one negative mode.

The fact that the fixed point we are trying to find is unstable should not stop us from using this method, especially if the fixed point is expected to have only one negative mode. More importantly, one of the main advantages of the Ricci flow method is that it can provide convincing evidence for the existence of a fixed point on a certain manifold in a coordinate invariant manner. This property of Ricci flow is especially attractive in the context of finding static and non-extremal braneworld black holes in RSII, since the existence of such solutions has been questioned [8, 9, 16].

Since we expect the solutions we seek will have one negative mode, we will have to introduce a parameter in our ansatz, eq. (3.7) or (3.8). Then we will have to fine-tune this parameter so that the initial data lies close enough to the hypersurface in the space of geometries on \mathcal{M} which is orthogonal to the negative mode. One way (certainly not the only one) of doing this is to replace in (3.7) or (3.8) the $\tau\tau$ and rr components of the metric by [23]

$$g_{\tau\tau} \rightarrow k(r) g_{\tau\tau}, \quad g_{rr} \rightarrow k(r) g_{rr}, \quad k(r) = 1 - \alpha(1 - r^2)^2, \quad (3.11)$$

where α is the parameter that we will fine-tune. Notice that with this parameter we can vary the surface gravity while keeping the size of the time-circle at infinity and hence the temperature fixed.

With this one-parameter generalisation of our ansatz we simulated (2.10), using the reference metric as our initial data. For the actual numerical implementation of the flow we evolved in time using simple forward Euler method and at every time along the flow we imposed the boundary conditions described in the previous subsection. This implies solving the Israel junction conditions (3.10), which are non-linear equations, at every time step. This is important in order to correctly simulate the flow on \mathcal{M} , which now

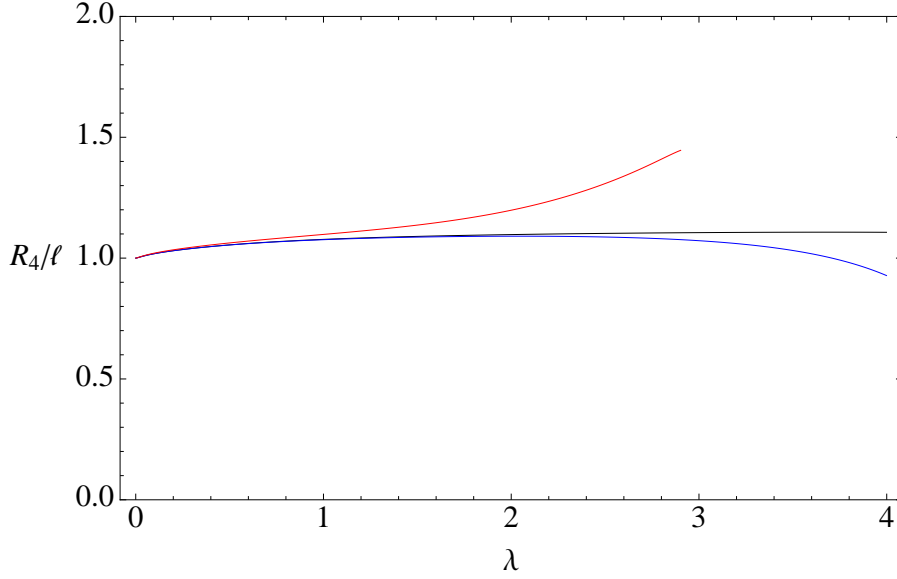


Figure 3: Radius of the black hole on the brane, R_4/ℓ , as a function of the Ricci flow time λ for $\alpha = 0.490583$ (black), 0.5 (red), 0.49 (blue), and fixed inverse temperature $\beta = 4\pi\ell$. For the flow with $\alpha \approx \alpha_*$, the radius of the black hole on the brane remains constant for an arbitrarily long time, and thus providing strong evidence for the existence of a fixed point and hence a braneworld black hole with this horizon radius.

has a brane as a boundary. To solve this non-linear problem numerically we used Newton's algorithm described in §2, now applied to the boundary conditions. This method has the advantage that it homes in the solution very quickly if one starts sufficiently close to it. Since as initial data we took the reference metric (with the same value of the parameter α) which satisfies all boundary conditions, including (3.10). Then, taking sufficiently small time-steps, we could efficiently use the previous solution as the initial guess and the latter was always close to the actual solution corresponding to the next time step.

For fixed horizon temperature, as we varied α we observed two markedly different flows depending on the value of this parameter: For $\alpha > \alpha_*$ the horizon expands indefinitely and for $\alpha < \alpha_*$ a singularity forms in finite flow time. On the other hand, for α sufficiently close to the critical value α_* the flow stays close to the fixed point for an arbitrarily long flow time. The existence of these flows provides strong evidence for the existence of a fixed point, and therefore a braneworld black hole. In Fig. 3 we present our results for the Ricci flow of a braneworld black hole of $R_4/\ell \approx 1.2$ and $\alpha_* \approx 0.490583$. In this case it is also worth noting that for the fine-tuned flow and in the region of the flow where R_4/ℓ is approximately constant, the DeTurck vector vanishes (within numerical accuracy) everywhere on the spacetime and in particular on the brane. Therefore, we conclude that the metric we are finding is *not* a Ricci soliton. Finally, we mention that as we vary the temperature of the black hole on the brane we have to fine-tune the parameter α so as to find the new critical value. In any case, we observed the existence of a critical flow for braneworld black holes of sizes $0.1 \lesssim R_4/\ell \lesssim 10$, thereby finding strong numerical evidence for the existence of such solutions.

We want to emphasise that this result is independent of the choice of reference metric and it provides global information on the space of geometries on \mathcal{M} . In particular it tells us about the existence of an Einstein metric on \mathcal{M} and therefore, a localised black hole on the brane.

3.2.4 Results: Newton's method

In the previous subsection we used Ricci flow to provide strong evidence for the existence of braneworld black holes of various sizes. However, the Ricci flow method is not very useful in practice to find the solutions to high accuracy since this requires a considerable amount of fine-tuning. In addition, for every

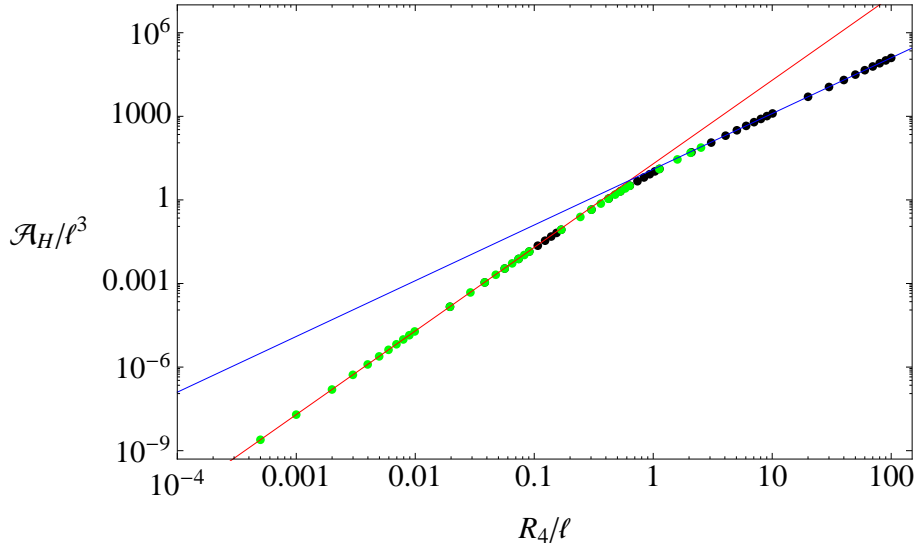


Figure 4: Area of the horizon as a function of its radius on the brane. The black (green) dots correspond to the data obtained with the ansatz (3.7) and (3.8) respectively. In the overlapping region both ansätze give same results for the various physical quantities. The red (blue) line corresponds the area of the horizon as a function of its radius for a 5d and 4d asymptotically flat Schwarzschild black hole respectively. Note that we have used log scale in both axes.

different temperature we have to do the fine-tuning again and therefore this method is not optimal for exploring the branch of solutions. In fact, as pointed out in [22], it may be that for certain black hole sizes our initial data (3.11) may fail to intersect the hypersurface in the space of geometries where the fixed point lies, and therefore we would not be able to find solutions.

To efficiently explore the branch of solutions we will use Newton's method. We find that for black holes whose radius on the brane is large ($R_4/\ell \gtrsim 10$) using (3.7) and the reference metric as the initial guess is sufficient for the algorithm to converge. Similarly, using the ansatz (3.8) and the reference metric as the initial guess Newton's method can find solutions for sufficiently small black holes ($R_4/\ell \lesssim 0.1$). We should point out that sometimes it may not be so easy to find a suitable initial guess which lies close enough to the solution. In those cases, one can use Ricci flow and with a fair amount of fine-tuning it is possible to construct a good enough initial guess so that Newton's method can home in the solution very quickly.

To numerically construct the solutions we have used a pseudospectral collocation approximation in both the r and x directions up to 40×40 points. This gives highly accurate results and the data presented here is based on this latter resolution. Once we had found one solution then we could easily find nearby ones by varying slightly the temperature, perturbing accordingly the reference metric and use the old solution as the new initial guess. Using this procedure and combining both ansätze, eqs. (3.7) and (3.8), we could find braneworld black holes whose radius on the brane was within the range $5 \times 10^{-3} \lesssim R_4/\ell \lesssim 100$. The results are displayed in Fig. 4, where we plot the full five-dimensional area of the horizon against the radius of the black hole on the brane obtained with the ansatz (3.7) (black dots) and (3.8) (green dots) respectively. We clearly see that in the overlapping region both ansätze give the same results. On that plot we also display the behaviour of the area as a function of its radius for a 5d (red) and 4d (blue) asymptotically flat Schwarzschild black hole. As one can clearly see from this plot, the geometry of braneworld black holes smoothly interpolates between a 5d behaviour when the black hole is small ($R_4 \ll \ell$) and a 4d behaviour when it is large ($R_4 \gg \ell$).³⁴ Therefore, we indeed find that standard 4d

³⁴In the context of Kaluza-Klein black holes there is a similar interpolation between 5d and 4d black hole physics, but in that case it is not smooth since there is a singular topology change transition.

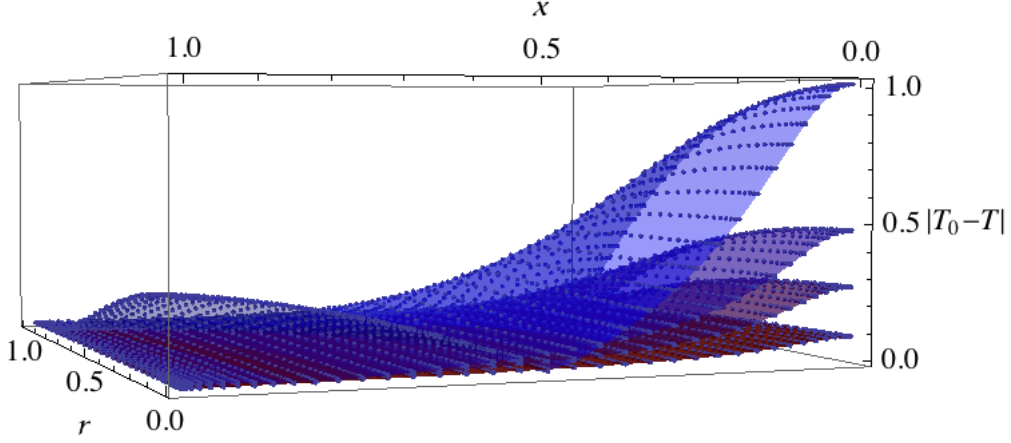


Figure 5: Difference $|T_0 - T|$ between the function T controlling the norm of ∂_τ in the AdS₅-CFT₄ (denoted by T_0) and in braneworld black holes (denoted by T) of sizes $R_4/\ell = 1, 5, 10, 30$ from top to bottom. As the black hole on the brane becomes larger the difference $|T_0 - T|$ converges uniformly to zero.

GR is recovered on the brane when the black holes are sufficiently large.

In §3.2.2 we argued that large braneworld black holes should be “close” to the AdS₅-CFT₄ solution discussed in 3.1. Now that we have constructed the solutions numerically we can make a more quantitative comparison. In Fig 5 we consider the difference between the function T appearing in the $\tau\tau$ component of metric in the AdS₅-CFT₄ solution and in braneworld black holes of sizes $R_4/\ell = 1, 5, 10, 30$. Since this function is associated to the norm of the Killing field ∂_τ it is a gauge invariant quantity. As we can see from this plot, as the black hole on the brane becomes larger it is better and better approximated by the AdS/CFT solution. This provides a nice confirmation of the correctness of the argument in §3.2.1.

Ref. [21] also considered the embeddings of the spatial cross sections of the horizon into \mathbb{H}^4 for braneworld black holes of various sizes. In Fig. 2 of this reference one can see that the intrinsic geometry of the horizon becomes closer to the AdS/CFT solution as the black hole on the brane becomes larger, which is yet another confirmation that large braneworld black holes are well-approximated by the AdS/CFT solution. One can check that the shape of the horizon is pancake-like in accordance with previous expectations [4, 6, 7], so that the extent of the horizon in the directions tangent to the brane is much larger than the extent into the bulk. This should imply that Gregory-Laflamme-type of instabilities [33, 34] that could cause ripples to develop along the directions transverse to the brane should not fit into the horizon. Therefore we expect that large braneworld black holes to be dynamically stable under this type of perturbations. We can provide evidence for this by computing the spectrum of the Harmonic Einstein equation about our solutions restricted to stationary and axisymmetric modes. Note that in Newton’s algorithm we already have to compute the linearisation of the Harmonic Einstein equation. In addition, for transverse and traceless modes, the spectrum of the Harmonic Einstein equation about an Einstein solution coincides with the spectrum of the Lichnerowicz operator. We display our results in Fig. 6. As can be seen from this plot, there exists one and only one negative mode, which tends to the negative mode of the asymptotically flat $5d$ Schwarzschild solution when the black hole on the brane is small. Small braneworld black holes are close to the latter solution and therefore they should be stable. The absence of zero modes and new negative modes as we move towards braneworld black holes

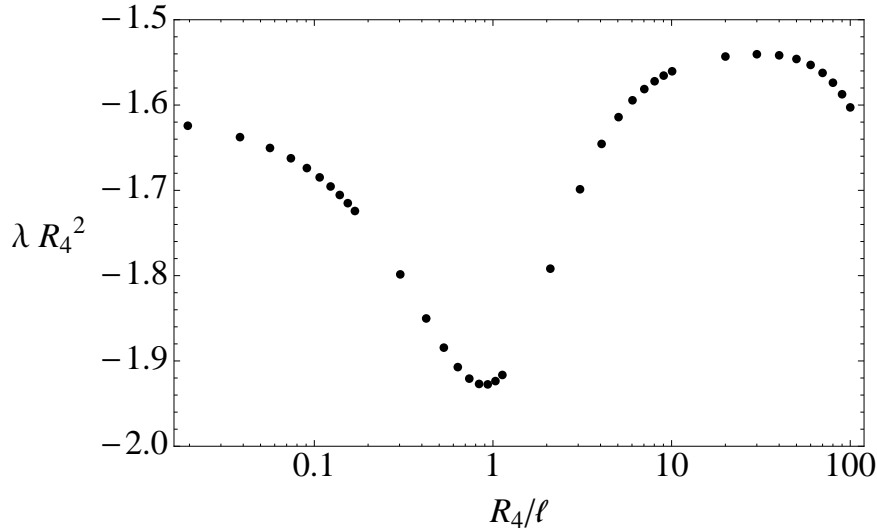


Figure 6: Spectrum of the Lichnerowicz operator computed about our solution. We find that there is one and only one negative mode, which provides evidence that braneworld black holes are dynamically stable under Gregory-Laflamme instabilities. Note that the negative mode tends to the negative mode of the asymptotically flat 5d Schwarzschild black hole when R_4/ℓ becomes sufficiently small.

of larger radius suggests that these should also be dynamically stable. It would be interesting to carry out a detailed analysis of the gravitational perturbations.

Finally present some results of the various numerical convergence tests that we have performed. Recall that with the boundary conditions (3.10) we could not analytically prove the non-existence of Ricci solitons. Therefore, a posteriori we have to check that indeed our solutions are Einstein. To check this we can monitor the quantity $\phi = \xi^\alpha \xi_\alpha$ as we increase the resolution of our code; if the solutions are Einstein, then this quantity should tend to zero in the continuum limit. If that is the case, then we can use it to measure the numerical error. In Fig. 7 we present the convergence tests for the ansatz (3.7) (the other ansatz (3.8) gives similar results). As this plot clearly shows, $\phi_{\max} R_4^2 \rightarrow 0$ in the continuum limit and in accordance with our discretisation scheme. Note that the numerical error is larger for very large or very small black holes, which is expected since we have to resolve widely separated scales, namely the horizon radius on the brane and the radius of AdS.

4 Conclusions

In this article we have reviewed the recent results of [20, 21] where the numerical construction of localised black holes on the brane of all sizes in the RSII model was done. A crucial aspect of these works was the use of the new method of [22, 23] for casting the Einstein equations in a manifestly elliptic form. We have reviewed this new approach in §2, together with two basic algorithms (Ricci flow and Newton’s method) for numerically solving the resulting non-linear equations as a boundary value problem. The Ricci flow method has the great advantage of being a geometric method that can provide invariant information about the existence of solutions to the equations (2.6). This is of special importance in the context of the braneworld black holes in RSII, whose existence was not clear before the previous works. Newton’s method, although more difficult to implement and being non-geometrical, converges very quickly and it allows to find solutions to a high accuracy.

In §3, firstly we have seen how to construct a solution in AdS₅ such that its boundary metric is conformal to 4d Schwarzschild and in the IR tends to the Poincare horizon of AdS. This solution is especially relevant for the braneworld black hole problem since large braneworld black holes can be very

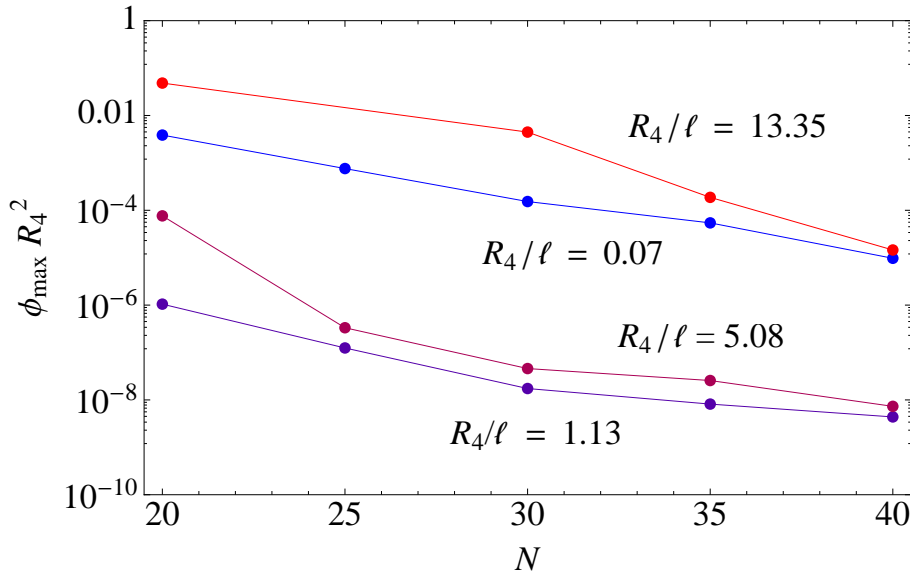


Figure 7: Maximum value of ϕ over the whole domain, including the brane, for braneworld black holes of radius $R_4/\ell = 13.35, 5.04, 1.13, 0.07$ as a function of the number of grid points N . This quantity tends to zero in the continuum limit, indicating that our solutions are indeed Einstein. A similar behaviour is observed for black holes of other sizes.

well approximated by this AdS/CFT solution. In addition, the non-existence arguments of [8, 9] could be applied to this solution as well, and its existence shows that they are not correct. In §3.2 we have reviewed (and extended) the results of [21], where black holes on the brane with radius $5 \times 10^{-3} \lesssim R_4/\ell \lesssim 100$ were constructed. This work settles down the issue of the existence of braneworld black holes. In addition, we have provided evidence that these objects should be dynamically stable.

Acknowledgements

It is a great pleasure to acknowledge the contributions of my collaborators, J. Lucietti and T. Wiseman, from whom I have benefited so much; without them the works reviewed here would not have been possible. I would also like to thank the organisers of the JGRG21 workshop for the invitation and for organising such a successful and enjoyable event. I would also like to thank all the Japanese people for their efforts in recovering from the Great East Earthquake. I am supported by an EPSRC postdoctoral fellowship [EP/H027106/1].

References

- [1] L. Randall, R. Sundrum, “A Large mass hierarchy from a small extra dimension,” *Phys. Rev. Lett.* **83** (1999) 3370-3373. [hep-ph/9905221].
- [2] L. Randall, R. Sundrum, “An Alternative to compactification,” *Phys. Rev. Lett.* **83** (1999) 4690-4693. [hep-th/9906064].
- [3] J. Garriga, T. Tanaka, “Gravity in the brane world,” *Phys. Rev. Lett.* **84** (2000) 2778-2781. [hep-th/9911055].
- [4] S. B. Giddings, E. Katz, L. Randall, “Linearized gravity in brane backgrounds,” *JHEP* **0003** (2000) 023. [hep-th/0002091].

- [5] A. Chamblin, S. W. Hawking, H. S. Reall, “Brane world black holes,” *Phys. Rev.* **D61** (2000) 065007. [hep-th/9909205].
- [6] R. Emparan, G. T. Horowitz, R. C. Myers, “Exact description of black holes on branes,” *JHEP* **0001**, 007 (2000). [hep-th/9911043].
- [7] R. Emparan, G. T. Horowitz, R. C. Myers, “Exact description of black holes on branes. 2. Comparison with BTZ black holes and black strings,” *JHEP* **0001** (2000) 021. [hep-th/9912135].
- [8] T. Tanaka, “Classical black hole evaporation in Randall-Sundrum infinite brane world,” *Prog. Theor. Phys. Suppl.* **148** (2003) 307-316. [gr-qc/0203082].
- [9] R. Emparan, A. Fabbri, N. Kaloper, “Quantum black holes as holograms in AdS brane worlds,” *JHEP* **0208** (2002) 043. [hep-th/0206155].
- [10] A. L. Fitzpatrick, L. Randall, T. Wiseman, “On the existence and dynamics of braneworld black holes,” *JHEP* **0611** (2006) 033. [hep-th/0608208].
- [11] T. Wiseman, “Relativistic stars in Randall-Sundrum gravity,” *Phys. Rev.* **D65** (2002) 124007. [hep-th/0111057].
- [12] T. Wiseman, “Static axisymmetric vacuum solutions and nonuniform black strings,” *Class. Quant. Grav.* **20** (2003) 1137-1176. [hep-th/0209051].
- [13] H. Kudoh, T. Tanaka, T. Nakamura, “Small localized black holes in brane world: Formulation and numerical method,” *Phys. Rev.* **D68** (2003) 024035. [gr-qc/0301089].
- [14] H. Kudoh, “Thermodynamical properties of small localized black hole,” *Prog. Theor. Phys.* **110** (2004) 1059-1069. [hep-th/0306067].
- [15] H. Kudoh, “Six-dimensional localized black holes: Numerical solutions,” *Phys. Rev.* **D69** (2004) 104019. [hep-th/0401229].
- [16] H. Yoshino, “On the existence of a static black hole on a brane,” *JHEP* **0901** (2009) 068. [arXiv:0812.0465 [gr-qc]].
- [17] B. Kleihaus, J. Kunz, E. Radu, D. Senkbeil, “Electric charge on the brane?,” *Phys. Rev.* **D83**, 104050 (2011). [arXiv:1103.4758 [gr-qc]].
- [18] A. Kaus, H. S. Reall, “Charged Randall-Sundrum black holes and N=4 super Yang-Mills in AdS(2) x S**2,” *JHEP* **0905** (2009) 032. [arXiv:0901.4236 [hep-th]].
- [19] A. Kaus, “Perturbations around the near horizon limit of charged Randall Sundrum black holes,” [arXiv:1105.4739 [hep-th]].
- [20] P. Figueras, J. Lucietti, T. Wiseman, “Ricci solitons, Ricci flow, and strongly coupled CFT in the Schwarzschild Unruh or Boulware vacua,” *Class. Quant. Grav.* **28**, 215018 (2011). [arXiv:1104.4489 [hep-th]].
- [21] P. Figueras, T. Wiseman, “Gravity and large black holes in Randall-Sundrum II braneworlds,” [arXiv:1105.2558 [hep-th]].
- [22] M. Headrick, S. Kitchen, T. Wiseman, “A New approach to static numerical relativity, and its application to Kaluza-Klein black holes,” *Class. Quant. Grav.* **27**, 035002 (2010). [arXiv:0905.1822 [gr-qc]].
- [23] T. Wiseman, “Numerical construction of static and stationary black holes,” [arXiv:1107.5513 [gr-qc]].
- [24] A. Adam, S. Kitchen, T. Wiseman, “A numerical approach to finding general stationary vacuum black holes,” [arXiv:1105.6347 [gr-qc]].

- [25] D. M. DeTurck, “Deforming metrics in the direction of their Ricci tensors,” *J. Differ. Geom.*, **18**:15762 (1983).
- [26] N. Koiso “On rotationally symmetric Hamilton’s equation for Kähler-Einstein metrics,” *Recent Topics in Differential and Analytic Geometry*, Adv. Stud. Pure Math. **18** (Boston, MA: Academic) pp 327-37 (1990).
X.-J. Wang and X. Zhu, “Kähler-Ricci solitons on toric manifolds with positive first Chern class,” *Adv. Math.* **188** 87-103 (2004).
H.-D. Cao, “Geometry of Ricci solitons,” *Chin. Ann. Math. Ser. B.* **27** 121-42 (2006).
M. Headrick and T. Wiseman, “Numerical Kähler-Ricci soliton on the second del Pezzo,” [arXiv:0706.2329].
- [27] J. P. Bourguignon, In *Global differential geometry and global analysis* (Berlin, 1979), vol. 838 of *Lecture notes in Math.* pp 42-63, Springer, Berlin 1981.
- [28] D. J. Gross, M. J. Perry, L. G. Yaffe, “Instability of Flat Space at Finite Temperature,” *Phys. Rev.* **D25** (1982) 330-355.
- [29] M. T. Anderson, P. T. Chrusciel, E. Delay, “Nontrivial, static, geodesically complete, vacuum spacetimes with a negative cosmological constant,” *JHEP* **0210** (2002) 063. [gr-qc/0211006].
- [30] S. de Haro, S. N. Solodukhin, K. Skenderis, “Holographic reconstruction of space-time and renormalization in the AdS / CFT correspondence,” *Commun. Math. Phys.* **217** (2001) 595-622. [hep-th/0002230].
- [31] P. Figueras, T. Wiseman, *in preparation*.
- [32] S. de Haro, K. Skenderis, S. N. Solodukhin, “Gravity in warped compactifications and the holographic stress tensor,” *Class. Quant. Grav.* **18** (2001) 3171-3180. [hep-th/0011230].
- [33] R. Gregory and R. Laflamme, “Black strings and p-branes are unstable,” *Phys. Rev. Lett.* **70** (1993) 2837 [hep-th/9301052].
- [34] R. Gregory, “Black string instabilities in Anti-de Sitter space,” *Class. Quant. Grav.* **17** (2000) L125 [hep-th/0004101].

Astrophysical censorship

Umpei Miyamoto^{35(a)}, Sanjay Jhingan^(b), Tomohiro Harada^(a)

^(a)*Department of Physics, Rikkyo University, Tokyo 171-8501, Japan*

^(b)*Centre for Theoretical Physics, Jamia Millia Islamia, New Delhi 110025, India*

Abstract

There are several solutions to the Einstein equation exhibiting naked-singularity formation in gravitational collapse, which could possibly serve as counterexamples to the cosmic censor hypothesis. It has not been examined seriously, however, whether or not such naked singularities are indeed visible to asymptotic observers in astrophysically realistic stellar collapse, such as the core collapse and the delayed collapse in the final stage of stellar evolution. In this study, we set the spherically symmetric mass distribution which is motivated by the astrophysical scenarios and evolve it with vanishing pressure for simplicity. We show that even if a naked singularity could appear at the centre, the naked singularity is hidden behind an event horizon and cannot be observed by a distant observer. With this illustration, we argue the existence of an “astrophysical censor” that prohibits singularities formed in astrophysical gravitational collapse from being observed by a distant observer.

1 Introduction

Singularity theorems have been one of the most important developments in the theory of classical general relativity [1]. These theorems ensure that under very general and physically reasonable conditions singularities are bound to occur in nature. To ensure the validity of classical laws of physics, a hypothesis that a physically realistic gravitational collapse within classical general relativity will never result in a naked singularity, called cosmic censorship [2], was proposed. By a globally naked singularity we mean the existence of future-directed non-spacelike curves from a singularity to a far-away observer, implying the violation of weak censorship. If all the future-directed non-spacelike curves fall back into the singularity we only have the violation of strong censorship, where the singularity is termed as a locally naked singularity.

If the cosmic censorship is violated in any sense, it would be important whether the violation can be tested experimentally or observationally. In this study we analyze the formation of singularity and its causal structure based on the astrophysically realistic collapse scenarios in the final stage of stellar evolution, such as the core collapse and the delayed collapse. One can say that naked singularities are harmless in a sense if they do not disturb an asymptotic observer. For the asymptotic observer the violation of strong censorship causes no harm. Therefore, as for the direct testability of the violation of the cosmic censorship, it is important whether or not the weak cosmic censorship conjecture is preserved or not. With this perspective we analyze here the well known Lemaître-Tolman-Bondi model [3] with the initial conditions where naked singularities are known to appear as an outcome of the evolution.

We begin with reviewing the basic framework of the dust-collapse model. The next section deals with the main results of this study. We work in the geometrized unit ($c = G = 1$), otherwise denoted.

2 Spherical dust (LTB) model as stellar collapse

The energy-momentum tensor of a pressureless fluid is written as $T^{\mu\nu} = \rho u^\mu u^\nu$, with the energy density ρ and the normalized velocity field u^μ ($u^\mu u_\mu = -1$). Solving the Einstein equations with the spherically symmetric ansatz, the Lemaître-Tolman-Bondi (LTB) solution is obtained in comoving synchronous

³⁵Email address: umpei@rikkyo.ac.jp

coordinates ($u^\mu = \delta_t^\mu$) as

$$ds^2 = -dt^2 + \frac{R^2}{1+f(r)} dr^2 + R^2(t,r) d\Omega^2, \quad \dot{R}^2 = f(r) + \frac{F(r)}{R}, \quad \rho(t,r) = \frac{F'}{8\pi R^2 R}, \quad (2.1)$$

where $X' = \partial_r X$, $\dot{X} = \partial_t X$, and $d\Omega^2$ is the line element of a unit two-sphere. $F(r)$ and $f(r)$ are integration constants, and fixed once the initial distributions of mass and velocity of the fluid are specified. Integrating equation of \dot{R} , we obtain $R = R(t,r)$ in an implicit form

$$t - t_s(r) = -\frac{R^{3/2}}{\sqrt{F}} G\left(-\frac{fR}{F}\right), \quad (2.2)$$

where $t_s(r)$ is a constant of integration and $G(y) = \frac{\text{Arcsin}\sqrt{y}}{y^{3/2}} - \frac{\sqrt{1-y}}{y}$ ($0 < y \leq 1$). With the coordinate degrees of freedom available, one can choose initial time at $t = 0$ and fix $R(0,r) = r$ without any loss of generality. Then, the expression for time when a fluid element defined by a particular $r = \text{const.}$ value plunges into the shell-focusing singularity, which is defined by $R = 0$, is given by

$$t_s(r) = \frac{r^{3/2}}{\sqrt{F}} G\left(-\frac{fr}{F}\right). \quad (2.3)$$

For spherically symmetric systems the condition for the existence of an apparent horizon (i.e., an inner boundary of the region containing trapped surfaces), corresponds to the existence of two-spheres whose outward normals are null, is given by $R = F$.

In LTB models, we have the following relation between the singularity and the apparent horizon (AH) curve $t_{\text{AH}}(r) = t_s(r) - FG(-f)$. This equation is crucial in understanding the causal structure of singularity in LTB models. Since G is a positive and convex function, the positivity of mass F implies $t_{\text{AH}}(r) < t_s(r)$ for the non-central shells ($r > 0$). It is only at the centre that the regularity condition on the initial data demands the mass function F should be zero and hence the singularity and the apparent horizon appear simultaneously, i.e., $t_{\text{AH}}(0) = t_s(0)$. Thus it is only the central singularity which can be a naked shell-focusing singularity. In what follows we shall be interested in the central shell-focusing singularity.

In this study, we assume the following simple form of the density profile at the initial time $t = 0$,

$$\rho(0,r) = \begin{cases} \rho_c \left(1 - \left(\frac{r}{L}\right)^n\right), & 0 \leq r \leq r_b, \\ 0, & r > r_b \end{cases}, \quad (2.4)$$

where ρ_c , L , and r_b ($\leq L$) are positive constants, and $n = 1, 2$, or 3 . Here, ρ_c is the central density; $r = r_b$ gives the boundary of the star; L is a parameter controlling the gradient of the density as well as n . Since $F(r)$ is twice the Misner-Sharp quasi-local mass, the above ansatz of density distribution fixes $F(r)$ as

$$\frac{1}{2}F(r) = 4\pi \int_0^r \rho(0,r) r^2 dr. \quad (2.5)$$

The LTB spacetime is connected to an outer Schwarzschild spacetime whose mass M is given by $M = \frac{1}{2}F(r_b)$. For our purpose, it is convenient to choose (M, ρ_c, r_b, n) as a set of parameters specifying a model. The remaining parameter L can be given in terms of these parameters

$$L = r_b \left(\frac{12\pi}{(n+3)(4\pi - 3M/\rho_c r_b^3)} \right)^{1/n}. \quad (2.6)$$

In addition to $F(r)$, the LTB solution has another arbitrary function $f(r)$, which is related to the initial velocity distribution of fluid elements $\dot{R}(0,r)$. We assume that all fluid elements are at rest $\dot{R}(0,r) = 0$ at the initial time, which is called the momentarily static case. Such a case is realized by taking $f = -\frac{F}{r}$. This condition is very different from the usual ‘marginally bound’ models, where collapsing shells are at rest at spatial infinity, corresponding to vanishing f . The momentarily static condition is astrophysically motivated because the collapse to a black-hole formation will begin when a dynamical instability sets in. Such an instability is due to: the electron-capture at a static massive stellar core; the photo-dissociation reactions at a core of very massive stars in the prompt core-collapse scenario; the cooling and mass fall-back at a newly born neutron star in the delayed collapse scenario [4].

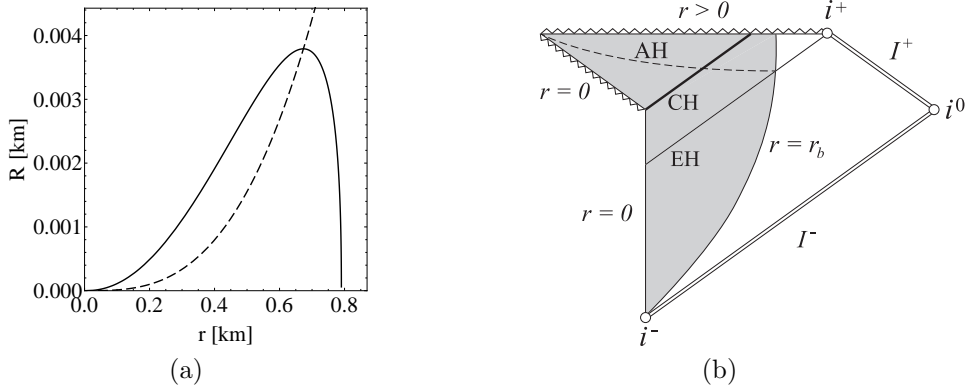


Figure 1: (a) The trapping of the Cauchy horizon (solid) by the apparent horizon (dashed) in the r - R plane. The Cauchy horizon emanating from the central singularity $R = r = 0$ is trapped by the apparent horizon at $(r_{\text{trap}}, R_{\text{trap}}) = (0.673, 0.00379)$, which is enough inside the stellar surface located at $r = r_b = 10.5$, and then plunges into the non-central singularity lying on $R = 0$ at $r = 0.790$. (b) A conformal diagram of the LTB solution mimicking the initial mass distribution of the astrophysically realistic collapse in the final stage of stellar evolution. The central ($r = 0$) singularity is locally naked but not globally. Namely, the Cauchy horizon (CH, thick solid) is trapped by the apparent horizon (AH, thin dashed) and plunges into the non-central ($r > 0$) singularity without reaching the surface of collapsing star ($r = r_b$). The line EH (thin solid) represents the event horizon.

3 Results: Astrophysical censorship

The nakedness of the central singularity is determined by examining the null rays locally around the singularity for given initial conditions F and f [5]. In our models F and f are characterized by the parameters (M, ρ_c, r_b, n) . It can be shown that for $n = 1$ and $n = 2$ the singularity is naked, while for $n = 3$ the singularity can be either naked or censored, depending on other factors. We stress here that the $n = 2$ profile is most physically plausible, since it models the mass distribution of stars in hydrostatic equilibrium. This is because in the presence of pressure $p = p(\rho)$, the pressure gradient can be balanced at the centre with the gravitational force, which is proportional to r , only for $n = 2$. For $n = 1$, the pressure gradient force dominates the gravitational force, while the situation is reversed for $n = 3$. Therefore, we show the results only in the $n = 2$ case.

Since we have a wide three-dimensional parameter space of (M, ρ_c, r_b) even if n is fixed, it is practical to take several sets of numerical values of (M, ρ_c, r_b) , each of which is realized by a typical equation of state of neutron star. In this article, we adopt $\rho_c = 2.00 \times 10^{15}$ [g/cm³], $M = 2M_\odot$, $r_B = 10.5$ [km], $n = 2$ (e.g., see [6]). For a given set of (M, ρ_c, r_b, n) , parameter L is determined through equation (2.6). Given the background spacetime parameters, what to do is to obtain the Cauchy horizon by integrating numerically the radial null geodesic equation from the central singularity.

The Cauchy horizon numerically obtained is shown in figure 1(a). One can see that R increases with r at first along the Cauchy horizon, but then encounters the apparent horizon at $R = R_{\text{trap}} = 3.79$ [m] and eventually plunges into the non-central singularity $R = 0$ at $r > 0$. In order to see that this trapping point is enough inside the collapsing star, we define the proper radius of collapsing star at the time of trapping by $R_b := R(t_{\text{trap}}, r_b)$, where t_{trap} is the time of trapping measured in the t -coordinate. In the present case, $R_b = 7.56$ [km]. Thus, $R_{\text{trap}}/R_b \simeq 0.05\%$ and we can say that the trapping happens enough inside the star. In other words, the naked singularity cannot be globally naked, preserving the weak cosmic censorship hypothesis. A conformal diagram is depicted in figure 1(b).

4 Concluding remarks

We saw above that the naked singularities appearing in the collapse of massive stars cannot be globally naked. Here, we illustrate that globally naked singularities can happen only for parameters that are unrealistic from an astrophysical point of view. As in the above argument we take $n = 2$, the same value of ρ_c as before, and set $r_b = L$. Then, only parameter left to be fixed is the mass M . Integrating null geodesic equation numerically up to the surface for various values of M , one can easily find that for $M \geq 0.2466M_\odot$ the Cauchy horizon is trapped by the apparent horizon before reaching the surface of star, whereas for $M < 0.2466M_\odot$ the Cauchy horizon is not trapped within the stellar interior. Thus, the globally naked singularities can appear only for collapse of the small-mass regime that is far below the masses of the observed neutron stars ($\sim 1.5M_\odot$) and the maximum mass ($\sim 1.5M_\odot$) of the neutron star for the extremely soft equation of state.

Finally, we would like to stress that we are not in the position to claim that there appear locally naked singularities in the astrophysically realistic collapse. The appearance of naked singularities in our analysis is entirely because we choose the dust as a matter model and the situation can be very different in other choice. Instead, our conclusion is that even if a naked singularity could appear at the centre of realistic stellar collapse, it will be hidden behind an event horizon and cannot be observed by a distant observer. Since the exposition of the central naked singularity to a distant observer depends on the dynamics of not central but surrounding region, our conclusion is not very sensitive to the choice of matter models.

Acknowledgments

UM and TH are supported by Research Center for Measurement in Advanced Science in Rikkyo University, and by the Grant-in-Aid for Scientific Research Fund of the Ministry of Education, Culture, Sports, Science and Technology, Japan [Young Scientists (B) 22740176 and 21740190].

References

- [1] R. Penrose, *Phys. Rev. Lett.* **14**, 57-59 (1965); S. Hawking, *Proc. Roy. Soc. Lond.* **A300**, 187-201 (1967); S. W. Hawking, R. Penrose, *Proc. Roy. Soc. Lond.* **A314**, 529-548 (1970); S. W. Hawking, G. F. R. Ellis, Cambridge University Press, Cambridge, 1973; J. M. M. Senovilla, "Singularity Theorems and Their Consequences," *Gen. Relativ. Grav.* **29**, 701-848 (1997).
- [2] R. Penrose, *Riv. Nuovo. Cimento Soc. Ital. Fis.* **1**, 252 (1969); in "Gravitational Radiation and Gravitational Collapse," IAU Symposium **64**, ed. C. DeWitt-Morette, Reidel, Dordrecht (1974).
- [3] G. Lemaître, *Ann. Soc. Sci. Bruxelles I A* **53**, 51 (1933); R. C. Tolman, *Proc. Nat. Acad. Sci.* **20**, 169-176 (1934); H. Bondi, *Mon. Not. Roy. Astron. Soc.* **107**, 410-425 (1947).
- [4] G. E. Brown, H. Bethe, *Astrophys. J.* **423**, 659 (1994).
- [5] P. S. Joshi and I. H. Dwivedi, *Phys. Rev. D* **47**, 5357 (1993) [arXiv:gr-qc/9303037].
- [6] S. L. Shapiro and S. A. Teukolsky, New York, USA, Wiley (1983) 645 p.

Cosmic censorship in overcharging a charged black hole with a charged particle

Soichiro Isoyama ^{36(a)}

^(a) *Yukawa institute for theoretical physics, Kyoto University, Sendai 606-8502, Japan.*

Abstract

There is a claim that a static charged black hole (Reissner-Nordström black hole) can be overcharged by absorbing a charged test particle. If it is true, it might give a counter example to the weak cosmic censorship conjecture. However, so far the proposed process has only been analyzed within a test particle approximation. We here argue that all the back reaction effects can be properly taken into account when we consider the trajectory of a particle on the border between the plunge and bounce orbits. In such marginal cases we find that the Reissner-Nordström black hole can never be overcharged via the absorption of a charged particle. Since all the plunge orbits are expected to have a higher energy than the marginal orbit, we conclude that there is no supporting evidence that indicates the violation of the cosmic censorship in the proposed overcharging process.

1 Introduction

General relativity is the most successful classical theory of gravity and it has brought us deep a understanding of spacetime. Nevertheless, when we evolve the Einstein equations with a well-posed initial condition, singularities, at which general relativity and all established theories lose their predictability, are known to form. However, in most cases singularities are hidden by event horizons as in the case of black holes and cannot be seen by a distant observer. This statement is known as the weak cosmic censorship conjecture proposed by Penrose [1] and has still been an open question in general relativity.

According to the uniqueness theorem, all stationary asymptotically flat black holes in Einstein-Maxwell system are described by Kerr-Newman solutions, which are specified uniquely by the mass M , the charge Q and the angular momentum J satisfying

$$M^2 \geq Q^2 + (J/M)^2. \quad (1.1)$$

When the equality is saturated, the black holes are called extremal, and a naked singularity appears when $M^2 < Q^2 + (J/M)^2$. If it were really possible, we would say that the black hole is overcharged or overspinned via matter absorption.

Recently, there arise some claims that Eq. (1.1) is indeed saturated if one consider the process of particle absorption with the initial black hole being prepared slightly below the extremal limit. However, as already mentioned in Refs. [3], these proposed processes were analysed within the test particle limit. That is, the back reaction effects due to the presence of a particle must be taken into account in these analyses before concluding that they were a genuine counterexample to the cosmic censorship conjecture.

To address the role of back reaction effects in the overcharging/overspinning issue, we discuss whether a Reissner-Nordström (RN) black hole can be overcharged or not by the capturing of a charged particle, taking into account all possible back reaction effects, which is originally proposed in Ref. [3]. ³⁷

2 Overcharging a Reissner-Nordström black hole without back reaction effects

We consider a point particle with rest mass μ and charge q radially falling toward a nearly extremal RN black hole with mass M and charge Q . By assumption, these parameters satisfy $\mu < q \ll Q < M$.

³⁶Email address: isoyama@yukawa.kyoto-u.ac.jp

³⁷In this article, we use the units in which $G = c = 1$, but we explicitly write $\kappa^2 = 8\pi G$ in Sec. 3.2, respecting the original notations in Ref. [4]. The sign convention of the metric as $(-, +, +, +)$.

Due to the spherical symmetry of a RN black hole, we can choose the coordinate system such that the trajectory of a particle is along the axis without loss of generality. Then, the trajectory is represented by $z^\alpha(s) = (T(s), R(s), 0, 0)$ with the proper time s along the world line of the particle in the (t, r, θ, ϕ) coordinate.

In the above setup, if the following two conditions are satisfied, we would say that a RN black hole is possibly overcharged. The first condition is that the particle is in a plunge orbit. For plunge orbits there is no turning point where the radial velocity becomes zero. Therefore the condition is

$$\left(\frac{dR}{ds}\right)^2 > 0, \quad \text{for } R \geq r_+, \quad (\text{absorption condition}) \quad (2.1)$$

where $r_+ := M + \sqrt{M^2 - Q^2}$ is the value of the radial coordinate of the event horizon. The second condition is on the total energy of the final state. After the absorption of the particle, the system will approach another RN geometry with mass $M_{\text{final}} = M + E$ and charge $Q_{\text{final}} = Q + q$. The condition that the final RN geometry exceeds the extremal bound is given by

$$M + E < Q + q. \quad (\text{overcharging condition}) \quad (2.2)$$

In Ref. [3], it was demonstrated that radial orbits in a rather wide range of parameter space satisfy the conditions (2.1) and (2.2) as long as the back reaction effects are neglected. In fact, both the absorption and overcharging conditions are satisfied under the parametrization, for $1 < b < a$, $c < \sqrt{a^2 - b^2}$,

$$M := 1 + 2\epsilon^2, \quad Q := 1, \quad E := a\epsilon - 2b\epsilon^2, \quad q := a\epsilon, \quad \mu := c\epsilon, \quad (2.3)$$

where $0 < \epsilon \ll 1$ and the coefficients a , b and c are assumed to be $O(1)$ real numbers.

3 Back reaction effects on the overcharging process

As was already emphasized in Ref. [3], the analysis in the previous section is not sufficient because the back reaction effects associated with particle presence in general also scales as $O(\epsilon^2)$. We have to compute the total amount of energy in the final state of the whole system to the accuracy of $O(\epsilon^2)$, taking into account the effects of back reaction. At the same time, we have to examine how the absorption condition (2.1) is modified once the back reaction effects are taken into account.

Given that the self-force calculation is still in its preliminary stage, here, we propose to bypass these difficult tasks by focusing on the marginal orbits that pass through an unstable equilibrium state. The basic strategy that we use here is to relate the unstable equilibrium state to an exact solution known as the double Reissner-Nordström (DRN) static solution [5, 6] that must include all the backreaction effects on the total energy of the system in equilibrium. At the same time, we also evaluate the energy loss of the system via radiation emitted to infinity through the infall of the particle from the equilibrium state to the black hole horizon to the accuracy of $O(\epsilon^2)$, which can be readily achieved using the standard black hole perturbation method.³⁸

3.1 Total energy of a charged black hole and a charged particle in equilibrium

As a first step to examine the overcharging condition (2.2) for the marginal orbits, we here extract the total energy of the system composed of a charged black hole and a charged particle in the equilibrium state, E_{eq} , using the DRN solution of the Einstein-Maxwell equations [5, 6].

The DRN solution is characterized by five parameters: masses of the RN sources m_1 , m_2 , their charges e_1 , e_2 , and the separation between them ℓ and by a constraint that assures the existence of the equilibrium state without any conical singularities between the two charged objects. The metric, the static electromagnetic potential and the relevant equation are all presented in the original paper [5].

³⁸ To extend our argument to more general cases, we assume that the other plunge orbits result in final states that have higher energies than the final state in the case of the marginal trajectory, whose energy is deduced under the conditions that the mass and charge of the initial black hole and the charge of the plunging particle are fixed. Once we accept this rather reasonable assumption, the avoidance of overcharging in the marginal cases is extended to general plunge orbits.

From the asymptotic form the metric and the electromagnetic potential, we find that the total energy of the DRN is $m_1 + m_2$ and the total charge is $e_1 + e_2$. Moreover, one can prove, under the assumptions $m_2 > m_1 > 0$ and $e_2 > e_1 > 0$,

$$E_{\text{eq}} > q + Q, \quad (3.1)$$

which means that the total energy never goes below the extremal bound in the equilibrium configuration.
39

3.2 Energy flux radiated from a charged particle

In the preceding section, with the help of the DRN solution, we showed that the total energy of the equilibrium state of a charged particle in a RN black hole cannot be less or equal to its total charge. Nevertheless, it is not sufficient yet to exclude the possibility that a RN black hole is overcharged by absorbing a charged particle. The energy loss via the electromagnetic and gravitational radiation can reduce the total energy as the particle falls from the equilibrium position to the event horizon of the black hole. Then the total energy in the final state will be given by $E_{\text{eq}} - E_{\infty}$ with E_{∞} being the energy radiated away to infinity.

To estimate E_{∞} , we here adopt a linear black hole perturbation formalism developed by Kodama and Ishibashi [4]. After decomposing the perturbations into the Fourier-Harmonic components, the energy flux carried by electromagnetic and gravitational waves to infinity is expressed as

$$E_{\infty} = \int_0^{+\infty} d\omega \sum_{\mathfrak{l}} \frac{8\pi\mathfrak{l}(\mathfrak{l}+1)\omega^2}{9\kappa^2\nu(M+\nu)} \left(\frac{|\mathcal{X}_+|^2}{|W_+|^2} + \frac{(\mathfrak{l}-1)(\mathfrak{l}+2)}{16} \frac{|\mathcal{X}_-|^2}{|W_-|^2} \right), \quad (3.2)$$

where $W_{\pm} := O(1)$ is a real number and \mathfrak{l} is the angular index of the scalar spherical harmonics $Y_{\mathfrak{l}\mathfrak{m}}(\theta, \phi)$. The expressions for \mathcal{X}_{\pm} given in Eq. (3.2) schematically takes the form [7]

$$O(\epsilon) \times \int_{r_+}^{r_0} I(r) e^{i\omega T(r)} dr, \quad (3.3)$$

where $I(r)$ is a certain regular function of r bounded above in the integrated region, whose typical scale of variation is $O(M^{-1})$, and r_0 is the radial position of the equilibrium configuration.

Actually, radiated energy is $O(\epsilon^4)$ or higher. It is obvious from Eq. (3.3) that $|\mathcal{X}_{\pm}(\omega)|$ is suppressed by a factor of $O(\epsilon)$. In addition, the particle's velocity (dR/ds) is always suppressed in the present setup given by Eqs (2.3). Since the back ground radial equation of motion of the particle takes ⁴⁰

$$\left(\frac{dR}{ds} \right)^2 = \frac{1}{\mu^2} \left(E - \frac{qQ}{R} \right)^2 - f(R) =: V^{(o)}(R). \quad (3.4)$$

Since $V^{(o)}(r)$ is a quadratic function of $1/r$ bounded from below and both $V^{(o)}$ and $dV^{(o)}/dr$ vanishes at $r = r_0$, $V^{(o)}$ takes its maximum value at $r = r_+$, in the interval of our interest between r_+ and r_0 . Hence, we have

$$V^{(o)}(r) \leq V^{(o)}(r_+) = \frac{1}{\mu^2} \left(E - \frac{qQ}{M + \sqrt{M^2 - Q^2}} \right)^2 = \frac{4(a-c)^2}{c^2} \epsilon^2 + O(\epsilon^3). \quad (3.5)$$

This implies that the velocity of a particle dR/ds given in Eq. (3.4) is always at most $O(\epsilon)$.

When the particle moves very slowly, the amount of emitted radiation is also expected to be small. This intuition can be made explicit in the expression for \mathcal{X}_{\pm} as follows. One can see that each expression

³⁹We would like to comment on the correspondence between the DRN solution and the equilibrium configuration of a test particle in a RN black hole. While these two picture are written in the very different manner, we found that they were uniquely identified with the accuracy of $O(\epsilon^2)$.

⁴⁰The energy of the particle E is defined by $E := -(\partial_t)^a(\mu u_a + qA_a)$ where (∂_t) is the Killing field associated with the time coordinate t , A_a is the vector electro-magnetic potential of the background RN black hole and $u^a := dz^a/ds$ is the four velocity of the particle.

in Eq. (3.3) is regular on the boundaries of the integral. Here we replace $e^{i\omega T(r)}$ with an equivalent expression

$$\frac{f}{i\omega} \left(\frac{dR}{ds} \right) \left(f \frac{dT}{ds} \right)^{-1} \left(\frac{\partial e^{i\omega T(r)}}{\partial r} \right), \quad (3.6)$$

and perform integration by parts. This additional suppression owing to the dR/ds factor guarantees that the total energy emitted to infinity is at most $O(\epsilon^4)$.

To summarize, the total energy emitted to infinity by a particle that falls from the unstable stationary point to the horizon, E_∞ , is always suppressed, and it cannot be as large as $O(\epsilon^2)$ for any parameter choice.

4 Conclusion

In this work, we have examined the back reaction effects of $O(\epsilon^2)$ when a charged particle whose mass and charge are of $O(\epsilon)$ is absorbed by a nearly extremal RN black hole. To avoid the technical difficulties related to the electromagnetic and gravitational self-force, we concentrated on the case of the marginal orbit, which is the separatrix dividing the plunge and recoil orbits. We first showed that, with the aid of an exact solution, the total energy of the system is always greater than the total charge for the equilibrium configuration that the marginal orbit passes through. Then, we demonstrated that the radiative energy loss as the particle is falling into the black hole from the equilibrium position is $O(\epsilon^4)$ or higher.

Combining these results, we succeeded in proving that the total energy of the system composed of a charged particle and a black hole is always greater than their total charge for the marginal orbit :

$$E_{\text{eq}} - E_\infty > q + Q. \quad (4.1)$$

In short, the back reaction effects prevent a nearly extremal RN black hole from being overcharged, and hence we conclude the cosmic censorship conjecture is not violated.

As was mentioned in Sec. 3, our discussion relies on the assumption that the marginal orbit passes through the unstable stationary configuration. Although it is difficult to imagine that this is not the case, to obtain a definitive answer to the question whether these assumptions are correct or not, it is necessary to solve the orbital evolution directly including the self-force effects. In the case of a charged particle in the non-vanishing electro-magnetic background, even the fundamental formulation describing the self-force effects has not yet been developed to the level applicable to the overcharging problem discussed in this paper. We hope we will return to this point in near future and draw a definitive conclusion whether or not the cosmic censorship conjecture is prevailed in this overcharging process.

References

- [1] R. Penrose, Phys. Rev. Lett. **14**, 57 (1965).
- [2] R. M. Wald, arXiv:gr-qc/9710068.
- [3] V. E. Hubeny, Phys. Rev. D **59**, 064013 (1999) [arXiv:gr-qc/9808043].
- [4] H. Kodama and A. Ishibashi, Prog. Theor. Phys. **111**, 29 (2004) [arXiv:hep-th/0308128]; A. Ishibashi and H. Kodama, arXiv:1103.6148 [hep-th].
- [5] G. A. Alekseev and V. A. Belinski, Phys. Rev. D **76**, 021501 (2007) [arXiv:0706.1981 [gr-qc]]; G. A. Alekseev and V. A. Belinski, arXiv:0710.2515 [gr-qc]; G. A. Alekseev and V. A. Belinski, arXiv:1103.0582 [gr-qc].
- [6] V. S. Manko, Phys. Rev. D **76**, 124032 (2007) [arXiv:0710.2158 [gr-qc]].
- [7] S. Isoyama, N. Sago and T. Tanaka, Phys. Rev. D **84**, 124024 (2011) [arXiv:1108.6207 [gr-qc]].

High-velocity collision of particles around a Kerr black hole

Tomohiro Harada⁴¹

Department of Physics, Rikkyo University, Toshima, Tokyo 171-8501, Japan

Abstract

We derive a general formula for the center-of-mass (CM) energy for the near-horizon collision of two general geodesic particles around a Kerr black hole. We find that if the angular momentum of the particle satisfies the critical condition, the CM energy can be arbitrarily high. We then apply the formula to the collision of a particle orbiting an innermost stable circular orbit (ISCO) and another generic particle near the horizon and find that the CM energy is arbitrarily high if we take the maximal limit of the black hole spin. In view of the astrophysical significance of the ISCO, this implies that particles can collide around a rapidly rotating black hole with a very high CM energy without any artificial fine-tuning. We next apply the formula to the collision of general inclined geodesic particles and show that, in the direct collision scenario, the collision with an arbitrarily high CM energy can occur near the horizon of maximally rotating black holes not only at the equator but also on a belt centered at the equator between latitudes $\pm 42.94^\circ$. This is also true in the scenario through the collision of a last stable orbit particle. This strongly suggests that if signals due to high-energy collision are to be observed, such signals will be generated primarily on this belt.

1 Introduction

Many black hole candidates have been observed in X-ray binaries and galactic centres. In the former case, electromagnetic radiation emitted from accretion disks around black holes of mass $\sim 10M_\odot$ is observed. In the latter case, the central objects are believed to be supermassive black holes of mass $\sim 10^6 - 10^9 M_\odot$. However, no direct signature of black hole horizons has been observed yet. In the near future, the observation with the resolution of the black hole horizon scale might catch the direct image of the black hole horizon, which is called a black hole shadow, in terms of the millimeter electromagnetic waves. Moreover, when gravitational radiation from black holes is observed, it will directly reveal the spacetime geometry in the vicinity of black hole horizons.

Astrophysical black holes are generally rotating and uniquely described by a Kerr metric, in which the line element is given by

$$ds^2 = -\left(1 - \frac{2Mr}{\rho^2}\right) dt^2 - \frac{4Mar \sin^2 \theta}{\rho^2} d\phi dt + \frac{\rho^2}{\Delta} dr^2 + \rho^2 d\theta^2 + \left(r^2 + a^2 + \frac{2Mra^2 \sin^2 \theta}{\rho^2}\right) \sin^2 \theta d\phi^2, \quad (1.1)$$

where $\rho^2 = r^2 + a^2 \cos^2 \theta$ and $\Delta = r^2 - 2Mr + a^2$. If $0 \leq |a| \leq M$, Δ vanishes at $r = r_\pm = M \pm \sqrt{M^2 - a^2}$. The horizon radius is given by $r_H = r_+$. The angular velocity of the horizon is given by

$$\Omega_H = \frac{a}{r_H^2 + a^2} = \frac{a}{2M(M + \sqrt{M^2 - a^2})}. \quad (1.2)$$

We define the nondimensional Kerr parameter $a_* = a/M$. We can assume $a \geq 0$ without loss of generality.

Bañados et al. [1] proposed a scenario where rapidly rotating black holes may act as particle accelerators. More precisely, they considered the following scenario. Let us drop two particles of the same rest mass at rest at infinity on the equatorial plane of a rotating black hole and assume that the two

⁴¹Email address: harada@rikkyo.ac.jp

particles collide near the horizon. If the maximum spin limit $a_* \rightarrow 1$ is taken and the angular momentum of either particle is fine-tuned, then the centre-of-mass (CM) energy, which is the invariant measure of the collision energy, can be arbitrarily high.

In this article, we discuss the robustness and the condition for this phenomenon in more general situations. This article is based on the collaboration with M. Kimura [2, 3].

2 The collision of general geodesic particles

The CM energy of particles 1 and 2 at the same spacetime point is defined by

$$E_{\text{cm}}^2 = -(p_1 + p_2)^a (p_1 + p_2)_a = m_1^2 + m_2^2 - 2g_{ab} p_1^a p_2^b, \quad (2.1)$$

where p_i^a and m_i are the four-momentum and the rest mass of particle $i (= 1, 2)$, respectively. This is a scalar quantity, therefore coordinate-independent and in principle observable. This is the energy of the two colliding particles observed by a local observer which is at rest in the centre-of-mass frame of the two particles.

The general geodesic equations are integrable with four conserved quantities [4]. The conserved quantities are the rest mass m , the energy E , the angular momentum L and the Carter constant \mathcal{Q} . The geodesic orbits are given by the following set of first-order ordinary differential equations:

$$\rho^2 \dot{t} = -a(aE \sin^2 \theta - L) + (r^2 + a^2)P/\Delta, \quad (2.2)$$

$$\rho^2 \dot{\phi} = -(aE - L/\sin^2 \theta) + aP/\Delta, \quad (2.3)$$

$$\rho^2 \dot{r} = \sigma_r \sqrt{R}, \quad (2.4)$$

$$\rho^2 \dot{\theta} = \sigma_\theta \sqrt{\Theta}, \quad (2.5)$$

where $\cdot = d/d\lambda$, $\sigma_r = \pm 1$, $\sigma_\theta = \pm 1$,

$$P = P(r) = (r^2 + a^2)E - aL, \quad (2.6)$$

$$R = R(r) = P^2 - \Delta[m^2 r^2 + (L - aE)^2 + \mathcal{Q}], \quad (2.7)$$

$$\Theta = \Theta(\theta) = \mathcal{Q} - \cos^2 \theta [a^2(m^2 - E^2) + L^2/\sin^2 \theta]. \quad (2.8)$$

The condition $\dot{t} > 0$ must be satisfied for physical particle orbits, which is called the ‘forward-in-time’ condition. In the near-horizon limit, this reduces to

$$L \leq \Omega_H^{-1} E \equiv L_c. \quad (2.9)$$

We consider the collision of two particles outside the event horizon. Then, we can show that the CM energy is bounded except in the limit to the horizon. For the near-horizon collision, the CM energy is given by

$$E_{\text{cm}}^2 = m_1^2 + m_2^2 + \frac{1}{r_H^2 + a^2 \cos^2 \theta} \left[(m_1^2 r_H^2 + \mathcal{K}_1) \frac{E_2 - \Omega_H L_2}{E_1 - \Omega_H L_1} + (m_2^2 r_H^2 + \mathcal{K}_2) \frac{E_1 - \Omega_H L_1}{E_2 - \Omega_H L_2} - \frac{2(L_1 - a \sin^2 \theta E_1)(L_2 - a \sin^2 \theta E_2)}{\sin^2 \theta} - 2\sigma_{1\theta} \sqrt{\Theta_1} \sigma_{2\theta} \sqrt{\Theta_2} \right], \quad (2.10)$$

where $\mathcal{K}_i \equiv \mathcal{Q}_i + (L_i - aE_i)^2$. Therefore, if the angular momentum of either of the particles is fine-tuned so that $L_i \rightarrow \Omega_H^{-1} E_i$, the CM energy E_{cm} can be arbitrarily high. We call particles with $L = \Omega_H^{-1} E$ *critical particles*.

We can define the effective potential as follows:

$$\frac{1}{2} \dot{r}^2 + \frac{r^4}{\rho^4} V(r) = 0, \quad (2.11)$$

where

$$V(r) = -\frac{R(r)}{2r^4}. \quad (2.12)$$

It is useful to classify critical particles in terms of the behaviour of the effective potential at the horizon. The classification is summarised in Table I.

Table 1: The classification of critical particles in terms of $V(r_H)$, $V'(r_H)$ and $V''(r_H)$.

Class	$V(r)$ at $r = r_H$	BH spin	Scenario
I	$V = V' = 0, V'' < 0$	$ a = M$	Direct collision
II	$V = V' = V'' = 0$	$ a = M$	LSO (ISCO) collision
III	$V = V' = 0, V'' > 0$	$ a = M$	Multiple scattering
IV	$V = 0, V' > 0$	$0 < a < M$	Multiple scattering

3 The collision of an ISCO particle

The Kerr black hole has an innermost stable circular orbit (ISCO) and its generalisation to non-equatorial orbits, which is called a last stable orbit (LSO). The ISCO is important in astrophysical contexts. The inner edge of the standard accretion disk is usually given by the ISCO. In the extreme-mass-ratio-inspirals (EMRIs), the transition of the adiabatic inspiral phase to the plunge phase occurs at the ISCO. We can see that the fine-tuning is naturally realised by an ISCO particle: as $a_* \rightarrow 1$, $r_{\text{ISCO}} \rightarrow r_H$ and $L \rightarrow \Omega_H^{-1} E$.

We consider the collision of an ISCO particle with another generic particle. We consider two distinct kinds of collision of an ISCO particle. The one is the near-horizon collision, where the ISCO particle plunges to the vicinity of the horizon and collide with a counterpart particle there. The other is the on-ISCO collision, where the ISCO particle collide with a counterpart at the ISCO radius. The schematic figures for these two kinds of collision are shown in Fig. 1. For the near-horizon collision of an ISCO

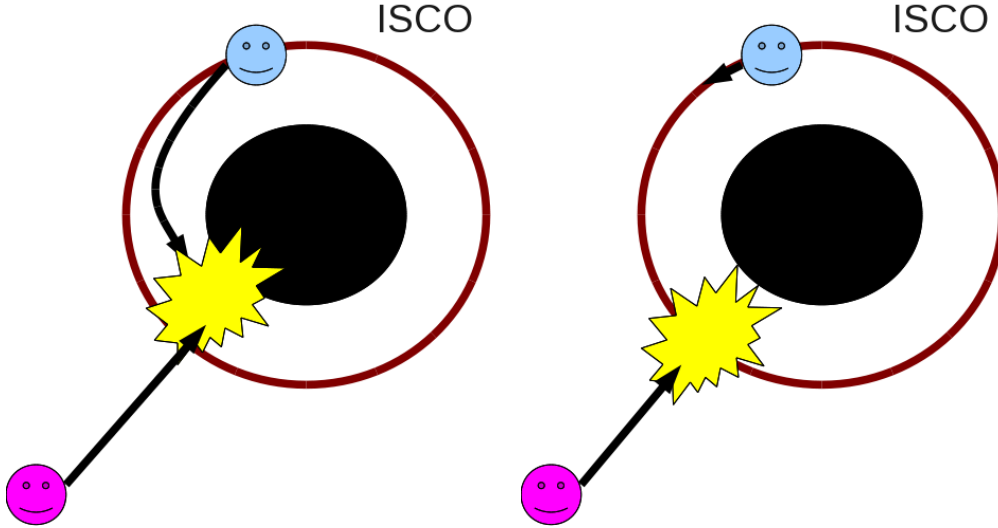


Figure 1: Left panel: the near-horizon collision of an ISCO particle plunging from the ISCO. Right panel: the collision of an ISCO particle at the radius of the ISCO

particle with a generic counterpart, we obtain

$$\frac{E_{\text{cm}}}{2m_0} \approx \frac{1}{2^{1/2}3^{1/4}} \frac{\sqrt{2e_2 - l_2}}{\sqrt[4]{1 - a_*^2}} \quad (3.1)$$

for $a_* \approx 1$. For the collision of an ISCO particle with a generic counterpart at the ISCO radius, we obtain

$$\frac{E_{\text{cm}}}{2m_0} \approx \frac{1}{2^{1/6}3^{1/4}} \frac{\sqrt{2e_2 - l_2}}{\sqrt[6]{1 - a_*^2}} \quad (3.2)$$

for $a_* \approx 1$.

4 High-velocity collision apart from the equatorial plane

It is intriguing whether the high-velocity collision is restricted to that on the equatorial plane or not. Here, we concentrate ourselves on the direct collision scenario and the ISCO collision scenario, for which the high-velocity collision with the critical particles is of classes I and II, respectively, because the physical relevance of the other cases is not clear. This implies that we can assume $V = V' = 0$ and $V'' \leq 0$ at $r = r_H$. Consequently, the black hole must be maximally rotating and θ is restricted. The allowed region is the belt centered at the equator between latitudes $\pm 42.94^\circ$.

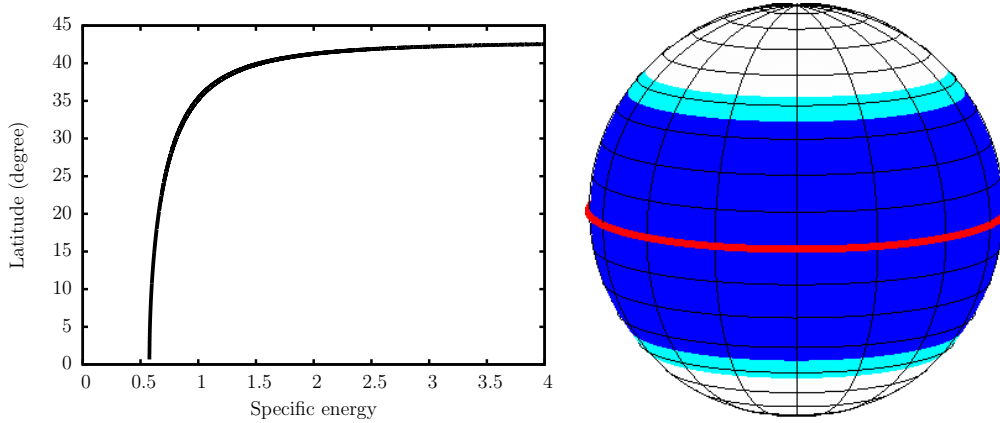


Figure 2: Left panel: the highest latitude as a function of the specific energy of the critical particle. Right panel: The allowed region of the high-velocity collision.

5 Summary

We reach the following conclusion. The CM energy of two colliding geodesic particles near the horizon can be arbitrarily high in the maximal rotation limit with the fine-tuning of the angular momentum. The required fine-tuning of the angular momentum is naturally realised by a particle orbiting the ISCO or LSO. The high-velocity collision can occur not only at the equator but also at the latitude between $\pm 43^\circ$ near the horizon in the maximal rotation limit of the black hole.

As future prospects, we would like to raise the investigation of the effects of gravitational radiation reaction and self-force and the theoretical predictions to astrophysical observation.

References

- [1] M. Bañados, J. Silk and S. M. West, *Phys. Rev. Lett.* **103** (2009) 111102.
- [2] T. Harada and M. Kimura, *Phys. Rev. D* **83** (2011) 084041.
- [3] T. Harada and M. Kimura, *Phys. Rev. D* **83** (2011) 024002.
- [4] B. Carter, *Phys. Rev.* **174**, 1559 (1968).

Bosenova collapse of axion cloud around a rotating black hole

Hiroataka Yoshino ^{42(a)} and Hideo Kodama ^(a,b)

^(a)*Theory Center, Institute of Particles and Nuclear Studies, KEK, Tsukuba, Ibaraki, 305-0801, Japan*

^(b)*Department of Particle and Nuclear Physics, Graduate University for Advanced Studies, Tsukuba 305-0801, Japan*

Abstract

Motivated by possible existence of stringy axions of ultralight mass, we study numerically the behavior of axion field around a rotating black hole (BH). Due to the superradiant instability, the axion field grows extracting the rotational energy of the BH. The nonlinear self-interaction becomes important as the field value gets large, and our result suggests that the nonlinear effect leads to an explosive phenomena, which is analogous to the bosenova observed in experiments of Bose-Einstein condensate.

1 Introduction

Recently, it was pointed out that the string theory may be probed through cosmology or astrophysics by observing the phenomena caused by “axions” [1]. In addition to the QCD axion, the stringy axions or axionlike particles have been proposed and discussed: In string theory, many moduli arise when extra dimensions are compactified, and some of them behave as axionlike scalar fields with ultralight mass. The typical number of the axionlike fields is 10-100, and it leads to a generic landscape of stringy axions, the so-called “axiverse”. An axion of mass $2 \times 10^{-20} \text{eV} \lesssim \mu \lesssim 3 \times 10^{-10} \text{eV}$ is expected to cause interesting phenomena around an astrophysical black hole (BH). The axion field would form a quasibound state and grow by the superradiant instability [2], which is caused by the fact that the energy of the field can be negative in the ergoregion (i.e., the superradiant mode). If the negative energy falls into the horizon, the outside energy increases in time. The growth rate normalized by BH mass, $M\omega_I$, depends on the ratio of half of the gravitational radius to the Compton wavelength of axion $M\mu$ (in the Planck units $c = G = \hbar = 1$). The instability is effective for $M\mu \sim 1$, and its typical time scale is $\tau \sim 10^7 M$.

One of the important effect in the BH-axion system is the nonlinear self-interaction of axions. The potential $U(\Phi)$ of the axion field is periodic as typically given by $U(\Phi) = f_a^2 \mu^2 [1 - \cos(\Phi/f_a)]$, where the equation of the axion is

$$\square\Phi - U'(\Phi) = 0. \quad (1.1)$$

Although the Klein-Gordon equation [$U(\Phi) = (1/2)\mu^2\Phi^2$] gives a good approximation for small Φ/f_a , as the field grows large, the nonlinear effects should become relevant. One of the expected nonlinear phenomena is the “bosenova”, which is explosive phenomena observed after collapse of Bose-Einstein condensates of Rb85 in experiments [3]. If the bosenova happens also in the BH-axion system, its details and the observational consequence have to be studied. This is the purpose of our work. We develop a 3D code to simulate nonlinear axion field in a Kerr spacetime. Here, the axion field is treated as a test field, and the background geometry is fixed to be the Kerr spacetime.

2 Numerical method and code

In developing a code, there were two difficulties. The first difficulty is that the numerical instability happens in the Boyer-Lindquist coordinates because the time coordinate basis is spacelike in the ergoregion. We solved this problem by adopting zero-angular-momentum observer (ZAMO) coordinates. The ZAMOs are observers such that they stay at fixed r and θ , but move in ϕ direction with angular velocity $\Omega(r, \theta)$ so that their angular momenta are zero. The ZAMO coordinates $(\tilde{t}, \tilde{\phi}, \tilde{r}, \tilde{\theta})$ are introduced via

$$\tilde{t} = t, \quad \tilde{\phi} = \phi - \Omega(r, \theta)t, \quad \tilde{r} = r, \quad \tilde{\theta} = \theta. \quad (2.1)$$

⁴²Email address: hyoshino@post.kek.jp

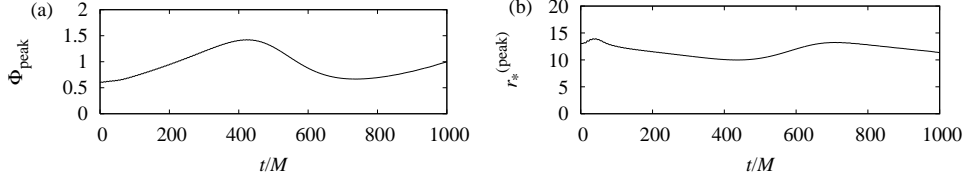


Figure 1: The peak value φ_{peak} of the field (left panel) and its location $r_*^{(\text{peak})}$ with respect to the tortoise coordinate (right panel) as functions of time in simulation (A).

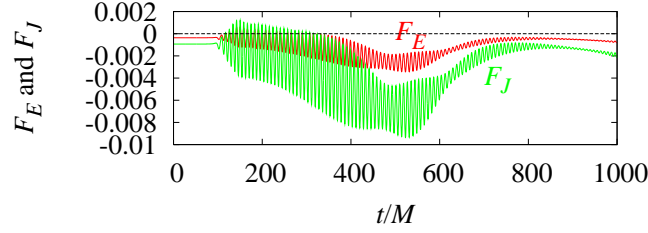


Figure 2: Fluxes F_E and F_J of energy and angular momentum, respectively, toward the horizon in simulation (A).

Since the coordinate basis of \tilde{t} is timelike everywhere, stable simulations become feasible. The second difficulty is that the ZAMO coordinates become gradually distorted, which causes growth of the numerical error. We solved this problem by “pulling back” the ZAMO coordinates. When the ZAMO coordinates become distorted, we introduce new ZAMO coordinates which are not distorted at that time, and continue time evolution with the new coordinates. Iterating these processes, longterm evolution was realized.

Our code is a three-dimensional code of the ZAMO coordinates $(\tilde{r}_*, \tilde{\theta}, \tilde{\phi})$. The sixth-order finite differencing is used in spatial directions, and time evolution is proceeded with the fourth-order Runge-Kutta method. Typically, we used the grid size $\Delta r_*/M = 0.5$ and $\Delta\theta = \Delta\phi = \pi/30$, and the Courant number $C := \Delta t/\Delta r_* = (3/2\pi)\Delta\theta$. In pulling back the coordinates, we applied the seventh-order Lagrange interpolation. The coordinate range of r_* is $r_*^{(\text{in})} \leq r_* \leq r_*^{(\text{out})}$, where $r_*^{(\text{in})}$ and $r_*^{(\text{out})}$ are typically adopted as $-200M$ and $300\text{--}1000M$, respectively. The pure ingoing boundary condition is imposed at $r_*^{(\text{in})}$, and the field value is fixed at $r_*^{(\text{out})}$. In order to assess the code, we checked the convergence with respect to grid size and the conservation of energy and angular momentum. We also simulated numerically the quasibound state of the linear Klein-Gordon equation, and confirmed that the numerical data agree well with the semianalytic solution. In particular, we could reproduce growth rate of the superradiant instability with the deviation of 1.7% from the semianalytic results. Therefore, our code has the ability to describe the energy extraction by superradiance fairly accurately.

3 Numerical results

We present the results of typical two simulations (A) and (B), for which the effect of nonlinearity is weak and strong, respectively. Both simulations are done under the parameter $a/M = 0.99$ and $M\mu = 0.4$, and as the initial condition, we chose $l = m = 1$ mode of the quasibound state of Klein-Gordon field, but with the different initial amplitude $\varphi_{\text{peak}}(0) = 0.6$ (A) and 0.7 (B).

3.1 Simulation (A): Weakly nonlinear case

The left panel of Fig. 1 shows the peak value of the field $\varphi_{\text{peak}} := \sup[\varphi]$, and the right panel shows the position $r_*^{(\text{peak})}$ of the peak with respect to the tortoise coordinate r_* as functions of t/M . Both φ_{peak} and $r_*^{(\text{peak})}$ oscillate with the period $\simeq 700M$, and φ_{peak} increases when the peak location approaches the horizon because the field gets compacted in a small region. Figure 2 shows the energy and angular

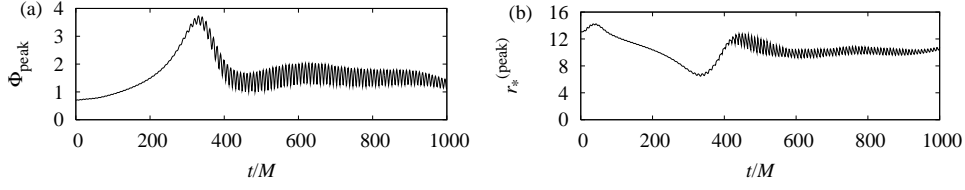
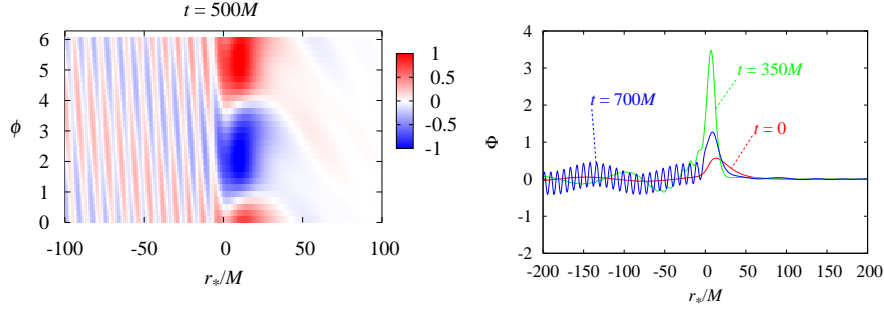


Figure 3: Same as Fig. 1 but for simulation (B).

Figure 4: Left panel: A snapshot of the field in the equatorial plane $\theta = \pi/2$ at $t = 500M$ [shown by the density plot in the plane $(r_*/M, \phi)$]. Right panel: Snapshots of the field ϕ as a function of r_*/M at $\phi = 0$ in the equatorial plane $\theta = \pi/2$ for $t/M = 0, 350, 700$.

momentum fluxes F_E and F_J toward the horizon evaluated at $r_* = -100M$. The nonlinear effect appears after $t/M \simeq 100$. Although both F_E and F_J oscillate, their mean values are always negative and their absolute values become larger around $t = 500M$: The extraction of energy and angular momentum becomes more efficient due to the nonlinear effect.

3.2 Simulation (B): Strongly nonlinear case

The left panel of Fig. 3 shows the peak value φ_{peak} , and the right panel shows the position of the peak $r_*^{(\text{peak})}$ as functions of t/M . In contrast to (A), $r_*^{(\text{peak})}$ approaches the horizon only once, and after that, it fluctuates around $r_* = 10M$: The bosenova is happening here. Left panel of Fig. 4 shows the density plot of the axion field φ at $t = 500M$ in the $(r_*/M, \phi)$ plane. During the bosenova, the peak periodically splits into two parts, one remaining around $r_* \simeq 10M$ and the other falling into the BH. This periodic split generates ingoing waves of angular frequency $\omega_{\text{NL}} \simeq 0.72/M$, which violates the superradiant condition $\omega < m\Omega_H = 0.434/M$. Right panel of Fig. 4 shows the snapshots of the field on the $\phi = 0$ line on the equatorial plane $\theta = \pi/2$ at time $t/M = 0, 350, 700$. At $t/M = 350$, the peak of the field becomes very high and around this time the bosenova begins to happen. At $t/M = 700$, the infalling waves of relatively high frequency can be seen for $r_* \lesssim 0$.

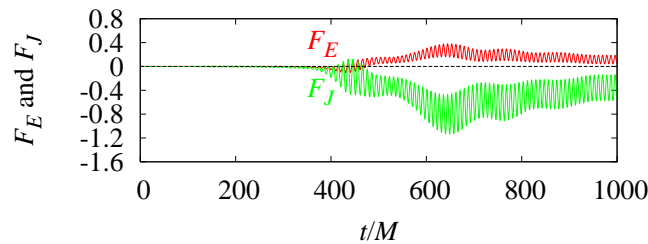


Figure 5: Same as Fig. 2 but for simulation (B).

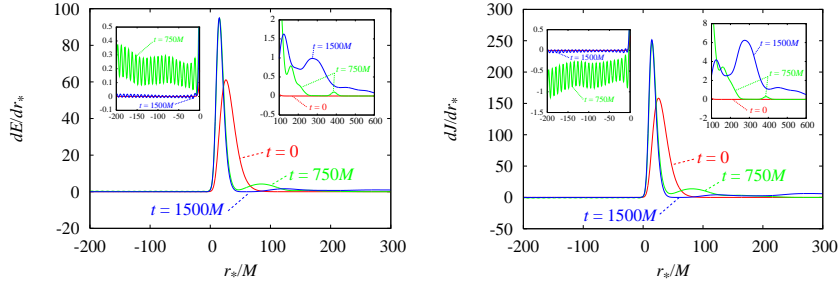


Figure 6: The energy density dE/dr_* (left) and the angular momentum density dJ/dr_* (right) with respect to the tortoise coordinate r_* at time $t/M = 0, 750,$ and 1500 for simulation (B).

Figure 5 shows the energy and angular momentum fluxes F_E and F_J toward the horizon. During the bosonova, F_E is positive up to $t = 1000M$. Here, the dominant contribution comes from the high-frequency waves generated by the nonlinear effect. Therefore, the extraction of energy is prevented by the bosonova. On the other hand, F_J continues to be negative, and the waves continue to extract the angular momentum from the BH. The left and right panels of Fig 6 show the energy and angular momentum densities with respect to r_* , dE/dr_* and dJ/dr_* , at $t/M = 0, 750,$ and 1500 . At $t/M = 750$ and 1500 , most of the energy is contained in $0 \lesssim r_*/M \lesssim 30$. In right inset of each panel that highlights the distant region, a small bump can be seen around $r_*/M = 400$ for $t/M = 750$. This bump is moving to outside approximately at the speed of light. Therefore, a small explosion happened in the bosonova. At $t/M = 1500$, more amount of energy and angular momentum can be seen at the distant place.

4 Summary

As the result of our simulations, we found the following: (A) When the initial peak value is small, the nonlinear effect causes periodic change of peak location and the peak value, and enhances the energy and angular momentum extraction; (B) When the initial peak value is large, the nonlinear effect causes an explosion, the bosonova. During the bosonova, high-frequency waves violating the superradiant condition are generated, and thus, the energy flux toward the horizon becomes positive terminating the superradiant instability. After JGRG21, we performed supplementary simulations in order to assess whether the bosonova happens or not taking account of the possibility that the nonlinear effect saturates the growth by superradiant instability. The result shows no evidence for saturation, and therefore, the bosonova is likely to happen as a result of the superradiant instability. Studying observational consequence of the bosonova, such as gravitational wave emission, is an interesting issue to be explored.

Acknowledgments

This work was supported by the Grant-in-Aid for Scientific Research (A) (22244030).

References

- [1] A. Arvanitaki, S. Dimopoulos, S. Dubovsky, N. Kaloper and J. March-Russell, *Phys. Rev. D* **81**, 123530 (2010) [arXiv:0905.4720 [hep-th]]; A. Arvanitaki and S. Dubovsky, *Phys. Rev. D* **83**, 044026 (2011) [arXiv:1004.3558 [hep-th]].
- [2] S. L. Detweiler, *Phys. Rev. D* **22**, 2323 (1980); T. J. M. Zouros and D. M. Eardley, *Annals Phys.* **118**, 139 (1979); S. R. Dolan, *Phys. Rev. D* **76**, 084001 (2007) [arXiv:0705.2880 [gr-qc]].
- [3] S. L. Cornish, N. R. Claussen, J. L. Roberts, E. A. Cornell and C. E. Wieman, *Phys. Rev. Lett.* **85**, 1795 (2000); E. A. Donley, N. R. Claussen, S. L. Cornish, J. L. Roberts, E. A. Cornell, and C. E. Wieman, *Nature* **412**, 295 (2001) [arXiv:cond-mat/0105019].

Constraints on Particle Dark Matter Models by the Presence of Primordial Black Holes

Ryo Saito^{43(a)}, Shigeki Matsumoto^(b), Satoshi Shirai^(c,d), and Tsutomu T. Yanagida^(b)

^(a) *Yukawa Institute for Theoretical Physics, Kyoto University, Kyoto 606-8502 Japan*

^(b) *IPMU, TODIAS, University of Tokyo, Kashiwa, 277-8583, Japan*

^(c) *Department of Physics, University of California, Berkeley, CA 94720*

^(d) *Theoretical Physics Group, Lawrence Berkeley National Laboratory, Berkeley, CA 94720*

Abstract

We show that cosmic-ray experiments impose a tight constraint on some particle dark matter models if the primordial black holes exist as a part of the dark matter in the Universe.

1 Introduction

The identity of dark matter (DM) is one of the challenging problems in contemporary cosmology. Since we do not have satisfactory DM candidates in the standard model of particle physics and inflationary cosmology, the existence of DM indicates that we need physics beyond the standard model of the Universe.

One approach is to introduce a new particle that is stable and neutral. A major class of such candidates is weakly interacting massive particles (WIMPs), which has mass roughly between 10 GeV and TeV, and weak-scale annihilation cross sections. In the standard scenario, the WIMPs are produced as thermal relics, which are in thermal equilibrium with the hot plasma in the early Universe and decouple when the annihilation rate falls below the expansion rate. Then, the present relic density is determined by its annihilation cross section as,

$$\Omega_{\text{WIMP}} h^2 \simeq 0.1 \left(\frac{\langle \sigma v \rangle}{3 \times 10^{-26} \text{ cm}^3 \text{ s}^{-1}} \right)^{-1}, \quad (1.1)$$

where $\langle \sigma v \rangle$ is thermal average of a product of the annihilation cross section and velocity. Hence, the annihilation cross section $\langle \sigma v \rangle \sim 3 \times 10^{-26} \text{ cm}^3 \text{ s}^{-1}$, which is the typical size of the weak-scale cross section, can provide the present DM density.

In some particle DM models, however, DM-candidate particles are predicted to have larger cross sections and then smaller abundance. In these models, DM should be mixture of WIMPs and another component. A candidate of such a component is primordial black holes (PBHs), which are black holes formed in the early Universe as a result of the gravitational collapse of the primordial density fluctuations. Though the mass of PBHs can have a wide range of values depending on the spectral shape of the density fluctuations, PBHs can be the dominant component of DM only if their masses are in the mass range 10^{20-26} g , where there are no constraints from gravitational lensing experiments and others [1].

If a part of DM consists of PBHs, WIMPs are accreted by PBHs and form minihalo around them. The minihalo formed around a PBH is called ultracompact minihalo (UCMH) [2–4]. The number density of WIMP in the UCMHs is so high that a small fraction of them can lead to significant enhancement of the cosmic ray signal from WIMP annihilations [5–7]. Therefore, we expect that the cosmic-ray experiments can provide stringent constraints on the number/annihilation rate of UCMHs and then a model of WIMP. In this paper, we investigate the constraint on models of WIMP from cosmic-ray experiments in the case that a fraction of DM in the Universe consists of PBHs and UCMHs are formed around them.

⁴³Email address: rsaito@yukawa.kyoto-u.ac.jp

2 Enhancement of annihilations by the primordial black holes

In this section, we briefly introduce the WIMP accretion process on the PBHs and estimate consequent enhancement of the annihilation rate in the galactic halo in the present Universe.

First, we estimate the enhanced WIMP abundance assuming that a fraction of the DM consists of PBHs at their formation time:

$$\rho_{\text{PBH},i} = (1 - f_{\text{WIMP}})\rho_{c,i}, \quad \rho_{\text{WIMP},i} = f_{\text{WIMP}}\rho_{c,i}, \quad (0 \leq f_{\text{WIMP}} \leq 1) \quad (2.1)$$

where $\rho_{c,i}$ is the DM density at the formation time. If the fraction of WIMPs is small, the accretion mostly occurs in the radiation-dominated era. In the radiation-dominated era, a mass shell with radius r feels force from the central PBH and the radiation in the inner region. Hence, the accretion is governed by the following equation,

$$\frac{d^2r}{dt^2} = -\frac{GM_{\text{PBH}}}{r^2} + \frac{L^2}{r^3} - \frac{8\pi G}{3}\rho_{\text{rad}}r, \quad (2.2)$$

where $L = \|\mathbf{r} \times \mathbf{v}\|$ is angular momentum per mass for a WIMP and ρ_{rad} is the energy density of the radiation. Since the forces from the PBH and radiation are the central force, the angular momentum is conserved during the accretion. The angular momentum of WIMPs is originated from peculiar velocity induced gravitationally and thermally. The former is irrelevant to the present analysis because the fluctuations in the gravitational potential do not grow much in the radiation-dominated era. The WIMPs have the thermal velocity dispersion $\sqrt{3T_{\text{kd}}/m_{\text{WIMP}}}$ at the kinetic decoupling and the velocity decreases as $\propto (1+z)$ after that. Hence, the thermal velocity is provided by the Maxwell distribution with a dispersion,

$$\sigma_t \simeq 35 \text{ cm/s} \left(\frac{m_{\text{WIMP}}}{100 \text{ GeV}}\right)^{-\frac{1}{2}} \left(\frac{T_{\text{kd}}}{10 \text{ MeV}}\right)^{-\frac{1}{2}} \left(\frac{1+z}{1+z_{\text{eq}}}\right), \quad (2.3)$$

where T_{kd} is temperature of the Universe at the kinetic decoupling, which is determined by scattering cross sections with light particles, and z_{eq} is redshift at the matter-radiation equality.

The WIMP density profile in the UCMHs can be estimated by solving Eq.(2.2) with initial conditions,

$$r = r_i, \quad \frac{dr}{dt} = H_i r_i + v_i \cos \theta, \quad (2.4)$$

where H_i and v_i are the Hubble parameter and the thermal velocity at the initial time and θ is angle between the radial direction and the initial velocity. Since the angular momentum is conserved, L can be written as $L = r_i v_i \sin \theta$ using the initial radius and velocity. After the WIMPs are decoupled from the Hubble expansion, their motion can be well approximated by the Keplerian motion with a definite energy and angular momentum. Hence, time-averaged energy density of WIMP is given by,

$$\rho_{\text{WIMP}} = \frac{1}{4\pi r^2} \int \frac{2d\mu}{T v_r}, \quad (2.5)$$

where $d\mu$ represents energy for WIMPs with initial radius $r_i - r_i + dr_i$ and velocity $v_i - v_i + dv_i$,

$$d\mu \equiv 4\pi r_i^2 \rho_{\text{WIMP},i} dr_i f(v_i) d^3 v_i, \quad (2.6)$$

and T and v_r are their period and radial velocity after the decoupling. Here, $f(v)$ is the Maxwell distribution with the dispersion (2.3). The energy density (2.5) becomes higher for smaller angular momenta because the centrifugal force prevent the WIMPs from being bound by the PBHs. Since the accretion is most efficient at the matter-radiation equality, the density is typically comparable to $f_{\text{WIMP}}\rho_{\text{eq}} \sim 10^5 f_{\text{WIMP}} \text{ GeV/cm}^3$ if the angular momentum is negligible and the accretion occurs efficiently.

In an inner high-dense region, the high annihilation rate reduces the density and the profile becomes shallower. This shallower profile develops from a radius R_a where the density becomes comparable to

$$\rho_a \equiv \frac{m_{\text{WIMP}}}{\langle \sigma v \rangle (t_0 - t_i)} = 8 \times 10^9 \text{ GeV/cm}^3 \left(\frac{m_{\text{WIMP}}}{100 \text{ GeV}}\right) \left(\frac{\langle \sigma v \rangle}{3 \times 10^{-26} \text{ cm}^3/\text{s}}\right)^{-1}, \quad (2.7)$$

where $t_0 - t_i$ is time elapsed from the formation of the UCMH, 4×10^{17} s.

Provided the WIMP density, we can estimate the the annihilation rate per PBH as,

$$\Gamma = \frac{1}{m_{\text{WIMP}}^2} \int dr 2\pi r^2 \rho_{\text{WIMP}}(r)^2 \langle \sigma v \rangle. \quad (2.8)$$

The density profile (2.5) is determined by mass, cross sections, and PBH mass. Hence we can unambiguously calculate it if a particle DM model and PBH mass are provided. Since the WIMP density in the UCMHs is typically $\mathcal{O}(10^{4-5})$ larger than the local density $\rho_{\odot} = 0.3 \text{ GeV/cm}^3$, a tiny fraction of PBHs can induce a large annihilation rate. Therefore, we expect that some models of WIMP are tightly constrained by cosmic-ray experiments in the presence of PBHs.

3 Gamma-ray constraints

Here, we consider the constraints from gamma-ray experiments as the Fermi gamma-ray space telescope [8]. The signals from the UCMHs are similar to that from the decaying DM with mass $2m_{\text{WIMP}}$. Hence it is convenient to introduce a corresponding life time defined by

$$\tau_c^{-1} \equiv \frac{n_{\text{PBH},\odot}}{\rho_{\odot}/2m_{\text{WIMP}}} \Gamma, \quad (3.1)$$

where $n_{\text{PBH},\odot}$ is local number density of PBHs. By using the corresponding lifetime (3.1), we can read the constraints on UCMHs from those on decaying DM. In Fig. 1, we have depicted the constraints on the corresponding lifetime for wino dark matter using the constraints on decaying DM in Ref. [9]. For PBH masses larger than 10^{24} g, where the angular momentum is negligible compared to the gravitational force from the PBHs, the resultant corresponding lifetime has a similar value and the wino dark matter is excluded for all parameter region. Though the constraint becomes weaker for smaller PBH masses, where the angular momentum is relevant, we can see that the wino dark matter is excluded for large parameter region in the PBH-DM window 10^{20-26} g.

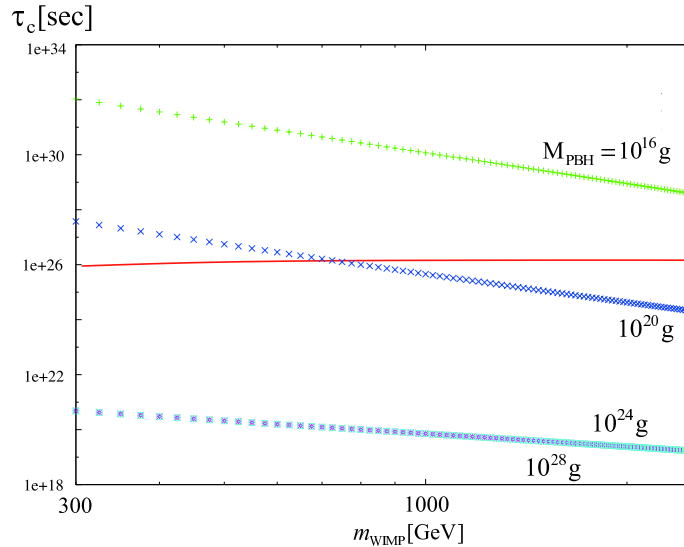


Figure 1: Gamma-ray constraints for wino dark matter. Each dots represent the corresponding lifetime for different PBH mass and wino mass. The parameter region below the red line is excluded by the Fermi observations of the isotropic diffuse gamma-ray.

4 Summary

In this paper, we have seen that some models of WIMP can be tightly constrained by cosmic-ray experiments as the Fermi gamma-ray space telescope in the presence of a tiny amount of PBHs. The PBHs produced at the early Universe can form a minisize halo called UCMH around them by accreting the surrounding WIMPs. The WIMP density in the UCMHs is so large that a tiny amount of the PBHs can induce a large annihilation rate and then the UCMHs become gamma-ray sources for the Fermi gamma-ray space telescope. The signal from the UCMHs depends on a model of WIMP and PBH mass. As an example, we have investigated the constraint from the Fermi gamma-ray space telescope for wino dark matter and found that it is excluded for large parameter region in the PBH-DM window 10^{20-26} g. Though we have considered wino dark matter here, similar tight constraints are expected to be obtained for models which predict smaller DM abundance. If the existence of PBHs are shown, it is expected that tight constraints are imposed on particle DM models by cosmic-ray experiments.

References

- [1] B. J. Carr, K. Kohri, Y. Sendouda and J. Yokoyama, *Phys. Rev. D* **81**, 104019 (2010)
- [2] K. J. Mack, J. P. Ostriker and M. Ricotti, *Astrophys. J.* **665**, 1277 (2007).
- [3] M. Ricotti, *Astrophys. J.* **662**, 53 (2007).
- [4] M. Ricotti and A. Gould, *Astrophys. J.* **707**, 979 (2009).
- [5] P. Scott, S. Sivertsson and S. Sivertsson, *Phys. Rev. Lett.* **103**, 211301 (2009) [Erratum-ibid. **105**, 119902 (2010)]
- [6] B. C. Lacki and J. F. Beacom, *Astrophys. J.* **720**, L67 (2010)
- [7] R. Saito and S. Shirai, *Phys. Lett. B* **697**, 95 (2011)
- [8] <http://fermi.gsfc.nasa.gov/>.
- [9] C. Chen, S. Mandal and F. Takahashi, *JCAP* **1001**, 023 (2010)

A quasi-radial stability criterion for rotating relativistic stars

Kentaro Takami⁴⁴, Luciano Rezzolla^{1,2} and Shin'ichirou Yoshida³

¹*Max-Planck-Institut für Gravitationsphysik, Albert Einstein Institut, Golm, Germany*

²*Department of Physics, Louisiana State University, Baton Rouge, LA USA*

³*Department of Earth Science and Astronomy, Graduate School of Arts and Sciences, University of Tokyo, Japan*

Abstract

The stability properties of relativistic stars against gravitational collapse to black hole is a classical problem in general relativity. A sufficient criterion for secular instability was established by Friedman, Ipser and Sorkin (1988), who proved that a sequence of uniformly rotating barotropic stars is secularly unstable on one side of a turning point and then argued that a stronger result should hold: that the sequence should be stable on the opposite side, with the turning point marking the onset of secular instability. We show here that this expectation is not met. By computing in full general relativity the F -mode frequency for a large number of rotating stars, we show that the neutral-stability point, *i.e.*, where the frequency becomes zero, differs from the turning point for rotating stars. Using numerical simulations we validate that the new criterion can be used to assess the dynamical stability of relativistic rotating stars.

1 INTRODUCTION

The stability of a relativistic star against collapse to black hole is one of the most important predictions of general relativity. While this problem is reasonably well understood for nonrotating stars, this is not the case for rotating stars and is particularly obscure when the stars are rapidly rotating. A milestone in this landscape is the criterion for secular stability proposed by Friedman, Ipser and Sorkin (1988), who proved that a sequence of uniformly rotating barotropic stars is secularly unstable on one side of a turning point. They then argued, based on an expectation that viscosity leads to uniform rotation, that the turning point should identify the onset of secular instability. While for nonrotating star the turning point coincides with the secular-instability point, for rotating stars it is only a sufficient condition for a secular instability. Lacking other guides, the turning point is routinely used to find a dynamical instability in simulations.

Our understanding of the dynamical instability of relativistic stars in uniform rotation can be improved by determining the neutral-stability line, that is the set of stellar models whose frequency of the fundamental mode of quasi-radial oscillation (F mode) is vanishingly small. While this problem is challenging from a perturbative point of view, especially when the rate of rotation becomes high, it can be tackled through numerical calculations. We have therefore simulated in full general relativity 54 stellar models and calculated accurately the corresponding F -mode frequency via a novel analysis of the power spectral density (PSD) of the central rest-mass density. We find that it coincides with the turning point for spherical stars, but not for rotating stars, with the difference increasing with the angular momentum.

Unless stated differently, we use units in which $c = G = M_{\odot} = 1$.

2 Numerical Setup and Initial Data

All of our calculations have been performed in full general relativity (GR) using the `Whisky2D` code described in detail in Kellerman et al. [1]. This is a 2-dimensional (2D) code based on the 3-dimensional (3D) `Whisky` code [2], and exploiting the condition of axisymmetry through the “cartoon” method [3]. In essence, the evolution of the spacetime is obtained using the 2D version of `Ccatie`, a finite-differencing

⁴⁴Email address: kentaro.takami@aei.mpg.de

code providing the solution of a conformal traceless formulation of the Einstein equations [4], while the equations of relativistic hydrodynamics are solved a flux-conservative formulation of the equations.

The initial equilibrium stellar models are built using the `rns` code [5] as isentropic, uniformly rotating relativistic perfect-fluid polytropes with equation of state $p = K\rho^\Gamma$, $e = \rho + \frac{p}{\Gamma-1}$, where p is the pressure, ρ the rest-mass density, K the polytropic constant, Γ the polytropic exponent, and e the energy density. We have here set $K = 100$ and $\Gamma = 2$. Furthermore, because we are not interested here in extracting gravitational-wave information, we place the outer boundary at a few stellar radii and use a uniform grid with spacing $\Delta x = \Delta z = h$ ranging between $h = 0.04 M_\odot$ for the rapidly rotating models and up to $h = 0.1 M_\odot$ for the slowly rotating ones.

As discussed by many authors, the truncation error in the initial data is sufficient to trigger perturbations in the star, which will start to oscillate in a number of eigenmodes. However, because we need to determine the eigenfrequency of the F mode, it is important that as much as possible of the initial perturbation energy goes into exciting that mode. For this reason we introduce an initial perturbation using the eigenfunction of the F mode for a nonrotating neutron star with the same central density, and which can be computed from linear perturbation theory.

3 Methodology and Accuracy

As customary, we extract the F -mode frequency by performing a discrete Fourier transform of the evolution of a representative hydrodynamical quantity, such as the central rest-mass density ρ_c , and by inspecting the corresponding PSD. Defining as F_N the frequency of the largest peak in the numerical PSD, previous studies determined the value of the F -mode frequency, F , by fitting the PSD with a known analytic function or by taking the derivative of the PSD. The frequency obtained in these ways depends sensitively on the fitting function used, on the shape of the PSD around F_N , and on the evolution time τ . We here use a different approach. Because F_N will tend to F as the evolution time $\tau \rightarrow \infty$, we simply consider the evolution of F_N for increasingly large values of τ . What we find in this way is that $F_N(\tau)$ is an oscillating function around F , whose amplitude is however bounded by two envelopes which have a clear $1/\tau$ dependence. Fitting for these envelopes and extrapolating for $\tau \rightarrow \infty$ we obtain a very accurate and possibly optimal value for F . This approach turns out to give an excellent measure of the F -mode eigenfrequency.

4 RESULTS

The space of parameters is spanned by central rest-mass density and the angular momentum of the rotating models. To cover the largest possible region of parameters we have evolved 54 stellar models of relativistic stars with ρ_c in the range $[\rho_{\min}, \rho_{\max}] = [8 \times 10^{-4}, 3.18 \times 10^{-3}]$ and dimensionless rotation parameter β between zero and the mass-shedding limit.

We show as filled blue circles in Fig. 1 all of the computed F -mode frequencies, where the squares of the F -mode frequencies $(F)^2$ are reported as function of ρ_c and β . Shown as a solid magenta line is the analytic fitting of the frequency for nonrotating stars, while dashed blue lines show sequences of rotating stars having the same rest-mass density. All models simulated have nonzero F -mode frequencies and their number diminishes for $(F)^2 \approx 0$. This is because for these models the oscillation timescale tends to become extremely large, thus becoming intractable in numerical simulations. In addition, models near the neutral point could also be artificially induced to collapse simply by the accumulation of the truncation error, thus preventing any reliable measure. As a result, our analysis has been constrained to values of the frequencies $F \gtrsim 2.2 \times 10^{-3} \simeq 0.45$ kHz. Fortunately, however, the quality of the data and the smoothness in which they appear in Fig. 1, allow us to compute an analytic fit of the function $(F)^2 = (F)^2(\rho_c, \beta)$ and thus determine analytically the neutral-stability line where $(F)^2 = 0$.

It is convenient to use a fitting function $(F_{\text{fit}})^2(\rho_c, \beta)$ that is linear in β and such that $(F_{\text{fit}})^2(\rho_{\max}, 0) = 0$ by construction

$$(F)_{\text{fit}}^2(\rho_c, \beta) = (F)_{\text{fit}}^2(\rho_c, 0) + \beta \sum_{n=0}^5 b_n(\rho_c)^n = \sum_{n=0}^5 a_n(\rho_c)^n + \beta \sum_{n=0}^5 b_n(\rho_c)^n, \quad (4.1)$$

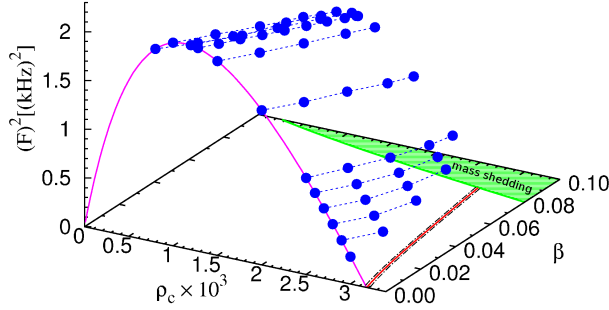


Figure 1: Square of the F -mode frequencies (blue filled circles) as a function of ρ_c and β . The dashed green area shows models above the mass-shedding limit, and the red solid line marks the neutral stability (*cf.* Fig. 2).

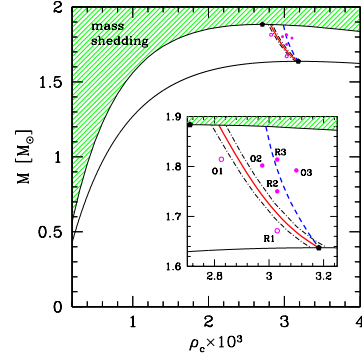


Figure 2: Stability lines in a (ρ_c, M) diagram. The two solid black lines mark sequences with either zero or mass-shedding angular momentum. The solid red line is the neutral-stability line, “thickened” by the error bar. The blue dashed line is instead the turning-point criterion for secular stability. Marked with empty or filled circles are representative models with constant angular velocity O1, O2, O3, or constant initial central rest-mass density R1, R2, R3.

where a_n, b_n are constant coefficients, which a least-square fitting with the data reveals to be

$$\begin{aligned} a_5 &= 6.978 \times 10^8, & a_4 &= -7.757 \times 10^6, & a_3 &= 3.621 \times 10^4, \\ a_2 &= -9.599 \times 10, & a_1 &= 1.172 \times 10^{-1}, & a_0 &= 2.110 \times 10^{-7}, \\ b_5 &= -5.599 \times 10^{10}, & b_4 &= 4.862 \times 10^8, & b_3 &= -1.612 \times 10^6, \\ b_2 &= 2.545 \times 10^3, & b_1 &= -1.896, & b_0 &= 3.357 \times 10^{-4}. \end{aligned}$$

Using expression (4.1), it is straightforward to compute the neutral-stability line in a (ρ_c, β) plane as the one at which $(F)_{\text{fit}}^2(\rho_c, \beta) = 0$. Of course this line will be “thickened” by the uncertainty associated to the fit which, to be conservative, we consider to be σ_{max} . While a neutral-stability line is already very informative in a (ρ_c, β) plane, its greatest impact can be appreciated in the more traditional (ρ_c, M) diagram. This is shown in Fig. 2, where the two solid black lines refer to sequences of nonrotating and mass-shedding models, respectively. Drawn as solid red is the neutral-stability line “thickened” by the error bar σ_{max} . Finally, shown as a blue dashed line is the turning-point criterion for secular stability along a sequence of constant angular momentum J , *i.e.*, $(\partial M / \partial \rho_c)_{J=\text{const}} = 0$.

Clearly, the new neutral-stability criterion does coincide with the turning-point criterion for nonrotating stars, but it differs from it as the angular momentum is increased, moving to smaller central rest-mass densities. While unexpected, this difference does not point to a conflict between the two criteria. This is because the turning-point criterion is only a *sufficient* condition for secular instability of rotating stars; stated differently, while a rotating stellar model which is at or to the right of the turning-point line is expected to be also secular unstable, the opposite is not true. Hence, the two criteria are compatible as long as the secular instability line lies to the left of the neutral-stability line. Therefore, along a $J = \text{const.}$ sequence of stellar models we expect the following order with increasing rest-mass density: secular instability, dynamical instability, turning-point.

To validate that the neutral-stability line should be used in place of the turning-point line to distinguish stellar models that are dynamically unstable from those that are instead stable, we have considered 6 models whose properties fall in a small region near the two stability lines. More specifically, we consider two different sequences having either constant angular velocity, *i.e.*, models O1, O2, O3 in Fig. 2, or

constant ρ_c , *i.e.*, models R1, R2, R3. The predictions for these models are different according to which criterion is used for stability. In fact, while models O1, R1 are expected to be stable for both criteria and models O3, R3 are expected to be unstable for both criteria, models O2, R2 are predicted to be stable on a dynamical timescale by the turning-point criterion but unstable by the neutral-stability criterion.

To test these predictions we have evolved these configurations maintaining the same computational setup (but without an initial perturbation). As expected, models O1, R1 are found to be stable over a few oscillations, while models O3, R3 are found to collapse to black holes within a oscillation. Similarly, models O2, R2 are also found to collapse to black holes over a timescale which is only slightly larger than that of models O3, R3. We conclude that the neutral-stability line can indeed be used to mark the boundary of a dynamically unstable region.

5 Conclusions

The stability of rotating relativistic stars against gravitational collapse to black hole is an old problem in general relativity, impacting all those astrophysical problems where a neutron star may be produced and induced to collapse as a result of mass accretion. Despite the importance of this problem, no analytic criterion is known for a dynamical stability of rotating stars. Important progress was made about 20 years ago, when a criterion for secular stability was proposed by Friedman et al. [6], who suggested that a turning point along a sequence of stellar models with constant angular momentum can be associated with the onset of a secular instability. Although this criterion is only a sufficient condition for the development of a secular instability, it has been systematically used to limit the region of dynamical instability in simulations of relativistic stars.

To improve our understanding of the dynamical instability of relativistic stars in uniform rotation, we have computed the neutral-stability point for a large class of stellar models, *i.e.*, the set of stellar models whose F -mode frequency is vanishingly small. These have allowed us to produce an analytic fit of the data and deduce from this the neutral-stability line. The latter coincides with the turning-point line of Friedman et al. [6] for nonrotating stars, but differs from it as the angular momentum is increased, being located at smaller central rest-mass densities as the angular momentum is increased. This difference does not contradict turning-point criterion since the latter is only a sufficient condition for secular instability.

To test this result we have evolved stellar models whose properties fall in a small region near the two stability lines, paying special attention to those stellar models that are predicted to be stable on a dynamical timescale by the turning-point criterion but unstable by the neutral-stability line. Numerical evidence that these model do collapse to black holes allows us to conclude that the neutral-stability line can be used effectively to mark the boundary to dynamical instability.

The details of this work appear in [7].

References

- [1] Kellerman T., Baiotti L., Giacomazzo B., Rezzolla L., 2008, *Classical and Quantum Gravity*, 25, 225007
- [2] Baiotti L., Hawke I., Montero P. J., Löffler F., Rezzolla L., Stergioulas N., Font J. A., Seidel E., 2005, *Phys. Rev. D*, 71, 024035
- [3] Alcubierre M., Brüggmann B., Holz D., Takahashi R., Brandt S., Seidel E., Thornburg J., Ashtekar A., 2001, *International Journal of Modern Physics D*, 10, 273
- [4] Pollney D., Reisswig C., Rezzolla L., Szilágyi B., Ansorg M., Deris B., Diener P., Dorband E. N., Koppitz M., Nagar A., Schnetter E., 2007, *Phys. Rev. D*, 76, 124002
- [5] Stergioulas N., Friedman J. L., 1995, *Astrophys. J.*, 444, 306
- [6] Friedman J. L., Ipser J. R., Sorkin R. D., 1988, *Astrophys. J.*, 325, 722
- [7] Takami K., Rezzolla L., Yoshida S., 2011, *Mon. Not. R. Astron. Soc.*, 416, L1

Effect of Pasta Phase on Oscillations in Neutron Stars

Hajime Sotani⁴⁵

*Division of Theoretical Astronomy, National Astronomical Observatory of Japan, 2-21-1 Osawa,
Mitaka, Tokyo 181-8588, Japan*

Abstract

We show that the shear modes in the neutron star crust are quite sensitive to the existence of nonuniform nuclear structures, the so-called “pasta”. Due to the existence of pasta phase, the frequencies of shear modes are reduced, where the dependence of fundamental frequency is different from that of overtones. Since the torsional shear frequencies depend strongly on the structure of pasta phase, through the observations of stellar oscillations, one can probe the pasta structure in the crust, although that is quite difficult via the other observations. Additionally, considering the effect of pasta phase, we show the possibility to explain the all observed frequencies in the SGR 1806-20 with using only crust torsional shear modes.

1 Introduction

The soft gamma repeaters (SGRs) are considered as one of the most promising candidate of magnetars, which are neutron stars with strong magnetic fields. The sporadic X- and gamma-ray bursts are radiated from SGRs, while SGRs rarely emit much stronger gamma-rays called “giant flares”. Up to now, at least three giant flares have been detected, which are the SGR 0526-66, the SGR 1900+14, and the SGR 1806-20. Through the timing analysis of these decaying tail, the quasi-periodic oscillations (QPOs) have discovered, which are in the range from tens Hz up to a few kHz [1]. Since the QPOs are believed as the outcomes of the neutron star oscillations, the observations of QPOs in SGRs could be first evidences to detect the neutron star oscillations directly.

It is considered that the neutron star crust exists from the bottom of the ocean of melted iron inward to the boundary with the inner fluid core at a density of order the saturation density of nuclear matter. Although nuclei in the crust form a bcc lattice due to Coulomb interactions, according to the recent studies, the nuclear structure in the bottom of crust could be nonuniform, i.e., with increasing the density, the shape of nuclear matter region is changing from sphere (bcc lattice) into cylinder, slab, cylindrical hole, and uniform matter (inner fluid core). This variation of nuclear structure is known as the so-called “pasta structure”. The density that the cylinder structure appears, ρ_p , depends on the nuclear symmetry energy expressed with the density symmetry coefficient L , which is suggested to be order $\rho_p \sim 10^{13}$ g/cm³ via the calculations of the ground state of matter in the crust. However, it might be quite difficult to verify the existence of pasta structure by using the observation of neutron star properties such as mass and radius, because the width of pasta phase is around 10% of the crust, which is less than a few hundred meters. In contrast, in this article, we will calculate the torsional oscillations of neutron star with pasta phase and show that the frequencies of shear modes depend strongly on the presence of pasta phase and on ρ_p . The more details of this study can be seen in [2].

2 Shear Modulus in Crust

Previously, there are many calculations about the oscillations of magnetars (e.g., [3–6]), where they assume that nuclei form bcc lattice in the crust when the crust torsional oscillations are considered. With this assumption, the shear modulus of the crust is suggested as

$$\mu = 0.1194 \times n_i (Ze)^2 / a, \quad (2.1)$$

⁴⁵Email address: sotani@astro.auth.gr

where n_i is the ion number density, $a = (3/4\pi n_i)^{1/3}$ is the average ion spacing, and $+Ze$ is the ion charge. On the other hand, it is pointed out that the elastic properties in the pasta phase could be liquid crystals rather than a crystalline solid [7]. That is, unlike the case of bcc lattice, the shear modulus should be decreasing in the pasta phase as increasing the density. This picture is thought to be natural, because the structure of nuclear matter changes gradually as mentioned the above and at last the shear modulus becomes zero in the fluid core. In order to realize such a relation about the shear modulus, we adopt Eq. (2.1) in the crust except for the pasta phase, while in the pasta phase it is assumed that the shear modulus can be expressed as the cubic function with respect to the density, which satisfies that μ should connect to Eq. (2.1) smoothly at $\rho = \rho_p$ and become zero smoothly at the boundary with the core, i.e., $\mu = c_1(\rho - \rho_c)^2(\rho - c_2)$, where c_1 and c_2 are some constants determined by the boundary conditions (see Fig. 1). Of course, this simple relation of μ in the pasta phase might be a kind of toy model, although expressed the rough behavior, because that should depend on the microscopic structure including the matter composition and/or the nuclear symmetry energy. Still, this relation is thought to be enough to examine the dependence of shear oscillations on the existence of pasta phase as a first step. Anyway, as a result of the fall-off of shear modulus, one can expect that the shear velocity will become smaller, and that the frequencies of shear modes will also decrease.

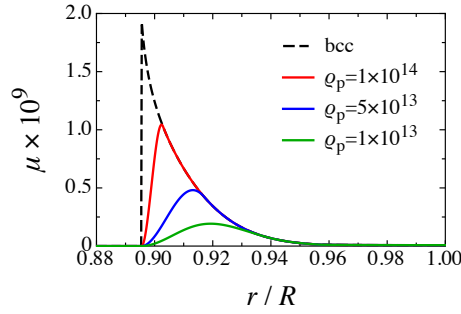


Figure 1: Adopted shear modulus μ as a function of relative radius r/R .

3 Torsional Shear Modes

The torsional shear modes can be described with using one perturbation variable, which is the angular displacement of the stellar matter, $\mathcal{Y}(t, r)$. The non-zero component of perturbed matter quantities is ϕ -component of the perturbed 4-velocity of fluid, δu^ϕ , which is expressed with \mathcal{Y} as

$$\delta u^\phi = e^{-\Phi} \partial_t \mathcal{Y}(t, r) \sin^{-1} \theta \partial_\theta P_\ell(\cos \theta). \quad (3.1)$$

Assuming that the perturbed variable has a harmonic time dependence, such that $\mathcal{Y}(t, r) = e^{i\omega t} \mathcal{Y}(r)$, the perturbation equation reduces to

$$\mathcal{Y}'' + \left[\left(\frac{4}{r} + \Phi' - \Lambda' \right) + \frac{\mu'}{\mu} \right] \mathcal{Y}' + \left[\frac{\epsilon + p}{\mu} \omega^2 e^{-2\Phi} - \frac{(\ell + 2)(\ell - 1)}{r^2} \right] e^{2\Lambda} \mathcal{Y} = 0, \quad (3.2)$$

where ϵ and p correspond to the energy density and pressure, respectively, and the prime denotes the derivative with respect to r . With appropriate boundary conditions, the problem to solve becomes the eigenvalue problem. We impose a zero traction condition at the boundary between the inner core and the crust, and the zero-torque condition at the stellar surface.

4 Numerical Results

We examine the frequencies of torsional shear modes, as varying the value of ρ_p in the range of $\rho_p = 10^{13} - 10^{14}$ g/cm³, because that value is not certain but suggested to be order 10^{13} g/cm³ as mentioned

before. The left panel of Fig. 2 shows the fundamental frequencies of torsional shear modes with $\ell = 2$ as a function of the stellar mass, where the broken line corresponds to the frequencies for the stellar model without pasta phase and the solid lines are corresponding to those with pasta phase with different values of ρ_p . Obviously, one can observe that the frequencies of shear modes depend strongly on the existence of pasta phase. In fact, compared with the frequency for the stellar model without pasta phase, those with pasta phase are reduced to 12.0%, 34.9%, and 49.3% for $\rho_p = 1 \times 10^{14}$, 4×10^{13} , and 1×10^{13} g/cm³, respectively. While, in the right panel of Fig. 2, the frequencies of 1st overtones of shear modes with $\ell = 2$ are plotted as a function of the stellar mass. Unlike the fundamental modes, the frequencies with higher ρ_p are almost same as that without pasta phase. Still, one can see the dependence of the frequency on the existence of pasta phase with lower ρ_p . In fact, the frequencies with pasta phase are different from that without pasta phase in 0.4%, 46.0%, and 67.0% for $\rho_p = 1 \times 10^{14}$, 4×10^{13} , and 1×10^{13} g/cm³, respectively. This dependence might be difficult to explain in analogy with the Newtonian limit, but one could be possible to obtain the additional information of the crust property via the observation of frequencies of overtones.

Since the both frequencies of fundamental and overtone shear modes depend strongly on the presence of pasta phase, whose effect has been neglected so far, one needs to consider this effect on the shear oscillations. Additionally, owing to this strong dependence, it could be possible to probe the properties of pasta phase via the observations of stellar oscillations and stellar mass, although the constraint on the pasta phase is quite difficult via the other observations of neutron stars. In contrast to simple relation of μ adopted in this article, we will make an examination with more realistic shear model in the pasta phase in the future.

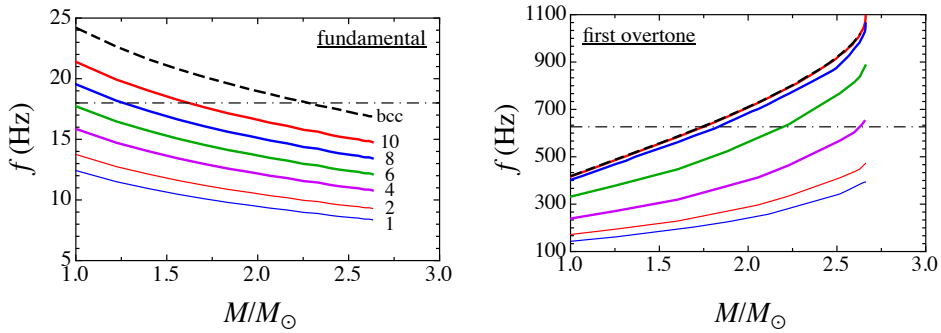


Figure 2: Frequencies of fundamental torsional shear modes (left) and first overtones (right) with $\ell = 2$ as a function of neutron star mass.

At last, we will compare the calculated frequencies of shear modes with the observed QPO frequencies in giant flare. Especially, in this article we focus on the QPO frequencies in the SGR 1806-20, i.e., 18, 26, 30, and 92.5 Hz in less than 100 Hz, because this phenomenon has the most observed frequencies among the detected giant flares in the past [1]. The previous calculations are shown the difficulty to explain the all observed frequencies with using only crust shear modes [3]. That is, the fundamental $\ell = 2$ mode, which is the possible lowest frequency, is considered to correspond to the observed frequency of 18 Hz and the fundamental $\ell = 3$ mode is corresponding to 26 or 30 Hz. But, the spacing of shear frequencies with different ℓ is larger than the spacing between the observed frequencies of 26 and 30 Hz. In practice, according to such a traditional identification, we can explain the observed frequencies with the crust shear modes with pasta phase as shown in the left panel of Fig. 3, i.e., 18, 30, 92.5 Hz can be identified as $\ell = 2, 3$, and 10 fundamental modes within a few percent accuracy, where the expected stellar mass is $M = 1.5M_\odot$. However, we find the possibility to explain the all observed frequencies with using only crust shear modes, if ρ_p would be small. As shown in the right panel of Fig. 3, the observed frequencies of 18, 26, 30, and 92.5 Hz can be identified as $\ell = 3, 4, 5$, and 16 fundamental shear modes within a few percent accuracy again, where the expected stellar mass is $M = 1.5M_\odot$. This is important suggestion to explain the observed QPO frequencies in giant flares, which could become a directing post in the asteroseismology with neutron stars.

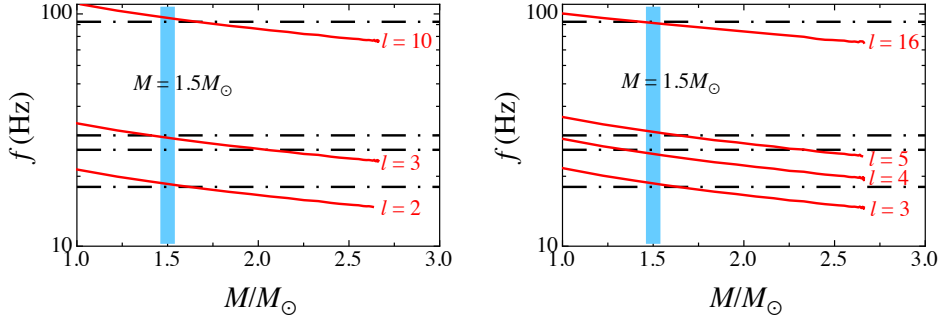


Figure 3: Comparison for the frequencies with the observed QPO frequencies in SGR 1806-20 with $\rho_p = 10^{14} \text{ g/cm}^{-3}$ (left) and with $\rho_p = 2 \times 10^{13} \text{ g/cm}^{-3}$ (right).

5 Conclusion

We consider the effect of nonuniform nuclear structure, the so-called “pasta”, in the neutron star crust on the torsional shear modes. Based on the suggestion that the elastic properties in the pasta phase could be liquid crystals, the frequencies of shear modes are calculated with simple relation of shear modulus. As a result, due to the existence of pasta phase, one can observe the smaller frequencies than those expected without pasta phase. This result indicates not only the importance to take into account the pasta phase, but also the possibility to probe the pasta structure via the observations of the stellar oscillations, such as the QPO frequencies in giant flares. Furthermore, we show the possibility to explain the observed QPO frequencies with using only crust shear modes with pasta phase, which is quite difficult with the traditional identification without pasta phase. In order to find the most suitable stellar model with the observations, we need to adopt more realistic pasta structure and to examine systematically with different EOSs, where the additional effects, such as superfluidity inside the star as well as the stellar magnetic field, should be also taken into account. Still, we believe that the pasta structure in the neutron star crust could play an important role in the stellar oscillations.

Acknowledgements

This work was supported by Grant-in-Aid for Scientific Research on Innovative Areas (23105711).

References

- [1] A. L. Watts, T. E. Strohmayer, *Adv. Space Res.*, **40**, 1446 (2006).
- [2] H. Sotani, *Mon. Not. R. Astron. Soc. Letter* **417**, L70 (2011).
- [3] H. Sotani, K. D. Kokkotas, N. Stergioulas, *Mon. Not. R. Astron. Soc.* **375**, 261 (2007).
- [4] H. Sotani, K. D. Kokkotas, N. Stergioulas, *Mon. Not. R. Astron. Soc. Letter* **385**, L5 (2008).
- [5] H. Sotani, A. Colaiuda, K. D. Kokkotas, *Mon. Not. R. Astron. Soc.* **385**, 2161 (2008).
- [6] H. Sotani, K. D. Kokkotas, *Mon. Not. R. Astron. Soc.* **395**, 1163 (2009).
- [7] C. J. Pethick, A. Y. Potekhin, *Phys. Lett. B* **427**, 7 (1998).

Dynamical Approaches for Secular Instabilities in Rotating Stars

Motoyuki Saijo^{46(a),(b)}

^(a)*Department of Physics, Rikkyo University, Toshima, Tokyo 171-8501, Japan*

^(b)*Research Measurement of Advanced Science, Rikkyo University, Toshima, Tokyo 171-8501, Japan*

Abstract

We propose a new method of investigating nonlinear dynamics focusing on the physical phenomena of rotating stars in Newtonian gravity which appear in secular timescale. Since acoustic waves normally interact with the surrounding material in dynamical timescale, we need a special technique to achieve secular timescale in dynamical approach. We particularly focus on r -mode instability and construct a numerical scheme of killing the effect of acoustic wave by imposing an anelastic condition at every timestep. Although we only explain the rotating star in Newtonian gravity here, this technique can be also applied to relativistic gravitation (conformally flat approximation in general relativity). Boundary condition for solving pressure Poisson equation and future extension from the anelastic conditions are also discussed.

1 Introduction

Various secular instabilities hidden in the rotating star may potentially grow, telling us full of internal structure of the star. r -mode instability occurs when the backward modes in the rotating frame amplify because of gravitational wave emission. g -mode instability occurs in the non-adiabatic evolution or convectively unstable case. It comes from the oscillation of the fluid elements because of the restoring force of buoyancy. Secular bar mode instability occurs when the magnitude of rotation exceeds some threshold. Energy dissipation such as gravitational radiation or viscosity plays a crucial role to trigger this instability. Kelvin-Helmholtz instability occurs when the deviation of the velocities between the different fluid layers exceeds some critical value. All instabilities occur in secular timescale are related in some way to the energy transition of the material in dissipative manner. Investigating these instabilities potentially tell us the local structure of rotating stars.

In order to understand the behaviour of these instabilities in secular timescale, dynamical approach is one way to explore the problem. However this is not at all an easy task, since the evolution period of the dynamics is restricted by the characteristic timescales of the system. For the neutron star, the shorter timescales are acoustic time and the rotation period of the star. These timescales are considered as dynamical since the characteristic timescale is in the order of $\sim 1/\sqrt{\rho_c}$, where ρ_c is the characteristic rest-mass density (central rest-mass density) of the star. The longer timescales is viscosity time, gravitational radiation reaction time and nonlinear growth time. These timescale are considered as secular, since the characteristic timescale is around $\sim 10^6$ times of dynamical time in the standard neutron star. In order to focus on the phenomena of the secular timescale, we have to kill the effect of dynamical one and relax the timestep restriction.

There are two representative attempts to investigate r -mode instability in dynamical approach. One is to find the saturation amplitude of r -mode instability. Lindblom, Tohline and Vallisneri [1] find that the saturation amplitude is in the order of unity, using the 3-D hydrodynamic simulation in Newtonian gravity with radiation reaction potential. In order to achieve secular timescale with dynamics, the authors have to impose large amplitude to the radiation reaction potential. While the computation from 1-D evolution with partially including three wave interaction leads the saturation amplitude in the order of 10^{-3} , depends on the property of the interaction term [2]. The other is to focus on the final fate of the r -mode instability. Gressman et al. [3] find that the energy dissipation of r -mode leads catastrophically decay to differentially rotating configuration in dynamical timescale, using the 3-D simulation in Newtonian

⁴⁶Email address: saijo@rikkyo.ac.jp

gravity. In fact they impose an initial condition of r -mode amplitude as unity. However, the computation from 1-D evolution with coupling network leads the conclusion that Kolmogorov-type cascade occurs in secular timescale after reaching the saturation amplitude around $\sim 10^{-3}$ [4]. From these two attempts of investigating the properties of r -mode instability in dynamical approach, it is useful to have an alternative approach to cover the linear regime to nonlinear regime, and to cover dynamical timescale to secular timescale.

Nowadays, we are in the stage to investigate the r -mode instability through gravitational wave detection in the ground base detector through the global cooperation of the gravitation wave detection network. At present the upper limit of the r -mode amplitude from the youngest known stars are around the order of 10^{-4} [5]. Once we detect gravitational waves from the unstable modes of neutron stars, we are able to investigate the interior structure of neutron stars in principle.

2 Anelastic approximation in linear regime

Here we assume that the rotating star is composed of perfect fluid in Newtonian gravity. The basic equations are continuity equation, Euler equation, the energy equation and the gravitational field equation as

$$\begin{aligned}\frac{\partial \rho}{\partial t} + \nabla_i(\rho v^i) &= 0, \\ \frac{\partial}{\partial t}(\rho v^i) + \nabla_j(\rho v^j v^i) &= -\nabla^i p - \rho \nabla^i \Phi, \\ \frac{\partial \varepsilon}{\partial t} &= -\frac{p}{\rho^2} \nabla_j(\rho v^j), \\ \Delta \Phi &= 4\pi \rho,\end{aligned}$$

where ρ is the rest-mass density, v^i the velocity, p the pressure, Φ the gravitational potential, and ε the specific internal energy. In order to close the system, we have to impose the equation of state of the matter $p = p(\rho, \varepsilon)$.

Next, we linearised the basic equations in order to control the acoustic wave easily [6]. Although we only introduce the case of Newtonian gravity here, we can extend the case automatically up to conformally flat approximation in general relativity [7]. We perturb the rest mass density ρ , velocity v^i , and the specific enthalpy $h(\equiv \varepsilon + p/\rho)$ from the equilibrium configuration as

$$\begin{aligned}\rho &= \rho_{\text{eq}} + \delta\rho, \\ v^i &= v_{\text{eq}}^i + \delta v^i, \\ h &= h_{\text{eq}} + \delta h.\end{aligned}$$

Then the linearised basic equations are

$$\frac{D}{Dt} \delta\rho = -\nabla_j(\rho_{\text{eq}} \delta v^j), \quad (2.1)$$

$$\frac{D}{Dt} \delta v^i = -v_{\text{eq}}^j \nabla_j v_{\text{eq}}^i - \delta v^j \nabla_j v_{\text{eq}}^i - \frac{1}{\rho} \nabla^i p - \nabla^i \Phi, \quad (2.2)$$

$$\frac{D}{Dt} \delta h = -\delta v^j \nabla_j h_{\text{eq}} - (\Gamma - 1) h_{\text{eq}} \nabla_j \delta v^j, \quad (2.3)$$

assuming Γ -law equation of state [$p = (\Gamma - 1)\rho\varepsilon$]. Note that we use the Lagrangian time derivative D/Dt as

$$\frac{D}{Dt} \equiv \frac{\partial}{\partial t} + v_{\text{eq}}^j \nabla_j.$$

assuming that the equilibrium configuration of the star is rotating uniformly. Here we kill the acoustic wave of δh in the rotating frame, that is to say, imposing the condition that the source term of Eq. (2.3) to be zero. This condition with no shock leads

$$\nabla_j(\rho_{\text{eq}} \delta v^j) = 0.$$

Therefore we do not need to evolve in time the fluctuation of the rest-mass density $\delta\rho$. Together with the divergence of the linearised Euler equation, we can formally have the elliptic type of equation for δh as

$$\Delta\delta h = S_h(\delta h, \delta v^i, \text{all force terms}).$$

Imposing a boundary condition to the equilibrium enthalpy h_{eq} at the surface of the star, we can achieve large timestep Δt for explicit time evolution (around 100 times efficient comparing with the existence of the acoustic waves in Ref. [6] using spectral method).

3 Anelastic approximation in nonlinear regime

Next we relax the condition of the linear perturbation in the previous section. We deviate the rest mass density, velocity, and the specific enthalpy from the equilibrium as

$$\begin{aligned}\rho &= \rho_{\text{eq}} + \Delta\rho, \\ v^i &= v_{\text{eq}}^i + \Delta v^i, \\ h &= h_{\text{eq}} + \Delta h.\end{aligned}$$

Note that the quantities $\Delta\rho$, Δv^i , Δh are not necessary small compared to those of equilibrium configuration. Then the basic equations are

$$\frac{D}{Dt}\rho + \nabla_j(\rho\Delta v^j) = 0, \quad (3.1)$$

$$\frac{D}{Dt}(\rho\Delta v^i) + \nabla_j(\rho\Delta v^j\Delta v^i) = -\rho v_{\text{eq}}^j\nabla_j v_{\text{eq}}^i - \rho\Delta v^j\nabla_j v_{\text{eq}}^i - \nabla^i p - \rho\nabla^i\Phi, \quad (3.2)$$

$$\frac{D}{Dt}\Delta h = -\Delta v^j\nabla_j h - (\Gamma - 1)h\nabla_j\Delta v^j. \quad (3.3)$$

The robust way of solving these equations is to kill the acoustic wave by replacing the source term of the specific enthalpy as zero, and evolve in time. However, propagation of Δh in acoustic wave is not completely killed because of the numerical fluctuation. In fact, the system is numerically unstable from $\nabla_i p$ term from my demonstration.

Next, we try to control the acoustic wave at each timestep. The source term for time evolution of the specific enthalpy equation [Eq. (3.3)] can be written as

$$\nabla_j(\rho\Delta v^j) = 0, \quad (3.4)$$

where we assume Γ -law equation of state with no shock. This anelastic condition makes the evolution equation simple. First we only need to perform time evolution in Euler equation. Second, taking the divergence of the Euler equation, we can derive the pressure Poisson equation as

$$\Delta p = -\nabla_i \left[\rho(\nabla^i\Phi + \Delta v^j\nabla_j v_{\text{eq}}^i + v_{\text{eq}}^j\nabla_j v_{\text{eq}}^i) + \nabla_j(\rho\Delta v^j\Delta v^i) + \frac{D}{Dt}(\rho\Delta v^i) \right].$$

Note that we do not impose anelastic condition here. We can impose two type of boundary condition for solving the pressure Poisson equation. One is the Dirichlet boundary condition $p = 0$ at stellar surface, and the other the Neumann boundary condition $(\partial p/\partial \mathbf{n}) = 0$, where \mathbf{n} is the orthogonal unit vector on the stellar surface configuration.

Since the anelastic condition [Eq. (3.4)] should be satisfied at each timestep, we have to add a trick in order to satisfy the constraint through evolution. Here we use the same technique which has been used in MAC (mark in cell) method for computing Navie-Stokes equations in incompressible fluid [8]. Instead of solving the pressure Poisson equation with anelastic condition, we impose time derivative part $[\nabla_i(\rho\Delta v^i)]$ in the source term with future finite time differencing. We also put a constraint that the every next time step of the quantity $\nabla_i(\rho\Delta v^i)$ is set to be zero. Imposing this time derivative part, we can control the constraints $[\nabla_i(\rho\Delta v^i) = 0]$, which is removed at every next timestep.

4 Discussion

We propose a method of investigating secular instabilities of rotating stars with a dynamical approach. This is a natural extension of the anelastic approximation in the linear regime to focus on the nonlinear dynamics in secular timescale.

Since we control the fluctuation of the acoustic wave propagation by introducing the pressure Poisson equation, constraint scheme seems to be stable through evolution. However the difficulty goes to the pressure Poisson equation. The boundary condition should be imposed on the stellar surface configuration. If the numerical error is crucial from the stellar surface, careful treatment of the boundary condition such as surface fitting coordinate or sophisticated extrapolation method from the interior of the star up to the surface should be necessary. The efficient technique for solving the pressure Poisson equation may be also required. Also there is no guarantee that the source term of the pressure Poisson equation is positive inside the star when imposing this anelastic condition, we have to be careful about the validity regime of this approximation.

Anelastic approximation is a first step for relaxing the incompressibility of the fluid, and it enables us to explore the phenomena of secular timescale through dynamics. The next step along this line is to take low Mach number approximation, which allows us to treat the thermodynamical variation partially, but still killing the propagation effect of the acoustic waves. Such case has been already discussed in combustion fluid. It may be useful when we investigate complicated equation of state of rotating star in secular timescale.

References

- [1] L. Lindblom, J. E. Tohline, M. Vallisneri, *Phys. Rev. Lett.* **65**, 1152 (2001).
- [2] A. K. Schenk, P. Arras, E. E. Flanagan, S. A. Teukolsky and I. Wasserman, *Phys. Rev. D* **65**, 024001 (2002).
- [3] P. Gressman, L.-M. Lin, W.-M. Suen, N. Stergioulas and J. L. Friedman, *Phys. Rev. D* **66**, 041303 (2002).
- [4] P. Arras, E. E. Flanagan, S. M. Morsink, A. K. Schenk, S. A. Teukolsky and I. Wasserman, *Astrophys. J.* **591**, 1129 (2003).
- [5] LIGO Scientific Collaboration, *Astrophys. J.* **722**, 1504 (2010).
- [6] L. Villain and S. Bonazzola, *Phys. Rev. D* **66**, 123001 (2002).
- [7] L. Villain, S. Bonazzola and P. Haensel, *Phys. Rev. D* **71**, 083001 (2005).
- [8] S. McKee, M. F. Tome, V.G. Ferreira, J. A. Cuminato, A. Castelo, F. S. Sousa and N. Mangiavacchi, *Comp. Fluid.* **37**, 907, (2008).

What are universal features of gravitating Q-balls?

Takashi Tamaki^{47(a)} and Nobuyuki Sakai^{48(b)}

^(a)*Department of Physics, Nihon University, Tokusada, Tamura, Koriyama, Fukushima 963-8642, Japan*

^(b)*Department of Education, Yamagata University, Yamagata 990-8560, Japan*

Abstract

We investigate how gravity affects Q-balls.

1 Introduction

Q-balls, a kind of nontopological solitons, appear in a large family of field theories with global U(1) (or more) symmetry. It has been argued that Q-balls with the Affleck-Dine (AD) potential could play important roles in cosmology. For example, Q-balls can be produced efficiently and could be responsible for baryon asymmetry and dark matter. Because Q-balls are typically supposed to be microscopic objects, their self-gravity is usually ignored.

However, if we contemplate the results on boson stars, we notice the possibility that self-gravity can be important even if it is very weak. For example, in the case of the potential $V_{\text{mini}} = m^2\phi^2/2$, equilibrium solutions, called (mini-)boson stars, exist due to self-gravity, though no equilibrium solution exists without gravity. From this motivation, we have investigated the following three models. The first one is $V_3(\phi) := \frac{m^2}{2}\phi^2 - \mu\phi^3 + \lambda\phi^4$ [1]. The second one is $V_4(\phi) := \frac{m^2}{2}\phi^2 - \lambda\phi^4 + \frac{\phi^6}{M^2}$ [2]. Interestingly, gravitating Q-balls (boson stars) in these two models have a common property that stable Q-balls with arbitrarily small charge exist no matter how weak self-gravity is, while Q-ball properties in flat spacetime fairly depend on the potentials.

From the theoretical point of view, however, models with logarithmic terms are more natural. Specifically, in the AD mechanism noted above, there are two types of potentials: gravity-mediation type and gauge-mediation type. The former type is described by the potential, $V_{\text{grav.}}(\phi) := \frac{m^2}{2}\phi^2 \left[1 + K \ln\left(\frac{\phi}{M}\right)^2\right]$. In flat spacetime equilibrium solutions for $K \geq 0$ are nonexistent while those for $K < 0$ are existent. If we take self-gravity into account, stable Q-balls exist even for $K = 0$ since the potential coincides with V_{mini} . In our previous paper [3], we have shown that gravitating “Q-balls” exist, which are surrounded by Q-matter, even for $K > 0$. Here, we extend our analysis to the gauge-mediation type [4],

$$V_{\text{gauge}}(\phi) := m^4 \ln\left(1 + \frac{\phi^2}{m^2}\right) \quad \text{with } m > 0. \quad (1.1)$$

We shall show that gravitating Q-balls with (1.1) have a common property with V_{mini} , V_3 and V_4 .

2 Analysis method of equilibrium Q-balls

We begin with $\mathcal{S} = \int d^4x \sqrt{-g} \left\{ \frac{\mathcal{R}}{16\pi G} - \frac{1}{2} g^{\mu\nu} \partial_\mu \phi \cdot \partial_\nu \phi - V(\phi) \right\}$, where $\phi = (\phi_1, \phi_2)$ is an SO(2)-symmetric scalar field and $\phi := \sqrt{\vec{\phi} \cdot \vec{\phi}} = \sqrt{\phi_1^2 + \phi_2^2}$. We assume a spherically symmetric and static spacetime, $ds^2 = -\alpha^2(r)dt^2 + A^2(r)dr^2 + r^2(d\theta^2 + \sin^2\theta d\varphi^2)$. For the scalar field, we assume $(\phi_1, \phi_2) = \phi(r)(\cos\omega t, \sin\omega t)$ and suppose V_{gauge} Model. We rescale the quantities as $\tilde{\phi} \equiv \frac{\phi}{m}$, $\tilde{V}_{\text{gauge}} \equiv \frac{V_{\text{gauge}}}{m^4} = \ln(1 + \tilde{\phi}^2)$, $\tilde{\omega} \equiv \frac{\omega}{m}$, $\kappa = Gm^2$, $\tilde{t} \equiv mt$, $\tilde{r} \equiv mr$.

We review their equilibrium solutions in flat spacetime ($\kappa = 0$). The scalar field equation reduces to $\tilde{\phi}'' = -\frac{2}{\tilde{r}}\tilde{\phi}' - \tilde{\omega}^2\tilde{\phi} + \frac{d\tilde{V}_{\text{gauge}}}{d\tilde{\phi}}$. This is equivalent to the field equation for a single static scalar field with

⁴⁷Email address: tamaki@ge.ce.nihon-u.ac.jp

⁴⁸Email address: nsakai@e.yamagata-u.ac.jp

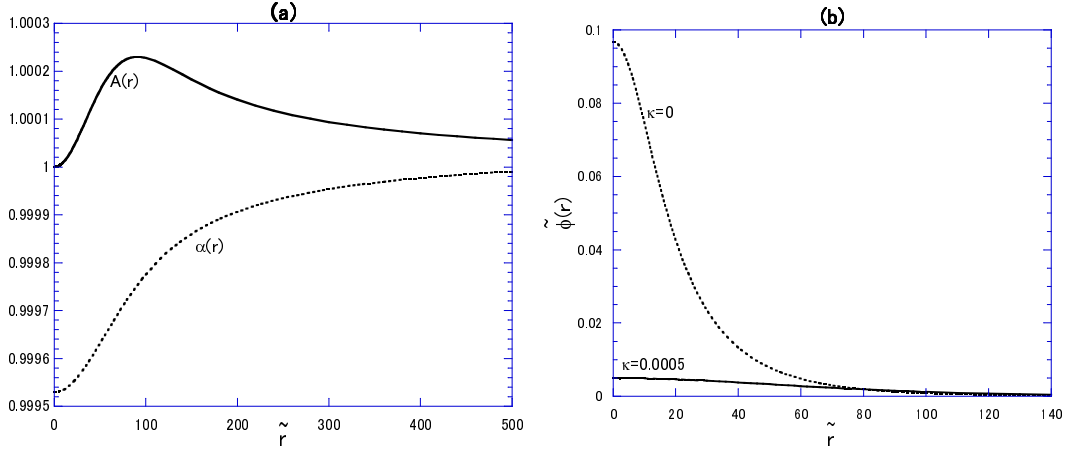


Figure 1: For a thick-wall Q-ball for $\tilde{\omega}^2 \simeq 1.999$.

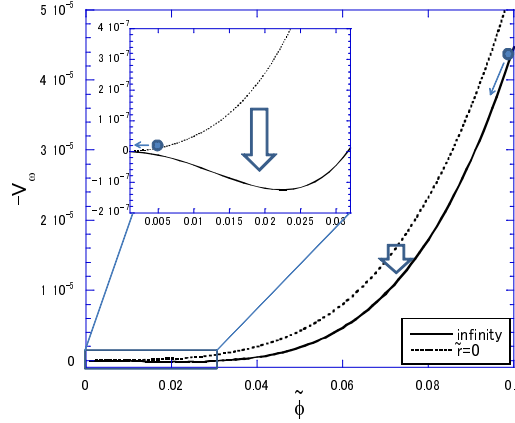


Figure 2: $-V_\omega$ for a thick-wall Q-ball $\tilde{\omega}^2 \simeq 1.999$.

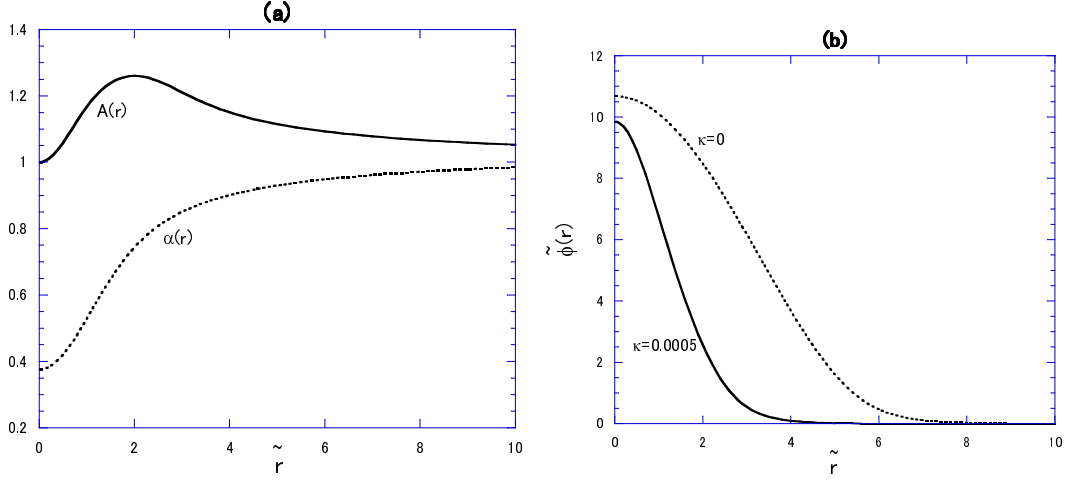
the potential $V_\omega := \tilde{V}_{\text{gauge}} - \tilde{\omega}^2 \tilde{\phi}^2/2$. If we introduce $\epsilon^2 := 2 - \tilde{\omega}^2$, the two limits $\epsilon^2 \rightarrow 2$ and $\epsilon^2 \rightarrow 0$ correspond to the thin-wall limit and the thick-wall limit, respectively.

If one regards the radius r as “time” and the scalar amplitude $\phi(r)$ as “the position of a particle”, one can understand Q-ball solutions in words of Newtonian mechanics. To discuss gravitational effects later, it is useful to estimate the central value $\phi_0 := \tilde{\phi}(0)$ in flat spacetime. Because $V_\omega \approx 0$ at $r = 0$, its order of magnitude is estimated as a solution of $V_\omega = 0$ ($\tilde{\phi}(0) \neq 0$). For V_{gauge} with the thick-wall condition $\epsilon^2 \ll 1$, we obtain $\phi_0^2 \left(1 - \frac{\tilde{\omega}^2}{2}\right) - \frac{\phi_0^4}{2} \simeq 0$, where we have used Maclaurin expansion of $\ln(1 + \tilde{\phi}^2)$ and neglected higher order terms $O(\phi_0^5)$. Then, we obtain $\phi_0 \simeq \epsilon$.

3 Gravitating Q-balls

The potential picture described above is effective in arguing equilibrium solutions also in curved spacetime. In this case, V_ω should be redefined by $V_\omega := \tilde{V}_{\text{gauge}} - \frac{\tilde{\omega}^2}{2\alpha^2} \tilde{\phi}^2$. “The potential of a particle”, $-V_\omega$, is now “time”-dependent, which sometimes plays an important role, as we see below.

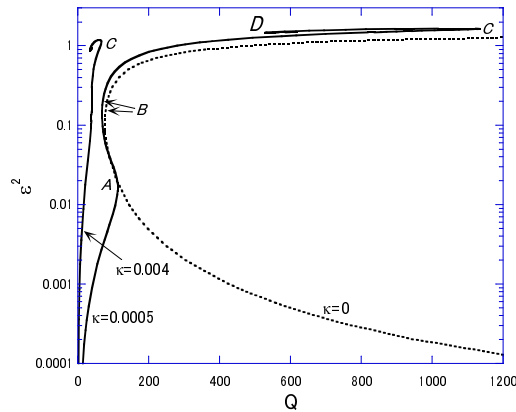
First, we show the result on a thick-wall Q-ball with $\tilde{\omega}^2 \simeq 1.999$ in Fig. 1. We put $\kappa = 0.0005$ for a gravitating Q-ball. The metric functions $\alpha(\tilde{r})$, $A(\tilde{r})$ and the field amplitude $\tilde{\phi}(\tilde{r})$ are shown in (a) and (b), respectively. Because $\alpha(\tilde{r})$ and $A(\tilde{r})$ are close to one, one may think that gravity acts as small perturbations. However, looking at $\tilde{\phi}(\tilde{r})$, we find that gravity changes its shape drastically.

Figure 3: For a Q-ball for $\tilde{\omega}^2 \simeq 0.35$.

We explain the reason for this result by using the potential $-V_\omega$, as shown in Fig. 2. For the flat case $\kappa = 0$, $-V_\omega$ is fixed as shown by a solid line. As a result, the scalar field with a relatively large value ($\tilde{\phi} \simeq 9.68 \times 10^{-2}$) at the initial time $\tilde{r} = 0$ rolls down and climb up the potential and finally reaches $\tilde{\phi} = 0$ at the time $\tilde{r} \rightarrow \infty$. On the other hand, for the gravitating case $\kappa = 0.0005$, $-V_\omega$ changes from a dotted line to a solid line as “time” \tilde{r} goes. An important point is that the sign of $-\frac{dV_\omega}{d\tilde{\phi}}$ changes near the origin. Therefore, the scalar field should take a sufficient small value ($\tilde{\phi} \simeq 4.96 \times 10^{-3}$) to satisfy $\tilde{\phi}(\infty) = 0$.

Second, we show the result on a relatively thin Q-ball with $\tilde{\omega}^2 \simeq 0.35$ in Fig. 3. The metric functions $\alpha(\tilde{r})$, $A(\tilde{r})$ and the field amplitude $\tilde{\phi}(\tilde{r})$ are shown in (a) and (b), respectively. (a) tells us that, compared with the case $\tilde{\omega}^2 \simeq 1.999$, the gravitational field is fairly stronger near the origin but approaches the flat spacetime faster as $\tilde{r} \rightarrow \infty$. (b) indicates that the size of the Q-ball becomes smaller due to self-gravity.

We can also explain the reason for this result by using the potential $-V_\omega$. $-V_\omega$ for a gravitating case $\kappa = 0.0005$ changes from a dotted line to a solid line as “time” \tilde{r} goes. An essential difference from the former thick-wall case is that this change occurs “quickly”. Thus, weaker gravity does not necessarily mean a smaller influence to Q-balls and it is interesting to investigate its influences for various $\tilde{\omega}^2$.

Figure 4: Q - ϵ^2 relation for $\kappa = 0, 0.0005$ and 0.004 .

It is instructive to depict the Q - ϵ^2 in Fig. 4. For the thick-wall solutions $\epsilon^2 \ll 1$ with gravity, as we explained using Fig. 2, Q-ball charge is very small because $\tilde{\phi}(0) \ll 1$, and there is no lower bound of Q , contrary to the flat case. It should be argued carefully whether or not there remain thick-wall solutions with $Q \rightarrow 0$ in the weak gravity limit $\kappa \neq 0$.

4 Thick-wall solutions for $\kappa \neq 0$

We consider thick-wall solutions ($\epsilon^2 \ll 1$) with weak gravity by expressing the metric functions as

$$\alpha^2 = 1 + h(r), \quad A^2 = 1 + f(r), \quad (|h| \ll 1, \quad |f| \ll 1), \quad (4.1)$$

and we shall take up to first order in h and f hereafter. As we discussed for the flat spacetime in Sec. II, we evaluate $\phi_0 := \tilde{\phi}(0)$ as a solution of $V_\omega = 0$ with (4.1), $\epsilon^2 + \tilde{\omega}^2 h(0) - \phi_0^2 \simeq 0$, where we have neglected higher order terms $O(\phi_0^5)$. Let us consider the limit $\epsilon^2 \rightarrow 0$. For the flat case $\kappa = 0$, $\phi_0 \simeq \epsilon$ since $h(0)$ can be taken to be zero identically. However, for any small $\kappa \neq 0$, it is not evident whether or not $h(0)$ can be negligible and we should compare the order of $h(0)$ with that of ϵ^2 . For this purpose, we should also estimate it by using the Einstein equations. To do this, we assume a top-hat configuration,

$$\tilde{\phi}(\tilde{r}) \sim \phi_0 \ll 1 \quad \text{for} \quad \tilde{r} < \frac{C}{\epsilon}, \quad C = \text{const.} \quad (4.2)$$

From the Einstein equations, we find

$$-G_t^t + G_i^i := \left(\frac{\tilde{r}^2 \alpha'}{A} \right)' = 8\pi\kappa\tilde{r}^2 A \alpha \left(\frac{\tilde{\omega}^2 \tilde{\phi}^2}{\alpha^2} - V \right), \quad (4.3)$$

where i denotes spatial components. If we take the weak field approximation (4.1) and the thick-wall approximation $\epsilon^2 \ll 1$, we obtain $(\tilde{r}^2 h')' \simeq 16\pi\kappa\tilde{r}^2 \tilde{\phi}^2$. With the central boundary condition $h'(0) = 0$ and the approximation (4.2), we can integrate as $h' \simeq \frac{16}{3}\pi\kappa\phi_0^2 \tilde{r}$, for $\tilde{r} < \frac{C}{\epsilon}$. With the outer boundary condition $h(\frac{C}{\epsilon}) \simeq h(\infty) = 0$, we can integrate it as $h(0) \simeq -\frac{8}{3}\pi\kappa\phi_0^2 \frac{C^2}{\epsilon^2}$. By using $V_\omega = 0$, we obtain

$$\phi_0^2 = \frac{3\epsilon^4}{8\pi\kappa C^2 + 3\epsilon^2}. \quad (4.4)$$

This formula clearly shows how ϕ_0 converges as $\epsilon \rightarrow 0$ and $\kappa \rightarrow 0$; it depends on their convergent rates. If $\epsilon^2 \gg \kappa C^2$, we have $\phi_0 \simeq \epsilon$, as in the flat case. If $\epsilon^2 \ll \kappa C^2$, we have $\phi_0 \simeq \frac{\epsilon^2}{2C} \sqrt{\frac{3}{2\pi\kappa}}$. In the real situation, κ is very small but a nonzero constant, while ϵ is variable and determined by initial conditions. Therefore, if we discuss the thick-wall limit in weak gravity, the latter result applies. In this case, because $Q \propto \tilde{\phi}^2 \tilde{r}^3 \sim \phi_0^2 \frac{1}{\epsilon^3} \sim \epsilon$, there is no lower bound of Q as expected. Moreover, the point A in Fig. 4 can be interpreted as the point when $\epsilon^2 \sim \kappa C^2$.

We want to examine what types of potentials we can apply the above results. To obtain the result for $\epsilon^2 \ll \kappa C^2$, we have only assumed that the leading order in V_ω (or that in the Maclaurin series) is quadratic, $\tilde{\phi}^2$. Therefore, the above results hold true not only for AD model but also general models in which a positive mass term is a leading order one.

5 Conclusion and discussion

We have investigated how gravity affects Q-balls by exemplifying the case with the AD potential $V(\phi) := m^4 \ln(1 + \frac{\phi^2}{m^2})$. Surprisingly, stable Q-balls with arbitrarily small charge exist, no matter how weak gravity is, contrary to the case of flat spacetime. The result for the gravitating case is a universal property which has been known to hold for various potentials [1–3]. Our results suggest that gravity may play an important role in the Q-ball formation process.

References

- [1] T. Tamaki and N. Sakai, Phys. Rev. D **81**, 124041 (2010).
- [2] T. Tamaki and N. Sakai, Phys. Rev. D **83**, 044027 (2011).
- [3] T. Tamaki and N. Sakai, Phys. Rev. D **83**, 084046 (2011).
- [4] T. Tamaki and N. Sakai, Phys. Rev. D **84**, 044054 (2011).

Gravitational Waves from Compact Binaries as Probes of the Universe

Nicolás Yunes ^{49(a)}

^(a)*Department of Physics, Montana State University, Bozeman, MT 59718, United States.*

Abstract

The future detection of gravitational wave forces us to consider the many ways in which astrophysics, gravitational wave theory and fundamental theory will interact. In this paper, I summarize some recent work done to develop such an interface. In particular, I concentrate on how non-vacuum astrophysical environments can modify the gravitational wave signal emitted by compact binary inspirals, and whether signatures from the former are detectable by current and future gravitational wave detectors. I also describe the interface between gravitational wave modeling and fundamental theory, focusing on the status of the parameterized post-Einsteinian framework (a general framework to detect deviations away from General Relativity in future gravitational wave data) and its current data analysis implementation.

1 Multi-Messenger Gravitational Wave Astrophysics

The future detection of gravitational waves opens fertile ground to develop a collaboration between astrophysics, gravitational wave theory and data analysis. The traditional way in which such interdisciplinary work was thought to happen was fairly sequential: astrophysics would predict which sources gravitational wave theorist should model; theorist would provide highly accurate models for such systems; and data analysts would take such models and implement them in pipelines to maximize the probability of detecting a signal. An accurate astrophysical system and waveform model are crucial as the first detections will consist of signals that are completely buried in instrumental noise.

Once a signal has been detected, feedback in this cycle can occur. That is, data analysts can extract the best-fit parameters for the signal detected and, given enough detections, create population models of the distribution of system parameters in the low-redshift universe. For example, given a sufficient number of compact binary signals, one could construct the distribution of masses, mass ratios, spins, etc. This information could then be returned to the astrophysics community to see how it matches predicted population models.

Another route in which feedback can occur is through the data placing constraints on General Relativity. Given a single detection, data analysts can determine the probability that the foundational assumptions of General Relativity remain valid in strongly gravitating, highly dynamical systems, where tests of Einstein's theory currently do not exist. The most stringent tests we have today come from binary pulsar observations (see e.g. [1]), but the gravitational compactness of such bodies, the characteristic mass of the system divided by its orbital separation, remains minuscule. Compact binary coalescences can in principle sample horizon-scale compactnesses, thus allowing for the most stringent tests yet.

The interaction of gravitational wave theory with astrophysics is a two-way street. One way to proceed is to focus on how the dynamical evolution of a gravitational system affects the astrophysical environment. An example of this is the evolution of a circumbinary accretion disk when its binary black hole nucleus coalesces. In this process, the binary emits $\sim 5 - 10\%$ its rest mass in gravitational waves, depending on the orbital characteristics of the system. A change in rest mass leads to a modification in the Newtonian potential that the circumbinary accretion disk is bounded to, forcing the latter to readjust and leading to shocks in the material that then emits electromagnetic radiation (see e.g. [2, 3]).

A different way to proceed is to focus on how the astrophysical environment modifies the gravitational wave evolution. Let us revisit the example given above, ie. that of a circumbinary accretion disk with a comparable-mass binary black hole in a quasi-circular inspiral. One could imagine that the mere presence

⁴⁹Email address: nyunes@physics.montana.edu

of the accretion disk might modify the evolution of the binary, for example due to angular momentum transport by the disk or the disk's self-gravity. Surely, these and other effects will have an impact on the binary's inspiral rate, but are such effects measurable by future gravitational wave detectors? For the current example, the answer is likely no. That is, the effect of the accretion disk is probably too small to be detectable by LISA, because the comparable mass binary's inertia is too great relative to the effect of the disk.

The effect of the astrophysical environment on the gravitational wave signal is not always negligible, however, and the prototypical system where the former matters is extreme mass-ratio inspirals. These systems consist of a solar-mass compact object spiraling into a supermassive black hole in a generic orbit. Due to the extreme mass-ratio, any small perturbation produced by a non-vacuum, astrophysical environment can have drastic effects on the small object's trajectory. Moreover, such systems can remain in the sensitivity band of low-frequency gravitational wave detectors for tens of years, depositing hundreds of thousands of radians of phase information in any given year. Thus, any small perturbation can accumulate over a year, leading to an observable effect. In this paper, I will describe a few papers [4–6] that have studied two possible astrophysical environment effects on extreme-mass ratio inspiral gravitational waves: the effect of accretion disks and the effect of massive perturbers.

The interaction of gravitational wave theory and data analysis with fundamental theory can also proceed in two different ways. Until very recently, the standard approach was *top-down*: one would pick a modified gravity theory, derive its equations of motion and solve them to find its predicted gravitational wave radiation. Once a prediction had been made, one could construct a template bank for this modified theory and then, given a gravitational wave detection consistent with General Relativity, constrain how large the parameters of the modified theory can be. Examples of this approach exist for Brans-Dicke theory [7–12, 14], dynamical Chern-Simons gravity [15, 16], phenomenological massive graviton propagation [8, 9, 13, 14, 17, 18], gravitational Lorentz-violation [19], and gravitational parity violation [20], violations of Local Position Invariance [21] and the existence of extra-dimensions [22].

The problem with any of these approaches is that the construction of template banks and subsequent analysis of detected signals is computationally expensive for each alternative theory. Moreover, it is unclear which modified theory effect to concentrate on, since none of the above models is particularly more theoretically appealing than General Relativity. For example, in the massive graviton case, there is no self-consistent theory at the level of the action that would lead to such massive graviton effects.

Lacking such a particular compelling model, a new framework to constrain deviations from General Relativity was recently proposed: the parameterized post-Einsteinian (ppE) framework [23]. This approach proposes to enhance the General Relativity template banks (spanned by system parameters) through the addition of new, well-motivated theory parameters. These parameters are such that when they acquire certain numerical values, they lead to waveforms predicted by all the modified gravity theories described above. The advantage of such an approach is that one need only concentrate on the construction of a single template bank. Matched filtering with elements from this bank would then allow the data to select the theory that best matches the signal, thus lifting the fundamental theoretical bias that General Relativity must be *a priori* correct. In this paper, I will summarize the current status of the ppE framework.

2 Gravitational Wave Modeling

Gravitational wave modeling has a long history and it would be quite pretentious and inappropriate to attempt a complete description here. Instead, I will only summarize the bits and pieces of gravitational wave modeling that will be necessary to understand the modeling of astrophysical and modified gravity effects, focusing on compact binary coalescences (inspiral-phase only) and ignoring any tidal deformation of the compact objects. I refer the interesting reader to the following review papers [24] for post-Newtonian, comparable-mass inspiral modeling, [25] for self-force, extreme-mass ratio modeling, [26] for approximate, extreme-mass ratio modeling, and references therein.

2.1 Comparable-Mass Compact Binary Quasi-Circular Inspirals

Let us begin with the modeling of gravitational waves emitted by comparable-mass, compact binary inspirals. The observed quantity at the detector is not the time-domain waveform, but the response function: a quantity constructed from the contraction of the response tensor with the (transverse-traceless) gravitational wave metric perturbation:

$$h(t) = F_+(\theta_S, \phi_S, \psi_S)h_+ + F_\times(\theta_S, \phi_S, \psi_S)h_\times, \quad (2.1)$$

where $h_{+,\times}$ are the plus- and cross-polarized gravitational wave metric perturbations, while $F_{+,\times}$ are beam-pattern functions. These functions characterize the response of the detector to an incoming gravitational wave and are slowly-varying.

The Fourier transform of the response function can be evaluated analytically if we assume that the phase varies on a much shorter time-scale than the amplitude, i.e. in the stationary phase approximation [27]. Let us define the cosine and sine responses for the dominant $\ell = 2$ mode

$$h(t) = h_C(t) + h_S(t), \quad h_C(t) = \mathcal{A} Q_C(\iota, \beta) \cos 2\phi, \quad h_S(t) = \mathcal{A} Q_S(\iota, \beta) \sin 2\phi, \quad (2.2)$$

where $\mathcal{A} = -\mathcal{M}/D_L (2\pi\mathcal{M}F)^{2/3}$ is a slowly-varying amplitude, while

$$Q_C(\iota, \beta) \equiv 2(1 + c_i^2) c_{2\beta} F_+ - 4c_i s_{2\beta} F_\times, \quad Q_S(\iota, \beta) \equiv 2(1 + c_i^2) s_{2\beta} F_+ + 4c_i c_{2\beta} F_\times, \quad (2.3)$$

and $c_i = \cos \iota$, $c_{2\beta} = \cos 2\beta$ and $s_{2\beta} = \sin 2\beta$, with ι and β the inclination and polarization angles respectively. Then, the Fourier transform in the stationary phase approximation is

$$\tilde{h}_C(f) = -\left(\frac{5}{384}\right)^{1/2} \pi^{-2/3} \frac{\mathcal{M}^{5/6}}{D_L} Q_C(\iota, \beta) [2F(t_0)]^{-7/6} e^{-i(\Psi+\pi/4)}, \quad (2.4)$$

while $\tilde{h}_S(f) = i\tilde{h}_{C \rightarrow S}(f)$. The phase of the gravitational wave Fourier transform is

$$\Psi[F(t_0)] = 2\pi \int^{F(t_0)} \frac{F'}{\dot{F}'} \left(2 - \frac{f}{F'}\right) dF'. \quad (2.5)$$

The quantity t_0 is the *stationary-point*, defined by $2\dot{\phi}(t_0) = 2\pi f$, essentially the region in which the Fourier transform does not average out. In Eq. (2.4), D_L is the luminosity distance, $\mathcal{M} = \eta^{3/5} m$ is the chirp mass, with $\eta = m_1 m_2 / m^2$ the symmetric mass ratio and $m = m_1 + m_2$ the total mass, while F is the orbital frequency.

Gravitational wave detectors are the most sensitive to the phase of the response function, Eq. (2.5), whose functional form is controlled by the orbital frequency's evolution equation. In vacuum General Relativity, the orbital frequency can only evolve due to the emission of gravitational waves. Using the balance law $\dot{E} = -\langle \mathcal{L}_{\text{GW}} \rangle$, i.e. the rate of change of the binary's binding energy is exactly balanced by the flux of gravitational wave energy-momentum suitably averaged over several wavelengths, one can derive

$$\frac{dF}{dt} \equiv \frac{\dot{E}}{dE/dF} \sim \frac{48}{5\pi\mathcal{M}^2} (2\pi\mathcal{M}F)^{11/3} \quad (2.6)$$

to leading order in $2\pi\mathcal{M}F \sim v^3$, where v is the binary's orbital velocity. Of course, if Kepler's third law is modified or if additional sinks of energy-momentum are present, for example due to scalar-field emission or to accretion-disk induced angular momentum transport, then the gravitational wave phase will be modified accordingly. Ignoring these effects for the moment, the Fourier transform is then

$$\tilde{h}_{(\text{circ})} = -\left(\frac{5}{384}\right)^{1/2} \pi^{-2/3} \frac{\mathcal{M}^{5/6}}{D_L} Q(\iota, \beta) f^{-7/6} \exp \left[i \left(2\pi f t_c - \bar{\phi}_c - \frac{\pi}{4} + \frac{3}{128} (\pi\mathcal{M}f)^{-5/3} \right) \right], \quad (2.7)$$

where $Q = Q_C + iQ_S$ and we have retained only the Newtonian term in the phase.

2.2 Extreme Mass-ratio, Compact Binary Quasi-Circular Inspirals

Let us now consider extreme-mass ratio inspirals in a quasi-circular orbit confined to the equatorial plane of the supermassive black hole. The dominant $\ell = 2$, gravitational wave mode accumulates a phase

$$\phi_{\text{GW}} = 2 \int_{t_f - T_{\text{obs}}}^{t_f} \Omega(t) dt = 2 \int_{R_0}^{R_f} \Omega(r) \frac{dr}{\dot{r}} = \frac{1}{16} \frac{M_{\text{SMBH}}}{m_{\text{CO}}} R_f^{5/2} \left[\left(1 + \frac{\tau}{R_f^4} \right)^{5/8} - 1 \right] \quad (2.8)$$

where T_{obs} is the observation time, Ω is the orbital angular frequency, M_{SMBH} is the supermassive black hole mass, m_{CO} is the stellar-mass compact object's mass and (R_0, R_f) are the M_{SMBH} -normalized initial and final orbital radius respectively. The quantity τ here is the dimensionless observation time defined by $\tau \equiv (256/5)(m_{\text{CO}} T_{\text{obs}} / M_{\text{SMBH}}^2)$. One can verify that for low-frequency gravitational wave detectors, with peak sensitivity in the micro- to deci-Hz band, the accumulated gravitational wave phase can reach millions of radians for separations in $(R_0, R_f) \in (30M_{\text{SMBH}}, R_{\text{ISCO}})$, where R_{ISCO} is the radius of the innermost stable circular orbit for a test-particle on a geodesic of the background spacetime.

The accumulation of gravitational wave phase information clearly depends on the rate of inspiral, \dot{r} . This quantity can be computed from $\dot{r} = \dot{E}/(dE/dr)$, which again depends both on the binary's binding energy $E(r)$ and its rate of change. If additional sinks of energy are present in the problem or if the binding energy is deformed, then the accumulated gravitational wave phase will be different than what one would expect for a vacuum inspiral.

The accumulated gravitational wave phase in Eq. (2.8) can be used as a quick measure of how important non-vacuum or non-General Relativity effects are, but this measure is only approximate since it uses Newtonian relations, which are highly inaccurate for extreme-mass ratio inspiral. A much more appropriate scheme is that of the *effective-one-body* approach, recently implemented for extreme-mass ratio inspirals in [28, 29] and references therein. In this scheme, one maps the two-body inspiral into an effective inspiral of a test-particle with mass η in orbit around a supermassive black hole with mass m . The equations of motion then reduce to the Hamilton-Jacobi equations

$$\frac{dr}{dt} = \frac{A(r)}{\sqrt{D(r)}} \frac{\partial \widehat{H}^{\text{real}}}{\partial p_{r^*}}, \quad \frac{d\Phi}{dt} = \frac{\partial \widehat{H}^{\text{real}}}{\partial p_{\Phi}}, \quad (2.9)$$

$$\frac{dp_{r^*}}{dt} = -\frac{A(r)}{\sqrt{D(r)}} \frac{\partial \widehat{H}^{\text{real}}}{\partial r}, \quad \frac{dp_{\Phi}}{dt} = \widehat{\mathcal{F}}_{\Phi}. \quad (2.10)$$

where $\widehat{H}^{\text{real}} \equiv H^{\text{real}}/\mu$ is the reduced (i.e., dimensionless) real Hamiltonian and $\widehat{\mathcal{F}}_{\Phi} := \mathcal{F}_{\Phi}/\mu$ is a reduced radiation-reaction force that controls the rate of inspiral (there is no radial component on average here because we are dealing with an equatorial, quasi-circular orbit). The azimuthal radiation-reaction force can be modeled via $\widehat{\mathcal{F}}_{\Phi} = \eta^{-1} \dot{L} = -\eta^{-1} \dot{L}_{\text{GW}} = -(\eta\Omega)^{-1} \dot{E}_{\text{GW}}$, where \dot{L} is the rate of change of the binary system's orbital angular momentum, while \dot{L}_{GW} and \dot{E}_{GW} are the angular momentum and energy radiated in gravitational waves.

The energy flux is composed of several contributions. The most accurate model for the average, energy flux radiated to infinity is the factorized resummation

$$\dot{E}_{\text{GW}} = \frac{2}{16\pi} \sum_{\ell=2}^{\ell=8} \sum_{m=1}^{m=\ell} (m\Omega)^2 |R h_{\ell m}|^2, \quad (2.11)$$

where R is the distance to the observer and $h_{\ell m}$ is the harmonically-decomposed gravitational wave metric perturbation. In addition to this, there is also energy flux into any trapped surfaces, black hole horizons, that can be modeled by solving the Teukolsky equation perturbatively in a post-Newtonian expansion (see e.g. [30, 31]). Of course, if there are additional sinks of energy, these must also be accounted for here by adding contributions to the total energy flux.

2.3 Gravitational Wave Signatures

In the previous sections, we have briefly summarized some salient features of gravitational wave modeling for comparable-mass and extreme mass-ratio quasi-circular inspirals, but are modifications in this

modeling observable? A plausible criterion to decide whether a certain gravitational wave modification is detectable by a given detector is the following:

$$\delta\phi_{\text{GW}} \geq \begin{cases} 10/\rho & \text{if } \rho \geq 10, \\ 0 & \text{if } \rho \leq 10, \end{cases} \quad (2.12)$$

where ρ^2 is the square of the signal-to-noise ratio (SNR), defined as

$$\rho^2(h) = 4 \int \frac{df}{S_h(f)} |\tilde{h}|^2. \quad (2.13)$$

As before, \tilde{h} is the Fourier transform of the measured gravitational wave response function, while $S_h(f)$ is the spectral noise density curve of the detector. The piece-wise nature of this criterion accounts for the fact that there is a threshold SNR below which the signal cannot be detected in the first place.

The above requirements give us a rough sense of when a certain modification might be detectable, but can such a modification be distinguishable from a vacuum waveform. To address this question, one can consider the SNR of the waveform difference

$$\rho^2(\delta h) \equiv \min_{\lambda_2} \left[4 \int \frac{df}{S_n(f)} \left| \tilde{h}_1(f) - \tilde{h}_2(f; \lambda_2) \right|^2 \right], \quad (2.14)$$

where \tilde{h}_1 and \tilde{h}_2 are the Fourier transforms of two waveforms (the ‘‘signal’’ and ‘‘template’’), normalized such that $\rho(h_1) = \rho(h_2) = 1$. The template depends on parameters $\vec{\lambda}_2$ that may be different from the true astrophysical ones, where the minimum difference corresponds to the best fit. One can then consider this SNR, minimized over template parameters, to construct a measure similar to that of Eq. (2.12). The minimization will partially account for the effect of possible template parameter degeneracies with non-vacuum or non-General Relativity effects.

3 Astrophysical Imprints

In this section, we consider two astrophysical environment effects in the modeling of gravitational waves. We begin with massive perturbers, summarizing the results of [4], and then move on to accretion disk effects, summarizing the results of [5, 6]. I refer the interested reader to these papers and the many references therein, which will not be included in this paper for simplicity.

3.1 Massive Perturbers

Let us consider an extreme-mass ratio inspiral, where the stellar-mass compact object is in a quasi-circular, equatorial orbit around a spinning supermassive black hole. Let us now imagine that there is a third compact object, with mass M_{Sec} and at a distance r_{Sec} from the supermassive black hole. We here imagine that M_{Sec} is comparable to M_{SMBH} and much greater than m_{CO} . This scenario is depicted in Fig. 1. Clearly, this is a three-body system, composed of two sub-binaries: the extreme-mass ratio system and the $M_{\text{SMBH}} - M_{\text{Sec}}$ system. Because of this, the extreme mass-ratio gravitational waves will be emitted from an *accelerated* frame (a frame that rotates due to the presence of the secondary).

The modifications to the trajectories of the small body can be modeled in the framework of the effective-one-body scheme described in Sec. 2.2. The dominant effect is simply a Doppler shift in the extreme mass-ratio inspiral gravitational wave frequencies, which then leads to an integrated modification in the gravitational wave phase. The implementation of this correction is simple: divide the right-hand-side of Eq. (2.10) by the appropriate Doppler factor

$$\dot{\Phi} \equiv \Omega \quad \rightarrow \quad \dot{\Phi} = \Omega [1 + v_{\text{los}}(t, \delta = \pi/2)], \quad (3.1)$$

where v_{los} is the velocity along the line of sight

$$v_{\text{los}}(t) = \left(\frac{M_{\text{Sec}}}{M_{\text{Tot}}} \right) v_{\text{Newt}} \cos(\omega_{\text{Newt}} t + \delta) \sin(\iota). \quad (3.2)$$

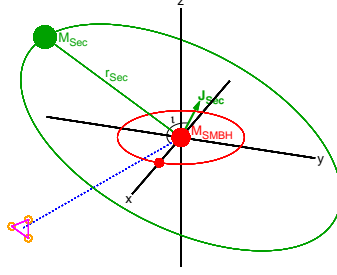


Figure 1: Schematic view of the extreme-mass ratio system (in the xy plane), the massive perturber M_{Sec} (at a distance r_{Sec}), and the line of sight. ι is the inclination between the primary-secondary supermassive black hole's orbital angular momentum vector and the line of sight.

with $v_{\text{Newt}} = (GM_{\text{Tot}}/r_{\text{Sec}})^{1/2}$ the Newtonian virial velocity, $\Omega_{\text{Newt}} = (GM_{\text{Tot}}/r_{\text{Sec}}^3)^{1/2}$ the Newtonian angular velocity for an object in a circular orbit, and δ an initial phase offset, with $(\Omega_{\text{Newt}}t + \delta)$ the orbital phase of the $M_{\text{SMBH}} - M_{\text{Sec}}$ system. A constant relative speed can be re-absorbed in a redefinition of the masses, and thus, it does not lead to a measurable correction. In Eq. (3.1), we have ignored the appropriate Lorentz factor Γ , since $v_{\text{Newt}}/c \ll 1$, and we have removed the constant velocity drift in v_{los} by choosing $\delta = \pi/2$.

This simple modeling neglects other gravitational wave generation effects. One could incorporate such effects by introducing an external, vectorial force (the product of the the total mass of the system and the time derivative of the velocity of Eq. (3.2)) to Hamilton's equations. Such a modeling would require a non-adiabatic evolution, which would lead to eccentric and inclined extreme-mass ratio trajectories. The magnitude of this correction, however, is small, as it scales with the tidal force of the perturber on the center of mass of the extreme mass-ratio inspiral, relative to the stellar-mass compact object's acceleration due to the secondary supermassive black hole. Since the tidal force scales as $\sim M_{\text{Sec}}/r_{\text{Sec}}^3$, this effect is suppressed relative to the acceleration by a factor of $r/r_{\text{Sec}} \sim 10^{-4}$ for an extreme-mass ratio inspiral with orbital separation $30M_{\text{SMBH}}$ and a primary-secondary binary orbital separation of 0.01 pc. This ratio would not be small if the perturber were in the near-zone (less than a gravitational wavelength away) from the center of mass of the extreme-mass ratio system.

We can now estimate what the distance and mass of the secondary black hole must be for its effect on extreme mass-ratio inspiral gravitational to be detectable by a LISA-like mission. The time-dependent Doppler shift described above leads to a correction in the gravitational wave phase of $\Delta\phi_{\text{GW}} = \dot{v}_{\text{los}}T_{\text{obs}}N/(2c)$, where N is the number of radians in the waveform, T_{obs} is the observation time. Let us further define ϵ as the detectable fractional phase shift: $\epsilon \equiv \Delta\phi_{\text{GW,detect}}/N$, a fiducial value of which is $\epsilon = 10^{-7}$, or 0.1 radians over $\sim 10^6$ radians for a typical one-year inspiral.

The definition of ϵ is a curve in $r_{\text{Sec}} - M_{\text{Sec}}$ space that delineates the secondary parameters that would lead to a sufficiently large dephasing to be detectable. This is shown in Fig. 2 for a range of ϵ values. Any secondary system with mass and separation above the curves would be observable. The solid curves plot the relation described in the previous paragraph, while the dashed curves account for the next $\ddot{v}_{\text{los}}t^2$ order effect. For comparison, the region of $(M_{\text{Sec}}, r_{\text{Sec}})$ space that falls in the pulsar-timing-array sensitivity band are also shown. Of course, the gravitational waves that would be detectable by pulsar-timing-arrays would be those generated by the $M_{\text{SMBH}} - M_{\text{Sec}}$ binary, and their distance to Earth would have to be sufficiently small. In principle, however, this scenario allows for the possibility of coincident future detection of gravitational waves from LISA-like detectors and pulsar-timing-arrays.

Just because an effect is sufficiently large to be in principle measurable does not imply that it can be distinguished from other vacuum effects. One must therefore worry about possible degeneracies of vacuum system parameters with those introduced by the secondary perturber (M_{Sec} and r_{Sec} in this case). We can get a sense of whether this is the case by computing the Fourier transform of the modified gravitational wave in the stationary-phase approximation. Following Sec. 2.1, one finds the following

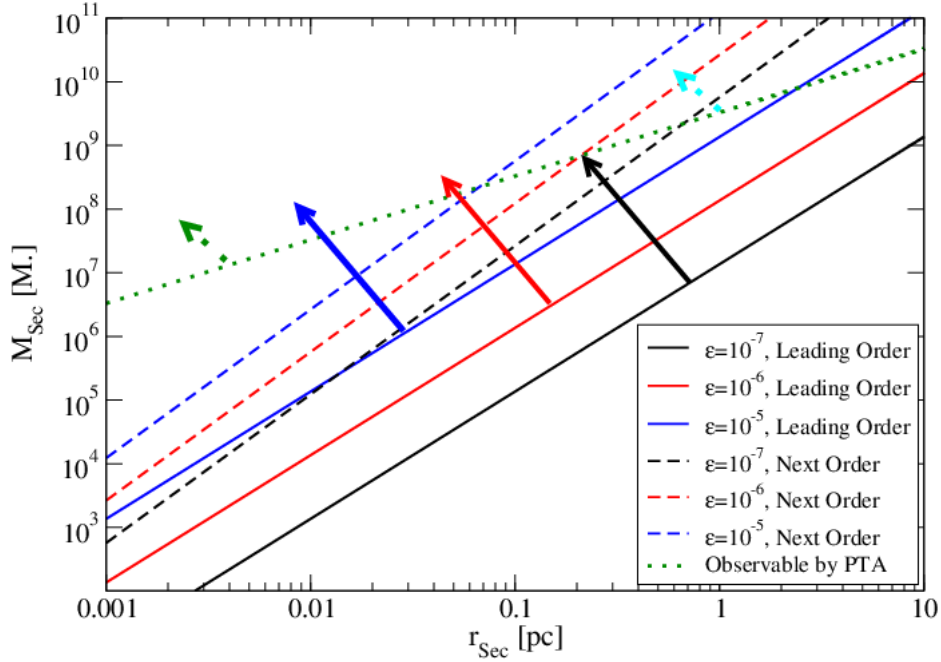


Figure 2: Range of secondary masses and separations that could be measurable by LISA given a sufficiently strong EMRI. The region above the solid and dashed lines would be observable. Measurement of the leading-order effect gives a determination of the combination $(M_{\text{Sec}} \sin \iota)/r_{\text{Sec}}^2$, while measuring the next-order effect gives a determination of the combination $(M_{\text{Sec}} \sin \iota)^{3/2}/r_{\text{Sec}}^{7/2}$. Thus measuring both effects together allows both $M_{\text{Sec}} \sin \iota$ and r_{Sec} to be determined.

correction to the phase

$$\Delta\Psi = \frac{3}{128} (\pi\mathcal{M}f)^{-5/3} \left[\left(\frac{25}{1248} \frac{\mathcal{M}M_{\text{Sec}}}{r_{\text{Sec}}^2} - \frac{25}{2496} \frac{\mathcal{M}M_{\text{Sec}}M_{\text{Tot}}t_c^2}{r_{\text{Sec}}^5} \right) (\pi\mathcal{M}f)^{-8/3} + \frac{125}{1032192} \frac{\mathcal{M}^2M_{\text{Sec}}M_{\text{Tot}}t_c}{r_{\text{Sec}}^5} (\pi\mathcal{M}f)^{-16/3} - \frac{625}{1094713344} \frac{\mathcal{M}^3M_{\text{Sec}}M_{\text{Tot}}}{r_{\text{Sec}}^5} (\pi\mathcal{M}f)^{-8} \right]. \quad (3.3)$$

where we have neglected a constant term that is no measurable. Observe that the corrections introduced by M_{Sec} cannot be re-absorbed by a redefinition of vacuum system parameters, which implies that the effect of the secondary are (at worst) weakly-correlated vacuum terms. Moreover, if one could independently constrain the coefficients in from of the dominant $f^{-8/3}$ term and also the $f^{-16/3}$ and f^{-8} terms, one would be able to break the degeneracy between M_{Sec} and r_{Sec} in the leading-order term.

3.2 Accretion Disks

Let us now consider a different astrophysical environment: an extreme mass-ratio system in a circular equatorial orbit that is embedded in the accretion disk associated with the supermassive black hole. We refer the interested reader to [5] for astrophysical scenarios that could lead to this configuration. Of course, the effect of such a disk on the extreme-mass ratio inspiral will depend on the disk properties, which are not accurately known. One must then think of all possible effects that could be present and determine which one leads to the largest correction to extreme-mass ratio inspirals.

The dominant effect is that induced by the gravitational torque induced by spiral density waves in the accretion disk (ie. *migration* torque in planetary dynamics). Migration can occur whether a gap is cleared out or not, with the former leading to the largest effects. One might naively think that the stellar-object's mass accretion would also greatly modify the object's motion, but this is not the case because of quenching by a variety of processes, predominantly limited gas supply and radiation pressure. Migration

then becomes dominant, but its effect on gravitational waves still depends on the disk's properties. If one models the latter as an α (Shakura-Sunyaev) disk (where viscosity is proportional to the total pressure), then all disk effects become negligible. But if the disk is better described by a β profile (where viscosity is proportional to gas pressure only) in the radiation-dominated (extreme-mass ratio) regime, then the effect of migration would be measurable. Therefore, if such an accretion disk effect is detected one would know that the disk associated with that particular extreme mass-ratio binary is of β type.

Figure 3 summarizes the impact of the main accretion disk effects on the gravitational wave. This figure plots the dephasing (the difference between the gravitational wave phase computed with and without disk effects) as a function of the final orbital radius, assuming a one year inspiral. The left and right panels show results for different extreme mass-ratios, while the different curve colors and styles correspond to different disk effects: black is for accretion onto the small compact object, blue is for migration and green is for azimuthal winds. The latter corresponds to a difference in the orbital compact object velocity and the gas velocity, which can push the former forward or backward. The total accumulated gravitational wave phase is denoted by a thin magenta line, while the thick magenta lines correspond to two (an optimistic and a pessimistic) measures of the accuracy of a classic LISA-like mission. Notice that migration can lead to dephasing of order $10^2 - 10^3$ radians for β disks, while the same effect is essentially negligible for α disks. Therefore, a measurement of such disk effects could allow us to infer disk properties related to migration.

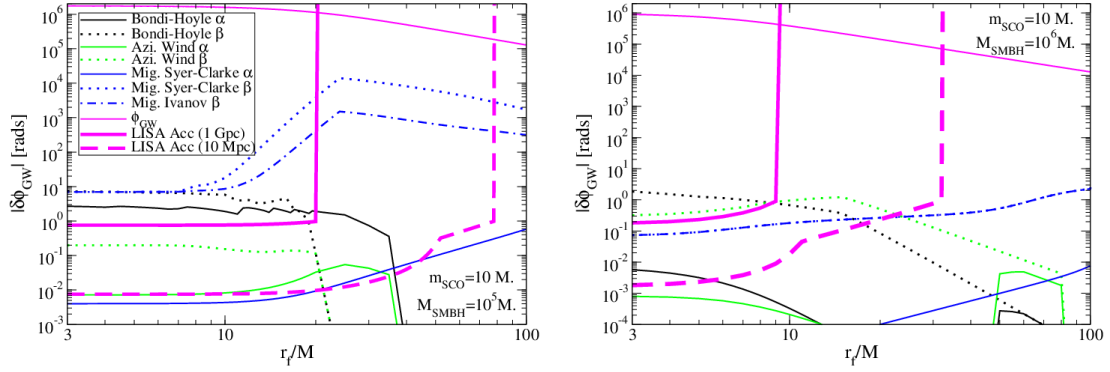


Figure 3: Gravitational wave dephasing as a function of final radius in units of M_{SMBH} induced by different disk effects. Solid (dotted) curves correspond to α (β) disks, with different colors indicating different disk effects: black corresponds to Bondi-Hoyle-Lyttleton (BHL) accretion onto the small object, green to azimuthal winds and blue to migration. The thin, solid magenta line is the total accumulated gravitational wave phase in vacuum. The thick, solid (dashed) magenta line corresponds to a measure of the accuracy to which LISA can measure the gravitational wave phase for a source at 1 Gpc (10 Mpc). Observe that certain disk effects, like migration, can leave huge imprints on the gravitational wave observable, inside the LISA accuracy bucket, provided the disk is a β one.

As before, a simple dephasing argument does not guarantee that disk effects can be disentangled from other vacuum system parameters. One can get a sense of whether such disentanglement is possible by computing the Fourier transform of the gravitational wave response function in the stationary-phase approximation:

$$\Psi/\Psi_{\text{vac}} = 1 - \tilde{A}_1 \alpha_1^{c_1} \dot{m}_{\text{SMBH},1}^{c_2} M_{\text{SMBH},5}^{\tilde{a}_3} q_0^{\tilde{a}_4} u_0^{\tilde{a}_5}, \quad (3.4)$$

and

$$|\tilde{h}|/|\tilde{h}|_{\text{vac}} = 1 - \tilde{B}_1 \alpha_1^{c_1} \dot{m}_{\text{SMBH},1}^{c_2} M_{\text{SMBH},5}^{\tilde{a}_3} q_0^{\tilde{a}_4} u_0^{\tilde{a}_5}, \quad (3.5)$$

where $\alpha_1 = \alpha/0.1$ is the normalized α -viscosity parameter, $\dot{m}_{\text{SMBH},1} \equiv \dot{m}_{\text{SMBH}}/0.1$ is the normalized supermassive black hole accretion rate $\dot{m} \equiv \dot{M}_{\text{SMBH}}/\dot{M}_{\text{SMBH,Edd}}$ with $\dot{M}_{\text{SMBH,Edd}}$ the Eddington rate. Similarly, $M_{\text{SMBH},5} = M_{\text{SMBH}}/(10^5 M_\odot)$ is a normalized supermassive black hole mass, $q_0 \equiv q/10^{-4}$ is the normalized mass-ratio $q = M_{\text{SMBH}}/m_{\text{CO}}$ and $u_0 \equiv (\pi \mathcal{M} f)/(6.15 \times 10^{-5})$ is a normalized reduced frequency for a gravitational wave frequency of 10^{-2} Hz. The parameters $(\tilde{A}_1, \tilde{B}_1, \tilde{a}_i, c_i)$ are given in

Table 1. Of course, these expressions are only valid when the accretion disk effects are small perturbations away from the vacuum evolution (ie. at sufficiently small separations).

		\tilde{A}_1	\tilde{B}_1	\tilde{a}_3	\tilde{a}_4	\tilde{a}_5	c_1	c_2
BHL	α	3(-8)	2(-7)	1	4	-20/3	-1	-5
BHL	β	1(-5)	1(-4)	6/5	79/25	-79/15	-4/5	-17/5
W	α	6(-17)	1(-16)	1	16/5	-16/3	-1	-3
W	β	6(-12)	4(-11)	6/5	59/25	-59/15	-4/5	-7/5
M1	α	3(-10)	4(-9)	1	16/5	-16/3	-1	-3
M1	β	1(-6)	3(-6)	6/5	59/25	-59/15	-4/5	-7/5
M2	α_{SC}	8(-6)	2(-5)	1	-2/5	-8/3	0	1
M2	β_{SC}	6(-3)	2(-2)	1/4	-1/8	-25/12	1/2	5/8
M2	β_{IPP}	6(-4)	2(-3)	4/7	-17/70	-7/3	2/7	11/4

Table 1: Columns are parameters in Eqs. (3.4) and (3.5) and rows are disk effects. The notation $x(y) = x \times 10^y$ in radians for \tilde{A}_1 and dimensionless for \tilde{B}_1 . Observe that the frequency exponent $\tilde{a}_5 < 0$, implying that these accretion disk effects are dominant at small frequencies (large radii).

The important result here is that the dependence of the disk effects with frequency, ie. the parameter \tilde{a}_5 , is of opposite sign with respect to those that arise in the vacuum gravitational wave phase. This is because disk corrections are largest for large radii, equivalent to weak-field vacuum effects, while post-Newtonian corrections to the vacuum gravitational wave phase are largest for small radii, equivalent to strong-field effects. This suggests that migration effects are weakly correlated with vacuum system parameters, as one could not reabsorb these disk effects by choosing different vacuum parameters.

4 Modified Gravity Imprints

In this section, we discuss how modified gravity imprints can manifest in the gravitational wave observable. We describe a scheme developed to constrain such imprints, the so-called parameterized post-Einsteinian (ppE) framework. We mainly follow the presentation in [16] and the recent results of [32].

4.1 Top-Down Approach

One approach to testing Einstein's theory with gravitational wave observations is a top-down one: pick a modified gravity theory, study its consequences and match-filter gravitational wave data with a template bank specifically constructed for that theory to test for possible deviations consistent with that theory. Most studies carried out so-far considered only quasi-circular coalescences in the inspiral phase. For such waveforms, the modified Fourier transform of the response function in the stationary-phase approximation can be modeled as

$$\tilde{h}(f) = \tilde{h}_{\text{GR}}(f) (1 + \alpha u^a) e^{i\beta u^b}, \quad (4.1)$$

where the GR transform was already described in Sec. 2.1, while (a, b) are numbers and (α, β) are functions of system parameters and parameters of the theory. We present their values in the Table 2.

Let us explain how the symbols of Table 2 are defined. In Brans-Dicke theory, S is the difference in the square of the sensitivities and ω_{BD} is the Brans-Dicke coupling parameter [9]. In the phenomenological massive graviton theory, D is a certain distance measure, z is redshift and λ_g is the Compton wavelength of the graviton [9]. In the parity violation case, the amplitude deformation depends on the inclination angle and the beam pattern angles via [20]

$$\delta\mathcal{A} = \frac{(F_+^2 + F_\times^2) c_i (1 + c_i^2)}{F_+^2 (1 + c_i^2) + 4F_\times^2 c_i^2}, \quad (4.2)$$

while v is a measure of parity violation. In non-dynamical Chern-Simons (CS) gravity [33], the quantity $\delta\dot{\vartheta}_{\text{CS}}$ is the time derivative of the CS scalar field (ie. the magnitude of the canonical embedding coordinate) [20]. In a varying Newton's constant theory, \dot{G}_c is the value of the time derivative of Newton's

Theory	α	a	β	b
Brans-Dicke	0	\cdot	$-\frac{5}{3584} \frac{S^2}{\omega_{\text{BD}}} \eta^{2/5}$	$-\frac{7}{3}$
Massive Graviton	0	\cdot	$-\frac{\pi^2 D \mathcal{M}}{\lambda_g^2 (1+z)}$	-1
Parity Violation	$4v\delta\mathcal{A}$	1	0	\cdot
Non-Dynamical CS Gravity	$4\pi\delta\dot{\vartheta}_{\text{CS}}\delta\mathcal{A}$	1	0	\cdot
$G(t)$ Theory	$-\frac{5}{512}\dot{G}\mathcal{M}$	$-\frac{8}{3}$	$-\frac{25}{65536}\dot{G}_c\mathcal{M}$	$-\frac{13}{3}$
Lorentz Violation	0	\cdot	$-\frac{\pi^{2-\gamma}}{(1-\gamma)} \frac{D_\gamma}{\lambda_{\text{LV}}^{2-\gamma}} \frac{\mathcal{M}^{1-\gamma}}{(1+z)^{1-\gamma}}$	$-\alpha_{\text{LV}} - 1$
Conservative EDGB	$\frac{5}{6}\eta^{-4/5}\zeta_{\text{EDGB}}$	$\frac{4}{3}$	$\frac{25}{64}\eta^{-4/5}\zeta_{\text{EDGB}}$	$-\frac{1}{3}$
Extra Dimensions	0	\cdot	$-\frac{75}{2554344} \frac{dM}{dt} \eta^{-4} (3 - 26\eta + 24\eta^2)$	$-\frac{13}{3}$

Table 2: Parameters that define the deformation of the response function in a variety of modified gravity theories. The notation \cdot means that a value for this parameter is irrelevant, as its amplitude is zero. All other parameters are defined in the text.

constant at coalescence [21]. In the phenomenological Lorentz-violating theory, λ_{LV} is a distance scale at which Lorentz-violation becomes important, while γ is the graviton momentum exponent in the deformation of the dispersion relation [19]. In Einstein-Dilaton-Gauss-Bonnet gravity, ζ_{EDGB} is the coupling parameter in the theory, and we here present only the modification in the response function introduced by the deformation of the background Schwarzschild metric [34]. In theories with extra dimensions, dM/dt is the mass loss due to gravitons leaking into the extra dimension.

As one can see from the above table, there are many possible deviations from General Relativity that one could consider, and none of the above has been sufficiently well-studied to determine whether any of them are compelling alternatives. A top-down approach would require us to construct as many template banks as there are alternative theories to consider. Of course, each of these banks would contain additional dimensions in parameter space (and thus many more templates), as one would have to allow for variations of the fundamental parameters of the modified theories. This might increase the computational cost beyond current capabilities.

But perhaps the biggest drawback of a top-down approach is that one must pick a theory beforehand, and this does not allow the data to select the theory that fits it best. Instead, this choice is made by the gravitational wave theorist or data analyst. It is entirely possible that, if General Relativity is incorrect in the strong field, none of the above theories will represent the correct modification. Thus, if one implements a top-down approach, one is forcing a certain fundamental bias into the analysis, ie. the fundamental bias that we, as theorists, know what modifications of gravity are possible.

4.2 Bottom-Up Approach

A new scheme has been proposed to alleviate this fundamental bias: the ppE framework [16]. In this scheme, one enhances General Relativity templates \tilde{h}_{GR} , which depend on system parameters $\vec{\lambda}_{\text{Sys}}$, through the introduction of theory parameters $\vec{\lambda}_{\text{ppE}}$:

$$\tilde{h}(f; \vec{\lambda}_{\text{Sys}}) \rightarrow \tilde{h}_{\text{GR}}(f; \vec{\lambda}_{\text{Sys}}) + \delta\tilde{h}(f; \vec{\lambda}_{\text{Sys}}; \vec{\lambda}_{\text{ppE}}). \quad (4.3)$$

When these parameters acquire certain values, the templates reduce exactly to those predicted in General Relativity, ie. $\delta\tilde{h}(f; \vec{\lambda}_{\text{Sys}}; \vec{\lambda}_{\text{ppE}}^{\text{GR}}) = 0$. When they acquire other values, the templates reduce to the predictions of modified gravity theories. The idea then is to match filter or perform Bayesian statistics with this enhanced template bank to allow the data to select the best-fit values of $\vec{\lambda}_{\text{ppE}}$ that best fit the signal.

This framework emerges from a generalization of the parameterized post-Newtonian scheme, developed in the 1970's to test modified gravity theories with Solar System experiments [35–40]. That scheme proposed the enhancement of the main quantity which all Solar System observables depend on, the weak-field expansion of the metric tensor in a certain coordinate system and gauge, by theory (ppN) parameters:

$$g_{\mu\nu}(x^\mu; \vec{\lambda}_{\text{Sys}}) \rightarrow g_{\mu\nu}(x^\mu; \vec{\lambda}_{\text{Sys}}, \vec{\lambda}_{\text{ppN}}). \quad (4.4)$$

When these parameters vanish, then the metric tensor reduces exactly to that predicted by General Relativity $g_{\mu\nu}(x^\mu; \vec{\lambda}_{\text{Sys}}, 0)$, while when they don't, they describe the weak-field expansion of the metric tensor in a plethora of modified gravity theories. The idea is then to constrain the values of $\vec{\lambda}_{\text{ppN}}$ by measuring Solar-System observables that depend on the metric tensor.

The ppN and ppE frameworks, however, differ in the priorities that drive the parameterized General Relativity deviations. While the former does not care about how many theory ppN parameters are introduced, in the latter we wish to minimize the number of ppE parameters. Otherwise, the inclusion of too many ppE parameters dilutes the information in the extracted best-fit, raising the false-alarm probability. One must then find a balance between the number of parameters introduced and the amount of bias contained in the templates.

The precise form of ppE templates clearly depends on the system under consideration and the level of theoretical complexity that one wishes to include. Keeping in line with the rest of this paper, we concentrate here on non-spinning, quasi-circular inspirals. In their original work, [16] also proposed ppE templates that contain the merger and ringdown phases in a hybrid fashion, but we will not discuss these here. As for the theoretical complexity, this depends on the number of additional ppE theory parameters one wishes to include.

The simplest ppE realization, which we refer to as the *restricted ppE templates*, is the following [41, 42]

$$\delta\tilde{h}(f; \vec{\lambda}_{\text{Sys}}; \alpha, \beta) = \tilde{h}_{\text{GR}}(\alpha u^{a_{\text{PN}}}) e^{i\beta u^{b_{\text{PN}}}}, \quad (4.5)$$

where the theory parameters (α, β) are to be searched over, while $(a_{\text{PN}}, b_{\text{PN}})$ are numbers equal to some of the post-Newtonian predictions for amplitude and phase frequency exponents, ie. $(a_{\text{PN}}, b_{\text{PN}})$ are not allowed to vary. For example, a Newtonian prediction for the amplitude and phase frequency exponents would be $a_{\text{Newt}} = -7/3$ and $b_{\text{Newt}} = -5/3$, while a 1.5PN prediction would be $a_{1.5\text{PN}} = 1$ and $b_{1.5\text{PN}} = -2/3$.

One can think of these tests as consistency checks of the post-Newtonian expansion. That is, given a detection of a gravitational-wave, one can in principle measure the chirp mass and the mass ratio by detecting the Newtonian and 1PN corrections to the phase. Allowing for a 1.5PN parameterized deviation in the phase then allows one to check whether this term is indeed as predicted by the post-Newtonian expansion. Alternatively, one can also think of these tests as straw-men indicators for GR consistency/inconsistency. That is, given a low signal-to-noise ratio detection, one can ask whether the signal detected is consistent with a General Relativity hypothesis $(\alpha, \beta) = (0, 0)$ [43].

The great disadvantage of the restricted ppE formalism is that, although one might be able to discern whether deviations are present, one cannot tell what kind of deviations those are. To alleviate this problem, one can introduce *free ppE templates*, the simplest version of which is [16]

$$\delta\tilde{h}(f; \vec{\lambda}_{\text{Sys}}; \alpha, \beta) = \tilde{h}_{\text{GR}}(\alpha u^a) e^{i\beta u^b}, \quad (4.6)$$

where now (α, β, a, b) are free ppE parameters. Observe that different choices of ppE parameters can recover all the modified theory predictions listed in Table 2. Furthermore, one can show that a generic power-series deformation of the binding energy or the gravitational wave luminosity will lead to a metric with the above ppE parameterization [16].

Given a stretch of gravitational wave data, one can then search via matched filtering with free ppE templates and allow the data to select the (α, β, a, b) ppE parameters that fit it best. If a deviation is present, such a procedure would not only signal the presence of a deviation, but it would also signal what type of phase or amplitude deformation is introduced. That is, one would know the best-fit numerical values of a and b , which encode what type of modified gravity effect is present. For example, as suggested by Table 2, a non-zero detection of β associated with $b = -7/3$ would signal the presence of a scalar dipolar mode, while one associated with $b = -13/3$ would signal the existence of an anomalous acceleration.

We have recently carried out a detailed Bayesian analysis with free ppE waveforms, whose main results are shown in Fig. 4 [32]. This figure shows the (3σ) -bounds on β for different values of b (ie. an exclusion plot for anything above the dotted curves), given gravitational wave detections consistent with General Relativity. The different dotted curves correspond to different binary systems, where we consider the inspiral phase only. For comparison, we also plot current bounds on β from the double binary pulsar, as well as a few Solar System constraints. Observe that for $b \gtrsim -2$, gravitational wave observations could

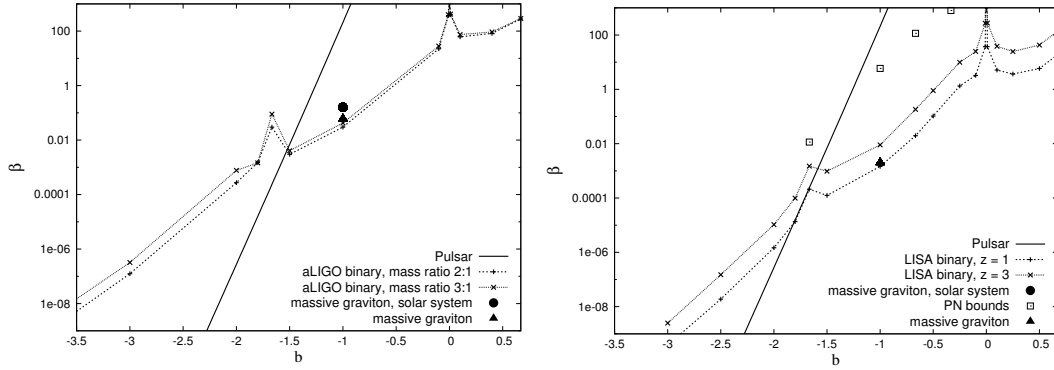


Figure 4: Left: (3σ) -bounds on β for different values of b for a single $\text{SNR} = 20$ aLIGO/aVirgo detection. The two dotted lines correspond to two sources with different mass ratios, total masses, and sky locations, but both at redshift $z = 0.1$ ($D_L = 462 \text{ Mpc}$). The solid line is the (3σ) -bound on β from the golden pulsar (PSR J0737-3039), while other symbols are bounds from Solar System experiments and other aLIGO analyses. Right: Same as left but for two classic-LISA sources at redshift $z = 1$ and $z = 3$.

rule out a large sector of (β, b) parameter space that is currently unconstrained. These results were confirmed using both a Fisher analysis as well as mapping out the likelihood surface with a Markov-Chain Monte-Carlo techniques.

Given a gravitational wave detection, one can also ask whether a General Relativity waveform (an Einstein hypothesis) or a non-General Relativity waveform (a non-Einstein hypothesis) best fits the data. This can be established by computing the Bayes factor or the odds-ratio of these two hypothesis. When using ppE templates, the hypothesis become nested, but the above described analysis can still be easily carried out. The Bayes factor will increase the larger (α, β) are, and so assuming a threshold Bayes factor of 10 (1 to 10 betting odds that one of the two hypothesis is incorrect and the other is correct) one can derive the accuracy to which (α, β) can be measured as a function of b . Implementing such a scheme, one obtains similar results to those already plotted in Fig. 4.

5 A Roadmap for the Future

The era of multi-messenger gravitational wave astrophysics is at our doorstep. A full exploitation of gravitational wave information will require a deep collaboration between astrophysicists, gravitational wave modelers, general relativists and data analysts. In this paper, I have described recent efforts to extract information about the astrophysical and theoretical environment in which compact binaries might be evolving.

On the astrophysical side, we have seen that the presence of a secondary perturber or an accretion disk can lead to observable effects in extreme-mass ratio inspiral gravitational waves. As for the former, these effects become non-negligible when secondary perturbers are at a distance of 0.1 pc or less from the center of mass of the extreme-mass ratio binary, given secondary masses of $10^7 M_\odot$. As for the latter, angular momentum transport due to density waves, analogous to planetary migration, can leave observable signatures in extreme-mass ratio binaries embedded in the thin disks, provided the latter are of β -type. These effects seem weakly degenerate with other system parameters, as suggested by a simple Fourier analysis.

On the fundamental theory side, we have seen that a top-down approach leads to a variety of waveform predictions. There is no particular modified gravity theory that is more compelling than General Relativity, which forces us to consider all theories on an equal footing. Performing a data analysis study for all such theories might be computationally prohibitive. Instead, one can carry out a bottom-up approach by match-filtering with ppE templates. These waveforms enhance General Relativity templates with certain well-motivated theory parameters, which then allows the data to select the parameters that best fit it, lifting some degree of fundamental bias.

A variety of paths present themselves for future studies. One could, for example, consider other astrophysical environment effects, or other specific top-down modified gravity theories, to discover what the corrections to the waveform are. Alternatively, one could consider whether the presence of an astrophysical environment could prohibit tests of Einstein's theory. This seems quite unlikely, given that modified gravity effects if present should be there always, while astrophysical environment effects should only affect a hand-full of sources. Finally, a realistic implementation of the ppE idea will require the generalization of the free ppE model to more complex and accurate waveforms. If this is not accomplished, mismodeling bias is likely to contaminate ppE studies, hindering the ability of gravitational waves to constrain Einstein's theory. Work along this lines is promising.

References

- [1] M. 2. Kramer *et al.*, *In the Proceedings of 22nd Texas Symposium on Relativistic Astrophysics at Stanford University, Stanford, California, 13-17 Dec 2004, pp 0038* [arXiv:astro-ph/0503386].
- [2] T. Bogdanovic, T. Bode, R. Haas, P. Laguna, D. Shoemaker, *Class. Quant. Grav.* **28**, 094020 (2011). [arXiv:1010.2496 [astro-ph.CO]].
- [3] T. Bode, R. Haas, T. Bogdanovic, P. Laguna, D. Shoemaker, *Astrophys. J.* **715**, 1117-1131 (2010). [arXiv:0912.0087 [gr-qc]].
- [4] N. Yunes, M. Coleman Miller, J. Thornburg, *Phys. Rev.* **D83**, 044030 (2011). [arXiv:1010.1721 [astro-ph.GA]].
- [5] B. Kocsis, N. Yunes, A. Loeb, *Phys. Rev.* **D84**, 024032 (2011). [arXiv:1104.2322 [astro-ph.GA]].
- [6] N. Yunes, B. Kocsis, A. Loeb, Z. Haiman, [arXiv:1103.4609 [astro-ph.CO]].
- [7] C. M. Will, *Phys. Rev.* **D50**, 6058-6067 (1994). [gr-qc/9406022].
- [8] C. M. Will, N. Yunes, *Class. Quant. Grav.* **21**, 4367 (2004). [gr-qc/0403100].
- [9] E. Berti, A. Buonanno, C. M. Will, *Class. Quant. Grav.* **22**, S943-S954 (2005). [gr-qc/0504017].
- [10] A. Stavridis, C. M. Will, *J. Phys. Conf. Ser.* **228**, 012049 (2010).
- [11] K. G. Arun, C. M. Will, *Class. Quant. Grav.* **26**, 155002 (2009). [arXiv:0904.1190 [gr-qc]].
- [12] D. Keppel, P. Ajith, *Phys. Rev.* **D82**, 122001 (2010). [arXiv:1004.0284 [gr-qc]].
- [13] E. Berti, J. Gair, A. Sesana, [arXiv:1107.3528 [gr-qc]].
- [14] K. Yagi, T. Tanaka, *Phys. Rev.* **D81**, 064008 (2010). [arXiv:0906.4269 [gr-qc]].
- [15] C. F. Sopuerta, N. Yunes, *Phys. Rev.* **D80**, 064006 (2009). [arXiv:0904.4501 [gr-qc]].
- [16] N. Yunes, F. Pretorius, *Phys. Rev.* **D79**, 084043 (2009). [arXiv:0902.4669 [gr-qc]].
- [17] C. M. Will, *Phys. Rev.* **D57**, 2061-2068 (1998). [gr-qc/9709011].
- [18] P. D. Scharre, C. M. Will, *Phys. Rev.* **D65**, 042002 (2002). [gr-qc/0109044].
- [19] S. Mirshekari, N. Yunes, C. M. Will, [arXiv:1110.2720 [gr-qc]].
- [20] N. Yunes, R. O'Shaughnessy, B. J. Owen, S. Alexander, *Phys. Rev.* **D82**, 064017 (2010). [arXiv:1005.3310 [gr-qc]].
- [21] N. Yunes, F. Pretorius, D. Spergel, *Phys. Rev.* **D81**, 064018 (2010). [arXiv:0912.2724 [gr-qc]].
- [22] K. Yagi, N. Tanahashi, T. Tanaka, *Phys. Rev.* **D83**, 084036 (2011). [arXiv:1101.4997 [gr-qc]].
- [23] N. Yunes, F. Pretorius, *Phys. Rev.* **D80**, 122003 (2009). [arXiv:0909.3328 [gr-qc]].

- [24] L. Blanchet, *Living Rev. Rel.* **9**, 4 (2006).
- [25] L. Barack, *Class. Quant. Grav.* **26**, 213001 (2009). [arXiv:0908.1664 [gr-qc]].
- [26] N. Yunes, *GW Notes*, Vol. 2, p. 3-47 (2009).
- [27] N. Yunes, K. G. Arun, E. Berti, C. M. Will, *Phys. Rev.* **D80**, 084001 (2009). [arXiv:0906.0313 [gr-qc]].
- [28] N. Yunes, A. Buonanno, S. A. Hughes, M. Coleman Miller, Y. Pan, *Phys. Rev. Lett.* **104**, 091102 (2010). [arXiv:0909.4263 [gr-qc]].
- [29] N. Yunes, A. Buonanno, S. A. Hughes, Y. Pan, E. Barausse, M. C. Miller, W. Thrope, *Phys. Rev.* **D83**, 044044 (2011). [arXiv:1009.6013 [gr-qc]].
- [30] T. Tanaka, Y. Mino, M. Sasaki, M. Shibata, *Phys. Rev.* **D54**, 3762-3777 (1996). [gr-qc/9602038].
- [31] Y. Mino, M. Sasaki, T. Tanaka, *Prog. Theor. Phys. Suppl.* **128**, 373-406 (1997). [gr-qc/9712056].
- [32] N. Cornish, L. Sampson, N. Yunes, F. Pretorius, [arXiv:1105.2088 [gr-qc]].
- [33] S. Alexander, N. Yunes, *Phys. Rept.* **480**, 1-55 (2009). [arXiv:0907.2562 [hep-th]].
- [34] N. Yunes, L. C. Stein, *Phys. Rev.* **D83**, 104002 (2011). [arXiv:1101.2921 [gr-qc]].
- [35] K. Nordtvedt Jr., *Astrophysical J.* **161**, 1059 (1970).
- [36] K. S. Thorne and C. M. Will, *Astrophysical J.* **163**, 595 (1971).
- [37] C. M. Will, *Astrophysical J.* **163**, 611 (1971).
- [38] C. M. Will, *Astrophysical J.* **169**, 125 (1971).
- [39] C. M. Will and K. Nordtvedt Jr. *Astrophysical J.* **177**, 757 (1972).
- [40] K. Nordtvedt Jr. and C. M. Will, *Astrophysical J.* **177**, 775 (1972).
- [41] K. G. Arun, B. R. Iyer, M. S. S. Qusailah, B. S. Sathyaprakash, *Class. Quant. Grav.* **23**, L37-L43 (2006). [gr-qc/0604018].
- [42] C. K. Mishra, K. G. Arun, B. R. Iyer, B. S. Sathyaprakash, *Phys. Rev.* **D82**, 064010 (2010). [arXiv:1005.0304 [gr-qc]].
- [43] T. G. F. Li, W. Del Pozzo, S. Vitale, C. V. D. Broeck, M. Agathos, J. Veitch, K. Grover, T. Sidery *et al.*, [arXiv:1110.0530 [gr-qc]].

Constraint propagation and constraint-damping in the C^2 -adjusted formulation

Takuya Tsuchiya^{50(a)}, Gen Yoneda^(a) and Hisa-aki Shinkai^(b)

^(a)*Department of Mathematical Sciences, Waseda University, Okubo, Shinjuku, Tokyo, 169-8555, Japan*

^(b)*Faculty of Information Science and Technology, Osaka Institute of Technology, 1-79-1 Kitayama, Hirakata, Osaka 573-0196, Japan.*

Abstract

In order to perform accurate and stable long-term numerical calculations, we construct new sets of ADM and BSSN evolution equations by adjusting constraints to their right-hand-sides. We apply a method suggested by Fiske (2004), which adds functional derivative of the norm of constraints, C^2 . We derive their constraint propagation equations (evolution equations of constraints) in flat spacetime, which show that C^2 itself evolve decaying. We also perform numerical tests with the polarized Gowdy-wave testbed, and show that the constraint-damping appears. The life-times of the standard ADM and BSSN simulations are improved as about twice as longer.

1 Introduction

In numerical relativity, the standard way to integrate the Einstein equations is 3+1 splitting of spacetime. The fundamental spacetime splitting is the Arnowitt-Deser-Misner (ADM) formulation [1]. However, it is known that the ADM formulation is not suitable formulation to perform long-term simulations in strong gravitational fields [2]. To perform simulations such as coalescences of binary neutron stars and/or black holes, many formulations are suggested, one of the most commonly used among the numerical relativists is the so-called Baumgarte-Shapiro-Shibata-Nakamura (BSSN) formulation [3].

The current formulations use the constraint-damping technique which is obtained by adding the constraint equation to the evolution equations. Fiske [4] suggested a method of constructing a set of evolution equations which we call “ C^2 -adjusted system”. We apply his system to the ADM and BSSN formulations. To see the effect of the adjustments, we analyze the constraint propagation of the C^2 -adjusted ADM and BSSN formulations, and we also perform some numerical tests to confirm the constraint-damping behaviors.

2 General Idea of C^2 -adjusted system

Suppose dynamical variables u^i obeys a set of evolution equations with constraint equations, C^a ;

$$\partial_t u^i = f(u^i, \partial_j u^i, \dots), \quad (2.1)$$

$$C^a = g(u^i, \partial_j u^i, \dots). \quad (2.2)$$

Fiske [4] proposed an adjustment of the evolution equations in the way of

$$\partial_t u^i = f(u^i, \partial_j u^i, \dots) - \kappa^{ij} \left(\frac{\delta C^2}{\delta u^j} \right), \quad (2.3)$$

where κ^{ij} is a positive-definite constant coefficient, and C^2 is the norm of constraints which is defined as $C^2 \equiv \int C_a C^a d^3x$. The term $(\delta C^2 / \delta u^j)$ is the functional derivative of C^2 with u^j . We call the set of (2.3) with (2.2) as “ C^2 -adjusted formulation”. The associated constraint propagation equation becomes

$$\partial_t C^2 = h(C^a, \partial_i C^a, \dots) - \int d^3x \left(\frac{\delta C^2}{\delta u^i} \right) \kappa^{ij} \left(\frac{\delta C^2}{\delta u^j} \right). \quad (2.4)$$

⁵⁰Email address: tsuchiya@akane.waseda.jp

If we set κ^{ij} so as the second term in the RHS of (2.4) becomes dominant than the first term, then $\partial_t C^2$ becomes negative, which indicates that constraint violations are expected to decay to zero.

3 Applications

Now, we apply the idea of C^2 -adjusted system to the ADM and BSSN formulations.

3.1 C^2 -adjusted ADM Formulation

3.1.1 Evolution Equations

We apply C^2 -adjusted system to the ADM formulation. The evolution equations are formally written as

$$\partial_t \gamma_{ij} = [\text{Original Terms}] - \kappa_{\gamma ijmn} \left(\frac{\delta(C^{\text{ADM}})^2}{\delta \gamma_{mn}} \right), \quad (3.1)$$

$$\partial_t K_{ij} = [\text{Original Terms}] - \kappa_{K ijmn} \left(\frac{\delta(C^{\text{ADM}})^2}{\delta K_{mn}} \right), \quad (3.2)$$

where $(C^{\text{ADM}})^2$ is the norm of the constraints, which we set

$$(C^{\text{ADM}})^2 \equiv \int \{(\mathcal{H}^{\text{ADM}})^2 + \gamma^{ij} \mathcal{M}_i^{\text{ADM}} \mathcal{M}_j^{\text{ADM}}\} d^3x, \quad (3.3)$$

and both coefficients, $\kappa_{\gamma ijmn}$ and $\kappa_{K ijmn}$, are supposed to be positive definite. The adjusted terms, $(\delta(C^{\text{ADM}})^2/\delta \gamma_{mn})$ and $(\delta(C^{\text{ADM}})^2/\delta K_{mn})$, are explicitly written as eqs. (A1) and (A2) in [5], respectively.

3.1.2 Constraint Propagation Equations

In order to investigate the effect of the constraint-damping due to the adjusted terms in (3.1)-(3.2), we show the constraint propagation equations in the flat spacetime:

$$\partial_t \mathcal{H}^{\text{ADM}} = [\text{Original Terms}] - 2\kappa_{\gamma} \Delta^2 \mathcal{H}^{\text{ADM}}, \quad (3.4)$$

$$\partial_t \mathcal{M}_i^{\text{ADM}} = [\text{Original Terms}] + \kappa_K \Delta \mathcal{M}_i^{\text{ADM}} + 3\kappa_K \partial_i \partial_j (\mathcal{M}^{\text{ADM}})^j, \quad (3.5)$$

where, we set the coefficients as $\kappa_{\gamma ijmn} = \kappa_{\gamma} \delta_{im} \delta_{jn}$ and $\kappa_{K ijmn} = \kappa_K \delta_{im} \delta_{jn}$. In both equations (3.4)-(3.5), we see the diffusion terms, $-2\kappa_{\gamma} \Delta^2 \mathcal{H}^{\text{ADM}}$ and $\kappa_K \Delta \mathcal{M}_i^{\text{ADM}}$, respectively. These terms contribute to the damping of the constraint violations.

3.2 C^2 -adjusted BSSN Formulation

3.2.1 Evolution Equations

Next, we apply the idea to the BSSN formulation. The evolution equations are formally written as

$$\partial_t \varphi = [\text{Original Terms}] - \lambda_{\varphi} \left(\frac{\delta(C^{\text{BSSN}})^2}{\delta \varphi} \right), \quad (3.6)$$

$$\partial_t K = [\text{Original Terms}] - \lambda_K \left(\frac{\delta(C^{\text{BSSN}})^2}{\delta K} \right), \quad (3.7)$$

$$\partial_t \tilde{\gamma}_{ij} = [\text{Original Terms}] - \lambda_{\tilde{\gamma} ijmn} \left(\frac{\delta(C^{\text{BSSN}})^2}{\delta \tilde{\gamma}_{mn}} \right), \quad (3.8)$$

$$\partial_t \tilde{A}_{ij} = [\text{Original Terms}] - \lambda_{\tilde{A} ijmn} \left(\frac{\delta(C^{\text{BSSN}})^2}{\delta \tilde{A}_{mn}} \right), \quad (3.9)$$

$$\partial_t \tilde{\Gamma}^i = [\text{Original Terms}] - \lambda_{\tilde{\Gamma}}^{ij} \left(\frac{\delta(C^{\text{BSSN}})^2}{\delta \tilde{\Gamma}^j} \right), \quad (3.10)$$

where all the coefficients λ_φ , λ_K , $\lambda_{\tilde{\gamma}ijmn}$, $\lambda_{\tilde{A}ijmn}$, and $\lambda_{\tilde{\Gamma}}^{ij}$ are positive definite. $(C^{\text{BSSN}})^2$ is a function of the constraints $\mathcal{H}^{\text{BSSN}}$, $\mathcal{M}_i^{\text{BSSN}}$, \mathcal{G}^i , \mathcal{A} , and \mathcal{S} , which we set as

$$(C^{\text{BSSN}})^2 = \int \{(\mathcal{H}^{\text{BSSN}})^2 + \gamma^{ij} \mathcal{M}_i^{\text{BSSN}} \mathcal{M}_j^{\text{BSSN}} + c_G \gamma_{ij} \mathcal{G}^i \mathcal{G}^j + c_A \mathcal{A}^2 + c_S \mathcal{S}^2\} d^3x, \quad (3.11)$$

where, c_G , c_A , and c_S are Boolean parameters (0 or 1). These three parameters are introduced to prove the necessity of the algebraic constraint terms in (3.11). The adjusted terms in (3.6)-(3.10) are then written down explicitly, as shown as eqs. (A1)-(A5) in [6], respectively.

3.2.2 Constraint Propagation Equations

In order to see the effect of the adjusted terms in (3.6)-(3.10), we derive the constraint propagation equations in the flat spacetime:

$$\begin{aligned} \partial_t \mathcal{H}^{\text{BSSN}} &= [\text{Original Terms}] + (-128\lambda_\varphi \Delta^2 - (3/2)\lambda_{\tilde{\gamma}} \Delta^2 + 2\lambda_{\tilde{\Gamma}} \Delta) \mathcal{H}^{\text{BSSN}} \\ &\quad + c_G (-1/2)\lambda_{\tilde{\gamma}} \Delta \partial_m - 2\lambda_{\tilde{\Gamma}} \partial_m) \mathcal{G}^m + 3c_S \lambda_{\tilde{\gamma}} \Delta \mathcal{S}, \end{aligned} \quad (3.12)$$

$$\partial_t \mathcal{M}_a^{\text{BSSN}} = [\text{Original Terms}] + \left\{ (8/9)\lambda_K \delta^{bc} \partial_a \partial_b + \lambda_{\tilde{A}} \Delta \delta_a^c + \lambda_{\tilde{A}} \delta^{bc} \partial_a \partial_b \right\} \mathcal{M}_c^{\text{BSSN}} - 2c_A \lambda_{\tilde{A}} \partial_a \mathcal{A}, \quad (3.13)$$

$$\begin{aligned} \partial_t \mathcal{G}^a &= [\text{Original Terms}] + \delta^{ab} ((1/2)\lambda_{\tilde{\gamma}} \partial_b \Delta + 2\lambda_{\tilde{\Gamma}} \partial_b) \mathcal{H}^{\text{BSSN}} \\ &\quad + c_G (\lambda_{\tilde{\gamma}} \Delta \delta^a_b + (1/2)\lambda_{\tilde{\gamma}} \delta^{ac} \partial_c \partial_b - 2\lambda_{\tilde{\Gamma}} \delta^a_b) \mathcal{G}^b - \lambda_{\tilde{\gamma}} c_S \delta^{ab} \partial_b \mathcal{S}, \end{aligned} \quad (3.14)$$

$$\partial_t \mathcal{A} = [\text{Original Terms}] + 2\lambda_{\tilde{A}} \delta^{ij} (\partial_i \mathcal{M}_j^{\text{BSSN}}) - 6c_A \lambda_{\tilde{A}} \mathcal{A}, \quad (3.15)$$

$$\partial_t \mathcal{S} = [\text{Original Terms}] + 3\lambda_{\tilde{\gamma}} \Delta \mathcal{H}^{\text{BSSN}} + c_G \lambda_{\tilde{\gamma}} \partial_\ell \mathcal{G}^\ell - 6c_S \lambda_{\tilde{\gamma}} \mathcal{S}. \quad (3.16)$$

where we set the coefficient parameters, $\lambda_{\tilde{\gamma}ijmn} = \lambda_{\tilde{\gamma}} \delta_{im} \delta_{jn}$, $\lambda_{\tilde{A}ijmn} = \lambda_{\tilde{A}} \delta_{im} \delta_{jn}$ and $\lambda_{\tilde{\Gamma}}^{ij} = \lambda_{\tilde{\Gamma}} \delta^{ij}$ for simplicity. In the above equations, we see the appearances of diffusion terms $(-128\lambda_\varphi \Delta^2 - (3/2)\lambda_{\tilde{\gamma}} \Delta^2 + 2\lambda_{\tilde{\Gamma}} \Delta) \mathcal{H}^{\text{BSSN}}$, $\lambda_{\tilde{A}} \Delta \mathcal{M}_a^{\text{BSSN}}$, $c_G (\lambda_{\tilde{\gamma}} \Delta - 2\lambda_{\tilde{\Gamma}}) \mathcal{G}^a$, $-6c_A \lambda_{\tilde{A}} \mathcal{A}$ and $-6c_S \lambda_{\tilde{\gamma}} \mathcal{S}$, respectively. These terms contribute to the damping of the violations. If we set the parameters, c_G , c_A and c_S , are zero, equations (3.14)-(3.16) turn not to include diffusion terms. Therefore, $(C^{\text{BSSN}})^2$ should include \mathcal{G}^i , \mathcal{A} and \mathcal{S} .

4 Numerical Tests

We perform simulations of the polarized Gowdy wave which is one of the testbeds for comparing formulations [7]. The numerical parameters are the same with those in [7].

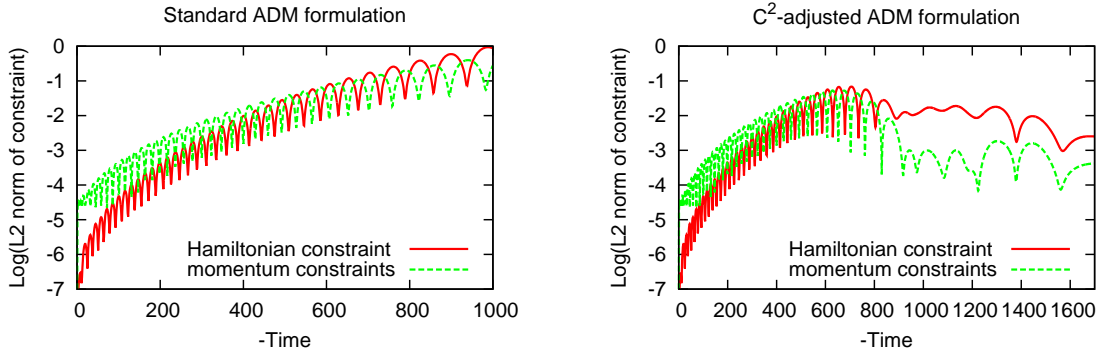


Figure 1: L2 norm of each constraint in the polarized Gowdy wave test with the ADM formulations. The L2 norm of the constraints are shown as a function of the backward time. We adopt the parameters same with the line (c) in Fig.2 of [5].

In Figure 1, we show that the constraint violations with the ADM formulations. We see that the adjusted cases decrease the violation, and the lifetime of simulations becomes about 1.7 times longer than that of the standard case. Next, in Fig.2, we show that the constraint violations with the BSSN

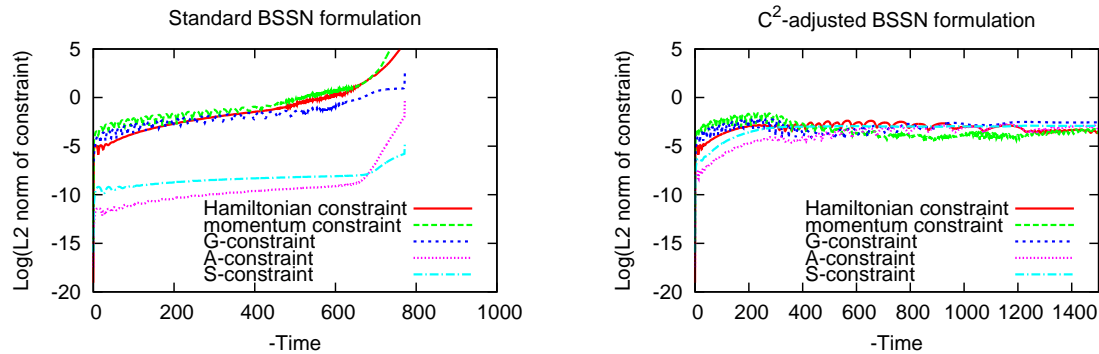


Figure 2: L2 norm of each constraint with the BSSN formulations. We adopt the parameters same with the line (C) in Fig.8 of [6].

formulations. We see the similar effects, and the lifetime of simulations of the adjusted case becomes more than twice longer than that of the standard case.

5 Summary

In this report, we reviewed the idea of the C^2 -adjusted system and applied the system to the ADM and BSSN formulations. We see the effect of constraint-damping due to the adjusted terms by showing the constraint propagation equations. We performed the simulations with these formulations in the Gowdy wave testbed and confirmed the constraint-damping behaviors and the life time of the simulations becomes longer than those of the standard cases. Please refer [6] for more details.

This work was partially supported by Grant-in-Aid for Scientific Research Fund of Japan Society of the Promotion of Science No. 22540293 (HS).

References

- [1] R. Arnowitt, S. Deser, and C. W. Misner, in *Gravitation: An Introduction to Current Research*, edited by L. Witten (Wiley, New York, 1962); J. W. York, Jr., in *Sources of Gravitational Radiation*, edited by L. Smarr (Cambridge University Press, Cambridge, 1979); L. Smarr and J.W. York, Jr., *Phys. Rev. D* **17**, 2529 (1978).
- [2] H. Shinkai and G. Yoneda, *Class. Quant. Grav.* **17**, 4799 (2000); H. Shinkai and G. Yoneda, [arXiv:gr-qc/0209111](#) (2002); H. Shinkai, *J. Korean Phys. Soc.* **54**, 2513 (2009).
- [3] M. Shibata and T. Nakamura, *Phys. Rev. D* **52**, 5428 (1995); T. W. Baumgarte and S. L. Shapiro, *Phys. Rev. D* **59**, 024007 (1998).
- [4] D. R. Fiske, *Phys. Rev. D* **69**, 047501, (2004).
- [5] T. Tsuchiya, G. Yoneda and H. Shinkai, *Phys. Rev. D* **83**, 064032, (2011).
- [6] T. Tsuchiya, G. Yoneda and H. Shinkai, [arXiv:gr-qc/1109.5782](#).
- [7] M. Alcubierre *et al.*, *Class. Quant. Grav.* **21**, 589 (2004).

Effects of hyperon in binary neutron star mergers

Yuichiro Sekiguchi⁵¹

Yukawa Institute for Theoretical Physics, Kyoto University, Kyoto 606-8502, Japan

Abstract

Numerical simulations for the merger of binary neutron stars are performed in full general relativity incorporating both nucleonic and hyperonic finite-temperature equations of state (EOS) and neutrino cooling for the first time. It is found that even for the hyperonic EOS, a hypermassive neutron star is first formed after the merger for the typical total mass $\approx 2.7M_{\odot}$, and subsequently collapses to a black hole (BH). It is shown that hyperons play a substantial role in the post-merger dynamics, torus formation around the BH, and emission of gravitational waves (GWs). In particular, the existence of hyperons is imprinted in GWs. Therefore, GW observations will provide a potential opportunity to explore the composition of the neutron star matter.

1 Introduction

The properties of the neutron star (NS) matter, in particular its equation of state (EOS), are still poorly understood. In recent years, the influence of non-nucleonic degrees of freedom, such as hyperons, meson condensations, and quarks, on properties of the NS matter has been discussed extensively [1]. Generally speaking, presence of such exotic particles results in softening of EOS. This effect reduces the maximum mass of NS. The recent mass measurement of PSR J1614-2230 ($M_{\text{J1614-2230}} = 1.97 \pm 0.04M_{\odot}$) [2] gave a strong impact on the properties of the NS matter, indicating that stiff EOSs are preferable. However, it does not still constrain the existence of exotic particles in NS [1, 3].

There are a number of numerical studies exploring effects of such exotic phases on stellar core collapse [4]. By contrast, effects of the exotic particles on dynamics and gravitational waves (GWs) from binary neutron stars (BNS) mergers and hypermassive neutron stars (HMNS) subsequently formed have not been studied in detail (but see recent studies in [5]), although the coalescence of BNS is one of the most promising sources for next-generation kilo-meter-size GW detectors.

Among exotic particles, Λ hyperons are likely to appear first in (cold) NS around the rest-mass density above several times of the nuclear matter density. We here present the first results of numerical-relativity simulations for the BNS merger performed incorporating a finite-temperature EOS including contributions of Λ hyperons [8] (Hyp-EOS). We ignore the contributions of Σ hyperons because recent experiments suggest that Σ hyperons feel a repulsive potential [7] while Λ hyperons feel an attractive potential [6], and hence, Λ hyperons are likely to appear first and to be dominant.

2 Setting

Numerical simulations in full general relativity are performed using the same method and formulation as in [9]⁵². In addition to the ordinary hydrodynamic equations, we solve evolution equations for the neutrino (Y_{ν}), electron (Y_e), and total lepton (Y_l) fractions per baryon, taking account of weak interaction processes and neutrino cooling employing a general relativistic leakage scheme [11, 12]. The results with Hyp-EOS are compared with those with a finite-temperature nucleonic EOS [13] (Shen-EOS). The maximum mass of zero-temperature spherical NS for Hyp-EOS is $M_{\text{max,Hyp}} \approx 1.8M_{\odot}$. This is smaller than that for Shen-EOS, $M_{\text{max,Shen}} \approx 2.2M_{\odot}$. Simulations with finite-temperature EOSs with exotic phases which can produce a stable NS with mass larger than $M_{\text{J1614-2230}}$ should be performed in the future studies.

⁵¹Email address: sekig@yukawa.kyoto-u.ac.jp

⁵²Einstein's equations are solved in the so-called Baumgarte-Shapiro-Shibata-Nakamura (BSSN)-puncture formulation [10] with dynamical gauge conditions for the lapse function and the shift vector; a fourth-order finite differencing in space and a fourth-order Runge-Kutta time integration are used; a conservative shock capturing scheme with third-order accuracy in space and fourth-order accuracy in time is employed for solving hydrodynamic equations

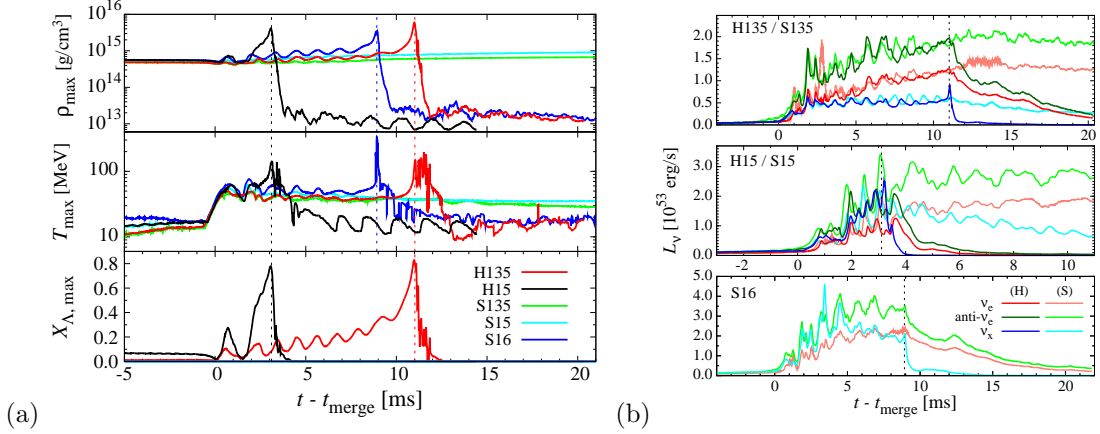


Figure 1: (a) Maximum rest-mass density, maximum matter temperature, and maximum mass fraction of hyperons as functions of time for H135 (solid red), H15 (dotted black), S135 (dashed green), S15 (short-dotted cyan), and S16 (dashed-dotted blue). The vertical thin lines show the time at which a BH is formed. (b) Neutrino luminosities for H135 and S135 (top), H15 and S15 (middle), and S16 (bottom). The dotted vertical lines show the time at which a BH is formed. The solid and dashed curves correspond to the result with the Hyp-EOS and Shen-EOS, respectively.

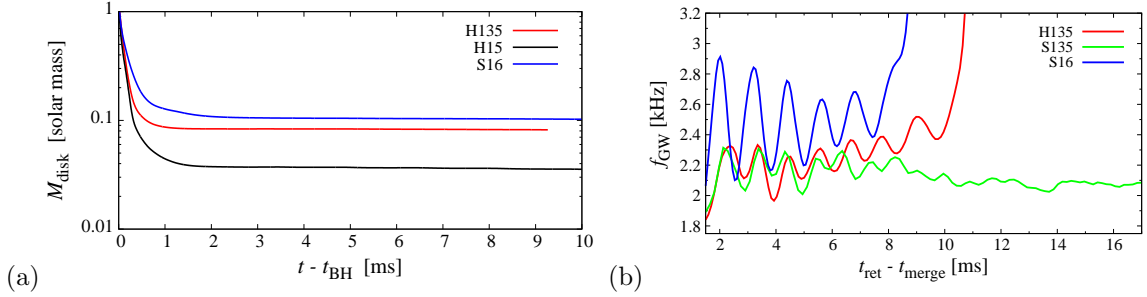


Figure 2: (a) The torus mass as a function of time after the BH formation. (b) $f_{\text{GW}}(t)$ in the HMNS phase, smoothed by a weighted spline.

Numerical simulations are performed in a non-uniform grid [9]⁵³, and we confirm that the convergence is achieved except for stochastic behaviors due to convective motions. Outer boundaries are located in a local wave zone. During the simulations, we check the conservation of baryon rest-mass, total gravitational mass, and total angular momentum, and find that the errors are within 0.2%, 1%, and 2%, respectively, for the high-resolution runs. We focus on the merger of equal-mass BNS. The gravitational mass of single NS in isolation is $M_{\text{NS}} = 1.35$ and $1.5M_{\odot}$ for Hyp-EOS (referred to as H135 and H15). We perform simulations with the initial condition of about 3–4 orbits before the onset of the merger until the system relaxes to a quasistationary state. We compare the simulation results with those for Shen-EOS with $M_{\text{NS}} = 1.35, 1.5,$ and $1.6M_{\odot}$ (referred to as S135, S15, and S16) obtained in [9].

3 Results

Figure 1(a) plots the evolution of maximum rest-mass density, ρ_{\max} , maximum temperature, T_{\max} , and maximum mass fraction of hyperons, $X_{\Lambda, \max}$ as functions of $t - t_{\text{merge}}$ where t_{merge} is an approximate onset time of the merger. After the merger sets in, $X_{\Lambda, \max}$ increases to be $\gtrsim 0.1$ in accordance with the

⁵³The inner domain is composed of a finer uniform grid and the outer domain of a coarser nonuniform grid. The grid resolution in the inner zone is chosen so that the major diameter of each neutron star in the inspiral orbit is covered by 60 and 80 grid points for low- and high-resolution runs, respectively

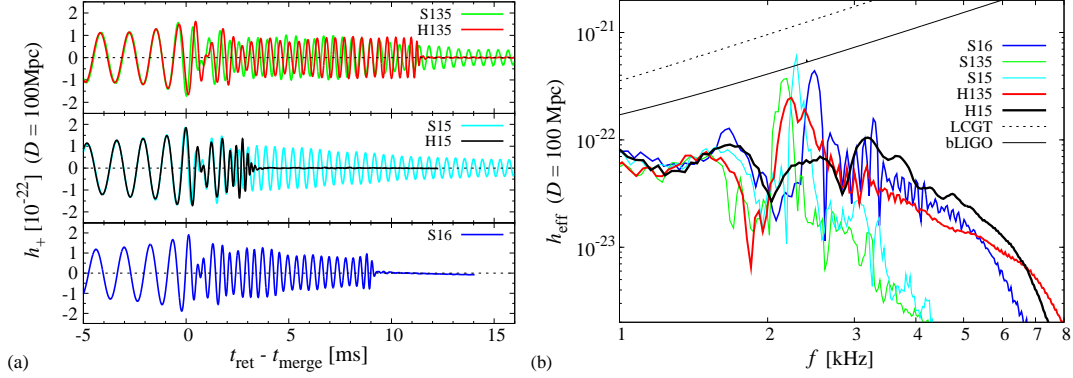


Figure 3: (a) GWs observed along the axis perpendicular to the orbital plane for the hypothetical distance to the source $D = 100$ Mpc. (b) The effective amplitude of GWs defined by $0.4f|h(f)|$ as a function of frequency for $D = 100$ Mpc. The noise amplitudes of a broadband configuration of broadband-LIGO and LCGT are shown together.

increase in ρ_{max} , and hyperons play a substantial role in the post-merger dynamics and emission of GWs.

A HMNS is first formed after the merger, supported by the centrifugal force and thermal contributions to the pressure [5, 9]. They subsequently contract by emission of GWs, and for H135, H15, and S16, they collapse to a black hole (BH) at $t = t_{\text{BH}}$ where $t_{\text{BH}} - t_{\text{merge}} \approx 11.0, 3.1,$ and 8.9 ms, respectively. After the BH formation for H135, H15, and S16, an accretion torus is formed around the BH. Figure 2(a) plots the torus mass, M_{torus} , as a function of time. M_{torus} in a quasistationary state is $\approx 0.082, 0.035,$ and $0.10M_{\odot}$ for H135, H15, and S16, respectively, with $\rho_{\text{max}} \approx 10^{13}$ g/cm³ (see Fig. 1(a)). Interestingly, M_{torus} is smaller for H135 than that for S16 in spite of the longer lifetime of the HMNS. This is likely because the HMNS for H135 just before the BH formation is more compact than that for S16. Our results suggest that the emergence of non-nucleonic degrees of freedom such as hyperons would have a negative impact for driving a short-gamma ray burst for which formation of a massive torus is preferred [14].

Figure 1(b) plots neutrino luminosities as functions of time. Electron antineutrinos are dominantly emitted for all the models as found in the previous studies [9, 15]. Soon after the BH formation, μ/τ neutrino luminosity steeply decreases because high temperature regions are swallowed into the BH, while luminosities of electron neutrinos and antineutrinos decrease only gradually because these neutrinos are emitted via charged-current processes from the massive accretion torus [9]. These features in neutrino luminosities are quantitatively the same for Hyp-EOS and Shen-EOS models, and hence, it would be difficult to extract information of the NS matter only from the neutrino signal.

Figure 3(a) plots the plus mode (h_+) of GWs as a function of $t_{\text{ret}} - t_{\text{merge}}$ where t_{ret} is the retarded time. GWs from the inspiral phase (for $t_{\text{ret}} \lesssim t_{\text{merge}}$) agree well with each other for the models with Hyp-EOS and Shen-EOS for the same mass. On the other hand, quasi-periodic GWs from the HMNS show differences. In particular, the characteristic GW frequency, f_{GW} , increases with time for Hyp-EOS models, as clearly observed in the effective amplitude [see Fig. 3(b)] defined by $h_{\text{eff}} \equiv 0.4f|h(f)|$ where $h(f)$ is the Fourier transform of $h_+ - ih_{\times}$ with h_{\times} being the cross mode and the factor 0.4 comes from taking average in terms of directions to the source and rotational axis of the HMNS. Reflecting the shift of the characteristic frequency, the prominent peak in the GW spectra for Hyp-EOS models (H135 and H15) is broadened. We here note that the lifetime of the HMNS is longer for H135 than that for S16. The reason for this broadening of the peak is described as follows in more detail.

In the case that hyperons are absent, the HMNS slightly contract simply due to the angular momentum loss (weakening centrifugal force) via GW emission. By contrast, in the case that hyperons are present, X_{Λ} increases with the contraction of the HMNS, resulting in the relative reduction of the pressure. As a result, the HMNS further contract. Recent studies showed that f_{GW} is associated with the frequency of f -mode which is approximately proportional to $\sqrt{M_{\text{H}}/R_{\text{H}}^3}$ where M_{H} and R_{H} are the mass and radius of the HMNS [16]. This indicates that f_{GW} should increase with time. To see that this is indeed the case, we show $f_{\text{GW}} (\equiv d\phi_{\text{NP}}/dt)$ calculated from a Weyl scalar $\Psi_4 \equiv \Psi e^{-i\phi_{\text{NP}}}$ in Fig. 2(b). It is clearly seen

that the mean value of f_{GW} in the HMNS phase is approximately constant for Shen-EOS models. By contrast, f_{GW} for H135 increases with time as the HMNS becomes compact.

4 Summary

We have reported effects of hyperons on the BNS merger in numerical-relativity simulations incorporating finite-temperature, both hyperonic and nucleonic EOS, microphysical processes, and neutrino cooling. We showed that for the adopted hyperonic EOS, a BH is not promptly formed and a HMNS is first formed for the typical total mass of BNS, as in the nucleonic Shen-EOS. The HMNS subsequently collapse to a BH and a massive torus is formed around the BH. The torus mass for the hyperonic EOS is smaller than that for the nucleonic EOS. We further showed that for the hyperonic EOS, the characteristic frequency of GWs, f_{GW} , from the HMNS increases by a factor of $\sim 20\text{--}30\%$ during their evolution via GW emission, by contrast with that for the nucleonic EOS in which f_{GW} is approximately constant. Our results open a possibility to constrain the composition of the NS matter via observation of GW from the HMNS.

Acknowledgments: Numerical simulations were performed on SR16000 at YITP of Kyoto University and on SX9 and XT4 at CfCA of NAOJ. This work was supported by Grant-in-Aid for Scientific Research (21018008, 21105511, 21340051, 22740178, 23740160), Grant-in-Aid on Innovative Area (20105004), and HPCI Strategic Program of Japanese MEXT.

References

- [1] F. Weber, Prog. Part. Nucl. Phys. **54**, 193 (2005). J. M. Lattimer and M. Prakash, Phys. Rep. **442**, 109 (2007); arXiv:1012.3208 (2010).
- [2] P. Demorest, et al., Nature **467**, 1081 (2010).
- [3] M. Alford et al., Astrophys. J. **629**, 969 (2005); J. R. Stone et al., Nucl. Phys. A **792**, 341 (2007); A. Kurkela, P. Romatschke, and A. Vuorinen, Phys. Rev. D **81**, 105021 (2010).
- [4] K. Nakazato, K. Sumiyoshi, and S. Yamada, Astrophys. J. **721**, 1284 (2010); I. Sagert et al., Phys. Rev. Lett. **102**, 081101 (2009); K. Sumiyoshi et al., Astrophys. J. Lett. **690**, L43 (2009).
- [5] K. Hotokezaka et al., Phys. Rev. D **83**, 124008 (2011). A. Bauswein and H.-T. Janka, arXiv:1106.1616 (2011).
- [6] C. Ishizuka et al., J. Phys. G **35**, 085201 (2008).
- [7] H. Noumi. et al. Phys. Rev. Lett. **89** 072301 (2002).
- [8] H. Shen et al., arXiv:1105.1666, (2011).
- [9] Y. Sekiguchi et al., Phys. Rev. Lett. **107**, 051102 (2011).
- [10] M. Shibata and T. Nakamura, Phys. Rev. D **52**, 5428 (1995); T. W. Baumgarte and S. L. Shapiro, Phys. Rev. D **59**, 024007 (1998); M. Campanelli, et al., Phys. Rev. Lett. **96**, 111101 (2006).
- [11] Y. Sekiguchi, Prog. Theor. Phys. **124**, 331 (2010); Class. Quant. Grav. **27**, 114107 (2010).
- [12] Y. Sekiguchi and M. Shibata, Astrophys. J. **737**, 6 (2011).
- [13] H. Shen, et al., Nucl. Phys. A **637**, 435 (1998).
- [14] T. Piran, Rev. Mod. Phys. **76**, 1143 (2005); E. Nakar, Phys. Rep. **442**, 166 (2007).
- [15] M. Ruffert, H.-Th. Janka, and G. Schäfer, Astron. Astrophys. **311**, 532 (1996); S. Rosswog and M. Liebendörfer, Mon. Not. R. Astron. Soc. **342**, 673 (2003).
- [16] N. Stergioulas, et al., arXiv:1105.0368 (2011).

Gravitational waves and neutrino emissions from the merger of binary neutron stars

Kenta Kiuchi,^(a) Yuichiro Sekiguchi,^(a) Koutarou Kyutoku,^(a) and Masaru Shibata,^(a)

^(a)*Yukawa Institute for Theoretical Physics, Kyoto University, Kyoto, 606-8502, Japan*

Abstract

Numerical simulations for the merger of binary neutron stars are performed in full general relativity incorporating both nucleonic and hyperonic finite-temperature equation of states and neutrino cooling for the first time. It is found that for the nucleonic and hyperonic equation of states, a hyper massive neutron star (HMNS) with a long lifetime ($\gtrsim 10$ ms) is the outcome for the total mass $2.7 M_{\odot}$. It is shown that the typical total neutrino luminosity of the HMNS is $\sim 3 \times 10^{53}$ erg/s and the effective amplitude of gravitational waves from the HMNS is $2 - 4 \times 10^{-22}$ at $f \approx 2.1$ kHz for a source of distance of 100 Mpc. We present the neutrino luminosity curve when a black hole is formed for the first time as well.

1 Introduction

Coalescence of binary neutron stars (BNS) are drawing attention of researchers in various fields because it is one of most promising source for next generation kilo-meter-size gravitational-wave (GW) detectors [1] and a possible candidate for the progenitor of short-hard gamma-ray bursts [2] as well as a high-end laboratory of the nuclear theory [3]. Motivated by these facts, numerical simulations have been extensively performed for the merger of BNS in the framework of full general relativity in the past decade since the first success in 2000 [4].

BNSs evolve due to gravitational radiation reaction and eventually merge. Before the merger sets in, each neutron star is cold, (i.e., thermal energy of constituent nucleons is much smaller than the Fermi energy), because thermal energy inside the neutron stars is significantly reduced by neutrino and photon coolings due to the long-term evolution (typically $\gtrsim 10^8$ yrs) until the merger. By contrast, after the merger, shocks are generated by hydrodynamic interactions, which heat a merged object, hyper massive neutron star (HMNS), up to $\sim 30 - 50$ MeV, and hence, copious neutrinos are emitted. So far, numerical relativity simulations in which both the nuclear theory based finite temperature equation of state (EOS) and neutrino cooling are properly taken into account have not been done yet. In addition, the properties of the neutron star matter are still poorly understood. In recent years, the influence of non-nucleonic degrees of freedom, such as hyperons, meson condensations, and quarks, on properties of the neutron star matter has been discussed extensively. Among exotic particles, Λ hyperon are believed to appear first in (cold) neutron star around the rest mass density of $\rho \sim 2 - 3 \rho_{\text{nuc}}$, where $\rho_{\text{nuc}} \approx 2.8 \times 10^{14} \text{g/cm}^3$ is the nuclear matter density. To explore the neutron star matter properties in BNS merger, we adopt Shen-EOS for the nucleonic EOS [5] and a finite-temperature EOS including contributions of Λ hyperons as the hyperonic EOS [6]. In this proceeding, we present the first results of numerical relativity simulation for the BNS merger performed incorporating both a finite-temperature EOS and neutrino cooling based on Sekiguchi et al. [7].

2 Framework

Numerical simulations in full general relativity are performed using the following formulation and numerical schemes: Einstein's equations are solved in the original version of Baumgarte-Shapiro-Shibata-Nakamura-puncture formulation; a fourth-order finite differencing in space and a fourth-order Runge-Kutta time integration are used; a conservative shock capturing scheme with third-order accuracy in space and fourth-order accuracy in time is employed for solving hydrodynamic equations. We solve evolution equations for neutrino (Y_{ν}), electron (Y_e), and total lepton (Y_l) fractions per baryon, taking into

account weak interaction processes and neutrino cooling employing a general relativistic leakage scheme for electron type (ν_e), electron anti-type ($\bar{\nu}_e$), and other types (μ/τ) of neutrinos (ν_x) [8] as well. We implement Shen-EOS, tabulated in terms of the rest-mass density (ρ), temperature (T), and Y_e or Y_l , as the nucleonic EOS and a finite-temperature EOS including contributions of Λ hyperons (Hyp-EOS) as the hyperonic EOS. These EOS produce a maximum mass of zero-temperature spherical NS of $\approx 2.2M_\odot$ for Shen-EOS and $\approx 1.8M_\odot$ for Hyp-EOS. Although Hyp-EOS cannot pass through the observational constraint of PSR J1614-2230 ($M_{J1614-2230} = 1.97 \pm 0.04M_\odot$), it deserves employing to explore the impact of hyperons on the BNS merger.

Numerical simulations are performed preparing a non-uniform grid as in [10]. The inner domain is composed of a finer uniform grid and the outer domain of a coarser nonuniform grid. The grid resolution in the inner zone is chosen to cover the major diameter of each neutron star in the inspiral orbit by 60 and 80 grid points for low- and high-resolution. Outer boundaries are located in a local wave zone at $\approx 560 - 600\text{km}$. As a monitor of the accuracy, we check the conservation of baryon rest-mass, total gravitational mass, and total angular momentum and find that they are preserved within the accuracy of 0.5%, 1%, and 3%, respectively, for the high-resolution runs.

Sekiguchi et al. [7] focuses on the merger of equal mass BNS with total mass ranging from $2.7M_\odot$ to $3.2M_\odot$. In this proceeding, we report the models with total mass $2.7M_\odot$. There are two possible fates of BNS: If its total mass M is greater than a critical mass M_c , a BH will be formed soon after the onset of the merger, while a differentially rotating HMNS will be formed for $M < M_c$. M_c for Shen-EOS (Hyp-EOS) is $2.8 - 2.9M_\odot$ ($2.3 - 2.4M_\odot$). Therefore, we expect that Shen-EOS model will form a HMNS and Hyp-EOS model will collapse to a BH.

2.1 Numerical results

Figure 1 plots the evolution of maximum rest-mass density, ρ_{max} , maximum temperature, T_{max} , and maximum mass fraction of hyperons, $X_{\Lambda, \text{max}}$ as functions of $t - t_{\text{merge}}$ where t_{merge} is an approximate onset time of the merger. Before the merger ($t < t_{\text{merge}}$), ρ_{max} and T_{max} for Hyp-EOS model agree well with those for the corresponding Shen-EOS model, because $X_{\Lambda, \text{max}}$ in this phase is small as $O(10^{-2})$ and effects of hyperons on dynamics are not significant. After the merger sets in ($t > t_{\text{merge}}$), on the other hand, $X_{\Lambda, \text{max}}$ increases to be $\gtrsim 0.1$ in accordance with the increase in ρ_{max} , and hyperons play a substantial role in the post-merger dynamics. Although the total mass, M , is larger than the maximum mass of the zero-temperature spherical NS for all the models, a HMNS is formed after the merger, supported by the centrifugal force and thermal contribution to the pressure [7, 9]. They subsequently contract by emission of GWs, which carry energy and angular momentum from the HMNS; ρ_{max} increases in the gravitational radiation timescale. For Hyp-EOS model, it collapses to a black hole (BH) at $t = t_{\text{BH}}$ where $t_{\text{BH}} - t_{\text{merge}} \approx 11.0$ ms. At $t - t_{\text{merge}} \sim 20$ ms for Shen-EOS model, the degree of its nonaxial symmetry becomes low enough that the emissivity of GWs is significantly reduced. Because no dissipation process except for the neutrino cooling is present, the HMNS will be alive at least for a cooling time, $t_{\text{cool}} \equiv E_{\text{th}}/L_\nu \sim 2-3$ s, where E_{th} is total thermal energy and L_ν is total neutrino luminosity [7].

Figure 3 plots neutrino luminosities as functions of time for three flavors (ν_e , $\bar{\nu}_e$, and sum of ν_x). It is found that electron anti neutrinos are dominantly emitted for any model. The reason for this is as follows: The HMNS has a high temperature, and hence, electron-positron pairs are efficiently produced from thermal photons, in particular in its envelope. Neutrons efficiently capture the positrons to emit anti neutrinos whereas electrons are not captured by protons as frequently as positrons because the proton fraction is much smaller than the neutron fraction. Such hierarchy in the neutrino luminosities was reported also in Ruffert et al. [11]. Soon after the BH formation, μ/τ neutrino luminosity steeply decreases because high temperature regions are swallowed into the BH, while luminosities of electron neutrinos and anti neutrinos decrease only gradually because these neutrinos are emitted via charged-current processes from the massive accretion torus. These features in neutrino luminosities are quantitatively the same for Hyp-EOS and Shen-EOS models, and hence, it would be difficult to extract information of the neutron star matter only from the neutrino signal.

The anti neutrino luminosity for the long-lived HMNS for Shen-EOS model is $L_{\bar{\nu}} \sim 2 \times 10^{53}\text{erg/s}$ with small time variability. It is greater than that from the protoneutron stars found after supernovae [12]. Averaged neutrino energy is $\epsilon_{\bar{\nu}} \sim 20 - 30$ MeV. The sensitivity of water-Cherenkov neutrino

detectors such as Super-Kaminokande and future Hyper-Kamiokande (HK) have a good sensitivity for such high-energy neutrinos in particular for electron anti neutrinos. The detection number for electron neutrinos is approximately estimated by $\sigma\Delta TL_{\bar{\nu}}/(4\pi D^2\epsilon_{\bar{\nu}})$ where σ is the total cross section of the detector against target neutrinos, ΔT is the lifetime of the HMNS, and D is the distance to the HMNS. For one-Mton detector such as HK, the expected detection number is $\gtrsim 10$ for $D \sim 5$ Mpc, neutrinos from the HMNS may be detected and its formation may be confirmed. Note that GWs from the HMNS will be simultaneously detected for such a close event, reinforcing the confirmation of the HMNS formation.

Figure 3(a) plots the plus and cross mode ($h_{+, \times}$) of GWs as a function of $t_{\text{ret}} - t_{\text{merge}}$ where t_{ret} is the retarded time $t_{\text{ret}} = t - D - 2M \log(D/M)$, extracted from the metric in the local wave zone. The waveforms are composed of the so-called chirp waveform, which is emitted when the BNS is in an inspiral motion (for $t_{\text{ret}} \lesssim t_{\text{merge}}$, and the merger waveform (for $t_{\text{ret}} \gtrsim t_{\text{merge}}$). The GW amplitude is $|h_{+, \times}| \lesssim 2 \times 10^{-22}$ for a source at a distance $D = 100$ Mpc. GWs from the inspiral phase (for $t_{\text{ret}} \lesssim t_{\text{merge}}$) agree well with each other for the models with Hyp-EOS and Shen-EOS. On the other hand, quasi-periodic GWs from the HMNS (for $t_{\text{ret}} \gtrsim t_{\text{merge}}$) show differences. First, the amplitude of quasi-periodic GWs damps steeply at the BH formation for Hyp-EOS model. This is because the HMNS collapses to a BH due to the softening of the EOS before relaxing to a stationary spheroid. Second, the characteristic GW frequency, f_{GW} , *increases* with time for Hyp-EOS model. These facts are clearly observed in the effective amplitude [see Fig. 3(b)] defined by $h_{\text{eff}} \equiv 0.4f|h(f)|$ where $h(f)$ is the Fourier transform of $h_+ - ih_{\times}$ and the factor 0.4 comes from taking average in terms of direction to the source and rotational axis of the HMNS. Reflecting a shorter lifetime of the HMNS in Hyp-EOS model, the peak amplitude of $h_{\text{eff}}(f)$ is smaller. Reflecting the shift of the characteristic frequency, the prominent peak in the GW spectrum for Hyp-EOS model is broadened. The effective amplitude $2 - 4 \times 10^{-22}$ for $D = 100$ Mpc suggests that for a specially-designed version of advanced GW detectors such as broadband LIGO, which has a good sensitivity for a high-frequency band, GWs from the HMNS oscillations may be detected with $S/N = 5$ if $D \lesssim 20$ Mpc or the source is located in an optimistic direction.

3 Summary

We have reported the first results of numerical-relativity simulation performed incorporating both a finite-temperature nucleonic EOS and hyperonic EOS as well as neutrino cooling effect. We showed that for both the nucleonic and hyperonic EOS, HMNS is the canonical outcome and BH is not promptly formed after the onset of the merger for the canonical value of the neutron star mass $1.35M_{\odot}$. For the nucleonic EOS, the lifetime of the formed HMNS is much longer than its dynamical timescale, $\gg 10\text{ms}$, and will be determined by the timescale of neutrino cooling. For the hyperonic EOS, the HMNS subsequently collapse to a BH. Neutrino luminosity of the HMNS was shown to be high as $\sim 3 \times 10^{53}\text{erg/s}$. The effective amplitude of GWs is $2 - 4 \times 10^{-22}$ at $f_{\text{peak}} \approx 2.1$ kHz for a source distance of 100 Mpc. If the BNS merger happens at a relatively short distance or is located in an optimistic direction, such GWs may be detected and HMNS formation will be confirmed.

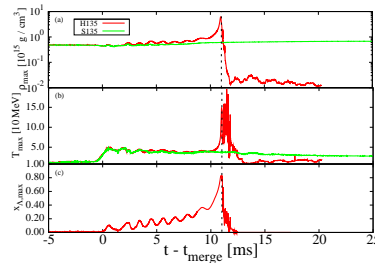


Figure 1: Maximum value of rest-mass density, after temperature, and mass fraction of hyperons as functions of time for H135 (red) and S135 (green). The vertical thin lines show the time at which a BH is formed.

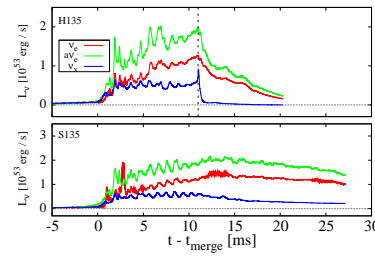


Figure 2: Neutrino luminosities for S135 and H135. The dashed vertical lines show the time at which a BH is formed.

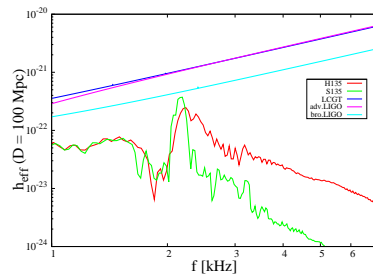


Figure 3: (a) GWs from the optimistic direction with the hypothetical distance to the source $D = 100$ Mpc. (b) The effective amplitude of GWs defined by $0.4f|h(f)|$ as a function of frequency for $D = 100$ Mpc. The noise amplitudes of a broadband configuration of Advanced Laser Interferometer Gravitational wave Observatories (bLIGO), and Large-scale Cryogenic Gravitational wave Telescope (LCGT) are shown together.

References

- [1] J. Abadie, et al., Nucl.Instrum.Methods Phys.Res.Sect., **A624**, 223 (2010); T. Accadia, et al., CQG, **28**, 025005 (2011); K. Kuroda, et al., CQG, **27**, 084004 (2010).
- [2] R. Narayan, B. Paczynski, T. Piran, Astrophys. J. **395**, L83-L86 (1992).
- [3] J. M. Lattimer and M. Prakash, Phys. Rept. **442**, 109 (2007)
- [4] M. Shibata and K. Uryu, Phys. Rev. D **61**, 064001 (2000)
- [5] H. Shen, H. Toki, K. Oyamatsu and K. Sumiyoshi, Prog. Theor. Phys. **100**, 1013 (1998), Nucl. Phys. A **637**, 435 (1998)
- [6] H. Shen, H. Toki, K. Oyamatsu and K. Sumiyoshi, arXiv:1105.1666 [astro-ph.HE].
- [7] Y. Sekiguchi, K. Kiuchi, K. Kyutoku and M. Shibata, Phys. Rev. Lett. **107**, 051102 (2011), Phys. Rev. Lett. **107**, 211101 (2011)
- [8] Y. Sekiguchi, Prog. Theor. Phys. **124**, 331 (2010)
- [9] K. Hotokezaka, K. Kyutoku, H. Okawa, M. Shibata and K. Kiuchi, Phys. Rev. D **83**, 124008 (2011)
- [10] K. Kiuchi, Y. Sekiguchi, M. Shibata and K. Taniguchi, Phys. Rev. D **80**, 064037 (2009)
- [11] M. Ruffert, H.-Th. Janka, and G. Schäfer, Astron. Astrophys. **311**, 532 (1996); M. Ruffert and H.-Th. Janka, *ibid* **380**, 544 (2001); S. Rosswog and M. Liebendörfer, Mon. Not. R. Astron. Soc. **342**, 673 (2003).
- [12] K. Sumiyoshi, S. Yamada, H. Suzuki, H. Shen, S. Chiba and H. Toki, Astrophys. J. **629**, 922 (2005)

Gravitational waves from cosmic string - domain wall networks

Takashi Hiramatsu,^{54(a)} Masahiro Kawasaki,^{55(b),(c)} Ken'ichi Saikawa^{56(b)} and Toyokazu Sekiguchi,^{57(d)}

^(a) *Yukawa Institute for Theoretical Physics, Kyoto University, Kitashirakawa Oiwake-cho, Sakyo-ku, Kyoto 606-8502, Japan*

^(b) *Institute for Cosmic Ray Research, The University of Tokyo, 5-1-5 Kashiwa-no-ha, Kashiwa City, Chiba 277-8582, Japan*

^(c) *Institute for Physics and Mathematics of the Universe, The University of Tokyo, 5-1-5 Kashiwa-no-ha, Kashiwa City, Chiba 277-8582, Japan*

^(d) *Department of Physics and Astrophysics, Nagoya University, Nagoya 464-8602, Japan*

Abstract

The networks of domain walls bounded by cosmic strings naturally arise in the theory of complex scalar field with a potential which has multiple degenerate minima. In particular, QCD axion models predict the formation of such string-wall networks in the early universe. Based on 3D lattice simulations, we investigate the radiation of axion particles and gravitational waves from these defect networks, and discuss its implications for axion cosmology.

1 Introduction

Topological defects are non-trivial field configurations which are formed if some symmetries are spontaneously broken in the early universe. These defects can be surface-like (domain walls) or vortex-like (cosmic strings), depending on the structure of symmetry groups (for review, see [1]). In this work, we consider a kind of hybrid defect which arises from some sequence of symmetry breaking. If a spontaneous breaking of some global U(1) symmetry is followed by a breaking of discrete symmetry, strings attached to domain walls will be formed. Such a series of symmetry breaking naturally occurs in some particle physics models, and we especially consider the model of axions.

Axion is a pseudo Nambu Goldstone boson which arises from the spontaneous breaking of the U(1) Peccei-Quinn (PQ) symmetry, introduced in order to solve the strong CP problem of the quantum chromodynamics (QCD) [2–5]. This U(1) symmetry is broken when the temperature of the universe becomes comparable to the axion decay constant F_a . Later, axion acquires a mass due to the non-perturbative effect in QCD, and discrete subgroup of U(1) is spontaneously broken. As a consequence, networks of domain walls bounded by strings are formed around the QCD era [6]. In some cases, these string-domain wall networks survive for a long time, and they can be another source of the stochastic background of gravitational waves [7].

2 Model of domain walls bounded by strings

We consider the model of a complex scalar field ϕ with the Lagrangian density given by

$$\mathcal{L} = \frac{1}{2} \partial_\mu \phi^* \partial^\mu \phi - V(\phi), \quad (2.1)$$

where the scalar potential is given by

$$V(\phi) = \frac{\lambda}{4} (\phi^* \phi - \eta^2)^2 + \frac{m^2 \eta^2}{N_{\text{DW}}^2} (1 - \cos N_{\text{DW}} \theta). \quad (2.2)$$

⁵⁴Email address: himatatz@yukawa.kyoto-u.ac.jp

⁵⁵Email address: kawasaki@icrr.u-tokyo.ac.jp

⁵⁶Email address: saikawa@icrr.u-tokyo.ac.jp

⁵⁷Email address: sekiguchi@a.phys.nagoya-u.ac.jp

Here, θ is the angular part of the scalar field (i.e. $\phi = |\phi|e^{i\theta}$). The first term in eq. (2.2) is usual mexican-hat potential, which causes spontaneous breaking of U(1) symmetry. In the early universe, U(1) symmetry is broken when the temperature of the universe falls below the energy scale $\sim \eta$. At this time, the scalar field gets a vacuum expectation value $|\langle\phi\rangle|^2 = \eta^2$, and cosmic strings are formed. The second term in eq. (2.2) may arise due to the non-perturbative effect of QCD. Because of the presence of this term, the U(1) symmetry is explicitly broken into its subgroup $Z_{N_{\text{DW}}}$. This term becomes non-negligible when the mass of the angular part of the scalar field m becomes greater than the friction term which comes from the cosmic expansion, $m \gtrsim H$, where H is the Hubble parameter. Then, the angular part of the scalar field begins to roll down to one of N_{DW} degenerate minima represented by

$$\theta = \frac{2\pi k}{N_{\text{DW}}}, \quad k = 0, 1, \dots, N_{\text{DW}} - 1. \quad (2.3)$$

At this stage, the discrete $Z_{N_{\text{DW}}}$ symmetry is spontaneously broken, and domain walls are formed, separating the N_{DW} vacua. These domain walls are attached to cosmic strings around their boundaries [1].

The value of N_{DW} depends on models, which we do not specify here. However, the evolution of the defect networks is different between the case with $N_{\text{DW}} = 1$ and others. If $N_{\text{DW}} = 1$, it can be shown that domain walls bounded by strings are unstable, and they disappear immediately after the formation [8]. On the other hand, if $N_{\text{DW}} > 1$, the string-wall networks are stable, and they eventually dominate the energy density of the universe. If it occurs after the era of big bang nucleosynthesis, it conflicts with standard cosmology [9].

In order to solve this problem, Sikivie [6] phenomenologically introduced a term

$$\delta V = -\Xi\eta^3(\phi e^{-i\delta} + \text{h.c.}) \quad (2.4)$$

in the potential (2.2), where Ξ is a dimensionless parameter which is assumed to be much less than unity. This term lifts degenerate vacua, breaking the discrete symmetry explicitly. If this kind of term exists in the potential, it affects as a pressure on walls, which eventually annihilate them. We can naively estimate the life time of the networks t_{dec} by the ratio between the surface energy density of domain walls σ and the difference of the potential energy between two neighboring vacua,

$$t_{\text{dec}} \sim \sigma / (\Xi\eta^4 / N_{\text{DW}}) \quad (2.5)$$

where $\sigma \simeq 9m\eta^2 / N_{\text{DW}}^2$ for axionic domain walls [10].

In our previous study [7], we found that string-wall networks actually disappears in the time scale given by eq. (2.5) and pointed out that it is possible to probe axion models with $N_{\text{DW}} > 1$ by observing gravitational waves produced by these defect networks. Also, the cosmological abundance of cold axions produced by string-wall networks gives another constraint on the model parameters. In this work, we are going to give a concrete analysis of gravitational waves and axion radiations from string-wall networks by numerically computing the spectrum of these radiations.

3 Spectrum of gravitational waves and radiated axions

In the numerical studies, we follow the evolution of two real scalar fields ϕ_1 and ϕ_2 which are defined by $\phi = \phi_1 + i\phi_2$. We solve the classical equations of motion derived from the Lagrangian density (2.1) on the 3-dimensional lattice with 512^3 points. Note that, this model has three parameters, λ , N_{DW} and m (η is fixed to be unity). In numerical simulations, we use the values $\lambda = 0.1$ and $m = 0.1$, and vary the value of N_{DW} .

To calculate the spectrum of gravitational waves, we use the formalism developed in [11]. Here, gravitational waves are described as spatial metric perturbations from the spatially flat Friedmann-Robertson-Walker background,

$$ds^2 = dt^2 - R^2(t)(\delta_{ij} + h_{ij})dx^i dx^j, \quad (3.1)$$

and they obey the linearized field equation

$$\ddot{h}_{ij} + 3H\dot{h}_{ij} - \frac{\nabla^2}{R^2}h_{ij} = \frac{16\pi G}{R^2}T_{ij}^{\text{TT}}, \quad (3.2)$$

where T_{ij}^{TT} is the transverse-traceless component of the stress-energy tensor. The solution of eq. (3.2) is formally given as a time integral of T_{ij}^{TT} convoluted with Green's functions [11]. Then the fraction of the energy density of gravitational waves is described by

$$\Omega_{\text{gw}}(k, t) \equiv \frac{d\rho_{\text{gw}}/d\ln k}{\rho_c(t)} = \frac{4}{3\pi V} \frac{G^2}{R^4 H^2} S_k(t), \quad (3.3)$$

where V is the volume of the simulation box, $\rho_c = 3H^2/8\pi G$ is the critical density of the universe, and $S_k(t)$ is some function of k and t which can be calculated by using the formal solutions of eq. (3.2).

Figure 1 (a) shows the result of the gravitational wave spectrum. The slope of the spectrum changes at two characteristic scales corresponding to the Hubble radius ($k/R \sim H$) and the width of the domain walls which is given by the mass of the axion ($k/R \sim m$). Also, there is nearly flat (but slightly red-tilted) spectrum extends between two relevant scales. These results are similar to the spectrum obtained in the context of simple model with real scalar field, investigated in [12].

We also compute the spectrum $P(t, k)$ of radiated axions which is defined by

$$\frac{1}{2} \langle \dot{a}(t, \mathbf{k})^* \dot{a}(t, \mathbf{k}') \rangle = \frac{(2\pi)^3}{k^2} \delta^{(3)}(\mathbf{k} - \mathbf{k}') P(t, k), \quad (3.4)$$

where $\langle \dots \rangle$ represents an ensemble average and $\dot{a}(t, \mathbf{k})$ is the Fourier component of the time derivative of the axion field, whose value is obtained from simulated data of ϕ . To give a precise estimation of $P(t, k)$, we excise the contaminations which come from the moving defects (strings and domain walls) by using the technology developed in [13].

Figure 1 (b) shows the result of the spectrum of radiated axions. The spectrum has a peak at comoving momentum $k \approx 3$, which roughly corresponds to the scale of the mass of the axion. Therefore, the radiated axions are mildly relativistic, and their contribution to the present abundance of the cold dark matter can be large [14].

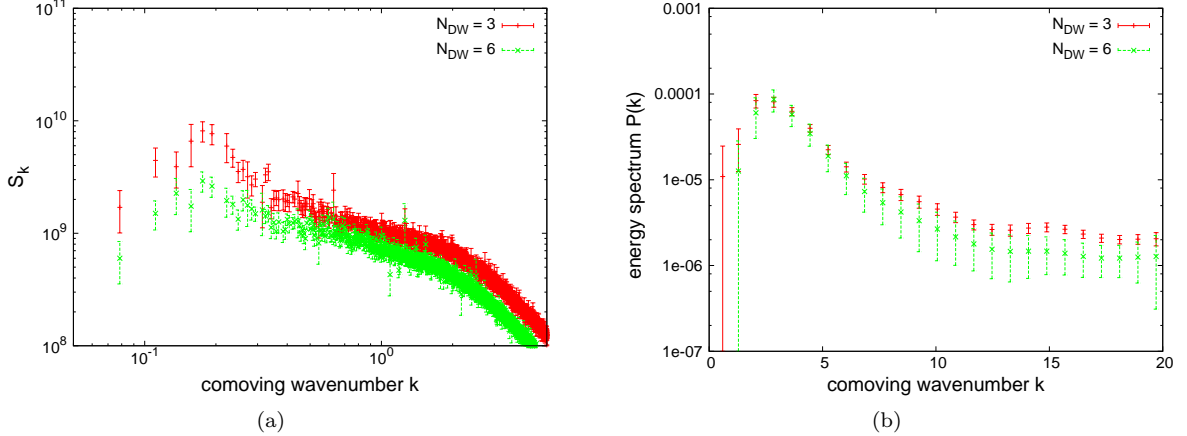


Figure 1: The spectra of (a) gravitational waves and (b) axions produced by string-wall networks, evaluated at the final time of numerical simulations with $N_{\text{DW}} = 3$ and 6.

4 Discussions

We investigated the cosmological scenario in which the networks of domain walls bounded by strings exist for a long time. Assuming that they disappear around the time given by eq. (2.5) without causing any cosmological disasters, we expect that significant amounts of gravitational waves and axions are produced from these defect networks before their annihilation. The present abundance of radiated axions can be estimated as

$$\Omega_a h^2 \simeq 6 \times \left(\frac{6}{N_{\text{DW}}} \right)^{3/2} \left(\frac{10^{-56}}{\Xi} \right)^{1/2} \left(\frac{10^{10} \text{GeV}}{F_a} \right)^{1/2}, \quad (4.1)$$

where h is the current value of the Hubble parameter in units of $100 \text{ km sec}^{-1} \text{ Mpc}^{-1}$ and $F_a \equiv \eta/N_{\text{DW}}$ is the axion decay constant. By requiring that it must not exceed the present abundance of cold dark matter $\Omega_{\text{CDM}} h^2 \simeq 0.11$, it is possible to constrain the model parameters such as F_a and Ξ . Also the present abundance of gravitational waves is estimated as

$$\Omega_{\text{gw}} h^2 \simeq 5 \times 10^{-15} \left(\frac{6}{N_{\text{DW}}} \right)^6 \left(\frac{10^{-56}}{\Xi} \right)^2 \left(\frac{10^{10} \text{ GeV}}{F_a} \right)^4. \quad (4.2)$$

From numerical studies, we found that the spectrum of gravitational waves extends between two relevant scales, the Hubble radius and the mass of axions. These scales correspond to the frequencies between $f \sim 10^{-10} \text{ Hz}$ and $f \sim 10 \text{ Hz}$, if we take $N_{\text{DW}} = 6$, $\Xi = 10^{-56}$ and $F_a = 10^{10} \text{ GeV}$. It might be possible to observe such a signal of gravitational waves in future space-borne interferometers with higher sensitivities, such as DECIGO [15]. Therefore, the observation of gravitational waves gives another constraint on the model parameters. More detailed analysis will be presented in future publications [16].

Numerical computation in this work was carried out at the Yukawa Institute Computer Facility. This work is supported by Grant-in-Aid for Scientific research from the Ministry of Education, Science, Sports, and Culture (MEXT), Japan, No.14102004 and No.21111006 (M. K.) and also by World Premier International Research Center Initiative (WPI Initiative), MEXT, Japan. K. S. and T. S. are supported by the Japan Society for the Promotion of Science (JSPS) through research fellowships. T. H. was supported by JSPS Grant-in-Aid for Young Scientists (B) No.23740186 and also by MEXT HPCI STRATEGIC PROGRAM.

References

- [1] A. Vilenkin and E. P. S. Shellard, *Cosmic strings and other topological defects* (Cambridge University Press, 1994).
- [2] R. D. Peccei and H. R. Quinn, *Phys. Rev. Lett.* **38**, 1440, (1977).
- [3] R. D. Peccei and H. R. Quinn, *Phys. Rev. D* **16**, 1791, (1977).
- [4] S. Weinberg, *Phys. Rev. Lett.* **40**, 223, (1978).
- [5] F. Wilczek, *Phys. Rev. Lett.* **40**, 279, (1978).
- [6] P. Sikivie, *Phys. Rev. Lett.* **48**, 1159, (1982).
- [7] T. Hiramatsu, M. Kawasaki and K. Saikawa, *JCAP* **08**, 030, (2011) [arXiv:1012.4558 [astro-ph.CO]].
- [8] S. M. Barr, K. Choi and J. E. Kim, *Nucl. Phys.* **B283**, 591, (1987).
- [9] Y. B. Zel'Dovich, I. Y. Kobzarev and L. B. Okun', *Sov. Phys. JETP* **40**, 1, (1974).
- [10] M. C. Huang and P. Sikivie, *Phys. Rev. D* **32**, 1560, (1985).
- [11] J. F. Dufaux, A. Bergman, G. N. Felder, L. Kofman and J. -P. Uzan, *Phys. Rev. D* **76**, 123517, (2007) [arXiv:0707.0875 [astro-ph]].
- [12] M. Kawasaki and K. Saikawa, *JCAP* **09**, 008, (2011) [arXiv:1102.5628 [astro-ph.CO]].
- [13] T. Hiramatsu, M. Kawasaki, T. Sekiguchi, M. Yamaguchi and J. Yokoyama, *Phys. Rev. D* **83**, 123531, (2011) [arXiv:1012.5502 [hep-ph]].
- [14] M. Nagasawa and M. Kawasaki, *Phys. Rev. D* **50**, 4821, (1994) [arXiv:astro-ph/9402066].
- [15] S. Kawamura et al., *Class. Quantum Grav.* **28**, 094011, (2011).
- [16] T. Hiramatsu, M. Kawasaki, K. Saikawa and T. Sekiguchi, in preparation.

Violation of the Rotational Invariance in the CMB Bispectrum

Maresuke Shiraishi^{58(a)} and Shuichiro Yokoyama^(a)

^(a)*Department of Physics and Astrophysics, Nagoya University, Nagoya 464-8602, Japan*

Abstract

We investigate a statistical anisotropy on the Cosmic Microwave Background (CMB) bispectrum, which can be generated from the primordial non-Gaussianity induced by quantum fluctuations of a vector field. We find new configurations in the multipole space of the CMB bispectrum given by $\ell_1 = \ell_2 + \ell_3 + 2$, $|\ell_2 - \ell_3| - 2$ and their permutations, which violate the rotational invariance, such as an off-diagonal configuration in the CMB power spectrum. We also find that in a model presented by Yokoyama and Soda (2008), the amplitude of the statistically anisotropic bispectrum in the above configurations becomes as large as that in other configurations such as $\ell_1 = \ell_2 + \ell_3$. As a result, it might be possible to detect these contributions in future experiments, which would give us novel information about the physics of the early Universe.

1 Introduction

The current cosmological observations, particularly Cosmic Microwave Background (CMB), tell us that the Universe is almost isotropic, and primordial density fluctuations are almost Gaussian random fields. However, in keeping with the progress of the experiments, there have been many works that verify the possibility of the small deviation of the statistical isotropy, e.g., the so-called ‘‘Axis of Evil’’. The analyses of the power spectrum by employing the current CMB data suggest that the deviation of the statistical isotropy is about 10% at most (e.g., Refs. [1]). Toward more precise measurements in future experiments, there are a lot of theoretical discussions about the effects of the statistical anisotropy on the CMB power spectrum, [2], e.g., the presence of the off-diagonal configuration of the multipoles in the CMB power spectrum, which vanishes in the isotropic spectrum.

As is well known, it might be difficult to explain such statistical anisotropy in the standard inflationary scenario. However, recently, there have been several works about the possibility of generating the statistically anisotropic primordial density fluctuations in order to introduce nontrivial dynamics of the vector field [3]. In Ref. [4], the authors considered a modified hybrid inflation model where a waterfall field couples not only with an inflaton field but also with a massless vector field. They have shown that, owing to the effect of fluctuations of the vector field, the primordial density fluctuations may have a small deviation from the statistical isotropy and also the deviation from the Gaussian statistics. If the primordial density fluctuations deviate from the Gaussian statistics, they produce the non-zero higher order spectra (corresponding to higher order correlation functions), e.g., the bispectrum (3-point function), the trispectrum (4-point function) and so on. Hence, in the model presented in Ref. [4], we can expect that there are characteristic signals not only in the CMB power spectrum but also in the CMB bispectrum.

With these motivations, in this work, we calculate the CMB statistically anisotropic bispectrum sourced from the curvature perturbations generated in the modified hybrid inflation scenario proposed in Ref. [4], on the basis of the useful formula presented in Ref. [5]. Then, we find the peculiar configurations of the multipoles which never appear in the isotropic bispectrum, like off-diagonal components in the CMB power spectrum. In this paper, in accordance with Ref. [6], we present these consequences.

2 Statistically anisotropic non-Gaussianity in curvature perturbations

In this section, we briefly review the mechanism of generating the statistically anisotropic bispectrum induced by primordial curvature perturbations proposed in Ref. [4], where the authors set the system

⁵⁸Email address: mare@nagoya-u.jp

like the hybrid inflation wherein there are two scalar fields: inflaton ϕ and waterfall field χ , and a vector field A_μ coupled with a waterfall field. The action is given by

$$S = \int dx^4 \sqrt{-g} \left[\frac{1}{2} R - \frac{1}{2} g^{\mu\nu} (\partial_\mu \phi \partial_\nu \phi + \partial_\mu \chi \partial_\nu \chi) - V(\phi, \chi, A_\nu) - \frac{1}{4} g^{\mu\nu} g^{\rho\sigma} f^2(\phi) F_{\mu\rho} F_{\nu\sigma} \right]. \quad (2.1)$$

Here, $F_{\mu\nu} \equiv \partial_\mu A_\nu - \partial_\nu A_\mu$ is the field strength of the vector field A_μ , $V(\phi, \chi, A_\mu)$ is the potential of fields and $f(\phi)$ denotes a gauge coupling. To guarantee the isotropy of the background Universe, we need the condition that the energy density of the vector field is negligible in the total energy of the Universe and we assume a small expectation value of the vector field. Therefore, we neglect the effect of the vector field on the background dynamics and also the evolution of the fluctuations of the inflaton. In the standard hybrid inflation (only with the inflaton and the waterfall field), the inflation suddenly ends owing to the tachyonic instability of the waterfall field, which is triggered when the inflaton reaches a critical value ϕ_e . In the system described using Eq. (2.1), however, ϕ_e may fluctuate owing to the fluctuation of the vector field and it generates additional curvature perturbations.

In this work, in order to calculate the CMB bispectrum explicitly, we focus on a case that the scale invariance is kept in the spectrum of the vector perturbations, which is realized for $f \propto a, a^{-2}$ with a being the scale factor. Furthermore, we adopt a simple model whose potential looks like an Abelian Higgs model in the unitary gauge as [4]

$$V(\phi, \chi, A^i) = \frac{\lambda}{4} (\chi^2 - v^2)^2 + \frac{1}{2} g^2 \phi^2 \chi^2 + \frac{1}{2} m^2 \phi^2 + \frac{1}{2} h^2 A^\mu A_\mu \chi^2, \quad (2.2)$$

where λ, g , and h are the coupling constants, m is the inflaton mass, and v is the vacuum expectation value of χ . Then, applying the δN formalism, the bispectrum of primordial curvature perturbations depending on \mathbf{A} is obtained as

$$\begin{aligned} \left\langle \prod_{n=1}^3 \zeta(\mathbf{k}_n) \right\rangle &= (2\pi)^3 F_\zeta(\mathbf{k}_1, \mathbf{k}_2, \mathbf{k}_3) \delta \left(\sum_{n=1}^3 \mathbf{k}_n \right), \\ F_\zeta(\mathbf{k}_1, \mathbf{k}_2, \mathbf{k}_3) &= C P_\zeta^{\text{iso}}(k_1) P_\zeta^{\text{iso}}(k_2) \hat{A}^a \hat{A}^b \delta^{cd} P_{ac}(\hat{\mathbf{k}}_1) P_{bd}(\hat{\mathbf{k}}_2) + 2 \text{ perms.}, \\ C &\equiv -g_\beta^2 \frac{\phi_e}{N_e} \left(\frac{g}{hA} \right)^2, \end{aligned} \quad (2.3)$$

where $N_e \equiv \partial N / \partial \phi_e$ with N being the e -folding number, $\phi_e^2 = (\lambda v^2 - h^2 A^2) / g^2$, $A \equiv |\mathbf{A}|$, $P_{ij}(\hat{\mathbf{k}}) \equiv \delta_{ij} - \hat{\mathbf{k}}_i \hat{\mathbf{k}}_j$, and $\hat{\cdot}$ denotes a unit vector. P_ζ^{iso} and g_β quantify the statistically isotropic and statistically anisotropic parts in the power spectrum of curvature perturbations given by

$$\left\langle \prod_{n=1}^2 \zeta(\mathbf{k}_n) \right\rangle = (2\pi)^3 P_\zeta^{\text{iso}}(k) \left[1 + g_\beta (\hat{\mathbf{A}} \cdot \hat{\mathbf{k}})^2 \right] \delta \left(\sum_{n=1}^2 \mathbf{k}_n \right). \quad (2.4)$$

These are expressed with respect to $\beta \equiv h^4 A^2 / (g^4 f_e^2 \phi_e^2)$, as $P_\zeta^{\text{iso}}(k) \approx P_\phi(k) (1 + \beta) / (2\epsilon)$ and $g_\beta \approx -\beta / (1 + \beta)$. Here, f_e, P_ϕ , and $\epsilon \equiv (\partial V / \partial \phi / V)^2 / 2$ denote f when the inflation ends, the power spectrum of inflatons, and a slow-roll parameter, respectively. Note that in the above expression, we have neglected the effect of the longitudinal polarization in the vector field for simplicity and the terms that are suppressed by a slow-roll parameter $\eta \equiv \partial^2 V / \partial \phi^2 / V$. Since the current CMB observations suggest $g_\beta < \mathcal{O}(0.1)$ (e.g., Refs. [1]) and $N_e^{-1} \simeq -\sqrt{2\epsilon}$, the overall amplitude of the bispectrum in this model, C , does not seem to be sufficiently large to be detected. However, even if $g_\beta \ll 1$ and $\epsilon \ll 1$, C can become greater than unity for $g^2 \phi_e / (hA)^2 \gg 1$. Thus, we expect meaningful signals also in the CMB bispectrum. Then, in the next section, we closely investigate the CMB bispectrum generated from the primordial bispectrum given by Eq. (2.3) and discuss a new characteristic feature of the CMB bispectrum induced by the statistical anisotropy of the primordial bispectrum.

3 Imprints on the CMB bispectrum and discussions

In this section, we show some results of the CMB bispectra generated from the primordial bispectrum, which has statistical anisotropy owing to the fluctuations of the vector field, given by Eq. (2.3). We also discuss the special signals of this CMB bispectrum, which vanish in the statistically isotropic bispectrum.

The CMB fluctuation can be expanded in terms of the spherical harmonic function as $\frac{\Delta X(\hat{\mathbf{n}})}{X} = \sum_{\ell m} a_{X,\ell m} Y_{\ell m}(\hat{\mathbf{n}})$, where $\hat{\mathbf{n}}$ is a unit vector pointing toward a line-of-sight direction, and X denotes the intensity ($\equiv I$) and polarizations ($\equiv E, B$). Then, the CMB bispectrum generated from the bispectrum of the primordial curvature perturbations can be expressed as [5]

$$\left\langle \prod_{n=1}^3 a_{X_n, \ell_n m_n} \right\rangle = \left[\prod_{n=1}^3 4\pi(-i)^{\ell_n} \int_0^\infty \frac{d^3 \mathbf{k}_n}{(2\pi)^3} \mathcal{T}_{X_n, \ell_n}(k_n) Y_{\ell_n m_n}^*(\hat{\mathbf{k}}_n) \right] (2\pi)^3 F_\zeta(\mathbf{k}_1, \mathbf{k}_2, \mathbf{k}_3) \delta\left(\sum_{n=1}^3 \mathbf{k}_n\right), \quad (3.1)$$

where $\mathcal{T}_{X,\ell}$ is the transfer function of the scalar mode [7]. By dealing with the complicated angular dependence, we can obtain an explicit form of this bispectrum [6]. That equation implies that, owing to the vector field \mathbf{A} , the CMB bispectrum has a direction dependence, and hence, the dependence on m_1, m_2, m_3 cannot be confined only to a Wigner-3j symbol, namely,

$$\left\langle \prod_{n=1}^3 a_{X_n, \ell_n m_n} \right\rangle \neq B_{X_1 X_2 X_3, \ell_1 \ell_2 \ell_3} \begin{pmatrix} \ell_1 & \ell_2 & \ell_3 \\ m_1 & m_2 & m_3 \end{pmatrix}. \quad (3.2)$$

This fact truly indicates the violation of the rotational invariance in the bispectrum of the primordial curvature perturbations and leads to the statistical anisotropy on the CMB bispectrum.

In the discussion of the CMB power spectrum, if the rotational invariance is violated in the primordial power spectrum as Eq. (2.4), the signals in the off-diagonal configurations of ℓ also have nonzero values [2]. Likewise, there are special configurations in the CMB bispectrum induced from the statistical anisotropy on the primordial bispectrum as Eq. (2.3). The selection rules of the Wigner symbols suggest that the CMB statistically anisotropic bispectrum in this case (3.1) could be nonzero in the multipole configurations given by

$$\ell_1 = |\ell_2 \pm \ell_3| \pm 2, \quad (3.3)$$

and two permutations of ℓ_1, ℓ_2, ℓ_3 . In contrast, in these configurations, the CMB isotropic bispectrum defined in Ref. [8] vanishes owing to the triangle condition of the Wigner-3j symbol $\begin{pmatrix} \ell_1 & \ell_2 & \ell_3 \\ m_1 & m_2 & m_3 \end{pmatrix}$ and the nonzero components arise only from

$$|\ell_2 - \ell_3| \leq \ell_1 \leq \ell_2 + \ell_3. \quad (3.4)$$

Therefore, the signals of the configurations (3.3) have the pure information of the statistical anisotropy on the CMB bispectrum.

Figure 1 shows the CMB anisotropic bispectra of the intensity mode given by Eq. (3.1) with $C = 1$ for the several configurations of ℓ 's and m 's as a function of ℓ_3 . The red solid line and green dashed line satisfy the special relation (3.3), namely, $\ell_1 = \ell_2 + \ell_3 + 2, |\ell_2 - \ell_3| - 2$, and the blue dotted line obeys a configuration of Eq. (3.4), namely, $\ell_1 = \ell_2 + \ell_3$. From this figure, we confirm that the signals in the special configuration (3.3) are comparable in magnitude to those for $\ell_1 = \ell_2 + \ell_3$. Therefore, if the rotational invariance is violated on the primordial bispectrum of curvature perturbations, the signals for $\ell_1 = |\ell_2 \pm \ell_3| \pm 2$ can also become beneficial observables. It might be possible to detect these contributions of the statistical anisotropy in future experiments, which would give us novel information about the physics of the early Universe. Of course, also for the E -mode polarization, we can give the same discussions and results.

Although we assume a specific potential of inflation to show the statistical anisotropy on the CMB bispectrum explicitly, the above calculation and discussion will be applicable to other inflation models where the rotational invariance violates ⁵⁹.

References

- [1] N. E. Groeneboom and H. K. Eriksen, *Astrophys. J.* **690** (2009), 1807 [arXiv:0807.2242 [astro-ph]].
N. E. Groeneboom, L. Ackerman, I. K. Wehus and H. K. Eriksen, *Astrophys. J.* **722** (2010), 452 [arXiv:0911.0150 [astro-ph.CO]].

⁵⁹After our paper [6], in Ref. [10], the statistically anisotropic CMB bispectra originated from other inflation models have also been analyzed.

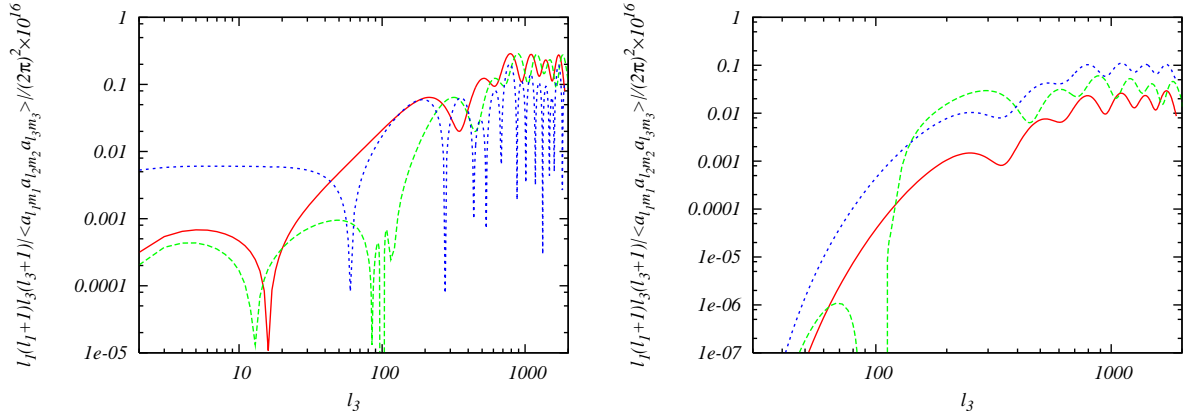


Figure 1: (color online) Absolute values of the CMB statistically anisotropic bispectra of the intensity mode given by Eq. (3.1) for $(m_1, m_2, m_3) = (0, 0, 0)$ (left figure) and $(10, 20, -30)$ (right one) as the function with respect to l_3 . The lines correspond to the spectra for $(\ell_1, \ell_2) = (102 + \ell_3, 100)$ (red solid line), $(|100 - \ell_3| - 2, 100)$ (green dashed line) and $(100 + \ell_3, 100)$ (blue dotted line). Here, we adopt $C = 1$ and fix the other parameters to the mean values limited from the WMAP-7yr data as reported in Ref. [9]

- [2] L. Ackerman, S. M. Carroll and M. B. Wise, *Phys. Rev. D* **75** (2007), 083502 [Erratum-ibid. *D* **80**, 069901 (2009)] [arXiv:astro-ph/0701357]. A. E. Gumrukcuoglu, B. Himmetoglu and M. Peloso, *Phys. Rev. D* **81**, 063528 (2010) [arXiv:1001.4088 [astro-ph.CO]]. M. A. Watanabe, S. Kanno and J. Soda, *Mon. Not. Roy. Astron. Soc.* **412** (2011), L83 [arXiv:1011.3604 [astro-ph.CO]].
- [3] K. Dimopoulos, *Phys. Rev. D* **74** (2006), 083502 [arXiv:hep-ph/0607229]. T. S. Koivisto and D. F. Mota, *JCAP* **0808** (2008), 021 [arXiv:0805.4229 [astro-ph]]. K. Dimopoulos, M. Karciauskas, D. H. Lyth and Y. Rodriguez, *JCAP* **0905** (2009), 013 [arXiv:0809.1055 [astro-ph]]. M. Karciauskas, K. Dimopoulos and D. H. Lyth, *Phys. Rev. D* **80** (2009), 023509 [arXiv:0812.0264 [astro-ph]]. N. Bartolo, E. Dimastrogiovanni, S. Matarrese and A. Riotto, *JCAP* **0910** (2009), 015 [arXiv:0906.4944 [astro-ph.CO]]. K. Dimopoulos, M. Karciauskas and J. M. Wagstaff, *Phys. Rev. D* **81**, 023522 (2010) [arXiv:0907.1838 [hep-ph]]. K. Dimopoulos, M. Karciauskas and J. M. Wagstaff, *Phys. Lett. B* **683** (2010), 298 [arXiv:0909.0475 [hep-ph]]. C. A. Valenzuela-Toledo and Y. Rodriguez, *Phys. Lett. B* **685** (2010), 120 [arXiv:0910.4208 [astro-ph.CO]]. C. A. Valenzuela-Toledo, arXiv:1004.5363 [astro-ph.CO]. E. Dimastrogiovanni, N. Bartolo, S. Matarrese and A. Riotto, *Adv. Astron.* **2010** (2010), 752670 [arXiv:1001.4049 [astro-ph.CO]]. K. Dimopoulos and J. M. Wagstaff, *Phys. Rev. D* **83**, 023523 (2011) [arXiv:1011.2517 [hep-ph]]. M. Karciauskas, arXiv:1104.3629 [astro-ph.CO].
- [4] S. Yokoyama and J. Soda, *JCAP* **0808** (2008), 005 [arXiv:0805.4265 [astro-ph]].
- [5] M. Shiraishi, D. Nitta, S. Yokoyama, K. Ichiki and K. Takahashi, *Prog. Theor. Phys.* **125** (2011), 795 [arXiv:1012.1079 [astro-ph.CO]].
- [6] M. Shiraishi and S. Yokoyama, *Prog. Theor. Phys.* **126**, 923 (2011) [arXiv:1107.0682 [astro-ph.CO]].
- [7] M. Zaldarriaga and U. Seljak, *Phys. Rev. D* **55** (1997), 1830 [arXiv:astro-ph/9609170]. M. Shiraishi, S. Yokoyama, D. Nitta, K. Ichiki and K. Takahashi, *Phys. Rev. D* **82** (2010), 103505 [arXiv:1003.2096 [astro-ph.CO]].
- [8] E. Komatsu and D. N. Spergel, *Phys. Rev. D* **63** (2001), 063002 [arXiv:astro-ph/0005036].
- [9] E. Komatsu *et al.* [WMAP Collaboration], *Astrophys. J. Suppl.* **192** (2011), 18 [arXiv:1001.4538 [astro-ph.CO]].
- [10] N. Bartolo, E. Dimastrogiovanni, M. Liguori, S. Matarrese and A. Riotto, arXiv:1107.4304 [astro-ph.CO].

Weak lensing of cosmic microwave background from a cosmic (super-)string network

Daisuke Yamauchi^{60(a)}, Keitaro Takahashi^{61(b)}, Yuuiti Sendouda^{62(c)}, Chul-Moon Yoo^{63(d)},

^(a)*Institute for Cosmic Ray Research, The University of Tokyo, Kashiwa 277-8582, Japan*

^(b)*Faculty of Science, Kumamoto University, 2-39-1, Kurokami, Kumamoto 860-8555, Japan*

^(c)*Graduate School of Science and Technology, Hirosaki University, Hirosaki, Aomori 036-8561, Japan*

^(d)*Yukawa Institute for Theoretical Physics, Kyoto University, Kyoto 606-8502, Japan*

Abstract

We present calculations of cosmic (super-)strings contribution to cosmic microwave background anisotropy and polarization spectrum due to gravitational weak lensing. We clarify the dependence of the CMB polarization due to weak lensing on the intercommuting probability explicitly. As the intercommuting probability decreases, the spectra of the convergence, the lensed temperature, and polarization increase because the number density of string segment becomes larger. An important feature for observing CMB polarizations is that the small scale lensed spectra due to cosmic (super-)string network could decay slowly, compared with primordial scalar perturbations.

1 Introduction and Summary

It is naturally expected that topological defects, appearing as solutions to the field equation in various models of particle physics, have formed during phase transitions in the early universe through spontaneous symmetry breakings. Recently cosmic strings have attracted a renewed interest in the context of string cosmology since it was pointed out that a new type of cosmic strings, so-called cosmic superstrings, may be formed at the end of stringy inflation (see e.g. [1]). One of observationally important features of cosmic superstrings compared to field-theoretic ones arises from the fact that, The intercommuting probability for field-theoretic strings, P , has been shown to be almost always unity, while the value of P can be significantly smaller for cosmic superstrings (see e.g. [2]).

The CMB polarizations, especially the B-mode could be a useful probe of cosmic strings through the future observations such as PLANCK, CMBPol, ACTPol, SPTPol, and LiteBIRD. In this paper, we investigate gravitational weak lensing due to cosmic (super-)strings as yet another source of the B and other modes. The BB polarizations are induced by lensing as the partial conversion of the primary EE polarizations. First we calculate the spectrum of the convergence field due to strings. Then we obtain the temperature and polarization spectra of the CMB, clarifying how they can vary according to the value of the intercommuting probability P . We find that the contributions from segments located at low redshifts are dominant and low multipole modes of lensing are essential even at high ℓ in CMB. The amplitude of the spectra increases as P decreases, because the smaller the probability P is, the larger the amplitude of the power spectrum of the induced scalar lensing potential is. An interesting feature observed in the small scale limit is that the string-lensed spectra decay more slowly than that of the primordial scalar perturbations. The characteristic power-law behavior will help us distinguish cosmic (super-)strings from other secondary effects. Even if the strings have only small tension, the string weak lensing could serve as the dominant source for the BB polarization on sufficiently small scales.

⁶⁰Email address: yamauchi@icrr.u-tokyo.ac.jp

⁶¹Email address: keitaro@sci.kumamoto-u.ac.jp

⁶²Email address: sendouda at cc.hirosaki-u.ac.jp

⁶³Email address: yoo@yukawa.kyoto-u.ac.jp

2 Convergence field due to a string network

We assume that strings can be well approximated as Nambu-Goto strings and the gravitational field of strings is sufficiently weak that we can solve the linearized Einstein equations. The convergence κ can be described by the stress-energy tensor $T_{\mu\nu}$ as

$$\kappa = 4\pi G \int_0^{\chi_S} d\chi \frac{(\chi_S - \chi)\chi}{\chi_S} T_{\mu\nu} \bar{K}^\mu \bar{K}^\nu \Big|_{\eta=\eta_0-\chi}, \quad (2.1)$$

where χ_S, η_0 denote the comoving distance from a lens object to last scattering surface and the conformal time at present, we have introduced $\bar{K}^\mu = (1, \hat{\mathbf{n}})$, and $\hat{\mathbf{n}}$ denotes the line-of-sight. To see the contribution due to string segments, we should evaluate the stress-energy tensor of a string. In this gauge, the stress-energy tensor in the transverse gauge can be described as

$$T^{\mu\nu}(\mathbf{r}, \eta_0 - \chi) = \mu \int d\sigma \begin{pmatrix} 1 & \dot{r}_L^k \\ \dot{r}_L^l & \dot{r}_L^k \dot{r}_L^l - r_L^{k'} r_L^{l'} \end{pmatrix} \delta^3(\mathbf{r} - \mathbf{r}_L(\sigma, \eta_c(\sigma))), \quad (2.2)$$

where we have introduced the three-dimensional coordinate with the origin O as \mathbf{r} , and the embedding function of the string position along the line-of-sight as $\mathbf{r}_L = \mathbf{r}_L(\sigma, \eta_c(\sigma))$. we introduce $\eta_c(\sigma)$ as the conformal time along the intersection of the observer's past light-cone and the string worldsheet, $\eta_c(\sigma) = \eta_0 - |\mathbf{r}_L(\sigma, \eta_c(\sigma))|$ [6].

In this paper, we use the formalism proposed in [6, 7] for the angular power spectrum due to cosmic (super-)strings. Since the observed sky map of the convergence due to string segments can appear as a superposition of those due to each segment, the total contributions of the convergence can be decomposed into each contribution of each string segment. In our treatment, we first introduce a segment index “ (i) ” to denote the contribution from each segment between the last scattering surface and the present. For simplicity, we also assume that the i -th lens object is localized at $\chi = \chi_L^{(i)}$, namely thin-lens approximation. Under this assumption, the distance between the observer and the i -th lens object can be approximated as $|\mathbf{r}_L^{(i)}(\sigma, \eta_c(\sigma))| \approx \chi_L^{(i)}$. Hence, the stress-energy of the string network along the ray, $\mathbf{r} = \chi \hat{\mathbf{n}}$, can be well approximated as

$$T_{\mu\nu}(\chi \hat{\mathbf{n}}, \eta_0 - \chi) \bar{K}^\mu \bar{K}^\nu \approx \sum_{(i) \in \text{segments}} \frac{1}{\chi_L^{(i)}} \Sigma^{(i)}(\hat{\mathbf{n}}) \delta(\chi - \chi_L^{(i)}), \quad (2.3)$$

where $\Sigma^{(i)}(\hat{\mathbf{n}})$ denotes surface energy density for the i -th segment [7]:

$$\Sigma^{(i)}(\hat{\mathbf{n}}) \approx \mu \int ds \delta(\hat{\mathbf{n}} - \hat{\mathbf{n}}_L^{(i)}(s)), \quad (2.4)$$

where we have introduced the angular position of the i -th segment along the ray as $\hat{\mathbf{n}}_L^{(i)}(s) \equiv \mathbf{r}_L^{(i)}(\chi_L^{(i)} s, \eta_0 - \chi_L^{(i)}) / \chi_L^{(i)}$, the worldsheet angular coordinate as $s = \sigma / \chi_L^{(i)}$. Substituting Eq. (2.3) into Eq. (2.1), the spherical coefficient of the convergence field is given by

$$\kappa_{\ell m} \approx \sum_{(i)} 4\pi G \mu \frac{\chi_S - \chi_L^{(i)}}{\chi_S} \int ds Y_{\ell m}^*(\hat{\mathbf{n}}_L^{(i)}) \equiv \sum_{(i)} \kappa_{\ell m}^{(i)}, \quad (2.5)$$

then the angular power spectrum of the convergence can be written as

$$C_\ell^{\kappa\kappa} = \frac{1}{2\ell + 1} \sum_m \left[\left\langle \sum_{(i)} |\kappa_{\ell m}^{(i)}|^2 \right\rangle + \left\langle \sum_{(i) \neq (j)} \kappa_{\ell m}^{(i)} \kappa_{\ell m}^{(j)*} \right\rangle \right], \quad (2.6)$$

Now the string segments are assumed to be distributed randomly between the last scattering surface and the present consistently with the string network model. This implies that there is no correlation between two different segments, $\langle \kappa_{\ell m}^{(i)} \kappa_{\ell m}^{(j)*} \rangle = 0$ for $(i) \neq (j)$. Then, the 1-segment contribution dominates the angular power spectrum and the power spectrum of the convergence can reduce to [7]

$$C_\ell^{\kappa\kappa} \approx \int_{z_{\min}}^{z_{\text{LSS}}} dz \frac{dV}{dz} \int d\Theta_L \cdot \frac{dn}{d\Theta_L} \mathcal{G}_\ell^{\kappa\kappa}(\Theta_L, z), \quad (2.7)$$

where $(dV/dz)dz$ is the differential comoving volume element at redshift z , $(dn/d\Theta_L) \cdot d\Theta_L$ is the comoving number density of string segments with the parameters in the range $[\Theta_L, \Theta_L + d\Theta_L]$. And $\mathcal{G}_\ell^{\kappa\kappa}$ is given by

$$\mathcal{G}_\ell^{\kappa\kappa}(z) \approx 2\pi \left(G\mu \frac{\chi_S - \chi_L^{(i)}}{\chi_S} \right)^2 \frac{2}{(1 - v_{\text{rms}}^2) \ell_{\text{co}}(z) \ell} \int_{-2\ell/\ell_{\text{co}}(z)}^{2\ell/\ell_{\text{co}}(z)} du P_\ell(\cos(u/\ell)). \quad (2.8)$$

where ℓ_{co} is the angular scale which corresponds to the correlation length of the string network [6]. This characteristic scale can be obtained by solving the velocity-dependent one-scale model with the intercommuting probability P [5, 6].

In order to investigate the dependence on the intercommuting probability P , the total angular power spectra of the convergence, $C_\ell^{\kappa\kappa}$, with various values of P are shown in Fig. 1. The typical amplitudes of the lensing power spectrum at $\ell = 10$ for are $C_{\ell=10}^{\kappa\kappa} \approx 6.0 \times 10^2 (G\mu)^2$ for $P = 1$, $4.6 \times 10^3 (G\mu)^2$ for $P = 10^{-1}$, $8.7 \times 10^4 (G\mu)^2$ for $P = 10^{-3}$, and $3.0 \times 10^6 (G\mu)^2$ for $P = 10^{-6}$. The spectrum for large ℓ behaves as ℓ^{-1} . The spectrum has a larger amplitude and a broader shape as P decreases. These properties can be understood by considering that the number density of string segments is larger and the correlation length for a string network is shorter for smaller P .

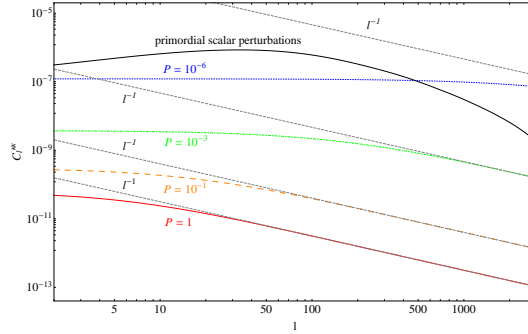


Figure 1: The all-sky total angular power spectrum $C_\ell^{\kappa\kappa}$ with $G\mu = 2 \times 10^{-7}$. The curves are, from bottom to top, for $P = 1, 10^{-1}, 10^{-3},$ and 10^{-6} . The gray dotted lines show the asymptotic behavior $\propto \ell^{-1}$ for large ℓ . For comparison, the power spectrum of the convergence due to primordial scalar perturbations is shown in black solid curve.

3 Lensed power spectra from cosmic (super-)strings

Lensing involves deflections that remap the temperature and polarization fields. The lensing effect is conventionally expressed as the change of the direction vector by an angular gradient of the scalar lensing potential ϕ and the a rotation of the pseudo-scalar lensing potential ϖ [8]:

$$\hat{\mathbf{n}} \rightarrow \hat{\mathbf{n}} + \nabla_{\hat{\mathbf{n}}} \phi(\hat{\mathbf{n}}) + (*\nabla_{\hat{\mathbf{n}}}) \varpi, \quad (3.1)$$

where $\nabla_{\hat{\mathbf{n}}}$ represents the angular derivative, i.e., the covariant derivative on the sphere, $*$ is the ninety-degree rotation operator. We will simply assume the pseudo-scalar lensing potential is negligible, and the lensing potential is given by

$$\kappa(\hat{\mathbf{n}}) = \frac{1}{2} \nabla_{\hat{\mathbf{n}}}^2 \phi(\hat{\mathbf{n}}). \quad (3.2)$$

Once the convergence field due to the cosmic (super-)string network is given, we can calculate the lensing potential through Eq. (3.2) and the angular power spectrum of the CMB temperature anisotropy and polarizations by using the formula developed in [4]. Figure 2 show the BB angular power spectra induced by the gravitational lensing due to cosmic (super-)strings. For the string components, the normalization

of the spectra is related to the string tension as $C_\ell^{\text{BB}} \propto (G\mu)^2$, and we took $G\mu = 2 \times 10^{-7}$ for all the plots. In this figure one can see that the amplitude of the spectra increases as P decreases. This is because the smaller the probability P is, the larger the amplitude of the power spectrum of the induced scalar lensing potential is. For comparison, contributions from the inflationary density perturbations are also shown. The cosmological parameters are chosen to match the current CMB data. For BB, in the large scale limit the differences between the lensed and unlensed spectrum can be well approximated by white spectrum, namely $\tilde{C}_\ell^{\text{BB}} - C_\ell^{\text{BB}} = \text{constant}$. On the other hand, an interesting feature observed in the small scale limit is that the string-lensed BB spectra decay more slowly than that of the primordial scalar perturbations. Actually, the spectra are approximately in proportion to the angular power spectrum of the convergence, $\ell^2(\tilde{C}_\ell^{\text{BB}} - C_\ell^{\text{BB}}) \propto C_\ell^{\kappa\kappa}$ [3], and therefore we have that $\ell^2(\tilde{C}_\ell^{\text{BB}} - C_\ell^{\text{BB}}) \propto \ell^{-1}$ (see Fig. 1). This characteristic power-law behavior will help us distinguish cosmic (super-)strings from other secondary effects. Even if the strings have only small tension, the string weak lensing could serve as the dominant source for the BB polarization on sufficiently small scales.

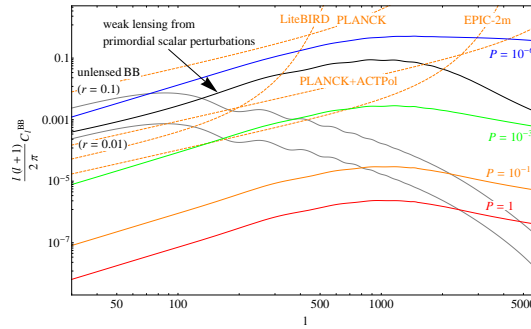


Figure 2: The BB polarization angular power spectrum in the units of μK^2 . The curves are, from bottom to top, the difference between the lensed and unlensed spectra for $P = 1$ (red), 10^{-1} (orange), 10^{-3} (green), and 10^{-6} (blue), with $G\mu = 2 \times 10^{-7}$. The spectrum due to the primordial density perturbations is shown as the black curve for comparison. The unlensed primordial spectra due to inflationary tensor perturbation with $r = 0.1$ (not lensed by density perturbations) is shown in gray solid line. For comparison, the spectrum with $r = 0.01$ is also shown in gray solid line. The dotted lines in orange are the sensitivity curve of PLANCK, EPIC-2m, combined PLANCK+SPTPol, and LiteBIRD.

References

- [1] S. Sarangi and S. -H. H. Tye, Phys. Lett. B **536**, 185 (2002) [arXiv:hep-th/0204074].
- [2] E. J. Copeland, R. C. Myers and J. Polchinski, JHEP **0406**, 013 (2004) [arXiv:hep-th/0312067].
- [3] A. Lewis and A. Challinor, Phys. Rept. **429**, 1 (2006) [arXiv:astro-ph/0601594].
- [4] W. Hu, Phys. Rev. D **62**, 043007 (2000) [arXiv:astro-ph/0001303].
- [5] K. Takahashi, A. Naruko, Y. Sendouda, D. Yamauchi, C. -M. Yoo, M. Sasaki, JCAP **0910**, 003 (2009). [arXiv:0811.4698 [astro-ph]], D. Yamauchi, Y. Sendouda, C. -M. Yoo, K. Takahashi, A. Naruko, M. Sasaki, JCAP **1005**, 033 (2010). [arXiv:1004.0600 [astro-ph.CO]].
- [6] D. Yamauchi, K. Takahashi, Y. Sendouda, C. M. Yoo and M. Sasaki, Phys. Rev. D **82**, 063518 (2010) [arXiv:1006.0687 [astro-ph.CO]].
- [7] D. Yamauchi, K. Takahashi, Y. Sendouda, C. -M. Yoo, [arXiv:1110.0556 [astro-ph.CO]].
- [8] T. Namikawa, D. Yamauchi, A. Taruya, [arXiv:1110.1718 [astro-ph.CO]].

Generation of the primordial magnetic fields from the non-adiabatic fluctuations at the pre-recombination era

Satoshi Maeda^{64(a)}

^(a)*Department of Physics, Kyoto University, Kyoto 606-8502, Japan.*

Abstract

In the pre-recombination era, cosmological density fluctuations can naturally generate magnetic fields through Thomson scatterings. In previous studies, only the magnetic field generation from the initially-adiabatic fluctuations has been considered. Here we investigate the generation of cosmological magnetic fields sourced by the primordial non-adiabatic fluctuations based on the cosmological perturbation theory, using the tight-coupling approximations between photon and baryon fluids. We will show that the magnetic fields are generated from the non-adiabatic density perturbation at the pre-recombination era and evaluate the power spectrum of generated magnetic fields in the case of the non-adiabatic perturbation with the blue power spectrum. Finally we obtain that the amplitude of the generated magnetic fields is about 10^{-20} Gauss on 1Mpc. This amplitude can be amplified up to the magnetic fields in galaxies.

1 Introduction

The magnetic fields in galaxies and in clusters of galaxies are observed and the typical strength is about $1\mu\text{Gauss}$. The origin of these fields is not clear yet [1]. This is one of the significant problem in the modern cosmology. It has been considered that very weak large-scale magnetic fields generated in the early universe are amplified by the dynamo mechanism after galaxy formation [2].

Many mechanisms generating primordial magnetic fields are proposed, such as the generation from the second-order density perturbation at the pre-recombination era [3–6]. In this era, protons and electrons move interacting with photons by the Thomson scattering. As the mass of electrons is much smaller than one of protons, the cross section of the Thomson scattering for electrons is larger and it causes the magnetic fields.

The primordial fluctuations are generated in the very early universe, for example, at the time of inflation. They evolve into anisotropies of the cosmic microwave background (CMB) and act as the seed of the large-scale structure. In a simplest single-field inflation model, only adiabatic fluctuations are produced. However in other models such as a multi-field inflation model inspired by the string theory, non-adiabatic fluctuations are also produced. Actually, adiabatic fluctuations are known as the main component of the fluctuations from the CMB observations. However, the non-adiabatic fluctuations can still exist as a sub-dominant component. For example, in ref. [7], it is indicated that the power spectrum of non-adiabatic fluctuations may have a very blue spectrum.

In previous studies, initially-adiabatic fluctuations are considered for the generation of magnetic fields. In this case, however, it has been shown that the fields can not be generated at the first order of the tight coupling approximation (TCA) for the Thomson scattering [4, 5].

We will show that the magnetic fields can be generated at the first-order expansion of the TCA if the primordial non-adiabatic fluctuations of baryons exist [8],

$$C(\vec{x}) := \frac{\delta\bar{n}^{(1)}}{\bar{n}^{(0)}} - \frac{3}{4} \frac{\delta\bar{\rho}_\gamma^{(1)}}{\bar{\rho}_\gamma^{(0)}}. \quad (1.1)$$

Then there is a possibility that the strength of the primordial magnetic fields is stronger than that of the fields only from adiabatic fluctuations if the non-adiabatic fluctuations have a blue spectrum. Therefore it is important to examine the magnetic fields generated by the non-adiabatic fluctuations.

⁶⁴Email address: smaeda@tap.scphys.kyoto-u.ac.jp

2 Generation of the magnetic fields from the non-adiabatic fluctuations

The EoMs for each species (γ, p, e) are

$$\nabla_\nu T_{(\gamma)i}{}^\nu = \kappa_i^{\gamma p} + \kappa_i^{\gamma e}, \quad (2.1)$$

$$\nabla_\nu T_{(p)i}{}^\nu = en_p E_i + \kappa_i^{pe} + \kappa_i^{p\gamma}, \quad (2.2)$$

$$\nabla_\nu T_{(e)i}{}^\nu = -en_e E_i + \kappa_i^{ep} + \kappa_i^{e\gamma}, \quad (2.3)$$

where κ_i^{ab} in the right-hand side are collision terms. κ_i^{ab} for the Thomson scattering between photons and charged particles are

$$\kappa_i^{\gamma e} = -\kappa_i^{e\gamma} = -\frac{4}{3}\sigma_T n_e \rho_\gamma \left[(u_{(\gamma)i} - u_{(e)i}) - \frac{1}{4}u_{(e)j} \Pi_{\gamma i}^j \right], \quad (2.4)$$

$$\kappa_i^{\gamma p} = -\kappa_i^{p\gamma} = -\frac{m_e^2}{m_p^2} \frac{4}{3}\sigma_T n_p \rho_\gamma \left[(u_{(\gamma)i} - u_{(p)i}) - \frac{1}{4}u_{(p)j} \Pi_{\gamma i}^j \right], \quad (2.5)$$

where Π_γ is anisotropic stress of photons. κ_i^{ab} for the Coulomb scattering between charged particles are

$$\kappa_i^{pe} = -\kappa_i^{ep} = -e^2 n_p n_e \eta_C (u_{(p)i} - u_{(e)i}). \quad (2.6)$$

The metric in the Poisson gauge is given by the flat-Friedmann spacetime:

$$ds^2 = a^2(\eta) \left[-(1 + 2\phi) d\eta^2 + 2\chi_i d\eta dx^i + (1 - 2\mathcal{R}) \delta_{ij} dx^i dx^j \right], \quad (2.7)$$

where $d\eta = dt/a$ is the conformal time.

Subtracting EoMs for proton and electron, we obtain “the Ohm’s law”,

$$E_i = \frac{1 - \beta^3}{1 + \beta} \frac{4\sigma_T}{3e} a \rho_\gamma (1 - 2\mathcal{R}) \left[\delta v_{(\gamma b)i} - \frac{1}{4}v_{(b)j} \Pi_{\gamma i}^j \right] := \frac{1 - \beta^3}{1 + \beta} \frac{4\sigma_T}{3e} a \rho_\gamma (1 - 2\mathcal{R}) \Delta v_{(\gamma b)i}, \quad (2.8)$$

where we use $\delta v_{b\gamma} \gg \delta v_{pe} \rightarrow 0$.

Substituting eq. (2.8) into the induction equation of the magnetic fields, we obtain

$$(a^3 B^i)' = -\frac{1 - \beta^3}{1 + \beta} \frac{4\sigma_T}{3e} \epsilon^{ijk} a^2 \left[\partial_j (\rho_\gamma \Delta v_{(\gamma b)k}) + \rho_\gamma \partial_j (\phi - 2\mathcal{R}) \Delta v_{(\gamma b)k} + \frac{1}{a^2} (\rho_\gamma v_j a^2 \Delta v_{(\gamma b)k})' \right] \quad (2.9)$$

It shows that the velocity difference between photons and baryons and anisotropic stress of photon generate the magnetic field.

We use the tight coupling approximation (TCA) for the Thomson scattering so as to represent $\Delta v_{(\gamma b)i}$ by the well-known perturbative quantities. When the dynamical timescale is longer than the timescale of the Thomson scattering, we can expand the physical quantities under the TCA. At zeroth order in the TCA, all fluid components move together with the same velocity v_i . We set the photon frame as the “background” in the TCA. In other words, physical quantity for zeroth-order TCA is the same as that of photon. The quantity $\Delta v_{(\gamma b)i}$ in eq. (2.9) is expressed

$$\Delta v_{(\gamma b)i} = \Delta v_{(\gamma b)i}^{(I)} + \Delta v_{(\gamma b)i}^{(II)} + \dots \quad (2.10)$$

The equation which determines the velocity difference between baryon and photon is provided from the subtraction of the EoM for photon from baryon

$$\begin{aligned} & \frac{\rho'_\gamma}{\rho_\gamma} (v_{(\gamma)i} + \chi_i) - \frac{n'}{n} (v_{(b)i} + \chi_i) + (\delta v_{(\gamma b)i})' + 4\mathcal{H} \delta v_{(\gamma b)i} \\ & - (\phi + 2\mathcal{R}) \left[\frac{\rho'_\gamma}{\rho_\gamma} v_{(\gamma)i} - \frac{n'}{n} v_{(b)i} + (\delta v_{(\gamma b)i})' + 4\mathcal{H} \delta v_{(\gamma b)i} \right] \\ & - 5\mathcal{R}' \delta v_{(\gamma b)i} + \frac{1}{4} \frac{\partial_i \rho_\gamma}{\rho_\gamma} + \partial_j (v_{(\gamma)i} v_{(\gamma)}^j) - \frac{1}{1 + \beta} \partial_j (v_{(p)i} v_{(p)}^j + \beta v_{(e)i} v_{(e)}^j) \\ & = -\alpha(1 - 2\mathcal{R}) \Delta v_{(\gamma b)i}, \end{aligned} \quad (2.11)$$

where α is defined as

$$\alpha := \frac{1 + \beta^2}{1 + \beta} (1 + R) \frac{4a\sigma_T \rho_\gamma}{3m_p}, \quad (2.12)$$

with $R := (3m_p(1 + \beta)n)/(4\rho_\gamma)$.

Using the TCA, we solve eq. (2.11) for $\Delta v_{(\gamma b)i}^{(I,1)}$ and $\Delta v_{(\gamma b)i}^{(I,2)}$ and obtain the evolution equation of the magnetic fields

$$(a^3 B^i)' = \frac{1 - \beta^3}{1 + \beta} \frac{4\sigma_T}{3e} a^2 \bar{\rho}_\gamma^{(0)} \epsilon^{ijk} \left[\frac{2a^2 \mathcal{H}}{\bar{\alpha}^{(0)}} \omega^{(2)i} + \frac{\bar{R}^{(0)}}{1 + \bar{R}^{(0)}} \epsilon^{ijk} \partial_j \bar{C}^{(1)} \Delta v_{(\gamma b)k}^{(I,1)} \right], \quad (2.13)$$

where $\omega^{(2)i}$ is defined as the photon's vorticity which follows

$$\left(a^2 \omega^{(2)i} \right)' + \frac{\mathcal{H} \bar{R}^{(0)}}{1 + \bar{R}^{(0)}} a^2 \omega^{(2)i} = \frac{\bar{R}^{(0)}}{2(1 + \bar{R}^{(0)})^2} \bar{\alpha}^{(0)} \epsilon^{ijk} \partial_j \bar{C}^{(1)} \Delta v_{(\gamma b)k}^{(I,1)}. \quad (2.14)$$

Here

$$\Delta v_{(\gamma b)i}^{(I,1)} = \frac{1}{\bar{\alpha}^{(0)}} \left[\mathcal{H} v_i^{(1)} - \frac{1}{4} \frac{\partial_i \delta \bar{\rho}_\gamma^{(1)}}{\bar{\rho}_\gamma^{(0)}} \right], \quad (2.15)$$

Eq. (2.13) tells us that the non-adiabatic fluctuations contribute as the source at the first-order TCA.

3 Power spectrum of the generated magnetic fields

In order to obtain the evolution of the perturbation and evaluate the power spectrum of the generated magnetic fields, we solve the linearized Einstein equations. Finally we obtain the power spectrum of the magnetic fields as

$$\begin{aligned} \frac{2\pi^2}{k^3} P_B(k) &= \left(\frac{1 - \beta^3}{1 + \beta} \frac{\sigma_T \bar{\rho}_{\gamma 0}^{(0)}}{ea^3} \right)^2 (2\pi^2)^2 \int d^3 p |\vec{k} \times \vec{p}|^2 P_{na}(p) P_a(|\vec{k} - \vec{p}|) \times \\ &\times \int_0^\eta d\eta_1 \int_0^\eta d\eta_2 a_1^{-2} a_2^{-2} \{ g(\vec{k}, \vec{p}, \eta_1) g(\vec{k}, \vec{p}, \eta_2) + f(\vec{k}, \vec{p}, \eta_1) f(\vec{k}, \vec{p}, \eta_2) \}, \end{aligned} \quad (3.1)$$

where

$$f(\vec{k}, \vec{p}, \eta) := \frac{1}{(2\pi)^{3/2}} \frac{\eta^2 \bar{R}^{(0)}}{2(1 + \bar{R}^{(0)})} \frac{1}{\bar{\alpha}^{(0)}} |\vec{k} - \vec{p}|^2 \frac{j_1(y)}{y}, \quad (3.2)$$

$$g(\vec{k}, \vec{p}, \eta) := \frac{1}{(2\pi)^{3/2}} \frac{1}{\bar{\alpha}^{(0)}} \frac{|\vec{k} - \vec{p}|^2}{2\eta(1 + \bar{R}^{(0)})} \int d\tilde{\eta} \frac{(\tilde{\eta})^2 \bar{R}^{(0)}}{1 + \bar{R}^{(0)}} \frac{j_1(\tilde{y})}{\tilde{y}} \quad (3.3)$$

and $y = |\vec{k} - \vec{p}| \eta / \sqrt{3}$.

$P_a(k)$ is the power spectrum of the adiabatic fluctuations. $P_{na}(k)$ is the power spectrum of the non-adiabatic fluctuations of baryon defined by

$$\frac{P_{na}}{P_a} := \left(\frac{\Omega_{\text{CDM}}}{\Omega_b} \right)^2 \frac{\mathcal{A}}{1 - \mathcal{A}} \left(\frac{k}{k_0} \right)^{n_2 - 1}, \quad (3.4)$$

where k_0 is a pivot scale. \mathcal{A} is represented as the ratio of the cold dark matter isocurvature fluctuation to the sum of the adiabatic and the isocurvature fluctuations.

We perform the numerical integration for $\mathcal{A} \simeq 0.1, 0.01$ and $n_2 \simeq 4$ to calculate the amplitudes of the magnetic fields at the radiation-matter equality time and show the result in Fig. 1. The circle and plus mark represent the contribution of the slip term $\langle SS^* \rangle$ (f term) for each \mathcal{A} and the square and cross mark represent the contribution of the vorticity term $\langle \Omega \Omega^* \rangle$ (g term) for each \mathcal{A} . From this figure we find that the vorticity term is less important at the generation of the magnetic fields at pre-recombination era. The physical magnetic field strength is about 10^{-20} Gauss at 1Mpc. The generated magnetic fields have a blue spectrum $k^{1.16}$ and so the larger strength is expected at the smaller scales.

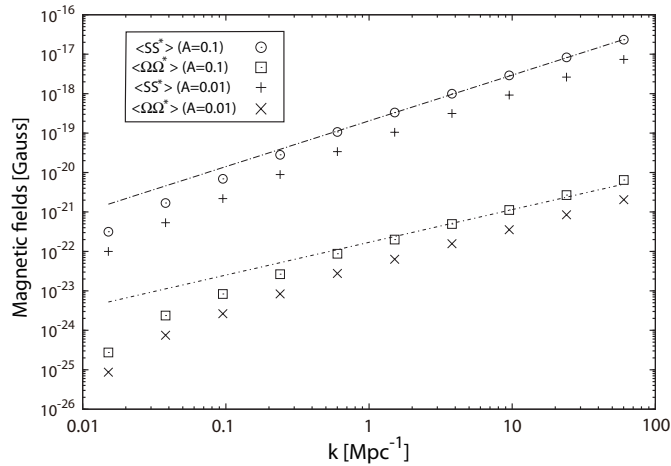


Figure 1: Calculated physical amplitudes of magnetic fields for several comoving wave numbers (k). The plus and cross mark represent the contributions of the slip term and vorticity term respectively. Here we set $\mathcal{A} \simeq 0.1$ (circle and square mark), $\mathcal{A} \simeq 0.01$ (plus and cross mark) and $n_2 = 4$.

4 Summary

We discussed the generation of magnetic fields by non-adiabatic fluctuations at the pre-recombination era. Firstly we showed that non-adiabatic fluctuations generate magnetic fields using the tight coupling approximation. We found that magnetic fields are generated at the first-order expansion of the tight coupling approximation. This result should be compared with the case of initially-adiabatic fluctuations, where magnetic fields are created only at the second order.

Secondly we calculated the power spectra of magnetic fields at the radiation-matter equality time considering the non-adiabatic fluctuations with a blue spectrum. We found that the fields have a blue spectrum $B \propto k^{1.16}$ for $n_2 = 4$, and the amplitude is about $B \sim 10^{-20}$ Gauss at the comoving scale of 1Mpc if the maximum amount of non-adiabatic fluctuations allowed from CMB observations is considered. Because the spectrum is bluer than those from the adiabatic fluctuations found in refs. [3, 6], this fields may dominate the primordial magnetic fields at small scales. The amplitude would be enough to be amplified to the present fields in galaxies by the dynamo mechanism [2].

References

- [1] L. M. Widrow, Rev. Mod. Phys. **74**, 775 (2002); M. Giovannini, Int. J. Mod. Phys. D **13**, 391(2004).
- [2] A. C. Davis, M. Lilley and O. Tornkvist, Phys. Rev. D **60**, 021301 (1999).
- [3] K. Ichiki, K. Takahashi, N. Sugiyama, H. Hanayama and H. Ohno, Science **311**, 827 (2006); K. Ichiki, K. Takahashi, N. Sugiyama, H. Hanayama and H. Ohno, arXiv:astro-ph/0701329;
- [4] T. Kobayashi, R. Maartens, T. Shiromizu and K. Takahashi, Phys. Rev. D **75**, 103501 (2007).
- [5] S. Maeda, S. Kitagawa, T. Kobayashi and T. Shiromizu, Class. Quant. Grav. **26**, 135014 (2009).
- [6] E. Fenu, C. Pitrou and R. Maartens, arXiv:1012.2958 [astro-ph.CO].
- [7] I. Sollom, A. Challinor and M. P. Hobson, Phys. Rev. D **79**, 123521 (2009) [arXiv:0903.5257 [astro-ph.CO]].
- [8] S. Maeda, K. Takahashi and K. Ichiki, JCAP **1111**, 045 (2011) [arXiv:1109.0691 [astro-ph.CO]].

Construction of gauge-invariant variables of linear metric perturbations on general background spacetime

Kouji Nakamura⁶⁵

*TAMA Project Office, Optical and Infrared Astronomy Division,
National Astronomical Observatory of Japan,
2-21-1, Osawa, Mitaka, Tokyo 181-8588, Japan*

Abstract

An outline of a proof of the decomposition of linear metric perturbations into gauge-invariant and gauge-variant parts on an arbitrary background spacetime which admits ADM decomposition is briefly discussed. We explicitly construct the gauge-invariant and gauge-variant parts of the linear metric perturbations based on some assumptions. This implies that we can develop the higher-order gauge-invariant perturbation theory on an arbitrary background spacetime.

Introduction — Higher-order general-relativistic perturbations have very wide applications. Among these applications, second-order cosmological perturbations are topical subject due to the precise measurements in recent cosmology. Higher-order black hole perturbations are also discussed in some literature. Moreover, as a special example of higher-order perturbation theory, there are researches on perturbations of a spherical star, which are motivated by researches into the oscillatory behaviors of a rotating neutron star. Thus, there are many physical situations to which general-relativistic higher-order perturbation theory should be applied.

As well-known, general relativity is based on the concept of general covariance. Due to this general covariance, the “gauge degree of freedom”, which is unphysical degree of freedom of perturbations, arises in general-relativistic perturbations. To obtain physical results, we have to fix this gauge degrees of freedom or to extract some invariant quantities of perturbations. This situation becomes more complicated in higher-order perturbation theory. Therefore, it is worthwhile to investigate higher-order gauge-invariant perturbation theory from a general point of view.

According to these motivations, in Ref. [1], we proposed a procedure to find gauge-invariant variables for higher-order perturbations on an arbitrary background spacetime. This proposal is based on the single assumption that *we already know the procedure to find gauge-invariant variables for linear-order metric perturbations* (Conjecture 1 in this article). Under this assumption, we summarize some formulae for the second-order perturbations of the curvatures and energy-momentum tensor for the matter fields in Refs. [2, 3]. Confirming that the above assumption is correct in the case of cosmological perturbations, in Refs. [4], the second-order gauge-invariant cosmological perturbation theory was developed. Through these works, we find that our general framework of higher-order gauge-invariant perturbation theory is well-defined except for the above assumption for linear-order metric perturbations. Therefore, we proposed the above assumption as a conjecture in Ref. [3]. If this conjecture is true, our general-relativistic higher-order gauge-invariant perturbation theory is completely formulated on an arbitrary background spacetime and has very wide applications. The main purpose of this article is to give a brief outline of a proof of this conjecture. Details of this issue is given in Ref. [5].

Perturbations in general relativity — The notion of “gauge” in general relativity arise in the theory due to the general covariance. There are two kinds of “gauges” in general relativity. These two “gauges” are called as the first- and the second-kind gauges, respectively. The distinction of these two different notion of “gauges” is an important premise of our arguments. *The first-kind gauge* is a coordinate system on a single manifold \mathcal{M} . The coordinate transformation is also called *gauge transformation of the first kind* in general relativity. On the other hand, *the second-kind gauge* appears in perturbation theories in a theory with general covariance. In perturbation theories, we always treat two spacetime manifolds. One is the physical spacetime \mathcal{M} which is our nature itself and we want to clarify the properties of

⁶⁵Email address: kouji.nakamura@nao.ac.jp

\mathcal{M} through perturbations. Another is the background spacetime \mathcal{M}_0 which has nothing to do with our nature but is prepared by hand for perturbative analyses. *The gauge choice of the second kind* is the point identification map $\mathcal{X} : \mathcal{M}_0 \mapsto \mathcal{M}$. We have to note that the correspondence \mathcal{X} between points on \mathcal{M}_0 and \mathcal{M} is not unique in the perturbation theory with general covariance. General covariance intuitively means that there is no preferred coordinate system in the theory. Due to this general covariance, we have no guiding principle to choose the identification map \mathcal{X} . Actually, as a gauge choice of the second kind, we may choose a different point identification map \mathcal{Y} from \mathcal{X} . This implies that there is degree of freedom in the gauge choice of the second kind. This is *the gauge degree of freedom of the second kind* in perturbation theory. *The gauge transformation of the second kind* is understood as a change $\mathcal{X} \rightarrow \mathcal{Y}$ of the identification map.

To define perturbations of an arbitrary tensor field \bar{Q} , we have to compare \bar{Q} on the physical spacetime \mathcal{M}_λ with Q_0 on the background spacetime \mathcal{M}_0 through the introduction of the above second-kind gauge choice $\mathcal{X}_\lambda : \mathcal{M}_0 \rightarrow \mathcal{M}_\lambda$. The pull-back \mathcal{X}_λ^* , which is induced by the map \mathcal{X}_λ , maps a tensor field \bar{Q} on \mathcal{M}_λ to a tensor field $\mathcal{X}_\lambda^* \bar{Q}$ on \mathcal{M}_0 . Once the definition of the pull-back of the gauge choice \mathcal{X}_λ is given, the perturbations of a tensor field \bar{Q} under the gauge choice \mathcal{X}_λ are simply defined by the evaluation of the Taylor expansion at \mathcal{M}_0 :

$${}^{\mathcal{X}}Q := \mathcal{X}_\lambda^* \bar{Q}_\lambda|_{\mathcal{M}_0} = Q_0 + \lambda {}^{(1)}_{\mathcal{X}}Q + \frac{1}{2} \lambda^2 {}^{(2)}_{\mathcal{X}}Q + O(\lambda^3), \quad (0.1)$$

where ${}^{(1)}_{\mathcal{X}}Q$ and ${}^{(2)}_{\mathcal{X}}Q$ are the first- and the second-order perturbations of \bar{Q} , respectively.

When we have two different gauge choices \mathcal{X}_λ and \mathcal{Y}_λ , we have two different representations of the perturbative expansion of the pulled-backed variables $\mathcal{X}_\lambda^* \bar{Q}_\lambda|_{\mathcal{M}_0}$ and $\mathcal{Y}_\lambda^* \bar{Q}_\lambda|_{\mathcal{M}_0}$. Although these two representations of the perturbations are different from each other, these should be equivalent because of general covariance. This equivalence is guaranteed by the *gauge-transformation rules* between two different gauge choices. The change of the gauge choice from \mathcal{X}_λ to \mathcal{Y}_λ is represented by the diffeomorphism $\Phi_\lambda := (\mathcal{X}_\lambda)^{-1} \circ \mathcal{Y}_\lambda$. This diffeomorphism Φ_λ is the map $\Phi_\lambda : \mathcal{M}_0 \rightarrow \mathcal{M}_0$ for each value of $\lambda \in \mathbb{R}$ and does change the point identification. Therefore, the diffeomorphism Φ_λ is regarded as the gauge transformation $\Phi_\lambda : \mathcal{X}_\lambda \rightarrow \mathcal{Y}_\lambda$. The gauge transformation Φ_λ induces a pull-back from the representation ${}^{\mathcal{X}}Q_\lambda$ of the perturbed tensor field Q in the gauge choice \mathcal{X}_λ to the representation ${}^{\mathcal{Y}}Q_\lambda$ in the gauge choice \mathcal{Y}_λ . Actually, the tensor fields ${}^{\mathcal{X}}Q_\lambda$ and ${}^{\mathcal{Y}}Q_\lambda$, which are defined on \mathcal{M}_0 , are connected by the linear map Φ_λ^* as ${}^{\mathcal{Y}}Q_\lambda = \Phi_\lambda^* {}^{\mathcal{X}}Q_\lambda$. According to generic arguments concerning the Taylor expansion of the pull-back of tensor fields on the same manifold [6], we obtain the order-by-order gauge-transformation rules for the perturbative variables ${}^{(1)}Q$ and ${}^{(2)}Q$ as

$${}^{(1)}_{\mathcal{Y}}Q - {}^{(1)}_{\mathcal{X}}Q = \mathcal{L}_{\xi_{(1)}} Q_0, \quad {}^{(2)}_{\mathcal{Y}}Q - {}^{(2)}_{\mathcal{X}}Q = 2\mathcal{L}_{\xi_{(1)}} {}^{(1)}_{\mathcal{X}}Q + \left\{ \mathcal{L}_{\xi_{(2)}} + \mathcal{L}_{\xi_{(1)}}^2 \right\} Q_0. \quad (0.2)$$

where the vector fields $\xi_{(1)}^a$ and $\xi_{(2)}^a$ are the generators of the gauge transformation Φ_λ .

The notion of gauge invariance considered in this article is the *order-by-order gauge invariance* proposed in Ref. [3]. We call the k th-order perturbation ${}^{(k)}_{\mathcal{X}}Q$ is gauge invariant iff ${}^{(k)}_{\mathcal{X}}Q = {}^{(k)}_{\mathcal{Y}}Q$ for any gauge choice \mathcal{X}_λ and \mathcal{Y}_λ . Through this concept of the order-by-order gauge invariance, we can develop the gauge-invariant perturbation theory.

Construction of gauge-invariant variables — First, we consider the metric perturbation. The metric \bar{g}_{ab} on \mathcal{M} , which is pulled back to \mathcal{M}_0 using a gauge choice \mathcal{X}_λ , is expanded in the form of Eq. (0.1): $\mathcal{X}_\lambda^* \bar{g}_{ab} = g_{ab} + \lambda \mathcal{X}^a h_{ab} + (\lambda^2/2) \mathcal{X}^a \mathcal{X}^b h_{ab} + O^3(\lambda)$, where g_{ab} is the metric on \mathcal{M}_0 . Although this expansion of the metric depends entirely on the gauge choice \mathcal{X}_λ , henceforth, we do not explicitly express the index of the gauge choice \mathcal{X}_λ if there is no possibility of confusion. Through these setup, in Ref. [1], we proposed a procedure to construct gauge-invariant variables for higher-order perturbations. Our starting point to construct gauge-invariant variables is the following conjecture for the linear-order metric perturbation h_{ab} defined by the above metric expansion:

Conjecture 1 *If there is a symmetric tensor field h_{ab} of the second rank, whose gauge transformation rule is $\mathcal{Y}^a h_{ab} - \mathcal{X}^a h_{ab} = \mathcal{L}_{\xi_{(1)}} g_{ab}$, then there exist a tensor field \mathcal{H}_{ab} and a vector field X^a such that h_{ab} is decomposed as $h_{ab} =: \mathcal{H}_{ab} + \mathcal{L}_X g_{ab}$, where \mathcal{H}_{ab} and X^a are transformed as $\mathcal{Y}^a \mathcal{H}_{ab} - \mathcal{X}^a \mathcal{H}_{ab} = 0$, $\mathcal{Y}^a X^a - \mathcal{X}^a X^a = \xi_{(1)}^a$ under the gauge transformation (0.2), respectively.*

In this conjecture, \mathcal{H}_{ab} and X^a are *gauge-invariant* and *gauge-variant* parts of the perturbation h_{ab} . In the case of the perturbation theory on an arbitrary background spacetime, this conjecture is a highly non-trivial statement due to the non-trivial curvature of the background spacetime, though its inverse statement is trivial.

An outline of a proof of Conjecture 1 — To give an outline of a proof of Conjecture 1 on an arbitrary background spacetime, we assume that the background spacetimes admit ADM decomposition. Therefore, the background spacetime \mathcal{M}_0 considered here is $n + 1$ -dimensional spacetime which is described by the direct product $\mathbb{R} \times \Sigma$. Here, \mathbb{R} is a time direction and Σ is the spacelike hypersurface ($\dim \Sigma = n$) embedded in \mathcal{M}_0 . This means that \mathcal{M}_0 is foliated by the one-parameter family of spacelike hypersurface $\Sigma(t)$, where $t \in \mathbb{R}F$ is a time function. Then, the metric on \mathcal{M}_0 is described by

$$g_{ab} = -\alpha^2(dt)_a(dt)_b + q_{ij}(dx^i + \beta^i dt)_a(dx^j + \beta^j dt)_b, \quad (0.3)$$

where α is the lapse function, β^i is the shift vector, and $q_{ab} = q_{ij}(dx^i)_a(dx^j)_b$ is the metric on $\Sigma(t)$.

Since the ADM decomposition (0.3) is a local one, we may regard that the arguments in this article are restricted to that for a single patch in \mathcal{M}_0 which is covered by the metric (0.3). Further, we may change the region which is covered by the metric (0.3) through the choice of the lapse function α and the shift vector β^i . The choice of α and β^i is regarded as the first-kind gauge choice, which have nothing to do with the second-kind gauge. Since we may regard that the representation (0.3) of the background metric is that on a single patch in \mathcal{M}_0 , in general situation, each Σ may have its boundary $\partial\Sigma$.

To prove Conjecture 1, we first consider the components of the metric h_{ab} as $h_{ab} = h_{tt}(dt)_a(dt)_b + 2h_{ti}(dt)_a(dx^i)_b + h_{ij}(dx^i)_a(dx^j)_b$. Under the gauge-transformation rule $\mathcal{Y}h_{ab} - \mathcal{X}h_{ab} = \mathcal{L}_{\xi_{(1)}}g_{ab}$, the components $\{h_{tt}, h_{ti}, h_{ij}\}$ are transformed as

$$\begin{aligned} \mathcal{Y}h_{tt} - \mathcal{X}h_{tt} &= 2\partial_t \xi_t - \frac{2}{\alpha} (\partial_t \alpha + \beta^i D_i \alpha - \beta^j \beta^i K_{ij}) \xi_t \\ &\quad - \frac{2}{\alpha} (\beta^i \beta^k \beta^j K_{kj} - \beta^i \partial_t \alpha + \alpha q^{ij} \partial_t \beta_j + \alpha^2 D^i \alpha - \alpha \beta^k D^i \beta_k - \beta^i \beta^j D_j \alpha) \xi_i, \end{aligned} \quad (0.4)$$

$$\mathcal{Y}h_{ti} - \mathcal{X}h_{ti} = \partial_t \xi_i + D_i \xi_t - \frac{2}{\alpha} (D_i \alpha - \beta^j K_{ij}) \xi_t - \frac{2}{\alpha} M_i^j \xi_j, \quad (0.5)$$

$$\mathcal{Y}h_{ij} - \mathcal{X}h_{ij} = 2D_{(i} \xi_{j)} + \frac{2}{\alpha} K_{ij} \xi_t - \frac{2}{\alpha} \beta^k K_{ij} \xi_k, \quad (0.6)$$

where M_i^j is defined by $M_i^j := -\alpha^2 K^j_i + \beta^j \beta^k K_{ki} - \beta^j D_i \alpha + \alpha D_i \beta^j$. Here, K_{ij} is the components of the extrinsic curvature of Σ in \mathcal{M}_0 and D_i is the covariant derivative associate with the metric q_{ij} ($D_i q_{jk} = 0$). The extrinsic curvature K_{ij} and its trace K are related to the time derivative of the metric q_{ij} by $K_{ij} = -(1/2\alpha) [\partial_t q_{ij} - D_i \beta_j - D_j \beta_i]$ and $K := q^{ij} K_{ij}$, respectively.

Inspecting gauge-transformation rules (0.4)–(0.6), we consider the decomposition of the components $\{h_{ti}, h_{ij}\}$ into the set of the variables $\{h_{(VL)}, h_{(V)i}, h_{(L)}, h_{(TV)i}, h_{(TT)ij}\}$ as follows:

$$h_{ti} =: D_i h_{(VL)} + h_{(V)i} - \frac{2}{\alpha} (D_i \alpha - \beta^k K_{ik}) (h_{(VL)} - \Delta^{-1} D^k \partial_t h_{(TV)k}) - \frac{2}{\alpha} M_i^k h_{(TV)k}, \quad (0.7)$$

$$\begin{aligned} h_{ij} =: & \frac{1}{n} q_{ij} h_{(L)} + D_i h_{(TV)j} + D_j h_{(TV)i} - \frac{2}{n} q_{ij} D^k h_{(TV)k} + h_{(TT)ij} \\ & + \frac{2}{\alpha} K_{ij} (h_{(VL)} - \Delta^{-1} D^k \partial_t h_{(TV)k}) - \frac{2}{\alpha} K_{ij} \beta^k h_{(TV)k}, \end{aligned} \quad (0.8)$$

$$D^i h_{(V)i} = 0, \quad q^{ij} h_{(TT)ij} = 0 = D^i h_{(TT)ij}. \quad (0.9)$$

Here, we assume the existence of Green functions of the elliptic derivative operators $\Delta := D^i D_i$ and $\mathcal{F} := \Delta - \frac{2}{\alpha} (D_i \alpha - \beta^j K_{ij}) D^i - 2D^i \left\{ \frac{1}{\alpha} (D_i \alpha - \beta^j K_{ij}) \right\}$, and the existence and the uniqueness of the solution A_i to the integro-differential equation

$$\mathcal{D}_j^k A_k + D^m \left[\frac{2}{\alpha} \tilde{K}_{mj} \left\{ \mathcal{F}^{-1} D^k \left(\frac{2}{\alpha} M_k^l A_l - \partial_t A_k \right) - \beta^k A_k \right\} \right] = L_j \quad (0.10)$$

for given a vector field L_j . Although the derivation of Eq. (0.7)–(0.9) is highly non-trivial, we only note that the relation (0.7)–(0.9) between the variables $\{h_{ti}, h_{ij}\}$ and $\{h_{(VL)}, h_{(V)i}, h_{(L)}, h_{(TV)i}, h_{(TT)ij}\}$

is invertible if we accept above three assumptions. In other words, the fact that we based on these assumptions implies that we have ignored perturbative modes which belong to the kernel of the above derivative operators and trivial solutions to Eq. (0.10) if there exists. These modes should be separately treated in different manner. We call these modes as *zero modes*. The issue concerning about treatments of these zero modes is called *zero-mode problem*, which is a remaining problem in our general framework on higher-order general-relativistic gauge-invariant perturbation theory.

Under these assumptions, the gauge-transformation rules for the variables $\{h_{(VL)}, h_{(V)i}, h_{(L)}, h_{(TV)i}, h_{(TT)ij}\}$ are summarized as follows:

$$\mathcal{Y}h_{(VL)} - \mathcal{X}h_{(VL)} = \xi_t + \Delta^{-1}D^k\partial_t\xi_k, \quad \mathcal{Y}h_{(V)i} - \mathcal{X}h_{(V)i} = \partial_t\xi_i - D_i\Delta^{-1}D^k\partial_t\xi_k, \quad (0.11)$$

$$\mathcal{Y}h_{(L)} - \mathcal{X}h_{(L)} = 2D^i\xi_i, \quad \mathcal{Y}h_{(TV)l} - \mathcal{X}h_{(TV)l} = \xi_l, \quad \mathcal{Y}h_{(TT)ij} - \mathcal{X}h_{(TT)ij} = 0. \quad (0.12)$$

From these gauge-transformation rules, we may define the components of the gauge-variant part X_a by $X_i := h_{(TV)i}$ and $X_t := h_{(VL)} - \Delta^{-1}D^k\partial_t h_{(TV)k}$. Then, we obtain the gauge-variant part X_a of the perturbation h_{ab} as $X_a := X_t(dt)_a + X_i(dx^i)_a$. Using the above variables X_t and X_i , we can construct gauge-invariant variables for the linear-order metric perturbation h_{ab} :

$$\begin{aligned} -2\Phi &:= h_{tt} + \frac{2}{\alpha}(\partial_t\alpha + \beta^i D_i\alpha - \beta^j\beta^i K_{ij})X_t - 2\partial_t X_t \\ &\quad + \frac{2}{\alpha}(\beta^i\beta^k\beta^j K_{kj} - \beta^i\partial_t\alpha + \alpha q^{ij}\partial_t\beta_j + \alpha^2 D^i\alpha - \alpha\beta^k D^i\beta_k - \beta^i\beta^j D_j\alpha)X_i, \end{aligned} \quad (0.13)$$

$$-2n\Psi := h_{(L)} - 2D^i X_i, \quad \nu_i := h_{(V)i} - \partial_t X_i + D_i\Delta^{-1}D^k\partial_t X_k, \quad \chi_{ij} := h_{(TT)ij}. \quad (0.14)$$

Actually, we can easily confirm that these variables Φ , Ψ , ν_i , and χ_{ij} are gauge invariant. We also note that the variable ν_i satisfies the property $D^i\nu_i = 0$ and the variable χ_{ij} satisfies the properties $\chi_{ij} = \chi_{ji}$, $q^{ij}\chi_{ij} = 0$, and $D^i\chi_{ij} = 0$. The original components $\{h_{tt}, h_{ti}, h_{ij}\}$ of the metric perturbation h_{ab} is rewritten in terms of these gauge-invariant variables and the variables X_t and X_i . These representation shows that we may define the gauge-invariant variables \mathcal{H}_{ab} so that $\mathcal{H}_{ab} := -2\Phi(dt)_a(dt)_b + 2\nu_i(dt)_a(dx^i)_b + (-2\Psi q_{ij} + \chi_{ij})(dx^i)_a(dx^j)_b$. This leads to assertion of Conjecture 1. \square

Summary — We proposed an outline of a proof of Conjecture 1 for an arbitrary background spacetime. Conjecture 1 states that we already know the procedure to decompose the linear-order metric perturbation h_{ab} into its gauge-invariant part \mathcal{H}_{ab} and gauge-variant part X_a . Conjecture 1 is the only non-trivial part when we consider the general framework of gauge-invariant perturbation theory on an arbitrary background spacetime. Although there will be many approaches to prove Conjecture 1, in this article, we just proposed an outline a proof. We also note that our arguments do not include zero modes. The existence of zero modes is also related to the symmetry of the background spacetime. To resolve this zero-mode problem, careful discussions on domains of functions for perturbations and its boundary conditions at $\partial\Sigma$ will be necessary. Besides this zero-mode problem, we have almost completed the general framework of the general-relativistic higher-order gauge-invariant perturbation theory. The outline of a proof of Conjecture 1 shown in this article gives rise to the possibility of the application of our general framework not only to cosmological perturbations [3, 4] but also to perturbations of black hole spacetimes or perturbations of general relativistic stars. Therefore, we may say that the wide applications of our gauge-invariant perturbation theory will be opened. We leave these development as future works.

References

- [1] K. Nakamura, Prog. Theor. Phys. **110**, (2003), 723.
- [2] K. Nakamura, Prog. Theor. Phys. **113** (2005), 481.
- [3] K. Nakamura, Phys. Rev. D **80** (2009), 124021.
- [4] K. Nakamura, Phys. Rev. D **74** (2006), 101301(R); K. Nakamura, Prog. Theor. Phys. **117** (2007), 17; K. Nakamura, Prog. Theor. Phys. **121** (2009), 1321.
- [5] K. Nakamura, arXiv:1105.4007 [gr-qc].
- [6] K. Nakamura, Advances in Astronomy, **2010** (2010), 576273.

Hawking temperature for near-equilibrium black holes

Shunichiro Kinoshita⁶⁶

Department of Physics, Kyoto University, Kitashirakawa Oiwake-Cho, 606-8502, Kyoto, Japan

Abstract

We discuss the Hawking temperature of near-equilibrium black holes using a semiclassical analysis. We introduce a useful expansion method for slowly evolving spacetime, and evaluate the Bogoliubov coefficients using the saddle point approximation. For a spacetime whose evolution is sufficiently slow, such as a black hole with slowly changing mass, we find that the temperature is determined by the surface gravity of the past horizon. We study the Hawking temperature of the AdS–Vaidya spacetime and discuss implications of our results in the context of the AdS/CFT correspondence.

1 Introduction

The fact that black holes possess thermodynamic properties has been intriguing in gravitational and quantum theories, and is still attracting interest. Nowadays it is well-known that black holes will emit thermal radiation with Hawking temperature proportional to the surface gravity of the event horizon [1]. This result plays a significant role in black hole thermodynamics. Moreover, the AdS/CFT correspondence opened up new insights about thermodynamic properties of black holes. In this context we expect that thermodynamic properties of conformal field theory (CFT) matter on the boundary would respect those of black holes in the bulk. In particular, stationary black holes correspond to thermal equilibrium of the dual field theory at finite temperature equal to the bulk Hawking temperature.

When time dependence is sufficiently weak, we may expect thermodynamic properties of a black hole to persist. This expectation partially stems from physical insight on ordinary thermodynamics systems, in which thermodynamic properties persists when the system is sufficiently near equilibrium and quasistationary. If black hole thermodynamics is robust enough, such insight on usual thermodynamic systems leads to the above expectation on dynamical spacetimes and black holes. Within the context of the AdS/CFT correspondence, thermodynamic properties of dynamical black holes lead to new insights into the dynamics of strongly coupled field theory on the boundary. One typical problem in this line is thermalization processes in the boundary field theory, which is holographically modeled by formation of the bulk black hole and its equilibration into a stationary state.

Based on these interests, we consider nonstationary spacetimes, and try to determine the Hawking temperature measured by observers in the asymptotic region. One naive way to do this would be to define a certain time coordinate to associate temperature of the black hole (future) horizon to that measured by asymptotic observers. Even though this procedure is seemingly natural from the viewpoint of black hole thermodynamics or horizon dynamics, it is puzzling from the viewpoint of causality, since this temperature is determined using information in the future region for that observer. In the AdS/CFT setup, if we were to define temperature at a point on the boundary in this way, we would need information in the bulk region, which is not causally accessible from that boundary point. Such a property would not be desirable if we care about causality in the bulk and boundary, especially when time dependence comes into the story.

To avoid such problems, we consider the conventional derivation of the Hawking radiation based on Bogoliubov transformations for nonstationary background. An advantage of this method is that we can naturally determine temperature measured by asymptotic observers using only information causally available to them. Particularly, we focus our attention on an eternal black hole rather than black hole formation by gravitational collapse [2] because we are interested in near-equilibrium system such as transition from an equilibrium state to another equilibrium state. We clarify how the Hawking temperature changes when a black hole becomes dynamical, for instance, due to mass accretion to the black hole, and

⁶⁶Email address: kinoshita@tap.scphys.kyoto-u.ac.jp

show that the Hawking temperature of dynamical black holes can be naturally associated with “surface gravity” of the past horizon. See also [3] in detail.

2 Estimation of Bogoliubov coefficients

We introduce two null coordinates u , which gives a natural time for observers in the asymptotic region, and U , which is the affine parameter on the past horizon. To probe a nonstationary spacetime, we use wave packets which are localized in both the time and frequency domains rather than plane waves spreading over the whole time. The wave packet is peaked around a time $u = u_0$ with width $\sim \Delta u$, which are the time and duration of the observation, respectively. The Bogoliubov coefficients between the wave packet modes and $\bar{u}_{\hat{\omega}} \propto e^{-i\hat{\omega}U}$ are given by

$$\left. \begin{array}{l} A_{\omega\hat{\omega}} \\ B_{\omega\hat{\omega}} \end{array} \right\} = \pm \frac{1}{2\pi} \sqrt{\frac{\hat{\omega}}{\omega}} \int_{-\infty}^{\infty} w_{\Delta u}(u - u_0) \frac{dU}{du} e^{\pm i\omega u - i\hat{\omega}U(u)} du, \quad (2.1)$$

where $w_{\Delta u}(x)$ is a window function which goes sufficiently fast to zero outside the interval Δu around $x = 0$. In addition, we assume that analytic continuation of $w_{\Delta u}(x)$ is varying slowly at least for $|x| < \Delta u$ in the complex plane. Using the Klein–Gordon product, these coefficients are written as $A_{\omega\hat{\omega}} = (\psi_{\omega}, \bar{u}_{\hat{\omega}})$ and $B_{\omega\hat{\omega}} = -(\psi_{\omega}^*, \bar{u}_{\hat{\omega}})$, where we have constructed the wave packet localized around time $u = u_0$ and frequency ω as $\psi_{\omega}(u) = \frac{1}{\sqrt{4\pi\omega}} w_{\Delta u}(u - u_0) e^{-i\omega u}$. We note that $A_{\omega\hat{\omega}}$ and $B_{\omega\hat{\omega}}$ satisfy the following relation $\int_0^{\infty} d\hat{\omega} (|A_{\omega\hat{\omega}}|^2 - |B_{\omega\hat{\omega}}|^2) = (\psi_{\omega}, \psi_{\omega})$, which follows from the completeness of $\{\bar{u}_{\hat{\omega}}\}$. The number density in terms of the wave packet mode ψ_{ω} is given by $\int_0^{\infty} d\hat{\omega} |B_{\omega\hat{\omega}}|^2 / (\psi_{\omega}, \psi_{\omega})$, which is roughly the number of particles generated in the frequency band of width $\sim 1/\Delta u$ around frequency ω .

Let us suppose that the evolution of the background spacetime is sufficiently slow around $u = u_0$ within time interval Δu . To clarify what slowly evolving is, we shall introduce the following quantity

$$\kappa(u) \equiv -\frac{d}{du} \log \frac{dU}{du}. \quad (2.2)$$

If the background spacetime is stationary, $\kappa(u)$ becomes a constant and it is nothing but the surface gravity of the black hole (Killing) horizon. Therefore, we may state that the spacetime is evolving slowly when $\kappa(u)$ is almost constant during Δu . In that case, we may express $\kappa(u)$ as $\kappa(u) = \kappa_0 [1 + \epsilon f(u)]$, where $f(u)$ is a real function which satisfies $f(u_0) = 0$ and $|f(u)| \leq 1$ for $|u - u_0| < \Delta u$, and ϵ is a small parameter. In other words, this assumption implies

$$\frac{\Delta\kappa}{\kappa_0} \leq \epsilon \quad \text{for } |u - u_0| < \Delta u, \quad (2.3)$$

where $\Delta\kappa \equiv |\kappa(u) - \kappa_0|$. For discussions below, we further assume that analytic continuation of $f(u)$ satisfies $|f(u)| \leq 1$ for any complex u such that $|u - u_0| < \Delta u$.

Then, we may expand $U'(u)$, $U(u)$ and $U''(u)$ with respect to ϵ as

$$\begin{aligned} U'(u) &= U'_0 \exp\left(-\int_{u_0}^u \kappa(x) dx\right) = U'_0 \exp\{-\kappa_0(\delta u + \epsilon g(u))\} = U'_0 e^{-\kappa_0 \delta u} (1 - \epsilon \kappa_0 g(u) + \mathcal{O}(\epsilon^2)), \\ U(u) &= U_0 + \int_{u_0}^u U'(x) dx = U_0 + U'_0 \left(\frac{1 - e^{-\kappa_0 \delta u}}{\kappa_0} - \epsilon \kappa_0 \int_{u_0}^u e^{-\kappa_0(x-u_0)} g(x) dx + \mathcal{O}(\epsilon^2)\right), \\ U''(u) &= -\kappa(u) U'(u) = -\kappa_0 (1 + \epsilon f(u)) U'_0 e^{-\kappa_0 \delta u} (1 - \epsilon \kappa_0 g(u) + \mathcal{O}(\epsilon^2)), \end{aligned} \quad (2.4)$$

where we defined $U_0 = U(u_0)$, $\delta u = u - u_0$ and $g(u) = \int_{u_0}^u f(x) dx$. Note that $|g(u)| \leq |\delta u|$ follows from the assumption $|f(u)| \leq 1$ for $|\delta u| < \Delta u$.

Now, to evaluate those coefficients (2.1) by the saddle point approximation, we will consider the integral $\int_{-\infty}^{\infty} \exp \phi(u) du$, where $\phi(u) \equiv \log \frac{dU}{du} \pm i\omega u - i\hat{\omega}U(u)$. Here, the saddle point $u = u_*$ is given by $\phi'(u_*) = 0$. We also expand the saddle point as $u_* = u_*^{(0)} + \epsilon u_*^{(1)} + \mathcal{O}(\epsilon^2)$. Solving $\phi'(u_*) = 0$ order by

order of ϵ , we find

$$\delta u_*^{(0)} = -\frac{1}{\kappa_0} \log \left(\frac{\kappa_0 r}{\hat{\omega} U'_0} \right) - \frac{i}{\kappa_0} \left(\frac{\pi}{2} \mp \theta \right), \quad u_*^{(1)} = -g(u_*^{(0)}) - \frac{f(u_*^{(0)})}{\kappa_0 r e^{\mp i \theta}}, \quad (2.5)$$

where we have defined $r e^{\mp i \theta} \equiv 1 \mp i \omega / \kappa_0$, which satisfies $r \gg 1$ because of the geometric optics approximation $\omega / \kappa_0 \gg 1$. We expand $\phi(u_*)$ and $\phi''(u_*)$ with respect to ϵ as $\phi(u_*) - \phi(u_0) \equiv \phi_0 + \epsilon \phi_1$ and $\phi''(u_*) \equiv \phi''_0 + \epsilon \phi''_1$ where $\mathcal{O}(\epsilon^2)$ terms are omitted. To guarantee that the perturbative expansion above is valid and that the calculation of the saddle point approximation is not affected by the correction terms, we should require each of correction terms to be much smaller than their leading term. Under these assumptions, we find that the integral in Eq. (2.1) can be evaluated by the saddle point approximation as

$$\left| \int_{-\infty}^{\infty} w_{\Delta u}(\delta u) e^{\phi(u)} du \right| \simeq U'_0 \left| w_{\Delta u}(\delta u_*^{(0)}) \right| e^{\text{Re} \phi_0} \sqrt{\frac{2\pi}{|\phi''_0|}}. \quad (2.6)$$

So that the suppression due to the window function, $w_{\Delta u}$, is weak and the integral value becomes close to that for the unwindowed function, the saddle point should satisfy $|\delta u_*| \lesssim \Delta u$. For the imaginary part of $u_*^{(0)}$ the condition $|\delta u_*| \lesssim \Delta u$ becomes $\Delta u^{-1} \lesssim \kappa_0$, and for the real part it becomes a condition on $\hat{\omega}$, given by $\kappa_0 r e^{-\kappa_0 \Delta u} / U'_0 \lesssim \hat{\omega} \lesssim \kappa_0 r e^{\kappa_0 \Delta u} / U'_0$. If $\hat{\omega}$ is out of this region, no saddle point exists between $|u - u_0| \lesssim \Delta u$, and then the integral will be suppressed due to the window function. This condition means that only the Kruskal modes of $\hat{\omega}$ with limited frequency band can have correlations with the wave packet mode ψ_ω due to its localization in the time domain.

Consequently, sufficient conditions for the saddle point approximation to be valid are given by

$$\epsilon \kappa_0 \ll \frac{1}{\Delta u} \lesssim \kappa_0 \ll \omega, \quad |f'(u)| \ll \kappa_0 r, \quad (2.7)$$

for $|u - u_0| < \Delta u$. Note that the condition on ϵ , $\epsilon \kappa_0 \ll \Delta u^{-1}$, can be rewritten as $\Delta \kappa \Delta u \ll 1$, where $\Delta \kappa$ is defined by Eq. (2.3). If we can take the time interval $\Delta u (\gtrsim \kappa_0^{-1})$ satisfying this condition, we have a sufficiently small $\epsilon \ll 1$ for which Eq. (2.7) holds. Roughly speaking, this condition is indicating that the time variation of $\kappa(u)$ should be sufficiently moderate to satisfy $\frac{1}{\kappa_0} \frac{d\kappa}{du} \ll 1$ between the interval $|u - u_0| \lesssim \kappa_0^{-1}$. Under these assumptions, at the leading order we have $|A_{\omega \hat{\omega}}|^2 / |B_{\omega \hat{\omega}}|^2 \simeq \exp(2\pi \omega / \kappa_0)$, which implies the spectrum observed at the time $u = u_0$ becomes a thermal one with temperature $\kappa(u_0) / 2\pi$ for high frequencies $\omega \gg \kappa_0$.

Now, we consider the geometrical meaning of $\kappa(u)$ defined by Eq. (2.2). Ingoing null vectors with respect to null coordinates u and U are written as $k^a = (\partial / \partial u)^a$ and $\bar{k}^a = (\partial / \partial U)^a$, respectively. Note that U is an affine parameter on the past horizon because it is one of the Kruskal coordinates. Using $k^a = U'(u) \bar{k}^a$, we have $k^a \nabla_a k^b = (k^a \nabla_a U'(u)) \bar{k}^b + (U')^2 \bar{k}^a \nabla_a \bar{k}^b$. The last term vanishes because U is the affine parameter. As a result, we obtain $k^a \nabla_a k^b = -\kappa(u) k^b$. We shall call $\kappa(u)$ ‘‘surface gravity’’ for the past horizon because it describes the inaffinity of the null generator k^a of the past horizon, which is defined by the asymptotic time at the null infinity. When the spacetime is stationary, the past horizon and $\kappa(u)$ coincide with the Killing horizon and its surface gravity, respectively. In this sense, $\kappa(u)$ is a natural extension of surface gravity of stationary spacetimes. (In Ref. [2], it was called ‘‘peeling properties’’ for gravitational collapse.) It is worth noting that the surface gravity for the past horizon is not determined only by local geometrical quantities on that horizon but also by the relation between the time coordinates on the horizon and in the asymptotic region. In fact, the Killing vector which defines the surface gravity of the Killing horizon is also determined using the asymptotic time in a stationary case.

Roughly speaking, the particles of the Hawking radiation observed in the asymptotic region start from the vicinity of the horizon and propagate along outgoing null geodesics. Every outgoing null ray arriving at the null infinity experiences the near-horizon region of the past horizon rather than the (future) event horizon. Based on this observation, it seems to be natural that the spectrum is affected by the surface gravity near the past horizon.

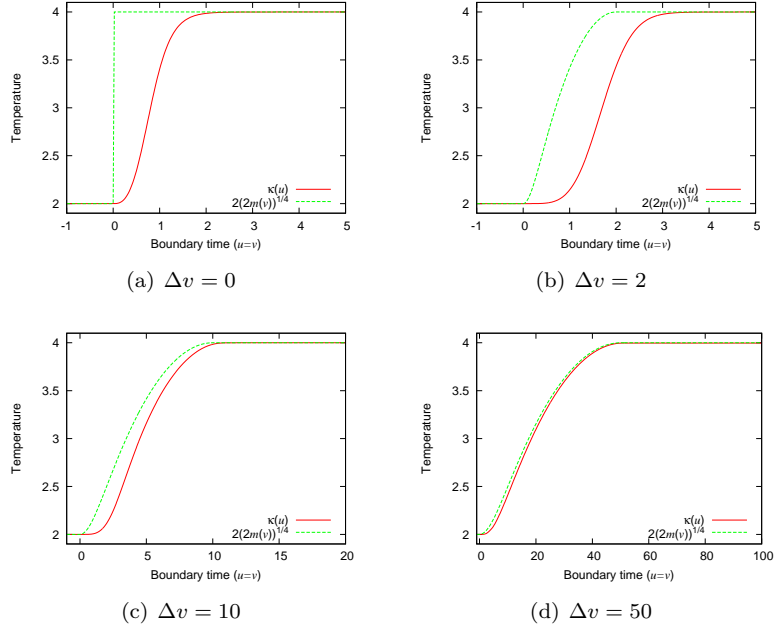


Figure 1: $\kappa(u)$ and a quasistatic temperature $2\pi T_{\text{qs}} = 2(2m(v))^{1/4}$ for various injection times Δv .

3 Application to AdS–Vaidya

In this section, we consider an explicit example of transitions from an initial equilibrium state to another equilibrium state. We will focus attention on the AdS–Vaidya spacetime. This is a toy model to describe a thermalization process in the AdS/CFT correspondence. We consider the 5D AdS–Vaidya spacetime $ds^2 = [-F(\bar{v}, z)d\bar{v}^2 - 2d\bar{v}dz + d\bar{x}_3^2]/z^2$, where $F(\bar{v}, z)$ is given by $F(\bar{v}, z) = 1 - 2m(\bar{v})z^4$, and the curvature radius of the AdS is set to unity. We suppose that the mass function $m(\bar{v})$ is m_0 ($\bar{v} < 0$), $m_0 + \Delta m \sin^2 \frac{\pi\bar{v}}{2\Delta v}$ ($0 \leq \bar{v} \leq \Delta v$) and $m_0 + \Delta m$ ($\bar{v} > \Delta v$). During an interval Δv , the null fluid is injected into the black hole with mass m_0 , and the mass eventually becomes $m_0 + \Delta m$. For the AdS–Vaidya, Bondi energy observed at the boundary is described by the mass function $m(\bar{v})$. Note that the time coordinate \bar{v} is nothing but asymptotic time at the boundary. In the context of the AdS/CFT correspondence, $m(\bar{v})$ corresponds to the energy density of the CFT matter. Therefore, the duration of the injection Δv will represent the time scale of energy density change.

Now we shall consider the Hawking temperature in the current case. We introduce double-null coordinates (u, v) as $z = z(u, v)$, $\bar{v} = v$. In these coordinates, the boundary $z = 0$ is described by $u = v$. An asymptotic time t at the boundary is given by $t = \frac{u+v}{2}$, and it is equal to v (or u) there. In Fig. 1, for $\Delta v = 0, 2, 10, 50$ we plot $\kappa(u)$ together with a quasistatic temperature $2\pi T_{\text{qs}} = 2(2m(v))^{1/4}$, which is naively determined from the mass functions $m(v)$ in a similar manner to static black holes. We can observe that both curves begin to coincide as the injection time becomes longer. In other words, the variation of the temperature $\kappa(u)$ tends to follow the variation of the black hole mass $m(v)$. These results lead us to the conclusion that, even if the mass injection is rapid, the temperature will gradually change over a time scale no shorter than the thermal time scale $\sim \kappa^{-1}$. In this sense, we may say that there is a finite relaxation time irrespective of the speed of energy injection. When energy injection and the resultant black hole evolution is slower than this relaxation time, the temperature tends to evolve in a similar way to the mass injection.

References

- [1] S. W. Hawking, *Commun. Math. Phys.* **43**, 199-220 (1975).

- [2] C. Barcelo, S. Liberati, S. Sonogo and M. Visser, *JHEP* **1102**, 003 (2011) [[arXiv:1011.5911 \[gr-qc\]](#)].
- [3] S. Kinoshita and N. Tanahashi, *Phys. Rev. D* **85**, 024050 (2012) [[arXiv:1111.2684 \[hep-th\]](#)].

Universal Property of Quantum Gravity implied by Uniqueness Theorem of Bekenstein-Hawking Entropy

Hiromi Saida⁶⁷

Department of Physics, Daido University, 10-3 Takiharuru Minami-ku, Nagoya, Japan

Abstract

We search for a universal property of quantum gravity, where “universal” means to be independent of any existing model of quantum gravity. To do so, we investigate deeply the basis of black hole thermodynamics. The uniqueness of Bekenstein-Hawking entropy lets us extract a reasonable universal property of quantum gravity from the conditions justifying Boltzmann formula. The universal property indicates a repulsive gravity at Planck length scale, otherwise stationary black holes can not be regarded as thermal equilibrium states of gravity. (This manuscript is based on [1])

1 Introduction

As mentioned in the abstract, we investigate the basis of black hole thermodynamics in order to search for universal properties of quantum gravity, where “universal” means to be independent of any existing model of quantum gravity (such as the super string theory, loop quantum gravity, causal dynamical triangulation, and so on). The basic concept of black hole thermodynamics is the following consideration: *Because a stationary black hole emits the thermal radiation (Hawking radiation), the black hole is in a thermal equilibrium state of gravity. And, usually, the micro-scopic origin of black hole (thermal state of gravity) is expected to be the quantum states of gravity.* This basic concept depends on the thermal radiation theory.

By accepting the above concept of black hole thermodynamics, it is reasonable to require that the quantum gravity satisfies the presupposition of thermal radiation theory, otherwise we can not regard black holes as thermal equilibrium states by observing the Hawking radiation. Here, the presupposition of thermal radiation theory (Planck spectrum of radiation emitted by thermal equilibrium body) is that the ordinary thermodynamics and quantum statistical mechanics work well on any thermal equilibrium body, at least in laboratory systems. Therefore, it is natural to require that *the basic idea of statistical mechanics is applicable to thermal equilibrium states of not only laboratory systems but also quantum gravity (black holes).* Here, the basic idea of statistical mechanics is, for example, the Boltzmann formula, $S_{BH} = \ln \Omega_g$, where S_{BH} is the Bekenstein-Hawking entropy and Ω is the number of states of black hole counted by the underlying quantum gravity.

From the above consideration, let us adopt the following two suppositions in order to search for a universal property of quantum gravity,

Supposition 1: A stationary black hole is a thermal equilibrium state composed of micro-states of underlying quantum gravity. This is based on the Hawking radiation.

Supposition 2: Basic formalism of statistical mechanics (e.g. Boltzmann formula, grand partition function and so on) is applicable to underlying quantum gravity so as to describe the thermal equilibrium states (black holes). This is based on the presupposition of thermal radiation theory.

The issues for each supposition are as follows:

Issue on Supposition 1 (Uniqueness of BH entropy): Note that, if the Boltzmann formula, $S_{BH} = \ln \Omega_g$, holds for black holes, then it defines the Bekenstein-Hawking entropy S_{BH} *uniquely* in micro-scopic point of view. This means that the Boltzmann formula can never work well unless the uniqueness of entropy is proven in macro-scopic point of view of thermodynamics (without using

⁶⁷Email address: saida@daido-it.ac.jp

any micro-scopic theory) [2-4]. In ordinary thermodynamics, the uniqueness of entropy is proven by some basic requirements of thermodynamics[2, 3]. However, as summarized in Sec.2, some basic requirements of ordinary thermodynamics do not hold in black hole thermodynamics [1, 5, 6]. Then, it is not necessarily manifest whether the uniqueness of S_{BH} holds in black hole thermodynamics. Hence, we have to prove the uniqueness of S_{BH} before the discussion of Boltzmann formula.

Issue on Supposition 2 (Justification of Boltzmann formula): Once the uniqueness of Bekenstein-Hawking entropy S_{BH} is proven in macro-scopic point of view, we can proceed to the investigation of Boltzmann formula. Note that the validity of Boltzmann formula in ordinary quantum statistical mechanics is justified by some intrinsic properties of Hilbert space of ordinary quantum mechanics. Those intrinsic properties appear in Ruelle-Tasaki theorem and Dobrushin theorem [4, 7, 8] as summarized in Sec.3. *Then, if S_{BH} is given by the Boltzmann formula, we can expect that those theorems of ordinary quantum mechanics are related with some property of underlying quantum gravity. Some universal property of quantum gravity may be extracted from those theorems.*

Sec.2 is for the uniqueness of S_{BH} , and Sec.3 is for the two theorems of ordinary quantum mechanics. Then, Sec.4 shows a conclusion about the universal property of quantum gravity.

2 Uniqueness Theorem of Bekenstein-Hawking Entropy

In the rigorous axiomatic formulation of ordinary thermodynamics (e.g. see Lieb and Yngvason [2] or Tasaki [3]), the basic axioms consist of not only the “four laws of thermodynamics” but also some more requirements. One of the axioms of ordinary thermodynamics modified in black hole thermodynamics is the classification requirement of state variables; all thermodynamic state variables are classified into two categories, extensive variables (e.g. energy, entropy and so on) and intensive variables (e.g. temperature, pressure and so on). Here the extensivity and intensivity are defined by the scaling behavior as follows: Under the scaling of “system’s size” $V \rightarrow \alpha V$ and $N \rightarrow \alpha N$ (where V is volume and N is mol-number for a gas in a container), the extensive variable X is scaled as $X \rightarrow \alpha X$, and the intensive variable Y is invariant $Y \rightarrow Y$. This classification of state variables is frequently used in many theorems of ordinary thermodynamics including the uniqueness theorem of entropy.

On the other hand, in the framework of black hole thermodynamics, e.g. for Schwarzschild black hole of radius R_{BH} , some representative state variables are as follows: The Bekenstein-Hawking entropy is $S_{BH} = \pi R_{BH}^2$, the Hawking temperature is $T_{BH} = (4\pi R_{BH})^{-1}$ and the internal energy is $E_{BH} = R_{BH}/2$, where we use the units $c = 1$, $G = 1$, $\hbar = 1$. For this Schwarzschild black hole, the basic scaling is given by the scaling of length size $R_{BH} \rightarrow \lambda R_{BH}$, and we find the scaling behaviors, $S_{BH} \rightarrow \lambda^2 S_{BH}$, $T_{BH} \rightarrow \lambda^{-1} T_{BH}$ and $E_{BH} \rightarrow \lambda E_{BH}$ [5]. *This implies that the state variables in black hole thermodynamics should be classified not into two categories, but into three categories; the extensive variables (e.g. S_{BH}), intensive variables (e.g. T_{BH}) and energy variables (e.g. E_{BH}). In this classification, the energy variables, which are extensive in ordinary thermodynamics, form one independent category in black hole thermodynamics, since the scaling behavior of energy is different from that of extensive variables. Furthermore, the scaling behavior of extensive and intensive variables are different from that of ordinary thermodynamics. But, the scaling behavior of [extensive variable]×[intensive variable] (e.g. $T_{BH}S_{BH}$) is the same with that of energy variables. [1, 6]*

Because the classification of state variables are changed, the uniqueness of S_{BH} in black hole thermodynamics is not manifest. However as shown in ref.[1], the uniqueness of S_{BH} can be proven with modifying the proof of uniqueness in ordinary thermodynamics. The statement of theorem is:

Uniqueness Theorem of Entropy: Let K be an extensive variable which increases along irreversible adiabatic processes. Then there exist two constants $a(> 0)$ and b such that $K = aS_{BH} + b$, where S_{BH} is the Bekenstein-Hawking entropy. (See ref.[1] for the proof.)

This statement is the same with that in ordinary thermodynamics. Once this theorem is proven, we can proceed to the investigation of Boltzmann formula. In this sense, we can regard the conclusion in Sec.4 as a result implied by the uniqueness of S_{BH} .

3 Conditions Justifying Boltzmann Formula

This section is not for black hole but for ordinary quantum mechanics. For simplicity in this section, consider the system of N identical particles in the region of volume V with no external field, and:

- Interaction potential : $\Phi(\vec{x}_1, \dots, \vec{x}_N) = \sum_{j=1}^{\infty} \phi^{(j)}(\vec{x}_{i_1}, \dots, \vec{x}_{i_j})$, where $i_j \in (1, \dots, N)$.
- Energy eigen value : $E_k(V, N)$, where $k = 0, 1, 2, \dots$ and $E_k \leq E_{k+1}$ (“=” is for degenerated states.)
- Number of states : $\Omega(V, N; U) :=$ “Number of eigen states satisfying $E_k \leq U$ ” = $\max_{E_k \leq U} k$.

For the first, let us show the Ruelle-Tasaki theorem which clarifies the sufficient conditions for the validity of Boltzmann formula [1, 4, 7]:

Ruelle-Tasaki Theorem: Suppose the following two conditions of interaction potential $\Phi(\vec{x}_1, \dots, \vec{x}_N)$:

Condition A: Arbitrary j -particle interaction, $\phi^{(j)}$, becomes negative for sufficiently large distribution of j particles. That is, there exists a constant $r_A (> 0)$, such that

$$\phi^{(j)}(\vec{x}_{i_1}, \dots, \vec{x}_{i_j}) \leq 0 \quad \text{for} \quad r_A \leq \min_{k,l=1,\dots,j} |\vec{x}_{i_k} - \vec{x}_{i_l}|. \tag{3.1}$$

Condition B: Interaction potential Φ is bounded below. That is, there exists a constant $\phi_B (> 0)$, such that

$$\Phi(\vec{x}_1, \dots, \vec{x}_N) \geq -N \phi_B. \tag{3.2}$$

Then, the following limit exists uniquely; $\sigma(\varepsilon, \rho) := \lim_{t.l.} \frac{\ln \Omega(V, N; U)}{V}$, where $\lim_{t.l.}$ means the thermodynamic limit defined by $V \rightarrow \infty$ with fixing $\rho := N/V$ and $\varepsilon := U/V$ at constant values.

By this theorem, the thermodynamics limit of $\ln \Omega(V, N; U)$ is defined well. Furthermore, it can be also proven that $\sigma(\varepsilon, \rho)$ is concave about its arguments (ε, ρ) and monotone increasing about ε , and remains constant along *reversible* adiabatic processes [4]. These behaviors are some characteristic properties of entropy already known in thermodynamics. Then, in statistical mechanics, it is assumed that $\ln \Omega(V, N; U)$ is equal to the entropy (the Boltzmann formula).

Obviously, the above conditions A and B are the sufficient conditions for the validity of Boltzmann formula. Furthermore, *a system, which holds Boltzmann formula but violates conditions A or B, has not been found experimentally. Hence, at least in laboratory systems, it is reasonable to require that any physical system satisfies the conditions A and B.*

Next, let us show the Dobrushin theorem which clarifies the necessary condition of the existence of thermal equilibrium states for the system under consideration [1, 7, 8]:

Dobrushin theorem: Consider the case satisfying following presuppositions:

Presupposition C: The j -particle interactions for $j \neq 2$ disappear, and the total interaction potential Φ is a sum of two-particle interactions, $\Phi(\vec{x}_1, \dots, \vec{x}_N) = \sum_{1 \leq i < j \leq N} \phi^{(2)}(\vec{x}_i, \vec{x}_j)$.

Presupposition D: $\phi^{(2)}(\vec{x}, \vec{y}) \propto |\vec{x} - \vec{y}|^{-\alpha}$, where $\alpha > 0$.

Under these presuppositions, if the ground partition function of the system can be defined uniquely (i.e. if thermal equilibrium states exist), then the following integral, $I_V^{(2)}$, is non-negative,

$$I_V^{(2)} := \frac{1}{V^2} \iint_V d^3x_1 d^3x_2 \phi^{(2)}(\vec{x}_1, \vec{x}_2) \geq 0. \tag{3.3}$$

Obviously, $I_V^{(2)} \geq 0$ is the necessary condition for the existence of thermal equilibrium states. Note that the presuppositions C and D are natural when we consider the gravity.

4 Conclusion

Our supposition 2 in Sec.1 implies that the ordinary quantum mechanics and quantum gravity shares the same properties which justify the validity of Boltzmann formula and the existence of thermal equilibrium states. The sufficient conditions A and B and the necessary condition $I_V^{(2)} \geq 0$ are expected to be such properties⁶⁸. Note that, these three conditions (A, B and $I_V^{(2)} \geq 0$) are for the interaction potential. On the other hand, although it is not clear whether the full quantum gravity is expressed by using the interaction potential Φ or Hamiltonian, but the semi-classical expression of quantum gravity should be expressed by an effective Lagrangian using an interaction potential. Hence, our suggestion is:

Implication from the above: The interaction potential in the effective Lagrangian of quantum gravity should satisfy the conditions A, B and $I_V^{(2)} \geq 0$, in order to regard a stationary black hole as a thermal equilibrium state of quantum gravity whose entropy is given by the Boltzmann formula. The typical form of the effective potential is shown in the figure below. This means that the semi-classical correction to Einstein-Hilbert action expresses a repulsive gravity at a short lengths scale (which may be the Planck scale).

In this manuscript, any existing model of quantum gravity is not used. (See ref.[1] for detail.) Therefore, this implication can be regarded as a universal property of quantum gravity.

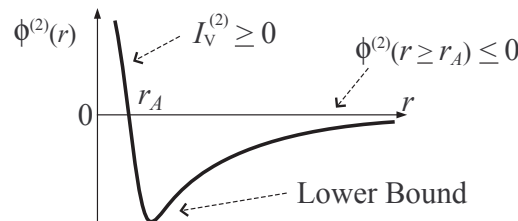


Figure 1: Effective potential of quantum gravity at semi-classical level. Thermal equilibrium states of gravity (black holes) may not exist unless a repulsive region appears, where r_A may be Planck scale.

References

- [1] H.Saida, *Universal Property of Quantum Gravity implied by Uniqueness Theorem of Bekenstein-Hawking Entropy*, Entropy 13 (2011) 1611–1647.
Invited as a feature (and refereed) paper for the special issue *black hole thermodynamics* edited by J.Bekenstein in the journal *Entropy*.
- [2] E.H.Lieb and J.Yngvason, *The Physics and Mathematics of the Second Law of Thermodynamics*, Phys.Rep.310 (1999) 1–96.
- [3] H.Tasaki, *Thermodynamics (Netus-Rikigaku)*, Baifu-kan Publ., 2000. [Published in Japanese]
- [4] H.Tasaki, *Statistical Mechanics (Tokei-Rikigaku)*, Baifu-kan Publ., 2008. [Published in Japanese]
- [5] J.W.,Jr.York, *Black-hole thermodynamics and the Euclidean Einstein action*, Phys.Rev.D33 (1986) 2092–2099
- [6] H.Saida, *To what extent is the entropy-area universal?*, Prog.Theor.Phys.122 (2010) 1515–1552.
- [7] D.Ruelle, *Statistical Mechanics –Rigorous Results–*, Imperial College Press and World Scientific Publ., 1999.
- [8] R.L.Dobrushin, *Investigation of the Conditions of the Asymptotic Existence of the Configuration Integral of the Gibbs Distribution*, Teorija Verojatn. i ee Prim.9 (1964) 626–643.

⁶⁸ So far, no counter-example to sufficient conditions A and B are found experimentally. Then, it may be reasonable to extend this fact to quantum gravitating systems, so that quantum gravity also satisfies the conditions A and B.

Time Evolution of Evaporating Black Rings

Mitsuhiro Matsumoto^{69(a)}, Hirotaka Yoshino^(b) and Hideo Kodama^{(a)(b)}

^(a)*Department of Particles and Nuclear Physics, The Graduate University for Advanced Studies (SOKENDAI), 1-1 Oho, Tsukuba, Ibaraki 305-0801, Japan*

^(b)*KEK Theory Center, Institute of Particle and Nuclear Studies, KEK, 1-1 Oho, Tsukuba, Ibaraki, 305-0801, Japan*

Abstract

It was shown that a five-dimensional Myers-Perry black hole loses its mass and angular momenta by Hawking radiation and evolves toward a state with nonvanishing nondimensional rotation parameters similarly to the case of a four-dimensional Kerr black hole. In order to extend this analysis to the case of a black ring, we derive a set of equations that determines time evolution of quasistationary evaporation of a black ring, by approximating a thin black ring by a boosted black string.

1 Introduction

In four spacetime dimensions, a stationary, asymptotically flat, vacuum black hole is completely characterized by its mass and spin. In particular, the topology of its event horizon must be a sphere. By contrast, in five dimensions, there are black objects with nonspherical topologies. In this paper, we focus on a black ring of the $S^1 \times S^2$ horizon topology. The black ring solution rotating in the direction of S^1 was found by Emparan and Reall [1]. Since a five-dimensional spacetime can have two angular momenta, Pomeransky and Sen'kov [2] extended it to black rings with two independent rotation parameters (i.e., rotating in both directions of S^1 and S^2).

A black hole is known to evaporate due to the effect of quantum fields in curved spacetime as shown by Hawking [3]. It is generally believed that by the Hawking radiation, a black hole loses its mass and angular momentum and approaches a nonrotating black hole regardless of its initial state. However, Chambers *et al.* [4] showed that a four-dimensional Kerr black hole evolves to a final evolutionary state with the nonvanishing nondimensional rotation parameter, $a/M \sim 0.555$, if only the massless scalar field is taken into account (i.e., in the absence of fields with nonzero spin). This analysis was extended to five-dimensional Myers-Perry black holes by Nomura *et al* [5]. They showed that any such black hole with nonzero rotation parameters a and b evolves toward an asymptotic state with $a/M^{1/2} = b/M^{1/2} \sim 0.1975(8/3\pi)^{1/2}$. Here, this value is independent of the initial values of a and b . It is interesting to extend these studies to the case of black rings, and this is the purpose of our work.

2 Black Ring

The metric of a Pomeransky-Sen'kov black ring is

$$ds^2 = -\frac{H(y,x)}{H(x,y)}(dt + \Omega)^2 + \frac{F(x,y)}{H(y,x)}d\psi^2 + 2\frac{J(x,y)}{H(y,x)}d\psi d\phi - \frac{F(y,x)}{H(y,x)}d\phi^2 - \frac{2R^2H(x,y)}{(x-y)^2(1-\nu)^2} \left(\frac{dx^2}{G(x)} - \frac{dy^2}{G(y)} \right), \quad (2.1)$$

where the 1-form Ω is

$$\Omega = -\frac{2R\lambda\sqrt{(1+\nu)^2 - \lambda^2}}{H(y,x)} \left[(1-x^2)y\sqrt{\nu}d\phi + \frac{1+y}{1-\lambda+\nu} \{1 + \lambda - \nu + x^2y\nu(1-\lambda-\nu) + 2\nu x(1-y)\} d\psi \right]. \quad (2.2)$$

The explicit form of the functions G , H , J and F can be found in Ref. [2]. Here, we follow the notation of Ref. [2], except that we choose the signature $(-, +, +, +, +)$ for the metric, exchange ϕ and ψ , and

⁶⁹Email address: matsu@post.kek.jp

use R instead of k . The coordinate ranges are $-\infty < t < +\infty$, $0 < \phi, \psi < 2\pi$, $-1 \leq x \leq 1$ and $-\infty < y < -1$. R is a parameter of dimension of length, which determines the characteristic scale. λ and ν are dimensionless parameters satisfying $0 \leq \nu < 1$ and $2\sqrt{\nu} \leq \lambda < 1 + \nu$, which determine two nondimensional rotational parameters. The regular event horizon exists at $y = (-\lambda + \sqrt{\lambda^2 - 4\nu})/2\nu$. The solution is asymptotically flat, and spacelike infinity is located at $x = y = -1$. The coordinates (x, ϕ) parametrize the two-sphere S^2 and ψ parametrizes the circle S^1 . One recovers the Emparan-Reall black ring by setting $\nu = 0$.

Here, we consider a thin black ring limit where the ratio of the S^1 radius to the S^2 radius becomes infinity,

$$\lambda \rightarrow 0, \quad R\lambda = \text{finite}, \quad (2.3)$$

and define new parameters $a(\equiv M_K a_*)$, M_K and coordinates r , z and θ as

$$\nu = a_*^2 \lambda^2 / 4, \quad R\lambda = \sqrt{2} M_K, \quad y = -\frac{\sqrt{2} R}{r}, \quad \psi = -\frac{z}{\sqrt{2} R}, \quad x = \cos \theta. \quad (2.4)$$

Here, a_* is fixed in taking the limit. Then the black ring solution is reduced to the so-called boosted Kerr string solution

$$ds^2 = -\left(1 - \frac{2M_K r \cosh^2 \sigma}{\rho^2}\right) dt^2 + \frac{2M_K r \sinh 2\sigma}{\rho^2} dt dz + \left(1 + \frac{2M_K r \sinh^2 \sigma}{\rho^2}\right) dz^2 + \frac{\rho^2}{\Delta} dr^2 + \rho^2 d\theta^2 \\ + \frac{(r^2 + a^2)^2 - \Delta a^2 \sin^2 \theta}{\rho^2} \sin^2 \theta d\phi^2 - \frac{4M_K r \cosh \sigma}{\rho^2} a \sin^2 \theta dt d\phi - \frac{4M_K r \sinh \sigma}{\rho^2} a \sin^2 \theta dz d\phi, \quad (2.5)$$

where $\rho^2 = r^2 + a^2 \cos^2 \theta$, $\Delta = r^2 - 2M_K r + a^2$. Here a is the rotation parameter, M_K is the mass density of the boosted Kerr string, and $\sigma := \operatorname{arctanh}(1/\sqrt{2})$ is the boost parameter. The outer and inner horizons are located at $r = r_{\pm} := M_K \pm \sqrt{M_K^2 - a^2}$.

3 Emission Rate

In this section, we consider the emission of massless scalar particles from the Pomenransky-Sen'kov black ring by Hawking radiation. The evolution of a scalar field is governed by the Klein-Gordon equation in curved spacetime

$$(-g)^{-1/2} \partial_{\mu} (\sqrt{-g} g^{\mu\nu} \partial_{\nu} \Phi) = 0, \quad (3.1)$$

where g is the determinant of the metric (2.1). To quantize the field, we expand it in terms of eigenmodes as $\Phi = e^{-i\omega t} e^{im\phi} e^{in\psi} \Psi(x, y)$. The expected number of particles emitted per unit time is formally given by

$$\langle N \rangle = \frac{\Gamma(\omega, \tilde{l}, m, n)}{e^{(\omega - n\Omega_{\psi} - m\Omega_{\phi})/T} - 1}, \quad (3.2)$$

where \tilde{l} is the eigenvalue of $\Psi(x, y)$ (which has not been determined as we will mention later), Ω_{ψ} is the angular velocity along ψ , Ω_{ϕ} is the angular velocity along ϕ , and $\Gamma(\omega, \tilde{l}, m, n)$ is the greybody factor, which is identical to the absorption probability of the incoming wave of the corresponding mode. We can evaluate the emission rates of the total mass and angular momenta, which give changes of the black ring mass M and angular momenta J_{ψ} and J_{ϕ} as

$$-\frac{d}{dt} \begin{pmatrix} M \\ J_{\psi} \\ J_{\phi} \end{pmatrix} = \frac{1}{2\pi} \sum_{\tilde{l}, m, n} \int_0^{\infty} d\omega \langle N \rangle \begin{pmatrix} \omega \\ n \\ m \end{pmatrix}, \quad (3.3)$$

where \sum means summing up over all modes. Note that it is difficult to estimate the emission rates generally because no one has succeeded in separating the coordinates x and y and two-dimensional numerical calculation of eigenfunctions is required.

Here, we consider the situation where the eigenvalue of \tilde{l} can be approximately evaluated: a black string limit discussed above. For the boosted black string (2.5), we can separate the wave equation, and

therefore, we approximate the evolution of a scalar field in a black ring spacetime by that in a boosted Kerr string spacetime. In this situation, the scalar field can be separated as

$$\Phi = e^{-i\omega t} R(r) e^{ikz} e^{im\phi} S_\ell^m(\theta), \quad (3.4)$$

where $S_\ell^m(\theta)$ is the spheroidal harmonic function. From the coordinate transformation (2.4), the relation between n of a black ring and k of a boosted black string is $n = 2kR \tanh \sigma$. The expected number of particles emitted per unit time is given by

$$\langle N' \rangle = \frac{\Gamma'(\omega, \ell, m, k)}{e^{(\omega - kV - m\Omega_\phi)/T'} - 1}, \quad (3.5)$$

where T' is the temperature of the horizon and V is the linear velocity of the horizon along the string direction,

$$T' = \frac{r_+ - r_-}{4\pi (r_+^2 + a^2) \cosh \sigma}, \quad V = \tanh \sigma. \quad (3.6)$$

$\Gamma'(\omega, \ell, m, k)$ is the greybody factor of the boosted Kerr string spacetime. The emission rates (3.3) is evaluated by summing over ℓ, k instead of \tilde{l}, n and using $\langle N' \rangle$ instead of $\langle N \rangle$. In order to determine the emission rates, we need to calculate the greybody factors.

4 Greybody Factor

In the following, we evaluate the greybody factors for a massless scalar fields in a boosted Kerr string spacetime. Substituting the ansatz (3.4) into the Klein-Gordon equation (3.1) in the background of (2.5), we get the following angular and radial wave equations for $S_\ell^m(\theta)$ and $R(r)$ [7],

$$0 = \frac{1}{\sin \theta} \partial_\theta (\sin \theta \partial_\theta S_\ell^m) + \left[a^2 (\omega^2 - k^2) \cos^2 \theta - \frac{m^2}{\sin^2 \theta} + \lambda_{\ell m} \right] S_\ell^m, \quad (4.1)$$

$$0 = \Delta \partial_r (\Delta \partial_r R) - \Delta [k^2 r^2 + a^2 \omega^2 - 2\omega m a \cosh \sigma + \lambda_{\ell m}] R + \left[[\omega (r^2 + a^2) - m a \cosh \sigma]^2 + 2M_K r (r^2 + a^2) \cosh^2 \sigma (\omega - k \tanh \sigma)^2 - 2M_K r (r^2 + a^2) \omega^2 - m^2 a^2 \sinh^2 \sigma + 4k m a M_K r \sinh \sigma \right] R, \quad (4.2)$$

where $\lambda_{\ell m}$ is the separation constant which is determined as an eigenvalue of (4.1). For small $a^2 (\omega^2 - k^2)$, the eigenvalues associated with the spheroidal wave functions S_ℓ^m are $\lambda_{\ell m} = \ell(\ell + 1) + \mathcal{O}(a^2 (\omega^2 - k^2))$ [8].

As we mentioned in the previous section, the greybody factor is calculated as the absorption probability of the incoming waves of the corresponding mode. Defining new parameters $\tilde{\omega}$, \tilde{k} , the tortoise coordinate r_* and a new wave function u as

$$\tilde{\omega} = \omega \cosh \sigma + k \sinh \sigma, \quad \tilde{k} = \omega \sinh \sigma + k \cosh \sigma, \quad dr_* = \frac{r_+^2 + a^2}{\Delta} dr, \quad u = (r_+^2 + a^2) R, \quad (4.3)$$

the radial wave equation (4.2) can be rewritten as the equation of Schrödinger type:

$$\left[\frac{d^2}{dr_*^2} + \tilde{\omega}^2 - V(r) \right] u = 0, \quad (4.4)$$

where $V(r)$ is the effective potential

$$V(r) = \frac{\Delta \{2M_K r (r^2 - 2a^2) + a^2 (r^2 + a^2)\}}{(r^2 + a^2)^4} + \frac{\Delta (\tilde{\omega}^2 a^2 + \lambda_{\ell m}) + 4m\tilde{\omega} M_K a r - m^2 a^2}{(r^2 + a^2)^2}. \quad (4.5)$$

As the boundary condition, we impose the ingoing condition at the horizon. Then, u behaves as

$$u(r_*) \sim \begin{cases} e^{-i\tilde{\omega} r_*} & \text{at } r \rightarrow \infty, \\ A_{in} e^{-i\tilde{\omega}' r_*} + A_{out} e^{i\tilde{\omega}' r_*} & \text{at } r \rightarrow r_+. \end{cases} \quad (4.6)$$

Here $\omega' = \omega - m\Omega'_\phi$, where $\Omega'_\phi = a/(2Mr_+)$. The greybody factor is written as

$$\Gamma = 1 - |A_{out}/A_{in}|^2, \quad (4.7)$$

which has to be evaluated numerically.

Now, let us consider the case of the Emparan-Reall black ring, i.e. $a = 0$. In this case, S_ℓ^m becomes the spherical harmonic function and the calculation becomes much simpler compared to the case $a \neq 0$. We developed a code to calculate the greybody factors in this situation. Here we show the example of the behavior of the greybody factors for the modes of three lowest even l numbers in Fig.1.

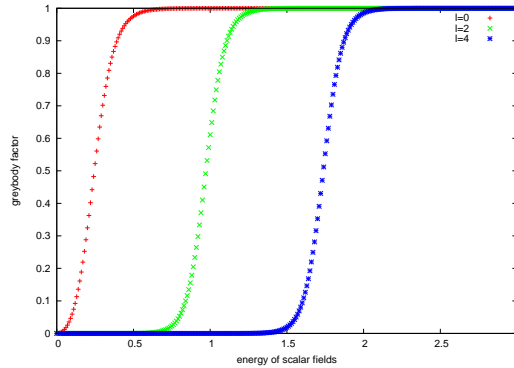


Figure 1: Greybody factors for the scalar modes $k = m = 0$, $\ell = 0, 2, 4$ (from left to right).

5 Summary

In this article, we have given a set of equations to calculate the quasistationary evaporation of large radius black rings. In our formulation, the behavior of a scalar field in a black ring spacetime is approximated by that in a boosted Kerr string spacetime. We showed a typical example of the numerical results of the greybody factors, and we are currently calculating the greybody factors for various other modes. The numerical determination of the evolution of a black ring by Hawking radiation will be completed soon.

Acknowledgments

This work is supported by the JSPS Grant-in-Aid for Scientific Research (A) No. 22244030.

References

- [1] R. Emparan and H. S. Reall, Phys. Rev. Lett. **88**, 101101 (2002).
- [2] A. A. Pomeransky and R. A. Sen'kov, [hep-th/0612005].
- [3] S. W. Hawking, Commun. Math. Phys. **43**, 199 (1975).
- [4] C. M. Chambers, W. A. Hiscock and B. Taylor, Phys. Rev. Lett. **78**, 3249 (1997).
- [5] H. Nomura, S. Yoshida, M. Tanabe and K. -i. Maeda, Prog. Theor. Phys. **114**, 707 (2005).
- [6] H. Elvang and R. Emparan, JHEP **0311**, 035 (2003).
- [7] O. J. C. Dias, Phys. Rev. D **73**, 124035 (2006)
- [8] S. A. Teukolsky, Astrophys. J. **185**, 635 (1973).

Quantum energy teleportation and black hole

Masahiro Hotta^{70(a)}

^(a)*Graduate School of Science, Tohoku University, Sendai 980-8578, Japan*

Abstract

Recently a protocol of quantum teleportation has been proposed which attains effective energy transportation by local operations and classical communication without breaking local energy conservation. This provides a new method of energy extraction from black holes. It is argued that information about zero-point fluctuation of quantum fields outside a black hole has a very close connection with black hole entropy.

1 Introduction

Interplay between quantum physics and quantum information theory has attracted much attention. Especially, quantum black hole is one of the striking examples. It is well known that black holes carry their own entropy, which is proportional to horizon area. It is shown that entanglement entropy of conformal fields in quantum information theory is equal to BTZ black hole entropy [1]. Recently, a protocol of quantum energy teleportation (QET) [2] sheds a new light on this entropy. This protocol reveals that information about zero-point fluctuation of quantum fields outside a black hole has a deep relationship with black hole entropy. This presentation is based on my recent paper [3].

2 Horizon shrinkage induced by QET

QET is a quantum protocol which effectively transports energy [2]. Performing a distant measurement of vacuum fluctuation, the zero-point energy becomes active and can be extracted by local operation dependent on the measurement result. This provides a new method of energy extraction from black holes. Outside a black hole, we perform a measurement of quantum fields and obtain information about the quantum fluctuation. Then positive-energy wave packets of the fields are generated during the measurement and fall into the black hole. Even after absorption of the wave packets by the black hole, we can retrieve a part of the absorbed energy outside the horizon by using QET. This energy extraction yields a decrease in the horizon area, which is proportional to the entropy of the black hole. However, if we accidentally lose the measurement information, we cannot extract energy anymore. The black-hole entropy is unable to decrease. Therefore, the obtained measurement information has a very close connection with the black hole entropy.

References

- [1] T. Azeyanagi, T. Nishioka and T. Takayanagi, Phys. Rev. D77, 064005, (2008).
- [2] M. Hotta, "Quantum Energy Teleportation: An Introductory Review", (2011), <http://www.tuhep.phys.tohoku.ac.jp/~hotta/extended-version-qet-review.pdf>
- [3] M. Hotta, Phys. Rev. D81, 044025, (2010).

⁷⁰Email address: hotta@tuhep.phys.tohoku.ac.jp

Multi-field open inflation and instanton

Kazuyuki Sugimura^{71(a)}, Daisuke Yamauchi^(b), Misao Sasaki^(a)

^(a) *Yukawa Institute for Theoretical Physics, Kyoto University, Kyoto 606-8502, Japan*

^(b) *Institute for Cosmic Ray Research, The University of Tokyo, Chiba 277-8582, Japan*

Abstract

In the open inflation scenario, phase transition from false vacuum inflation at a local minimum to slow-roll inflation is mediated by the quantum tunneling. In this work, we present a concrete multi-field open inflation model, explicitly showing how the bubble is nucleated by tunneling of scalar fields, and how slow-roll inflation in the nucleated bubble follows. This model is the first viable open inflation model with a simple potential. Multi-field tunneling is described by multi-field instanton method, which is a natural extension to the Coleman-De Luccia(CDL) instanton method. Evolution of the universe in the bubble obeys equations of motion for the open Friedmann-Lemaître-Robertson-Walker(FLRW) universe.

1 Introduction

Recently, quantum tunneling of a scalar field in inflationary era is keenly studied in the context of string landscape, which predicts many local minima in the potential for scalar fields, where scalar fields are stable classically but unstable due to quantum effects [1–3]. Quantum tunneling of a scalar field with gravity was first studied by Coleman and De Luccia[4, 5], and they found that the tunneling proceed via bubble nucleation, inside of which can be regarded as open FLRW universe because of the O(4)-symmetry of the instanton. In the case slow-roll inflation after the tunneling lasts for moderate number of e-foldings, say, about 50 or 60, the universe becomes almost flat at the end of the inflation but small curvature remains, and $\Omega_{K,0} \sim 10^{-2} - 10^{-3}$ might be observed in future observation. In fact, Freivogel et al. suggested that this kind of situation is preferred in string landscape[6]. The inflation scenario in which the universe bears small negative curvature because of the tunneling before slow-roll inflation is often called open inflation[7, 8]. Since open infalction can be seen as the outcome of string landscape, studies of open inflation might give us some indication about string landscape.

It is known that there has been a trouble in constructing a single-field open inflation model, that only a model with very artificial potential is possible[9]. This is because the condition for existence of a CDL instanton require the potential barrier to be steep, however, the condition for slow-roll inflation require flat potential tilt, and very artificial potential is needed in order to match these two oppsitley oriented condition at the same time.

However, let us consider a model with two scalar fields. One of which called “tunneling field” plays a major role in quantum tunneling, and the other called “inflaton” plays a major role in slow-roll inflation. In this case, it is expceted that open infalction is realized with simple potential by choosing the potential barrier for the tunneling field steep while the potential for the inflaton after the tunneling flat. Systems with many scalar fields in inflationary era are also motivated by string landscape.

In this study, we propose a concrete multi-field model with simple potential, and make sure that open inflation scenario is indeed realized by explicitly studying the evolution, which includes quantum tunneling and slow-roll inflation after the tunneling. This multi-field open inflation model is the first open inflation model with simple potential.

2 Scenario and Model

The brief scenario of our multi-field open inflation model is as follows. In the begining, two scalar fields are trapped at a false vacuum for a long time. Then, quantum tunneling happens where the tunneling

⁷¹Email address: sugimura@yukawa.kyoto-u.ac.jp

field play a main role. On the other side of the potential barrier, the inflaton starts to roll slowly due to the coupling between the two scalar fields, and causes slow-roll inflation. The slow-inflation continues until the inflaton reach the true vacuum where reheating occurs in the usual manner. The schematic picture of this scenario is drawn in the Fig. 1.

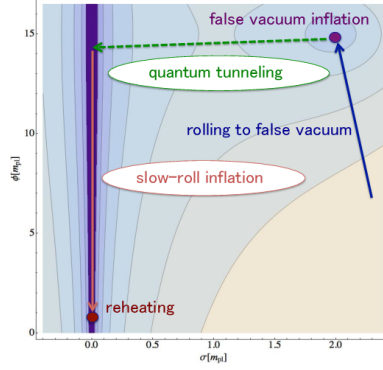


Figure 1: The schematic picture of our multi-field open inflation scenario. The color corresponds to the potential: lighter region is higher and darker region is lower. The vertical axis is inflaton's field value, and the horizontal axis is tunneling field's field value.

To realize this multi-field open inflation scenario, we propose a concrete model with a simple potential,

$$V(\sigma, \phi) = \alpha\sigma^2 \left\{ (\sigma - \sigma_0)^2 + M_V^2 \right\} + \left(\frac{1}{2}m_\phi^2\phi^2 + \frac{\beta}{2}\sigma^2(\phi - \phi_0)^2 \right). \quad (2.1)$$

Here, σ is the tunneling field and ϕ is the inflaton, first part of the potential is important in tunneling, and second part makes it possible for ϕ to slow-roll only after the tunneling by the coupling to σ . We take the parameters as $\alpha = 0.1$, $\sigma_0 = 2m_{pl}$, $M_V = 0.2m_{pl}$, $\beta = 0.1$, $m_\phi = 10^{-6}m_{pl}$, $\phi_0 = 15m_{pl}$. The false vacuum is located near (σ_0, ϕ_0) , and the true vacuum is located at $(0, 0)$.

3 Bubble Nucleation and Multi-filed Instanton

In this section, we study the quantum tunneling of scalar fields via bubble nucleation. Multi-field tunneling with gravity is expected to be described with multi-field instanton method, which is a natural extension to the CDL instanton method[10]. In the multi-field instanton method, we solve equations of motion for an instanton,

$$\begin{aligned} \frac{\bar{a}''}{\bar{a}} + \frac{1}{3m_{pl}^2} (\bar{\sigma}'^2 + \bar{\phi}'^2 + V(\bar{\sigma}, \bar{\phi})) &= 0, \\ \bar{\sigma}'' + 3\frac{\bar{a}'}{\bar{a}}\bar{\sigma}' - V_{\bar{\sigma}}(\bar{\sigma}, \bar{\phi}) &= 0, \quad \bar{\phi}'' + 3\frac{\bar{a}'}{\bar{a}}\bar{\phi}' - V_{\bar{\phi}}(\bar{\sigma}, \bar{\phi}) &= 0, \end{aligned} \quad (3.1)$$

with boundary condition,

$$\bar{a}(0) = \bar{a}(\tau_{\text{end}}) = 0, \quad \bar{a}'(0) = -\bar{a}'(\tau_{\text{end}}) = 1, \quad \bar{\sigma}'(0) = \bar{\sigma}'(\tau_{\text{end}}) = 0, \quad \bar{\phi}'(0) = \bar{\phi}'(\tau_{\text{end}}) = 0. \quad (3.2)$$

Here, τ is imaginary time and $'$ is derivative with respect to τ , \bar{a} is an instanton for the scale factor of the universe in Euclidean spacetime, and $\bar{\phi}$ and $\bar{\sigma}$ are instantons for ϕ and σ , respectively. It is known from the CDL argument[5] that the action for the instanton gives the tunneling rate and that the inside of the bubble is written as an open FLRW universe which starts with scalar fields whose values are given by the instanton's value at $\tau = 0$.

We numerically find the solution which satisfies these equations with the potential given by Eq. (2.1), and the result is plotted in Fig. 2.

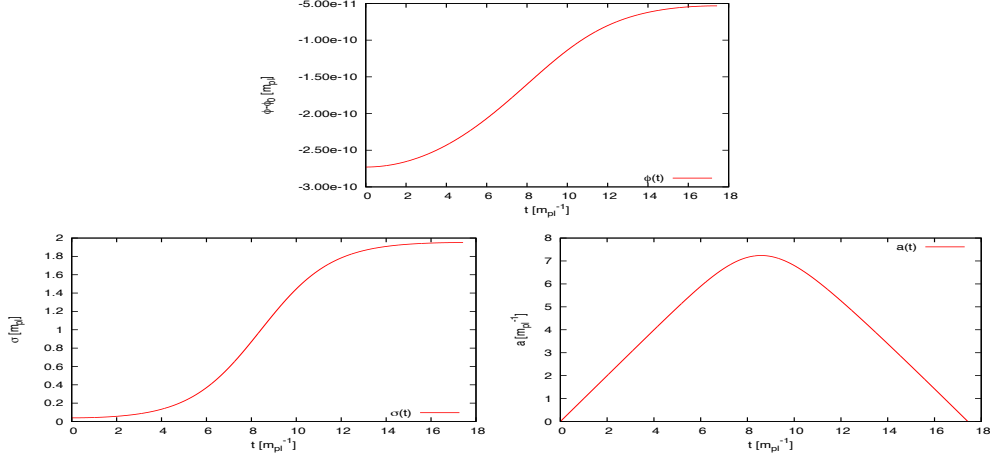


Figure 2: Multi-field instanton for the potential given by Eq. (2.1)[10].

4 Slow-roll Inflation Inside the Bubble

In this section, we study the evolution of the universe inside the bubble. The evolution equations are those for an open FLRW universe,

$$\begin{aligned} \ddot{a} + \frac{1}{3m_{pl}^2} (\dot{\sigma}^2 + \dot{\phi}^2 - V(\sigma, \phi)) &= 0, \\ \ddot{\sigma} + 3\frac{\dot{a}}{a}\dot{\sigma} + V_{\sigma}(\sigma, \phi) &= 0, \quad \ddot{\phi} + 3\frac{\dot{a}}{a}\dot{\phi} + V_{\phi}(\sigma, \phi) = 0, \end{aligned} \quad (4.1)$$

where $\dot{}$ denotes a derivative with respect to t and a is the scale factor of the open FLRW universe. The initial conditions at $t = 0$ are given from the multi-field instanton method as $a(0) = 0$, $\sigma(0) = \bar{\sigma}(0)$, $\phi(0) = \bar{\phi}(0)$, as we mentioned before.

We calculated these equations numerically with the potential given by Eq. (2.1), and the result is plotted in Fig. 3. Contribution to the Hubble square H^2 , or the energy density of the universe, from each component are plotted in Fig. 4, and it is apparent that the inflaton indeed causes slow-roll inflation.

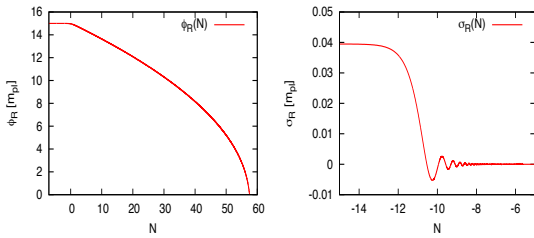


Figure 3: The evolution of the scalar fields in the nucleated bubble[10]. left: evolution of the inflaton. right: evolution of the tunneling field. The inflaton slowly rolls down the potential for about 60 numbers of e-foldings, from the nucleation point, $\phi \sim 15m_{pl}$, to the bottom of the potential, $\phi = 0$. The tunneling field soon reaches its potential minimum and it doesn't play a role in the evolution of the universe since then.

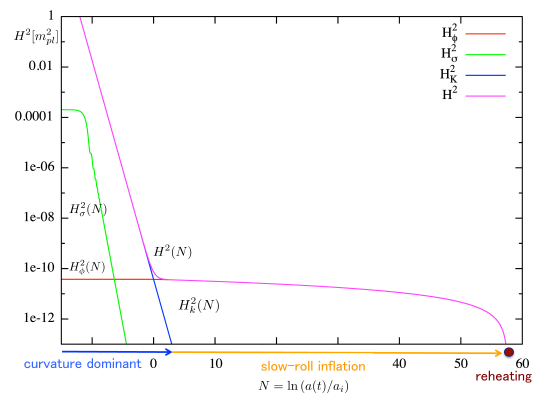


Figure 4: The contribution to Hubble square H^2 from each component, H_{ϕ}^2 , H_{σ}^2 , H_k^2 which are from inflaton, tunneling field, and curvature of the universe, respectively. Curvature dominance after the bubble nucleation soon comes to an end, and then slow-roll inflation by the inflaton follows.

5 Conclusion

We proposed a multi-field open inflation in Sec. 2 which is expected to realize multi-field open inflation scenario. The tunneling via bubble nucleation and the slow-roll inflation inside the bubble is explicitly calculated in Sec. 3 and Sec. 4, respectively. In Sec. 4, we can see that slow-roll inflation indeed occurs in the bubble, and now we are sure that open inflation scenario is indeed realized in our model of multi-field open inflation model. In this model, we assume two scalar fields, one is a tunneling field the other is an inflaton, which plays a major role in tunneling and slow-roll inflation, respectively. Since the potential for these two scalar fields has simple form, it can be said that we succeed in constructing a open inflation model with simple potential for the first time.

Now, we have a concrete model for the multi-field open inflation and know how the evolution of the universe proceeds in this model. Thus, it is possible to calculate some observable quantity in our model like the powerspectrum for the curvature perturbation, which is already known for a single field model[11, 12].

It is also interesting to study the bispectrum for the curvature perturbation in open inflation model, which is now we are working for, since the bispectrum is now getting available thanks to the development of the technology [13, 14]. A trace of open inflation might be found in the bispectrum, and as we mentioned in introduction, it might be a trace of string landscape.

References

- [1] S. Kachru, R. Kallosh, A. D. Linde, S. P. Trivedi, Phys. Rev. **D68**, 046005 (2003). [hep-th/0301240].
- [2] L. Susskind, In *Carr, Bernard (ed.): Universe or multiverse?* 247-266. [hep-th/0302219].
- [3] B. Freivogel, L. Susskind, Phys. Rev. **D70**, 126007 (2004). [hep-th/0408133].
- [4] S. R. Coleman, Phys. Rev. **D15**, 2929-2936 (1977).
- [5] S. R. Coleman, F. De Luccia, Phys. Rev. **D21**, 3305 (1980).
- [6] B. Freivogel, M. Kleban, M. Rodriguez Martinez, L. Susskind, JHEP **0603**, 039 (2006). [hep-th/0505232].
- [7] M. Bucher, A. S. Goldhaber and N. Turok, Phys. Rev. D **52**, 3314 (1995) [arXiv:hep-ph/9411206].
M. Bucher and N. Turok, Phys. Rev. D **52**, 5538 (1995) [arXiv:hep-ph/9503393].
- [8] M. Sasaki, T. Tanaka, K. Yamamoto, Phys. Rev. **D51**, 2979-2995 (1995). [gr-qc/9412025].
- [9] A. D. Linde, Phys. Lett. **B351**, 99-104 (1995). [hep-th/9503097].
A. D. Linde, A. Mezhlumian, Phys. Rev. **D52**, 6789-6804 (1995). [astro-ph/9506017].
- [10] K. Sugimura, D. Yamauchi and M. Sasaki, JCAP **1201**, 027 (2012) [arXiv:1110.4773 [gr-qc]].
- [11] J. Garriga, X. Montes, M. Sasaki and T. Tanaka, Nucl. Phys. B **513**, 343 (1998) [arXiv:astro-ph/9706229].
J. Garriga, X. Montes, M. Sasaki and T. Tanaka, Nucl. Phys. B **551**, 317 (1999) [arXiv:astro-ph/9811257].
- [12] A. D. Linde, M. Sasaki and T. Tanaka, Phys. Rev. D **59**, 123522 (1999) [arXiv:astro-ph/9901135].
- [13] E. Komatsu *et al.* [WMAP Collaboration], Astrophys. J. Suppl. **192**, 18 (2011) [arXiv:1001.4538 [astro-ph.CO]].
- [14] E. Komatsu and D. N. Spergel, Phys. Rev. D **63**, 063002 (2001) [arXiv:astro-ph/0005036].

Non-Gaussianity from Hilltop Curvaton

Fuminobu Takahashi⁷²

Particle Theory and Cosmology Group, Department of Physics, Tohoku University, 6-3, aza-Aoba, Aramaki, Aoba-ku, Sendai 980-8578, Japan

Abstract

We investigate density perturbations sourced by a curvaton with a generic energy potential. The key feature of a curvaton potential which deviates from a quadratic is that the curvaton experiences a non-uniform onset of its oscillation. This sources additional contributions to the resulting density perturbations, and we especially find that the non-Gaussianity parameter f_{NL} can become large: $10 \lesssim f_{\text{NL}} \lesssim 30$ in a hilltop Nambu-Goldstone curvaton scenario.

We explore density perturbations sourced by a curvaton rolling along an arbitrary energy potential. The key feature of a curvaton potential which deviates from a quadratic one is that the curvaton field with large-scale field fluctuations starts its oscillation at different times at different patches of the universe. Such behaviour contributes to the curvaton energy density perturbations in addition to that sourced directly from the original field fluctuations. We find that such non-trivial conversion processes of the field fluctuations into the density perturbations can lead to strong enhancement/suppression of the density perturbations of the universe, as well as for their non-Gaussianities.

It is worthwhile to investigate curvaton potentials which deviate from simple quadratic ones, both from observational and theoretical reasons: Considering a curvaton whose field fluctuations were generated during the inflationary era (which is the case studied in this paper), in order for the curvaton to produce the density perturbation spectrum which is red-tilted (i.e. with negative spectral index n_s-1) as suggested by latest CMB observations [1–3] without relying on specific inflation mechanisms, the curvaton needs to be located along a potential with negative curvature during inflation. This obviously suggests the curvaton potential to take non-trivial forms. Furthermore, explicit curvaton models constructed in the framework of microscopic physics can naturally possess intricate energy potentials, e.g., curvatons in supersymmetric models [5], a stringy curvaton model in [6] from a D-brane moving along the internal compactified space giving rise to a multi-dimensional periodic curvaton potential. [7] also discusses a string realization of the curvaton, where the potential is a linear combination of exponential terms.

We also apply our general results to the case where the curvaton is a pseudo-Nambu-Goldstone (NG) boson [8] of a broken U(1) symmetry. The periodic curvaton potential necessarily possesses not only minima but also maxima, around which the potential curvature is negative so that the resulting density perturbation spectrum can become red-tilted. We explore the parameter space of NG curvatons producing a red-tilted density perturbation spectrum as suggested by observations, and show that the allowed regions for the inflationary energy scale and the reheating temperature (i.e. when the inflaton decays) are strongly constrained, unless the NG curvaton is located close to the maximum of its potential during inflation. In such hilltop cases, the resulting density perturbations are extremely enhanced, thus relaxing the bounds on the inflation/reheating scales. Non-Gaussianity of the density perturbations also increases in the hilltop limit to values $10 \lesssim f_{\text{NL}} \lesssim 30$ in most part of the allowed parameter window, which will be tested by upcoming CMB measurements. Such mild increase of non-Gaussianity towards the hilltop limit is actually a rather generic feature of hilltop curvatons. The detailed calculations and discussion can be found in Ref. [10].

Let us comment on initial conditions of hilltop curvaton models. So far we have simply assumed that the curvaton sits near the local maximum. This may be justified if the curvaton is charged under some symmetry, which is unbroken during early stage of the inflation or pre-inflationary epoch. This ameliorates the amount of fine-tuning of the initial condition for the hilltop curvaton. On the other hand, in the NG curvaton model, there is no special point in its field space since the curvaton has an approximate shift symmetry. Then, a priori, there is no particular reason to believe that the curvaton

⁷²Email address: fumi@tuhep.phys.tohoku.ac.jp

initially sits near the local maximum. However, we do not know whether the conventional naturalness argument can be really applied to the determination of parameters in the early universe. For example, the parameters may be determined in a similar fashion as in the anthropic argument for explaining the present value of the cosmological constant [9]. Suppose that the prior probability of the initial position of the NG curvaton has a flat distribution in the field space. Assuming that all the other parameters are fixed, it is conceivable that only the universe with the curvaton initially sitting near the local maximum is anthropically selected, if it does not lead to the habitable universe otherwise. For instance, this is expected to be the case, if the inflaton mainly decays into the hidden sector while the curvaton decays into the standard model particles. Thus, the apparent fine-tuning of the initial condition of the NG curvaton based on the conventional naturalness argument may be due to our ignorance of the mechanism about how those parameters are determined.

Both from observational and theoretical reasons, it is important to investigate in detail the conversion process of the curvaton field fluctuations into the resulting density perturbations. In this work, we have provided generic analytic expressions incorporating effects due to non-uniform onset of the curvaton oscillation, which open up new possibilities for the curvaton paradigm.

References

- [1] D. Larson *et al.*, “Seven-Year Wilkinson Microwave Anisotropy Probe (WMAP) Observations: Power Spectra and WMAP-Derived Parameters,” *Astrophys. J. Suppl.* **192**, 16 (2011) [arXiv:1001.4635 [astro-ph.CO]].
- [2] J. Dunkley *et al.*, “The Atacama Cosmology Telescope: Cosmological Parameters from the 2008 Power Spectra,” arXiv:1009.0866 [astro-ph.CO].
- [3] R. Hlozek *et al.*, “The Atacama Cosmology Telescope: a measurement of the primordial power spectrum,” arXiv:1105.4887 [astro-ph.CO].
- [4] D. H. Lyth, “What would we learn by detecting a gravitational wave signal in the cosmic microwave background anisotropy?,” *Phys. Rev. Lett.* **78**, 1861 (1997) [arXiv:hep-ph/9606387].
- [5] K. Hamaguchi, M. Kawasaki, T. Moroi, F. Takahashi, “Curvatons in supersymmetric models,” *Phys. Rev.* **D69**, 063504 (2004). [hep-ph/0308174].
- [6] T. Kobayashi, S. Mukohyama, “Curvatons in Warped Throats,” *JCAP* **0907**, 032 (2009). [arXiv:0905.2835 [hep-th]].
- [7] C. P. Burgess, M. Cicoli, M. Gomez-Reino, F. Quevedo, G. Tasinato and I. Zavala, “Non-standard primordial fluctuations and nongaussianity in string inflation,” *JHEP* **1008**, 045 (2010) [arXiv:1005.4840 [hep-th]].
- [8] K. Dimopoulos, D. H. Lyth, A. Notari, A. Riotto, “The Curvaton as a pseudoNambu-Goldstone boson,” *JHEP* **0307**, 053 (2003). [hep-ph/0304050].
- [9] S. Weinberg, “Anthropic Bound on the Cosmological Constant,” *Phys. Rev. Lett.* **59**, 2607 (1987).
- [10] M. Kawasaki, T. Kobayashi and F. Takahashi, *Phys. Rev. D* **84**, 123506 (2011) [*Phys. Rev. D* **85**, 029905 (2012)] [arXiv:1107.6011 [astro-ph.CO]].

Beyond δN formalism

Atsushi Naruko ^{73(a)}, Yu-ichi Takamizu ^{74(b)} and Misao Sasaki ^{75(a)}

^(a) *Yukawa Institute for Theoretical Physics Kyoto University, Kyoto 606-8502, Japan*

^(b) *Research Institute for Science and Engineering, Waseda University, Tokyo 169-8555, Japan*

Abstract

We develop a theory of nonlinear cosmological perturbations on superhorizon scales for a multi-component scalar field in the context of inflationary cosmology. We employ the ADM formalism and the spatial gradient expansion approach. We provide a formalism to obtain the solution in the multi field case up to the order of ϵ^2 where $\epsilon = 1/(HL)$ is a small parameter representing the ratio of the Hubble radius to the characteristic length scale L of perturbation. This formalism can be applied to the calculation of the superhorizon evolution of the primordial non-Gaussianity beyond the so-called δN formalism, equivalent to $\mathcal{O}(\epsilon^0)$.

1 Introduction

The CMB anisotropy observation by WMAP [1] clearly showed us that the primordial curvature perturbations are nearly scale invariant and their statistics is Gaussian to very high accuracy. This is perfectly in agreement with the predictions of the standard, canonical single-field, slow-roll inflation. Nevertheless, an indication was found in the CMB data as well as in the large scale structure data that there may be a detectable level of non-Gaussianity in the curvature perturbation. Consequently a lot of attention has been paid in recent years to possible non-Gaussian features in the primordial curvature perturbation from inflation. Apparently this direction of research involves nonlinear cosmological perturbations.

There are mainly two approaches to nonlinear cosmological perturbations. One is the standard perturbative approach. This is basically straightforward and can in principle deal with most general situations as long as the perturbation expansion is applicable. But the equations can become very much involved and quite often the physical transparency may be lost.

The other is the spatial gradient expansion approach [2]. In this approach, the field equations are expanded in powers of spatial gradients and hence this is applicable only to perturbations on superhorizon scales. Nevertheless, it has a big advantage that the full nonlinear effects are taken into account at each order of the gradient expansion. Actually, non-Gaussianities in numerous models have been investigated in the last decade using the δN formalism, which corresponds to the lowest order in gradient expansion.

However, there are cases where the δN formalism is not applicable as is reported in [3]. Although we have neglected the spatial gradient terms in the δN formalism, those spatial gradient terms become important if a temporary violation of the slow-roll condition occurs. And hence, we need to further develop the theory of non-linear cosmological perturbation applicable to a wider class of inflation model taking into account the higher order in gradient expansion, which is dubbed the ‘‘Beyond δN formalism’’.

2 Leading order in gradient expansion

Firstly, we revisit the lowest order in gradient expansion and see that the lowest order equations coincide with the background equations. This means once we obtain the background homogeneous solutions, the solution at the lowest order in gradient expansion will be automatically given in terms of those solutions.

We use the ADM metric

$$ds^2 = g_{\mu\nu} dx^\mu dx^\nu = -\alpha^2 dt^2 + \hat{\gamma}_{ij} (dx^i + \beta^i dt)(dx^j + \beta^j dt), \quad (2.1)$$

⁷³Email address: naruko@yukawa.kyoto-u.ac.jp

⁷⁴Email address: ytakamizu@aoni.waseda.jp

⁷⁵Email address: misao@yukawa.kyoto-u.ac.jp

where α , β^i and $\hat{\gamma}_{ij}$ are the lapse function, the shift vector and the spatial three metric respectively. (Greek indices μ, ν run over $\mu, \nu = 0, 1, 2, 3$, and Latin indices $i, j = 1, 2, 3$.) The spatial metric is further decomposed as

$$\hat{\gamma}_{ij} = a^2(t)e^{2\Psi}\gamma_{ij}, \quad (2.2)$$

where $a(t)$ is the scale factor for our local universe and the determinant of γ_{ij} is normalised to be unity. The extrinsic curvature K_{ij} is defined by

$$K_{ij} = \frac{1}{2\alpha} \left(\partial_t \hat{\gamma}_{ij} - \hat{\gamma}_{jk} \hat{D}_i \beta^k - \hat{\gamma}_{ik} \hat{D}_j \beta^k \right), \quad (2.3)$$

where \hat{D} is the covariant derivative compatible with the spatial metric $\hat{\gamma}_{ij}$ and also is decomposed as

$$K_{ij} = a^2(t)e^{2\Psi} \left(\frac{1}{3} K \gamma_{ij} + A_{ij} \right), \quad (2.4)$$

where K and A_{ij} are the trace and traceless components of K_{ij} . It is known that we can assume $A_{ij} = \mathcal{O}(\epsilon^2)$ because A_{ij} rapidly decays on superhorizon scales in the inflationary universe [2]. Hereinafter, using the degree of freedom of the choice of spatial coordinates, we drop the shift vector, which is called as the time-orthogonal threading.

As for matter field, we consider a \mathcal{M} component scalar field whose action is given by

$$S = - \int d^4x \sqrt{-g} \left[\frac{1}{2} g^{\mu\nu} \delta_{IJ} \partial_\mu \phi^I \partial_\nu \phi^J + V(\phi) \right]; \quad (I, J, K = 1, 2, \dots, \mathcal{M}) \quad (2.5)$$

where although we restrict the scalar field metric to a simple one δ_{IJ} , the generalisation will be straightforward. From this action, the energy momentum tensor of this scalar field is obtained

$$T_{\mu\nu} = \delta_{IJ} \partial_\mu \phi^I \partial_\nu \phi^J + \left[-\frac{1}{2} g^{\alpha\beta} \delta_{IJ} \partial_\alpha \phi^I \partial_\beta \phi^J - V(\phi) \right] g_{\mu\nu}. \quad (2.6)$$

Now we write down the Einstein equations. At the leading order in gradient expansion where all spatial gradient terms and A_{ij} are neglected, we have only three equations, two constraints and one evolution equation for K ,

$$K^2 = \frac{3}{2} \delta_{IJ} \partial_\tau \phi^I \partial_\tau \phi^J + 3V, \quad (2.7)$$

$$\partial_i K = \frac{3}{2} \delta_{IJ} \partial_i \phi^I \partial_\tau \phi^J, \quad (2.8)$$

$$\partial_\tau K = \frac{3}{2} \delta_{IJ} \partial_\tau \phi^I \partial_\tau \phi^J. \quad (2.9)$$

where τ is the proper time τ defined as

$$\tau(t, x^i) \equiv \int_{x^i = \text{const.}} dt \alpha(t, x^i), \quad (2.10)$$

On the other hand, the explicit form of K under the time-orthogonal threading is

$$K = -\frac{1}{\alpha} \frac{\partial_t (a^3 e^{3\Psi})}{a^3 e^{3\Psi}} = -3 \frac{\partial_\tau (a e^\Psi)}{a e^\Psi}. \quad (2.11)$$

With the following two identifications,

$$a e^\Psi \Leftrightarrow a, \quad \tau \Leftrightarrow t, \quad (2.12)$$

we can see the correspondence between K and $-3H$ and also the correspondence between the structure of the lowest order equations and that of the background equations. Therefore, if we obtain the background

solution, $\phi(t)|_{\text{background}} = \phi_0(t)$, we can give the solution at the lowest order in gradient expansion just by changing the time coordinate t by τ , $\phi^g(t, x^i)|_{\text{gradient}} = \phi_0(\tau)$. Thus the solution are given by a function of τ by using the background solutions.

In passing, in the standard cosmological perturbation theory, the e -folding number N , $N = -\int dt H(t)$, is more convenient than the cosmic time t . Then, we change the time coordinate and use the e -folding number as the time coordinate below. And also the non-linear e -folding number \mathcal{N} is defined as,

$$\mathcal{N} \equiv -\frac{1}{3} \int_{x^i=\text{const.}} d\tau K(t, x^i) = - \int_{x^i=\text{const.}} dt \left(H + \partial_t \Psi(t, x^i) \right). \quad (2.13)$$

Rewriting equations (2.7) and (2.9) with the time coordinate \mathcal{N} , we again see the correspondence between those equations and the background equations with the time coordinate N .

3 Uniform \mathcal{N} slicing

It is known that, in the case of a single scalar field, the non-linear curvature perturbation on the comoving slicing is conserved on superhorizon scales at the lowest order in gradient expansion. At this order, we can show the coincidence among four common slices using the Einstein equations,

$$\text{comoving} = \text{uniform } K = \text{uniform energy} = \text{uniform } \mathcal{N} \quad (3.1)$$

As we have seen in the last section, the lowest-order solutions are expressed in terms of functions of \mathcal{N} . According to the above coincidence, especially the coincidence between the comoving and uniform \mathcal{N} slices, we can change \mathcal{N} by N in solutions on the comoving slicing.

On the other hand, at the next-leading order in gradient expansion, we need to take into account the spatial gradient terms, which are given spatial derivatives of the lowest order solutions. If the lowest order solutions are given by functions of N , we can easily evaluate them, which is the case in single field models. However, if the above coincidence does not hold, we cannot calculate them any more because the lowest order solutions are given by functions of \mathcal{N} , and \mathcal{N} is inhomogeneous in general, which will happen in multi-field case.

Therefore, the choice of slicing becomes crucial when we go to higher order in gradient expansion and we need to appropriately choose the time coordinate. Especially, in order to evaluate spatial gradient terms, we have to choose the uniform \mathcal{N} slicing. On this slicing, the curvature perturbation does not evolve from Eq (2.13) and is given by a time-independent function $f(x^i)$,

$$\Psi_{\mathcal{N}} = f(x^i). \quad (3.2)$$

4 Beyond δN formalism

In the uniform \mathcal{N} slicing and time-orthogonal threading, the scalar field equation is given as

$$\frac{K}{3} \partial_N \left(\frac{K}{3} \partial_N \phi^I \right) - \frac{K^2}{3} \partial_N \phi^I - \frac{1}{a^2 e^{2\Psi}} \left(D_i - \frac{D_i K}{K} + D_i \Psi \right) D^i \phi^I + \delta^{IJ} \frac{\partial V}{\partial \phi^J} = 0, \quad (4.1)$$

where D is the covariant derivative compatible with the spatial metric γ_{ij} . Using the Einstein equations, we can rewrite Eq (4.1) as,

$$\begin{aligned} & \frac{V}{3} \left(1 - \frac{1}{6} \partial_N \phi_J \partial_N \phi^J \right)^{-1} \partial_N^2 \phi^I - V \partial_N \phi^I + \delta^{IJ} \frac{\partial V}{\partial \phi^J} \\ &= \frac{1}{a^2 e^{2\Psi}} \left[\frac{\partial_N^2 \phi^I}{6 - \partial_N \phi_J \partial_N \phi^J} - 4 \partial_N \phi^I \right] \left(R - 4D^2 \Psi - 2D^i \Psi D_i \Psi \right) \\ & \quad + \frac{1}{a^2 e^{2\Psi}} \left(D_i - \frac{D_i K}{K} + D_i \Psi \right) D^i \phi^I - \frac{1}{a^2 e^{2\Psi}} \left[D_i \Psi D^i \left(\frac{1}{K} \right) - D^2 \left(\frac{1}{K} \right) + D_i \phi_J D^i \phi^J \right] \partial_N \phi^I. \end{aligned} \quad (4.2)$$

The lowest-order equation is obtained when the RHS is neglected because it involves the two spatial derivatives. Although we need to take into account the RHS at this order, it is regarded as the source term. Since they are given by spatial derivatives of the lowest order solutions, we can solve Eq (4.2) by integrating the RHS once the lowest order solutions are obtained. And then, we can express the next-leading order solution of the scalar field as a function of e-folds N , the initial conditions of scalar field and spatial metric,

$$\phi_{\mathcal{N}}^{I(2)}(t, x^i) = \phi_{\mathcal{N}}^{I(2)} \left[N, \phi(t_{\text{ini}}), \gamma_{ij}(t_{\text{ini}}) \right]. \quad (4.3)$$

Inserting this into the Hamiltonian constraint, we can also express the extrinsic curvature, $K^{(2)}$ on the uniform \mathcal{N} slice as a function of e-folds and the initial conditions of ϕ and γ_{ij} as

$$K_{\mathcal{N}}^{(2)} = K_{\mathcal{N}}^{(2)} \left[N, \phi(t_{\text{ini}}), \gamma_{ij}(t_{\text{ini}}) \right]. \quad (4.4)$$

Now we consider the gauge transformation from the uniform \mathcal{N} slice to the uniform K slice and evaluate the curvature perturbation on the uniform K slicing using the solutions on the uniform \mathcal{N} slice. We determine the generator $n \equiv \tilde{N} - N$ from the uniform \mathcal{N} to uniform K slices by Eq (4.4). Since K is uniform on the uniform K slice, n satisfies the following equation

$$K_{\mathcal{N}}^{(2)} \left[N, \phi(t_{\text{ini}}), \gamma_{ij}(t_{\text{ini}}) \right] = K_{\mathcal{N}}^{(2)} \left[N + n, \phi(t_{\text{ini}}) + \delta\phi(t_{\text{ini}}), \gamma_{ij}(t_{\text{ini}}) + \delta\gamma_{ij}(t_{\text{ini}}) \right]. \quad (4.5)$$

By solving Eq (4.5), we can determine the generator n . The gauge transformation for Ψ is given by

$$\tilde{\Psi}^{(2)}(N + n^{(0)}) = \Psi^{(2)} - (\Psi_N^{(0)} + n_N^{(0)})n^{(2)} - \frac{\alpha^{(0)2}}{6a^2 e^{2\Psi^{(0)}} (1 + n_N^{(0)})^2 H^2} \gamma^{ij(0)} \partial_i n^{(0)} \partial_j n^{(0)}. \quad (4.6)$$

Inserting n into Eq (4.6), we obtain the solution of Ψ on the uniform K slice.

At the lowest order in gradient expansion, Ψ can be regarded as the curvature perturbation. However, at the next-leading order, we need to take into account the contribution from the scalar part \mathcal{C} in γ_{ij} , which is subtracted from γ_{ij} as

$$\mathcal{C} = \gamma_{ij} \Big|_{\text{scalar}} \equiv -\frac{3}{4} \Delta^{-1} \left\{ \partial^i \left[e^{-3\Psi^{(0)}} \partial^j (e^{3\Psi^{(0)}} \gamma_{ij}^{(2)}) \right] \right\}, \quad (4.7)$$

By applying the gauge transformation for γ_{ij} ,

$$\tilde{\gamma}_{ij}^{(2)}(N + n^{(0)}) = \gamma_{ij}^{(2)} - \gamma_{ijN}^{(0)} n^{(2)} - \frac{\alpha^2}{a^2 e^{2\Psi} (1 + n_N^{(0)})^2 H^2} \left(n_i^{(0)} n_j^{(0)} - \frac{1}{3} \gamma^{kl} n_k^{(0)} n_l^{(0)} \gamma_{ij} \right), \quad (4.8)$$

we can also evaluate the spatial metric γ_{ij} on the uniform K slice. Finally, by subtracting the \mathcal{C} part from γ_{ij} , we can give the explicit form of the curvature perturbation on the uniform K slice,

$$\mathfrak{R}_K \equiv \Psi_K + \frac{1}{3} \mathcal{C}_K \quad (4.9)$$

References

- [1] WMAP Collaboration, E. Komatsu *et. al.*, *Astrophys. J. Suppl.* **192** (2011) 18.
- [2] D. H. Lyth *et. al.*, *JCAP* **0505** (2005) 004.
- [3] Y. Takamizu *et. al.*, *JCAP* **1006** (2010) 019.

Gradient expansion approach to multi-field inflation

Yuichi Takamizu^{76(a)} Atsushi Naruko^{77(b)} Misao Sasaki^{78(b)}

^(a) *Research Institute for Science and Engineering, Waseda University, Tokyo 169-8555*

^(b) *Yukawa Institute for Theoretical Physics Kyoto University, Kyoto 606-8502*

Abstract

We develop a theory of nonlinear cosmological perturbations on superhorizon scales for a multi-component scalar field with a general kinetic term and a general form of the potential in the context of inflationary cosmology. We employ the ADM formalism and the spatial gradient expansion approach, characterised by $O(\epsilon^2)$, where $\epsilon = 1/(HL)$ is a small parameter representing the ratio of the Hubble radius to the characteristic length scale L of perturbations. We provide a formalism to obtain the solution in the multi field case, if we know a complete set of solution of scalar fields. This formalism can be applied to the calculation of the superhorizon evolution of a primordial non-Gaussianity beyond the so-called δN formalism, equivalent to $O(\epsilon^0)$.

1 Introduction

The PLANCK satellite launched last year is expected to bring us much finer data and it is hoped that non-Gaussianity may actually be detected. As a consequence, non-Gaussianity from inflation has been a focus of much attention in recent years. To study possible origins of non-Gaussianity, the δN -formalism [2–4] turned out to be a powerful tool for the estimation of non-Gaussianity. We investigate a possible origin of non-Gaussianity, namely, non-Gaussianity due to a temporary non-slow roll stage on superhorizon scales. In order to investigate such a case, however, the δN -formalism is not sufficient since it is equivalent to the leading order approximation in the spatial gradient expansion. Thus, to evaluate such situation, it is necessary to develop a nonlinear theory of cosmological perturbations valid up through the next-leading order in the gradient expansion.

2 Single-field case

In this section, we will briefly review the nonlinear theory of cosmological perturbations valid up to $O(\epsilon^2)$ in the spatial gradient expansion for a single scalar field and follow the previous works [5, 6], where ϵ is the ratio of the Hubble length scale $1/H$ to the characteristic length scale of perturbations L , used as a small expansion parameter, $\epsilon \equiv 1/(HL)$, of the superhorizon scales. First of all, we show the main result in our formula for the nonlinear curvature perturbation, $\mathcal{R}_c^{\text{NL}}$,

$$\mathcal{R}_c^{\text{NL}''} + 2\frac{z'}{z}\mathcal{R}_c^{\text{NL}'} + \frac{c_s^2}{4}K^{(2)}[\mathcal{R}_c^{\text{NL}}] = O(\epsilon^4), \quad (2.1)$$

which shows two full-nonlinear effects;

1. Nonlinear variable: $\mathcal{R}_c^{\text{NL}}$ including full-nonlinear curvature perturbation, δN
2. Source term: $K^{(2)}[\mathcal{R}_c^{\text{NL}}]$ is a nonlinear function of curvature perturbations.

In (2.1), the prime denotes conformal time derivative and z is a well-known Mukhanov-Sasaki variable: $z = \frac{a}{H}\sqrt{\frac{\rho+P}{c_s^2}}$. The definition of $\mathcal{R}_c^{\text{NL}}$ will be also seen later, in (2.3) and the source term $K^{(2)}[X]$ is the Ricci scalar of the metric X , respectively. Of course, in the linear limit, it can be reduced to the well-known equation for the curvature perturbation on comoving hypersurfaces; $\mathcal{R}_c^{\text{Lin}''} + 2\frac{z'}{z}\mathcal{R}_c^{\text{Lin}'} - c_s^2\Delta[\mathcal{R}_c^{\text{Lin}}] = 0$.

We will briefly summarize our formula and show the above results in the following. We consider a minimally-coupled single scalar field described by an action of the form $S = \int d^4x\sqrt{-g}P(X, \phi)$, where

⁷⁶Email address: ytakamizu@aoni.waseda.jp

⁷⁷Email address: naruko@yukawa.kyoto-u.ac.jp

⁷⁸Email address: misao@yukawa.kyoto-u.ac.jp

$X = -g^{\mu\nu} \partial_\mu \phi \partial_\nu \phi$. Note that we do not assume the explicit forms of both kinetic term and its potential, that can be given as arbitrary function of $P(X, \phi)$. We adopt the ADM decomposition and employ the gradient expansion. In the ADM decomposition, the metric is expressed as $ds^2 = -\alpha^2 dt^2 + \gamma_{ij}(dx^i + \beta^i dt)(dx^j + \beta^j dt)$, where α is the lapse function, β^i is the shift vector and Latin indices run over 1, 2, 3. We introduce the extrinsic curvature K_{ij} defined by $K_{ij} = -\frac{1}{2\alpha} (\partial_t \gamma_{ij} - D_i \beta_j - D_j \beta_i)$, where D is the covariant derivative compatible with the spatial metric γ_{ij} . As a result, the basic equations are reduced to the first-order equations for the dynamical variables (γ_{ij}, K_{ij}) , with the two constraint equations. We further decompose them as $\gamma_{ij} = a^2 e^{2\zeta} \tilde{\gamma}_{ij}$ and $K_{ij} = a^2 e^{2\zeta} \left(\frac{1}{3} K \tilde{\gamma}_{ij} + \tilde{A}_{ij} \right)$ where $a(t)$ is the scale factor of the background FRW universe and $\det \tilde{\gamma}_{ij} = 1$. Next, we will employ the gradient expansion. In this approach we introduce a flat FRW universe $(a(t), \phi_0(t))$ as a background. As discussed, we consider the perturbations on superhorizon scales, therefore we consider $\epsilon \equiv 1/(HL)$ as a small expansion parameter and systematically expand equations by ϵ . We assume the condition for the gradient expansion; $\partial_t \tilde{\gamma}_{ij} = O(\epsilon^2)$. This corresponds to assuming the absence of any decaying modes at the leading-order in the expansion. This is justified in taking FRW spacetime as a background.

When we focus on a contribution arising from the scalar-type perturbations, we may choose the gauge in which $\tilde{\gamma}_{ij}$ approaches the flat metric. We take the *comoving slicing, time-orthogonal* gauge: $\delta\phi_c(t, x^i) = \beta_c^i(t, x^i) = O(\epsilon^3)$, where $\delta\phi \equiv \phi - \phi_0$ denotes a fluctuation of a scalar field. The subscript c denotes this gauge throughout this paper. Now we turn to the problem of properly defining a nonlinear curvature perturbation to $O(\epsilon^2)$ accuracy. Hereafter we will use the expression \mathcal{R}_c on comoving slices to denote it. Let us consider the linear curvature perturbation which is given as $\mathcal{R}^{\text{Lin}} = \left(H_L^{\text{Lin}} + \frac{H_T^{\text{Lin}}}{3} \right) Y$, where, following the notation in [1], the spatial metric in the linear limit is expressed as $\gamma_{ij} = a^2(\delta_{ij} + 2H_L^{\text{Lin}} Y \delta_{ij} + 2H_T^{\text{Lin}} Y_{ij})$. These expressions in the linear theory correspond to the metric components in our notation as $\zeta = H_L^{\text{Lin}} Y$ and $\tilde{\gamma}_{ij} = \delta_{ij} + 2H_T^{\text{Lin}} Y_{ij}$. Notice that the variable ζ_c reduces to $\mathcal{R}_c^{\text{Lin}}$ at leading-order in the gradient expansion, but not at second-order and it will be also similar to the nonlinear theory. Thus to define a nonlinear generalization of the linear curvature perturbation, we need nonlinear generalizations of $H_L Y$ and $H_T Y$. Our nonlinear ζ is an apparent natural generalization of $H_L^{\text{Lin}} Y$ as $H_L Y = \zeta$. As for $H_T Y$, however, the generalization is non-trivial. It corresponds to the $O(\epsilon^2)$ part of $\tilde{\gamma}_{ij}$. As shown in [6], it can be done by introducing the inverse Laplacian operator Δ^{-1} on the flat background and we defined the nonlinear generalization of $H_T Y$ as

$$H_T Y = E \equiv -\frac{3}{4} \Delta^{-1} \left[\partial^i e^{-3\ell^{(0)}} \partial^j e^{3\ell^{(0)}} (\ln \tilde{\gamma})_{ij} \right]. \quad (2.2)$$

With these definitions of $H_L Y$ and $H_T Y$, we can define the nonlinear curvature perturbation valid up through $O(\epsilon^2)$ as

$$\mathcal{R}_c^{\text{NL}} \equiv \zeta_c + \frac{E_c}{3}. \quad (2.3)$$

It is easy to show that this nonlinear quantity can be reduced to $\mathcal{R}_c^{\text{Lin}}$ in the linear limit. As clear from (2.2), finding $H_T Y$ generally requires a spatially non-local operation, however, in the comoving slicing, time-orthogonal gauge with the asymptotic condition on the spatial coordinates, we find it is possible to obtain the explicit form of $H_T Y$ without any non-local operation as seen in [6]. Finally, we can derive a nonlinear second-order differential equation that $\mathcal{R}_c^{\text{NL}}$ (2.3) satisfies at $O(\epsilon^2)$ accuracy by introducing the conformal time η , defined by $d\eta = dt/a(t)$ and the Mukhanov-Sasaki variable. The result can be reduced to a simple equation of the form (2.1) as a natural extension of the linear version.

3 Multi-field case

We consider a minimally-coupled multi-component scalar field described by an action of the form

$$S = \int d^4x \sqrt{-g} P(X^{IJ}, \phi^K), \quad X^{IJ} \equiv -g^{\mu\nu} \partial_\mu \phi^I \partial_\nu \phi^J \quad (3.1)$$

where I, J and K run over 1, 2, \dots , \mathcal{M} denoting \mathcal{M} -components scalar field. Note that we do not assume the explicit form of both kinetic terms and their potentials, that can be given as arbitrary function of $P(X^{IJ}, \phi^K)$. The stress energy tensor of the scalar fields is obtained by $T_{\mu\nu} = P_{(IJ)} \partial_\mu \phi^I \partial_\nu \phi^J + P g_{\mu\nu}$,

where $P_{(IJ)} = \frac{1}{2} \left(\frac{\partial P}{\partial X^{IJ}} + \frac{\partial P}{\partial X^{JI}} \right)$. Notice that it can not be a perfect fluid form, that is different from a single scalar system. We introduce the proper time τ and its definition is

$$\tau(t, x^i) \equiv \int_{x^i = \text{const.}} dt \alpha(t, x^i) \quad (3.2)$$

since the expression of K at leading-order in gradient expansion with the time-orthogonal threading, $K \equiv -\frac{1}{\alpha} \frac{\partial_t(a^3 \psi^6)}{a^3 \psi^6} = -3 \frac{\partial_\tau(a \psi^2)}{a \psi^2}$, where $\psi = e^{\zeta/2}$, if we associate $a \psi^2$ and τ with a and t respectively, we can check the correspondence between K and $-3H$. Based on these facts, the structure of the above equations is same as that of background equations. Hereafter we assume that we have already solved the background equations and have known their solutions since in general speaking, it is difficult to construct a solution of a multi-scalar system in a analytic treatment. If we know the background solution, $\phi(t)|_{\text{background}} = \phi_0(t)$ using this solution, we can give the solution of leading-order in gradient expansion as $\phi^g(t, x^i)|_{\text{gradient}} = \phi_0(\tau)$.

At the next order, the spatial derivative of the leading solution will appear in the equation and they are regarded as source terms. Then, if we can give the leading order solution, we can solve the equation at any order in gradient expansion just by integrating the source term. In the standard cosmological perturbation, the e-folding number N is often used as a time coordinate, which is defined by $N = -\int dt H(t)$. We can generalise this and define the general e-folding number \mathcal{N} using extrinsic curvature,

$$\mathcal{N} \equiv \frac{1}{3} \int_{x^i = \text{const.}} d\tau K(t, x^i) \quad (3.3)$$

If we also rewrite basic equation using \mathcal{N} as a time coordinate, we can again easily check that the structure of equations exactly coincide with that of background equations using N as a time coordinate.

As for a gauge choice, we consider the uniform K slicing which is taken in multi field case. After inflation, a single component (radiation or matter) will dominate the universe and during those era we can expect the above coincidence. Therefore, uniform K slice will be also one of the interesting slicings. At the leading order in the gradient expansion, the evolution equation for the extrinsic curvature can be used in order to obtain the solution of lapse as

$$\alpha^{(0)} = -\frac{2\dot{H}(t)}{E^{(0)}(t) + P^{(0)}(t, x^i)} + \mathcal{O}(\epsilon^3), \quad (3.4)$$

where the superscript: (0) means the order of the expansion. We can express $\alpha^{(0)}$ as a function of τ using $E^{(0)}$ and $P^{(0)}$. On the other hands, in a single-scalar system, it reads $\alpha^{(0)} = 1$ and it is the main difference between single and multi case. Since we have assumed that we can solve the scalar field equation and express the scalar field as a function of τ , we know the expressions of $E^{(0)}$ and $P^{(0)}$ as a function of τ . This equation means the inhomogeneity of α is related with that of $P^{(0)}$. The time evolution of the curvature perturbation: ψ can be obtained only by the perturbation (inhomogeneity) of the lapse α ,

$$\frac{\partial_t \psi}{\psi} = \frac{H}{2} (\alpha - 1). \quad (3.5)$$

Using the solution of Eq (3.4), we can obtain $\psi^{(0)}$ from (3.5),

$$\log \left[\frac{\psi^{(0)}(t, x^i)}{\psi^{(0)}(t_0, x^i)} \right] = \frac{1}{2} \int_{t_0}^t dt' H(\alpha^{(0)} - 1) + \mathcal{O}(\epsilon^2). \quad (3.6)$$

From Eq (3.5), the inhomogeneity of α derive the evolution of curvature perturbation. This corresponds to the fact that if the non-adiabatic exist, the curvature perturbation is not conserved. We need to resolve Eq (3.4), because the scalar field is the function of proper time, which is given by the time integration of lapse. Notice that there is a big problem. By solving the Einstein equations, we can express the lapse function on uniform K slice as a function of scalar field which is also the function of proper time. From the definition, the proper time is given by the time integral of lapse. We need to solve the following kind of equation,

$$\alpha = f \left[\phi(\tau) \right] = f \left[\phi \left(\int dt \alpha \right) \right] \quad (3.7)$$

It will be almost impossible to solve this equation, at least, in an analytic way. We may need the numerical calculation. In order to get the solution on uniform K slice, we need to solve the Einstein equations on uniform \mathcal{N} slice since on which the scalar field is expressed by a function of t or N not by τ or \mathcal{N} .

Then we have to solve the Einstein equations on uniform \mathcal{N} slice. From Eq (3.3), we can reread the condition of this slice as

$$\alpha(t, x^i)K(t, x^i) = -3H(t) \quad \Leftrightarrow \quad \partial_t \psi(t, x^i) = 0. \quad (3.8)$$

It shows on this slice, curvature perturbation becomes constant which is expressed by a function of x^i only. It is easy to obtain the solution in this gauge. If we have the solution as a function of a cosmic time t or background e -folding number, then we take gauge a transformation from this gauge to uniform expansion slice.

4 Summary

We have developed a theory of nonlinear cosmological perturbations on superhorizon scales for a single and multi-scalar field with a general kinetic term and a general form of the potential to the second-order in the spatial gradient expansion. The solution to this order is necessary to evaluate correctly the final amplitude of the curvature perturbation for models of inflation with a temporary violation of the slow-roll condition. For the single case, we have introduced a reasonable variable that represents the nonlinear curvature perturbation on comoving slices $\mathcal{R}_c^{\text{NL}}$, which reduces to the comoving curvature perturbation $\mathcal{R}_c^{\text{Lin}}$ in the linear limit. Then we have found that $\mathcal{R}_c^{\text{NL}}$ satisfies a nonlinear second-order differential equation, (2.1), as a natural extension of the linear second-order differential equation. Since the evolution of superhorizon curvature perturbations is genuinely due to the $O(\epsilon^2)$ effect, our formulation can be used to calculate the primordial non-Gaussianity beyond the δN formalism which is equivalent to leading order in the gradient expansion.

Different from the single field case, there is a difficulty in obtaining the solution in multi-field case. As we have seen, at the leading order in gradient expansion, the equations take the similar forms as background equations. Then, if we know the solutions of background equations, we can automatically give the solution at leading-order in gradient expansion. But, there is a pitfall in the multi-field case. Fortunately, in the case of single field, we can show the coincidence of slices between comoving, uniform expansion. Thanks to this splendid property, we can change the proper time by cosmic time in the scalar field solution. Then, we can express the metric by scalar field and the function of time. However, in the case of multi field, we cannot show this coincidence of slices. This means, for example, by solving the Einstein equations, we can express the lapse by the function of scalar field, which is also the function of proper time. The proper time is given by the time integration of lapse. To give the solution properly, we need to resolve this equation and it will be almost impossible.

We give the formalism to obtain the solution in the case of multi-field. First, we solve the Einstein equations on uniform e -folding number slice, the solution of scalar fields are given by the function of cosmic time or background e -folding number. Next, we consider the gauge transformation from above slice to uniform expansion slice. Applying the derived gauge transformation rules to the solution on above slice, we can find out the solution on uniform expansion slice.

References

- [1] H. Kodama and M. Sasaki, Prog. Theor. Phys. Suppl. **78** 1 (1984).
- [2] A. A. Starobinsky, JETP Lett. **42**, 152 (1985).
- [3] Y. Nambu and A. Taruya, Class. Quant. Grav. **13**, 705 (1996).
- [4] M. Sasaki and E. D. Stewart, Prog. Theor. Phys. **95**, 71 (1996).
- [5] Y. Takamizu and S. Mukohyama, JCAP **0901**, 013 (2009).
- [6] Y. Takamizu, S. Mukohyama, M. Sasaki and Y. Tanaka, JCAP **1006**, 019 (2010).

Parity Violation in Graviton Non-gaussianity

Jiro Soda^(a) and Hideo Kodama^(b,c) and Masato Nozawa^(b)

^(a) *Department of Physics, Kyoto University, Kyoto, 606-8502, Japan*

^(b) *Theory Center, KEK, Tsukuba 305-0801, Japan*

^(c) *Department of Particles and Nuclear Physics, The Graduate University for Advanced Studies, Tsukuba 305-0801, Japan*

Abstract

We study parity violation in graviton non-gaussianity generated during inflation. We develop a useful formalism to calculate graviton non-gaussianity. Using this formalism, we explicitly calculate the parity violating part of the bispectrum for primordial gravitational waves in the exact de Sitter spacetime and prove that no parity violation appears in the non-gaussianity. We also extend the analysis to slow-roll inflation and find that the parity violation of the bispectrum is proportional to the slow-roll parameter. We argue that parity violating non-gaussianity can be tested by the CMB. Our results are also useful for calculating three-point function of the stress tensor in the non-conformal field theory through the gravity/field theory correspondence.

1 Introduction

The most promising candidate for unifying particle interactions is string theory. String theory predicts a parity-odd gravitational Chern-Simons interactions in the low energy limit. Thus, experimental or observational detections of parity violation in the gravity sector certainly provide us with direct information concerning the UV completion of general relativity or the ultimate unified theory.

A prospective and reliable route to this end is to explore parity violation in relics of inflation in the early universe. In particular, measurements of parity violation in the primordial gravitational waves produced during inflation are expected to bring us valuable information about the Planck scale physics. From this standpoint, it has been intensively discussed how to observe the parity violation in the power spectrum directly using the laser interferometer and indirectly using $\langle TB \rangle$ correlation in the cosmic microwave background (CMB). Remarkably, some speculative gravitational theories with a parity violating term produce significant parity violation in the power spectrum of primordial gravitational waves. Unfortunately, in the conventional inflationary scenario a parity violating term leads to only very small amount of circular polarization in the power spectrum of primordial gravitational waves (see, e.g. [1, 2] and references therein).

In principle, we can also seek parity violation in higher-order correlation functions [3, 4]. Since the power spectrum and the higher-order statistics are often sensitive to different kinds of parity violating interactions, they may have different correlations with other revealing statistical features. For example, in a recent paper of Maldacena and Pimentel, they discussed graviton non-gaussianity in the exact de Sitter spacetime and found that the pattern of parity violating bispectrum is severely constrained by the conformal invariance [5]. One might then be tempted to deduce that their result implies the unsuppressed parity-violation in the bispectrum. We argue that this is not immediately obvious since they have not calculated observable quantities explicitly. In this short article, we develop a new tool to analyze graviton correlation functions and show that parity violation does *not* show up in the case of the exact de Sitter spacetime. A more detailed discussion can be found in [6].

2 A new formalism for graviton correlators

With the aid of the helicity basis, we present a useful method to evaluate graviton non-gaussianity generated by a parity-violating Weyl cubic term. Tensor perturbations on the Friedmann-Lemaître-

Robertson-Walker (FLRW) universe are given by

$$ds^2 = a^2(\eta) [-d\eta^2 + (\delta_{ij} + h_{ij}) dx^i dx^j], \quad h_{ii} = \partial_i h_{ij} = 0. \quad (2.1)$$

The gravitational action and the corresponding equations of motion are given by

$$S = \frac{M_{\text{pl}}^2}{8} \int d\eta d^3x a^2 (h'_{ij} h'_{ij} - \partial_k h_{ij} \partial_k h_{ij}), \quad h''_{ij} + 2 \frac{a'}{a} h'_{ij} - \Delta h_{ij} = 0. \quad (2.2)$$

We have two physical degrees of freedom for tensor perturbations which are characterized by the symmetric polarization tensors. Since we are interested in the presence/absence of parity-violation, it is of use to expand in a helicity basis $e_{ij}^{(\pm)}(\mathbf{k})$ satisfying

$$e_{ii}^{(s)}(\mathbf{k}) = 0, \quad k_j e_{ij}^{(s)}(\mathbf{k}) = 0, \quad \epsilon_{ijl} \frac{\partial}{\partial x^l} [e_{mj}^{(s)}(\mathbf{k}) e^{i\mathbf{k}\cdot\mathbf{x}}] = s k e_{im}^{(s)}(\mathbf{k}) e^{i\mathbf{k}\cdot\mathbf{x}}. \quad (2.3)$$

The index $s = \pm$ specifies two helicity states. We choose the normalization and the phase of polarization tensors in such a way that

$$e_{ij}^{(s)}(\mathbf{k}) e_{ij}^{*(s')}(\mathbf{k}) = \delta_{ss'}, \quad e_{ij}^{*(s)}(\mathbf{k}) = e_{ij}^{(-s)}(\mathbf{k}) = e_{ij}^{(s)}(-\mathbf{k}). \quad (2.4)$$

In this article we focus on the pure gravity parity-violating sector where the action is composed of the Weyl tensor $W_{\mu\nu\rho\sigma}$ and its Hodge dual. Since the quadratic term is topological, the leading term comes from the cubic interactions

$$S_{\text{PV}} = -b \int d\eta d^3x \sqrt{-g} \epsilon^{\mu\nu\lambda\rho} W_{\mu\nu}{}^{\alpha\beta} W_{\alpha\beta}{}^{\gamma\delta} W_{\lambda\rho\gamma\delta}. \quad (2.5)$$

Since the FLRW universe is conformally flat, this term does not affect the equations of motion (2.2) and the power spectrum. They could contribute to the non-gaussianity, which we now turn to discuss.

In order to simplify computations, introduce a new variable γ_{ij} as $\gamma'_{ij} := a h'_{ij}$, in terms of which we notice a useful relation $W^\mu{}_{\nu\lambda\rho}(h) = a^{-1} W^\mu{}_{\nu\lambda\rho}(\gamma)|_{\text{Minkowski}}$. We define

$$\gamma_{ij}^\pm := \frac{1}{2} (\gamma'_{ij} \mp i \epsilon_{jkl} \partial_l \gamma_{ik}), \quad (2.6)$$

which is symmetric, transverse and traceless. We find that a simple relation $(W^\pm)^3 = 64a^{-9}(\gamma^\pm)^3$ holds irrespective of the expanding history of the universe. Here $W^\pm = W \pm i \star W$ are the complexified self-dual and anti-self-dual Weyl tensors $\star W^\pm = \mp i W^\pm$. In the flat spacetime, the solutions γ_{ij} with two helicity states of fixed $|\mathbf{k}|$ form a unitary representation of three-dimensional Euclid group [7]. This representation decomposes into two irreducible representations, which are nothing but helicity states described by γ_{ij}^\pm . The same is true for the de Sitter spacetime. In [5], another useful method—a spinor helicity formalism—was invented.

Utilizing above, we can write the parity-violating cubic action (2.5) in a general FLRW background in terms of these new perturbation variables γ_{ij}^\pm as

$$S_{\text{PV}} = 8ib \int d\eta d^3x a^{-5} [(\gamma_{ij}^+) (\gamma_{jk}^+) (\gamma_{ki}^+) - (\gamma_{ij}^-) (\gamma_{jk}^-) (\gamma_{ki}^-)]. \quad (2.7)$$

From this, we can read off the interaction Hamiltonian $H_{\text{PV}}(\eta)$ as

$$H_{\text{PV}} = -\frac{8ib}{(2\pi)^6} a^{-5} \int d^3k_1 d^3k_2 d^3k_3 \delta(\mathbf{k}_1 + \mathbf{k}_2 + \mathbf{k}_3) \\ \times [(\gamma_{ij}^+(\eta, \mathbf{k}_1))' (\gamma_{jk}^+(\eta, \mathbf{k}_2))' (\gamma_{ki}^+(\eta, \mathbf{k}_3))' - (\gamma_{ij}^-(\eta, \mathbf{k}_1))' (\gamma_{jk}^-(\eta, \mathbf{k}_2))' (\gamma_{ki}^-(\eta, \mathbf{k}_3))']. \quad (2.8)$$

We should emphasize that $\gamma_{ij} = \gamma_{ij}^+ + \gamma_{ij}^-$ does not represent gravitational waves in Minkowski spacetime but an auxiliary field. From the definition $\gamma'_{ij} := a h'_{ij}$, we can give an explicit mode expansion expression

for γ_{ij}^\pm as:

$$\begin{aligned} (\gamma_{ij}^\pm)' = \int \frac{d^3\mathbf{k}}{(2\pi)^{3/2} M_{\text{pl}} \sqrt{2k}} \sum_{s=\pm} \left[e_{ij}^{(s)}(\mathbf{k}) (\partial_\eta \mp isk) (au'_k(\eta)) a_s(\mathbf{k}) \right. \\ \left. + e_{ij}^{*(s)}(-\mathbf{k}) (\partial_\eta \mp isk) (au'_k(\eta))^* a_s^\dagger(-\mathbf{k}) \right] e^{i\mathbf{k}\cdot\mathbf{x}}, \end{aligned} \quad (2.9)$$

wher u_k is the mode function. The main utility of our formalism is that a concise expression (2.7) considerably simplifies calculations of bispectrum in a general expanding universe.

3 Parity violation

Using the formulation summarized in the previous section, we compute the graviton non-gaussianity. Let us first consider the simplest case in which the back ground spacetime is pure de Sitter. The mode function in a de Sitter background reads $u_k = Hk^{-1} (1 + ik\eta) e^{-ik\eta}$, where H is a constant Hubble parameter. It is worth noting here the following property

$$\gamma_{ij}^\pm(\eta, \mathbf{k}) = (\gamma_{ij}^\mp(\eta, -\mathbf{k}))^\dagger. \quad (3.1)$$

This traces back to the property of helicity basis (2.4) and plays a key rôle in proving no parity violation in the exactly de Sitter universe.

Introducing the projection operators $\Pi_{ij,kl}^\pm(\mathbf{p}) = e_{ij}^{(\pm)}(\mathbf{p}) e_{kl}^{*(\pm)}(\mathbf{p})$, we can compute the bispectrum as

$$\begin{aligned} \langle \gamma_{i_1 j_1}^\pm(0, \mathbf{p}_1) \gamma_{i_2 j_2}^\pm(0, \mathbf{p}_2) \gamma_{i_3 j_3}^\pm(0, \mathbf{p}_3) \rangle \\ = \pm 384 i b M_{\text{pl}}^{-6} H^5 (2\pi)^3 p_1^2 p_2^2 p_3^2 \delta(\mathbf{p}_1 + \mathbf{p}_2 + \mathbf{p}_3) \frac{5!}{(p_1 + p_2 + p_3)^6} \\ \times \left[\Pi_{i_1 j_1, k_1 l_1}^\pm(\mathbf{p}_1) \Pi_{i_2 j_2, l_2 m}^\pm(\mathbf{p}_2) \Pi_{i_3 j_3, m k}^\pm(\mathbf{p}_3) + \Pi_{i_1 j_1, k_1 l_1}^\pm(\mathbf{p}_1) \Pi_{i_2 j_2, l_2 m}^\pm(\mathbf{p}_2) \Pi_{i_3 j_3, m k}^\pm(\mathbf{p}_3) \right]. \end{aligned} \quad (3.2)$$

Note that the mixed terms $\langle \gamma^+ \gamma^+ \gamma^- \rangle$ and $\langle \gamma^- \gamma^- \gamma^+ \rangle$ vanish as expected. These results are in agreement with those obtained by Maldacena and Pimentel [5].

Even if these correlators are nonvanishing, this does not immediately imply that the parity violation can be observed. This is due to the fact that neither $\langle (\gamma^+)^3 \rangle$ nor $\langle (\gamma^-)^3 \rangle$ themselves are direct observables. To see this more concretely, let us define the right-handed and left-handed circular polarizations by

$$h^R := h_{ij} e_{ij}^{*(+)}, \quad h^L := h_{ij} e_{ij}^{*(-)}, \quad (3.3)$$

respectively. A possible observable quantity in which a parity violation is encoded is their difference $\langle (h^R)^3 \rangle - \langle (h^L)^3 \rangle$. Using the relation $h_{ij}(0, \mathbf{k}) = -Hk^{-2} [\gamma_{ij}^+(0, \mathbf{k}) + \gamma_{ij}^-(0, \mathbf{k})]$, It is straightforward to verify that

$$\langle h^R(0, \mathbf{p}_1) h^R(0, \mathbf{p}_2) h^R(0, \mathbf{p}_3) \rangle = 0, \quad \langle h^L(0, \mathbf{p}_1) h^L(0, \mathbf{p}_2) h^L(0, \mathbf{p}_3) \rangle = 0. \quad (3.4)$$

It turns out that there exists no parity violation in a pure de Sitter universe.

Next, let us analyze the case in which the universe undergoes a slowly rolling inflationary expansion. Since the variable γ_{ij}^\pm does not correspond to the helicity decomposition when the spacetime departs from de Sitter, we can expect the appearance of parity violation.

When we expand every term up to the first order in the slow roll parameter $\epsilon := -\dot{H}/H^2$ where H is now defined by $H := \dot{a}/a$, the possible sources of parity violation stem from the following three parts: (i) change in the asymptotic mode function, (ii) change of γ_{ij}^\pm and (iii) change of the cosmic expansion. Putting all contributions together, we find that the contribution from (i) is higher-order. Hence the main cause of parity violation is due to (ii) and (iii). An elementary but lengthy calculation reveals that

$$\begin{aligned} h^L(0, \mathbf{p}_1) h^L(0, \mathbf{p}_2) h^L(0, \mathbf{p}_3) \rangle = -\langle h^R(0, \mathbf{p}_1) h^R(0, \mathbf{p}_2) h^R(0, \mathbf{p}_3) \rangle \\ = 6! (2\pi)^4 \epsilon (bH_*^2) (H_*/M_{\text{pl}})^6 \delta^{(3)}(\mathbf{p}) \frac{(p_1 + p_2 - p_3)(p_2 + p_3 - p_1)(p_3 + p_1 - p_2)}{p^3 (p_1 p_2 p_3)^2}, \end{aligned} \quad (3.5)$$

where $\mathbf{p} = \mathbf{p}_1 + \mathbf{p}_2 + \mathbf{p}_3$ is the total momentum. Hence parity violation shows up in the bispectrum and its magnitude is proportional to the slow roll parameter. It is interesting to observe that the bispectrum of curvature perturbations is also proportional to the slow-roll parameter in the conventional single inflationary scenario [3].

It should be stressed that this kind of parity violation can be observed in the CMB through the three-point correlators $\langle TTB \rangle$, etc. In the conventional slow-roll inflationary scenario, the amplitude might be too small to be detected in near future. However, in the non-conventional scenarios, we might have much larger parity violation.

4 Conclusions

We have developed a useful formalism to evaluate graviton correlation functions. The present formalism enables us to calculate higher-order parity violating correlation functions rather straightforwardly. As an illustrating application of this formalism, we studied parity violation in the early universe through non-gaussianity of gravitons and found that that no parity violation arises in the bispectrum for the exact de Sitter background. This does not mean that the $W^2 \star W$ term fails to produce any parity violating interaction. We have shown that the parity violation is not encoded in the graviton non-gaussianity. The situation is different when the spacetime departs from the exact de Sitter. In slow-roll inflationary case we have found parity violation in the graviton bispectrum proportional to the slow roll parameter. This is attributable to the fact that the boost generator in general FLRW spacetime is not the isometry of the background, thence both of the helicity components would mix except for de Sitter.

We also discussed that parity violation in the bispectrum can be observed e.g., in the $\langle TTB \rangle$ correlation in the CMB [8]. It might be also possible to detect the signature of parity violation through direct observations of primordial gravitational waves using a space interferometer observatory.

It is known that exact de Sitter correlation function is related to correlation function of stress tensor in the conformal field theory through analytic continuation [3]. Hence, the graviton non-gaussianity has an interesting application. Similarly, our results would be useful for calculating three-point functions of stress tensor in the non-conformal field theory using gravity/field theory correspondence [9].

References

- [1] M. Satoh, S. Kanno and J. Soda, Phys. Rev. D **77**, 023526 (2008) [arXiv:0706.3585 [astro-ph]]; M. Satoh and J. Soda, JCAP **0809**, 019 (2008) [arXiv:0806.4594 [astro-ph]]; M. Satoh, JCAP **1011**, 024 (2010) [arXiv:1008.2724 [astro-ph.CO]].
- [2] L. Sorbo, JCAP **1106**, 003 (2011). [arXiv:1101.1525 [astro-ph.CO]].
- [3] J. M. Maldacena, JHEP **0305**, 013 (2003) [arXiv:astro-ph/0210603].
- [4] M. Kamionkowski and T. Souradeep, arXiv:1010.4304 [astro-ph.CO].
- [5] J. M. Maldacena and G. L. Pimentel, arXiv:1104.2846 [hep-th].
- [6] J. Soda, H. Kodama and M. Nozawa, JHEP **1108**, 067 (2011) [arXiv:1106.3228 [hep-th]].
- [7] A. Higuchi, Class. Quant. Grav. **8**, 2005 (1991).
- [8] M. Shiraishi, D. Nitta and S. Yokoyama, Prog. Theor. Phys. **126**, 937 (2011) [arXiv:1108.0175 [astro-ph.CO]].
- [9] P. McFadden and K. Skenderis, JCAP **1106**, 030 (2011) arXiv:1104.3894 [hep-th]; A. Bzowski, P. McFadden and K. Skenderis, arXiv:1112.1967 [hep-th].

The estimation of black-hole masses in distant radio galaxies

Maragrita Khabibullina⁷⁹

Kazan (Volga region) federal university, Kremlevskaja Str., 18, Russia

Abstract

We have estimated the masses of the central supermassive black holes of 2442 radio galaxies from a catalog. Mass estimates based on optical photometry and radio data are compared. Relationships between the mass of the central black hole M_p^{bh} and the redshift z_p are constructed for both wavelength ranges (radio and optic). Upper-envelope cubic regression fits are obtained using the maximum estimates of the black-hole masses. The optical and radio upper envelopes show similar behavior, and have very similar peaks in position, $z_p \simeq 1.9$ and amplitude, $\log M_p^{bh} = 9.4$. This is consistent with a model in which the growth of the supermassive black holes is self-regulating, with this redshift corresponding to the epoch when the accretion-flow phase begins to end and the nuclear activity falls off.

1 Introduction

Radio galaxies, which are among the most powerful cosmic objects, allow us to study the evolution of matter and the dynamics of the expansion of the Universe at different cosmological epochs. Investigations of these radio sources are linked to several cosmological tests, which permit estimating the parameters and evolutionary characteristics of the Universe. Radio galaxies are identified with giant elliptical galaxies.

One of the central questions in studies of distant radio galaxies (redshifts $z > 0.3$) is the origin and growth rate of supermassive black holes (SMBHs) in their nuclei. The discovery of radio galaxies and quasars at high redshifts has raised the need to explain the rapid formation of SMBHs in early epochs of the evolution of the Universe.

An important result obtained from measurements of black-hole masses in nearby galaxies is the existence of an appreciable correlation between the mass of the central black hole and the mass of the bulge of the host galaxy, which gives rise to correlations between the black-hole mass and the luminosity of the bulge [1],[2] and between the black-hole mass and the stellar velocity dispersion σ (e.g. [3]-[6]). The existence of these correlations can provide constraints on the evolution of AGNs, and can be used to test whether AGNs precisely follow these relations or not.

Here, we verify two dependences of the black-hole masses on the radio and optical luminosities that are used in the literature in studies of radio galaxies. We calculated the luminosities using optical data in the R filter and 5-GHz radio flux densities. We assumed a Λ CDM cosmology with $H_0 = 71 \text{ km s}^{-1} \text{ Mpc}^{-1}$, $\Omega_M = 0.27$, and $\Omega_\Lambda = 0.73$. We used a catalog of distant radio galaxies with spectroscopic redshifts $z > 0.3$, which were selected based on data from the largest available databases [7]-[9].

2 Estimating the SMBH Masses

2.1 Optical Data

To estimate the SMBH mass, we used the relationship between the black-hole masses and R absolute magnitudes ($M_{bh} - M_R$) from [6], which was obtained via an analysis of the magnitudes and stellar velocities in AGNs: $\log(\frac{M_{bh}}{M_\odot}) = -0.50(\pm 0.02)M_R - 2.27(\pm 0.48)$, where M_R is the absolute R magnitude of the bulge, assuming that the bulge of an elliptical galaxy essentially represents the entire galaxy.

Since R observations are not available for all the catalog radio galaxies, we estimated the R luminosities of a number of objects based on data in other filters using the database of galactic spectral-energy distributions (SEDs) [10]. Photometric data were used to estimate the ages of the radio galaxies, assuming

⁷⁹Email address: rita@sao.ru

that their SEDs corresponded to the SEDs of elliptical galaxies. We determined the R magnitude using the redshift and the age of the corresponding model SED track. We used the GISSEL model data [11], which contains synthetic spectra of elliptical galaxies for ages from 200 million years to 14 billion years, as the basic library of tracks. This library can be accessed both in the HyperZ package [12] and at the site <http://sed.sao.ru>.

The luminosity was calculated using the formula [13]: $L = 4\pi F d_L^2(z)$, where F is the measured flux, $d_L(z) = (1+z) \int_0^z \frac{dz'}{H(z')}$, is the luminosity distance, and $H(z) = H_0[\Omega_R(1+z)^4 + \Omega_m(1+z)^3 - (\Omega_0 - 1)(1+z)^2 + \Omega_\Lambda]^{1/2}$ is the Hubble parameter. The resulting luminosity (more precisely, absolute magnitude) was used to estimate the masses of the central black holes of the galaxies.

2.2 Radio Data

To calculate the estimated black-hole masses based on radio data, we used the relationship between the radio luminosity and black-hole mass ($P_{5\text{GHz}} - M_{bh}$) from [14]: $P_{5\text{GHz}} \propto \left(\frac{M_{bh}}{M_\odot}\right)^{2.2 \div 3.0}$, where $P_{5\text{GHz}}$ is the total power at 5 GHz. Our calculations used the formula: $P_{5\text{GHz}} \propto \left(\frac{M_{bh}}{M_\odot}\right)^{3.0}$. We calculated the radio power using the standard formula [13]: $P_\nu = 4\pi d_L^2 S\left(\frac{\nu}{(1+z)}\right)(1+z)^{-1}$, where $S\left(\frac{\nu}{(1+z)}\right)$ is the source flux density at frequency ν taking into account the redshift and d_L is the photometric distance. The value $S\left(\frac{\nu}{(1+z)}\right)$ was determined from the continuum radio spectrum of each source, constructed via fitting with a standard set of functions. We used the spg program [15] of the RATAN-600 continuum data-reduction system for this purpose. For radio galaxies with measurements at only one frequency, we took the spectral index to be equal to the median value for our sample [7] at 1.4 GHz ($\alpha_{med} = -0.63$).

3 Discussion

In spite of the two-peaked form of the mass distribution, the radio data provide a smaller scatter in the redshift distribution (Fig.1). Figure shows the least-squares regression fits and upper envelopes for both types of data.

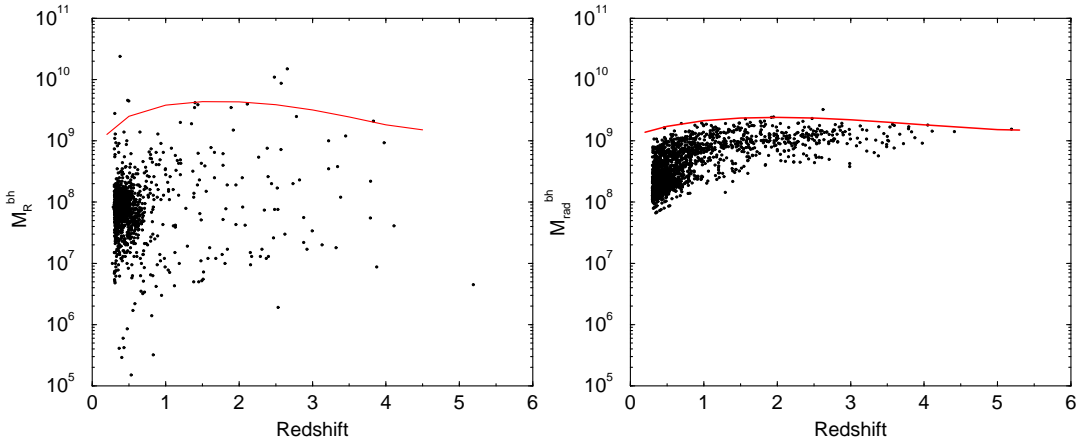


Figure 1: Plots of black-hole mass versus redshift for the radio galaxies, based on R optical data (left) and 5-GHz radio data (right). Regression fits were constructed for the mean and maximum black-hole masses in intervals $\Delta z = 0.5$.

The range of black-hole masses derived using the radio data is two orders of magnitude smaller than that for the optically derived masses. The mean radio masses in individual redshift intervals ($\Delta z = 0.5$) are higher than the corresponding optical masses.

In spite of the difference in the dispersion of the mass estimates, the positions and amplitudes of the maxima of both upper envelopes are similar: the peak is at $z_p = 1.78$ and $\log M_p^{bh} = 9.67$ for the optical data, and at $z_p = 1.92$ and $\log M_p^{bh} = 9.38$ for the radio data. The location of the maxima in the redshift range $1.5 < z < 2$ could be associated with some sort of systematic effect reflecting real physical processes. This range of z corresponds to an epoch of massive "ignition" of radio sources as a result of mergers between galaxies in galaxy clusters. In this case, due to selection effects, we will most likely detect objects with the maximum luminosity, which means those with the maximum estimated black-hole masses, in this range.

Note that this result obtained for our list of radio galaxies is consistent with the results of [16], where a sample of broad-line quasars from the SDSS was considered. Kelly et al. [16] found that the peak number density of SMBHs in broad-line quasars occurs at $z \sim 2$. The location of the mass-distribution peak at $z \sim 2$ is consistent with a self-regulating growth model for the SMBHs, with this being the epoch when the end of the accretion-flow phase begins and the nuclear activity starts to fall off.

The $M_{opt}^{bh} - M_{rad}^{bh}$ relation indicates the region in which the two methods used to estimate the masses of the SMBHs are statistically applicable, and shows the amount of scatter obtained using these methods (Fig.2).

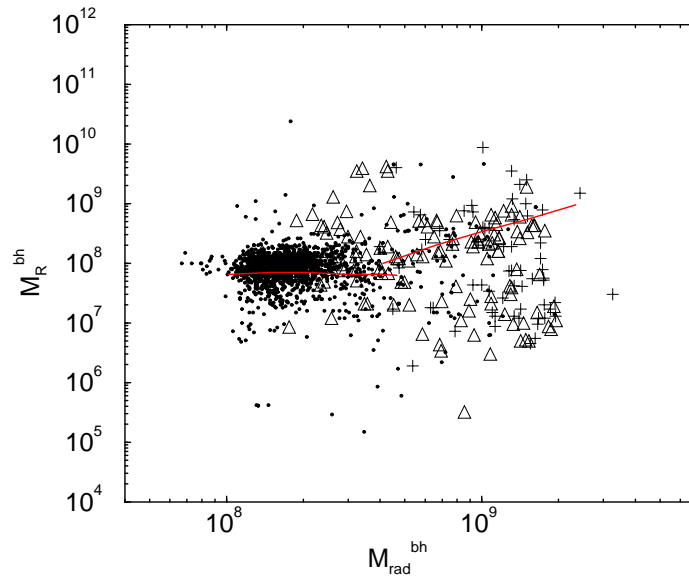


Figure 2: Plot of M_{opt}^{bh} versus M_{rad}^{bh} for R-band and 5-GHz data fits were obtained for two regions where the points are concentrated. Data for radio galaxies from different redshift ranges are denoted with different symbols: $0.3 \leq z < 0.7$ (points), $0.7 \leq z < 1.5$ (crosses), and $1.5 \leq z$ (triangles).

Three regions of clustering can be distinguished on this plot. The data for radio galaxies from different redshift ranges are shown by different symbols: $0.3 \leq z < 0.7$ (points), $0.7 \leq z < 1.5$ (crosses), and $1.5 \leq z$ (triangles). The high concentration of points in the left part of the diagram is due to the large number of comparatively nearby radio galaxies in the SDSS, for which relatively similar black hole masses were obtained. Nearly all the radio galaxies in the sample have $M_{opt}^{bh} \leq M_{rad}^{bh}$. For a second group, many of which are distant radio galaxies with $z \geq 1.5$ we observe a correlation between the two mass estimates for the central objects. The objects in the lower right part of Fig.2 have low optical and high radio mass estimates. These low estimates from the region of the lower envelope on the left $M^{bh}(z)$ diagram in Fig.1 and the corresponding estimates in the right diagram may be associated with non-elliptical subclasses of radio galaxies.

We can distinguish several selection effects that are inevitable when estimating the central black-hole masses, even when care is taken in selecting galaxies according to their optical and radio properties. Their manifestation can explain differences between results obtained using different methods to determine the central black-hole masses. These selection effects include the following:

1) more distant objects tend to be more powerful; i.e., a sample of distant objects contains, on average, galaxies with higher black-hole masses;

2) although the sample has been cleaned of objects with the properties of quasars (such as broad H α emission), some such objects with relatively weak lines may remain in the subsample of comparatively nearby ($z < 0.7$) sources;

3) the SDSS objects in our catalog should not include Seyfert 2 galaxies with narrow lines; in spite of their radio emission, these galaxies have low ratios of their bolometric to Eddington luminosities (see, e.g., [17]);

4) the presence of evolutionary effects that are strongly manifest in the radio, such as the fact that some radio galaxies may be observed in early phases of their activity, and that galaxies with central black holes of the same mass may have radio fluxes differing by an order of magnitude;

5) some comparatively nearby objects whose peak activity in the radio has passed have black-hole mass estimates derived from velocity dispersions calibrated based on the radio fluxes; in this case, the use of dependences for more distant galaxies can lead to overestimation of the black-hole masses.

Nevertheless, the similarity of the behaviors of the mass upper envelopes (Fig. 1) suggests that these estimates are trustworthy for objects with the highest luminosities (close to the Eddington values). The comparatively small scatter of the radio masses for various z makes it possible to use this diagram to estimate masses with a mean accuracy of less than an order of magnitude, or even half an order of magnitude at $z > 1.5$.

Acknowledgments This research was had made use of the NASA/IPAC Extragalactic Database. It was had also used the CATS database of radio astronomy catalogs and the FADPS system for radio-astronomical data reduction.. This work was supported by the Program of State Support for Leading Scientific Schools of the Russian Federation (School of S.M. Khaikin) and the Russian Foundation for Basic Research (projects 09-02-00298, 09-02-92659-IND, 08-02-00486).

Also I'd like to thank the Organizing Committee for the financial support.

References

- [1] J. Magorrian et al., *Astron. J.* **115**, 2285 (1998).
- [2] J. Kormendy and K. Gebhardt, *AIP Conf. Proc.* **586**, 363 (2001).
- [3] L. Ferrarese and D. Merritt, *Astrophys. J.* **539**, L9 (2000).
- [4] K. Gebhardt, R. Bender, G. Bower, et al., *Astrophys. J.* **539**, L13 (2000).
- [5] T.R. Lauer, S.M. Faber, D. Richstone, et al., *Astrophys. J.* **662**, 808 (2007).
- [6] J. Kormendy and R. Bender, *Astrophys. J.* **691**, 142 (2009).
- [7] M.L. Khabibullina and O.V. Verkhodanov, *Astrophys. Bull.* **64**, 123 (2009).
- [8] M.L. Khabibullina and O.V. Verkhodanov, *Astrophys. Bull.* **64**, 276 (2009).
- [9] M.L. Khabibullina and O.V. Verkhodanov, *Astrophys. Bull.* **64**, 340 (2009).
- [10] O.V. Verkhodanov, A.I. Kopylov, O.P. Zhelenkova, et al., *Astron. Astrophys. Trans.* **19**, 663 (2000).
- [11] G. Bruzual and S. Charlot, *Astrophys. J.* **405**, 538 (1993).
- [12] M. Bolzonella, J.-M. Miralles, and R. Pello, *Astron. Astrophys.* **363**, 476 (2000).
- [13] C. Lang, *Astrophysical Formulae* (Springer, New York, 1999; Mir, Moscow, 1978).
- [14] A. Franceschini, S. Vercellone, and A.C. Fabian, *Mon. Not. R. Astron. Soc.* **297**, 817 (1998).
- [15] O.V. Verkhodanov, in *Proceedings of the 27th Radioastron. Conference on Modern Radioastronomy (IPARAN, S.-Peterburg, 1997)*, vol. 1, p. 322..
- [16] B.C. Kelly, M. Vestergaard, Xi. Fan, et al., *Astrophys J.* **719**, 1315 (2010).
- [17] Yu Lu, Ting-Gui Wang, Xiao-Bo Dong, and Hong-Yan Zhou, *Mon. Not. R. Astron. Soc.* **1761**, 404 (2010).

Oscillation phenomena in the disk around the massive black hole Sagittarius A*

Makoto Miyoshi^(a), Zhi-Qiang Shen^(b), Tomoaki Oyama^(a), Rohta Takahashi^(c), Yoshiaki. Kato^(a)

^(a)*National Astronomical Observatory of Japan, Mitaka, Tokyo, 181-8588, Japan.*

^(b)*Shanghai Astronomical Observatory, 80 Nandan Road, Shanghai, 200030, China.*

^(c)*Department of Natural and Physical Sciences, Tomakomai National College of Technology, Tomakomai 059-1257, Japan.*

Abstract

The existence of black holes has been definitely established while zooming-in the relativistic region is still in difficulty though promising in near future. Sagittarius A* (Sgr A*), the most convincing massive black hole at the Galactic center, shows short time flares with quasi-periodic oscillations (QPO) with $P = 17, 22, \& 33$ min in near-infrared and X-ray regions originated from near the central black hole. Here we report the detection of radio QPOs with structure changes using the Very Long Baseline Array (VLBA) at 43 GHz. We found conspicuous patterned changes of the structure with $P = 16.8, 22.2, 31.4, \& 56.4$ min, roughly in a 3 : 4 : 6 : 10 ratio. The first two periods show a rotating one-arm structure, while the $P = 31.4$ min shows a rotating 3-arm structure, as if viewed edge-on. At the central $50 \mu\text{as}$ the $P = 56.4$ min period shows a double amplitude variation of those in its surroundings. Spatial distributions of the oscillation periods indicate that the disk of Sgr A* is presumably almost edge-on, rotating around an axis with $PA = -10^\circ$. The observed VLBI images of Sgr A* remain several features of the black hole accretion disk of Sgr A* in spite of being obscured and broadened by scattering of surrounding plasma. Details of our research are described in [1].

Our VLBA observations at 43 GHz were performed from 9 : 30 to 16 : 30(UT) on 2004 March 8th, 37 ~ 44 hours just after a millimeter wave flare of Sgr A* detected with the Nobeyama Millimeter Array. We did the standard amplitude calibrations using antenna gains and system temperatures with opacity corrections in AIPS (NRAO). At the last stage of the data calibrations we applied solutions of amplitude and phase from self-calibration with an image model of the average size and shape of Sgr A* at 43 GHz (single elliptical Gaussian with full width at half maximum of $712 \mu\text{as} \times 407 \mu\text{as}$, $PA = 79.8^\circ$ with 1 Jy in flux density). This manner substantially reduced the effect of atmospheric variations on the observed visibilities.

We investigated the spatial distributions of oscillations in flux density with two independent methods. The first one is the comparisons of power spectra of time variations of intensities in 209 small rectangles areas of the image. We produced 360 snapshot maps from 5-minute integrations with a starting time increment of 30 seconds. Each map area is 3 mas (east-west) \times 6 mas (north-south), divided into 1024×2048 cells, produced from CLEAN with a loop gain of 0.005 down to 10 mJy level. The same restoring beam of 0.15 mas (east-west) \times 0.4 mas (north-south) was applied to each map. We then measured flux density variation in each small rectangle. The time variations show small pitches similar to, but not the same as, those of other rectangles. We then calculated their power spectra using a maximum entropy method (MEM). We found confinements of the powers in spatial distributions of some periods around $P = 12.9, 17.2, 30.1, \text{ and } 55.8$ min. Shallower confinements appear around $P = 128.4, \text{ and } 268$ min though they are under-sampled. This method, however, tends to be affected by differences of u-v sampling between snapshot maps.

We hence used a new method, slit-modulation-imaging (SMI)[2] which is a way of examining the existence of the periodic structural change with an assuming period and almost free from u-v sampling differences. We tested around these confined periods of $P = 12.9, 17.2, 30.1, \text{ and } 55.8$ min, adding with the $P = 22.2$ min detected at X ray flares. Except for $P = 12.9$ min, we found conspicuous periodic change patterns from $P = 16.8, 22.2, 31.4, \text{ and } 56.4$ min which are roughly commensurable in a 3 : 4 : 6 : 10 ratio (see the figure).

In the case of $P = 16.8$ min, the peak is in the west of the image at the 1st and the 2nd phase frames, but shifts eastward, stays in the east at the 3rd, 4th and 5th phase frames, and after that, moves westward again. In the case of $P = 22.2$ min, at the 1st phase frame the peak is in the east, moves towards the west at the 2nd phase frame, shifts further west at the 4th and 5th phase frames, and then moves back towards the east from the 6th to 8th phase frames. Namely, in the $P = 16.8$ and 22.2 min structure changes, the brightest position oscillates

mostly in the east-west direction with the respective period, which looks like a one-arm structure ($m = 1$) motion viewed edge-on. Assuming the motions to be projected circular ones, we found the $P = 16.8$ min orbit is 0.18 mas while that of the $P = 22.2$ min is 0.15 mas in diameter, both are tilted with $PA = 82^\circ$ nearly the same position angle as the major axis of the average Sgr A* image at 43 GHz. The viewing angles are almost edge-on, 87.0° ($P = 16.8$ min) and 87.7° ($P = 22.2$ min) respectively.

In the $P = 31.4$ min change, one or two peaks appear in each phase frames. The numbers of peaks are $2 \rightarrow 1 \rightarrow 2 \rightarrow 2 \rightarrow 1 \rightarrow 2 \rightarrow 1 \rightarrow 1$ with phase frame change. At first glance this seems random, but a relation exists. The sum of peak numbers in the two SMI maps just half a period away from each other is always three, which can be explained by the existence of a three-arm pattern ($m = 3$) with evenly separation angle rotating with the period, which we view edge-on.

In the $P = 56.4$ min change, one peak appears during a half period (the 6th to 8th, and 1st phase frames) and two peaks appear during the last half period from the 2nd to the 5th phase frame. This is due to the amplitude of variation at the central 50 μ as being twice as large as those of the surroundings. One peak appears when the central part becomes bright, and two peaks, one on the east and one on the west, appear when the central part darkens. Unlike other periods, the $P = 56.4$ min component seems concentrated and excited at the radius close to the black hole where the relativistic effect are not negligible, and hence it can be a key to distinguishing the origin of QPOs.

The detected pattern changes are not from noise effects: we simulated changes using faked data with noise levels showing the comparable amplitude fluctuations with those of real visibility data. SMI images from faked data show larger variations in not east-west but south-north direction that the spatial resolution is worse, while those from the observations show the opposite tendency. From the faked data, changes appeared in the image but none of the periodic regular patterns could be found. Also the faked data showed no coincident occurrence between spreading size minima and amplitude peaks in the spectra of the whole 209 area. Further, the observed periodic changes of real data basically did not disappear in SMI-maps with shorter total integration times (195 min) while different changes appeared from faked data.

The radio QPOs reported here have a delay of 1.5 days from the millimeter wave flare, and the distributions extended to 100 R_s in apparent diameter while the QPOs in NIR and X-ray are just at the flaring time and estimated to occur around a marginally stable orbit (MSO). The flaring events at MSO would vibrate the whole system to excite fundamental disk oscillation modes, which would last for several days.

There are features that cannot be explained as Keplerian motions directly governed by centripetal force, but that are easily interpretable as disk oscillation features. First, The counter rotations occurred simultaneously between the $P = 16.8$ min and $P = 22.2$ min periods, which is difficult to be explained by a single body motion like hot spot models. Second, the orbit of the shorter period $P = 16.8$ min is larger than that of the $P = 22.2$ min, which cannot be realized by a Keplerian motion.

If QPOs originate in a strong gravity field where the relativistic effect plays an important role, the periods of QPOs should depend on the mass and the spin of a massive black hole. Recent theories of disk seismology predict that peak frequencies of QPOs can be scaled by a mass of central black holes as an analogy to QPOs in black hole X-ray binaries (BXB). For example, in GRO J1655-40, a peak frequency of high frequency QPOs is about $3 \times 10^2 (6.0 - 6.6 M_\odot / M_{\text{BH}})$ Hz (where M_\odot is a solar mass), with the result that a corresponding peak frequency using the mass of Sgr A* derived from the orbital motions of surrounding stars ($3.6 \pm 0.3 \times 10^6 M_\odot$) is about 5.1×10^{-4} Hz ($P = 32$ min), which is one of our findings. Detailed analysis with the obtained four QPO periods and wave-warp resonant oscillation model predicts the spin of Sgr A* to be 0.44 ± 0.08 and the black hole mass to be $(4.2 \pm 0.4) \times 10^6 M_\odot$ [3].

The apparent angular size of 0.1 mas corresponds to $10.4 R_s$ ($1 R_s$ is Schwarzschild radius) assuming the Galactic center distance to be 7.6 kpc, which scale give us that the orbital velocities of bright peak positions are $v_{P=16.8\text{min}} = 2.1 c$ at $8.8 R_s$ and $v_{P=22.2\text{min}} = 1.4 c$ at $7.4 R_s$, both are superluminal, but can be explained as follows.

It is well-known that the VLBI images of Sgr A* are obscured and broadened by the scatterings of surrounding plasma. If we consider the broadening ratio of $2.6 \sim 3.0$ at 43 GHz by scattering, and the magnifying ratio ~ 1.23 by self-gravitational lensing effect at $3 R_s$, the apparent 0.1 mas observed at 43 GHz is equal to 2.8 to 3.3 R_s in the intrinsic image of Sgr A*. Taking into these effects, we find that $v'_{P=16.8\text{min}} = 0.43 c$ at $2.7 R_s$ and $v'_{P=22.2\text{min}} = 0.68 c$ at $2.3 R_s$, which velocities are comparable to the Keplerian velocities at $r = 2 - 4 R_s$ from a black hole.

The amplitude of the QPOs were 22 mJy ($P = 16.8$ min), 24mJy ($P = 22.2$ min), 25mJy ($P = 31.4$ min), and 20 mJy ($P = 56.4$ min) respectively, the total reached 90 mJy, nearly 10 % of the constant flux density component of the image (= 980 mJy). Such structural changes will cause fluctuations in fringe phase, rate and amplitude. Existence of oscillations with periods shorter than the whole observing time will be one of the reasons why the VLBI imaging of Sgr A* is difficult so far. However at the same time, the detection of these periodic

pattern changes means the obscured radio image of Sgr A* still bears the imprint of the intrinsic figure. The VLBA observations of Sgr A*, together with oscillation analysis, will provide us a unique chance to investigate the strong gravity field around the massive black hole Sgr A* with order of R_s resolutions.

References

- [1] Miyoshi, M., Shen, Z.-Q., Oyama, T., Takahashi, R., & Kato, Y., *PASJ*, **63**, 1093-1116 (2011)
- [2] Miyoshi, M., *PASJ*, **60**, 1371-1386 (2008)
- [3] Kato, Y., Miyoshi, M., Takahashi, R., Negoro, H., & Matsumoto, R. *MNRAS*, **402**, L74-L78 (2010)

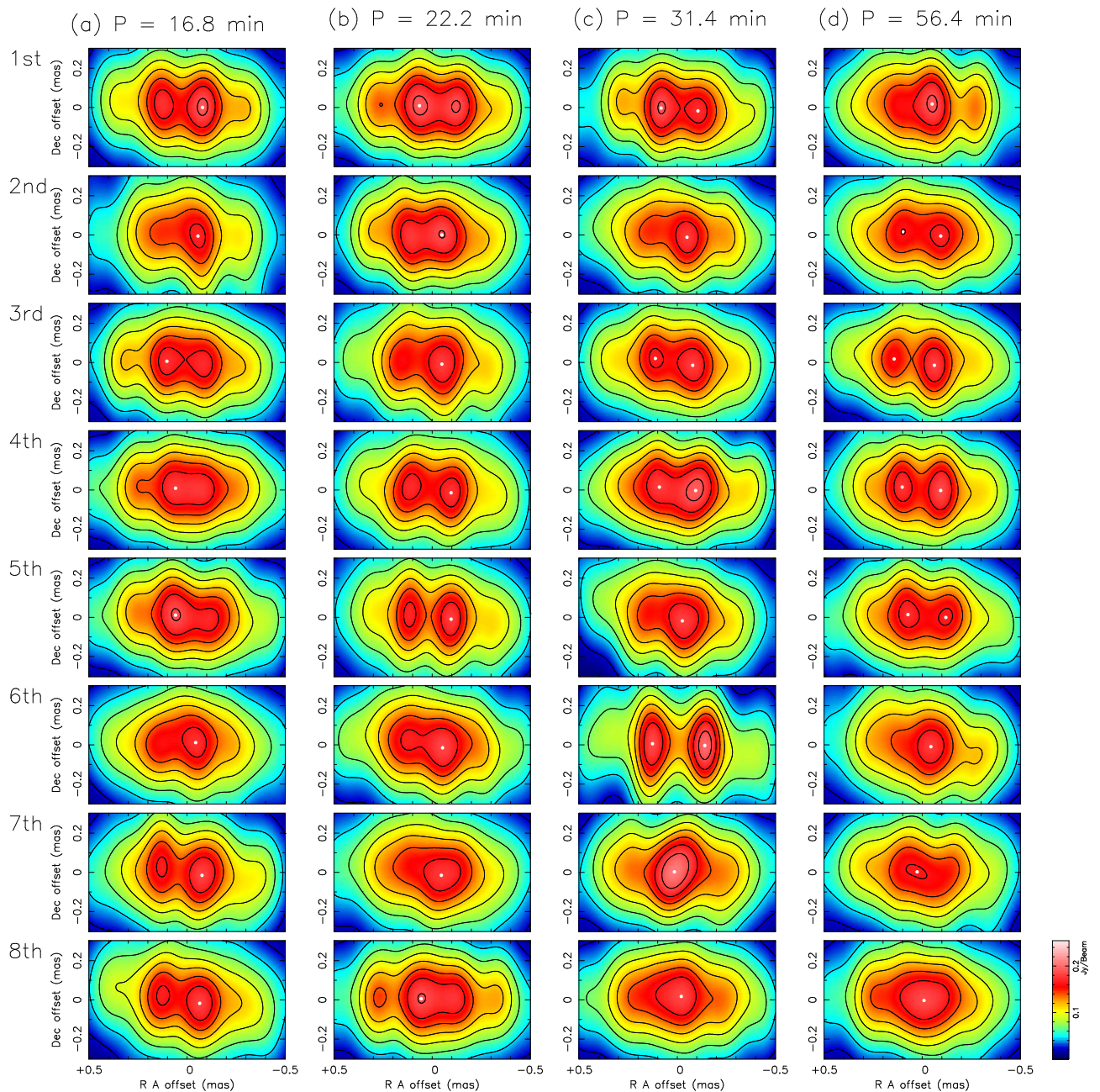


Figure 1: The slit-modulation-imaging (SMI) maps with the 4 periods $P = 16.8(a)$, $22.2(b)$, $31.4(c)$, and 56.4 min (d). The 8 maps show the images in phase frame series with respective periods. The white filled circles mark the intensity peak position in each map. In $P = 31.4$ & 56.4 min, second peaks are also marked with circles. Total amplitudes of respective periods are 22 mJy ($P = 16.8$ min), 24 mJy ($P = 22.2$ min), 24 mJy ($P = 31.4$ min), and 20 mJy ($P = 56.4$ min), which obtained by Fourier transform.

Effect of cosmological constant on light deflection

Hideyoshi Arakida^{80(a)}

^(a) *Iwate University, Ueda, Morioka 020-8550, Japan*

Abstract

We revisit the role of the cosmological constant Λ in the deflection of light by means of the Schwarzschild-de Sitter metric. In order to obtain the deflection angle α , the time transfer function approach is adopted, instead of solving the photon geodesic equation which is frequently used. We show that the cosmological constant does appear in the deflection angle and it diminishes light bending due to the mass of the central body M . However in contrast to previous results, for example Rindler and Ishak (Phys. Rev. D. 76:043006 2007), the leading order effect due to the cosmological constant does not couple with the mass of the central body M .

1 Introduction

It is popularly considered that the cosmological constant Λ or dark energy in a more general has the highest potential for explaining the observed accelerating expansion of Universe. However, its details are still far from clear; therefore this hypothesis must be verified in terms of not only cosmological observations but also other astronomical/astrophysical measurements.

Among such efforts, it is the most straightforward way to investigate the role of cosmological constant Λ in the classical tests of general relativity, such as the perihelion advance of planetary orbits and the bending of light rays. Thus far, it was found that the cosmological constant Λ contributes to the perihelion shift in principle even though it is presently difficult to detect because of its very small effect (See [1–3] and the references therein).

On the other hand, it has been believed for a long time that the cosmological constant Λ is not related to the motion of photons, namely light deflection, since the second-order geodesic equation of a photon does not contain Λ . However recently, Rindler and Ishak [4] pointed out that Λ does affect the bending of light by means of Schwarzschild-de Sitter or Kottler metric and the invariant formula for the cosine. Subsequently many authors argued its appearance in many different ways and the generality of these advocated the appearance of Λ in the deflection angle α . Nevertheless at the moment, it seems a conclusion has not yet been reached; for instance whether the leading order effect due to Λ is coupled with the mass of the central body M or not. See [5] for a review and also [6–11].

As we look at the circumstances, the origin of confusion, e.g., the appearance/disappearance of Λ or the coupling/uncoupling with the mass of the central body M , is essentially attributable to using the standard geodesic equation of photon to describe light deflection due to Λ because Λ does not appear. Therefore it is worthy to revisit this problem in terms of another theoretical approach.

In this paper, we will revisit the role of the cosmological constant Λ in terms of the time transfer function recently proposed in [12, 13], which is originally related to Synge’s world function $\Omega(x_A, x_B)$ and enables us to circumvent the integration of the null geodesic equation.

2 Outline of the time transfer function

Before calculating the light deflection due to the cosmological constant Λ , let us briefly summarize the time transfer function method presented in [12, 13].

Synge’s world function is defined by [14],

$$\Omega(x_A, x_B) \equiv \frac{1}{2}(\lambda_B - \lambda_A) \int_{\lambda_A}^{\lambda_B} g_{\mu\nu} \frac{dx^\mu}{d\lambda} \frac{dx^\nu}{d\lambda} d\lambda \quad (2.1)$$

where $g_{\mu\nu}$ is a metric tensor of spacetime, $x_A = (x_A^0 = ct_A, x_A^i = \vec{x}_A)$ and $x_B = (x_B^0 = ct_B, x_B^i = \vec{x}_B)$ are the coordinates of the two end points A and B , respectively, on the geodesic world-line, and λ is the affine parameter. Then, the world function $\Omega(x_A, x_B)$ is defined as the half length of the world-line between A and B .

⁸⁰Email address: arakida@iwate-u.ac.jp

It is generally difficult to acquire the world function concretely. Nonetheless, in the case of Minkowskian flat spacetime, the world function is obtained easily using the parameter equation $x(\lambda) = (x_B - x_A)\lambda + x_A$ and by setting $\lambda_A = 0$ and $\lambda_B = 1$ [12, 14],

$$\Omega^{(0)}(x_A, x_B) = \frac{1}{2}\eta_{\mu\nu}(x_B^\mu - x_A^\mu)(x_B^\nu - x_A^\nu) \quad (2.2)$$

where x^μ ($\mu = 0, 1, 2, 3$) are the Minkowskian coordinates with respect to the Minkowski metric $\eta_{\mu\nu} = \text{diag}(-1, 1, 1, 1)$. For the null geodesic, the world function $\Omega(x_A, x_B)$ satisfies the condition,

$$\Omega(x_A, x_B) = 0 \quad (2.3)$$

because $ds^2 = 0$. Hence, from (2.2) and (2.3), the travel time between A and B , i.e., $t_B - t_A$, in the Minkowski spacetime becomes,

$$c^2(t_B - t_A)^2 = \delta_{ij}(x_B^i - x_A^i)(x_B^j - x_A^j) = R_{AB}^2 \quad (2.4)$$

where δ_{ij} is Kronecker's delta symbol. The time transfer function starts from (2.4), and the weak-field approximation is developed recursively with respect to the gravitational constant G .

If the metric has the form, $g_{\mu\nu} = \eta_{\mu\nu} + h_{\mu\nu}$, $|h_{\mu\nu}| \ll 1$ (here $h_{\mu\nu}$ is a perturbation to $\eta_{\mu\nu}$), the time transfer functions that give the travel time of the light ray are formally expressed as follows:

$$t_B - t_A = \mathcal{T}_e(t_A, \vec{x}_A, \vec{x}_B) = \frac{1}{c}[R_{AB} + \Delta_e(t_A, \vec{x}_A, \vec{x}_B)] \quad (2.5)$$

$$= \mathcal{T}_r(\vec{x}_A, t_B, \vec{x}_B) = \frac{1}{c}[R_{AB} + \Delta_r(\vec{x}_A, t_B, \vec{x}_B)] \quad (2.6)$$

where $\mathcal{T}_e(t_A, \vec{x}_A, \vec{x}_B)$ is the emission time transfer function for the spatial coordinates \vec{x}_A, \vec{x}_B and signal emission time t_A , $\mathcal{T}_r(\vec{x}_A, t_B, \vec{x}_B)$ is the reception time transfer function for the spatial coordinates \vec{x}_A, \vec{x}_B and signal reception time t_B , $R_{AB} = |\vec{x}_B - \vec{x}_A|$, and Δ_e and Δ_r are the emission time delay function and reception time delay function, respectively. Δ_e and Δ_r characterize the gravitational time delay. In (2.5) and (2.6), R_{AB} comes from (2.4). Henceforth, A denotes the emission and B denotes the reception.

In general, the time transfer function depends on either the emission time t_A or reception time t_B and this feature is applied to obtaining the gravitational time delay in the McVittie spacetime [15]. However if the spacetime is static, the first order formulae reduce to

$$\Delta^{(1)}(\vec{x}_A, \vec{x}_B) = \frac{R_{AB}}{2} \int_0^1 \left[g_{(1)}^{00} - 2N_{AB}^i g_{(1)}^{0i} + N_{AB}^i N_{AB}^j g_{(1)}^{ij} \right] d\mu. \quad (2.7)$$

We use Eq. (2.7) in this paper and integration of Eq. (2.7) is carried out along the parameter equation $\vec{x}(\mu) = \vec{x}_A + \mu(\vec{x}_B - \vec{x}_A)$. It is found that from Eq. (2.7) in this method, the time delay is calculated with the remaining form of the metric $g_{\mu\nu}$.

Once the time transfer function \mathcal{T} is determined, the direction of the light ray can be obtained by

$$(k_0)_A = 1, \quad (k_i)_A = c \frac{\partial \mathcal{T}}{\partial x_A^i}, \quad (k_0)_B = 1, \quad (k_i)_B = -c \frac{\partial \mathcal{T}}{\partial x_B^i}. \quad (2.8)$$

3 Effect of the cosmological constant on light deflection

Now, let us revisit the contribution of Λ to the light deflection based on the time transfer function. To this end, we adopt the Schwarzschild-de Sitter or Kottler metric [16],

$$\begin{aligned} ds^2 &= - \left(1 - \frac{r_g}{r} - \frac{\Lambda}{3} r^2 \right) c^2 dt^2 + \left(1 - \frac{r_g}{r} - \frac{\Lambda}{3} r^2 \right)^{-1} dr^2 + r^2 d\Omega^2 \\ &= - \left(1 - \frac{r_g}{r} - \frac{\Lambda}{3} r^2 \right) c^2 dt^2 + \left(1 + \frac{r_g}{r} + \frac{\Lambda}{3} r^2 + \mathcal{O}(r_g^2, \Lambda^2) \right) dr^2 + r^2 d\Omega^2 \end{aligned} \quad (3.1)$$

where $r_g = 2GM/c^2$ is the Schwarzschild radius, $d\Omega^2 = d\theta^2 + \sin^2 \theta d\phi^2$, and the dr^2 component is linearized from the first line to the second.

It is beneficial to transform the spherical coordinates into rectangular ones since it is easy to set up the rectilinear line as the first approximation of the light path. By the coordinate transformation, $x = r \sin \theta \cos \phi$, $y = r \sin \theta \sin \phi$, $z = r \cos \theta$ Eq. (3.1) is rewritten as (see for example [17]),

$$ds^2 = - \left(1 - \frac{r_g}{r} - \frac{\Lambda}{3} r^2 \right) c^2 dt^2 + \left[\delta_{ij} + \left(\frac{r_g}{r} + \frac{\Lambda}{3} r^2 \right) \frac{x^i x^j}{r^2} + \mathcal{O}(r_g^2, \Lambda^2) \right] dx^i dx^j. \quad (3.2)$$

For the sake of simplicity, let us set up the coordinate system in such a way that the light path used to integrate the actual light path is parallel to x -axis and the motion of the photon is restricted to the x - y plane. Hence, Eq. (3.2) becomes

$$ds^2 = -\left(1 - \frac{r_g}{r} - \frac{\Lambda}{3}r^2\right) c^2 dt^2 + \left[1 + \left(\frac{r_g}{r} + \frac{\Lambda}{3}r^2\right) \frac{x^2}{r^2} + \mathcal{O}(r_g^2, \Lambda^2)\right] dx^2 \quad (3.3)$$

in which $r = \sqrt{x^2 + b^2}$ and b corresponds to the impact factor. Using Eq. (2.7), the time transfer function can be readily calculated as

$$\mathcal{T} = \frac{1}{c} (R_{AB} + \Delta\mathcal{T}_{\text{GR}} + \Delta\mathcal{T}_{\Lambda}), \quad (3.4)$$

$$\Delta\mathcal{T}_{\text{GR}} = \frac{GM}{c^2} \left[2 \ln \frac{x_B + \sqrt{x_B^2 + b^2}}{x_A + \sqrt{x_A^2 + b^2}} - \left(\frac{x_B}{\sqrt{x_B^2 + b^2}} - \frac{x_A}{\sqrt{x_A^2 + b^2}} \right) \right], \quad (3.5)$$

$$\Delta\mathcal{T}_{\Lambda} = \frac{\Lambda}{18} [2(x_B^3 - x_A^3) + 3b^2(x_B - x_A)]. \quad (3.6)$$

From Eqs. (3.4), (3.5) and (3.6), the direction of the light at the emission point A and the reception point B are computed using Eq. (2.8), noting that $y_A = y_B = b$ in our case. Moreover, since the differences between the directions of the actual light $(k_i)_A, (k_i)_B$ at the emission and reception points A, B and those of the straight line used in the integration are small such that

$$\tan \psi_A \simeq \psi_A = \frac{k_{bA}}{k_{xA}}, \quad \tan \psi_B \simeq \psi_B = \frac{k_{bB}}{k_{xB}}. \quad (3.7)$$

From the fact that $\mathcal{T}(\vec{x}_A, \vec{x}_B)$ is the two-point function at A and B based on Synge's world function $\Omega(x_A, x_B)$, the deflection angle observed at reception point B is equivalent to ψ_B . Thus, the deflection angle α is given by

$$\alpha \equiv \psi_B = \alpha_{\text{GR}} + \alpha_{\Lambda} + \mathcal{O}(r_g^2, \Lambda^2), \quad (3.8)$$

$$\alpha_{\text{GR}} = \frac{GMb}{c^2} \left(\frac{2}{x_B \sqrt{x_B^2 + b^2} + x_B^2 + b^2} - \frac{2}{x_A \sqrt{x_A^2 + b^2} + x_A^2 + b^2} + \frac{x_B}{\sqrt{x_B^2 + b^2}^3} - \frac{x_A}{\sqrt{x_A^2 + b^2}^3} \right), \quad (3.9)$$

$$\alpha_{\Lambda} = \frac{\Lambda}{3} b(x_B - x_A). \quad (3.10)$$

Eq. (3.9) can be rewritten as

$$\alpha_{\text{GR}} = \frac{GM}{c^2 b} [2(\cos \phi_A - \cos \phi_B) + \sin^2 \phi_A \cos \phi_A - \sin^2 \phi_B \cos \phi_B] \quad (3.11)$$

where $\sin \phi_A = b/\sqrt{x_A^2 + b^2}$, $\cos \phi_A = x_A/\sqrt{x_A^2 + b^2}$, $\sin \phi_B = b/\sqrt{x_B^2 + b^2}$, $\cos \phi_B = x_B/\sqrt{x_B^2 + b^2}$. For $\phi_A \rightarrow \pi$ (the emission point A is located at $-\infty$ along x axis), $\phi_B \rightarrow 0$ (the reception point B is located at $+\infty$ along x axis),

$$\alpha_{\text{GR}} = -\frac{4GM}{c^2 b}. \quad (3.12)$$

Eq. (3.12) means that the incoming light ray is bent in the negative direction with respect to the ϕ coordinate. On the other hand, from Eq. (3.10) the light deflection due to Λ occurs in the positive sense in reference to the ϕ coordinate. Therefore if we choose the sign of the deflection angle α in such a way that the deflection angle from the mass of the central body M takes a positive value, then α_{GR} and α_{Λ} can be rewritten as

$$\alpha_{\text{GR}} = \frac{GM}{c^2 b} [2(\cos \phi_B - \cos \phi_A) + \sin^2 \phi_B \cos \phi_B - \sin^2 \phi_A \cos \phi_A], \quad (3.13)$$

$$\alpha_{\Lambda} = -\frac{\Lambda}{3} b(x_B - x_A). \quad (3.14)$$

As mentioned above, Eq. (3.13) recovers the deflection angle obtained in the standard manner and the bending angle due to Λ in Eq. (3.14) seems to be equivalent to the result (see [5] again and the references therein)

$$\alpha_{\Lambda} = -\frac{\Lambda}{3} R r_b \quad (3.15)$$

where R corresponds to the impact factor b in Eq. (3.14) and r_b is the boundary radius of Schwarzschild-de Sitter/Kottler vacuole which can be regarded as $x_B - x_A$ in Eq. (3.14). Therefore in terms of the calculation based on the time transfer function, we conclude that the leading order term of the light deflection due to Λ is not coupled with the mass of the central body M .

References

- [1] A. W. Kerr, J. C. Hauck, B. Mashhoon, *Class. Quant. Grav.*, **20**, 2727 (2003).
- [2] W. Rindler, *Relativity: Special, General, and Cosmological* (2nd Ed.), Oxford Univ. Press, New York (2006).
- [3] L. Iorio, *Adv. Astron.*, id. 268647 (2008).
- [4] W. Rindler, M. Ishak, *Phys. Rev. D*, **76**, id. 043006 (2007).
- [5] M. Ishak, W. Rindler, *Gen. Rel. Grav.*, **42**, 2247 (2010).
- [6] M. Park, *Phys. Rev. D*, **78**, id. 023014 (2008).
- [7] I. B. Khriplovich, A. A. Pomeransky, *Int. J. Mod. Phys. D*, **17**, 2255 (2008).
- [8] F. Simpson, J. A. Peacock, *Heavens, MNRAS*, **402**, 2009 (2010).
- [9] A. Bhadra, S. Biswas, K. Sarkar, *Phys. Rev. D*, **82**, id. 063003 (2010).
- [10] H. Miraghaei, M. Nouri-Zonoz, *Gen. Rel. Grav.* **42**, 2947 (2010)
- [11] T. Biressa, J. A. de Freitas Pacheco, *Gen. Rel. Grav.*, **43**, 2649 (2011).
- [12] C. Le Poncin-Lafitte, B. Linet, P. Teyssandier, *Class. Quant. Grav.*, **21**, 4463 (2004).
- [13] P. Teyssandier, C. Le Poncin-Lafitte, *Class. Quant. Grav.*, **25**, 145020 (2008).
- [14] J. L. Synge, *Relativity: The General Theory*, North-Holland, Amsterdam (1964).
- [15] H. Arakida, *Gen. Rel. Grav.*, **43**, 2127 (2011).
- [16] F. Kottler, *Annalen. Phys.*, **361**, 401 (1918).
- [17] V. A. Brumberg, *Essential Relativistic Celestial Mechanics*, Adam Hilger, Bristol, Philadelphia and New York (1991).

Numerical simulation of quantum gravity

Takayuki Hikichi^{81(a)}, Yasusada Nambu^{82(a)}, Hiromi Saida^{83(b)}

^(a)*Department of Physics, Nagoya University, Chikusa-ku, Nagoya, 464-8602, Japan*

^(b)*Department of Physics, Daido University, Minami-ku, Nagoya, 457-8530, Japan*

Abstract

We performed a nonperturbative sum over geometries in (2+1)-dimensional causal dynamical triangulation through the help of Monte Carlo simulations, where the spacial topologies are assumed to be S^2 for simplicity. We also studied a case where the spacial topologies are T^2 . The numerical results imply these emerging quantum universes can be described by solutions of the Einstein equation at macroscopic scales. We also found that spectral dimensions of these spacetime are roughly 3.

1 Introduction

Causal dynamical triangulation (CDT) is a discrete regularization method for gravitational path integral [1]. In CDT, Lorentzian spacetime geometry is approximated by a simplicial manifold. The simplicial manifold is constructed by gluing “simplex” in such a way so as to have global proper-time foliation (cf. fig. 1). The simplex is the Lorentzian tetrahedron (in 2+1-dim) in which some edges are fixed to be space-like and the others are time-like (cf. fig. 2). The squared length of space-like links is $l_s^2 = a^2$ and the squared length of time-like links is $l_t^2 = -\alpha a^2$ ($\alpha > 0$), where α is a relative scaling of space-like and time-like links. Because the spacial topology change induces causality violation, we forbid the spacial topology to change in time. Then, in (2+1)-dimension the spacetime topology may be written as a product $M = I \times \Sigma^{(2)}$, where I denotes an interval and $\Sigma^{(2)}$ denotes two dimensional surfaces. For convenience, we chose $\Sigma^{(2)} = S^2$ or T^2 , where S^2 is a two-sphere and T^2 is a torus. Moreover, we set periodic boundary conditions in the time direction. Therefore, we assume spacetime topology to be $M = S^1 \times S^2$ or $S^1 \times T^2$.

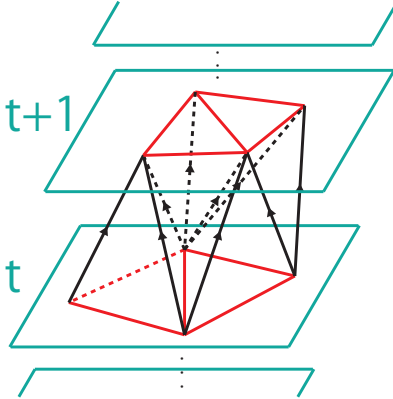


Figure 1: Global proper-time foliation in 3-dimension.

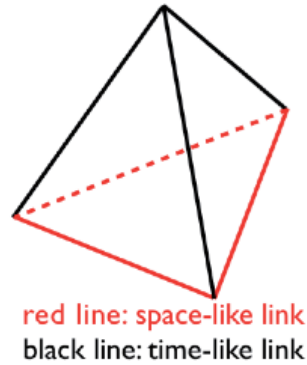


Figure 2: A 3-dimensional simplex with space-like links and time-like links.

In CDT the continuum path integral for gravity is represented by a sum over all discrete spacetime geometries T .

$$Z_L = \int \mathcal{D}g e^{iS_L[g]} \rightarrow Z_L = \sum_T e^{iS_L^{\text{Regge}}[T]}, \quad (1.1)$$

⁸¹Email address: hikichi@gravity.phys.nagoya-u.ac.jp

⁸²Email address: nambu@gravity.phys.nagoya-u.ac.jp

⁸³Email address: saida@daido-it.ac.jp

where S_L denotes the Einstein Hilbert action and S_L^{Regge} denotes that of discretized version. In an analogy with quantum field theory, one might hope to define the gravitational path integral by rotating to the Euclidean signature [2]

$$\alpha \rightarrow -\alpha, \quad S_E^{\text{Regge}} := -iS_L^{\text{Regge}}, \tag{1.2}$$

$$Z_E = \sum_T e^{-S_E^{\text{Regge}}[T]}. \tag{1.3}$$

For a technical reason, we have performed the simulations with (approximately) constant three-volume. We choose $\alpha = 1$, and the Euclidean Regge action can be written in the following form [3]

$$S_E^{\text{Regge}} = -\kappa_0 N_0 + \kappa_3 N_3, \tag{1.4}$$

$$\kappa_0 = \frac{a}{4G}, \quad \kappa_3 = \frac{a}{4G} \left(\frac{3}{\pi} \arccos \frac{1}{3} - 1 \right) + \frac{a^3 \Lambda}{48\sqrt{2}\pi G}, \tag{1.5}$$

where N_0 is the number of vertices, N_3 is the number of simplices, G and Λ are respectively Newton’s gravitational constant and the cosmological constant. Just like statistical mechanics, one can compute various geometric quantities from this partition function Z_E in principle. We computed the partition function Z_E by performing the Monte Carlo simulation.

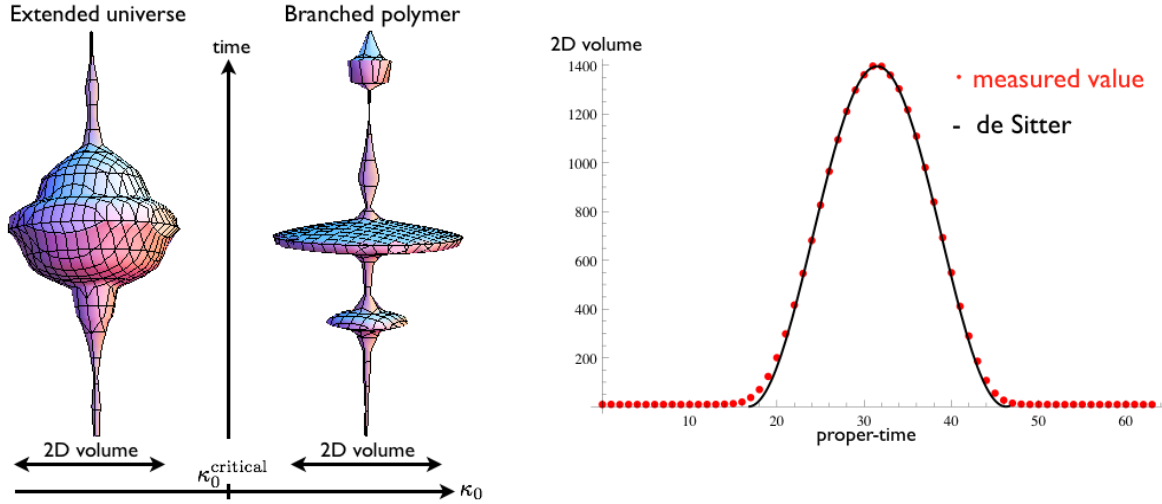


Figure 3: Monte Carlo snapshot of a typical sphere universe

Figure 4: Averaged spacial volume in the extended universe phase, measured for $N_3 = 64000$ and $\kappa_0 = 0.4$.

2 Emergence of de Sitter spacetime

We assume spacial topologies S^2 . Therefore the relevant spacetime topology is $S^1 \times S^2$. In 3D CDT, there appears two phases (cf. fig. 3) [4]. Which one emerges depends on the value of κ_0 (inverse of gravitational coupling constant). For sufficiently small κ_0 , the the averaged 2D spacial volume $\langle V_2(t) \rangle$ at proper time t can be described by that of the de Sitter instanton (cf. fig. 4)

$$\langle V_2(t) \rangle \propto \cos^2\left(\frac{t}{B}\right), \tag{2.1}$$

where B is a constant. We provide further evidence that the emergent universe in the extended universe phase is de Sitter spacetime at macroscopic scales. By studying a diffusion process on the discrete spacetime, we obtain an effective dimension, that is, the spectral dimension D_S . We will check whether the large-scale effective dimension is consistent with 3 in the extended universe phase (left part of fig. 3). The measuring method is described in detail in [5], [6]. We consider a randomly walking test particle in a given discrete spacetime configuration. The particle starts from a given tetrahedron and moves to nearest neighbor tetrahedra at a step. We measure the return probability $P(\sigma)$, which is the probability that the particle returns to the initial tetrahedron at σ steps.

We average over the return probabilities with randomly choosing tetrahedra and on different discrete spacetime configurations. When the diffusion step σ is not so large, the return probability for diffusion on fractal geometry is well-studied and is given by the formula as follows

$$P(\sigma) \propto \sigma^{-D_S/2}. \tag{2.2}$$

We can estimate the spectral dimension D_S by taking the logarithmic derivative

$$D_S = -2 \frac{d \log P(\sigma)}{d \log \sigma} + \text{finite-size correction}, \tag{2.3}$$

as long as the diffusion step σ is not so large. The ansatz, $D_S = a - be^{-c\sigma}$, gives the best fit with the measured spectral dimension $D_S(\sigma)$, where a, b, c are the fitting parameters. For the simulation with $N_3 = 64000$ and $\kappa_0 = 0.4$, the best fit become

$$D_S = 2.808 - 0.710e^{-0.026\sigma}. \tag{2.4}$$

Then, we obtained the extrapolating values

$$D_S(\sigma = \infty) = 2.81, \quad D_S(\sigma = 0) = 2.10. \tag{2.5}$$

The spectral dimension in the extended universe phase is approximately 3 at macroscopic scales.

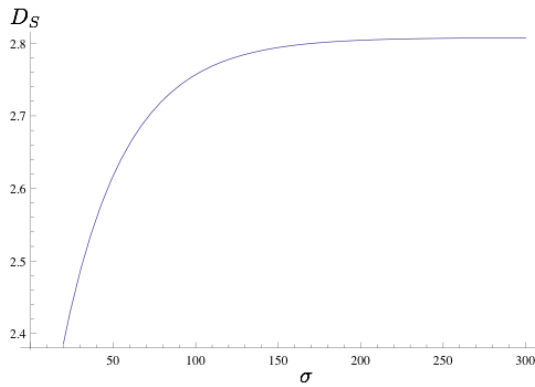


Figure 5: Spectral dimension in the extended universe phase, measured for $N_3 = 64000$ and $\kappa_0 = 0.4$.

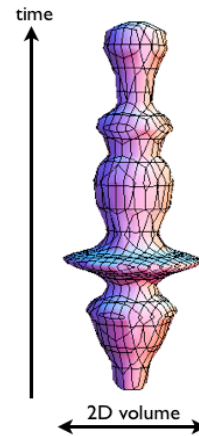


Figure 6: Monte Carlo snapshot of a typical torus universe, measured for $N_3 = 64000$ and $\kappa_0 = 0.4$.

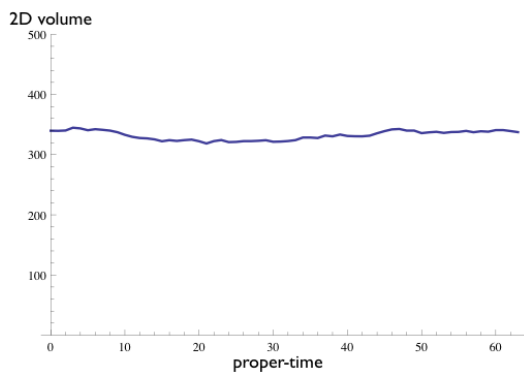


Figure 7: Averaged spatial volume of the torus universe, measured for $N_3 = 64000$ and $\kappa_0 = 0.4$.

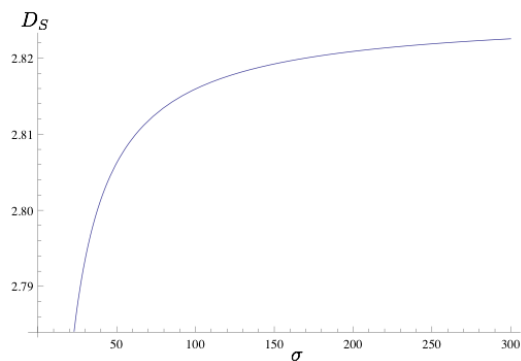


Figure 8: Spectral dimension of the torus universe, measured for $N_3 = 64000$ and $\kappa_0 = 0.4$.

3 The torus universe

Now, we consider a universe with spacial topology T^2 . Monte Carlo snapshot of a typical torus universe and the averaged 2D spacial volume $\langle V_2(t) \rangle$ at proper time t are shown in Figure 6, 7. This spacetime corresponds to the following metric at macroscopic scales

$$ds^2 = d\tau^2 + e^{2\{\alpha(\tau)+\beta(\tau)\}} dx^2 + e^{2\{\alpha(\tau)-\beta(\tau)\}} dy^2. \quad (3.1)$$

The corresponding Euclidean Einstein equations are as follows

$$\dot{\alpha}^2 - \dot{\beta}^2 = -\frac{\Lambda}{2}, \quad \ddot{\alpha} + 2\dot{\alpha}^2 = -\frac{\Lambda}{2}, \quad \ddot{\beta} + 2\dot{\alpha}\dot{\beta} = 0, \quad (3.2)$$

where $\dot{}$ denotes a proper-time derivative. Our simulation result seems to correspond to $\alpha = \text{const}$, $\beta = \text{const}$. So the effective cosmological constant $\Lambda_{\text{eff}} = 0$ is expected.

In this case, the following fit agrees with the data (cf. fig. 8)

$$D_S = a - \frac{b}{c + \sigma} = 2.826 - \frac{1.001}{1.001 + \sigma}, \quad (3.3)$$

where a, b and c are the fitting parameters. We obtained the asymptotic value for $N_3 = 64000$ and $\kappa_0 = 0.4$

$$D_S(\sigma = \infty) = 2.83, \quad D_S(\sigma = 0) = 1.83. \quad (3.4)$$

The spectral dimension of the torus universe is approximately 3 at macroscopic scales.

4 Summary

We found that the quantum universe emerging from a nonperturbative sum over geometries can be described the solutions of Euclidean Einstein equation on large scales in both cases of spacetime topologies are $S^1 \times S^2$ and $S^1 \times T^2$. Moreover, we obtained the effective dimension $D_S \approx 3$ by studying the diffusion process on the discrete spacetime ensemble.

References

- [1] J. Ambjørn, J. Jurkiewicz and R. Loll, [Phys. Rev. D 72, 064014 \(2005\)](#).
- [2] S. W. Hawking, [Phys. Lett 60A \(1977\) 81](#).
- [3] J. Ambjørn, J. Jurkiewicz and R. Loll, [Nucl. Phys. B 610 \(2001\) 347-382](#).
- [4] J. Ambjørn, J. Jurkiewicz and R. Loll, [Phys. Rev. D 64, 044011 \(2001\)](#).
- [5] D. Benedetti, J. Henson, [Phys. Rev. D 80, 124036 \(2009\)](#).
- [6] J. Ambjørn, J. Jurkiewicz and R. Loll, [Phys. Rev. Lett. 95, 171301 \(2005\)](#).

Constraining Galileon gravity from observational data with growth rate

Koichi Hirano^{84(a)} and Zen Komiya^(b)

^(a)*Department of Physics, Ichinoseki National College of Technology, Ichinoseki 021-8511, Japan*

^(b)*Department of Physics, Tokyo University of Science, Tokyo 162-8601, Japan*

Abstract

We studied the cosmological constraints on the Galileon gravity obtained from observational data of the growth rate of matter density perturbations, the supernovae Ia (SN Ia), the cosmic microwave background (CMB), and baryon acoustic oscillations (BAO). For the same value of the energy density parameter of matter $\Omega_{m,0}$, the growth rate f in Galileon models is enhanced, relative to the Λ CDM case, because of an increase in Newton's constant. The smaller $\Omega_{m,0}$ is, the more growth rate is suppressed. Therefore, the best fit value of $\Omega_{m,0}$ in the Galileon model, based only the growth rate data, is quite small. This is incompatible with the value of $\Omega_{m,0}$ obtained from the combination of SN Ia, CMB, and BAO data. On the other hand, in the Λ CDM model, the values of $\Omega_{m,0}$ obtained from different observational data sets are consistent. In the analysis of this paper, we found that the Galileon model is less compatible with observations than the Λ CDM model. This result seems to be qualitatively the same in most of the generalized Galileon models in which Newton's constant is enhanced.

1 Introduction

The modifications to gravity at cosmological distances have recently received much attention as a possible explanation for the current accelerated expansion of the universe.

We compare observed data of the growth rate of matter density perturbations to theoretical predictions. Whereas the background expansion history in modified gravity is nearly identical to that of dark energy models, the evolution of matter density perturbations in modified gravity is different from that of dark energy models (the cosmological constant is the standard candidate for dark energy). Thus, it is important to study the growth history of perturbations to distinguish modified gravity from models based on the cosmological constant or dark energy. Therefore, we computed the growth rate of matter density perturbations in Galileon cosmology and compared it to observational data. In addition, we studied the cosmological constraints on the Galileon model obtained from SN Ia, CMB anisotropies, and BAO observations so as to test the validity of the model.

2 Model

The action we consider is of the form

$$S = \int d^4x \sqrt{-g} \left[\frac{M_{\text{pl}}^2}{2} F(\phi) R + K(\phi, X) - G(\phi, X) \square\phi + L_m \right], \quad (2.1)$$

where g is the determinant of the space-time metric $g_{\mu\nu}$, $M_{\text{pl}} = (8\pi G)^{-1/2}$ is the reduced Planck mass, R is the Ricci scalar, and ϕ is a scalar field with a kinetic term $X \equiv -(1/2)(\nabla\phi)^2$. The function $F(\phi)$ depends on ϕ only, whereas $K(\phi, X)$ and $G(\phi, X)$ are functions of both ϕ and X . L_m is the matter Lagrangian. We have used the notation: $(\nabla\phi)^2 = g^{\mu\nu}\nabla_\mu\phi\nabla_\nu\phi$, $\square\phi = g^{\mu\nu}\nabla_\mu\nabla_\nu\phi$.

Variation with respect to the metric produces the Einstein equations; variation with respect to the Galileon field ϕ yields the equation of motion. For Friedmann–Robertson–Walker spacetime, the Einstein equations give

$$3M_{\text{pl}}^2 F H^2 = \rho_m + \rho_r - 3M_{\text{pl}}^2 H \dot{F} - K + 2X K_{,X} + 6H \dot{\phi} X G_{,X} - 2X G_{,\phi}, \quad (2.2)$$

$$-M_{\text{pl}}^2 F (3H^2 + 2\dot{H}) = p_r + 2M_{\text{pl}}^2 H \dot{F} + M_{\text{pl}}^2 \ddot{F} + K - 2X G_{,X} \ddot{\phi} - 2X G_{,\phi}, \quad (2.3)$$

⁸⁴Email address: hirano@ichinoseki.ac.jp

and the equation of motion for the Galileon field gives

$$\begin{aligned} & (K_{,X} + 2XK_{,XX} + 6H\dot{\phi}G_{,X} + 6H\dot{\phi}XG_{,XX} - 2XG_{,\phi X} - 2G_{,\phi})\ddot{\phi} \\ & + (3HK_{,X} + \dot{\phi}K_{,\phi X} + 9H^2\dot{\phi}G_{,X} + 3\dot{H}\dot{\phi}G_{,X} + 6HXG_{,\phi X} - 6HG_{,\phi} - G_{,\phi\phi}\dot{\phi})\dot{\phi} \\ & - K_{,\phi} - 6M_{\text{pl}}^2H^2F_{,\phi} - 3M_{\text{pl}}^2\dot{H}F_{,\phi} = 0, \end{aligned} \quad (2.4)$$

where an overdot represents differentiation with respect to cosmic time t and $H = \dot{a}/a$ is the Hubble expansion rate. Note that we have used the following partial derivative notation: $K_{,X} \equiv \partial K/\partial X$ and $K_{,XX} \equiv \partial^2 K/\partial X^2$ (and similarly for other variables). ρ_m and ρ_r are the energy densities of matter and radiation, respectively, and p_r is the pressure of the radiation.

In this paper, as we are interested in the basic parameters of Galileon theory, we consider the following functions

$$F(\phi) = \frac{2}{M_{\text{pl}}^2}\phi, \quad (2.5)$$

$$K(\phi, X) = 2\frac{\omega}{\phi}X, \quad (2.6)$$

$$G(\phi, X) = 2\xi(\phi)X, \quad (2.7)$$

where ω is the Brans–Dicke parameter and $\xi(\phi)$ is a function of ϕ . This model is the Brans–Dicke theory with the following self-interaction term: $\xi(\phi)(\nabla\phi)^2\Box\phi$. [1, 2]

For the numerical analysis in this paper, we adopt a specific model in which

$$\xi(\phi) = \frac{r_c^2}{\phi^2}, \quad (2.8)$$

where r_c is the crossover scale.

3 Density perturbations

The evolution equation for the cold dark matter overdensity δ in linear theory is governed by

$$\ddot{\delta} + 2H\dot{\delta} - 4\pi G_{\text{eff}}\rho\delta \simeq 0, \quad (3.1)$$

where G_{eff} represents the effective Newton's constant in Galileon gravity. For the model specified by Eqs. (2.5), (2.6), and (2.7), the effective Newton's constant is given by

$$G_{\text{eff}} = \frac{1}{16\pi\phi} \left[1 + \frac{(1 + \xi(\phi)\dot{\phi}^2)^2}{J} \right], \quad (3.2)$$

where

$$J = 3 + 2\omega + \phi^2\xi(\phi) \left[4\frac{\ddot{\phi}}{\phi} - 2\frac{\dot{\phi}^2}{\phi^2} + 8H\frac{\dot{\phi}}{\phi} - \phi^2\xi(\phi)\frac{\dot{\phi}^4}{\phi^4} \right]. \quad (3.3)$$

We plot the growth rate $f = d \ln \delta / d \ln a$ in Galileon gravity in Fig. 1 and Fig. 2. ω is the (constant) Brans–Dicke parameter and $\Omega_{m,0}$ is the energy density parameter of matter at the present day. We set $\Omega_{m,0} = 0.30$ for the Galileon model in Fig. 1 and $\omega = -10000$ for the Galileon model in Fig. 2. $\Omega_{m,0}$ for the Λ CDM model is 0.30 in these figures.

4 Observational constraints

In Fig. 1 and Fig. 2, for the same value of $\Omega_{m,0}$, the growth rate f in a Galileon model is enhanced compared to the Λ CDM case, because of the enhancement of Newton's constant. The smaller $\Omega_{m,0}$ is, the more suppressed the growth rate is. Therefore, comparing these with observational data of the growth rate, the best fit value of $\Omega_{m,0}$ in the Galileon model is quite small.

In Fig. 3, we plot the probability contours in the $(\Omega_{m,0}, |\omega|)$ -plane in the Galileon model. The contours show the 1σ (68.3%) and 2σ (95.0%) confidence limits, from the growth rate data, and from the combination of SN Ia, CMB, and BAO data. ($|\omega|$ is the absolute value of the Brans–Dicke parameter; $\omega < 0$.)

In the Galileon model, the allowed parameter region obtained using only the growth rate data does not overlap with the allowed parameter region obtained from the combination of SN Ia, CMB, and BAO data at all.

In Fig. 4, we plot the probability distribution of the energy density parameter of matter $\Omega_{m,0}$ in the Galileon model from observational data of (individually) growth rate, SN Ia, CMB, and BAO, and also the combination

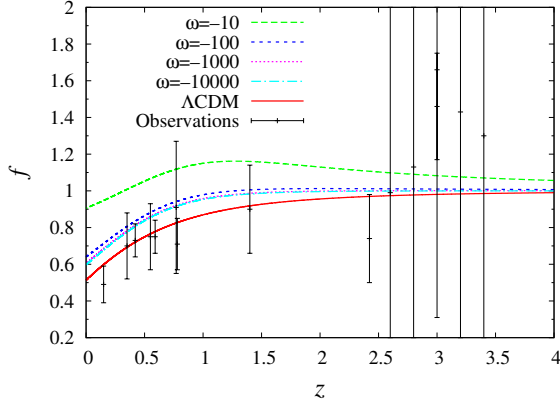


Figure 1: Growth rate f in Galileon gravity as a function of redshift z for various values of the Brans–Dicke parameter ω . The parameters are given by $\Omega_{m,0} = 0.30$.

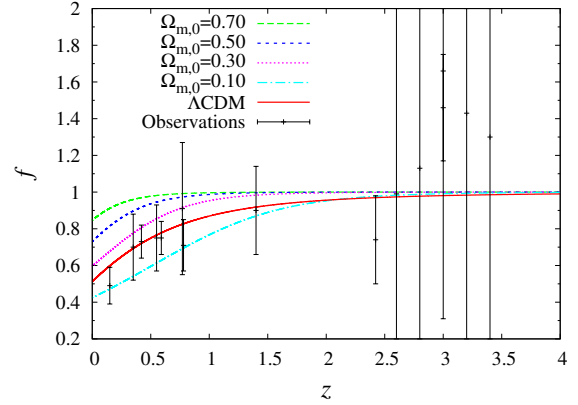


Figure 2: Growth rate f in Galileon gravity as a function of redshift z for various values of today's energy density parameter of matter $\Omega_{m,0}$. The parameters are given by $\omega = -10000$.

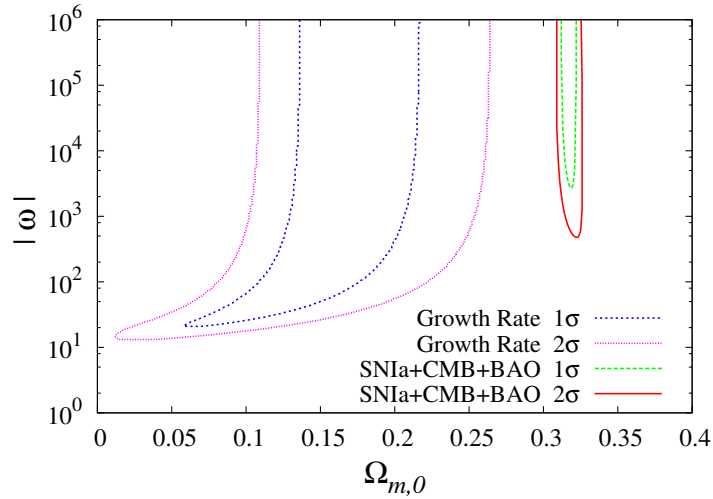


Figure 3: Probability contours in the $(\Omega_{m,0}, |\omega|)$ -plane for the Galileon model. The contours show the 1σ (68.3%) and 2σ (95.0%) confidence limits, from the growth rate data, and from the combination of SN Ia, CMB, and BAO data, respectively.

of all data, where the other parameter is marginalized. In the Galileon model, the bounds produced by each set of observations are inconsistent.

On the other hand, in Fig. 5, we plot the probability distribution of $\Omega_{m,0}$ for the Λ CDM model from observational data of (individually) growth rate, SN Ia, CMB, and BAO, and also the combination of all data. In the Λ CDM model, the bounds from each observational data set are consistent.

In Table 1, we list the best fit parameters, the χ^2 values, and the differences of the Akaike information criteria (AIC) and the Bayesian information criteria (BIC) for both the Galileon model and the Λ CDM model. Here, we use the combination of growth rate, SN Ia, CMB, and BAO data (all data).

5 Conclusions

Galileon gravity is a fascinating model that can induce the accelerated expansion of the present Universe, meets the requirements of solar system experiments, and can avoid ghost and instability problems. However, through

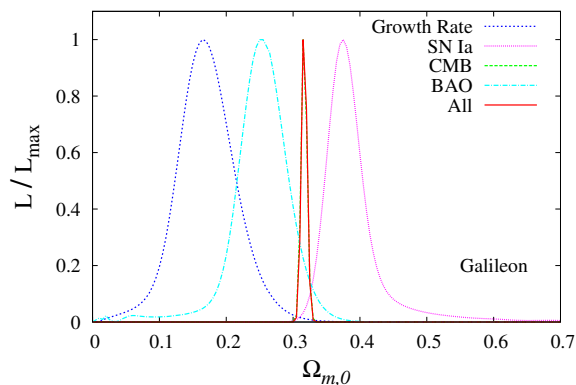


Figure 4: 1D probability distribution of $\Omega_{m,0}$ for the Galileon model from observational data of Growth Rate, SN Ia, CMB, BAO, respectively, and the combination of All data. The line of CMB almost overlaps with the line of All.

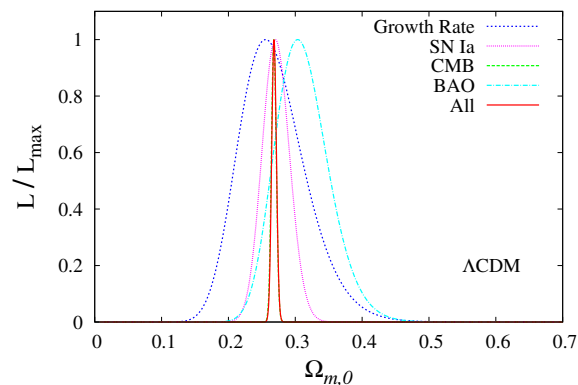


Figure 5: 1D probability distribution of $\Omega_{m,0}$ for the Λ CDM model from observational data of growth rate, SN Ia, CMB, and BAO, individually, and the combination of all data. The line of CMB almost overlaps with the line of All.

Model	Best fit parameters	χ^2	ΔAIC	ΔBIC
Λ CDM	$\Omega_{m,0} = 0.268$	550.674	0.00	0.00
Galileon	$\Omega_{m,0} = 0.316,$ $\omega = -2.69 \times 10^6$	582.013	33.339	37.697

Table 1: Results of observational tests using growth rate, SN Ia, CMB, and BAO data (all data).

the analysis presented in this paper, we found that the Galileon model is less compatible with observations than the Λ CDM model.

References

- [1] F. P. Silva and K. Koyama, *Phys. Rev. D* **80**, 121301, (2009).
- [2] T. Kobayashi, H. Tashiro, and D. Suzuki, *Phys. Rev. D* **81**, 063513, (2010).

Perturbative solutions to the lens equation for multiple lens planes

With some numerical examples

Koji Izumi ^{85(a)}

^(a)*Hirosaki University, Japan*

Abstract

We make a systematic attempt to determine, as a function of lens and source parameters the positions of images by multi-plane gravitational lenses. Numerical tests are done to investigate if the Taylor expansion method is robust. The method with a small mass ratio works well for changing a plane separation, whereas it breaks down in the inner domain near the caustics.

1 Lens equation

Two lens equation for two point masses is

$$w = z - \left(\frac{1 - \nu}{z^*} + \frac{\nu d_2}{z^* - \epsilon^* - \frac{(1 - \nu)\delta_2}{z}} \right), \quad (1.1)$$

where

$$d_2 \equiv \frac{D_1 D_{2s}}{D_2 D_{1s}}, \quad (1.2)$$

$$\delta_2 \equiv \frac{D_S D_{12}}{D_2 D_{1S}}. \quad (1.3)$$

2 Iterative solutions

Formal solutions are expressed in Taylor series as

$$z = \sum_{p_2=0}^{\infty} \sum_{p_3=0}^{\infty} \cdots \sum_{p_N=0}^{\infty} \nu_2^{p_2} \nu_3^{p_3} \cdots \nu_N^{p_N} z_{(p_2)(p_3)\cdots(p_N)}, \quad (2.1)$$

where the coefficients $z_{(p_2)(p_3)\cdots(p_N)}$ are independent of any ν_i . What we have to do is to determine each coefficient $z_{(p_2)(p_3)\cdots(p_N)}$ iteratively.

3 Numerical tests

$$\Delta \equiv \left| \frac{z_{Taylor} - z_{Num}}{z_{Num}} \right|, \quad (3.1)$$

where z_{Taylor} denotes a root obtained by the Taylor expansion method (including the third order corrections) and z_{Num} denotes the root that is obtained by numerically solving the lens equation. Δ_{Max} denotes the largest error among four image positions (for double planes) for the chosen parameter values.

⁸⁵Email address: elym.koji@gmail.com

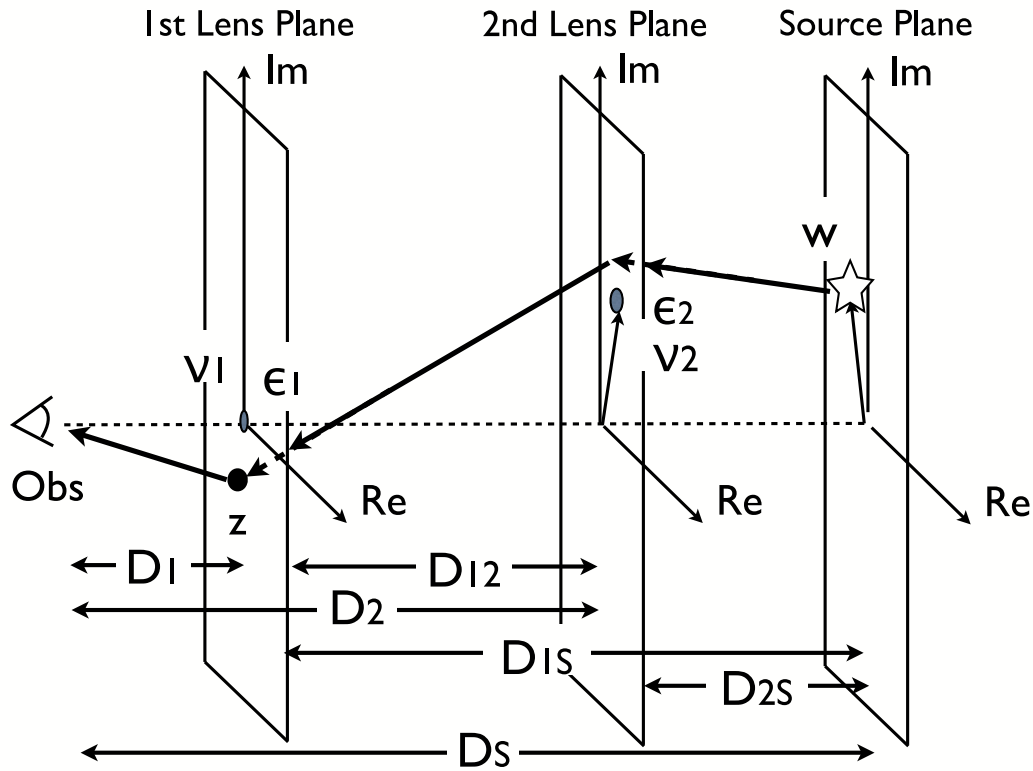


Figure 1: Notation: The source and image positions on complex planes are denoted by w and z , respectively. Locations of N masses are denoted by ϵ_i for $i = 1, \dots, N$. Here, we assume the thin lens approximation for each deflector. The several distances among the observer, source and each lens object are also defined.

4 Conclusion

We presented a method of Taylor series expansion to solve the multi-plane lens equation in terms of mass ratios except for the neighbourhood of the caustics.

Future works: Compare the present result with state-of-art numerical simulations.

References

- [1] Witt, A & A **236**, 311, (1990).
- [2] Asada, MNRAS **394**, 818, (2009).
- [3] Izumi, Asada, arXive1012.0070.

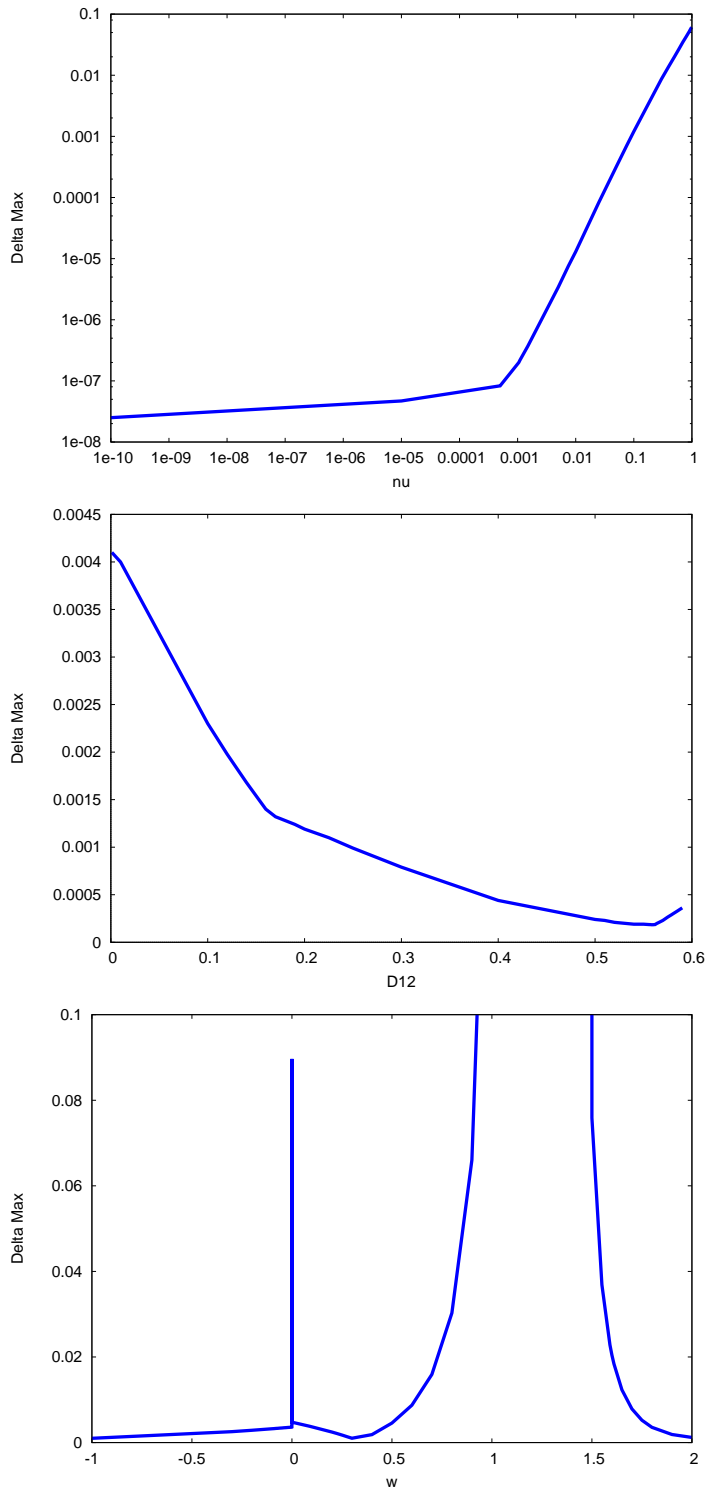


Figure 2: Numerical tests of the accuracy of the Taylor expansion method with different parameter values. The vertical axis denotes the largest relative error Δ_{Max} of the four images. The horizontal axis denotes the mass ratio ν (top panel), the plane separation D_{12} (middle panel), the source position w along the real axis (bottom panel), respectively.

Equations of motion in Double Field Theory: from classical particles to quantum cosmology

Nahomi Kan^{86(a)}, Koichiro Kobayashi^{87(b)}, and Kiyoshi Shiraishi^{88(b)}

^(a) Yamaguchi Junior College, Hofu-shi, Yamaguchi 747-1232, Japan

^(b) Yamaguchi University, Yamaguchi-shi, Yamaguchi 753-8512, Japan

Abstract

The equation of motion for a point particle in the background field of double field theory is considered. We find that the motion is described by a geodesic flow in the doubled geometry. Inspired by analysis on the particle motion, we propose a modified model of quantum string cosmology, which includes two scale factors. The report is based on [arXiv:1108.5795](https://arxiv.org/abs/1108.5795), to appear in Physical Review D.

1 Introduction

Double Field Theory (DFT) [1] is the theory of the massless field with a higher symmetry of spacetime including dual coordinates. Through this theory, Hull, Zwiebach, and Hohm clarified the T-duality symmetry of the massless field, and new symmetry related to the theory. More recently Jeon, Lee, and Park studied the structure of DFT using projection-compatible differential geometrical methods in [2].

The present report consists of two parts. In the first part, the motion of the particle in the background field in DFT is investigated. We show that the geodesic in the $2D$ -dimensional doubled-spacetime cannot be the geodesic in the D -dimensional spacetime. The geodesic equation in the D -dimensional spacetime is found to be the geodesic flow equation. In the second part, we consider the string cosmology with a bimetric model inspired by the constraint method discussed in the first part. Our method for the restriction on the metrics functions well, at least in the present reduced model for cosmology.

2 Review of projection-compatible approach

Coordinates are combined with dual coordinates to be $X^A = (\tilde{x}_a, x^\mu)^T$, where the suffixes A, B, \dots range over $1, 2, \dots, 2D$, while μ, ν, \dots as well as a, b, \dots range over $1, 2, \dots, D$. The constant metric is assumed to be expressed as the following $2D \times 2D$ matrix,

$$\eta_{AB} = \begin{pmatrix} 0 & \delta^a_\nu \\ \delta_\mu^b & 0 \end{pmatrix}. \quad (2.1)$$

The suffixes are entirely raised and lowered by this constant metric. Of course, $\eta^{AC}\eta_{CB} = \delta^A_B$ is satisfied.

The generalized metric is defined as follows:

$$\mathcal{H}_{AB} = \begin{pmatrix} g^{ab} & -g^{a\sigma}b_{\sigma\nu} \\ b_{\mu\sigma}g^{\sigma b} & g_{\mu\nu} - b_{\mu\rho}g^{\rho\sigma}b_{\sigma\nu} \end{pmatrix}. \quad (2.2)$$

Here, $g_{\mu\nu}$ and $b_{\mu\nu}$ are the metric in D dimensions and the antisymmetric tensor, respectively. It should be noted that \mathcal{H}^{AB} satisfies $\mathcal{H}^{AC}\mathcal{H}_{CB} = \delta^A_B$.

The following projection matrices are defined on the basis of the existence of two kinds of metrics. $P \equiv \frac{1}{2}(\eta + \mathcal{H})$, $\bar{P} \equiv \frac{1}{2}(\eta - \mathcal{H})$ which satisfy $P^2 = P$, $\bar{P}^2 = \bar{P}$, $P\bar{P} = \bar{P}P = 0$. From these, one can derive the identities $\bar{P}(\partial_A P)P = \bar{P}(\partial_A \bar{P})\bar{P} = 0$ or $P_D^B(\partial_A \mathcal{H}_{BC})P^C_E = \bar{P}_D^B(\partial_A \mathcal{H}_{BC})\bar{P}^C_E = 0$.

Now, the projection-compatible derivative is defined. In other words, both the metrics are ‘‘covariantly constant,’’ i.e., $\nabla_A \eta_{BC} = \nabla_A \mathcal{H}_{BC} = 0$. So, the covariant derivative of the projection of an arbitrary tensor coincides with the projection of the covariant derivative of the tensor. Jeon et al.[2] found that the covariant derivatives including the following connection have the character,

$$\Gamma_{ABC} \equiv 2P_{[A}^D \bar{P}_{B]}^E \partial_C P_{DE} + 2(\bar{P}_{[A}^D \bar{P}_{B]}^E - P_{[A}^D P_{B]}^E) \partial_D P_{EC}. \quad (2.3)$$

⁸⁶Email address: kan@yamaguchi-jc.ac.jp

⁸⁷Email address: m004wa@yamaguchi-u.ac.jp

⁸⁸Email address: shiraish@yamaguchi-u.ac.jp

They also obtained the action for the generalized metric, which was previously found by Hohm et al. [1]

$$S = \int dx d\tilde{x} e^{-2d} \left(\frac{1}{8} \mathcal{H}^{AB} \partial_A \mathcal{H}^{CD} \partial_B \mathcal{H}_{CD} - \frac{1}{2} \mathcal{H}^{AB} \partial_B \mathcal{H}^{CD} \partial_D \mathcal{H}_{AC} - 2 \partial_A d \partial_B \mathcal{H}^{AB} + 4 \mathcal{H}^{AB} \partial_A d \partial_B d \right),$$

from the consideration of the projection-compatible geometrical quantities. Here, $e^{-2d} = \sqrt{-g} e^{-2\phi}$ and ϕ is the dilaton field. If we set all the derivatives on the fields with respect to the dual coordinate zero ($\tilde{\partial}^a = 0$), the action for the effective theory for the zero-mode field in string theory is obtained as

$$S = \int dx \sqrt{-g} e^{-2\phi} \left[R + 4(\partial\phi)^2 - \frac{1}{12} H^2 \right],$$

where the three-form field $H = db$ is the field strength of the Kalb-Ramond 2-form b_{ij} .

3 The geodesic equation is not the equation of motion for a particle

Next, we consider the equation of motion for a particle. The geodesic equation is given by the following expression $U^\mu \nabla_\mu U^\nu = 0$, where $U^\mu \equiv \frac{dx^\mu}{ds} = \dot{x}^\mu$, s being a parameter.

The corresponding equation in the projection compatible geometry of Jeon et al. is considered to be

$$U^A \nabla_A U^B = U^A (\partial_A U^B + \Gamma_A{}^B{}_C U^C) = 0, \quad (3.1)$$

where $U^A = (\tilde{U}_a, U^\mu)^T = \frac{dX^A}{ds}$. From the project space ansatz $\bar{P}U = 0$, we are forced to use $\tilde{U}_a = g_{a\nu} U^\nu$. Moreover, we set $\tilde{\partial}g = 0$ as in the interpretation of DFT. Now, we find that the above equation reads

$$U^\mu \partial_\mu U^\nu + \frac{1}{2} g^{\nu\mu} (\partial_\rho g_{\mu\sigma} + \partial_\sigma g_{\mu\rho}) U^\rho U^\sigma = 0. \quad (3.2)$$

It is obviously different from the usual geodesic equation in general relativity (or differential geometry). In general, it is understood that the usage of the projection has a problem.

4 Projection and geodesic flow

The following Lagrangian is adopted, and the mechanics derived from it are considered:

$$L = \frac{1}{2} \mathcal{H}_{AB} \dot{X}^A \dot{X}^B + \lambda^A \bar{P}_{AB} \dot{X}^B. \quad (4.1)$$

Here, λ^A is an undecided multiplier. The Euler-Lagrange equation leads to the constraint $\bar{P}\dot{X} = 0$.

We find that the Hamiltonian is defined as

$$H = \frac{1}{2} \mathcal{H}^{AB} (p_A - \lambda^C \bar{P}_{CA}) (p_B - \lambda^D \bar{P}_{DB}). \quad (4.2)$$

The multiplier can be determined from the Hamilton equation as $\lambda_A = p_A + P_{AB} M^B$, where M^B is an arbitrary vector. When this is substituted into the above Hamiltonian, we obtain a new Hamiltonian

$$H_\star = \frac{1}{2} P^{AB} p_A p_B. \quad (4.3)$$

Using the new Hamiltonian, we obtain

$$\dot{X}^A = \frac{\partial H_\star}{\partial p_A} = P^{AB} p_B, \quad \dot{p}_A = -\frac{\partial H_\star}{\partial X^A} = -\frac{1}{2} \partial_A P^{BC} p_B p_C = -\frac{1}{4} \partial_A \mathcal{H}^{BC} p_B p_C. \quad (4.4)$$

These equations describe the geodesic flow in the system. The combined equation is found to be

$$\ddot{X}^A = \dot{X}^C (\partial_C P^{AB}) p_B - \frac{1}{2} P^{AB} \partial_B P^{CD} p_C p_D. \quad (4.5)$$

Now, let us take the condition $\tilde{\partial}^a = 0$ for the correspondence with DFT. If we consider $\tilde{p}^a = 0$, we obtain $\ddot{x}^\mu + \left\{ \begin{smallmatrix} \mu \\ \rho\sigma \end{smallmatrix} \right\} \dot{x}^\rho \dot{x}^\sigma = 0$, the geodesic equation in a usual D dimensional spacetime. We have obtained the geodesic equation in the D -dimensional spacetime from the geodesic flow in the $2D$ -dimensional space described by the generalized metric with natural assumptions.

5 A simple bi-metric model

We apply a similar method to a modified model for cosmology, which is related to the string cosmology [3]. In the model here, we consider two metrics, g and \tilde{g} . Though our model describes a bi-metric theory, the degree of freedom is to be mildly restricted. For simplicity of the discussion, we consider $b_{\mu\nu} = 0$. The cosmological action we consider is

$$S = -\frac{\lambda_s}{2} \int d\tau \left[\frac{1}{8} \text{Tr}(M' \eta M' \eta) + \Phi'^2 + e^{-2\Phi} V \right], \quad \text{with} \quad M_{AB} \equiv \begin{pmatrix} \tilde{G} & 1 \\ 1 & G \end{pmatrix}, \quad (5.1)$$

where G and \tilde{G} are the spatial parts of the metrics and $\Phi \equiv 2d$. Here, we add the constant potential V to the Lagrangian and λ_s is the constant that represents the scale of string theory [3]. The prime denotes differentiation with respect to τ .

We now define the ‘‘pseudo’’-projection matrices $P = \frac{\eta+M}{2}$, $\bar{P} = \frac{\eta-M}{2}$ and we wish to enforce $PM'P = \bar{P}M'\bar{P} = 0$ using some constraints. Now, the Lagrangian L_Λ with the constraint term is

$$L_\Lambda = \frac{\lambda_s}{2} \left[-\frac{1}{8} M'^{AB} M'_{AB} + \bar{\Lambda}_{AB} \bar{P}^{AC} M'_{CD} \bar{P}^{DB} + \Lambda_{AB} P^{AC} M'_{CD} P^{DB} - \Phi'^2 - e^{-2\Phi} V \right]. \quad (5.2)$$

The Hamiltonian of the system becomes

$$H_\Lambda = -\frac{4}{\lambda_s} \left[\Pi^{AB} - \frac{\lambda_s}{2} \left(\bar{P}^{AC} \bar{\Lambda}_{CD} \bar{P}^{DB} + P^{AC} \Lambda_{CD} P^{DB} \right) \right]^2 - \frac{1}{2\lambda_s} \Pi_\Phi^2 + \frac{\lambda_s}{2} e^{-2\Phi} V, \quad (5.3)$$

where the conjugate momentum for M_{AB} and Φ are represented by Π^{AB} and Π_Φ , respectively. We consider simplification by using the assumed relation, $P^2 \simeq P$ and $\bar{P}^2 \simeq \bar{P}$. The symbol \simeq is used to indicate this assumed approximation adopted by us. Finally, we obtain the Hamiltonian

$$H_* \equiv -\frac{8}{\lambda_s} \Pi^{AB} P_{BC} \Pi^{CD} \bar{P}_{DA} - \frac{1}{2\lambda_s} \Pi_\Phi^2 + \frac{\lambda_s}{2} e^{-2\Phi} V. \quad (5.4)$$

6 ‘‘Minisuperspace’’ version of the bi-metric model

Next, we examine the previous procedure of modification in the minisuperspace model. We suppose

$$M_{AB} = \begin{pmatrix} \tilde{A}(\tau) \delta^{ab} & 0 \\ 0 & A(\tau) \delta_{\mu\nu} \end{pmatrix}. \quad (6.1)$$

The Hamiltonian for the minisuperspace version of our modified model is found to be

$$H_* = -\frac{2}{\lambda_s D} (\pi \tilde{\pi} + \tilde{\pi} \pi - A \pi A \pi - \tilde{A} \tilde{\pi} \tilde{A} \tilde{\pi}) - \frac{1}{2\lambda_s} \Pi_\Phi^2 + \frac{\lambda_s}{2} e^{-2\Phi} V. \quad (6.2)$$

A special solution can be found for the Hamilton equations. The solution is

$$\tilde{A}(\tau) = \frac{1}{A_0} \exp \left[-\frac{2}{\sqrt{D}} C(\tau - \tau_0) \right], \quad A(\tau) = A_0 \exp \left[\frac{2}{\sqrt{D}} C(\tau - \tau_0) \right] + \delta, \quad (6.3)$$

where A_0 , τ_0 , and δ are constants. The similarity to the known string cosmological solution [3] is obvious, up to the possible constant deviation δ in A . For the solution, we find that $A\tilde{A} \rightarrow 1$ when $\tau \rightarrow +\infty$.

7 Quantum cosmology of the bi-metric model

Quantum cosmological treatment of the string cosmology has been widely studied [3]. In our model, the minisuperspace Wheeler-DeWitt equation is obtained as

$$\left[\frac{2}{\lambda_s D} \left(2 \frac{\partial}{\partial A} \frac{\partial}{\partial \tilde{A}} - A \frac{\partial}{\partial A} A \frac{\partial}{\partial A} - \tilde{A} \frac{\partial}{\partial \tilde{A}} \tilde{A} \frac{\partial}{\partial \tilde{A}} \right) + \frac{1}{2\lambda_s} \frac{\partial^2}{\partial \Phi^2} + \frac{\lambda_s}{2} e^{-2\Phi} V \right] \Psi = 0, \quad (7.1)$$

where Ψ is the wave function of the universe. To simplify the description of the system, we use the following variables: $x = \frac{\sqrt{D}}{4} \ln A/\tilde{A}$, $y = \frac{\sqrt{D}}{4} \ln A\tilde{A}$. Up to the ordering, we have

$$\left[-\frac{1 + e^{-(4/\sqrt{D})y}}{2} \frac{\partial^2}{\partial x^2} - \frac{\partial}{\partial y} \frac{1 - e^{-(4/\sqrt{D})y}}{2} \frac{\partial}{\partial y} + \frac{\partial^2}{\partial \Phi^2} + \lambda_s^2 e^{-2\Phi} V \right] \Psi = 0. \quad (7.2)$$

If we assume a solution of the form, $\Psi(x, y, \Phi) = X_k(x)Y_{kK}(y)Z_K(\Phi)$, we find the non singular real solution for $Y_{kK}(y)$ at $y = 0$ as follows:

$$Y_{kK}(y) = e^{-\sqrt{k^2-2K^2}y} F\left(\frac{1 + \sqrt{1-k^2} + \sqrt{k^2-2K^2}}{2}, \frac{1 - \sqrt{1-k^2} + \sqrt{k^2-2K^2}}{2}, 1; 1 - e^{-2y}\right), \quad (7.3)$$

where $F(\alpha, \beta, \gamma; z)$ is the Gauss' hypergeometric function.

If $K = \pm k$, $Y_{k\pm k}(y)$ has a maximum at $y = 0$ (see Figure 1). When we construct a wave packet for the cosmological wave function [3], the peak of this wave packet in terms of parameter y is naturally located at $y = 0$. Thus, the approximate scale factor duality $A\dot{A} \simeq 1$ is expected even at the ‘‘beginning’’ of the quantum universe. The detailed investigation on the behavior of the universe is left for future research.

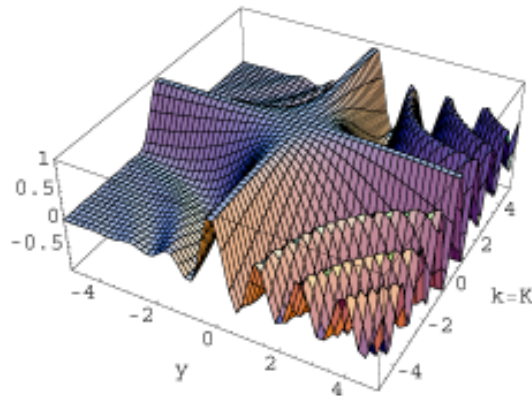


Figure 1: 3D-plot of $Y_{kk}(y)$.

References

- [1] C. Hull and B. Zwiebach, JHEP **0909** (2009) 099; JHEP **0909** (2009) 090.
- [2] I. Jeon, K. Lee and J.-H. Park, JHEP **1104** (2011) 014.
- [3] For a review, M. Gasperini and G. Veneziano, Phys. Rep. **373** (2003) 1.

Astrometric microlensing by the Ellis Wormhole

Takao Kitamura

Faculty of Science and Technology, Hirosaki University, Hirosaki 036-8561, Japan

Abstract

We study the gravitational microlensing effects of the Ellis wormhole in the weak-field limit. First, we find a suitable coordinate transformation, such that the lens equation and analytic expressions of the lensed image positions can become much simpler. Second, we prove that two images always appear for the weak-field lens by the Ellis wormhole. By using these analytic results, we discuss astrometric image centroid displacements due to gravitational microlensing by the Ellis wormhole. The astrometric image centroid trajectory by the Ellis wormhole is different from the standard one by a spherical lensing object that is expressed by the Schwarzschild metric. The anomalous shift of the image centroid by the Ellis wormhole lens is smaller than that by the Schwarzschild lens, provided that the impact parameter and the Einstein ring radius are the same. Therefore, the lensed image centroid by the Ellis wormhole moves slower. Such a difference, although it is very small, will be, in principle, applicable for detecting or constraining the Ellis wormhole by using future high-precision astrometry observations. In particular, the image centroid position gives us additional information, so that the parameter degeneracy existing in photometric microlensing can be partially broken.

1 Introduction

A peculiar feature of general relativity is that the theory admits a nontrivial topology of a spacetime. A solution of the Einstein equation that connects distant points of space-time was introduced by Einstein & Rosen [1]. This solution called the Einstein-Rosen bridge was the first solution to later be referred to as a wormhole. Initially, this type of solution was just a trivial or teaching example of mathematical physics. However, Morris & Thorne [2] proved that some wormholes are “traversable”, i.e., space and time travel can be achieved by passing through the wormholes. However, it is hard to observe wormholes. Therefore, we consider the gravitational microlensing effects by wormholes for find them. In this study, we used the Ellis wormhole metric for simplicity to compare Schwarzschild one because this metric is also spherical symmetry.

2 The Ellis wormhole

The Ellis wormhole is expressed by the line element

$$ds^2 = dt^2 - dr^2 - (r^2 + a^2)(d\theta^2 + \sin^2\theta d\phi^2),$$

where a is the throat radius of the wormhole. The Ellis wormhole is known to be a massless wormhole. However, this wormhole deflect light by gravitational lensing because of its curved space-time structure.

The deflection angle $\alpha(r)$ of the Ellis wormhole was derived by Dey & Sen(2008) to be

$$\alpha(r) = \pi \left(\sqrt{\frac{2(r^2 + a^2)}{2r^2 + a^2}} - 1 \right),$$

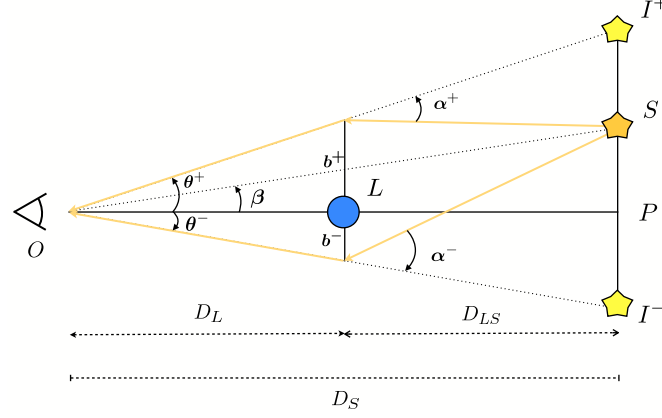
where r is the closest approach of the light. In the weak-field limit($r \rightarrow \infty$), the deflection angle becomes

$$\alpha(r) \rightarrow \frac{\pi}{4} \frac{a^2}{r^2} + O\left(\frac{a}{r}\right)^4.$$

For the Schwarzschild is

$$\alpha(r) = \frac{4GM}{r}$$

3 Lens equation for the Ellis wormhole



The lens equation for the Ellis wormhole is

$$\beta = \frac{r}{D_L} - \frac{\pi D_{LS}}{4 D_S} \frac{a^2}{r^2} \quad (r > 0)$$

$$\beta = \frac{r}{D_L} + \frac{\pi D_{LS}}{4 D_S} \frac{a^2}{r^2} \quad (r < 0).$$

They are rewritten as

$$\theta^3 - \beta\theta^2 - 1 = 0 \quad (\theta > 0)$$

$$\theta^3 - \beta\theta^2 + 1 = 0 \quad (\theta < 0),$$

in the units of $\theta_E = \sqrt[3]{\frac{\pi D_{LS}}{4 D_S D_L^2} a^2}$.

By using Cardano's formula, we obtained the solutions as[3]

$$\theta_+ = \left(\sqrt[3]{\frac{1}{2} + \sqrt{\frac{1}{4} + \frac{\beta^3}{27}}} + \sqrt[3]{\frac{1}{2} - \sqrt{\frac{1}{4} + \frac{\beta^3}{27}}} \right)^{-1}$$

$$\theta_- = \left(-\sqrt[3]{\frac{1}{2} - \sqrt{\frac{1}{4} - \frac{\beta^3}{27}}} - \sqrt[3]{\frac{1}{2} + \sqrt{\frac{1}{4} - \frac{\beta^3}{27}}} \right)^{-1}.$$

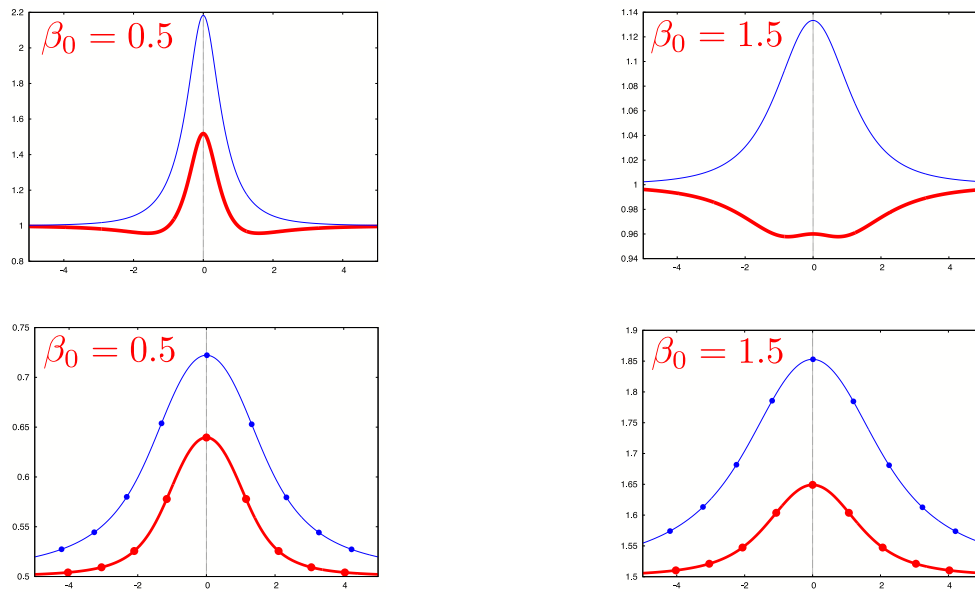
The previous paper also used Cardano's formula[4], however those solutions are complicated. Therefore, we simplified the expressions by appropriate coordinate transformation.

4 Magnification and Image photo centroid

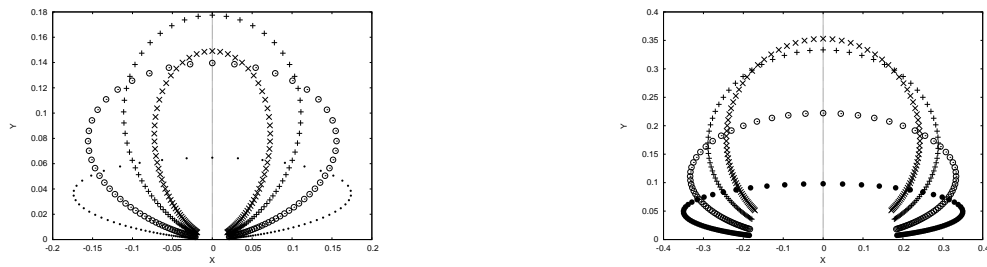
- The magnification of the brightness
- Photon center
- $\Delta\theta_{PC}$

Blue line is the Schwarzschild lines, and red line is the Ellis wormhole lines. β_0 is the closest distance from lens to source in units of θ_E .

In the bottom figures, the dot (\cdot), circle (\circ), plus ($+$), cross (\times) denote the positions for $\frac{\beta}{\theta_E} = 0.2, 0.5, 1.0, 1.5$, respectively, where the horizontal axis denotes the direction of the source motion.



The relative displacement trajectory by the Schwarzschild lens is known to be an ellipse. The bottom figure, which is Astrometric image centroid displacements ($\Delta\theta_{PC}$), shows that the relative trajectory by the Ellis lens looks like an ellipse but has a small difference. The shape is symmetric along the x -axis but slightly asymmetric along the y -axis like a tree leaf.



5 Summary

We studied the gravitational microlensing effects of the Ellis wormhole in the weak-field limit. First, we performed a suitable coordinate transformation, such that the lens equation and analytic expressions of the lensed image positions can become much simpler than the previous ones. Second, we proved that two images always appear for the weak-field lens by the Ellis wormhole. By using these analytic results, we investigated astrometric image centroid displacements due to gravitational microlensing by the Ellis wormhole. The anomalous shift of the image centroid by the Ellis wormhole lens is smaller than that by the Schwarzschild lens, provided that the impact parameter and the Einstein ring radius are the same. Therefore, the lensed image centroid by the Ellis wormhole moves slower.

References

- [1] A. Einstein, N. Rosen., *Phys. Rev* **48**, 73, (1935).
- [2] S. M. Moris, S. K. Thorne., *Am. J. Phys* **56**, 395, (1988).
- [3] Y. Toki, T. Kitamura, H. Asada, F. Abe ., *Astrophys. J.* **740**, 121, (2011).
- [4] F. Abe ., *Astrophys. J.* **725**, 787, (2011).

Flux vacua in DBI type Einstein Maxwell theory

Takuya Maki^{89(a)}, Nahomi Kan^{90(b)}, Koichiro Kobayashi^{91(c)} and Kiyoshi Shiraishi^{92(c)}

^(a) *Japan Women's College of Physical Education, Setagaya, Tokyo 157-8565, Japan*

^(b) *Yamaguchi Junior College, Hohn-shi, Yamaguchi 747-1232, Japan*

^(c) *Yamaguchi University, Yamaguchi-shi, Yamaguchi 753-8512, Japan*

Abstract

We study compactification of extra dimensions in a theory of Dirac-Born-Infeld (DBI) type gravity. We investigate the solution for Minkowski spacetime with an S^2 extra space. The solution is derived by the effective potential method in the presence of the magnetic flux on the extra sphere. We find that, in a certain model, the radius of the extra space has a minimum value independent of the higher-dimensional Newton constant in weak-field limit.

1 Introduction

Recently, models including the higher derivative terms are widely studied as a modified version of Einstein gravity. Moreover, various works are reported about compactification with an extra space in the higher derivative gravity (for example [1]).

The Dirac-Born-Infeld (DBI) type gravity has been considered by Deser and Gibbons [2] and studied by many authors. It is expected that the nonlinear nature of the model may remove the possible singularity of spacetime.

In our recent work, we considered a model of Weyl invariant Dirac-Born-Infeld (DBI) type gravity. This model contains the Weyl gauge field. It is natural to put the gauge field into DBI type gravity, since originally DBI theory aimed at relaxing the singularity of the electric field.

In the DBI electromagnetism, the Lagrangian is

$$\mathcal{L} = -\sqrt{-\det(\eta_{\mu\nu} + \beta F_{\mu\nu})}. \quad (1.1)$$

In the four-dimensional spacetime they are satisfied that $-\det(\eta_{\mu\nu} + \beta F_{\mu\nu}) = 1 - \beta^2(E^2 - B^2) - \beta^4(E \cdot B)^2$,

$$\nabla \cdot D = \nabla \cdot \frac{E}{\sqrt{1 - \beta^2 E^2}}. \quad (1.2)$$

In the case of the point charge, the electric field is $E \propto \frac{1}{\sqrt{r^4 + \beta^2}}$. The energy density is also finite.

2 Spacetime metric and flux

We first consider the theory with the massless gauge field in six dimensions (thus in the flat spacetime, it seems to be the DBI electromagnetism), and compactification of the extra dimensions. The Lagrangian of our model is the following:

$$\mathcal{L} = -\sqrt{-\det(f^2 g_{MN} - \alpha_1 R_{MN} + \beta F_{MN})} + (1 - \lambda)f^6 \sqrt{-g}, \quad (2.1)$$

where f is a mass scale. α_1 , β and λ are dimensionless parameters. M, N range over 0, 1, 2, 3, 5 and 6.

Note that one can rewrite the Lagrangian as in the form

$$\begin{aligned} \mathcal{L} &= -\sqrt{-\det \mathcal{M}_{MN}} + (1 - \lambda)f^6 \sqrt{-g} \\ &= -\sqrt{-g} \sqrt{\det \mathcal{M}^M{}_N} + (1 - \lambda)f^6 \sqrt{-g}, \end{aligned}$$

where it is satisfied that

$$\mathcal{M}^M{}_N = f^2 \delta^M{}_N - \alpha_1 R^M{}_N + \beta F^M{}_N. \quad (2.2)$$

⁸⁹Email address: maki@jwcpe.ac.jp

⁹⁰Email address: kan@yamaguchi-jc.ac.jp

⁹¹Email address: m004wa@yamaguchi-u.ac.jp

⁹²Email address: shiraish@yamaguchi-u.ac.jp

Now we assume that the spacetime is described by a direct product of four-dimensional spacetime and an extra space, i.e., the line element is written by

$$ds^2 = g_{\mu\nu}^{(4)} dx^\mu dx^\nu + g_{mn}^{(2)} dx^m dx^n, \quad (2.3)$$

where $\mu, \nu = 0, 1, 2, 3$ while $m, n = 5, 6$. We will omit the index within the parentheses which indicates the dimension, as long as confusion would not occur.

We suppose that the four-dimensional spacetime is a maximally symmetric space. The Ricci tensor of the spacetime is expressed as

$$R_{\mu\nu} = \frac{1}{4} R^{(4)} g_{\mu\nu}, \quad (2.4)$$

where $R^{(4)}$ is the scalar curvature of the four-dimensional spacetime. For the Minkowski spacetime, $R^{(4)}$ equals to zero. We adopt S^2 as the extra space. Then we find

$$R_{mn} = \frac{1}{2} R^{(2)} g_{mn} = \frac{1}{b^2} g_{mn}, \quad (2.5)$$

where $R^{(2)}$ and b are the scalar curvature and the radius of the two-sphere, respectively.

We suppose that the constant magnetic flux penetrates the extra sphere, just as in the model of Ranjbar-Daemi, Salam and Strathdee (RSS) [3]. Namely we set

$$F_{mn} = B \sqrt{g^{(2)}} \varepsilon_{mn}, \quad (2.6)$$

where $g^{(2)} = \det g_{mn}$. The totally antisymmetric symbol ε_{mn} takes the value 1 for $(m, n) = (5, 6)$. The strength of flux is rewritten as $B = \tilde{B}/b^2$ where \tilde{B} is a constant determined from a topological number. Substituting above ansatz into the Lagrangian, we get the reduced Lagrangian as

$$\mathcal{L}_0 = -\sqrt{-g^{(4)}} (4\pi b^2) \times \left\{ \sqrt{\left(f^2 - \frac{\alpha_1}{4} R^{(4)}\right)^4 \left[\left(f^2 - \frac{\alpha_1}{b^2}\right)^2 + \beta^2 \frac{\tilde{B}^2}{b^4}\right]} - (1 - \lambda) f^6 \right\}.$$

In this model, the effective Newton constant G in four dimensional spacetime can be read from the expansion of the Lagrangian in the small curvature limit,

$$\mathcal{L} = \sqrt{-g^{(4)}} \left[\text{const.} + \frac{1}{16\pi G} R^{(4)} + \dots \right]. \quad (2.7)$$

Thus we find $(16\pi G)^{-1}$ for the constant radius b_0 as

$$\frac{1}{16\pi G} = 4\pi b_0^2 f^2 \left(\frac{\alpha_1}{2}\right) \sqrt{\left(f^2 - \frac{\alpha_1}{b_0^2}\right)^2 + \frac{\beta^2 \tilde{B}^2}{b_0^4}}. \quad (2.8)$$

3 Four dimensional flat spacetime and compactification

We seek the solution for the four-dimensional flat spacetime. According to Wetterich [1], we use the method of the effective potential for a static solution, instead of solving the equation of motion derived from the Lagrangian directly. We now define a potential

$$V(y) = y \left\{ \sqrt{\left(1 - \frac{\alpha_1}{y}\right)^2 + \beta^2 \frac{\tilde{B}^2}{y^2}} - (1 - \lambda) \right\} \quad (3.1)$$

where $y = f^2 b^2$. Then the equation of motion and the stability condition are equivalent to

$$\begin{aligned} \frac{dV}{dy} \Big|_{y=y_0} &= V(y_0) = 0, \\ \frac{d^2V}{dy^2} \Big|_{y=y_0} &> 0 \end{aligned} \quad (3.2)$$

for the solution $y = y_0$. To make the equations simultaneously satisfied, we must tune the value of λ to be specific value λ_0 .

We consider further scaling of the variable and parameters become convenient. This yields a scaled potential

$$\frac{1}{|\beta\tilde{B}|}V(y) \rightarrow U(Y) = Y \left\{ \sqrt{\left(1 - \frac{A_1}{Y}\right)^2 + \frac{1}{Y^2}} - (1 - \lambda) \right\}, \quad (3.3)$$

where $Y = y/|\beta\tilde{B}|$ and $A_1 = \alpha_1/|\beta\tilde{B}|$. In Figure 1, we show the U - Y graph of potentials in the DBIE model and the RSS model.

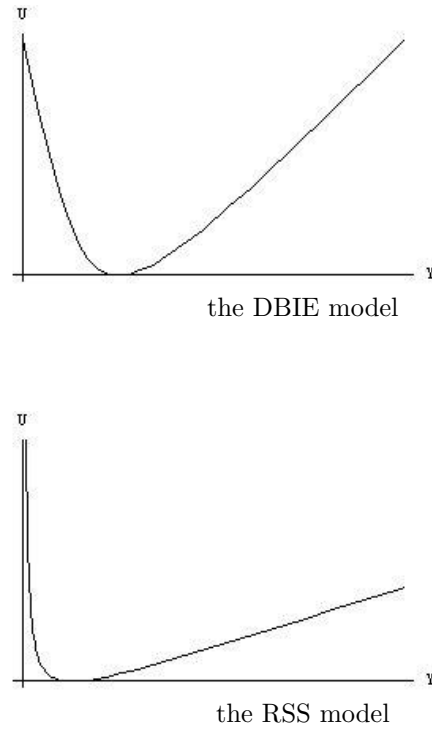


Figure 1: Effective potentials in the DBIE model and the RSS model.

Finally we find the solution for

$$\frac{dU}{dY}\Big|_{Y=Y_0} = U(Y_0) = 0 \quad \text{and} \quad \frac{d^2U}{dY^2}\Big|_{Y=Y_0} > 0 \quad (3.4)$$

is given by

$$\begin{aligned} Y_0 &= A_1 + \frac{1}{A_1}, \\ 1 - \lambda_0 &= \frac{1}{\sqrt{1 + A_1^2}} \end{aligned} \quad (3.5)$$

for $A_1 > 0$. It is interesting to see the minimal value of the radius of S^2 is $\frac{\sqrt{|\beta\tilde{B}|}}{f}$, which is independent of the value of α_1 .

The inverse of the Newton constant is then given by

$$\frac{1}{16\pi G} = 2\pi f^2 |\beta\tilde{B}|^2 \sqrt{1 + A_1^2}. \quad (3.6)$$

The squared ratio of the compactification scale and the four-dimensional Planck length is

$$\frac{b_0^2}{G} = 32\pi^2 |\beta\tilde{B}|^3 \sqrt{\frac{(1 + A_1^2)^3}{A_1^2}} \geq 32\pi^2 |\beta\tilde{B}|^3 \frac{3\sqrt{3}}{2}. \quad (3.7)$$

Comparing with the result of the RSS model

$$\frac{b_0^2}{G} = 32\pi^2 |\beta \tilde{B}|^3 \frac{1}{A_1}, \quad (3.8)$$

we find that, in our DBI gravity model, the compactification scale cannot be extremely smaller than the Planck length, provided that $|\beta \tilde{B}| \sim 1$.

4 Summary and outlook

The compactification in the DBI gravity with flux in the extra space has been investigated. The parameter region which allows the compactification has been revealed. We have shown that the small couplings attached to the curvature realize similar compactification to that of the RSS model.

An interesting dependence of the radius of the extra space on the parameter α_1 was found in our model. This will be of more importance if we consider the parameter as a dynamical variable, or we generalize our model to include the term such as $\phi^2 R_{MN}$, where ϕ is a scalar degree of freedom.

The analysis on stability against perturbation of higher modes, which deforms the spherical shape of the extra space, is important, even though the analysis on those modes will be complicated because of the higher-derivative terms in our model. This issue is left for future works.

Spontaneous compactification to a football-shaped internal space in the presence of a brane is also worth studying in the framework of the DBI type gravity models, because the higher curvature terms affect the geometrical aspects of conical or nearly conical points on the compact space.

The cosmological evolution of scale factors in our model is an important subject. Since the effective potential has a finite value at $b = 0$ in our DBI type model, the initial state of the universe may located at $b = 0$. The simple condition is suitable for quantum cosmology, although the derivative terms in our model make the canonical approach very complicated. (The quantum cosmology of the RSS model was studied by Halliwell [4].)

References

- [1] C. Wetterich, Phys. Lett. **B113** (1982) 377.
- [2] S. Deser and G. W. Gibbons, Class. Quant. Grav. **15** (1998) L35 [[arXiv:hep-th/9803049](#)].
- [3] S. Randjbar-Daemi, A. Salam and J. Strathdee, Nucl. Phys. **B214** (1983) 491.
- [4] J. J. Halliwell, Nucl. Phys. **B266** (1986) 228.

Off-equatorial orbits of charged particles in strong gravity with magnetic dipole field

Yasufumi Kojima⁹³

Department of Physics, Hiroshima University, Higashi-Hiroshima 739-8526

Abstract

Interplay between gravitational and electromagnetic action allows for stable, energetically bound off-equatorial motion of charged particles in the case of non-relativistic dynamics. We study such possibility and the characteristic, if exists, in the Bonnor spacetime, which is an exact solution of Einstein-Maxwell equations, and may describe the exterior solution for a massive object with magnetic dipole moment.

1 Introduction

Classical study of charged particles motion in a purely dipole magnetic field by Störmer[1] provides us with the basic physical description of radiation belts surrounding a magnetized planet. Radiation belts are known to be composed of individual ions and electrons whose motion is governed by magnetic forces only. In order to describe the dynamics of charged dust grains in planetary magnetospheres, when there are much smaller charge to mass ratios, one may take into account both the planetary gravity and electromagnetic fields [2]. Such studies point out the existence of the dust grains halo orbits near, e.g. Saturn [3].

The situation is not obvious in case of exact solutions of Einstein-Maxwell equations, where the gravitational and electromagnetic fields are mutually interconnected. The relativistic counterpart is recently investigated e.g. [4, 5]. They derived a semi-analytic condition for the halo orbits existence for pseudo-Newtonian model, Schwarzschild and Kerr-Newman black holes. Their exact location should depend on the type of particles, i.e. the charge to mass ratio. Possible chaotic motion in the halo orbits may have some astrophysical consequences [5, 6]. In this short article, we briefly discuss the existence of off-equatorial orbits in Bonnor spacetime [7]. Detailed discussion is in preparation[8].

2 Orbits in Bonnor spacetime

Bonnor[7] derived a solution for Einstein-Maxwell equations, which is given by

$$ds^2 = -\left(\frac{P}{Y}\right)^2 dt^2 + \frac{P^2 Y^2}{Q^3 Z} (dr^2 + Z d\theta^2) + \frac{Y^2 Z \sin^2 \theta}{P^2} d\phi^2, \quad (2.1)$$

where

$$P = r^2 - 2ar - b^2 \cos^2 \theta, \quad (2.2)$$

$$Q = (r - a)^2 - (a^2 + b^2) \cos^2 \theta, \quad (2.3)$$

$$Y = r^2 - b^2 \cos^2 \theta, \quad (2.4)$$

$$Z = r^2 - 2ar - b^2. \quad (2.5)$$

The solution contains two independent parameters. The constant a is related to the gravitational mass M , $a = GM/2$ and the other one b is to the magnetic dipole moment μ , $b = \mu G^{1/2}/(2a) = \mu/(G^{1/2}M)$. The ϕ -component of the electromagnetic potential is given by

$$A_\phi = \frac{\mu r \sin^2 \theta}{P}. \quad (2.6)$$

We consider charged particle motion with mass m and charge q . There are two conserved quantities, angular momentum and energy. They are written as

$$mL = mZ \sin^2 \theta \left(\frac{Y}{P}\right)^2 \frac{d\phi}{d\tau} + qA_\phi, \quad (2.7)$$

⁹³Email address: kojima@theo.phys.sci.hiroshima-u.ac.jp

$$mE = m \left(\frac{P}{Y} \right)^2 \frac{dt}{d\tau}, \quad (2.8)$$

where constants L and E denote specific angular momentum and energy. Using them, the motion in meridian plane is limited as

$$E^2 = \frac{P^4}{Q^3 Z} \left[\left(\frac{dr}{d\tau} \right)^2 + Z \left(\frac{d\theta}{d\tau} \right)^2 \right] + V_{\text{eff}}^2. \quad (2.9)$$

The effective potential is given by

$$V_{\text{eff}}^2 = \frac{P^2}{Y^2} \left[1 + \frac{P^2}{Y^2 Z \sin^2 \theta} \left(L - \frac{q\mu}{m} \frac{r \sin^2 \theta}{P} \right)^2 \right]. \quad (2.10)$$

The condition for off-equatorial orbit is derived by $\partial_r V_{\text{eff}} = 0$ and $\partial_\theta V_{\text{eff}} = 0$. After some calculations, we have

$$\left(\frac{q\mu}{m} \right)^2 = \frac{aY^2 S^2}{rZ\Lambda \sin^2 \theta (r^2 + b^2 \cos^2 \theta)}, \quad (2.11)$$

where

$$S = r^4 - 2ar^3 - 3b^2 r^2 \sin^2 \theta + 2ab^2 r (2 \sin^2 \theta - 1) - b^4 \cos^2 \theta, \quad (2.12)$$

$$\Lambda = 3r^4 - 10ar^3 - 2b^2 r^2 \cos^2 \theta - 6ab^2 r \cos^2 \theta - b^4 \cos^4 \theta. \quad (2.13)$$

The angular momentum L is given by

$$L = \left(\frac{q\mu}{m} \right) \frac{r \sin^2 \theta}{P} \pm \frac{2[arZ(r^2 + b^2 \cos^2 \theta)]^{1/2} Y \sin \theta}{P\Lambda^{1/2}}. \quad (2.14)$$

It is clear that the gravitational field is necessary for the off-equatorial orbit. The condition becomes meaningless in the limit of no gravity, i.e, $mG \rightarrow 0$. The existence of 'halo' orbits in the Bonnor spacetime outside the singularity $Z > 0$ is determined by the following condition

$$\Lambda > 0. \quad (2.15)$$

In order to understand derived condition, we consider weak gravity limit. The effective potential for large r is given by

$$V_{\text{eff}}^2 = \left(1 - \frac{4a}{\rho} \right) \left[1 + \frac{1}{\rho^2 \sin^2 \theta} \left(L - \frac{q\mu}{m} \left(1 + \frac{3a}{\rho} \right) \frac{\sin^2 \theta}{\rho} \right)^2 \right]. \quad (2.16)$$

where $\rho = r + a + O(a^2)$ represents the circular radius. This expression agrees with that for non-relativistic dynamics with Newton gravity and dipole magnetic field. For large radius, the condition (2.11) reduces to

$$\left(\frac{q\mu}{m} \right)^2 = \frac{GM r^3}{6 \sin^2 \theta}. \quad (2.17)$$

Gravity, centrifugal and Lorentz forces are balanced for it. The potential minimum corresponds to the circular motion along ϕ direction at (r_0, θ_0) , which should satisfy the above relation. With increase of energy E , $r(\tau)$ and $\theta(\tau)$ of the particle are no longer constant. There are bound orbits in vicinity of (r_0, θ_0) . Some numerical works are necessary to study the transition of bound to unbound orbits by further increasing E [8].

We next consider the existence condition (2.15). The condition for $\Lambda > 0$ in general depends on the polar angle θ . Two explicit examples are given below. The existence on the equatorial plane ($\theta = \pi/2$) is limited as

$$r > \frac{10}{3}a = \frac{5}{3}GM \approx 1.666GM. \quad (2.18)$$

The existence on the pole ($\theta = \pi/2$) depends on the parameter b^2 . The lower limit increases with it. For example, we have for $b^2 = a^2 = (GM/2)^2$

$$r > r_* \approx 1.835GM \quad (2.19)$$

Finally, detailed analysis of the existence condition for smaller radius is complicated and will be discussed elsewhere[8].

References

- [1] Störmer C 1955 *The Polar Aurora* (Clarendon Press, Oxford)
- [2] Dullin H R, Horányi M and Howard J E 2002 *Physica D* **171** 178
- [3] Howard J E, Horányi M and Stewart G R 1999 *Phys. Rev. Letters* **83** 3993
- [4] Kovář J, Karas V and Stuchlík Z 2008 *Class. Quantum Grav.* **25** 095011
- [5] Kopáček O, Karas V, Kovář J and Stuchlík Z 2010 *Astrophysical Journal* **722** 1240
- [6] Takahashi M and Koyama H 2009 *Astrophysical Journal* **693** 472
- [7] Bonnor W B, 1966 *Zeit. für Rhys.* **190** 444
- [8] Kojima Y, Kovář J and Karas V, *in preparation*

Extracting equations of state parameters from black hole-neutron star mergers

Koutarou Kyutoku^(a), Benjamin D. Lackey^(b), Masaru Shibata^(a), Patrick R. Brady^(b), John L. Friedman^(b)

^(a)*Yukawa Institute for Theoretical Physics, Kyoto University, Kyoto 606-8502, Japan*

^(b)*Department of Physics, University of Wisconsin-Milwaukee, P.O. Box 413,, Milwaukee, WI 53201, USA*

Abstract

The late inspiral, merger, and ringdown of a black hole-neutron star (BH-NS) system can provide information about the neutron-star equation of state (EOS). Candidate EOSs can be approximated by a parametrized piecewise-polytropic EOS above nuclear density, matched to a fixed low-density EOS; and we report results from a large set of BH-NS merger simulations that systematically vary two parameters. To within the accuracy of the simulations, we find that, apart from the neutron-star mass, a single physical parameter Λ , describing its deformability, can be extracted from the late inspiral, merger, and ringdown waveform. This parameter is related to the radius, mass, and $l = 2$ Love number, k_2 , of the neutron star by $\Lambda = 2k_2 R^5 / 3M_{\text{NS}}^5$, and it is the same parameter that determines the departure from point-particle dynamics during the early inspiral. Observations of gravitational waves from BH-NS coalescences thus restrict the EOS to a surface of constant Λ in the parameter space, thickened by the measurement error. Using various configurations of a single Advanced LIGO detector, we find that neutron stars are distinguishable from black holes of the same mass and that $\Lambda^{1/5}$ or equivalently R can be extracted to 10–40% accuracy from single events for mass ratios of $Q = 2$ and 3 at a distance of 100 Mpc, while with the proposed Einstein Telescope, EOS parameters can be extracted to accuracy an order of magnitude better.

1 Introduction

Construction of second-generation Advanced LIGO detectors is underway, and will soon begin for Advanced VIRGO and KAGRA, making it likely that gravitational waves from compact binaries will be observed in this decade. Plans are also in development for the third generation Einstein Telescope (ET) detector with an order-of-magnitude increase in sensitivity over Advanced LIGO. A major goal of the gravitational-wave program is to extract from observed waveforms the physical characteristics of their sources and, in particular, to use the waveforms of inspiraling and merging black hole (BH)-neutron star (NS) binaries to constrain the uncertain equation of state (EOS) of the NS matter. During inspiral the tidal interaction between the two objects leads to a small drift in the phase of the gravitational waveform relative to a point particle system. Specifically the tidal field \mathcal{E}_{ij} of one star will induce a quadrupole moment Q_{ij} in the other star given by $Q_{ij} = -\lambda \mathcal{E}_{ij}$ where λ is an EOS dependent quantity that describes how easily the star is distorted.

Numerical BH-NS simulations have been done to examine the dependence of the waveform on mass ratio, BH spin, NS mass, and the neutron-star EOS [2, 3]. The stronger information of the NS is found to be given by a sharp cutoff of the gravitational-wave spectrum at the merger. We perform an analysis of the detectability of EOS information with gravitational-wave detectors using these simulations [1], and find that, to within numerical accuracy, the EOS parameter extracted from the waveform is the same tidal parameter Λ that determines the departure from point particle behavior during inspiral; here Λ is a dimensionless version of the tidal parameter:

$$\Lambda := G\lambda \left(\frac{c^2}{GM_{\text{NS}}} \right)^5 = \frac{2}{3} k_2 \left(\frac{c^2 R}{GM_{\text{NS}}} \right)^5, \quad (1.1)$$

where M_{NS} , R , and k_2 are the NS mass, NS radius, and $l = 2$ quadrupole Love number, respectively.

2 Numerical simulations and merger waveforms

Gravitational waveforms at the late inspiral and merger stages are computed by numerical relativity simulations [2]. The initial condition is computed using LORENE and the simulation is performed using the AMR code, SACRA.

Gravitational waves are extracted using the Weyl scalar Ψ_4 , and the time integration is performed by the so-called fixed-frequency integration method [3].

To understand the dependence of the BH-NS waveform on the EOS we systematically vary the free parameters of a parametrized EOS, or the piecewise polytropic EOS, and then simulate the BH-NS binary coalescence for each set of parameters. We use a simplified two-parameter version of the piecewise-polytrope parametrization and uniformly vary each of these parameters. For our two parameters we use the pressure p_1 as well as a single fixed adiabatic index Γ for the core EOS. The crust EOS is given by a single polytrope with the constants $K_0 = 3.5966 \times 10^{13}$ in cgs units and $\Gamma_0 = 1.3569$ so that the pressure at 10^{13} g/cm^3 is $1.5689 \times 10^{31} \text{ dyne/cm}^2$. In total, 21 EOS models are adopted. In this work, we only focus on nonspinning BH-NS binaries and the NS mass M_{NS} is typically chosen to be $1.35M_\odot$, with some simulations for $1.2M_\odot$. The mass ratio, $Q \equiv M_{\text{BH}}/M_{\text{NS}}$, is taken typically to be 2, and some models are chosen to be $Q = 3$. Namely, our fiducial models are $M_{\text{NS}} = 1.35M_\odot$ and $Q = 2$. See Ref. [1] for the details of the EOS and BH-NS models.

3 Hybrid waveforms

Because our numerical simulations typically begin ~ 5 orbits before the merger, it is necessary to join the numerical waveforms to analytic waveforms representing the earlier inspiral. We match the numerical waveforms to the effective-one-body (EOB) waveforms that include inspiral, merger, and ringdown phases (see Ref. [1] and references therein) instead of post-Newtonian waveforms which are often not reliable during the last few cycles for higher mass ratios. This choice also allows us to use longer matching windows that average over numerical noise and the effects of eccentricity. For simplicity, and because it appears that an accurate description of the late inspiral dynamics just before merger requires 2PN tidal corrections which are not yet known, we will use the EOB waveforms without tidal corrections. Our results will therefore be lower limits on the measurability of EOS parameters, because the EOS dependence is coming solely from the numerical waveforms.

Denote a complex numerical waveform by $h_{\text{NR}}(t) = h_+^{\text{NR}}(t) - ih_\times^{\text{NR}}(t)$ and an EOB waveform with the same Q and M_{NS} by $h_{\text{EOB}}(t) = h_+^{\text{EOB}}(t) - ih_\times^{\text{EOB}}(t)$. A constant time-shift τ and phase-shift Φ can be applied to the EOB waveform to match it to a section of the numerical waveform by rewriting it as $h_{\text{EOB}}(t - \tau)e^{-i\Phi}$. We hold the numerical waveform fixed, because we must specify a matching window $T_I < t < T_F$, and there is only a small region of the numerical waveforms over which a valid match can be performed. Once the values of τ and Φ are determined, we will then choose to instead hold the EOB waveform fixed and shift the numerical waveform in the opposite direction by rewriting it as $h_{\text{NR}}^{\text{shift}}(t) = h_{\text{NR}}(t + \tau)e^{+i\Phi}$. This is done so that all of the numerical waveforms with the same Q and M_{NS} are aligned relative to a single fixed reference EOB waveform.

Over a matching window $T_I < t < T_F$, the normalized match between the waveforms is defined as

$$m(\tau, \Phi) = \frac{\text{Re} [z(\tau)e^{i\Phi}]}{\sigma_{\text{NR}}\sigma_{\text{EOB}}(\tau)}, \quad (3.1)$$

where

$$z(\tau) = \int_{T_I}^{T_F} h_{\text{NR}}(t)h_{\text{EOB}}^*(t - \tau) dt \quad (3.2)$$

and the normalizations for each waveform in the denominator are defined as

$$\sigma_{\text{NR}}^2 = \int_{T_I}^{T_F} |h_{\text{NR}}(t)|^2 dt \quad (3.3)$$

and

$$\sigma_{\text{EOB}}^2(\tau) = \int_{T_I}^{T_F} |h_{\text{EOB}}(t - \tau)|^2 dt. \quad (3.4)$$

The time-shift τ and phase Φ are chosen to maximize the match $m(\tau, \Phi)$ for a fixed matching window. Explicitly, the phase is determined analytically to be $\Phi = -\arg[z(\tau)]$; plugging this result back into Eq. (3.1), the time-shift is given by maximizing $|z(\tau)|/[\sigma_{\text{NR}}\sigma_{\text{EOB}}(\tau)]$ over τ . As stated above, once τ and Φ are found we shift the numerical waveform in the opposite direction to generate $h_{\text{NR}}^{\text{shift}}(t) = h_{\text{NR}}(t + \tau)e^{+i\Phi}$.

A hybrid waveform is generated by smoothly turning off the EOB waveform and smoothly turning on the shifted numerical waveform over a splicing window $S_I < t < S_F$ which can be chosen independently of the matching window. We employ Hann windows

$$w_{\text{off}}(t) = \frac{1}{2} \left[1 + \cos \left(\frac{\pi[t - S_I]}{S_F - S_I} \right) \right] \quad (3.5)$$

$$w_{\text{on}}(t) = \frac{1}{2} \left[1 - \cos \left(\frac{\pi[t - S_I]}{S_F - S_I} \right) \right]. \quad (3.6)$$

The hybrid waveform is then written

$$h_{\text{hybrid}}(t) = \begin{cases} h_{\text{EOB}}(t) & t < S_I \\ w_{\text{off}}(t)h_{\text{EOB}}(t) + w_{\text{on}}(t)h_{\text{NR}}^{\text{shift}}(t) & S_I < t < S_F \\ h_{\text{NR}}^{\text{shift}}(t) & t > S_F \end{cases} . \quad (3.7)$$

4 Parameter estimation

The output of a gravitational-wave detector $s(t) = n(t) + h(t)$ is the sum of detector noise $n(t)$ and a possible gravitational-wave signal $h(t)$. Stationary, Gaussian noise is characterized by its power spectral density (PSD) $S_n(|f|)$ defined by

$$\langle \tilde{n}(f)\tilde{n}^*(f') \rangle = \frac{1}{2}\delta(f - f')S_n(|f|) . \quad (4.1)$$

The gravitational wave signal is given in terms of the two polarizations of the gravitational wave by

$$h(t) = F_+h_+(t) + F_\times h_\times(t), \quad (4.2)$$

where $F_{+,\times}$ are the detector response functions and depend on the location of the binary and the polarization angle of the waves. We assume the binary is optimally located at the zenith of the detector and optimally oriented with its orbital plane parallel to that of the detector. This condition is equivalent to averaging h_+ and h_\times ($F_+ = F_\times = 1/2$).

It is well known that the optimal statistic for detection of a known signal $h(t)$ in additive Gaussian noise is

$$\rho = \frac{(h|s)}{\sqrt{(h|h)}} \quad (4.3)$$

where the inner product between two signals h_1 and h_2 is given by

$$(h_1|h_2) = 4\text{Re} \int_0^\infty \frac{\tilde{h}_1(f)\tilde{h}_2^*(f)}{S_n(f)} df. \quad (4.4)$$

In searches for gravitational-wave signals from compact binary mergers, a parametrized signal $h(t; \theta^A)$ is known in advance of detection, and the parameters θ^A must be estimated from the measured detector output $s(t)$. The parameters θ^A of an inspiral are estimated by maximizing the inner product of the signal $s(t)$ over the template waveforms $h(t; \theta^A)$. In the high signal-to-noise limit, the statistical uncertainty in the estimated parameters $\hat{\theta}^A$ arising from the instrumental noise can be estimated using the Fisher matrix

$$\Gamma_{AB} = \left(\frac{\partial h}{\partial \theta^A} \left| \frac{\partial h}{\partial \theta^B} \right) \right) \Big|_{\hat{\theta}^A} . \quad (4.5)$$

Note that $\hat{\theta}^A$ are the parameter values that maximize the signal-to-noise. The variance $\sigma_A^2 = \sigma_{AA} = \langle (\Delta\theta^A)^2 \rangle$ and covariance $\sigma_{AB} = \langle \Delta\theta^A \Delta\theta^B \rangle$ of the parameters are then given in terms of the Fisher matrix by

$$\langle \Delta\theta^A \Delta\theta^B \rangle = (\Gamma^{-1})^{AB} . \quad (4.6)$$

For hybrid waveforms, the partial derivatives in the Fisher matrix must be approximated with finite differences. It is most robust to compute the derivatives of the Fourier transforms used in the inner product. We rewrite the Fourier transform of each waveform in terms of the amplitude A and phase Φ as $\exp[\ln A - i\Phi]$. The derivatives $\partial \ln A / \partial \theta^A$ and $\partial \Phi / \partial \theta^A$ are then evaluated with finite differencing.

In general, errors in the parameters θ^A are correlated with each other forming an error ellipsoid in parameter space determined by the Fisher matrix Γ_{AB} . The uncorrelated parameters that are best extracted from the signal are found by diagonalizing Γ_{AB} . These new parameters are linear combinations of the original parameters θ^A . We focus attention below on the two parameters $\log(p_1)$ and Γ , and fix all other parameters as follows. We use the masses and spins determined from the numerical simulations and fix the time and phase shifts as determined during the hybrid waveform construction. We therefore construct the error ellipses in $\{\log(p_1), \Gamma\}$ parameter space and identify the parameter with the smallest statistical errors. We will leave an analysis of correlations due to uncertainty in masses and BH spin to future work.

5 Results

For the BHNS systems discussed here, the greatest departure from binary BH behavior occurs for gravitational-wave frequencies in the range 500–5000 Hz. As a result, detector configurations optimized for detection of BH-NS systems with low noise in the region below 500 Hz are not ideal for estimating EOS parameters. We therefore present results for the broadband aLIGO and the ET-D configurations.

We find that the resulting $1\text{-}\sigma$ error ellipses in the 2-dimensional parameter space $\{\log(p_1), \Gamma\}$ for an optimally oriented BH-NS with $Q = 2$ and $M_{\text{NS}} = 1.35M_{\odot}$ at a distance of 100 Mpc are aligned with surfaces of constant $\Lambda^{1/5}$. This indicates that, as expected, $\Lambda^{1/5}$ is the parameter that is best extracted from BH-NS gravitational-wave observations. Because $\Lambda^{1/5}$ and R are so closely aligned, we will use these two parameters interchangeably. The uncertainty in these quantities is $\sim 10\text{--}40\%$ for broadband aLIGO and $\sim 1\text{--}4\%$ for ET-D. The uncertainties for the higher mass ratio $Q = 3$ are somewhat larger than for $Q = 2$, but not significantly so. It is not clear how rapidly the uncertainty in $\Lambda^{1/5}$ and R will increase as the mass ratio is increased toward more realistic values. On the one hand the tidal distortion is likely to be much smaller for larger Q . On the other hand the overall signal will be louder, and the merger and ringdown will occur at lower frequencies where the noise is lower. Additional simulations for higher Q are needed to address this question.

References

- [1] B. D. Lackey, K. Kyutoku, M. Shibata, P. R. Brady, J. L. Friedman, *Phys. Rev. D* in press..
- [2] K. Kyutoku, M. Shibata, K. Taniguchi *Phys. Rev. D* **82**, 044049, (2010); erratum-ibid *D* **84**, 049902(E), (2011).
- [3] K. Kyutoku, H. Okawa, M. Shibata, K. Taniguchi *Phys. Rev. D* **84**, 064018, (2011).

Oscillating Bianchi IX Universe in Hořava-Lifshitz Gravity

Yosuke Misonoh^{94(a)}, Kei-ichi Maeda^{95(a)(b)} and Tsutomu Kobayashi^{96(c)(d)}

^(a)*Department of Physics, Waseda University, Okubo 3-4-1, Shinjuku, Tokyo 169-8555, Japan*

^(b)*Waseda Research Institute for Science and Engineering, Okubo 3-4-1, Shinjuku, Tokyo 169-8555, Japan*

^(c)*Hakubi Center, Kyoto University, Kyoto 606-8302, Japan*

^(d)*Department of Physics, Kyoto University, Kyoto 606-8502, Japan*

Abstract

We study a vacuum Bianchi IX universe in the context of Hořava-Lifshitz (HL) gravity. In particular, we focus on the classical dynamics of the universe and analyze how anisotropy changes the history of the universe. If the initial anisotropy is large, we find the universe which ends up with a big crunch after oscillations if a cosmological constant Λ is zero or negative. For $\Lambda > 0$, we find a variety of histories of the universe, that is de Sitter expanding universe after oscillations in addition to the oscillating solution and the previous big crunch solution. This fate of the universe shows sensitive dependence of initial conditions, which is one of the typical properties of a chaotic system. If the initial anisotropy is near the upper bound, we find the universe starting from a big bang and ending up with a big crunch for $\Lambda \leq 0$, while de Sitter expanding universe starting from a big bang for $\Lambda > 0$.

1 Introduction

Among attempts to construct a complete quantum gravitational theory, Hořava-Lifshitz (HL) gravity has been attracted much interest as a candidate for such a theory over the past years. HL gravity is characterized by its power-counting renormalizability, which is brought about by a Lifshitz-like anisotropic scaling as $t \rightarrow \ell^z t$, $\vec{x} \rightarrow \ell \vec{x}$, with the dynamical critical exponent $z = 3$ in the ultra-violet (UV) limit [1]. In order to recover general relativity (or the Lorentz invariance) in our world, one expects that the constant λ converges to unity in the infrared (IR) limit in the renormalization flow. Although it has been argued that there exist some fundamental problems in HL gravity, some extensions are proposed to remedy these difficulties. It is intriguing issue whether or not HL gravity can be a complete theory of quantum gravity.

As pointed out by earlier works, a big bang initial singularity may be avoided in the framework of HL cosmology due to the higher order terms in the spatial curvature R_{ij} in the action[2]. In this context, many researchers have studied the dynamics of the Friedmann-Lemaître-Robertson-Walker (FLRW) universe in HL gravity. Although we have also shown a singularity avoidance in HL cosmology[3], the following question may arise: Is this singularity avoidance generic? Is such a non-singular spacetime stable against anisotropic and/or inhomogeneous perturbations? In order to answer for these questions, we have to study more generic spacetime than the FLRW universe.

Therefore it is important to study whether or not non-singular universes in the present HL cosmology still exist with anisotropy and/or inhomogeneity. In the present paper, we shall investigate the possibility of the singularity avoidance in homogeneous but anisotropic Bianchi IX universe. Since we are interested in a singularity avoidance, we focus on an oscillating universe and analyze how anisotropy changes the history of the universe.

2 Bianchi IX universe in Hořava-Lifshitz gravity

First we introduce our Lagrangian of HL gravity, by which we will discuss the Bianchi IX universe. The basic variables in HL gravity are the lapse function, N , the shift vector, N_i , and the spatial metric, g_{ij} . These variables are subject to the action [1, 4]

$$S_{\text{HL}} = \frac{1}{2\kappa^2} \int dt d^3x \sqrt{g} N (L_K - V_{\text{HL}}[g_{ij}]) \quad (2.1)$$

⁹⁴Email address:y"underscore"misonou@moegi.waseda.jp

⁹⁵Email address:maeda"at"waseda.jp

⁹⁶Email address:tsutomu"at"tap.sphys.kyoto-u.ac.jp

where $\kappa^2 = 1/M_{\text{PL}}^2$ (M_{PL} : the Planck mass) and the kinetic term is given by

$$L_K = K_{ij}K^{ij} - \lambda K^2 \quad (2.2)$$

with

$$K_{ij} := \frac{1}{2N} (\partial_t g_{ij} - \nabla_i N_j - \nabla_j N_i) \quad (2.3)$$

$$K := g^{ij} K_{ij} \quad (2.4)$$

being the extrinsic curvature and its trace. The potential term V_{HL} will be defined shortly. In GR we have $\lambda = 1$, only for which the kinetic term is invariant under general coordinate transformations. In HL gravity, however, Lorentz symmetry is broken in exchange for renormalizability and the theory is invariant under the foliation-preserving diffeomorphism transformations,

$$t \rightarrow \bar{t}(t), \quad x^i \rightarrow \bar{x}^i(t, x^j). \quad (2.5)$$

As implied by the symmetry (2.5), it is most natural to consider the projectable version of HL gravity, for which the lapse function depends only on t : $N = N(t)$ [1]. Since the Hamiltonian constraint is derived from the variation with respect to the lapse function, in the projectable version of the theory, the resultant constraint equation is not imposed locally at each point in space, but rather is an integration over the whole space. In the cosmological setting, the projectability condition results in an additional dust-like component in the Friedmann equation [5].

The most generic form of the potential V_{HL} is given by [4]

$$\begin{aligned} V_{\text{HL}} = & 2\Lambda + g_1 R + \kappa^2 \left(g_2 R^2 + g_3 R^i_j R^j_i \right) + \kappa^3 g_4 \epsilon^{ijk} R_{i\ell} \nabla_j R^\ell_k \\ & + \kappa^4 \left(g_5 R^3 + g_6 R R^i_j R^j_i + g_7 R^i_j R^j_k R^k_i + g_8 R \Delta R + g_9 \nabla_i R_{jk} \nabla^i R^{jk} \right), \end{aligned} \quad (2.6)$$

where Λ is a cosmological constant, R^i_j and R are the Ricci and scalar curvatures of the 3-metric g_{ij} , respectively, and g_i 's ($i = 1, \dots, 9$) are the dimensionless coupling constants. By a suitable rescaling of time we set $g_1 = -1$. We also adopt the unit of $\kappa^2 = 1$ ($M_{\text{PL}} = 1$) throughout the paper.

Let us consider a Bianchi IX spacetime, which metric is written as

$$ds^2 = -dt^2 + \frac{a^2}{4} e^{2\beta_{ij}} \omega^i \omega^j, \quad (2.7)$$

where the invariant basis ω^i is given by

$$\begin{aligned} \omega^1 &= -\sin x^3 dx^1 + \sin x^1 \cos x^3 dx^2, \\ \omega^2 &= \cos x^3 dx^1 + \sin x^1 \sin x^3 dx^2, \\ \omega^3 &= \cos x^1 dx^2 + dx^3. \end{aligned} \quad (2.8)$$

A typical scale of length of the universe is given by a , which reduces to the usual scale factor in the case of the FLRW universe. We shall call it a scale factor in Bianchi IX model as well. The traceless tensor β_{ij} measures the anisotropy of the universe. The spacelike sections of the Bianchi IX is isomorphic to a three-sphere S^3 , and a closed FLRW model is a special case of the above metric in the isotropic limit ($\beta_{ij} \rightarrow 0$).

For a vacuum spacetime, without loss of generality, we can assume that β_{ij} is diagonalized as

$$\beta_{ij} = \text{diag} \left(\beta_+ + \sqrt{3}\beta_-, \beta_+ - \sqrt{3}\beta_-, -2\beta_+ \right). \quad (2.9)$$

The basic equations describing the dynamics of Bianchi IX spacetime in HL gravity are now given by the followings:

$$H^2 = \frac{2}{3(3\lambda - 1)} \left[\sigma^2 + \frac{64}{a^6} V(a, \beta_\pm) + \frac{8C}{a^3} \right], \quad (2.10)$$

$$\dot{H} + 3H^2 = \frac{8}{3(3\lambda - 1)} \left[\frac{8}{a^5} \frac{\partial V}{\partial a} + \frac{3C}{a^3} \right], \quad (2.11)$$

$$\dot{\beta}_\pm = \sigma_\pm \quad (2.12)$$

$$\dot{\sigma}_\pm + 3H\sigma_\pm + \frac{32}{3a^6} \frac{\partial V}{\partial \beta_\pm} = 0, \quad (2.13)$$

where

$$\sigma^2 := \frac{1}{2}\sigma_{\alpha\beta}\sigma^{\alpha\beta} = 3(\sigma_+^2 + \sigma_-^2). \quad (2.14)$$

$(\sigma_{\alpha\beta}) = \text{diag}(\sigma_+ + \sqrt{3}\sigma_-, \sigma_+ - \sqrt{3}\sigma_-, -2\sigma_+)$ is the shear tensor of a timelike normal vector perpendicular to the homogeneous three-space, and σ is its magnitude. It may be convenient to introduce the dimensionless shear by

$$\Sigma_{\pm} = \frac{\sigma_{\pm}}{H} \quad \text{and} \quad \Sigma = \frac{\sigma}{H}, \quad (2.15)$$

which measure the relative anisotropies to the expansion rate H . We also introduce the phase variable φ defined by

$$\varphi := \arctan\left(\frac{\sigma_-}{\sigma_+}\right), \quad (2.16)$$

which parameterizes the direction of the anisotropic expansion. The constant C arises from the projectability condition and it could be “dark matter” [5], but here we assume $C = 0$ just for simplicity. The potential V , which depends on a as well as β_{\pm} , is defined in [6].

We have performed numerical calculations to investigate the stability of oscillating FLRW universe against anisotropy. As a result, we have found five types of the fate of the universe.

- (A) Anisotropic oscillation : This oscillating solution shows only small deviation from the isotropic FLRW universe. The scale factor a (and then the volume) oscillates very regularly.
- (B) Big crunch after oscillations : An initially oscillating universe eventually collapses into a big crunch ($a = 0$) after many oscillations because of increase of the anisotropy. This is a singular solution.
- (C) From big bang to big crunch : The spacetime starts from a big bang and ends up with a big crunch. This type of solution cannot avoid singularity.
- (D) de Sitter expansion after oscillation : An initially oscillating universe eventually evolves into an exponentially expanding de Sitter universe because of a cosmological constant.
- (E) de Sitter expansion from big bang : the spacetime evolves into de Sitter phase without oscillation. The large anisotropy makes a jump from the oscillating phase to de Sitter phase in the beginning.

We summarize the results in Figure 1 (the coupling constants are chosen as $\lambda = 1, g_1 = 1, \Lambda = 3/10, g_3 = 1, g_5 = -3/100, g_9 = 1/100$ and $g_2 = g_4 = g_6 = g_7 = 0$).

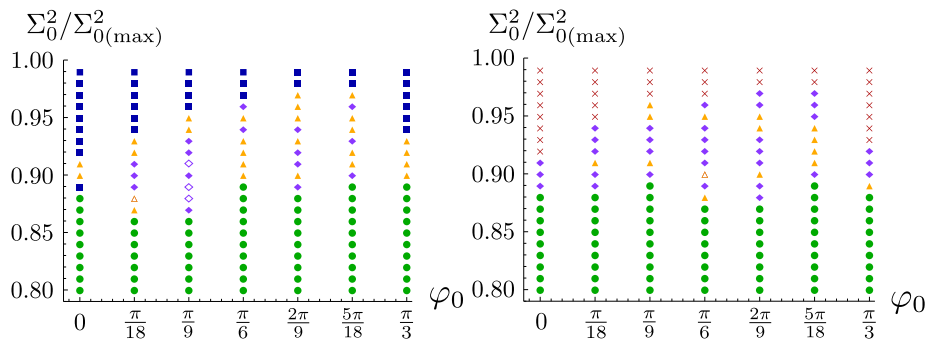


Figure 1: The fate of Bianchi IX universe in terms of initial anisotropy Σ_0^2 and φ_0 . We judge the fate of the universe at $t = 100t_{\text{PL}}$ (t_{PL} : the Planck time). The histories (A), (B), (C), (D) and (E) are represented by a filled green circle, yellow triangle, red cross, purple diamond and blue square, respectively. The empty yellow triangle and purple diamond are classified to the histories (B) and (D), respectively, but those oscillating periods are longer than $100t_{\text{PL}}$. We have set $a_0 = 1.0758$. \dot{a}_0 is fixed by the constraint equation [(a) $\dot{a}_0 > 0$ and (b) $\dot{a}_0 < 0$].

3 Conclusion

If the initial anisotropy is large, we find the universe which ends up with a big crunch after oscillations if a cosmological constant Λ is zero or negative. For $\Lambda > 0$, we find a variety of histories of the universe, that is de Sitter expanding universe after oscillations in addition to the oscillating solution and the previous big crunch solution. This fate of the universe shows sensitive dependence of initial conditions, which is one of the typical properties of a chaotic system. If the initial anisotropy is near the upper bound, we find the universe starting from a big bang and ending up with a big crunch for $\Lambda \leq 0$, while de Sitter expanding universe starting from a big bang for $\Lambda > 0$.

References

- [1] P. Hořava, Phys. Rev. D **79**, 084008 (2009) [arXiv: 0901.3775 [hep-th]].
- [2] R.H. Brandenberger, Phys. Rev. D **80**, 043516 (2009) [arXiv:0904.2835 [hep-th]]; arXiv: 1003.1745 [hep-th].
- [3] K. Maeda, Y. Misonoh and T. Kobayashi, Phys. Rev. D **82**, 064024 (2010) [arXiv:1006.2739 [hep-th]].
- [4] T.P. Sotiriou, M. Visser and S. Weinfurtner, Phys. Rev. Lett. **102**, 251601 (2009) [arXiv:0904.4464 [hep-th]]; T.P. Sotiriou, M. Visser and S. Weinfurtner, JHEP **0910**, 033 (2009) [arXiv:0905.2798 [hep-th]].
- [5] S. Mukohyama, Phys. Rev. D **80**, 064005 (2009) [arXiv: 0905.3563 [hep-th]].
- [6] Y. Misonoh, K. Maeda and T. Kobayashi, Phys. Rev. D **84**, 064030 (2011) [arXiv:1104.3978 [hep-th]].

Geometry and symmetry of target space of 5-dimensional Einstein-Maxwell-Chern-Simons theory with non-SUGRA coupling

Yoshiyuki Morisawa⁹⁷

*Faculty of Liberal Arts and Sciences, Osaka University of Economics and Law,
Gakuonji 6-10, Yao, Osaka 581-8511, Japan*

Abstract

We investigate the geometrical property and the symmetry of the target space of the five-dimensional Einstein-Maxwell-Chern-Simons system admitting two commuting spacelike Killing vector fields whose Chern-Simons coupling constant is the non-SUGRA value.

1 Introduction

As well known, the five-dimensional Einstein-Maxwell-Chern-Simons system admitting two commuting spacelike Killing vector fields whose Chern-Simons coupling constant is the SUGRA value can be reduced to the three-dimensional gravity-coupled sigma-model. Then the target space is the homogeneous space $G_{2(2)}/SO(4)$ [1, 2]. The solution generating methods using target space symmetry yield fruitful results. Assuming one more timelike symmetry, one can discuss black hole uniqueness as a boundary value problem using the Mazur identity [3].

However, this is not the case of the non-SUGRA value coupling constant. Although the five-dimensional Einstein-Maxwell-Chern-Simons system admitting two commuting spacelike Killing vector fields can also be reduced to the three-dimensional gravity-coupled sigma-model, the target space is not homogeneous and the symmetry of the target space cannot be described by a semisimple Lie algebra.

In this short article, we investigate the geometry and symmetry of this non-homogeneous target space. The target space is derived in Sec. 2. We show the symmetry of target space in Sec. 3 and investigate the non-semisimple Lie algebra which associates this symmetry in Sec. 4.

2 Reduction of 5D EMCS system with 2KVs

We consider the five-dimensional Einstein-Maxwell-Chern-Simons system and assume that the spacetime admits two commuting spacelike Killing vector fields ξ_1, ξ_2 . Then, the metric can be written in the form

$$g = f^{-1}\gamma_{ij}dx^i dx^j + f_{IJ}(dx^I + w^I{}_i dx^i)(dx^J + w^J{}_j dx^j), \quad (2.1)$$

where $I, J = 1, 2$, $i, j = 3, 4, 5$, $f = \det(f_{IJ})$ and γ_{ij} , $w^I{}_i$ and the gravitational potential $f_{IJ} = g(\xi_I, \xi_J)$ are independent on the coordinates x^I . We define the twist 1-form ω_I by

$$\omega_I = *(\xi_1 \wedge \xi_2 \wedge d\xi_I), \quad (2.2)$$

and then we obtain

$$d\omega_I = 2 *(\xi_1 \wedge \xi_2 \wedge R(\xi_I)). \quad (2.3)$$

Using these f_{IJ} and ω_I , the Ricci tensor R with respect to g and the Ricci tensor ${}^{(\gamma)}R$ with respect to the three-metric γ_{ij} are related to each other by

$$\begin{aligned} {}^{(\gamma)}R_{ij} &= f^{-2}\gamma_{im}\gamma_{jn}R^{mn} + f^{-1}f^{IJ}R_{IJ}\gamma_{ij} \\ &\quad + \frac{1}{4}f^{-2}f_{,i}f_{,j} + \frac{1}{4}f^{IJ}f^{KL}f_{IK,i}f_{JL,j} + \frac{1}{2}f^{-1}f^{IJ}\omega_{Ii}\omega_{Jj}. \end{aligned} \quad (2.4)$$

Next, we consider the Maxwell field $F = dA$ and assume that $\mathcal{L}_{\xi_I}A = 0$. We define the electric 1-forms E_I and the magnetic 1-form B by

$$E_I = -\iota_I F, \quad (2.5)$$

$$B = *(\xi_1 \wedge \xi_2 \wedge F). \quad (2.6)$$

⁹⁷Email address: morisawa@keiho-u.ac.jp

The Maxwell equation $dF = 0$ ensures the local existence of the electric potentials Φ_I such that

$$d\Phi_I = E_I. \quad (2.7)$$

From the Maxwell equation $d * F = -4\beta F \wedge F$, we can show that there locally exists the magnetic potential Ψ such that

$$d\Psi + 4\beta\epsilon^{PQ}\Phi_P d\Phi_Q = B, \quad (2.8)$$

where ϵ^{PQ} is the totally skew-symmetric symbol such that $\epsilon^{12} = 1$. Using these potentials Φ_I , Ψ , and the Einstein equation $R = \alpha(T - \frac{tr T}{3}g)$ (where T is the stress-energy tensor of the Maxwell field), Eq. (2.4) can be written by

$$\begin{aligned} {}^{(\gamma)}R_{ij} &= \frac{1}{4}f^{-2}f_{,i}f_{,j} + \frac{1}{4}f^{IJ}f^{KL}f_{IK,i}f_{JL,j} + \frac{1}{2}f^{-1}f^{IJ}\omega_{Ii}\omega_{Jj} \\ &\quad + \alpha \left[f^{IJ}\Phi_{I,i}\Phi_{J,j} + f^{-1}(\Psi_{,i} + 4\beta\epsilon^{IJ}\Phi_I\Phi_{J,i})(\Psi_{,j} + 4\beta\epsilon^{KL}\Phi_K\Phi_{L,j}) \right], \end{aligned} \quad (2.9)$$

and Eq. (2.3) ensures the local existence of the twist potentials λ_I such that

$$\omega_I = d\lambda_I + \alpha(\Psi d\Phi_I - \Phi_I d\Psi) - \frac{8}{3}\alpha\beta\epsilon^{PQ}\Phi_I\Phi_P d\Phi_Q. \quad (2.10)$$

We can also derive the equation of motion of the potentials f_{IJ} , λ_I , Φ_I and Ψ .

Finally, the Einstein-Maxwell-Chern-Simons system reduces to the equations derived from the action

$$S = \int d^3x \sqrt{|\gamma|} \gamma^{ij} \left({}^{(\gamma)}R - G_{AB} \frac{\partial X^A}{\partial x^i} \frac{\partial X^B}{\partial x^j} \right), \quad (2.11)$$

which describes the three-dimensional gravity-coupled sigma-model with the eight scalar fields $X^A = \{f_{11}, f_{12}, f_{22}, \lambda_1, \lambda_2, \Phi_1, \Phi_2, \Psi\}$ and the target space metric G . Here G_{AB} is given by

$$\begin{aligned} G_{AB} dX^A \otimes dX^B &= \frac{1}{4}f^{IJ}f^{KL}(df_{IJ} \otimes df_{KL} + df_{IK} \otimes df_{JL}) + \frac{1}{2}f^{-1}f^{IJ}\omega_I \otimes \omega_J \\ &\quad + \alpha[f^{IJ}d\Phi_I \otimes d\Phi_J + f^{-1}B \otimes B], \end{aligned} \quad (2.12)$$

where

$$B = d\Psi + 4\beta\epsilon^{PQ}\Phi_P d\Phi_Q, \quad (2.13)$$

$$\omega_I = d\lambda_I + \alpha(\Psi d\Phi_I - \Phi_I d\Psi) - \frac{8}{3}\alpha\beta\epsilon^{PQ}\Phi_I\Phi_P d\Phi_Q. \quad (2.14)$$

Here α is the parameter to absorb the normalization of the gauge field, β is related to the coupling constant of the Chern-Simons term, and $\alpha = 24\beta^2$ means the SUGRA value.

3 Target space symmetry with non-SUGRA value coupling constant

For the SUGRA value coupling constant $\alpha = 24\beta^2$, the target space has the fourteen Killing vector fields which are generators of $G_{2(2)}$ symmetry, and the target space is the homogeneous space $G_{2(2)}/SO(4)$.

On the other hand, the target space with $\alpha \neq 24\beta^2$ has only nine Killing vector fields:

$$K_1 = \frac{\partial}{\partial \lambda_1}, \tag{3.1}$$

$$K_2 = \frac{\partial}{\partial \lambda_2}, \tag{3.2}$$

$$K_3 = \Phi_1 \frac{\partial}{\partial \Phi_1} + \Psi \frac{\partial}{\partial \Psi} + 2\lambda_1 \frac{\partial}{\partial \lambda_1} + \lambda_2 \frac{\partial}{\partial \lambda_2} + 2f_{11} \frac{\partial}{\partial f_{11}} + f_{12} \frac{\partial}{\partial f_{12}}, \tag{3.3}$$

$$K_4 = \Phi_2 \frac{\partial}{\partial \Phi_2} + \Psi \frac{\partial}{\partial \Psi} + \lambda_1 \frac{\partial}{\partial \lambda_1} + 2\lambda_2 \frac{\partial}{\partial \lambda_2} + f_{12} \frac{\partial}{\partial f_{12}} + 2f_{22} \frac{\partial}{\partial f_{22}}, \tag{3.4}$$

$$K_5 = \Phi_1 \frac{\partial}{\partial \Phi_2} + \lambda_1 \frac{\partial}{\partial \lambda_2} + f_{11} \frac{\partial}{\partial f_{12}} + 2f_{12} \frac{\partial}{\partial f_{22}}, \tag{3.5}$$

$$K_6 = \Phi_2 \frac{\partial}{\partial \Phi_1} + \lambda_2 \frac{\partial}{\partial \lambda_1} + 2f_{12} \frac{\partial}{\partial f_{11}} + f_{22} \frac{\partial}{\partial f_{12}}, \tag{3.6}$$

$$K_7 = \frac{\partial}{\partial \Psi} - \alpha \Phi_I \frac{\partial}{\partial \lambda_I}, \tag{3.7}$$

$$K_8 = \frac{\partial}{\partial \Phi_1} - 4\beta \Phi_2 \frac{\partial}{\partial \Psi} + \alpha \Psi \frac{\partial}{\partial \lambda_1} + \frac{4}{3} \alpha \beta \Phi_2 \Phi_J \frac{\partial}{\partial \lambda_J}, \tag{3.8}$$

$$K_9 = \frac{\partial}{\partial \Phi_2} + 4\beta \Phi_1 \frac{\partial}{\partial \Psi} + \alpha \Psi \frac{\partial}{\partial \lambda_2} - \frac{4}{3} \alpha \beta \Phi_1 \Phi_J \frac{\partial}{\partial \lambda_J}. \tag{3.9}$$

We obtain the commutation relations as follows:

	K_1	K_2	K_7	K_8	K_9	$K_3 + K_4$	$K_3 - K_4$	K_5	K_6
K_1						$3K_1$	K_1	K_2	
K_2						$3K_2$	$-K_2$		K_1
K_7				$2\alpha K_1$	$2\alpha K_2$	$2K_7$			
K_8			$-2\alpha K_1$		$8\beta K_7$	K_8	K_8	K_9	
K_9			$-2\alpha K_2$	$-8\beta K_7$		K_9	$-K_9$		K_8
$K_3 + K_4$	$-3K_1$	$-3K_2$	$-2K_7$	$-K_8$	$-K_9$				
$K_3 - K_4$	$-K_1$	K_2		$-K_8$	K_9			$2K_5$	$-2K_6$
K_5	$-K_2$			$-K_9$			$-2K_5$		$K_3 - K_4$
K_6		$-K_1$			$-K_8$		$2K_6$	$-K_3 + K_4$	

These form a non-semisimple Lie algebra. Hereafter, we denote by g_9 this algebra.

4 Non-semisimple Lie algebra g_9

4.1 As subalgebra of g_2

Now we investigate the non-semisimple Lie algebra g_9 . First, we show that g_9 is a subalgebra of g_2 . It is easily confirmed that $(K_1, K_2, K_3 + K_4, K_3 - K_4, K_5, K_6, K_7, K_8, K_9)$ obeys the same algebra as the 9 generators $(X_1, X_2, X_7, X_6, X_{11}, X_4, X_3, X_5, X_8)$ of the $G_{2(2)}$ symmetry of the target space of the $D = 5$ minimal supergravity in Bouchareb *et al.* [2] upto constant coefficients. The root systems of g_2 and g_9 are given in Figure 1.

4.2 Ideals of g_9

$g_9 (= \{K_1, K_2, K_3 + K_4, K_3 - K_4, K_5, K_6, K_7, K_8, K_9\})$ has non-trivial ideals:

- $\{K_1, K_2\}$
- $\{K_1, K_2, K_7\}$
- $\{K_1, K_2, K_7, K_8, K_9\}$
- $\{K_1, K_2, K_3 - K_4, K_7, K_8, K_9\}$
- $\{K_1, K_2, K_3 - K_4, K_5, K_6, K_7, K_8, K_9\}$

where first four are the solvable ideals, and first three are the nilpotent ideals.

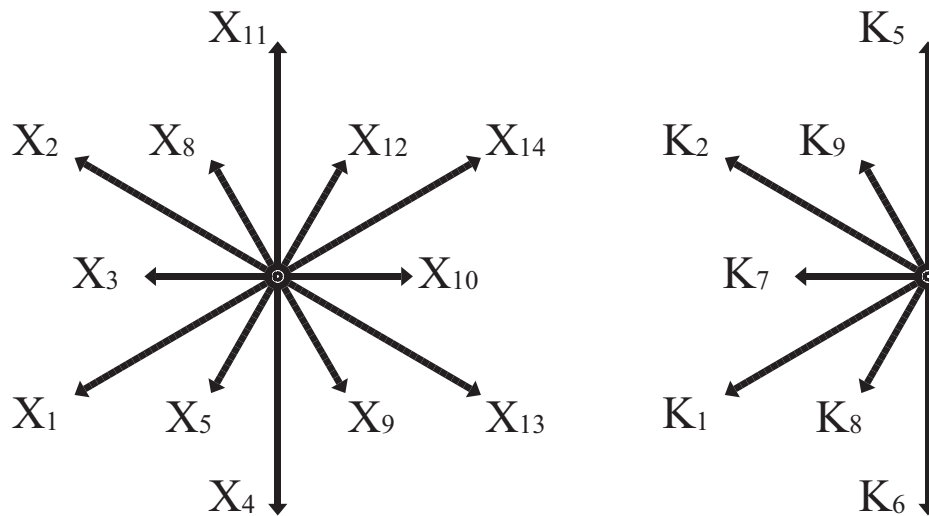


Figure 1: (left) The root system of g_2 [2], and (right) the root system of g_9

4.3 As parabolic subalgebra of g_2

Then, we show that g_9 is the parabolic Lie subalgebra of g_2 . The eight Killing vectors $\{X_1, \dots, X_8\}$ span the Borel subalgebra of g_2 , they are included in the 9 generators $\{X_1, \dots, X_8, X_{11}\}$. Here, $\{X_1, X_2, X_3, X_5, X_8\}$ is perpendicular to $\{X_1, \dots, X_8, X_{11}\}$ and corresponds to $\{K_1, K_2, K_7, K_8, K_9\}$ which is the maximal nilpotent ideal of g_9 . So, g_9 is the parabolic Lie subalgebra of g_2 .

5 Summary

We investigate the geometry and symmetry of the target space of the five-dimensional Einstein-Maxwell-Chern-Simons theory with non-SUGRA value coupling constant admitting two commuting spacelike Killing vector fields. The target space has the nine Killing vector fields and is not homogeneous. These nine Killing vector fields span the non-semisimple Lie algebra g_9 , which is the parabolic Lie subalgebra of g_2 .

Acknowledgement

This short article is based on the collaboration with Daisuke Ida, and Yukinori Yasui.

References

- [1] S. Mizoguchi and N. Ohta, Phys. Lett. B **441**, 123 (1998) [arXiv:hep-th/9807111].
- [2] A. Bouchareb, G. Clement, C. M. Chen, D. V. Gal'tsov, N. G. Scherbluk and T. Wolf, Phys. Rev. D **76**, 104032 (2007) [Erratum-ibid. D **78**, 029901 (2008)] [arXiv:0708.2361 [hep-th]].
- [3] S. Tomizawa, Y. Yasui and A. Ishibashi, Phys. Rev. D **79**, 124023 (2009) [arXiv:0901.4724 [hep-th]].

Quantum interference in Chern-Simons gravity

Hiroki Okawara

*Faculty of Science and Technology,
Hirosaki University, Hirosaki 036-8561, Japan*

Abstract

We discuss the quantum interference effects in a curved spacetime, and consider the Chern-Simons gravity as a particular example.

1 Quantum interference effect

The relativistic Lagrangian for a particle with mass m in a curved spacetime is given by

$$\mathcal{L} = -mc\sqrt{g_{\mu\nu}\dot{x}^\mu\dot{x}^\nu} \quad (1.1)$$

where an overdot denotes d/dt . We consider a system that is weakly gravitating, such that we can expand the metric about a fixing Minkowski background $\eta_{\mu\nu}$. Let us write $g_{\mu\nu} = \eta_{\mu\nu} + h_{\mu\nu}$, with $h_{\mu\nu}$ a small perturbation.

At 1PN order [1]

$$\begin{aligned} \mathcal{L} &= -mc^2 \left(1 + h_{00} + 2h_{0i} \frac{\dot{x}^i}{c} - \frac{(\dot{x}^i)^2}{c^2} + h_{ij} \frac{\dot{x}^i \dot{x}^j}{c^2} \right)^{\frac{1}{2}} \\ &\simeq -mc^2 \left(1 + \frac{1}{2}h_{00} + h_{0i} \frac{\dot{x}^i}{c} - \frac{(\dot{x}^i)^2}{2c^2} \right). \end{aligned} \quad (1.2)$$

Schrödinger equation

$$i\hbar \frac{\partial}{\partial t} \psi = \left(\frac{1}{2m} (\vec{p} + m\vec{h}_0)^2 + \frac{1}{2}mc^2 h_{00} \right) \psi. \quad (1.3)$$

Phase difference in quantum interferometry

$$\begin{aligned} \Delta &= \frac{mc}{\hbar} \left(\int_{\text{path } ACD} \vec{h}_0 \cdot d\vec{r} - \int_{\text{path } ABD} \vec{h}_0 \cdot d\vec{r} \right) \\ &= \frac{mc}{\hbar} \oint_C \vec{h}_0 \cdot d\vec{r} \\ &= \frac{mc}{\hbar} \int_S (\vec{\nabla} \times \vec{h}_0) \cdot d\vec{S}. \end{aligned} \quad (1.4)$$

2 Chern-Simons (CS) gravity

2.1 CS correction

CS gravity modifies GR by the addition of a new term to the action,

$$S_{CS} = \frac{1}{16\pi G} \int d^4x \frac{1}{4} f R^* R, \quad (2.1)$$

where G is Newton's gravitational constant, f is a prescribed external quantity (with units of squared length in geometrized units) that acts as a coupling constant, R is the Ricci scalar, and the star stands for the dual operation. The modified field equations can be obtained by varying the action with respect to the metric. The CS correction to the metric becomes [2]

$$\delta g_{0i} = 2 \sum_A \frac{f}{r_A} \left[\frac{m_A}{r_A} (v_A \times n_A)^i - \frac{J_A^i}{2r_A^2} + \frac{3}{2} \frac{(J_A \cdot n_A)}{r_A^2} n_A^i \right]. \quad (2.2)$$

The gyroscope acquire the precessional $\Omega^i = (\nabla \times g)^i$, where $g^i = g_{0i}$.

The CS modification to the precession angular velocity is given by

$$\delta \Omega^i = 2 \sum_A f \frac{m_A}{r_A^3} [3(v_A \cdot n_A) n_A^i - v_A^i], \quad (2.3)$$

and defined via $\delta \Omega^i = \Omega^i - \Omega_{GR}^i$, where Ω_{GR}^i is the GR prediction.

2.2 A particular example

When the number of bodies $A=2$, we set up the neutron interferometer in the Earth's surface. v the velocity is orbital speed of the Earth around the Sun.

The phase difference in Chern-Simons gravity

$$\Delta = \frac{mc}{\hbar} \int_S 2f \frac{M}{r^3} [3(\vec{v} \cdot \vec{n})\vec{n} - \vec{v}] \vec{N} dS, \quad (2.4)$$

where \vec{n} is the unit position vector of the interferometer from the center of the Earth, and \vec{N} is the unit vector of the interferometry loop.

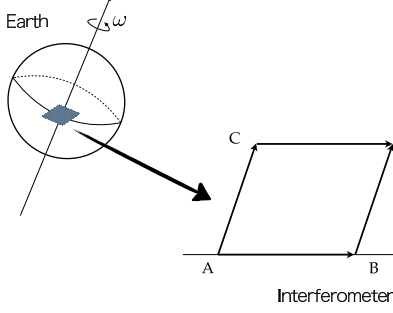


Figure 1: The neutron interferometer on the Earth

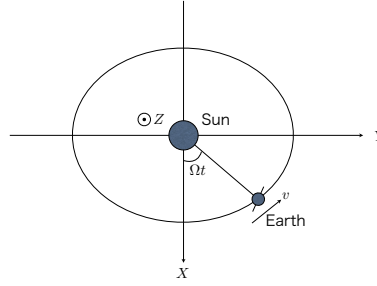


Figure 2: Earth motion

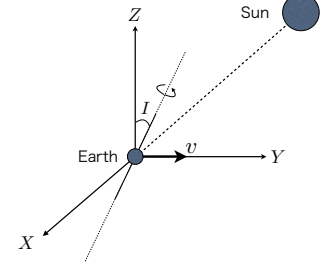


Figure 3: Inclination and velocity

3 Time variation

Coordinate rotation

$$\vec{N}(t) = R(t)\vec{N}_0, \quad \vec{n}(t) = R(t)\vec{n}_0, \quad R(t) = \begin{pmatrix} \cos(\omega t) & -\sin(\omega t) & 0 \\ \sin(\omega t) & \cos(\omega t) & 0 \\ 0 & 0 & 1 \end{pmatrix}. \quad (3.1)$$

Adding a Daily and Seasonal variation,

$$[3(\vec{v} \cdot \vec{n})\vec{n} - \vec{v}]\vec{N} = (R^{-1}\vec{v})^T (3(\vec{n}_0 \cdot \vec{N}_0)\vec{n}_0 - \vec{N}_0) \quad (3.2)$$

$$\vec{v}(t) = \begin{pmatrix} \cos(\Omega t) & \sin(\Omega t) & 0 \\ -\sin(\Omega t) & \cos(\Omega t) & 0 \\ 0 & 0 & 1 \end{pmatrix} \begin{pmatrix} 1 & 0 & 0 \\ 0 & \cos(I) & -\sin(I) \\ 0 & \sin(I) & \cos(I) \end{pmatrix} \begin{pmatrix} \cos(\Omega t) \\ \sin(\Omega t) \\ 0 \end{pmatrix} v, \quad (3.3)$$

where Ω is one year cycle and ω is one day cycle. I is axial tilt ; the angle between the Earth's rotational axis.

$$(R^{-1}\vec{v})_x = [\cos(\Omega t) \sin(\Omega t) \cos(I) - \cos(\Omega t) \sin(\Omega t)] \sin(\omega t) + [\sin^2(\Omega t) \cos(I) + \cos^2(\Omega t)] \cos(\omega t) \quad (3.4)$$

$$(R^{-1}\vec{v})_y = [\cos(\Omega t) \sin(\Omega t) \cos(I) - \cos(\Omega t) \sin(\Omega t)] \cos(\omega t) - [\sin^2(\Omega t) \cos(I) + \cos^2(\Omega t)] \sin(\omega t) \quad (3.5)$$

$$(R^{-1}\vec{v})_z = \sin(\Omega t) \sin(I) \quad (3.6)$$

Equatorial plane

4 Conclusion

We obtain quantum interference effects in Chern-Simons gravity.

- Daily and seasonal variation by the Earth's spin and revolution

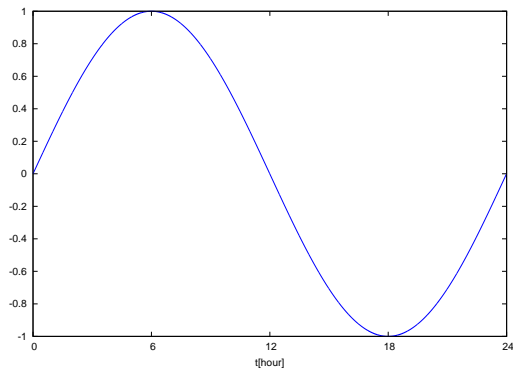


Figure 4: Daily variation

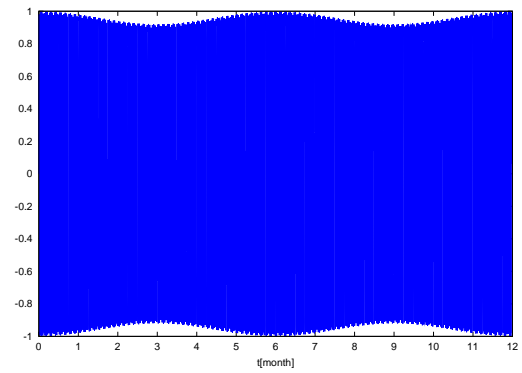


Figure 5: Seasonal variation

References

- [1] L. D. Landau and E. M. Lifshitz, *The Classical Theory of Fields* (Pergamom Press, Oxford, 1962).
- [2] Stephon Alexander and Nicolas Yunes, *Phys. Rev. Lett.* **99**, 241101 (2007).
- [3] H. Okawara, K. Yamada, H. Aasada, in preparation.

Effectiveness of Empirical Mode Decomposition in Search for Gravitational Wave Signals II

— An Possibility of Constructing an Alert System —

Ken-ichi Oohara^{98(a)}, Jordan B. Camp^(b), Yuta Hiranuma^(a), Alexander Stroeer^(c)
and Hiroataka Takahashi^{(d),(e)}

^(a)Department of Physics, Niigata University, Niigata 950-2181, Japan

^(b)Laboratory for Gravitational Physics, Goddard Space Flight Center, Greenbelt, Maryland 20771, USA

^(c)Center for Gravitational Wave Astronomy, The University of Texas at Brownsville, Brownsville, Texas 78520, USA

^(d)Department of Humanities, Yamanashi Eiwa College, Yamanashi, 400-8555 Japan

^(e)Earthquake Research Institute, The University of Tokyo, Tokyo 113-0032, Japan

Abstract

The Hilbert-Huang transform is the combination of the empirical mode decomposition and the Hilbert spectral analysis. Here we investigate a possibility of constructing an alert system with the Hilbert-Huang transform in search for gravitational wave signals.

1 Instruction

The Hilbert-Huang transform (HHT), proposed by Huang et al.[1]–[3], is novel data analysis technique used to detect and characterize physical oscillatory modes in time series data. It can be applied to non-linear and non-stationary time series data, while traditional analysis methods such as the Fourier transform and the wavelet transform presume the data is linear and stationary. The HHT has been applied to various fields; biomedical engineering, financial engineering, image processing, geophysics etc.

The HHT consists of the empirical mode decomposition (EMD), followed by the Hilbert Spectral Analysis (HSA). The EMD decomposes the data into intrinsic mode function (IMF), each representing a locally monochromatic frequency scale of the data. The HSA derives the instantaneous amplitude (IA) and frequency (IF) from the analytical complex representation of each IMF; the IMF itself and the Hilbert transform of the IMF are the real and imaginary parts, respectively. The IA and the IF are given by taking the absolute value and by differentiating the phase.

The IA of some of the IMFs will stand out for a few moments if the noisy data from a detector contains a real signal of the gravitational waves. Thus we will investigate a possibility of constructing an alert system with the HHT.

2 The Hilbert Spectral Analysis and the Empirical Mode Decomposition

The Hilbert transform $\hat{u}(t)$ of a function $u(t)$ is defined by

$$\hat{u}(t) = \frac{1}{\pi} P \int_{-\infty}^{\infty} \frac{u(t')}{t-t'} dt' = u(t) * \left(\frac{1}{\pi t} \right), \quad (2.1)$$

where P and $*$ denote the Cauchy principal value and the convolution, respectively. By the theory of the Poisson integral, $F(t) = u(t) + i\hat{u}(t)$ is the boundary value of a holomorphic function $F(z) = F(t + iy) = a(t)e^{i\theta(t)}$ in the upper half-plane, if $u(t) \in L^p(\mathbf{R})$. Then the instantaneous amplitude (IA) $a(t)$ and the instantaneous frequency (IF) $f(t)$ is, respectively, defined by

$$a(t) = \sqrt{u(t)^2 + \hat{u}(t)^2} \quad (2.2)$$

and

$$f(t) = \frac{1}{2\pi} \frac{d\theta(t)}{dt} \quad \text{where} \quad \theta(t) = \tan^{-1} \left(\frac{\hat{u}(t)}{u(t)} \right). \quad (2.3)$$

⁹⁸Email address: oohara@astro.sc.niigata-u.ac.jp

However, for $u(t) \notin L^p(\mathbf{R})$, the IF obtained using the above method is not necessarily physically meaningful. For example, $u(t) = \cos \omega t + C$, where C and ω are constants, does not yield a constant frequency of ω . To explore the applicability of the Hilbert transform, Huang et al. [2] showed that the necessary conditions to define a meaningful IF are that the functions are symmetric with respect to the local zero mean and have the same numbers of zero crossings and extrema. Thus they applied the empirical mode decomposition (EMD) to the original data $u(t)$ to decompose it into intrinsic mode functions (IMFs) and the residual. Each IMF satisfies the following conditions: (1) in the whole data set, the number of extrema and the number of zero crossings must either equal or differ at most by one; and (2) at any point, the mean value of the envelope defined by the local maxima and the envelope defined by the local minima is zero. The EMD is a series of high-pass filters in a sense. The algorithm is summarized in the following outline:

- $h_0(t) = u(t)$
- for $i = 0$ to i_{\max}
 - ★ $h_{i,0}(t) = h_i(t)$
 - ★ for $k = 0$ to k_{\max}
 - Identify the local maxima and minima of $h_{i,k}(t)$.
 - $U_{i,k}(t)$ = the upper envelope joining the local maxima using a cubic spline
 - $L_{i,k}(t)$ = the lower envelope joining the local minima using a cubic spline
 - $m_{i,k}(t) = (U_{i,k}(t) + L_{i,k}(t))/2$
 - $h_{i,k+1}(t) = h_{i,k}(t) - m_{i,k}(t)$
 - Exit from the loop k if $\sum_j |m_{i,k}(t_j)| < \varepsilon \sum_j |h_{i,k}(t_j)|$ with a small parameter ε .
 - ★ $\text{IMF}_i(t) = h_{i,k}(t)$
 - ★ $h_{i+1} = h_i(t) - c_i(t)$
- residual: $r(t) = h_{i_{\max}+1}(t)$

The parameter i_{\max} specifies the number of IMFs to be extracted from $u(t)$, which is in general set depending on the characteristics of the signal. The parameter k_{\max} must be a sufficiently large number, namely several thousand or more, according to the value of ε , since it means failure in the mode decomposition that k exceeds k_{\max} without satisfying the stoppage criterion.

The EMD can be applied to decompose an observed data into signals and noises. In the original EMD, however, mode mixing appears frequently. Mode mixing is defined as a single IMF either consisting of signals of widely disparate scale, or a signals of a similar scale residing in different IMF components. It is a consequence of signal intermittency, which could not only cause serious aliasing in the time-frequency distribution, but also make the individual IMF devoid of physical meaning. To overcome the drawback, Wu and Huang [4] proposed the ensemble EMD (EEMD), which defines the true IMF components as the mean of an ensemble of trials, each consisting of the signal plus a white noise of finite amplitude. The signal usually appears in an IMF of a small value of i with the EMD, namely $i = 1$ in the following case, while it shifts to $i = 3$ with the EEMD since the IMF1 and IMF2 contain only noises. Thus we specify $i_{\max} = 6$ in the following.

For example, we applied the EMD and the EEMD to a sine-Gaussian signal plus a Gaussian noise;

$$u(t) = s(t) + n(t) = a \exp[-(t/\tau)^2] \sin(2\pi ft) + n(t), \quad (2.4)$$

where $f = 300$ Hz, $\tau = (0.1 \text{ sec})/(2\pi) = 0.016$ sec. The noise $n(t)$ is generated by Gaussian random variates with mean zero and standard deviation $\sigma = 1$. Figure 1 shows the signal $s(t)$ and $u(t)$ of $a = 3.12$ (SNR = 20) and $a = 1.56$ (SNR = 10), as well as the noise $n(t)$ (SNR = 0), where SNR is defined by $\text{SNR} = \sqrt{\sum_i h(t_i)}/\sigma$. The

IMF 1 and its IA with the EMD are shown in Fig.2 and 3, and the IMF 3 and its IA with the EEMD in Fig.4 and 5.

3 Signal Search with the HHT

We consider the possibility of constructing an alert system with the HHT in search for gravitational wave signals. Here we will call an alert if we find an excess power in an IMF, that is, the IA is greater than a certain critical value IA_c for the duration $\delta t > \delta t_c$. Then further analysis will be carried out to investigate whether a real signal is contained.

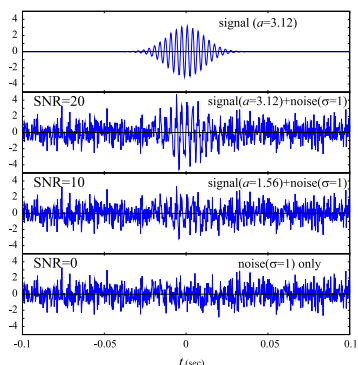


Fig.1: The signal + the Gaussian noise of $\sigma = 1$.

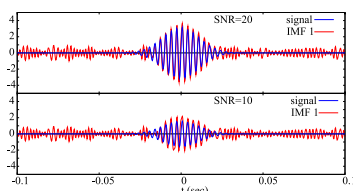


Fig.2: The IMF1 with the EMD.

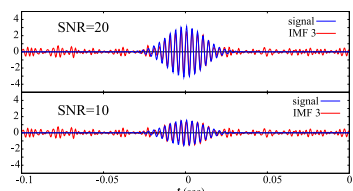


Fig.4: The IMF3 with the EEMD.

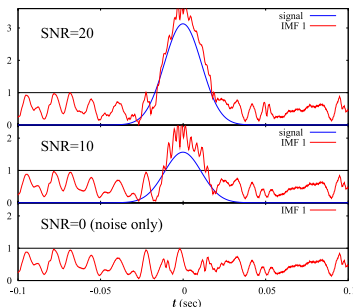


Fig.3: The instantaneous amplitude of IMF1 with the EMD.

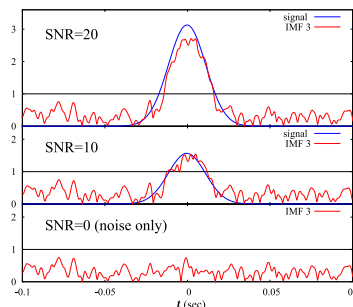


Fig.5: The instantaneous amplitude of IMF3 with the EEMD.

There are some parameters to be fixed in the EMD and the EEMD for this purpose. The most important parameter is the stoppage criterion ε of the EMD. We look for the optimal values of ε , IA_c and δt_c with the signal given by Eq.(2.4). For each parameter set of ε , IA_c and δt_c , we examine the rate of missing signals for SNR = 10 and 20 as well as the rate of false alert for SNR = 0 or noise only, using 400 samples, each of which is generated by adding a Gaussian random variate with a different seed to the signal of 1 second long. The sampling frequency of the data is 4096 Hz. We choose the parameters for the EEMD as follows; the size of ensemble $N = 100$, the standard deviation of the Gaussian noise to be added to each trial $\sigma_e = 2$. We tried other values of σ_e but we found that this value is optimal. As for N , we verified that the results hardly change even with $N > 100$ but the value $N \approx 50$ is too small.

First, we performed the EMD procedure for 400 samples of each data with the EMD stoppage criteria $\varepsilon = 10^{-2}, 10^{-3}$ and 10^{-4} . The alert criteria was examined for $IA_c = 0.5, 0.8$ and 1.0 ; $\delta t_c = 0.005$ sec and 0.01 sec. The results are shown in Tables 1. The column ‘false’ shows the number of false alert in 400 sample data for noise only data (SNR=0), while the numbers of missing signals for 400 sample data including signal of SNR=10 and 20 are shown in the column ‘miss10’ and ‘miss20’, respectively. If we accept false alert less than 10% and missing signals less than 1%, only $IA_c=1.0$ and $\delta t_c = 0.01$ sec is acceptable for SNR=20, while no acceptable parameter set is found for SNR=10.

Then we applied the EEMD, the results shown in Table 2. Parameter sets of $IA_c = 0.8$ with $(\delta t_c, \varepsilon) = (0.005, 10^{-3}), (0.005, 10^{-4})$ and $(0.01, 10^{-3})$ are suitable for searching signal of SNR ≥ 10 .

4 Conclusion

We investigated the possibility of the HHT for the alert system of the gravitational wave search. The EEMD procedure with some optimal parameters may be promising. The CPU time is less than 5 seconds with Intel Core i7 920 (2.67 GHz) for analysing 1 sec data using the EEMD with $\varepsilon = 10^{-3}$ and the size of each ensemble $N = 100$. However, it is reduced to about 0.05 seconds if 64 core of the latest CPU are used, since calculation in each trial of the ensemble can be fully parallelized via the message passing interface (MPI).

The instantaneous frequency is not used here, but it may be possible to reduce the rate of false alert with it. Although we considered only the signal of a fixed frequency here, we found that the above parameter sets are applicable for signals of time-varying frequencies as well. These results will be given elsewhere.

Acknowledgments

This work was in part supported by JSPS KAKENHI, Grant-in-Aid for Scientific Research (No. 23540293; K. Oohara and H. Takahasi) and Grant-in-Aid for Young Scientists (No. 23740207; H. Takahashi).

Table 1: The numbers of false alert and missing signals in 400 sample data with the EMD. False denotes false alert for noise only data, while miss10 and miss20 denote missing signals for data including signal of SNR=10 and 20, respectively.

$IA_c = 0.5, \delta t_c = 0.005$				$IA_c = 0.8, \delta t_c = 0.005$				$IA_c = 1.0, \delta t_c = 0.005$			
ε	false	miss10	miss20	ε	false	miss10	miss20	ε	false	miss10	miss20
10^{-2}	400	0	0	10^{-2}	399	2	0	10^{-2}	219	5	0
10^{-3}	400	0	0	10^{-3}	399	0	0	10^{-3}	178	7	0
10^{-4}	400	0	0	10^{-4}	398	0	0	10^{-4}	127	4	0
$IA_c = 0.5, \delta t_c = 0.01$				$IA_c = 0.8, \delta t_c = 0.01$				$IA_c = 1.0, \delta t_c = 0.01$			
ε	false	miss10	miss20	ε	false	miss10	miss20	ε	false	miss10	miss20
10^{-2}	400	14	0	10^{-2}	179	102	0	10^{-2}	13	133	0
10^{-3}	400	5	0	10^{-3}	201	73	0	10^{-3}	9	134	0
10^{-4}	400	0	0	10^{-4}	232	38	0	10^{-4}	13	97	0

Table 2: The same table of Table 1 with the EEMD.

$IA_c = 0.5, \delta t_c = 0.005$				$IA_c = 0.8, \delta t_c = 0.005$				$IA_c = 1.0, \delta t_c = 0.005$			
ε	false	miss10	miss20	ε	false	miss10	miss20	ε	false	miss10	miss20
10^{-2}	400	0	0	10^{-2}	120	52	0	10^{-2}	4	336	0
10^{-3}	400	0	0	10^{-3}	35	0	0	10^{-3}	1	12	0
10^{-4}	400	0	0	10^{-4}	3	1	0	10^{-4}	0	15	0
$IA_c = 0.5, \delta t_c = 0.01$				$IA_c = 0.8, \delta t_c = 0.01$				$IA_c = 1.0, \delta t_c = 0.01$			
ε	false	miss10	miss20	ε	false	miss10	miss20	ε	false	miss10	miss20
10^{-2}	323	6	0	10^{-2}	2	174	0	10^{-2}	0	392	2
10^{-3}	268	0	0	10^{-3}	2	1	0	10^{-3}	0	76	0
10^{-4}	147	3	0	10^{-4}	0	23	0	10^{-4}	0	120	0

References

- [1] N. E. Huang, S. R. Long and Z. Shen, *Adv. Appl. Mech.*, **32**, 59, (1996).
- [2] N. E. Huang et al., *Proc. R. Soc. London*, **454**, 903 (1998).
- [3] N. E. Huang, Z. Shen and S. R. Long, *Annu. Rev. Fluid. Mech.*, **31**, 417 (1999).
- [4] Z. Wu and N. E. Huang, *Adv. Adapt. Data Anal.*, **1**, 1 (2009).

Cosmic microwave background anisotropy produced by network of nonlinear super-structures

Nobuyuki Sakai⁹⁹

Department of Education, Yamagata University, Yamagata 990-8560, Japan

Abstract

Cross-correlation between the cosmic microwave background radiation (CMB) and galaxy distribution have indicated that nonlinear supervoids and superclusters with $> 100h^{-1}\text{Mpc}$ located at $z < 0.75$ make cold and hot spots of CMB, respectively. It is therefore natural to suppose that similar voids and clusters are distributed in the whole universe. In this paper we study the effect of a supervoid network on the CMB anisotropy in the ΛCDM model. First, we show that supervoids in high- z produce smaller effects, contrary to the case of Einstein-de Sitter universe. Next, we calculate the CMB angular power spectrum C_l , and find it is consistent with that obtained by WMAP observational data.

1 Introduction

While the cosmic microwave background radiation (CMB) reflects density fluctuations on the last-scattering surface, it also includes the secondary anisotropy produced by large scale structure, which is called the integrated Sachs-Wolfe (ISW) effect [1]. Although the secondary anisotropy may be smaller than the primordial anisotropy, it is important to estimate it not only to evaluate primordial fluctuations precisely but also to explore the large-scale distribution of dark matter. In fact, Granett, Neyrinck & Szapudi found hot and cold spots on the CMB associated with void and cluster structures at redshifts $0.4 < z < 0.75$ identified in the Sloan Digital Sky Survey luminous red galaxy catalog [2]. Also, Francis & Peacock showed that the ISW effect due to local structures at redshift $z < 0.3$ significantly affects the large-angle CMB anisotropies [3]. These results based on the galaxy-CMB cross-correlation may suggest an existence of anomalously large perturbations or new physics on scales $> 100\text{Mpc}$.

Motivated by these recent works, Inoue, Sakai & Tomita evaluated the nonlinear ISW effect produced by a single supervoid or supercluster in several methods [4]: thin-shell approximation (only for a void), a second-order perturbation method, and use of the Lemaitre-Tolman-Bondi metric. These analyses not only confirmed that supervoids and superclusters produce cold and hot spots, respectively, but also revealed their nonlinear effects, which had not obtained in the linear perturbations theory: a supervoid produces a hot ring around a cold spot, and a supercluster produces a temperature-dip in the center of a cold spot. Because these quantitative features agree with the measurement by Granett *et al.* they strongly indicate that cold and hot spots are evidence of supervoids and superclusters, respectively, on scales $> 100\text{Mpc}$.

If many supervoids and superclusters are located at $z < 0.75$, as indicated by the above studies, it is natural to suppose that similar voids and clusters are distributed in the whole universe. It was shown that, in the model of a network of empty voids in the Einstein-de Sitter (EdS) universe, voids at high redshift make a dominant contribution [5]. If this is the case for the present model, nonlinear super-structures at high redshift may give severe constraint on their abundance. In this paper, as a first step of statistical study of super-structures, we analyze the ISW effect produced by a supervoid network.

2 CMB anisotropy produced by a single supervoid

In preparation for statistical analysis of a supervoid-network model, we consider a single void in a Friedmann-Robertson-Walker (FRW) universe with a cosmological constant. We assume that a homogeneous low-density region is surrounded by a spherical thin shell. The general relativistic equations of motion of the shell were originally derived by Maeda and Sato [6] and were later rewritten in a more convenient expression [7], which we use here. Their observational consequences were discussed by Maeda, Sakai & Triay [8].

In this model the integration of the equations of motion require five initial values: the radius of the shell R , its peculiar velocity v , the density contrast δ_m , the Hubble parameter contrast δ_H as well as the background density

⁹⁹Email address: nsakai@e.yamagata-u.ac.jp

parameter Ω . Because the initial values of v and δ_H when $|\delta_m| \ll 1$ are determined by the linear perturbation theory, the initial values we can choose arbitrary are only R and δ_m .

For an empty void in the EdS universe, Thompson & Vishniac derived an analytic expression of the ISW effect of the thin-shell model [9]. Inoue & Silk generalize it for a dust-filled void in a flat FRW universe with a cosmological constant [10]:

$$\begin{aligned} \frac{\Delta T}{T} = & \frac{1}{3}(HR)^3 \cos \psi \left[-2\delta_H^2 - \delta_H^3 + (3 + 4\delta_m)\delta_H\Omega + \delta_m\Omega \left(-\frac{6v}{HR} + 1 \right) \right. \\ & \left. + \cos 2\psi \{ 2\delta_H^2 + \delta_H^3 + \delta_m\Omega + (3 + 2\delta_m)\delta_H\Omega \} \right], \end{aligned} \quad (2.1)$$

where ψ is the angle between the normal of the shell and the photon leaving the void. In the following analysis we choose

$$\Omega_0 = 0.27, \quad \lambda_0 = 0.73, \quad H_0 R_0 = 0.07, \quad \text{and} \quad \delta_0 = -0.3, \quad (2.2)$$

as indicated by the previous work [4]. Then all variables in the RHS of (2.1) are determined by numerical integration of the equations of motion described above.

In Fig. 1 we demonstrate how the ISW effect of a void depends on z , which characterizes both the evolution and the location of the void. (a) shows $(HR)^3\delta_m$, as a first approximation of the maximum amplitude of (2.1). In the case of the EdS universe, $R \propto t^{0.8}$ and $H \propto t^{-1}$, and therefore $(HR)^3$ decreases monotonically. In the present model, on the other hand, after the cosmological constant becomes dominant at $z \approx 3$, H and R gradually approach to constant and an exponential function, respectively, and hence $(HR)^3$ begins to increase. The effect of this rapid expansion also changes the apparent radius of temperature fluctuations after $z \approx 3$, as shown in Fig. 2(b). This indicates that only supervoids located in $z < 3$ produce large scale anisotropies of CMB.

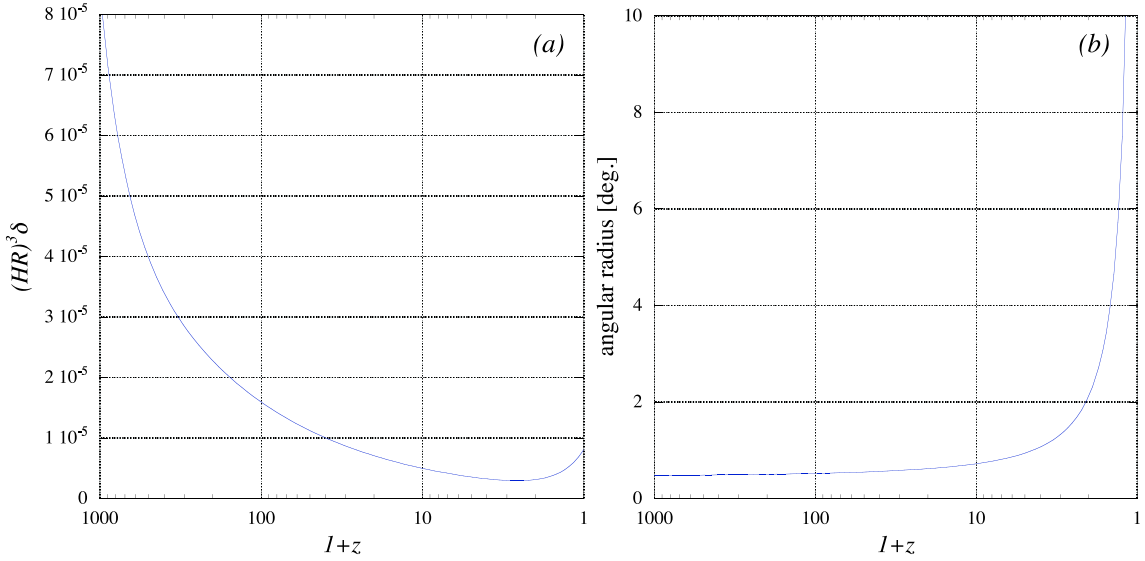


Figure 1: ISW effect of a single supervoid. (a) and (b) show the maximum amplitude ($\psi = 0$) and the apparent radius, respectively.

3 CMB anisotropy produced by a supervoid network

Next, we consider a model of a supervoid network in a FRW universe with a cosmological constant. The void-network model in the EdS universe was studied in [5, 9]. The model consists of randomly distributed, equally sized, and non-overlapped voids, which formed at some time simultaneously. Divide the universe into shells of the comoving thickness $2r_v(t_0)$, as depicted in Fig. 2. For each shell, the probability of a ray intersecting a void is given by

$$P = \frac{3}{2}F_0 \left\{ \frac{r_v(t)}{r_v(t_0)} \right\}^2, \quad (3.1)$$

where F_0 is the fractional volume of space occupied by voids and normalized at the present t_0 .

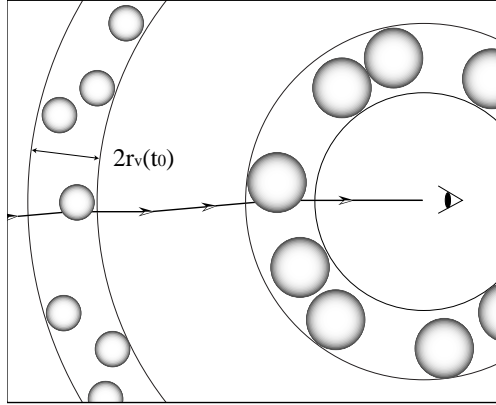


Figure 2: Schematic sketch of a supervoid network model. This structure is the same as in [5, 9]. Divide the universe into shells of comoving thickness $2r_v(t_0)$.

The angular correlation function of the CMB anisotropy $C(\theta)$ and its power spectrum C_l are, respectively, defined by

$$C(\theta) \equiv \left\langle \frac{\Delta T}{T}(\boldsymbol{\theta}_A) \frac{\Delta T}{T}(\boldsymbol{\theta}_B) \right\rangle_{\theta} \equiv \sum_l \frac{(2l+1)C_l}{4\pi} P_l(\cos \theta), \tag{3.2}$$

where $\boldsymbol{\theta}_A$ and $\boldsymbol{\theta}_B$ are angular positions with the separation angle θ . To calculate $C(\theta)$, first we take an average for each shell defined in Fig. 2, $C(\theta)_{\text{shell}}$, and then we sum up them over all shell: $C(\theta) = \sum C(\theta)_{\text{shell}}$. The angular power spectrum are obtained from

$$C_l = 2\pi \int_{-1}^1 C(\theta) P_l(\cos \theta) d(\cos \theta). \tag{3.3}$$

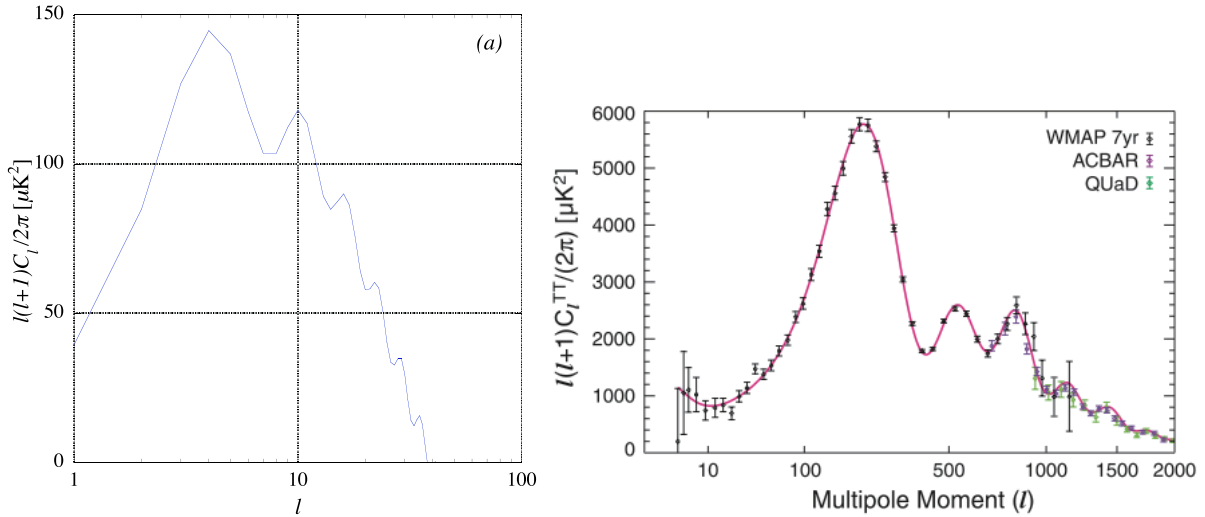


Figure 3: CMB angular power spectrum as a function of l . (a) shows the ISW effect of our void-network model with (2.2). (b) shows the observational results, which are quoted from Komatsu et al. [11]

In Fig. 3(a) we plot C_l for the parameter set (2.2). A peak appears at a large angular scale, $l < 10$, and amplitudes at a small angular scale, $l > 30$, are negligible. This is in contrast to the case of a network model of empty voids in the EdS universe, where a peak appears at very small scale, $l > 1000$. For comparison, we quote observational results from Komatsu et al. [11] in Fig. 3(b). Because our theoretical results in (a) does not include primordial fluctuations, their amplitudes of all scales should be smaller than those in the observational data in (b). In this sense the observational data at present does no exclude our void-network model.

To complete the statistical analysis of a super-structure model, it is necessary to estimate the ISW effect of a supercluster network model and the ordinary SW effect of both models. This is in progress.

The author thanks K. T. Inoue and K. Tomita for useful comments. This work was supported by Grant-in-Aid for Scientific Research on Innovative Areas No. 22111502.

References

- [1] R. K. Sachs & A. M. Wolfe, *ApJ* **147**, 73 (1967); M. J. Rees & D. W. Sciama, *Nature* **217**, 511 (1968).
- [2] B. R. Granett, M. C. Neyrinck & I. Szapudi, *ApJ* **683**, L99 (2008).
- [3] C. L. Francis & J. A. Peacock, *MNRAS* **406**, 14 (2019).
- [4] K. T. Inoue, N. Sakai & K. Tomita, *ApJ* **724**, 12 (2011).
- [5] N. Sakai, N. Sugiyama & J. Yokoyama, *ApJ* **510**, 1 (1999).
- [6] K. Maeda & H. Sato, *Prog. Theor. Phys.* **70**, 772 (1983); *ibid.* **70**, 1273 (1983).
- [7] N. Sakai, K. Maeda & H. Sato, *Prog. Theor. Phys.* **89**, 1193 (1993).
- [8] K. Maeda, N. Sakai & R. Triay, *JCAP* **08**, 026 (2011).
- [9] K. L. Thompson & E. T. Vishniac, *ApJ* **313**, 517 (1987).
- [10] K. T. Inoue & J. Silk, *ApJ* **664**, 650 (2007).
- [11] E. Komatsu et al., *ApJS* **192**, 18 (2011).

Ghost-free Lorentz-violating Weyl gravity

Yuuiti Sendouda¹⁰⁰

Graduate School of Science and Technology, Hirosaki University, Hirosaki, Aomori 036-8561, Japan

Abstract

We present a model of gravity that includes Weyl tensors in the action but can avoid the emergence of ghost degrees of freedom thanks to spontaneous Lorentz-symmetry breaking. Within the model, we consider the quantisation of the cosmological tensor perturbations in the early, Lorentz-violating stage of the inflationary universe, and find how the spectrum of primordial gravitational waves can be modified compared to General Relativity.

1 Introduction and summary

Since Stelle's work in 1978 [1], it has been considered that the addition of the Weyl curvature terms to Einstein's General Relativity (GR) leads to pathological instabilities through the emergence of *ghost* degrees of freedom (dofs) with negative kinetic terms.

The aim of this presentation is to propose a mechanism that serves to avoid the emergence of ghosts in the presence of Weyl terms in the action. This is achieved by an introduction of an extra dof that breaks the (local) Lorentz symmetry of spacetimes spontaneously.

Our simplest ghost-free Weyl gravity model is described in section 2. First of all, it will be shown that in the regions of spacetime where a unit vector field u^a becomes timelike, the equations of motion (eoms) (2.5) for the metric remain second order in timelike derivatives (i.e., derivatives along u^a), so that no new, most probably dangerous dofs emerge. The model, however, would have novel and observationally relevant features in comparison with GR as we shall see.

In section 3, first, it will be checked that the gravitons themselves do not become ghost if the sign of the coupling constant is appropriately chosen. Equation (3.2) for the action of the gravitons on cosmological backgrounds indicates how the kinetic term of the gravitons is modified from that in GR.

Then we will obtain the growing and decaying solutions on a de Sitter background, as shown in figure 1. The notable point is that the behaviour of the modes departs from the Minkowski one in the earliest times when the wavelength of the modes becomes shorter than the scale of Lorentz violation.

Finally we second quantise the gravitons in the Lorentz-violating regime. Our proposal is that the appropriate "positive frequency" modes are those reducing to harmonic oscillators in the small Hubble limit, $H \rightarrow 0$. This choice of the vacuum state leads to the expression (3.9) for the power spectrum of the primordial gravitational waves, which appears to depend on the ratio of the Hubble H to the energy scale of Lorentz violation.

We expect that the proposed mechanism can be applied to construct more general higher-curvature gravity models that are ghost free. Possible modification of the vacuum state will serve as a clue to distinguish this kind of Lorentz-violating gravity models from GR and between each other.

2 A Weyl gravity model without ghosts

Our model is specified by the action

$$S[g_{ab}, \chi] = S_{\text{EH}}[g_{ab}] + S_C[g_{ab}, \chi] + S_\chi[g_{ab}, \chi], \quad (2.1)$$

where

$$S_{\text{EH}}[g_{ab}] \equiv \frac{M_{\text{Pl}}^2}{2} \int d^4x \sqrt{-g} R \quad (2.2)$$

is the standard Einstein–Hilbert action,

$$S_C[g_{ab}, \chi] \equiv \gamma^2 \int d^4x \sqrt{-g} C_{abcd} C_{efgh} \gamma^{ae} \gamma^{bf} \gamma^{cg} u^d u^h \quad (2.3)$$

¹⁰⁰Email address: [sendouda\(a\)cc.hirosaki-u.ac.jp](mailto:sendouda(a)cc.hirosaki-u.ac.jp)

with

$$u_a \equiv \frac{\partial_a \chi}{\sqrt{-\partial_a \chi \partial^a \chi}} \quad \text{and} \quad \gamma_{ab} \equiv g_{ab} + u_a u_b \quad (2.4)$$

is an apparently hazardous ‘‘Weyl’’ term but now augmented by a scalar field χ , and $S_\chi[g_{ab}, \chi]$ is the action for χ , the form of which we need not specify for the present purpose.

The full Einstein equations read

$$M_{\text{Pl}}^2 G^{ab} - \gamma^2 B^{ab} = T_\chi^{ab}, \quad (2.5)$$

where G_{ab} is the Einstein tensor, B_{ab} is an analogue of the Bach tensor, whose form is presented elsewhere [2], and $T_\chi^{ab} \equiv 2(-g)^{-1/2} \delta S_\chi / \delta g_{ab}$ is the energy-momentum tensor of χ . The equation of motion for χ is

$$\frac{1}{\sqrt{-g}} \frac{\delta S_\chi}{\delta \chi} - \gamma^2 \nabla_a \Gamma^a = 0, \quad (2.6)$$

where $\nabla_a \Gamma^a \equiv -(-g)^{-1/2} \delta S_C / \delta \chi|_{\gamma^2=1}$ and its form will also be given in [2].

It can be checked that the tensor B_{ab} actually contains derivatives of the metric up to fourth order, the fact warning the emergence of ghost dofs and all the possible pathologies associated. The appearance of ghost dofs is, nonetheless, avoided if u^a is timelike. This notable property of our model is all thanks to the fact that the maximum order of the derivative along u^a appearing in B_{ab} is two, the remaining two out of the four being along the directions orthogonal to u^a .

3 Cosmological tensor perturbations

3.1 The action

We assume that a flat Friedmann–Lemaître–Robertson–Walker spacetime with the ansatz $g_{ab} dx^a dx^b = a(\tau)^2 (-d\tau^2 + \delta_{ij} dx^i dx^j)$ and $\chi = \chi(\tau)$ is a solution to the eoms. Hereafter a prime denotes derivative with respect to the conformal time τ .

Let us consider perturbations about a cosmological background. The second-order perturbation of the higher-curvature term S_C depends on the gauge-invariant tensor and vector variables, H_{ij} and $\Sigma_i \equiv B_i - V'_i$, which are defined via the decomposition of the perturbed metric: $\delta g_{ij} = a^2 (2H_{ij} + \partial_i V_j + \partial_j V_i)$ and $\delta g_{0i} = a B_i$ with the transverse–traceless conditions $H^i{}_i = \partial^i B_i = \partial^i V_i = 0, \partial_j H^{ij} = 0$ satisfied. The perturbed action in fact reads

$$\begin{aligned} {}^{(2)}S_C[H_{ij}, \Sigma_i] &= \gamma^2 \int d\tau d^3x {}^{(1)}C_{ijk0} {}^{(1)}C^{ijk0}|_{a(\tau)=1} \\ &= \gamma^2 \int d\tau d^3x \left(2\partial_k H'_{ij} \partial^k H'^{ij} + \frac{1}{4} \Delta \Sigma_i \Delta \Sigma^i \right), \end{aligned} \quad (3.1)$$

where $\Delta \equiv \partial_i \partial^i$.

The vector perturbation remains nondynamical as no time derivative have appeared, whereas the tensor part now acquires an additional kinetic term with extra spatial derivatives. The action for the tensor perturbations has, after using the background eoms, the form

$$\begin{aligned} S_T[H_{ij}] &\equiv {}^{(2)}(S_{\text{EH}} + S_C + S_\chi)[H_{ij}] \\ &= \frac{M_{\text{Pl}}^2}{2} \int d\tau d^3x a^2 \left(H'_{ij} H'^{ij} - \partial_k H_{ij} \partial^k H'^{ij} + \frac{1}{M_\gamma^2 a^2} \partial_k H'_{ij} \partial^k H'^{ij} \right), \end{aligned} \quad (3.2)$$

where we have introduced an energy scale of Lorentz violation $M_\gamma \equiv M_{\text{Pl}}/(2\gamma)$. We assume γ and M_γ are positive real so that the kinetic term of the graviton remains positive definite.

3.2 Mode functions and their asymptotic behaviour

The tensor perturbation is expanded as

$$H_{ij}(\tau, \vec{x}) = \frac{1}{M_{\text{Pl}} a(\tau)} \sum_{\lambda=1,2} \int \frac{d^3k}{(2\pi)^{3/2}} a_k^\lambda (e_k^\lambda)_{ij} \frac{\chi_k^\lambda(\tau)}{n_k(\tau)} e^{i\vec{k}\cdot\vec{x}}, \quad (3.3)$$

where $n_k(\tau) \equiv \sqrt{1 + y(\tau)^2}$ with $y(\tau) \equiv k/(a(\tau) M_\gamma)$. The reality conditions have been implicitly imposed. In particular, the polarisation tensors are transverse–traceless, and satisfy $(e_k^\lambda)_{ij}^* = (e_{-\vec{k}}^\lambda)_{ij}$ and $(e_k^\lambda)_{ij} (e_k^{\lambda'})^{ij*} = \delta_{\lambda\lambda'}$. Hereafter we concentrate on one of the polarisations and omit the index λ .

The eom for χ_k then reads

$$\chi_k''(\tau) + \Omega_k(\tau)^2 \chi_k(\tau) = 0 \quad \text{with} \quad \Omega_k(\tau)^2 \equiv \frac{k^2 - \mathcal{H}^2 - \mathcal{H}'}{1 + y^2} - \frac{y^2 \mathcal{H}^2}{(1 + y^2)^2}, \quad (3.4)$$

where $\mathcal{H} \equiv a'/a$. On de Sitter background, where $a = -1/(H\tau)$ with H being constant, the eom reduces to

$$\frac{d^2 \chi_k}{dz^2} + \frac{1 - 2z^{-2} + 4\epsilon^2(z^2 - 3)}{(1 + 4\epsilon^2 z^2)^2} \chi_k = 0, \quad (3.5)$$

where we have introduced a Hubble-normalised time coordinate $z \equiv -k\tau = k/(aH) > 0$ and a parameter $\epsilon \equiv H/(2M_\gamma)$, which we assume is within the range $0 < \epsilon < 1$. The two linearly independent solutions to the de Sitter eom (3.5), denoted by $\chi_k^{(1)}$ and $\chi_k^{(2)}$, are given in terms of the hypergeometric functions [2] whose form is plotted in figure 1.

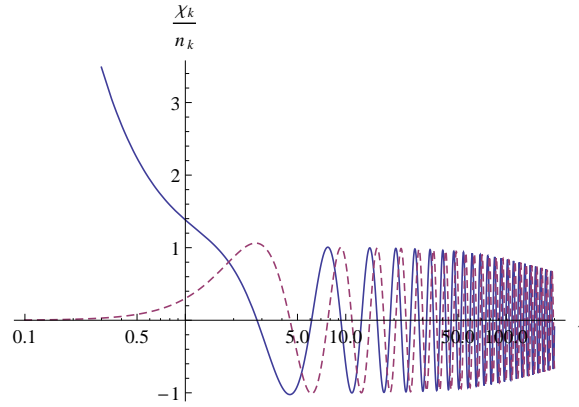


Figure 1: The behaviour of the growing and decaying mode functions $\chi_k^{(1)}$ (solid) and $\chi_k^{(2)}$ (dashed) for $\epsilon = 0.005$.

The late-time asymptotic behaviour of the above two modes, as $z \rightarrow 0$, is $\chi_k^{(1)}/n_k \sim 1/z$ and $\chi_k^{(2)}/n_k \sim z^2/3$, respectively, so one concludes that $\chi_k^{(1)}$ is the *growing* mode whereas $\chi_k^{(2)}$ being *decaying*. The amplitude of the growing tensor perturbation after horizon exit, $z \lesssim 1$, behaves as $\chi_k^{(1)}/(n_k a) \rightarrow \text{const.}$, i.e., *freezes out*, as in standard inflation. Note also that the above growing and decaying modes are found to be (at least numerically) fit very well by sinusoidal functions as $\chi_k^{(1)}/n_k \sim \sin z$ and $\chi_k^{(2)}/n_k \sim -\cos z$, respectively, in the subhorizon Lorentz-symmetric regime $1 \ll z \ll (2\epsilon)^{-1}$.

In the Lorentz-violating regime, $z \gtrsim (2\epsilon)^{-1}$, however, the two modes depart from simple harmonic motion. The early-time asymptotic expansion of the modes as $y \equiv 2\epsilon z \rightarrow \infty$ is obtained as

$$\frac{\chi_k^{(1)}}{n_k} \sim c_1 y^{-1/2-i\nu/2} + c_1^* y^{-1/2+i\nu/2} \quad \text{and} \quad \frac{\chi_k^{(2)}}{n_k} \sim c_2 y^{-1/2-i\nu/2} + c_2^* y^{-1/2+i\nu/2}, \quad (3.6)$$

where $\nu \equiv \sqrt{\epsilon^{-2} - 1}$, which is positive real for $\epsilon < 1$, and where c_1 and c_2 are complex constants depending on ϵ [2]. This expression implies that neither of the solutions obeys simple harmonic motion but, as going back to earlier times, their amplitude decays and the frequency decreases logarithmically.

3.3 Primordial gravitational waves from quantum fluctuations

We second quantise the tensor perturbations as

$$H_{ij}(\tau, \vec{x}) \rightarrow \hat{H}_{ij}(\tau, \vec{x}) = \frac{1}{M_{\text{Pl}} a(\tau)} \sum_{\lambda=1,2} \int \frac{d^3 k}{(2\pi)^{3/2}} \left[\hat{a}_{\vec{k}}^\lambda (e_{\vec{k}}^\lambda)_{ij} \frac{\chi_k^\lambda(\tau)}{n_k(\tau)} e^{i\vec{k}\cdot\vec{x}} + \text{h.c.} \right]. \quad (3.7)$$

Again we shall omit the index λ . The quantum vacuum state $|0\rangle$ is specified via the conditions $\hat{a}_{\vec{k}}|0\rangle = 0$ and $\langle 0|0\rangle = 1$. The standard procedure of the canonical quantisation leads to the usual commutation relations $[\hat{a}_{\vec{k}}, \hat{a}_{\vec{k}'}^\dagger] = \delta^3(\vec{k} - \vec{k}')$ and $[\hat{a}_{\vec{k}}, \hat{a}_{\vec{k}'}] = [\hat{a}_{\vec{k}}^\dagger, \hat{a}_{\vec{k}'}^\dagger] = 0$ if the modes are so normalised that Wronskian $\chi_k(\tau) \chi_k'(\tau)^* - \chi_k(\tau)^* \chi_k'(\tau)$ is i (see [2] for details).

Here we propose that the suitable positive frequency modes in our de Sitter setup are, modulo a phase factor, given by

$$\chi_k^+ = \frac{c_1^{-1} \chi_k^{(1)} - c_2^{-1} \chi_k^{(2)}}{2\sqrt{2k} \epsilon \nu \tanh(\pi \nu/2)}, \quad (3.8)$$

which is based on the observation that, in the “adiabatic” limit where $H \rightarrow 0$, the above defined function turns out to have a positive frequency with respect to the cosmic time, $\chi_k^+/n_k \propto e^{-i M_\gamma t}$. Accordingly, we suppose that the vacuum state of the universe is specified by this particular choice of the positive frequency modes.

A possible signature of our model would therefore be imprinted in the quantum fluctuations of the vacuum. Its computation leads to the power spectrum of the primordial gravitational waves after the freeze-out:

$$\mathcal{P}(k) = \frac{2}{\pi^2} \frac{H^2}{M_{\text{Pl}}^2} \Xi \quad \text{where} \quad \Xi \equiv \frac{2k z^2 |\chi_k^+|^2}{n_k^2} \Big|_{z \rightarrow 0}. \quad (3.9)$$

We find that the spectrum $\mathcal{P}(k)$ is scale-invariant as in standard inflation, whereas the amplitude changes depending the value of ϵ ; it once decreases down to about 65% as ϵ increases beyond 0.1, while it diverges as ϵ further approaches 1, see figure 2.

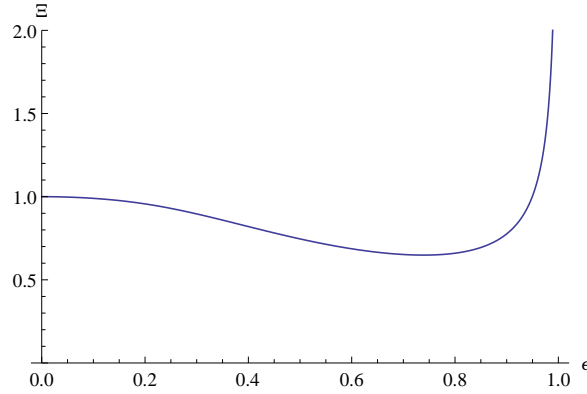


Figure 2: The modification factor Ξ for the amplitude of the power spectrum of the tensor perturbations as a function of $\epsilon = H/(2M_\gamma)$.

References

- [1] K. S. Stelle, *Gen. Rel. Grav.* **9**, 353 (1978).
- [2] N. Deruelle, M. Sasaki, Y. Sendouda, and A. Youssef, [arXiv:1202.3131](https://arxiv.org/abs/1202.3131) [gr-qc].

Einstein Universe under Deconstruction: the case with degenerate fermions

Nahomi Kan^{101(a)}, Koichiro Kobayashi^{102(b)}, and Kiyoshi Shiraishi^{103(b)}

^(a) *Yamaguchi Junior College, Hofu-shi, Yamaguchi 747-1232, Japan*

^(b) *Yamaguchi University, Yamaguchi-shi, Yamaguchi 753-8512, Japan*

Abstract

We study self-consistent static solutions for an Einstein universe in a graph-based induced gravity. In the generalization of the deconstruction model based on the graph, the eigenvalues of the graph Laplacian and the adjacent matrix gives the mass spectrum of the particles. Thus we can easily control UV divergences at one-loop level in such a model. We use the calculation method with the spectrum distribution function of the graph and search for the static solution supported by the degenerate pressure of the fermion (at zero temperature). The report is based on [arXiv:1110.5697](https://arxiv.org/abs/1110.5697).

1 Introduction

In our previous work [1], the induced gravity [2] model without UV divergences at one-loop level has been constructed by a generalized method of Dimensional Deconstruction (DD) [3] and a self-consistent solution for an Einstein static universe has been obtained.

In this brief report, we show the existence of a self-consistent Einstein universe in which strongly degenerate fermions by the calculation method using the spectral density function of graphs.

2 Induced gravity

Induced gravity has been studied by many authors [2]. The one-loop effective action can systematically be expressed by an integral form using Schwinger's proper time method as

$$\frac{1}{2} \text{Tr} \ln H = -\frac{1}{2} \int_0^\infty \frac{dt}{t} \text{Tr} \left[e^{-tH} \right], \quad (2.1)$$

where H is a Hessian operator which appears in the free-field action of a matter field. The expansion in terms of the Seeley-DeWitt coefficients can be written as

$$\text{Tr} \left[e^{-tH} \right] = \frac{1}{(4\pi t)^2} \int d^4x \sqrt{|\det g_{\mu\nu}|} \left[\text{Tr} a_0 + t \text{Tr} a_1 + t^2 \text{Tr} a_2 + o(t^3) \right], \quad (2.2)$$

where $g_{\mu\nu}$ denotes the spacetime metric and Tr means the trace over the spacetime indices. The one-loop effective action for the background fields is given by the collection of the contribution of various matter fields.

The UV divergences arise from the integration in the vicinity of $t = 0$. If we introduce a UV-cutoff scale Λ , the lower bound of the integration on t is replaced to $1/\Lambda^2$. The divergent parts in terms of the cut-off Λ are

$$\frac{1}{64\pi^2} (N_0 - 2N_{1/2} + 2N_1) \Lambda^4 \quad \text{and} \quad \frac{1}{192\pi^2} (N_0 + N_{1/2} - 4N_1) \Lambda^2 R, \quad (2.3)$$

where N_0 is the number of minimal scalar degrees of freedom, $N_{1/2}$ is the number of two-component fermion fields, N_1 is the number of massless vector fields, and R is the scalar curvature constructed from the metric $g_{\mu\nu}$.

The conditions for their cancelations are solved by $N_0 = 2N$, $N_{1/2} = 2N$, and $N_1 = N$, where $N = 1, 2, 3, \dots$. For massive fields, since

$$\sum_{i=1}^{N_s} e^{-(m_s^2)_i t} = N_s - t \sum_{i=1}^{N_s} (m_s^2)_i + t^2 \frac{1}{2} \sum_{i=1}^{N_s} (m_s^4)_i + \dots \equiv N_s - t \text{Tr} M_s^2 + t^2 \frac{1}{2} \text{Tr} M_s^4 + \dots, \quad (2.4)$$

¹⁰¹Email address: kan@yamaguchi-jc.ac.jp

¹⁰²Email address: m004wa@yamaguchi-u.ac.jp

¹⁰³Email address: shiraish@yamaguchi-u.ac.jp

(where M_s^2 is the mass-squared matrix for spin- s field), the condition on mass-squared matrix for the cancelation of divergences should be $\text{Tr } M_S^2 - 4 \text{Tr } M_D^2 + 3 \text{Tr } M_V^2 = 0$, where M_S^2 is the mass-squared matrix for the scalar fields, M_D^2 is that for the Dirac fields, and M_V^2 is that for the vector fields.

Now, we construct the field theories with mass matrices which satisfy the cancelation conditions.

3 Graph and mass matrices

We remember the concept of DD [3]. A moose diagram is used to describe this theory, and is no more than a graph. The N -sided polygon is identified as an example of simple graphs, a cycle graph C_N . A graph G consists of a vertex set \mathcal{V} and an edge set \mathcal{E} , where an edge is a pair of distinct vertices of G . The graph with directed edges is dubbed as a directed graph. An oriented edge $e = [u, v]$ connects the origin $u = o(e)$ and the terminus $v = t(e)$.

Now we introduce several matrices that are naturally associated with a graph [4, 5]. They are the incidence matrix $E(G) = (E)_{ve}$, the adjacency matrix $A(G) = (A)_{vv'}$, the degree matrix $D(G) = (D)_{vv'}$, and the graph Laplacian (or combinatorial Laplacian) $\Delta(G) = (\Delta)_{vv'}$. The relations among them are $\Delta = D - A$, and $\Delta = EE^T$. The important identities are $\text{Tr } A = 0$, and $\text{Tr } A^2 = \text{Tr } D$. Thus the relations $\text{Tr } \Delta = \text{Tr } D$ and $\text{Tr } \Delta^2 = \text{Tr } D^2 + \text{Tr } D$ hold.

The model of vector fields, whose mass-squared matrix is $f^2 \Delta$, is [5]

$$\mathcal{L}_V = -\frac{1}{4} \sum_{v \in \mathcal{V}} F_{\mu\nu}^v F_v^{\mu\nu} - \sum_{e \in \mathcal{E}} (\mathcal{D}_\mu U_e)^\dagger (\mathcal{D}^\mu U_e), \quad (3.1)$$

where the covariant derivative is $\mathcal{D}^\mu U_e \equiv (\partial^\mu + iA_{i(e)}^\mu - A_{o(e)}^\mu)U_e$ with $|U_e| = f$. Here f is a constant with the dimension of mass. Similarly, any kind of fields can be associated with a graph and their mass-squared matrix can be written by using the graph Laplacian. For scalar fields, we assign a scalar field ϕ_v to each vertex v of G . A mass term for scalar fields can be constructed as $f^2 \sum_{v, v' \in \mathcal{V}} \phi_v \Delta_{vv'} \phi_{v'}$. For spinor fields, the mass term can be expressed by using the incidence matrix E . For example, the Lagrangian density of fermion fields can be written as [5]

$$-\sum_{v \in \mathcal{V}} \bar{\psi}_{Rv} \not{D} \psi_{Rv} - \sum_{e \in \mathcal{E}} \bar{\psi}_{Le} \not{D} \psi_{Le} - f \sum_{e \in \mathcal{E}} \sum_{v \in \mathcal{V}} [(\bar{\psi}_{Le} (E^T)_{ev} \psi_{Rv} + h.c.)], \quad (3.2)$$

where the subscripts L and R denote left-handed and right-handed fermions, respectively. Namely, the left-handed fermions are assigned to the edges while the right-handed ones are assigned to the vertices. The mass spectrum of fermions governed by the Lagrangian (3.2) is also given by the eigenvalues of the graph Laplacian [5].

Therefore, the UV divergences can be controlled using the graph Laplacian and we can construct the models of UV-finite induced gravity. We prepare three graphs, G_S , G_D and G_V . All these graphs have N vertices. If the graphs associated to their field have the same degree matrix, we find [5]

$$\text{Tr } M_S^2 = \text{Tr } M_D^2 = \text{Tr } M_V^2 \quad \text{and} \quad \text{Tr } M_S^4 = \text{Tr } M_D^4 = \text{Tr } M_V^4. \quad (3.3)$$

Therefore we find that the induced vacuum energy and the inverse of the Newton constant at one-loop can be calculated for selected graphs [6]. Suppose that we select a type of non-simple graphs $G_{\{n_i\}} = C_{n_1} \cup C_{n_2} \cup \dots$, which has N vertices. Then we can choose different sets $\{n_i\}$ for scalar, Dirac, and vector fields in a model in order to obtain non-zero value for the Newton and cosmological constants [6].

4 The effective action in an Einstein universe

We assume that the background geometry is given by a static Einstein universe. Carrying out the integration over t , we expand the effective action in terms of the modes of Laplacian on S^3 (with the radius a). The regularized mode sum for a scalar field with mass m is found to be

$$\Sigma'_S(m^2 a^2) = \sum_{\ell=1}^{\infty} \ell^2 \left[\sqrt{\ell^2 + m^2 a^2} - 1 - \ell \left(1 + \frac{m^2 a^2 - 1}{2\ell^2} - \frac{(m^2 a^2 - 1)^2}{8\ell^4} \right) \right] - \frac{5m^2 a^2 - 6}{120} - \frac{1}{8} \gamma, \quad (4.1)$$

(where γ is the Euler-Mascheroni constant), and similar expressions are obtained for the fermion field and the vector field.

Using these expressions, we obtain the effective action

$$\frac{1}{2a} \sum_i [\Sigma'_S((m_0^2)_i a^2) - \Sigma'_D((m_{1/2}^2)_i a^2) + \Sigma'_V((m_1^2)_i a^2)]. \quad (4.2)$$

5 Spectral density function of a graph

For C_N , eigenvalues of the adjacency matrix are $\lambda_k = 2 \cos \frac{2\pi k}{N}$, ($k = 0, 1, \dots, N - 1$). For a large N , we find

$$\lim_{N \rightarrow \infty} \frac{1}{N} \sum_{k=0}^{N-1} f(\lambda_k) = \int_0^1 f(2 \cos \pi t) dt = \frac{1}{\pi} \int_{-2}^2 f(x) \frac{dx}{\sqrt{4-x^2}}, \tag{5.1}$$

then we can define the spectral density function of the cycle graph [7] as

$$\rho_\infty(x) = \begin{cases} \frac{1}{\pi} \frac{1}{\sqrt{4-x^2}}, & \text{for } -2 < x < 2 \\ 0, & \text{others} \end{cases} \quad \text{for cycle graphs.} \tag{5.2}$$

A large N means that the part of the effective action for a small a (the radius of the universe) is dominant. Then we approximate the effective action for a small a as

$$\Omega_0(fa) \equiv \frac{1}{2a} \int_{-2}^2 [\Sigma'_S(f^2 a^2(2-x)) - \Sigma'_D(f^2 a^2(2-x)) + \Sigma'_V(f^2 a^2(2-x))] \frac{N}{\pi \sqrt{4-x^2}} dx. \tag{5.3}$$

The graphs of the type of $C_n \cup C_m \cup \dots$ have the same spectral density function for a large N .

6 Strongly degenerate fermions

The thermodynamical potential with strongly degenerate fermions ($T = 0$) can be expressed only by the chemical potential μ and the mass spectrum of fermions.

Applying the spectral density function to this, we get

$$\begin{aligned} \Omega_D = & -\frac{2\pi^2 a^3}{12\pi^2} \int_{-2}^2 \theta(\mu - m(x)) \\ & \times \left[\mu \sqrt{\mu^2 - m^2(x)} \left(\mu^2 - \frac{5}{2} m^2(x) \right) + \frac{3}{2} m^4(x) \ln \left(\frac{\mu}{m(x)} + \sqrt{\frac{\mu^2}{m^2(x)} - 1} \right) \right] \frac{N}{\pi \sqrt{4-x^2}} dx, \end{aligned} \tag{6.1}$$

where $m^2(x) \equiv f^2(2-x)$ and $\theta(y)$ is the step function. This is the main contribution for a large N .

The Einstein equations can be written by using the thermodynamical potential Ω , which includes the vacuum contribution:

$$\frac{\partial(\mu^{-1}\Omega)}{\partial(\mu^{-1})} = 0 \quad \text{and} \quad \frac{\partial(\mu^{-1}\Omega)}{\partial a} = 0. \tag{6.2}$$

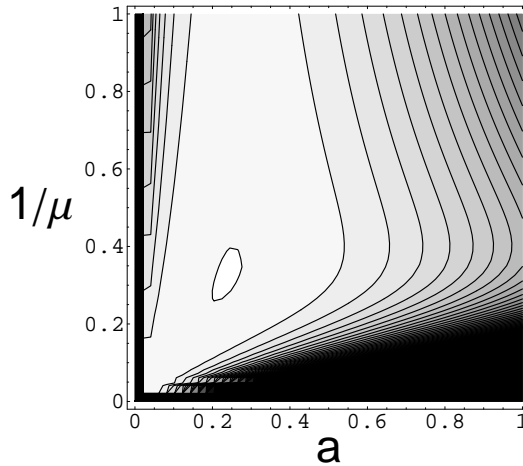


Figure 1: A contour plot of $\frac{1}{N} \mu^{-1} \Omega$.

In Figure 1, we show the contour plots for Ω/μ obtained by numerical calculations, whose extremum provides a self-consistent solution. The horizontal axis indicates the scale factor a , while the vertical one $1/\mu$, in the unit of f . One (unstable) solution for a self-consistent Einstein universe can be found. The Casimir effects is essential in this case.

7 Summary and prospects

We have shown the construction of Graph-based (calculable) induced gravity models. For a large N (the number of fields), a small a (the radius of the universe), the effective potential (mainly the Casimir energy) and the thermodynamical potential for the degenerate fermions are evaluated by using the spectral density function of graphs. We found the existence of a self-consistent solution for a static Einstein universe.

In future work, the trace formula for graph spectrum will be directly applied to the one-loop calculations.

References

- [1] N. Kan and K. Shiraishi, *Prog. Theor. Phys.* **121** (2009) 1035.
- [2] For a review, M. Visser, *Mod. Phys. Lett.* **A17** (2002) 977.
- [3] N. Arkani-Hamed, A. G. Cohen and H. Georgi, *Phys. Rev. Lett.* **86** (2001) 4757; C. T. Hill, S. Pokorski and J. Wang, *Phys. Rev.* **D64** (2001) 105005.
- [4] B. Mohar, "The Laplacian spectrum of graphs", in *Graph Theory, Combinatorics, and Applications*, ed. Y. Alavi *et al.* (Wiley, New York, 1991), p. 871; R. Merris, *Linear Algebra Appl.* **197** (1994) 143.
- [5] N. Kan and K. Shiraishi, *J. Math. Phys.* **46** (2005) 112301.
- [6] N. Kan and K. Shiraishi, *Prog. Theor. Phys.* **111** (2004) 745.
- [7] A. Hora and N. Obata, *Quantum Probability and Spectral Analysis of Graphs*, Springer, Berlin Heidelberg, 2007.

Asymptotic rigidity of black holes

Kentaro Tanabe^{104(a)}, Tetsuya Shiromizu^{105(b)}, and Shunichiro Kinoshita^{106(b)}

^(a) *Yukawa Institute for Theoretical Physics, Kyoto University, Kyoto 606-8502, Japan*

^(b) *Department of Physics, Kyoto University, Kyoto 606-8502, Japan.*

Abstract

It is expected that black holes are formed dynamically under gravitational collapses and approach stationary states. In this paper, we show that the asymptotic Killing vector at late time should exist on the horizon and then that it can be extended outside black holes under the assumption of the analyticity of spacetimes. This fact implies that if there is another asymptotic Killing vector which becomes a stationary Killing at a far region and spacelike in the “ergoregion,” the rotating black holes may have the asymptotically axisymmetric Killing vector at late time. Thus, we may expect that the asymptotic rigidity of the black holes holds.

1 Introduction

Black holes in our Universe are expected to be formed under gravitational collapses, and to finally approach stationary and vacuum states by radiating and absorbing energy, momentum, and angular momentum. Then the uniqueness theorem [1] guarantees that the black hole candidates in our Universe are the Kerr black holes. The key ingredient for the proof of the uniqueness theorem is the rigidity theorem [2–5]. The rigidity theorem shows that the stationary rotating black holes have axisymmetric Killing vectors. The outline of the proof is as follows: The stationarity of spacetime implies that there are no gravitational waves around a black hole. Then the expansion and shear of the event horizon must vanish by virtue of the Raychaudhuri equation and stationarity. Using the Einstein equations, then, we can find that the null geodesic generator of the event horizon is a Killing vector. If the black hole is rotating, this new Killing vector may deviate from the stationary Killing vector which becomes spacelike in the ergoregion. This means that the stationary black holes might have two Killing vectors, that is, the stationary and axisymmetric Killing vectors. Hence the stationary black holes should rotate rigidly.

However, the late-time phase of black holes produced by gravitational collapses would not be exactly stationary but nearly stationary. “Nearly stationary” means that the black holes are surrounded by the gravitational waves at late time. Then we cannot apply the rigidity theorem to such black holes because the expansion and shear of the null geodesic generator on the event horizon do not vanish due to the presence of the gravitational waves on the event horizon. Note that the late-time behaviors of the perturbations around the Schwarzschild and Kerr black holes were examined and it was shown that the perturbations decay at late time both on the horizon and null infinity at the same rate (for examples, see Refs. [6–8]). In the dynamical processes in gravitational collapses, however, it is quite nontrivial whether the formed black hole approaches the Kerr black hole. In this paper, we show that the asymptotic Killing vector, which will asymptotically approach a Killing vector at late time, should exist on the horizon without assuming any symmetries and then that it can be extended outside of the event horizon using the Einstein equations. This indicates that if there is another asymptotic Killing vector which will be an asymptotically stationary Killing vector at a far region, the rotating black hole may have the asymptotically axisymmetric Killing vector at late time.

2 Bondi-like coordinate and Einstein equations

In this section, introducing the Bondi-like coordinate near the event horizon, we investigate the initial value problem.

The event horizon is the boundary of the black hole and it is a null hypersurface. Then, we can introduce the Bondi-like (Gaussian null) coordinates $x^A = (u, r, x^a)$ near the event horizon as

$$ds^2 = g_{AB}dx^A dx^B = -Adu^2 + 2dudr + h_{ab}(dx^a + U^a du)(dx^b + U^b du), \quad (2.1)$$

¹⁰⁴Email address: tanabe@yukawa.kyoto-u.ac.jp

¹⁰⁵Email address: shiromizu@tap.scphys.kyoto-u.ac.jp

¹⁰⁶Email address: kinoshita@tap.scphys.kyoto-u.ac.jp

where u is a time coordinate. In this coordinate, the horizon position is taken to be $r = 0$. We assume that a cross section of the event horizon is compact in the $u = \text{constant}$ hypersurface and its topology is S^2 . x^a are coordinates on S^2 . Since the event horizon is a null hypersurface, g_{uu} must vanish on the event horizon and $l = \partial/\partial u$ is the null geodesic generator on the event horizon. Furthermore we can choose the coordinate u so that $l_a = 0$ on the event horizon. Then, we have $A \hat{=} 0$ and $U^a \hat{=} 0$ where $\hat{=}$ means the evaluation on the event horizon $r = 0$.

To solve the vacuum Einstein equations, we formulate the initial value problem in the Bondi coordinates. In the following, we solve the Einstein equations as the evolution equations in the direction of r . Thus, the initial value of the metric should be set on the $r = \text{constant}$ surface and we take the event horizon $r = 0$ as the initial surface. The evolution equations are given by

$$R_{rr} = -\frac{1}{2}(\log h)'' - \frac{1}{4}h^{ac}h^{bd}(h_{ab})'(h_{cd})' = 0, \quad (2.2)$$

$$R_{rB}h^{aB} = \frac{1}{2}U^{a''} + \frac{1}{2}h^{ac}h'_{bc}U^{b'} + \frac{1}{4}(\log h)'U^{a'} + \frac{1}{2}h^{ab}\bar{D}^c[h'_{bc} - h_{bc}(\log h)'] = 0 \quad (2.3)$$

and

$$\begin{aligned} R_{AB}h^A_a h^B_b &= -\frac{1}{2}Ah''_{ab} - \frac{1}{2}A'h'_{ab} - (\dot{h}_{ab})' + {}^{(h)}R_{ab} + \frac{A}{2}h^{cd}h'_{ac}h'_{bd} + \mathcal{L}_U h'_{ab} \\ &\quad + \frac{1}{2}h^{cd}(h'_{ac}\dot{h}_{bd} + h'_{bd}\dot{h}_{ac}) - \frac{1}{2}h'_{ac}(\bar{D}_b U^c + \bar{D}^c U_b) - \frac{1}{2}h'_{bc}(\bar{D}_a U^c + \bar{D}^c U_a) \\ &\quad - \frac{1}{2}h_{ac}h_{bd}U^c U^{d'} - \frac{1}{4}[(\log h) - 2\bar{D}_a U^a]h'_{ab} - \frac{1}{4}(\log h)'(Ah'_{ab} + \dot{h}_{ab} - \bar{D}_a U_b - \bar{D}_b U_a) \\ &\quad + \frac{1}{2}(h_{bc}\bar{D}_a U^{c'} + h_{ac}\bar{D}_b U^{c'}) = 0, \end{aligned} \quad (2.4)$$

where the prime and dot denote the r and u derivative, respectively, \bar{D}_a is a covariant derivative with h_{ab} and $h = \det h_{ab}$. Also, ${}^{(h)}R_{ab}$ is the Ricci tensor with respect to h_{ab} . The evolutions of the metric functions A , U^a and h_{ab} are determined by Eqs. (2.2), (2.3) and (2.4) completely.

The other components of the Einstein equations are constraint equations on the initial surface. For convenience, we provide the following constraint equation at $r = 0$

$$R_{uu} \hat{=} -\frac{1}{2}(\log \ddot{h}) + \frac{A'}{4}(\log \dot{h}) - \frac{1}{4}h^{ac}h^{bd}\dot{h}_{ab}\dot{h}_{cd} = 0. \quad (2.5)$$

3 Late-time symmetry on and near event horizon

In this section, we show that there is late-time symmetry on the event horizon. Then we will extend it outside of black hole regions.

3.1 Late-time behaviors on event horizon

To investigate late-time behaviors of the event horizon, we introduce the expansion and shear of the null geodesic generator $l = \partial/\partial u$ of the event horizon. The expansion θ and shear σ_{ab} are defined as

$$\begin{aligned} \sigma_{ab} + \frac{1}{2}\theta h_{ab}^{(0)} &\hat{=} h_a^A h_b^B \nabla_A l_B \\ &\hat{=} \frac{1}{2}\dot{h}_{ab}^{(0)}, \end{aligned} \quad (3.1)$$

where $h_{ab}^{(0)} \hat{=} h_{ab}$. σ_{ab} is the traceless part of $\dot{h}_{ab}^{(0)}$ with respect to $h_{ab}^{(0)}$. Then we can rewrite Eq. (2.5), one of the constraint equations as

$$\partial_w \theta_{(w)} = -\frac{1}{2}\theta_{(w)}^2 - \sigma_{(w)ab}\sigma_{(w)}^{ab}, \quad (3.2)$$

where we used the affine parameter w defined by $dw/du = \exp\left(\int^u A^{(1)}/2du'\right)$. $\theta_{(w)}$ and $\sigma_{(w)ab}$ are expansion and shear with respect to w . Here we remember that the area law of the event horizon holds for spacetimes satisfying the null energy condition, that is, $\theta_{(w)} \geq 0$. Since $\sigma_{(w)ab}\sigma_{(w)}^{ab} \geq 0$, Eq. (3.2) implies the inequality

$$\partial_w \theta_{(w)} + \frac{1}{2}\theta_{(w)}^2 \leq 0. \quad (3.3)$$

Then the integration over w gives us

$$\theta_{(w)} \leq \frac{1}{1/\theta_{(0)} + (w - w_0)/2} \rightarrow 0 \quad (\text{as } w \rightarrow \infty), \tag{3.4}$$

where we used the fact of $\theta_{(0)} = \theta_{(w)}(w = w_0) \geq 0$. In addition, Eq. (3.2) shows that the shear $\sigma_{(w)ab}$ should also vanish as $w \rightarrow \infty$. This is shown as a part of the proof of another theorem [9]. From now on, we assume that $w \rightarrow \infty$ corresponds to $u \rightarrow \infty$. Then, we see that θ and σ_{ab} should also vanish as $u \rightarrow \infty$. It is natural to assume that the cross section of the event horizon is compact. Then the vanishing of the expansion implies that the horizon area approaches a constant and finite value.

Altogether we see the behavior of the metric at late time as $\mathcal{L}_l g_{AB}|_{\text{horizon}} \rightarrow 0$ ($u \rightarrow \infty$). Here we impose the following decaying condition on the event horizon for the metric:

$$\mathcal{L}_l g_{AB} \hat{=} O\left(\frac{1}{u^n}\right), \tag{3.5}$$

which explicitly means $\dot{h}_{ab}^{(0)} = O(u^{-n})$. This equation means that the null geodesic generator of the event horizon l should be an asymptotic Killing vector at late time ($u \rightarrow \infty$). Thus there is a late-time symmetry on the event horizon.

3.2 Extension of late-time symmetry

We consider that the decaying condition of Eq. (3.5) can be extended outside of the event horizon as

$$\mathcal{L}_l g_{AB} = O\left(\frac{1}{u^n}\right). \tag{3.6}$$

We assume the analyticity of g_{AB} .

Under the presence of the analyticity of spacetimes, the above is equivalent with

$$(\mathcal{L}_n)^m \mathcal{L}_l g_{AB} \hat{=} O\left(\frac{1}{u^n}\right), \tag{3.7}$$

where $n = \partial/\partial r$ and $m = 0, 1, 2, \dots$.

In fact, we can show that this equation holds using the induction. Assuming that Eq. (3.7) holds for all $m < k$ where k is some positive integer and applying $(\mathcal{L}_n)^{k-1}$ to Eqs. (2.2), (2.3), and (2.4), we can obtain

$$\mathcal{L}_l A^{(k)} = O\left(\frac{1}{u^n}\right), \mathcal{L}_l U^{(k)a} = O\left(\frac{1}{u^n}\right), \mathcal{L}_l h_{ab}^{(k)} = O\left(\frac{1}{u^n}\right), \tag{3.8}$$

where $^{(m)}$ means the evaluation on the event horizon of the m -th derivatives with respect to r . For example, $h_{ab}^{(m)} = (\mathcal{L}_n)^m h_{ab}|_{r=0}$. Therefore, Eq. (3.8) describes $m = k$ equations of Eq. (3.7).

Using the Einstein equations, we can show that Eq. (3.7), equivalently Eq. (3.6) holds if the spacetime is real analytic. Hence this fact means that the null geodesic generator l of the event horizon is the asymptotic Killing vector at late time in the sense of Eq. (3.6).

4 Summary and discussion

We have confirmed that the expansion and shear of the event horizon should decay at late time in the vacuum spacetimes. Then, assuming the compactness of the cross sections of the event horizon, the null geodesic generators on the horizon give us an asymptotic Killing vector l at late time. This means that the horizon has late-time symmetry. By solving the Einstein equations, then, we have found that this late-time symmetry can be extended outside of the black holes. Therefore, at late time, there is the asymptotic symmetry outside of black holes.

If the black hole rotates and there is another asymptotic Killing vector at late time, k , which will be a stationary Killing vector at a far distance and spacelike near the horizon, $k - l$ is also an asymptotic Killing vector expected to correspond to axisymmetry. In this sense, we would expect that the rigidity holds in gravitational collapse at late time. In these discussions, we assume the compactness of the event horizon. Thus this result cannot be applied to other null hypersurfaces which do not have a compact cross section.

There is a remaining issue. In the proof of the rigidity theorem, the exact stationarity does show that the null geodesic generators of the horizon are Killing orbits. On the other hand, our argument could show us that the null geodesic generators of the horizon is a Killing orbit without assuming the presence of asymptotically stationary Killing vectors. It is likely that this difference suggests the existence of important and new points in black hole physics.

References

- [1] W. Israel, Phys. Rev. **164**, 1776 (1967); B. Carter, Phys. Rev. Lett. **26**, 331 (1971); S. W. Hawking, Commun. Math. Phys. **25**, 152 (1972); D. C. Robinson, Phys. Rev. Lett. **34**, 905 (1975); P. O. Mazur, J. Phys. **A15**, 3173 (1982); For a review, see M. Heusler, *Black Hole Uniqueness Theorems*, (Cambridge University Press, London, 1996); P. O. Mazur, hep-th/0101012; G. L. Bunting, PhD thesis, Univ. of New England, Armidale (1983).
- [2] S. W. Hawking and G. F. R. Ellis, *The Large scale structure of space-time*, (Cambridge Univ. Press, Cambridge, 1973).
- [3] S. W. Hawking, Commun. Math. Phys. **25**, 152-166 (1972).
- [4] H. Friedrich, I. Racz, R. M. Wald, Commun. Math. Phys. **204**, 691-707 (1999).
- [5] I. Racz, Class. Quant. Grav. **17**, 153-178 (2000).
- [6] C. Gundlach, R. H. Price, J. Pullin, Phys. Rev. **D49**, 883-889 (1994).
- [7] L. Barack, A. Ori, Phys. Rev. Lett. **82**, 4388 (1999).
- [8] L. Barack, A. Ori, Phys. Rev. **D60**, 124005 (1999).
- [9] S. A. Hayward, T. Shiromizu, K. -i. Nakao, Phys. Rev. **D49**, 5080-5085 (1994).

Three-body-interaction effects on the relativistic perihelion precession

Kei Yamada and Hideki Asada

*Faculty of Science and Technology,
Hirotsaki University, Hirotsaki 036-8561, Japan*

Abstract

The relativistic perihelion precession due to the three-body interaction is derived. We consider a hierarchical coplanar three-body system like the Sun-Jupiter-Saturn one: Both the secondary object as the largest planet corresponding to Jupiter (mass m_2) and the third one corresponding to Saturn (mass m_3) orbit around the primary object corresponding to Sun (mass $m_1 \gg m_2 \gg m_3$), where the mean orbital radius of the third body is larger than that of the secondary one (denoted as ℓ). We investigate the post-Newtonian effects on the motion of the third body (semimajor axis a , eccentricity e for the Keplerian orbital elements). Under some assumptions with a certain averaging, the relativistic perihelion precession of the third mass by the three-body interaction at the post-Newtonian order is expressed as $6Gm_2\ell^2c^{-2}a^{-3}n(1+9e^2/16)(1-e^2)^{-3}$, where we take the temporal averaging of the secondary position, G and c denote the gravitational constant and the speed of light, respectively, and n denotes the mean motion for the third body defined as $2\pi\sqrt{a^3G^{-1}(m_1+m_2)^{-1}}$.

1 Three-body system like Sun-Jupiter-Saturn

Motivation: Iorio pointed out the anomaly in Saturn's perihelion precession [1], however it is controverted by updated reports of planetary observations [2, 3]. Although, the researches of three-body interaction for the relativistic perihelion precession are based only on the numerical integrations. Therefore, it is interesting to investigate the analytical expression of the perihelion precession due to the relativistic three-body interaction.

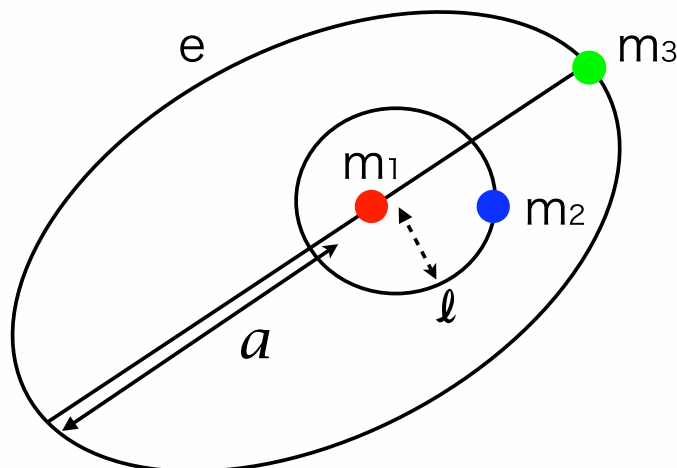


Figure 1: Schematic figure of the hierarchical coplanar three-body system with masses m_1 , m_2 and m_3 .

We consider a hierarchical coplanar three-body system like Sun-Jupiter-Saturn system.

In order to investigate such system, four assumptions are made upon the hierarchical three-body system:

- (i) $m_1 \gg m_2 \gg m_3$
- (ii) $r \gg \ell$
- (iii) the same orbital plane (coplanar)
- (iv) a circular motion for m_2

2 The effective metric acting on the third mass

In the post-Newtonian approximation, the line element for N masses is expressed as [4]

$$\begin{aligned}
 ds^2 &= g_{\mu\nu}(t, \mathbf{r}) dx^\mu dx^\nu \\
 &= \left[-1 + 2 \sum_A \frac{m_A}{r_A} - 2 \left(\sum_A \frac{m_A}{r_A} \right)^2 + 3 \sum_A \frac{m_A v_A^2}{r_A} - 2 \sum_A \sum_{B \neq A} \frac{m_A m_B}{r_A r_{AB}} \right] dt^2 \\
 &\quad + 2 \times \left[- \sum_A \frac{m_A}{r_A} \left\{ \frac{7}{2} v_{Aj} + \frac{1}{2} \frac{(\mathbf{v}_A \cdot \mathbf{r}_A) r_{Aj}}{r_A^2} \right\} \right] dt dx^j \\
 &\quad + \left[1 + 2 \sum_A \frac{m_A}{r_A} \right] \delta_{ij} dx^i dx^j,
 \end{aligned} \tag{2.1}$$

where $(x^\mu) = (t, \mathbf{r})$ for $\mu = 0, 1, 2, 3$, the position of each mass m_A is denoted as \mathbf{R}_A , the relative vectors and distances are defined as $\mathbf{r}_A \equiv \mathbf{r} - \mathbf{R}_A$, $\mathbf{R}_{AB} \equiv \mathbf{R}_A - \mathbf{R}_B$, $r_A \equiv |\mathbf{r}_A|$, $R_{AB} \equiv |\mathbf{R}_{AB}|$.

By using four assumptions, we finally obtain the effective (averaged) metric acting on the third mass as [5]

$$\begin{aligned}
 \langle ds^2 \rangle &= \left(-1 + \frac{2m_{tot}}{r} + \frac{m_2 \ell^2}{2r^3} + \frac{m_{tot} m_2 \ell^2}{r^4} - \frac{m_{tot} m_2 \ell^2}{\ell^3 r} \right) dt^2 \\
 &\quad + \left(1 + \frac{2m_{tot}}{r} + \frac{3m_2 \ell^2}{2r^3} \right) dr^2 + r^2 d\varphi^2 \\
 &= \left(-1 + \frac{r_s}{r} \left(1 - \frac{Q}{\ell^3} \right) + \frac{Q}{r^3} + \frac{r_s Q}{r^4} \right) dt^2 + \left(1 + \frac{r_s}{r} + \frac{3Q}{r^3} \right) dr^2 + r^2 d\varphi^2,
 \end{aligned} \tag{2.2}$$

which looks like an effective one-body metric with quadrupole moments. Here, we have already used $\theta = \pi/2 = \text{const.}$ and we defined the total mass as $m_{tot} = m_1 + m_2$, the effective Schwarzschild radius as

$$r_s = 2m_{tot}, \tag{2.3}$$

and the effective moment induced by the secondary body as

$$Q \equiv \frac{m_2 \ell^2}{2}. \tag{2.4}$$

It follows that the line element given by Eq. (2.2) agrees with the Schwarzschild metric on the equatorial plane if $Q = 0$.

3 Perihelion precession for three-body system in GR

As a result, the total deviation from the Newtonian value ($= 2\pi$) due to linear Q becomes [5]

$$\Delta\varphi_Q = \frac{3}{2} \frac{(16 + 9e^2)\pi}{(1 - e^2)^3} \frac{Q}{a^3}. \tag{3.1}$$

This is a correction to the perihelion (and aphelion) precession per revolution (perihelion \rightarrow aphelion \rightarrow perihelion). By dividing this by the orbital period P of the third body, we obtain the corresponding perihelion precession rate as [5]

$$\begin{aligned}
 \dot{\omega}_Q &= \frac{\Delta\varphi_Q}{P} \\
 &= 24 \frac{(1 + \frac{9}{16}e^2)}{(1 - e^2)^3} \frac{Q}{a^3} \frac{\pi}{P} \\
 &= 6 \frac{(1 + \frac{9}{16}e^2)}{(1 - e^2)^3} \frac{m_2 \ell^2}{a^3} n,
 \end{aligned} \tag{3.2}$$

where $n = 2\pi P^{-1}$ is the mean motion of the third mass.

Table 1: $\dot{\omega}_{Sat}$ by planets inside the Saturn's orbit. Eq. (3.2) is used for this evaluation.

planet	m_2 [kg]	ℓ [AU]	$\dot{\omega}_{Sat}$ [arcsec/cy]
Mercury	3.30×10^{23}	0.387	7.50×10^{-12}
Venus	4.87×10^{24}	0.723	3.86×10^{-10}
Earth	5.98×10^{24}	1.00	9.08×10^{-10}
Mars	6.42×10^{23}	1.52	2.26×10^{-10}
Jupiter	1.90×10^{27}	5.20	7.80×10^{-6}

4 Conclusion

We derived the relativistic perihelion precession due to the three-body interaction for a hierarchical coplanar three-body system corresponding to the Sun-Jupiter-Saturn one. For the Sun-Jupiter-Saturn system, this precession yields 7.8×10^{-6} arcsec/cy, which is larger than the Lense-Thirring effect by Sun ($O(10^{-7})$ arcsec/cy). As for the relativistic three-body-interaction perihelion precession of Saturn, the Jovian contribution is the most dominant among those by the planets inside the Saturn's orbit.

References

- [1] L. Iorio, *Astron. J.* **137**, 3615 (2009).
- [2] E. V. Pitjeva, private communication, (2011).
- [3] Agnes Fienga, et al., [arXiv:1108.5546 \[astro-ph\]](#), (2011).
- [4] C. W. Misner, K. S. Thorne, J. A. Wheeler, *Gravitation*, (Freeman, New York, 1973).
- [5] K. Yamada and H. Asada, [arXiv:1105.2998 \[gr-qc\]](#), (2011).

Gravitational collapse of ring objects in five-dimensional space-time

Yuta Yamada¹⁰⁷ and Hisa-aki Shinkai¹⁰⁸

*Faculty of Information Science and Technology, Osaka Institute of Technology,
Hirakata, Osaka 573-0196, Japan*

Abstract

Numerical studies of gravitational collapses of ring objects are reported. We followed dynamics of collisionless particles which are distributed in toroidal configurations in non-rotating space-time, comparing their evolutions both in four and five-dimensional space-time. All the models evolve into a single spherical black-hole, while we observed a formation of ring-shaped ($S^2 \times S^1$) apparent horizon in their earlier stage for large radius ring matter in five-dimensional cases. The topology change of apparent horizon occurs as their area gradually increases. Since we do not include any rotations of space-time, all collapses proceed so quickly that no observer can be escaped from the center of the ring if he/she observed an appearance of a ring black hole.

1 Introduction

In recent years, the so-called “large extra-dimensional models” have been investigated as a consequence of brane-world pictures. It is expected that the LHC detects productions (and evaporations) of mini black-holes if our universe is constructed with higher dimension more than four. With this background, black-holes in higher dimensional space-time are extensively studied for a decade.

In such studies of higher dimensional black-hole, one of the most interesting aspects is the discovery of black-ring solution[1] with horizon of $S^2 \times S^1$ topology in $U(1) \times U(1)$ space. Discovery of black-ring solution indicates that there is no uniqueness theorem under the assumption of stationary and axisymmetry in higher dimensional space-time. Furthermore, many interesting discoveries of new black-hole solutions which are called “black objects” have been reported and their properties are being revealed.

Recently, it was suggested that fat black-ring might be unstable because of the existence of initial data which violates the local Penrose inequality[2]. However, fully relativistic dynamical features of black-ring, such as the formation processes and topological transition, are still unknown. We plan to investigate dynamical features of black-objects using numerical simulations.

In our previous work, we investigated the initial data sequences of non-rotating spheroidal and ring matter configurations[3]. We numerically solved the Hamiltonian constraint under the assumption of momentarily static and conformally flat. We found a critical ring radius for ring-shaped apparent horizon (AH) and this results indicate that a dynamical transition of horizon’s topology from toroidal to spherical may be observed in a time evolution. We also discussed the validity of the hyper-hoop conjecture using minimum area around matter. We concluded that hyper-hoop conjecture is valid for the formation of spherical (S^3) apparent horizon. Furthermore, we performed the simulation of gravitational collapses with initial data sequences of spheroidal configurations using our full general relativity code[4].

In this article, we report the gravitational collapses of non-rotating ring objects in five-dimensional space-time (5D). Our simulations does not include angular momentum, but the model would be helpful for understandings of black-ring space-time. We search both AH of spherical and ring-shaped during time evolution.

2 Our numerical approach

2.1 Initial data

The initial data are constructed on four-dimensional space-like hypersurface $\Sigma^{(4)}$. By assuming the time symmetry, non-trivial equation is only the Hamiltonian constraint equation. We apply the standard conformal approach to

¹⁰⁷Email address: yamada@is.oit.ac.jp

¹⁰⁸Email address: shinkai@is.oit.ac.jp

obtain the spatial metric γ_{ij} . The equations would be simplified with a conformal transformation,

$$\gamma_{ij} = \psi^2 \hat{\gamma}_{ij} \quad \text{for } \Sigma^{(4)}, \quad (2.1)$$

where $\hat{\gamma}_{ij}$ is a trial base metric which we assume conformal flatness as,

$$d\ell^2 = \hat{\gamma}_{ij} dx^i dx^j = dX^2 + X^2 d\theta_1^2 + dZ^2 + Z^2 d\theta_2^2, \quad \text{for } \Sigma^{(4)}. \quad (2.2)$$

The Hamiltonian constraint equation, then, becomes

$$\hat{D}_i \hat{D}^i \psi = -\frac{1}{3} \kappa^2 \hat{\rho} \quad \text{for } \Sigma^{(4)}. \quad (2.3)$$

where D_i , κ^2 and $\hat{\rho}$ express the covariant derivative, gravitational constant and total energy density, respectively. We impose the asymptotically flatness as the outer boundary condition and reflection symmetry as the inner boundary condition as following

$$\psi = 1 + \frac{M_{\text{ADM}}}{r^{N-2}} \quad (\text{at outer boundaries}), \quad (2.4)$$

$$\nabla \psi = 0 \quad (\text{at inner boundaries}), \quad (2.5)$$

where $r = \sqrt{X^2 + Z^2}$, and M_{ADM} can be interpreted as the ADM mass of the configuration.

2.2 Evolution

We developed our evolution code using the standard 4 + 1 ADM formalism. In the $N + 1$ ADM formalism, the metric $g_{\mu\nu}$ is written as

$$g_{\mu\nu} = \begin{pmatrix} -\alpha^2 + \beta_k \beta^k & \beta_i \\ \beta_j & \gamma_{ij} \end{pmatrix}, \quad (2.6)$$

where μ and ν run from 0 to $N + 1$ and i, j, k run from 0 to N . Evolution equations for the spatial metric γ_{ij} and the extrinsic curvature K_{ij} are written as

$$\frac{\partial \gamma_{ij}}{\partial t} = -2\alpha K_{ij} + D_i \beta_j + D_j \beta_i, \quad (2.7)$$

$$\begin{aligned} \frac{\partial K_{ij}}{\partial t} &= \alpha^{(N)} R_{ij} + K K_{ij} - 2\alpha K_{il} K^{lj} - \kappa^2 \alpha \left(S_{ij} + \frac{1}{N-1} \gamma_{ij} (\rho - S) \right) \\ &\quad - D_i D_j \alpha + D_i \beta^m K_{mj} + D_j \beta^m K_{mi} + \beta^m D_m K_{ij}, \end{aligned} \quad (2.8)$$

where α and β_i are the lapse function and shift vector, S is the trace of stress tensor, respectively. We assume the asymptotical flatness,

$$\gamma_{ij} = \delta_{ij} + \frac{\text{const}}{r^{N-2}}, \quad (2.9)$$

at the outer boundary. We also impose the reflection symmetry on the inner boundary.

For the lapse condition, we apply the maximal time slicing condition ($K = 0$) at $t = 0$ (for the first time step), and K-driver condition during time evolution. In 5D, the condition is given by

$$D_i D^i \alpha = \alpha \left(K_{ij} K^{ij} + 2\kappa^2 \rho - \kappa^2 S - \frac{4\kappa^2}{3} (\rho - S) \right). \quad (2.10)$$

We solve this elliptic equation by imposing the asymptotically flatness. Solving Eq.(2.10) is computationally expensive since it is an elliptic partial differential equation. During time evolution, we adopt the K-driver condition, $\partial_t K = -cK$, (where c is a positive constant) which drives K back to zero so that the lapse function approximately satisfies the maximal time slicing condition. The K-driver for 5D is written down as

$$\frac{\partial \alpha}{\partial t} = \epsilon D_i D^i \alpha - \epsilon \alpha \left(K_{ij} K^{ij} + 2\kappa^2 \rho - \kappa^2 S - \frac{4\kappa^2}{3} (\rho - S) \right) - \epsilon \beta^i D_i K - \epsilon c K, \quad (2.11)$$

where ϵ acts as an effective diffusion constant. We also use zero shift condition $\beta^i = 0$ since we assume non-rotating space-time.

We use the 5D Cartoon method[5] for expressing the axisymmetric system for both the initial data set and time evolution. This method was proposed as a prescription for constructing a symmetric space-time numerically, in which the essence is not to use curvilinear coordinates but to use the Cartesian coordinates. This idea simplifies the treatment on the axis.

We express ring configurations by distributing a collisionless particles. Each particle follows the geodesic equation which we solved using the fourth-order Runge-Kutta method.

3 Numerical results

Figure 1 shows snapshots of 5D axisymmetric evolutions of ring matter which is described with 5000 particles and same ADM mass for all cases. We see that when initial ring radius is $R_c/M = 0.75$, common AH is observed at $t/M = 1.1$. While we see that when initial ring radius is $R_c/M = 1.5$, ring-shape AH is observed at $t/M = 1.7$. We also find that topological transition occur to spherical (S^3) from ring-shape ($S^2 \times S^1$) at $t/M = 2.7$.

In Fig.2, we show the area of both common and ring AHs as a function of coordinate time. We show three cases of the initial ring radius; $0.5M$, $1.5M$ and $2.0M$. Common or ring AH is formed for all cases. We see that the area of AHs monotonically increases in all cases. Furthermore, we find that the area of common AH is larger than that of ring AHs, when the topological transition is observed.

For the case of $R_c(t=0)/M = 1.5$ (right panel in Fig.1), we check whether the observer at the origin who watched the appearance of the ring AH can escape outside or not. Fig.3 shows the snapshots of the hypersurfaces on x and z axis with the proper-time. In Fig.3, solid lines colored by red, blue and green express a common and ring AH and light ray, respectively. For this case, the light ray which emitted from the inner ring AH reaches to origin at proper-time $t = 1.6$ (left panel in Fig.3). Even if the observer tries to escape with the speed of light just after that time, he/she can not move outside of the common AH.

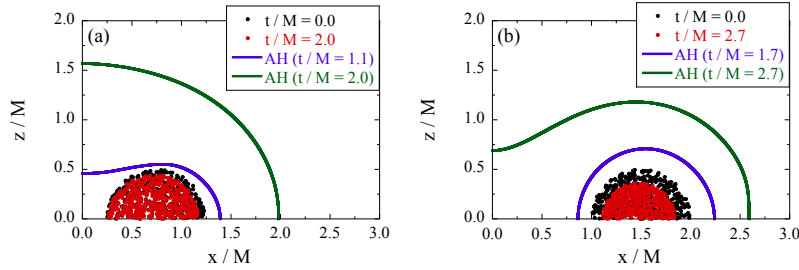


Figure 1: Snapshots of time evolutions plotting particles and location of AH. Number of particles are reduced to 1/10 for figures. We set initial ring radius to $R_c/M = 0.75$ (left panel) and $R_c/M = 1.5$ (right panel). We see that a common AH is directly formed at $t/M = 1.1$ in the left panel, while we see a topological transition of AHs to spherical from ring-shape at $t/M = 2.7$ in the right panel.

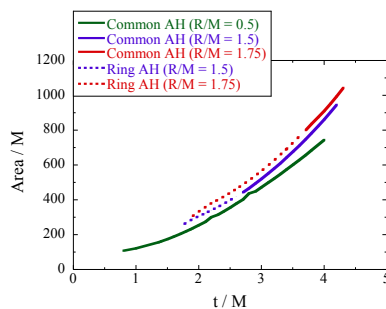


Figure 2: Area of AHs is shown for three cases that initial ring radius is $0.5M$, $1.5M$ and $2.0M$. Area is normalized with ADM mass M_{ADM} . Dotted lines express ring AH's area. Common AH's areas are expressed by solid lines. AHs monotonically increase in time. We see that the area of common AH is larger than that of the ring AHs, when the topological transition is observed.

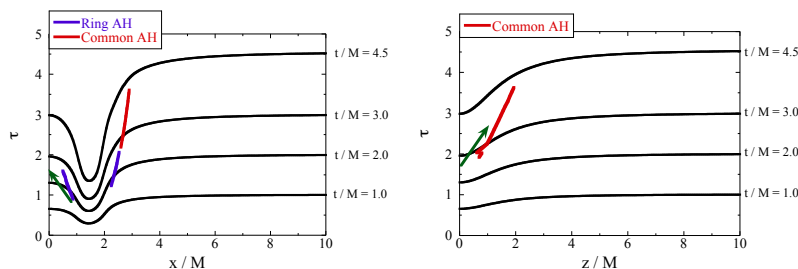


Figure 3: The snapshots of the hypersurfaces on x and z axis in the proper-time. The arrow indicates the path of light, which shows the observer at the origin cannot escape if he/she sees the appearance of a ring-shaped horizon.

4 Discussion

In this paper, we reported gravitational collapses of non-rotating ring configurations in 5D space-time. We found that topological transition of AH during the ring matter collapses where we observed monotonical increase of the area of AHs both common and ring AHs. We also found that no observer can escape from the center of the ring if he/she observed an appearance of a ring black hole since all collapses proceed so rapidly. Up to this moment, we only checked the existence of apparent horizons, and not the event horizons. The system does not include any angular momentums. We are implementing our code to cover these studies. This work was supported partially by the Grant-in-Aid for Scientific Research Fund of Japan Society of the Promotion of Science, No. 22540293. Numerical computations were carried out on SR16000 at YITP in Kyoto University, and on the RIKEN Integrated Cluster of Clusters (RICC).

References

- [1] R. Emparan and H. S. Reall, Phys. Rev. Lett. **88**, 101101 (2002).
- [2] P. Figueras, K. Murata and H. S. Reall, arXiv : 1107.5785 (2011).
- [3] Y. Yamada and H. Shinkai, Class. Quant. Grav. **27**, 045012 (2010).
- [4] Y. Yamada and H. Shinkai, Phys. Rev. D **83**, 064006 (2011).
- [5] M. Shibata and H. Yoshino, Phys. Rev. D. **80**, 084028 (2009).

Screening the Cosmological Constant in non-local gravity

Ying-li Zhang^{109(a)} and Misao Sasaki^{110(a)}

^(a) *Yukawa Institute for Theoretical Physics, Kyoto University, Kyoto 606-8502, Japan*

Abstract

In this paper, we consider a class of model of non-local gravity with a large bare cosmological constant, Λ , and study its cosmological solutions. In the absence of matter, we find a power-law expanding universe solution $a \propto t^n$ with $n < 1$, that is, a universe with decelerated expansion without any fine-tuning of the parameter. So the effect of the cosmological constant is effectively screened in this solution. Also it is found that the solution is ghost-free for a very wide range of parameters. Thus our solution opens up new possibilities for solution to the cosmological constant problem.

1 Introduction

Since the discovery of the accelerated expansion of the current universe, there arise extensive discussions on the mechanism to explain the observation within or beyond the Einstein gravity. One of the simplest model is to modify the right-hand side of the Einstein gravity where a cosmological constant term Λ and other unknown matter terms are added. Another popular approach involves the modification of gravity, so that the late-time accelerated expansion can be obtained 'naturally'. Among them, one of the most extensively studied of such modifications is $F(R)$ theory, where F is an arbitrary function of Ricci scalar R . Recently, inspired by the study of string/M theory or conventional quantum gravity, another type of the modification of gravity, called non-local gravity, attracts more and more attentions. In this theory, a non-local term $f(\square^{-1}R)$ is added into the action, where f is an arbitrary function and \square^{-1} is the inverse of d'Alembertian operator. Its cosmological effect and other various aspects has been studied in [1].

Here we concern on another aspect of non-local gravity. It is proposed in [2] that there is some hope to solve the cosmological constant problem in this framework. Inspired by their claim, a detailed mechanism to screen the cosmological constant in the non-local gravity is presented in [3]. However, like the situation of any other theories with higher-derivatives, here the non-local operator \square^{-1} often involves a wrong sign in the kinetic term, that is a ghost which will lead to the instability of the system. Some attempts have been made to avoided this problem around the flat or deSitter spacetime, but now successful up to now.

In this paper, we consider a simple one-parameter family of non-local gravity models with bare cosmological constant Λ and study their cosmological solutions. The models are characterized by a function $f(\psi) = f_0 e^{\alpha\psi}$ where $\psi \equiv \square^{-1}R$, with α being the real, dimensionless parameter. We assume the universe is spatially flat, and consider the case where there is no matter contribution. Interestingly, we find a power-law solution $a \propto t^n$, where a is the cosmic scale factor, with $n < 1$. This implies that the effect of the cosmological constant is completely shielded to render the expansion of the universe decelerated. To be specific, as α varies from $-\infty$ to $+\infty$, n increases monotonically from 0 to 1/2. Thus the universe behaves like a radiation-dominated universe for $\alpha \gg 1$. Then we examine if the solution is free from a ghost. To our happy surprise, it is found that for a very wide range of the parameter α , namely for $\alpha > \alpha_{cr} \approx 0.17$, the solution is found to be ghost-free. For this range of α , we find $n > n_{cr} \approx 0.35$.

2 Non-local gravity and ghost-free condition

We consider a class of non-local gravity whose action is given by

$$S = \int d^4x \sqrt{-g} \left\{ \frac{1}{2\kappa^2} [R(1 + f(\square^{-1}R)) - 2\Lambda] + \mathcal{L}_{\text{matter}}(Q; g) \right\}, \quad (2.1)$$

where $\kappa^2 = 8\pi G$, f is a function that characterizes the nature of non-locality with \square^{-1} being the inverse of the d'Alembertian operator, Λ is a (bare) cosmological constant and Q stands for matter fields. For definiteness, we

¹⁰⁹Email address: yingli@yukawa.kyoto-u.ac.jp

¹¹⁰Email address: misao@yukawa.kyoto-u.ac.jp

assume matter is coupled minimally to gravity. Therefore, the above may be regarded as an action in the Jordan frame.

In this simple class of non-local gravity, we rewrite the action into a local form by introducing two scalar fields ψ and ξ as

$$\begin{aligned} S &= \int d^4x \sqrt{-g} \left[\frac{1}{2\kappa^2} \{R(1+f(\psi)) - \xi(\square\psi - R) - 2\Lambda\} + \mathcal{L}_{\text{matter}} \right] \\ &= \int d^4x \sqrt{-g} \left[\frac{1}{2\kappa^2} \{R(1+f(\psi)+\xi) + g^{\mu\nu} \partial_\mu \xi \partial_\nu \psi - 2\Lambda\} + \mathcal{L}_{\text{matter}} \right]. \end{aligned} \quad (2.2)$$

Assuming a spatially flat FLRW universe with the metric,

$$ds^2 = -dt^2 + a^2(t) \delta_{ij} dx^i dx^j, \quad (2.3)$$

by varying the action with respect to $g_{\mu\nu}$, ξ and ψ , respectively, one obtains the field equations as

$$0 = -3H^2(1+f(\psi)+\xi) - \frac{1}{2}\dot{\xi}\dot{\psi} - 3H(f'(\psi)\dot{\psi} + \dot{\xi}) + \Lambda + \kappa^2\rho, \quad (2.4)$$

$$0 = (2\dot{H} + 3H^2)(1+f(\psi)+\xi) - \frac{1}{2}\dot{\xi}\dot{\psi} + \left(\frac{d^2}{dt^2} + 2H\frac{d}{dt}\right)(f(\psi)+\xi) - \Lambda + \kappa^2 P, \quad (2.5)$$

$$0 = \ddot{\psi} + 3H\dot{\psi} + 6\dot{H} + 12H^2, \quad (2.6)$$

$$0 = \ddot{\xi} + 3H\dot{\xi} + (6\dot{H} + 12H^2)f'(\psi), \quad (2.7)$$

where a dot denotes the time derivative $\dot{} = d/dt$, $H = \dot{a}/a$, and $\rho = -T_0^0$ and $P = T_i^i/3$ are the energy density and pressure of the matter fields, respectively.

To examine whether the theory contains a wrong sign in the kinetic term (ghost) or not, in the following we take an unperturbed approach, that is to make a conformal transformation of the metric to bring the action into the one in the Einstein frame, namely the conformal frame in which the gravitational part of the action (2.2) becomes purely Einstein. For this purpose, from now on, we denote the metric in the Jordan frame by $g_{\mu\nu}$ while the one in the Einstein frame is labeled by the index (E) as $g_{\mu\nu}^{(E)}$ and consider a conformal transformation,

$$g_{\mu\nu} = \Omega^2 g_{\mu\nu}^{(E)}, \quad (2.8)$$

and identify the conformal factor as

$$\Omega^{-2} = 1 + f(\psi) + \xi, \quad (2.9)$$

then the gravitational part of the action becomes Einsteinian as

$$\begin{aligned} S &= \int d^4x \sqrt{-g^{(E)}} \left\{ \frac{1}{2\kappa^2} \left(R^{(E)} - 6\nabla^{\mu(E)} \phi \nabla_{\mu}^{(E)} \phi - 2\nabla^{\mu(E)} \phi \nabla_{\mu}^{(E)} \psi - e^{2\phi} f'(\psi) \nabla^{\mu(E)} \psi \nabla_{\mu}^{(E)} \psi - 2e^{4\phi} \Lambda \right) \right. \\ &\quad \left. + e^{4\phi} \mathcal{L}_{\text{matter}}(Q; e^{2\phi} g^{(E)}) \right\}. \end{aligned} \quad (2.10)$$

It is now easy to derive the ghost-free condition. Since there are only two scalar fields, the condition for the absence of a ghost is that the trace and the determinant of the kinetic term matrix are both positive. In the present case, it is readily seen that only the positivity of the determinant is sufficient, that is,

$$\det \begin{vmatrix} 6 & 1 \\ 1 & e^{2\phi} f'(\psi) \end{vmatrix} > 0. \quad (2.11)$$

In terms of the original fields, this condition is expressed as

$$f'(\psi) > \frac{1}{6}(1+f(\psi)+\xi) > 0, \quad (2.12)$$

where $1+f(\psi)+\xi > 0$ is a necessary condition from Eq. (2.9). Later the above condition is used to examine if our cosmological solutions are free from ghosts or not.

3 Cosmological solutions

As a class of simple non-local gravity models, we consider the case when $f(\psi)$ is given by an exponential function,

$$f(\psi) = f_0 e^{\alpha\psi}. \quad (3.1)$$

we look for cosmological solutions with the assumption that the scale factor is a power-law function of time t , $a \propto t^n$. We also assume the absence of matter fields, $\rho = P = 0$. By solving the system of equations (2.4) - (2.7), one obtains the following solutions for scalar fields $\psi(t)$ and $\xi(t)$:

$$\psi(t) = \frac{1}{\alpha} \ln \left[\frac{\Lambda t^2}{6f_0 n(n+1)} \right], \quad \xi(t) = -1 - \frac{(2n-1)\alpha\Lambda t^2}{2(3n+1)(n+1)}, \quad (3.2)$$

where the index n is determined by the second equation in terms of parameter α as

$$6\alpha n^2 + 3(1-\alpha)n - 1 = 0. \quad (3.3)$$

so in principle there exist two solutions for n as

$$n_1 = \frac{-3 + 3\alpha + \sqrt{3(3\alpha^2 + 2\alpha + 3)}}{12\alpha}, \quad n_2 = \frac{-3 + 3\alpha - \sqrt{3(3\alpha^2 + 2\alpha + 3)}}{12\alpha}. \quad (3.4)$$

which are plotted in fig.1 in terms of real parameter α . From the figure, we notice that an expanding solution is given by $n = n_1$ for any α and by $n = n_2$ for $\alpha < 0$. In both cases, n approaches $1/2$ for $|\alpha| \gg 1$, that is, the evolution of the universe looks like a radiation-dominated one.

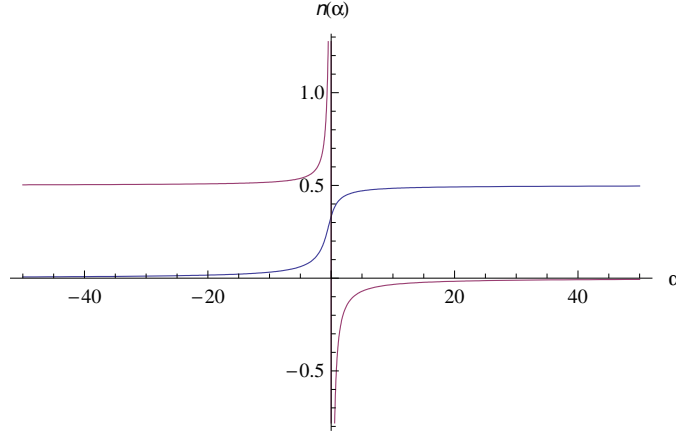


Figure 1: Index n as a function of parameter α . Here the blue line (the one in the middle, which is regular at $\alpha = 0$) denotes $n = n_1$ and the red line $n = n_2$.

Inserting solutions eq.(3.2) and (3.4) into the ghost-free condition eq.(2.12), one finds that n_2 is excluded, while for n_1 , the parameter α is constrained by

$$\alpha > \alpha_{cr} = \frac{1}{15} (7 - 2^{\frac{1}{3}} - 2^{\frac{5}{3}}) \approx 0.17 \implies 1/2 > n(=n_1) > n_{cr} \approx 0.35, \quad (3.5)$$

which implies a decelerated expanding universe in the absence of matter. Thus without any fine-tuning, the solution successfully screens the effect of the cosmological constant that would have led to accelerated expansion. It should be noted that Eq. (2.12) implies $f'(\psi) > 0$, which reduces to the constraint on the parameter $f_0 > 0$ for a positive α . Thus the solution we have obtained in the above is meaningful only for a positive cosmological constant Λ .

To explore the behavior of corresponding solutions in the Einstein frame, under the conformal transformation eq.(2.8), the cosmic proper time t_E in the Einstein frame is related to t by $dt = \Omega dt_E$, so that

$$t_E = \int_0^t \frac{dt}{\Omega} = \frac{\sqrt{\Lambda} t^2}{2\sqrt{(n+1)(3n+1)}}, \quad (3.6)$$

$$H_E = \frac{1}{a_E} \frac{da_E}{dt_E} = \frac{\Omega}{a} \frac{d}{dt_E} \left(\frac{a}{\Omega} \right) = \frac{\Omega^2}{a} \frac{d}{dt} \left(\frac{a}{\Omega} \right) = \frac{n_E}{t_E}, \quad (3.7)$$

where $n_E = (n + 1)/2$. Thus, inserting these relationship into solutions in the Jordan frame, eq.(3.2) and (3.5), one soon obtains the corresponding solutions in the Einstein frame as

$$\psi(t) = \frac{1}{\alpha} \ln \left[\frac{1}{3f_0(2n_E - 1)} \sqrt{\frac{\Lambda(3n_E - 1)}{n_E}} t_E \right], \quad (3.8)$$

$$\xi(t) = -1 - \frac{\alpha(4n_E - 3)}{2} \sqrt{\frac{\Lambda}{n_E(3n_E - 1)}} t_E, \quad (3.9)$$

where $0.75 > n_E > n_{E,cr} \approx 0.675$. Thus we conclude that the screening mechanism is also valid in the Einstein frame.

Before closing this section, an important comment is in order. As we demonstrated, the theory can be recasted in the form of a scalar-tensor theory or in the form of Einstein gravity plus two scalar fields. Therefore one might consider our theory to be simply a scalar-tensor theory that gives rise to a decaying cosmological constant. Technically this is true. But it should be emphasized that the form of the action for these scalar fields in either the original frame or the Einstein frame is completely fixed by the original form of non-local gravity given by eq.(2.1): There is no freedom in maneuvering the form of the Lagrangian for these scalar fields. In other words, even if one were to regard this theory as a scalar-tensor theory with two non-minimally coupled scalar fields (in the original Jordan frame), it would be highly non-trivial to find a theory that would lead to a solution with a decaying cosmological constant which decays sufficiently fast in the original frame as well as in the Einstein frame.

4 Conclusion

We have studied cosmological solutions in a simple class of non-local gravity with cosmological constant. The model is characterized by a function $f(\psi) = f_0 e^{\alpha\psi}$ where $f_0 > 0$ and α is a real parameter, and ψ is the inverse of the d'Alembertian acting on the scalar curvature, $\psi = \square^{-1}R$. In the absence of matter fields, we have found power-law solutions $a \propto t^n$ with $n < 1$, that is, with decelerated expansion. We have found that for $\alpha > \alpha_{cr} \approx 0.17$, the solution is ghost-free. Thus without any fine-tuning, the solution successfully screens the effect of the cosmological constant that would have led to accelerated expansion.

References

- [1] S. Deser and R. P. Woodard, Phys. Rev. Lett. **99**, 111301 (2007) [arXiv:0706.2151 [astro-ph]].
- [2] N. Arkani-Hamed, S. Dimopoulos, G. Dvali and G. Gabadadze, arXiv:hep-th/0209227.
- [3] S. Nojiri, S. D. Odintsov, M. Sasaki and Y. I. Zhang, Phys. Lett. B **696**, 278 (2011) [arXiv:1010.5375 [gr-qc]].
- [4] K. Bamba, S. Nojiri, S. D. Odintsov and M. Sasaki, arXiv:1104.2692 [gr-qc].
- [5] Y. I. Zhang and M. Sasaki, Int. J. Mod. Phys. D**21**, 1250006 (2012) [arXiv:1108.2112 [gr-qc]].
- [6] T. Koivisto, Phys. Rev. D **77**, 123513 (2008) [arXiv:0803.3399 [gr-qc]].

